STRUCTURAL AND METAMORPHIC EVOLUTION OF THE ARTHUR LINEAMENT, NORTHWESTERN TASMANIA, AUSTRALIA

by

Oliver Håkan Holm B.Sc. (Hons.)
University of New England

UNIVERSITY OF TASMANIA

Submitted in fulfilment of the requirements
for the degree of Doctor of Philosophy (Geology)
University of Tasmania, Hobart
July 2002

STATEMENT

This thesis contains the result of research carried out at the Centre for Ore Deposit Research, University of Tasmania, between 1998 and 2001, and contains no material which has been accepted for a degree or diploma by the University or any other institution, except by way of background information and duly acknowledged in the thesis, and to the best of the candidate's knowledge and belief no material previously published or written by another person except where due acknowledgement is made in the text of the thesis.

This thesis may be made available for loan and limited copying in accordance with the *Copyright Act 1968*.

Oliver H. Holm
University of Tasmania
July 2002

TABLE OF CONTENTS

LIST OF FIGURES

ABSTRACT

The aim of this project is to investigate the origin and deformational history of the Arthur Lineament, using a multi-disciplinary approach. The field-based research concentrated on the structural deformation of the study area. Laboratory-based research included microstructural investigations, whole-rock geochemistry to investigate the mafic igneous rocks in the study area, and metamorphic petrology and geochronology to characterise the timing and nature of the metamorphic events that affected the lineament and surrounding region.

The Arthur Lineament is a Cambrian age, high strain metamorphic belt located in northwest Tasmania, Australia. It is east-dipping, NE-trending, 5 to 10 km wide and approximately 110 km long. The lineament consists of phyllitic to schistose lithologies that have been subject to medium- to high strain, and variably metamorphosed to blueschist, or greenschist grade. The high strain belt comprises several different units. The major lithological unit in the southern Arthur Lineament is the Late Neoproterozoic "eastern" Ahrberg Group, which comprises metamorphosed psammite and psammopelite units, transitional to tholeiitic metabasalts and mafic volcanogenic metasediments. The southern Arthur Lineament also contains the Bowry Formation, which contains basalt/dolerite-derived tholeiitic amphibolites that are intruded by minor deformed 777±7 Ma granitoids, a unit correlated with the Ahrberg Group (AGC) and Neoproterozoic high strain turbidite sequences (Burnie and Oonah Formations).

Whole rock geochemistry of the metabasites in the "eastern" and "western" Ahrberg Groups, the Bowry Formation and the AGC have been examined in order to enable an understanding of the tectonic setting, into which the igneous rocks were emplaced. The "eastern" and "western" Ahrberg Group sequences, and the AGC, are interpreted to be lithostratigraphic correlates. The units have sequences of transitional tholeiites, that are enriched relative to MORB, and are increasingly tholeiitic towards the top of the stratigraphic pile. The Bowry Formation also comprises transitional tholeiites, however they are more evolved than the other units, and have REE patterns only slightly enriched relative to MORB.

The main orogeny to affect northwestern Tasmania was in the Early to Middle Cambrian. This event (the Tyennan Orogeny) consisted of three deformational episodes. The first two episodes ($Ca D_1$ and $Ca D_2$) were high strain events, related to arc-continent collision. These

involved the emplacement of allochthonous slices, and the structural repetition of units within the lineament. CaD_1 produced isoclinal folding, a schistose axial planar fabric and shearing parallel to the CaF_1 axial plane. CaD_2 was more pervasive than CaD_1, and produced tight to isoclinal folds with a schistose axial planar fabric. The CaS_1 and CaS_2 axial planar foliations are commonly sub-parallel, and the fold axes are close to parallel. The orientation of CaF_1 and CaF_2 folds changes from the low to high strain domains. In the low strain domains, CaF_1 folds are variable in their orientation. CaF_2 folds in the low strain domains are gently east- and west-plunging, with south-dipping axial planes. In the high strain domains, CaF_1 and CaF_2 folds have east-southeast dipping axial planes, and south-plunging fold axes. This is consistent in both the north and the south of the lineament. Structural analysis suggests that the change in orientation is due to a strongly rotational shear component during the CaD_2 event, and this is interpreted as evidence for south-directed transport.

The subsequent CaD_3 event, in the latest Cambrian, involved east-directed thrust. It produced asymmetric folds with gently west-dipping long limbs and steeply east-dipping short limbs. The CaF_3 are gently south plunging, with gently west-dipping axial planes and associated thrust faults. During the Devonian, and associated with extensive granitoid intrusion, two episodes of open, east-west trending folding occurred.

Metamorphic investigations show that two metamorphic events occurred in the Arthur Lineament. The earliest event corresponds to CaD_1. This event has been pervasively overprinted by the CaD_2 event, which has largely obliterated CaD_1 metamorphic textures. Where observed, CaD_1 occurred at greenschist grade in allochthonous units. However in units that are interpreted to be allochthonous, in the Bowry Formation and within part of the "eastern" Ahrberg Group, CaD_1 occurred at blueschist grade with amphibole cores recording conditions of approximately 700-1000 MPa and 450-500°C. Syn-CaD_2 metamorphism varies across the Arthur Lineament. Early in the CaD_2 event in the western parts of the lineament, amphibole compositions indicate that pressures were around 500 MPa, and the metamorphic grade was in the upper greenschist facies. However in parts of the Bowry Formation and the AGC, early CaD_2 temperatures were around 460 ± 40°C, and pressures were around 500-600 MPa. In these rocks, hornblende was stable in the metabasites, and syn-CaD_2 garnet, indicative of localised temperatures of approximately 500°C (greenschist-amphibolite facies transition) were found. During late CaD_2, pressures were around 300-400 MPa and the metamorphic grade was lower greenschist facies. Outside of the lineament, metamorphic conditions during CaD_1 and CaD_2 did not exceed greenschist grade, with temperatures of approximately 400°C and pressures of around 350 MPa.

Metamorphic monazites in northwestern Tasmania and King Island were investigated to define the extent of the Cambrian deformation, and provide insight into other metamorphic events. King Island has experienced a complex metamorphic history. There is no evidence of the Cambrian deformation, however a pronounced 1270 Ma regional metamorphic event, contact metamorphism related to the 760 Ma Wickham Orogeny, and localised, mylonite zone-related metamorphism at 380 Ma were observed. In the Arthur Lineament, the dominant metamorphic event occurred between 510-540 Ma. Monazite growth in metasedimentary samples from within the lineament is attributed to the early-$Ca D_2$ event. However, away from the lineament the Cambrian event is much weaker and significantly older monazites of detrital origin, are common. No strong Devonian peak was observed.

In summary, in northwestern Tasmania, following the Cambrian arc-continent collision, the blueschist grade ($\boldsymbol{Ca}D_1$) allochthonous slices were obducted and transported to the south of the subduction zone, in a progressive deformational event. Other parautochthonous rocks were also transported to the south during this high strain event, with associated shearing and folding occurring at greenschist grade metamorphic conditions. Sequential to this, a near coaxial high strain deformational event took place, detaching other parautochthonous slices that were variably metamorphosed to greenschist and upper greenschist-amphibolite facies (early $\boldsymbol{Ca}D_2$), and overthrusting the different grade slices to the south. During these events, strain-related rotation of the developing folds took place, resulting in a change in orientation of the fold axes from east-west to north south, and foliations from south-dipping to east-dipping, from the low strain zones into the high strain zones. The revised metamorphic geochronology of the Arthur Lineament indicates the early $\boldsymbol{Ca}D_2$ event occurred around 505-510 Ma. During $\boldsymbol{Ca}D_1$ and early $\boldsymbol{Ca}D_2$, the allochthonous and parautochthonous lithologies were structurally emplaced on top of the less deformed, autochthonous units. In the final stage of assembling the tectonostratigraphic 'pile', the various slices were stacked together, and lower greenschist facies metamorphic conditions were developed uniformly in all allochthonous, parautochthonous and autochthonous blocks (late $\boldsymbol{Ca}D_2$). Subsequent to this, the $\boldsymbol{Ca}D_3$ event caused the tilting of the tectonostratigraphy, to complete the evolution of the Arthur Lineament.

ACKNOWLEDGEMENTS

The author would firstly like to express his sincere gratitude to his supervisors, Drs Ron Berry and Tony Crawford, as well as Nic Turner for the guidance, encouragement, support and helpful advice that they have provided over the course of the PhD. This project was made possible through their in depth knowledge and wide-ranging understanding of the issues surrounding Tasmania's geology, and has benefited enormously from the many fruitful discussions about the complex issues surrounding the research topic. From CODES and the Geology Department, Dave Selley, Rob Scott, Stu Bull and Clive Burrett provided useful dialogue on different aspects of the project. Alistair Reed, Dave Seymour, Johnny Everard and Clive Calver from Mineral Resources Tasmania are thanked for their valuable insights into Tasmanian geology. The helpful advice of David Steele from the Central Science Laboratory, during the analytical component of the project is greatly appreciated.

Goldstream Pty Ltd are thanked for logistical support, including access to remote areas by heli-camps during the first field season, and access to drill core from their exploration workings in the Rocky River and Lucy Spur areas. Accommodation provided by Australian Bulk Minerals Savage River Mine during the second and third field seasons was greatly appreciated, making possible the extended fieldwork in the southern part of the study area. Hydro Tasmania is acknowledged for providing access to maintenance tracks around Reece Dam. Hugh Nolan is thanked for his support and malt whisky during the field seasons.

Technical and administrative staff at the University of Tasmania provided much help over the course of the PhD. From the Geology Department and CODES, I would like to thank June Pongratz, Peter Cornish, Lyn Starr, Lynne Vaudrey, Simon Stephens, Christine Higgins, Dianne Steffens, Phil Robinson, Nilar Hlaing and Katie McGoldrick for their various assistance.

Fellow PhD students, in particular Andrew Rae, Rick (and Mel) Squire, Meng Limtrakun, Sarah Jones, Dene Carroll and Owen Hatton are thanked for their camaraderie, and many discussions outside geology.

I would especially like to thank my parents Virginia and Håkan, my brother Rick, as well as my extended family, Sally, Norman, Angela and Jeremy Bakker, and Adam Hartnett, for their constant support and enthusiasm. Finally, I would like to dedicate this work to my wife Vanessa Bakker, who has encouraged me to fulfil my goals, and helped make them possible.

CHAPTER 1

INTRODUCTION

1.1 Preamble

1.1.1 Location and Access

The Arthur Lineament is situated in northwestern Tasmania and extends from the north coast near Somerset (390000 mE, 5460000 mN), to the west coast, near Granville Harbour (335000 mE, 5370000 mN), covering an area 5 to 10 km wide and 110 km long (Figure 1.1). Parts of the lineament are covered by Permian, Tertiary and Quaternary sequences. Access to various parts of the Arthur Lineament can be gained by several different roads and disused forestry tracks, although a vast area of the Arthur Lineament is quite remote and only accessible on foot by traversing up creeks, or by boat or helicopter, due to the dense vegetation, and steep terrain.

The southern Arthur Lineament is accessed by the C249 and C252 and Granville Harbour roads to the north of Zeehan, and the B23 and C247 roads between Waratah, Savage River and Corinna townships. The northern Arthur Lineament is primarily accessed by the National Highway (1) and A2 road on the north coast.

Mapping during the first field season (2/1998-4/1998) was carried out with logistical support from Goldstream Pty Ltd, in part using a helicopter-camp at Lucy Spur, to the north of the Paradise River, using tracks cut for a soil sampling and drilling exploration program.

1.1.2 Geomorphology, Climate, Flora and Fauna

The study area ranges in elevation from sea level to around 200m a.s.l on average, with peaks reaching 500m a.s.l. Although there is only moderate elevation, the contrast in relief is marked. Rivers and creeks typically have permanent flow, and are deeply incised.

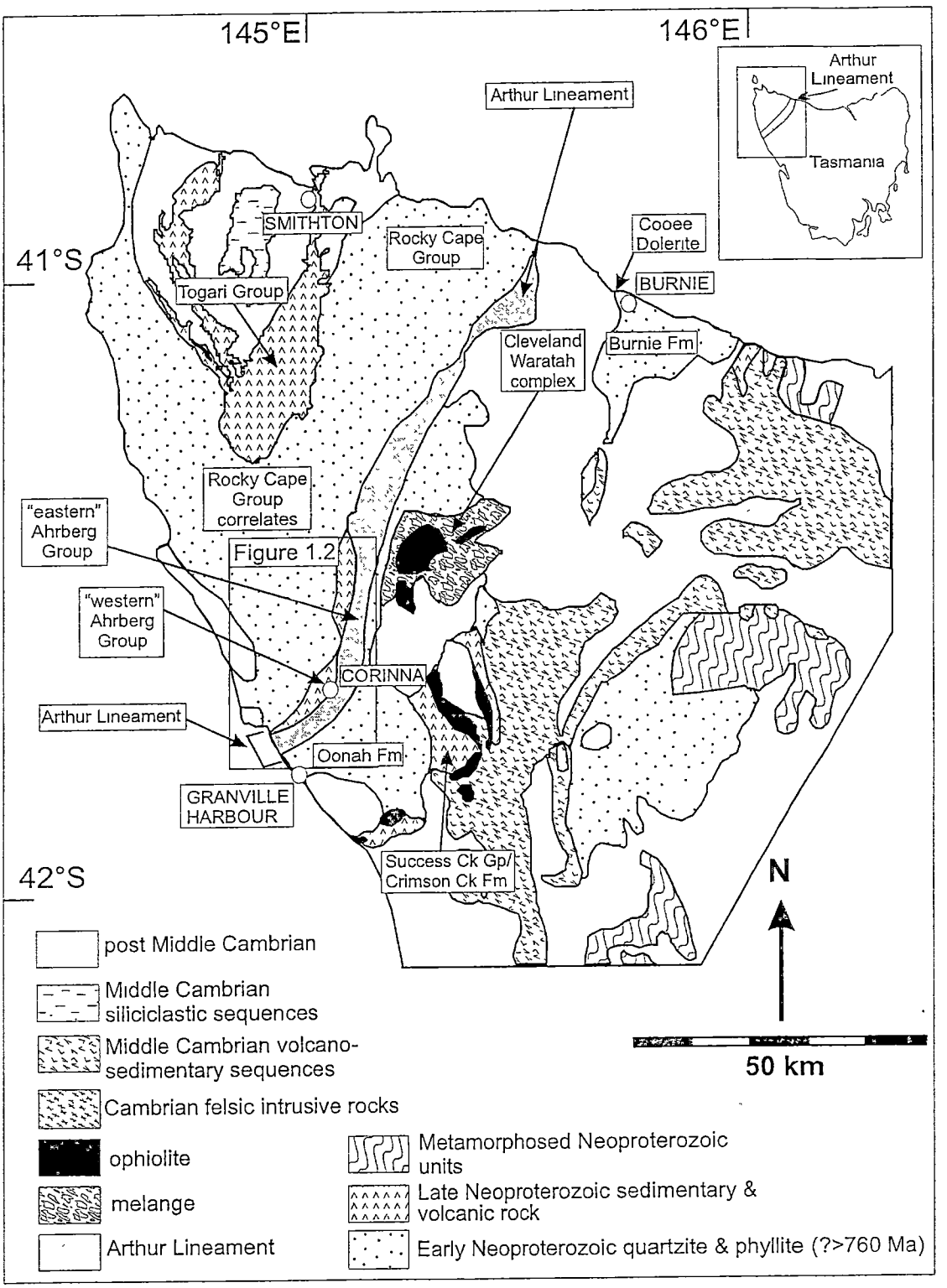

Figure 1.1. Setting of the Arthur Lineament, NW Tasmania (modified after Brown *et al.* 1995). The Arthur Lineament consists of the high strain (metamorphosed) Burnie and Oonah Formations, the "eastern" Ahrberg Group, the Bowry Formation, and other uncorrelated fault bounded units.

Northwestern Tasmania receives between 1200 and 2400 mm of rainfall per annum. The majority of the field area is in the range 1800 to 2400 mm. Maximum and minimum temperatures are in the range of 12 to 25 °C, and 3 to 9 °C, respectively, per annum (courtesy of the Commonwealth of Australia, Bureau of Meteorology). Maximum temperatures and minimum rainfall coincide between January and March, whereas minimum temperatures and maximum rainfall coincide in June to September. The west coast features stunted coastal heath due to prevailing westerly winds that are frequently rain-bearing, coming from the Southern Ocean. Away from the coast, the river valleys feature cool-temperate rainforest, whereas the plateau areas are dominated by sedgeland due to poor, peaty, acid soils with a high water table.

1.2 Objective and Scope of Study

The primary objective of this study is to document the geological history of the Late Neoproterozoic to Early Palaeozoic Arthur Lineament, as defined by Gee (1967a), with a focus on the tectonic setting, structure and metamorphism of this important and poorly documented feature. This has involved the detailed mapping of the Arthur Lineament and the units that bound it to the east and to the west. This has been carried out in order to establish whether the lineament boundaries and the lithologies within it are conformable or fault-bounded, and whether the metamorphic boundaries are transitional or sharp in nature.

Further objectives are to:

- Use whole rock geochemical analysis to compare the compositions of the different mafic sequences within the Rocky Cape Group correlates, "eastern" Ahrberg Group, Ahrberg Group correlate (AGC), Bowry Formation and "western" Ahrberg Group;
- Define structural domains and attempt correlation of deformational events between the different units;
- Carry out detailed metamorphic texture and strain analysis across the lineament;
- Undertake a geochronological study using metamorphic monazites in variably metamorphosed mudstones and pelites in the Rocky Cape Group correlates, "eastern" and "western" Ahrberg Groups, Bowry Formation, and the Burnie and

Oonah Formations, in order to establish the metamorphic ages of the different units.

1.3 Geological Setting and Proposed Model

The Arthur Lineament (Gee 1967a) is a NE-trending, east-dipping Early Palaeozoic high strain metamorphic belt in northwestern Tasmania (Figures 1.1 to 1.3). The lithologies in the Arthur Lineament are phyllitic to schistose and have been subject to medium- to high strain, and variably metamorphosed to blueschist, or lower to upper greenschist grade.

Turner *et al.* (1991) interpreted the southern part of the Arthur Lineament to consist of the "Timbs Group", and the strongly deformed Oonah Formation (Figure 1.2). The term "Timbs Group" was first used by Turner *et al.* (1991), but was not formally defined. Furthermore the "Timbs Group" is not a viable stratigraphic unit. It was interpreted to be a correlate of the Neoproterozoic Togari and Ahrberg Groups in northwestern Tasmania, based on its similar stratigraphy and identical chemistry of the tholeiitic mafic sequences (Crawford 1992, Turner & Crawford 1993). However, the "Timbs Group" (Turner *et al.* 1991) includes the Bowry Formation, that contains relict glaucophane, indicating an early blueschist metamorphic history (Chapter 3 and Turner & Bottrill 2001). This is atypical of the remainder of the "Timbs Group", and the unit is interpreted to be allochthonous. Rare blueschist assemblages have been found outside of the Bowry Formation; however these are also considered to be allochthonous (discussed in Chapter 3). Furthermore, the Bowry Formation contains a 777±7 Ma granitoid (Turner *et al.* 1998). Granitoids of this age are unknown elsewhere on mainland Tasmania. The maximum possible age for the base of the Togari Group (correlate of the Ahrberg Group) is <750 Ma (Calver & Walter 2000). The Bowry Formation amphibolites that are interlayered with the granitoid have previously been correlated with the Kanunnah Subgroup, which has a preferred age of 650-580 Ma (Crawford 1992, Calver & Walter 2000) (Figure 1.4(a)). Therefore, the Bowry Formation cannot be a lithostratigraphic correlate of the Kanunnah Subgroup or any part of the Ahrberg Group. Turner & Bottrill (2001) discussed the problems associated with large differences in

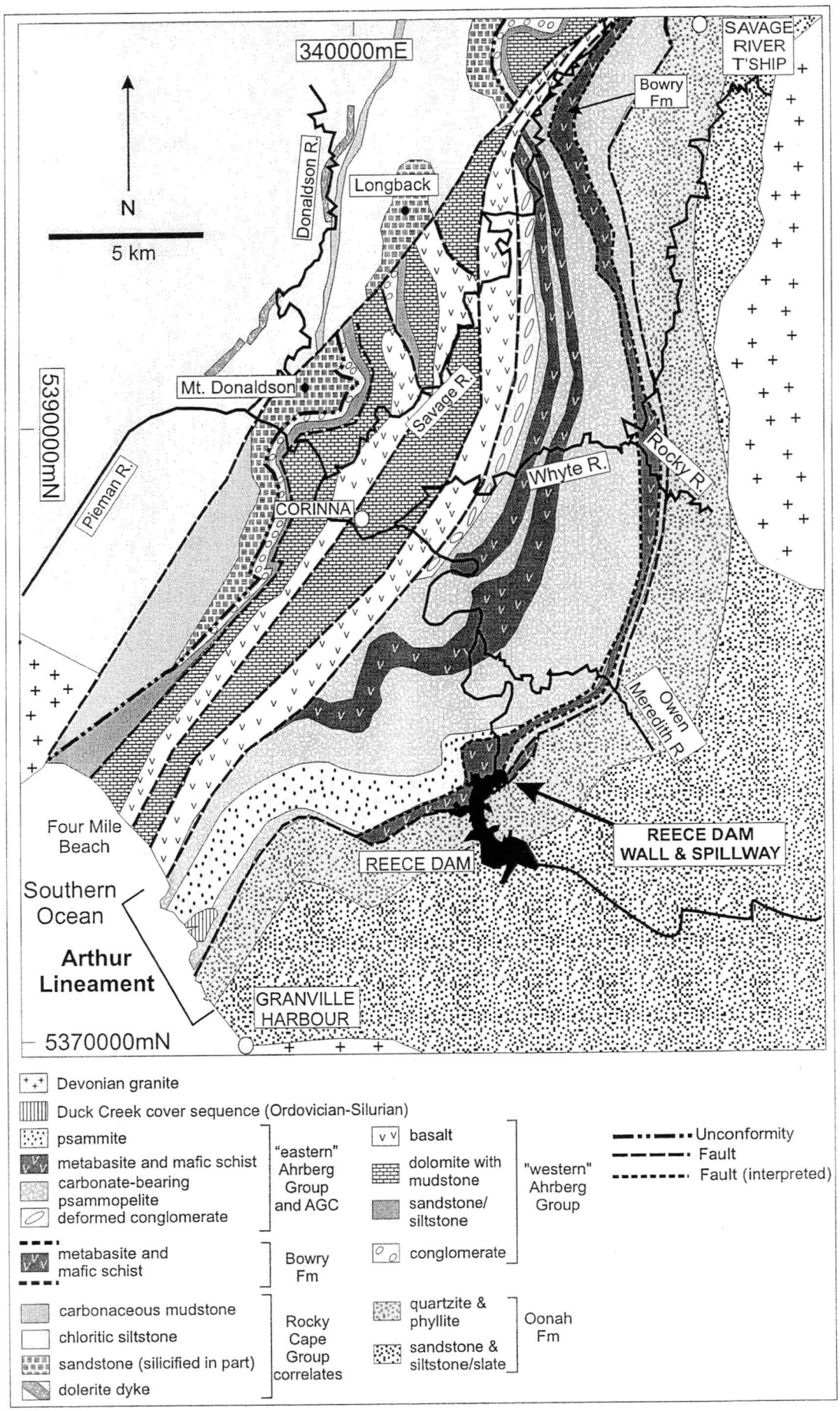

Figure 1.2. Simplified geology of the southern Arthur Lineament (from Turner *et al.* 1991).

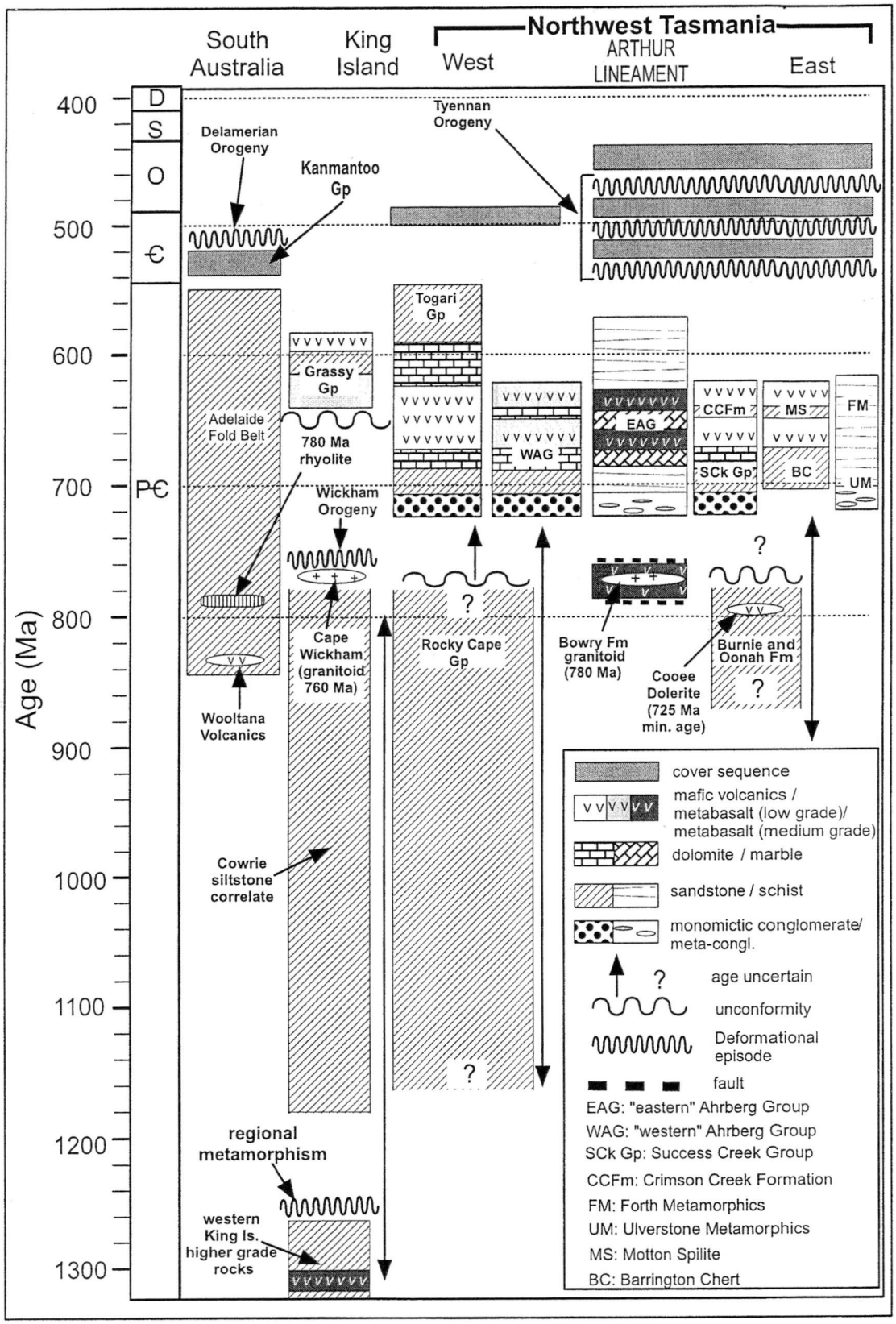

Figure 1.3. Space-time diagram displaying the contemporaneous rock packages in northwestern Tasmania, King Island and South Australia (modified from Calver & Walter 2000).

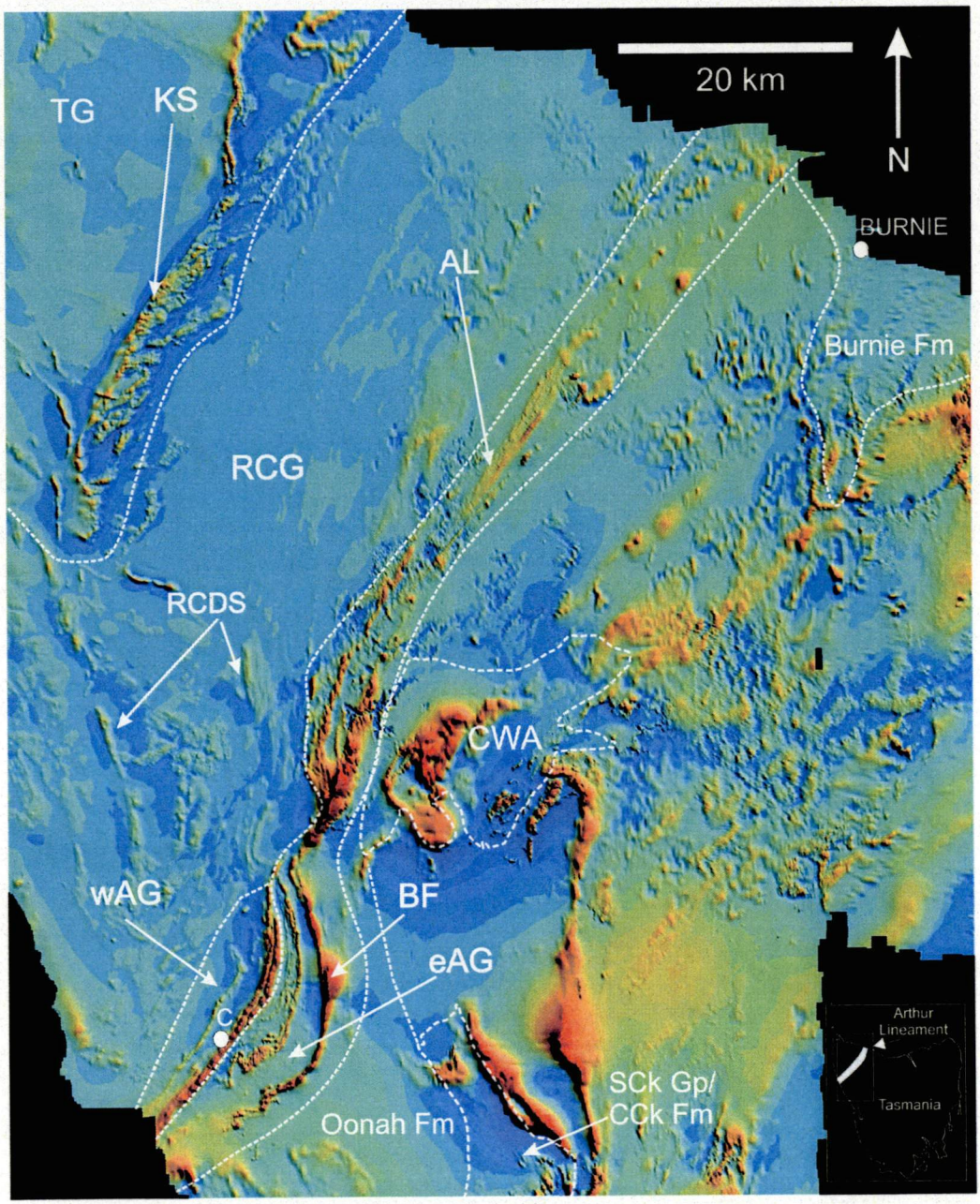

Figure 1.4(a). Total magnetic intensity aeromagnetic image of northwest Tasmania. Units in red are anomalously magnetic, whereas blue units have minimal magnetic component. AL = Arthur Lineament, eAG = "eastern" Ahrberg Group, wAG = "western" Ahrberg Group, RCG = Rocky Cape Group (and correlates), RCDS = Rocky Cape Dyke Swarm, TG = Togari Group, KS = Kanunnah Subgroup, SCk Gp / CCk Fm = Success Creek Group / Crimson Creek Formation, CWA = Cleveland-Waratah Association, C = Corinna. Image courtesy of AGSO.

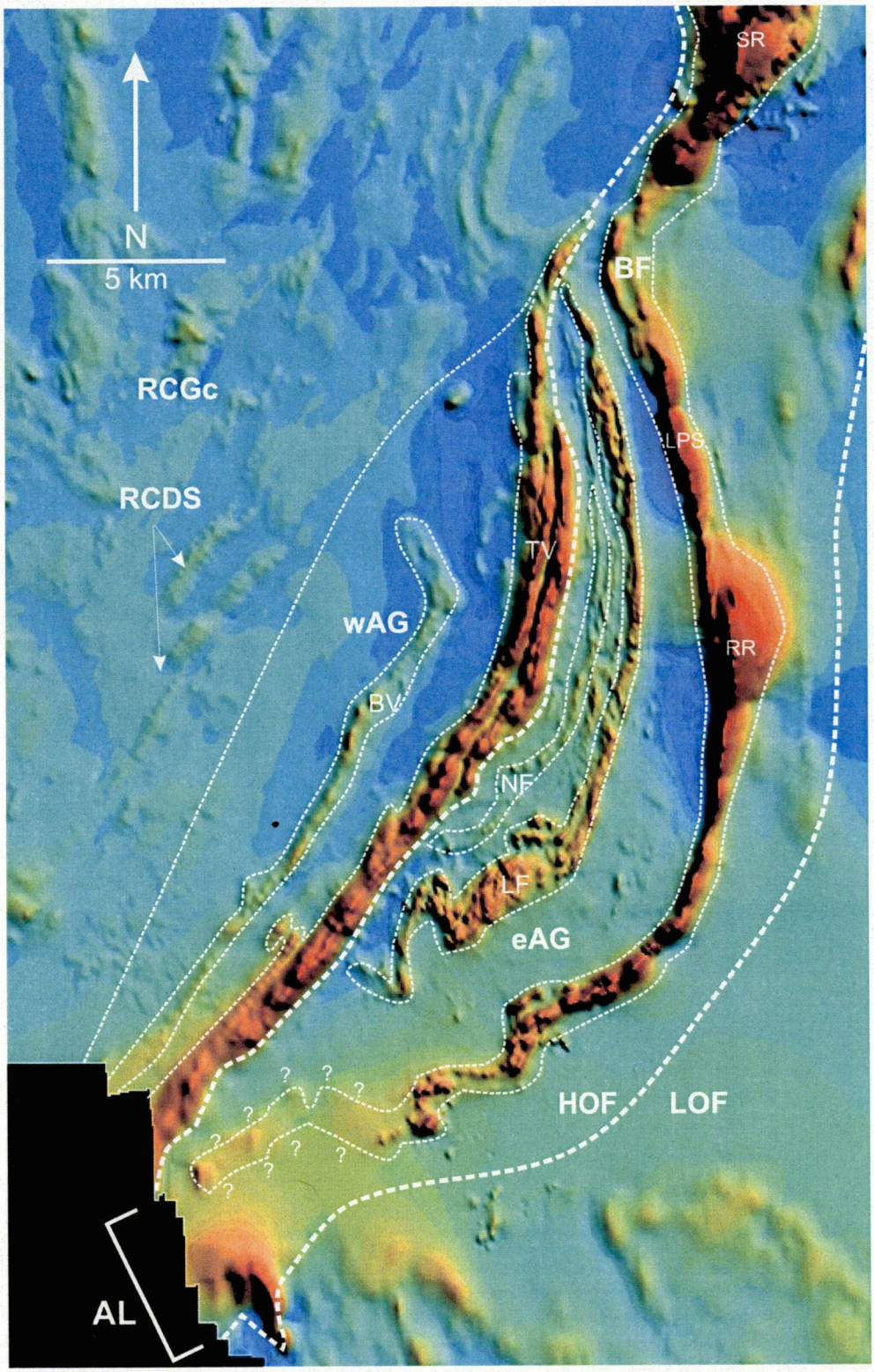

Figure 1.4(b). Total magnetic intensity aeromagnetic image of northwest Tasmania. Units in red are anomalously magnetic, whereas blue units have minimal magnetic component. AL = Arthur Lineament,eAG = "eastern" Ahrberg Group, HOF = high strain Oonah Formation, LOF = low strain Oonah Formation, wAG = "western" Ahrberg Group, BV = Bernafai Volcanics, TV = Tunnelrace Volcanics, NF = Nancy Formation, LF = Lucy Formation, BF = Bowry Formation, RR = Rocky River, SR = Savage River, LPS = Long Plains South, RCGc = Rocky Cape Group correlates, RCDS = Rocky Cape Dyke Swarm. Image courtesy of AGSO.

metamorphic history between the Bowry Formation and other parts of the "Timbs Group". They concluded the Bowry Formation had a faulted margin against the remainder of the "Timbs Group" with a metamorphic grade difference across the fault. The Bowry Formation, therefore, is fault bounded within the southern Arthur Lineament, has internal evidence of a different metamorphic history (Turner & Bottrill 2001) and is probably much older. The western section of the "Timbs Group" is interpreted here as a parautochthonous slice of the Ahrberg Group, and is referred to in this work as the "eastern" Ahrberg Group. The autochthonous Ahrberg Group is referred to as the "western" Ahrberg Group. The Bowry Formation is referred to here as a separate unit with no specific correlates. There are other fault bounded units within the Arthur Lineament. In particular, east of the Bowry Formation and faulted against the high strain Oonah Formation is a block composed of lithologies similar in appearance to the "eastern" Ahrberg Group. This unit is referred to as the Ahrberg Group correlate (AGC).

The "eastern" Ahrberg Group is the major lithological unit in the Arthur Lineament and is dominated by metamorphosed psammite and psammopelite units that contain carbonates. Some units of the "eastern" Ahrberg Group contain magnetically anomalous basalt/dolerite-derived tholeiitic amphibolites (Figure 1.4(b)). The Bowry Formation contains abundant basalt/dolerite-derived tholeiitic amphibolites, massive and banded magnetite, as well as minor deformed *ca.* 780 Ma granitoids (Figure 1.4(b)). To the west of the Arthur Lineament lie shallow marine siliciclastic sediments of the Neoproterozoic Rocky Cape Group and correlates (which are intruded by *ca.* 600 Ma dolerite sills/dykes (Adams *et al.* 1985)). The Rocky Cape Group and correlates are unconformably overlain by carbonates, shelf sediments, metabasalts and mafic volcanogenic metasediments of the Late Neoproterozoic "western" Ahrberg Group (to the east) (Figure 1.3). The "western" Ahrberg Group is faulted against the Arthur Lineament. To the east of the Arthur Lineament lie the mildly deformed Neoproterozoic turbidites of the moderate- to low strain Burnie and Oonah Formations.

Northwestern Tasmania (including King Island) underwent several changes in tectonic setting, and experienced multiple orogenic events in the Mesoproterozoic, Neoproterozoic and Early Palaeozoic (Figure 1.3). King Island was deformed during

a Grenville-age event (*ca.* 1250 Ma), and the Wickham Orogeny at *ca.* 780 Ma. Mainland northwestern Tasmania underwent its main phase of deformation during the Tyennan Orogeny at 510 ±10 Ma (Turner *et al.* 1998).

Prior to the Wickham Orogeny, northwestern Tasmania was in a passive continental margin setting. The Wickham Orogeny on King Island is represented by the 760 ±12 Ma King Island Granitoid, multiple episodes of ductile deformation and metamorphism (Cox 1973, 1989). In Tasmania the Wickham Orogeny is represented by an intrusive 777 ± 7 Ma granitoid in the Bowry Formation, outcropping in the Rocky River, Owen Meredith River, and in lower Stringer Creek; however, this granitoid may be part of what is considered to be an allochthonous slice that also contains relict blueschist facies assemblages. A low angle unconformity between the Rocky Cape Group and the overlying "western" Ahrberg and Togari Group correlates is the only other interpreted representation of the Wickham Orogeny in Tasmania (Turner *et al.* 1998).

The subsequent 510±10 Ma Tyennan Orogeny has been interpreted to represent the aborted subduction of the Late Neoproterozoic passive margin in an arc-continent collision, followed by exhumation and post-collisional re-equilibration (Berry & Crawford 1988, Crawford & Berry 1992, Turner *et al.* 1998). The Tyennan Orogeny involved crustal collision and was associated with emplacement of ultramafic-bearing allochthons and early high P, low T metamorphism (Turner *et al.* 1998). The Tyennan Orogeny produced high strain deformation and is interpreted to have resulted in the formation of the Arthur Lineament. It is regionally significant in western Tasmania, and has been correlated with the Ross Orogeny in Antarctica, the Delamerian Orogeny in South Australia and episodes of the Pan-African Orogeny (Berry 1994). The latest event of the Tyennan Orogeny in the Late Cambrian led to west over east folding and thrusting and was followed much later by the Middle Devonian Tabberabberan Orogeny (intrusion of granitoids, contact metamorphism and mild deformation). These subsequent deformational episodes resulted in a series of complex faulting and folding patterns.

For some time, the origin of the Arthur Lineament has been contentious. It was regarded by Berry (1994) to be a product of the 760-770 Ma Wickham Orogeny,

representing a major detachment between the weakly folded upper thrust sheet (Rocky Cape Group) and the strongly deformed footwall (Burnie and Oonah Formations). However, Turner *et al.* (1998) showed that, based on amphibole-derived K-Ar ages from amphibolites within the Bowry Formation in the Arthur Lineament, the main episode of deformation in the lineament occurred as part of the Tyennan Orogeny at 510 ± 10 Ma. Berry (1994) interpreted parts of the Bowry Formation to be allochthonous, emplaced at *ca* 500 Ma.

The Arthur Lineament is host to several styles of ore deposit. The Bowry Formation has numerous magnetite lenses along the eastern margin of the Arthur Lineament. The largest lens occurs at Savage River (351000 mE, 5404000 mN), with numerous other smaller lenses occurring along strike, at Rocky River (349500 mE, 5389000 mN), and Long Plains South (348000 mE, 5396000 mN) (Figure 1.4(b)). Associated with the magnetite is minor Cu-Au mineralisation. Also within the Bowry Formation is magnesite mineralisation, forming potentially economic deposits at Main Creek (347000 mE, 5399000 mN), Savage River (351000 mE, 5404000 mN) and at the Arthur-Lyons Rivers in the north. Within the Lucy Formation of the "eastern" Ahrberg Group there is also minor Middle Devonian-age, granite-related Au mineralisation (Figure 1.4(b)) (Turner *et al.* 1998). To the west of the "eastern" Ahrberg Group, in the "western" Ahrberg Group, silicification and subsequent leaching of dolomite has resulted in silica flour deposits that are currently being mined.

1.4 Previous Work

Several Tasmanian government geologists in the late 1800's and the early 1900's mentioned the presence of metamorphic schists in northwestern Tasmania, within what is now known as the Arthur Lineament. Thureau (1884) recorded the presence of micaceous schists in the Specimen Reef region, and Montgomery (1894) described of a range of lithologies including schists in the Corinna district. Harcourt Smith (1897) discussed Cu and Fe mineralisation in association with mafic schists in the Rocky River area and Twelvetrees (1900, 1903) recorded the presence slates and sandstones, which are separated by schistose rocks in the Whyte and Rocky River area.

In the 1920's and 1930's Tasmanian government geologists made further references in Mines Department reports to the schistose rocks and their association with mineralisation in area (Reid 1924, Scott 1926, Blake 1939). During the 1950's the Hydro-Electric Commission Tasmania commissioned reconnaissance geological mapping of areas of western and northwestern Tasmania, for the purpose of identifying prospective dam sites.

The schistose lithologies were named as the Corinna Beds and briefly described by Spry & Ford (1957), who grouped all lithologies bounded by the Bald Hill pyroxenite to the northeast of Corinna and by the granite of the Meredith Range to the east, including the schistose lithologies. Lithologies to the west of these were briefly described, and defined as the Donaldson Beds, the Interview Beds and the Rupert Beds; however the "Donaldson Beds" did not account for all lithologies in the Mt Donaldson area. .

Subsequent to this, Spry (1957a) redefined the schistose lithologies as the Whyte Schist, disregarding the term "Corinna Beds". Spry (1957a) considered the Whyte Schist and Rupert Beds to be older Precambrian in age, and also renamed the Oonah Quartzite defined by Hills & Carey (1949) as the Oonah Quartzite and Slate.

Spry (1958a) discontinued use of the term "Donaldson Beds", preferring the term Donaldson Formation, and addressed all units in the Mt Donaldson area, naming them the Delville Chert, Savage Dolomite, Bernafai Volcanics and the Corinna Slate. Further to this, Spry (1958a) redefined the Interview Beds as the Interview Slate and Quartzite, and disregarded the term Rupert Beds, proposing they were part of the Donaldson Group. The Rocky Cape Group was defined by Spry (1957b) as consisting of the sediments previously referred to by Twelvetrees (1903, 1905) as the "Rocky Cape quartzites". Spry (1962) suggested correlation between the Oonah Quartzite and Slate and the Burnie Quartzite and Slate, and also made correlations between units within the Rocky Cape Group and the Donaldson Group.

Spry (1957a) tentatively proposed that the more highly deformed and metamorphosed rocks belonged to a group of older Precambrian rocks that had undergone a Precambrian tectonic event, therein named the "Loddernian

Metamorphic Disturbance". The author also introduced the term "Penguin Movement", defining the tectonic event which separated what was considered younger Precambrian from the Upper Middle Cambrian. This terminology was partly revised by Spry (1962), who introduced the term "Frenchman Orogeny" to define the tectonic event that produced extensive regional metamorphism and minor basic igneous activity. The author emphasised the complexity of the geology in northwestern Tasmania, and outlined the difficulty in establishing the relationship between the strongly deformed and relatively undeformed rocks due to their lithological similarity. On this basis, Spry (1962) put forward an alternative hypothesis to explain the differing degree of deformation in the Precambrian rocks. He proposed that the metamorphosed older Precambrian rocks possibly represented the younger Precambrian rocks, but in a more deformed condition, as was first suggested by Spry (1957c) and supported by Burns (in Spry, 1962). Further to this, Spry (1962) interpreted the Frenchman Orogeny as separating the older and younger Precambrian rocks, and further defined the "Penguin Movement" as the late Precambrian tectonic event in the that separated all of the Precambrian rocks from the Cambrian.

Spry (1964) discussed the Whyte Schist in detail, and attempted to resolve on the basis of petrographic observations the relationship between rocks that were considered to be part of the Rocky Cape Geanticline, including the Whyte Schist, and those elsewhere in the state. Spry (1964) recorded the presence of relatively undeformed lithologies on either side of the Whyte Schist, and considered the Whyte Schist to represent a remnant Precambrian basement high, against which the younger Precambrian was deposited. He attributed this metamorphism and deformation to the Frenchman Orogeny.

Gee (1967a) claimed that based on sedimentary facing directions within the Rocky Cape Group (overturned and facing east) and the Burnie Formation (overturned and facing east) adjacent to the Arthur Lineament, it was impossible for the lineament to represent a basement high. The Penguin Movement was renamed the Penguin Orogeny by Gee (1967a) who interpreted the associated structural deformation to represent the southeast-directed transport of the Rocky Cape Group and Burnie Formation towards the Precambrian Tyennan Nucleus. Further to this, he noted the

similarity in mineral assemblages between the Whyte Schist and the Keith Metamorphics, thereby proposing their correlation. Gee (1967a) introduced the term 'Arthur Lineament' to describe the metamorphic units, referring to the lineament as "a ribbon-like belt of sheared metamorphic rocks", and proposed the Arthur Lineament represented the "fundamental tectonic structure of the Proterozoic in northwestern and western Tasmania".

Gee (1967a) and Turner (1984, 1989) proposed that based on field evidence, the metamorphosed lithologies of the Arthur Lineament are transitional with the adjacent less deformed units. Turner (1989) suggested that as the term 'Arthur Lineament' is a tectonic term, the name 'Arthur Metamorphic Complex' should be used as a stratigraphic term to describe the rocks within the lineament.

1.5 Lithostratigraphy of the Arthur Lineament and surrounding area

1.5.1 Introduction

The Arthur Metamorphic Complex consists of the highly deformed, schistose meta-sedimentary and meta-igneous "eastern" Ahrberg Group ("Timbs Group" of Turner *et al.* (1991)), previously known as the Whyte Schist (Spry 1964), and the highly deformed turbiditic Burnie and Oonah Formations (Spry 1964) which lie to the east of the AGC (Figure 1.2).

Correlation between the Burnie and Oonah Formations was suggested by Spry (1962) based on lithological similarities and further supported by Gee (1967a), who also considered the Burnie Formation to be contemporaneous with the Smithton Dolomite. Turner (1989) and Turner *et al.* (1992) made a tentative correlation (based on lithological similarities) between the Oonah Formation and the basal unit of the Ahrberg Group (Donaldson Group of Spry 1958a). Turner (1989) noted that despite the lithological similarities between the Oonah Formation and the Ahrberg Group, the tholeiitic Bernafai Volcanics of the Ahrberg Group were unrelated to the intraplate alkaline pillow basalts in the upper Oonah Formation. Due to the tholeiitic whole rock chemistry, the mafic rocks of the Ahrberg Group were tentatively

correlated with the basalts of Crimson Creek Formation and Smithton Volcanics (Turner 1989) (Figure 1.1).

Turner *et al.* (1992) noted the absence of a strict definition of the Oonah Formation, and defined it as the rocks described by Hills & Carey (1949) at Oonah Hill, the continuation of those rocks to the west (Spry 1958a) and to the north (Brown 1986). Turner *et al.* (1991) observed a decrease in strain of the strongly deformed Oonah Formation to the east of the Arthur Lineament over the distance of several kilometres.

In the southern part of the Arthur Lineament to the west of the "eastern" Ahrberg Group lies the weakly deformed and metamorphosed, slaty to phyllitic metasedimentary and meta-igneous "western" Ahrberg Group (Figures 1.1 to 1.4). The boundary between the "western" and "eastern" Ahrberg Groups was previously interpreted to be faulted (Turner *et al.* 1991), defined by a sharp transition in metamorphic grade and texture. The "western" Ahrberg Group unconformably overlies the weakly deformed, slaty, siliciclastic Rocky Cape Group (to the west) at a low angle (15 degrees). To the north, in the Smithton Synclinorium the basal unit of the Togari Group (Ahrberg Group correlate), also unconformably overlies the Rocky Cape Group at low angle (22°)(Gee 1967a, 1968). This was suggested by Gee (1967a) to have possibly resulted from a depositional dip component in the overlying conglomerate, although more recent mapping would suggest that the unconformity represents a period of gentle regional folding (Seymour & Calver 1995). Unit symbols given below refer to Turner *et al.* (1991).

1.5.2 Rocky Cape Group

The Rocky Cape Group consists of four main lithologies in its type section on the north coast (Gee 1968; Gee 1989):

TOP	(Not exposed)
Jacob Quartzite	Supermature quartzarenite with silica cement, with abundant planar cross-bedding.
Irby Siltstone	Siltstone with minor black shale, dolomite, sub-greywacke and hematitic breccia.
Detention Subgroup	Supermature cross-bedded quartz sandstone with minor interbedded siltstone.
Cowrie Siltstone	Black pyritic shale with interbedded siltstone.
BASE	(Not exposed)

The Rocky Cape Group correlate lithologies in the Crescent Hills – Longback – lower Pieman River area consist of an upwards coarsening, eastward younging, siliciclastic shallow marine sequence. Lowermost in the sequence studied is a variably chloritic and pyritic, laminated to thinly bedded micaceous, slaty siltstone and mudstone (***Prs***, ***Prsg***) (338400 mE, 5393750 mN). This is overlain by chloritic, fine-grained, thin- to medium-bedded sandstone with interbeds with a micaceous matrix and medium to coarse-grained, medium- to thickly-bedded white to silicified quartz sandstone (***Prq***, ***Prqq***) (341040 mE, 5398900 mN). No specific correlation has been made between the lithologies in the southern study area and the north coast, however a broad lithological comparison can be made between the Detention Subgroup and Cowrie Siltstone from the north coast, and units ***Prq*** and ***Prs***. The maximum age of the Rocky Cape Group is 1200 Ma based on a SHRIMP U-Pb date from detrital zircons (Black *et al.* 1997).

1.5.3 Burnie and Oonah Formations

The Burnie Formation consists predominantly of sandy turbidite-facies quartzose wacke and slaty mudstone, intruded by minor altered mafic dykes and containing occasional basaltic pillow lavas (eg. 398790 mE, 5457875 mN). The quartzwacke consists of quartz grains with minor detrital muscovite and chert fragments, in a chloritic-sericitic matrix. Sedimentary structures indicate deposition by northeasterly-directed turbidity currents and reworking by transverse traction currents (Gee 1989). Tholeiitic dolerite sills and transgressive sheets are common within the Burnie Formation (Spry 1957b, Gee 1967a, Gee 1989). At Cooee on the northwest coast a syn-sedimentary alkaline dolerite intrusion originally reported by Spry (1957a) was reported by Crook (1979) to have a minimum age of 725 ± 35 Ma based on a K-Ar ratios in biotite (Spry 1957a, Gee 1967b). The Oonah Formation is similar in character, although it displays more lithological variation (***Pou***, ***Poq***, ***Pom***, ***Pos***). It is made up of relatively clean quartz sandstone, dolomite, chert and conglomerate (Turner 1989, Seymour & Calver 1995). Turner *et al.* (1998) proposed that the Burnie and Oonah Formations and the Ahrberg Group were sourced from the Rocky Cape Group to the west, as a result of the Wickham Orogeny.

With increase in strain the Oonah Formation undergoes a gradual transition in texture, from phyllitic to schistose (***Posm***). This is best illustrated along the Lower Pieman Rd, from the Stanley River bridge (357580 mE, 5381380 mN) where the Oonah Formation is weakly cleaved, to the southeast Reece Dam spillway abutment (344930 mE, 5378880 mN) where the lithology is phyllitic to schistose, with strong development of two cleavages. The lithology in this transect is dominated by a fine- to medium-grained quartz sandstone, with minor interbeds of mudstone and chert. It is typically fine- to medium-bedded, with common grading features.

1.5.4 "Eastern" Ahrberg Group and the Ahrberg Group correlate (AGC)

The "eastern" Ahrberg Group ("Timbs Group" of Turner *et al.* 1991) is an east-dipping package of meta-sedimentary and meta-igneous rocks that together with the high strain Burnie and Oonah Formations make up the Arthur Metamorphic Complex. The meta-igneous predominantly comprise of amphibolitised tholeiitic metabasalts, interlayered with minor mafic volcanogenic psammopelites. Turner *et al.* (1991) named the easternmost metabasalt-dominated unit the Bowry Formation, and the other two metabasalt-dominated units to the west of the Bowry Formation were referred to as the Lucy and Nancy Formations, based on their status as mappable units (Turner 1992) (Figure 1.4(b)). Turner *et al.* (1991) assigned them the map symbol ***Pta***. The position of the formation boundaries are inferred, and accurate to approximately 250 m, based on aeromagnetic imaging, which clearly defines the units as magnetically anomalous (Figure 1.4(b)). Creek transects through these units confirmed the abundance of magnetite-bearing metabasalts within the units. Metabasalts vary between boudinaged pod-shaped bodies several metres in diameter, and less commonly dyke-like bodies. They are interpreted to be intrusive, although chilled margins are not evident, as their rims are commonly strongly foliated and sheared due to competency contrast. The centres of the large metabasalts display little or no foliation. They are predominantly fine- to medium-grained and variably retrogressed, with the predominant mineral assemblage actinolite-hornblende-chlorite-quartz-albite-epidote-sphene-magnetite ± biotite-pyrite-garnet. Chlorite and actinolite occur in greater proportions in more heavily retrogressed samples. The psammopelite dominated metasedimentary units of Turner *et al.* (1991) feature minor

tholeiitic metabasalts and have been assigned the unit symbol ***Pts*** by Turner *et al.* (1991). The metabasalts of ***Pts*** are indistinguishable from those within ***Pta***. The composition of the different psammopelitic ***Pts*** units is broadly consistent, comprising fine-grained quartz-muscovite-albite-chlorite-titanomagnetite ± dolomite schist. Albite is porphyroblastic, and has grown syn-tectonically.

Turner *et al.* (1991) indicated variation in the composition of the metasedimentary sequences by use of suffixes. ***Ptsq*** denotes units wherein micaceous quartz schist is dominant, with minor porphyroblastic schist, whereas ***Ptsqg*** denotes units dominated by grey phyllite. ***Ptsl*** is assigned to a unit of strongly deformed, boudinaged, predominantly monomictic metaquartzite-clast conglomerate, which forms the lowermost (far west) metasedimentary unit of the "eastern" Ahrberg Group. To the east of the Bowry Formation, and to the west of the high strain Oonah Formation, the AGC comprises minor metagabbro (***Pg***), that intrudes along the eastern margin of ***Ptsqg***, in the vicinity of the Reece Dam spillway (345140 mE, 5379190 mN) (Figure 1.2). This unit was analysed by Crawford (1992) and displays tholeiitic affinities.

The precursors of the "eastern" Ahrberg Group are interpreted to reflect a basinal sequence, with initial deposition of locally derived siliclastics and conglomerate, transgressing upwards into a calcareous, psammopelite-dominated, shallow marine sequence. Sub-alkalkine rift tholeiites were repeatedly extruded in the sequence, with input from associated volcaniclastic sediments.

1.5.5 Bowry Formation

Turner *et al.* (1991) named the easternmost metabasalt-dominated unit the Bowry Formation, based on its status as a mappable unit (Turner 1992) (Figure 1.4(b)). Turner *et al.* (1991) also assigned the Bowry Formation the map symbol ***Pta***. Interlayered with the mafic metasediments and meta-igneous rocks are several massive magnetite bodies (***Ptam***, ***Ptamd***) (eg. Savage River ore body, 349500 mE, 5405000 mN), magnesite-rich zones (***Ptac***) (eg. Main Creek deposit, 347000 mE, 5390000 mN), felsic albite schists and associated intrusive granitoids (***Ptaa***) (eg. Rocky River, 349140 mE, 5389360 mN).

The psammopelite-dominated metasedimentary units of Turner *et al.* (1991) feature minor tholeiitic metabasalts and have been assigned the unit symbol ***Pts*** by Turner *et al.* (1991). The metabasalts of ***Pts*** are indistinguishable from those within ***Pta***. The composition of the different psammopelitic ***Pts*** units is broadly consistent, comprising fine-grained quartz-muscovite-albite-chlorite-titanomagnetite ± dolomite schist. Albite is porphyroblastic, and has grown syn-tectonically.

1.5.6 "Western" Ahrberg Group

The "western" Ahrberg Group lies to the west of the "eastern" Ahrberg Group (Figure 1.1 to 1.4). The contact between the two is interpreted to be a major faulted boundary, due to the increase in strain and intensity of structural fabrics within the "western" Ahrberg Group proximal to the fault, and the corresponding prominent linear magnetic anomaly evident on aeromagnetic imaging (Figure 1.4(b)). The precise direction of displacement along the fault is uncertain due to lack of outcrop at the contact (344850 mE, 5392020 mN). The "western" Ahrberg Group unconformably overlies the Rocky Cape Group at low angle (5-15°) along the "western" Ahrberg Group's western boundary (339060 mE, 5392080 mN). The "western" Ahrberg Group is east facing and interpreted to represent a transgressing basinal sequence. The westernmost, basal unit of the "western" Ahrberg Group (the Donaldson Group) is a coarse-grained quartzose sandstone and conglomerate (***Pdc***), and was interpreted by Turner (1990) to represent a proximal marine fan deposit (339500 mE, 5392000 mN). This grades upwards into a sequence of sandstone interbedded with graphitic, pyrite-bearing mudstones (***Pds***) (339200 mE, 5390500 mN), becoming interbedded with minor oolitic carbonate bands towards the top (***Pdo***) (340000 mE, 5391000 mN). This is conformably overlain by the Savage Dolomite which features oolitic dolomite with minor interbeds of siltstone (***Psd***)(340250 mE, 5391000 mN). Silicification of ***Psd*** is common (***Psds***)(342000 mE, 5388500 mN), with the remaining lag products of silicification resulting in silica flour deposits (***Psdss***)(340500 mE, 5392000 mN) (Turner 1990, Khin Zaw *et al.* 1992).

The overlying Bernafai Volcanics (***Pbu, Pbt, Pbm, Pbg, Pbgw***) features tholeiitic metabasalts and associated volcaniclastic metasediments that have been

metamorphosed to sub-greenschist facies. The intrusive rocks contain actinolite-chlorite-epidote-albite, whereas the metasediments commonly contain chlorite-quartz-mica-±albite-tourmaline.

Above the Bernafai Volcanics lies the poorly exposed Corinna Dolomite (***Psd***, ***Psds***, ***Psdss***, ***Pdg***), which has undergone silicification (Turner 1992), and displays botryoidal, banded silicification textures resembling colloform textures (Turner 1992). The uppermost unit of the "western" Ahrberg Group is the Tunnelrace Volcanics, which comprises tholeiitic metabasalts and associated volcaniclastic metasediments (***Pbu***, ***Pbt***, ***Pbb***, ***Pbd***, ***Pbq***)(Turner & Crawford 1993). The unit has been subject to greater strain and a slightly higher level of metamorphism (mid greenschist facies) than the Bernafai Volcanics and is interpreted to be fault-bound (Turner & Crawford 1993). The Tunnelrace Volcanics has a stronger aeromagnetic signature than the Bernafai Volcanics, due to a greater magnetite content (Figure 1.4). This was suggested by Turner & Crawford (1993) to be a reflection of a higher metamorphic grade.

1.6 Discussion and Correlation

Previous workers have proposed varying regional correlations between the Precambrian lithologies in northwestern Tasmania. Spry (1962) made correlations between the Donaldson Group (now the lowermost unit of the Ahrberg Group) and units of the Rocky Cape Group, and between the Burnie and Oonah Formations. Spry (1962, 1964) proposed that the Burnie and Oonah Formations were correlates of the Rocky Cape Group, forming the basal sequence, but interpreted the Whyte Schist as deformed Precambrian basement. In contrast, Gee (1967a) suggested the Rocky Cape Group represented the oldest exposed sequence in northwestern Tasmania and that it was deposited in a shallow marine setting on a continental shelf initially starved of clastic input, whereas the Burnie and Oonah Formations were younger and contemporaneous. Further to this Gee (1967a) suggested that the Burnie and Oonah Formations as deeper water correlates of the Smithton Dolomite of the Togari Group, and interpreted the Cooee Dolerite to be equivalent to the deformed amphibolites within the Keith Metamorphics (the central northern exposure of the Arthur Lineament). Gee (1967a) also recommended against correlation between the

dolomites of the Success Creek Group and the Smithton Dolomite, as the two sequences were interpreted to have been deposited in separate basins.

Turner (1992) correlated the conglomeratic basal unit of the Ahrberg Group with the Burnie and Oonah Formations, as did Gee (1967a). Further to this, Turner *et al.* (1992, 1994) were in agreement with Gee (1967a), suggesting that the Burnie and Oonah Formations were coeval, and deposited at around 700 Ma. This was based on the syn-sedimentary interpretation of the 725 ±35 Ma Cooee Dolerite (Crook 1979), and the 690 ±10 Ma K-Ar muscovite-derived ages from the Burnie Formation (Adams *et al.* 1985). Turner *et al.* (1992, 1994) interpreted the Rocky Cape Group to be significantly older, with a maximum age of 1100 Ma, based on a U-Pb age from detrital zircon (Råheim & Compston 1977).

1.6.1 Rocky Cape Group and Burnie and Oonah Formations

A temporal correlation between the Rocky Cape Group and the Burnie and Oonah Formations is suggested herein, with the Rocky Cape Group being deposited in a shallow marine setting on a continental shelf, and the Burnie and Oonah Formations forming the offshore extension. There are several lines of argument that support this correlation:

- The eastern margin of the Rocky Cape Group has previously been interpreted to be a passive continental margin in Precambrian time (eg. Solomon & Griffiths 1974, Crawford & Berry 1992). As pointed out by Crook (1979), studies of modern passive continental margins (eg. Burk & Drake 1974) imply that the site of the Precambrian passive margin in northwestern Tasmania should be marked by a sedimentary prism, featuring large amounts of quartz-rich, shallow water and flysch facies. This work supports the finding of Crook (1979), who noted that the thickness, composition and facies of the Rocky Cape Group and Burnie Formation are consistent with this model.
- In the study area, the Rocky Cape Group correlates is an east-younging sequence that reflects a regressive, shallow marine depositional environment with a gradual increase in sediment transport velocity. The oldest part of the sequence is dominated by a medium- to thickly-bedded weakly chloritic siltstone with

minor mudstone (***Prs***). This grades up into a cyclical, interbedded sequence of a mature, medium-grained, thin- to medium-bedded quartz sandstone with a silty matrix with minor truncated crossbeds, and interbeds of laminated- to thinly-bedded, variably carbonaceous siltstone (***Prq***). The Oonah Formation is also an east-younging sequence, predominantly comprising thin- to medium-bedded, fine- to medium-grained mature quartz sandstones with interbeds of mudstone. Brown (1989) noted the presence of Bouma B and C units, indicative of deposition by turbidity currents. Mueller (1998) suggested that based on facies types within the Oonah Formation, sediment was transported by turbidity currents; debris flows; and suspension settling.

- The predominance of mature quartz sands in both the Rocky Cape Group and the Burnie and Oonah Formations suggests a common source. Mueller (1998) claimed from provenance studies that the Oonah Formation has a similar geochemical signature to the Rocky Cape Group, both being deposited in a continental margin setting. This supports Gee's (1967a) interpretation, that the Rocky Cape Group sediments were derived from a distant granitic or gneissic source.
- A comparison of palaeocurrent data for the Rocky Cape Group and the Burnie and Oonah Formations suggests similar palaeocurrent directions for the two groups. Gee (1967a) found bimodal palaeocurrent patterns to be indicative of northwest- and southeast-directed dispersal currents in the Rocky Cape Group. Mueller (1998) noted the presence of both northeast- and southeast-directed palaeocurrent directions in the Oonah Formation, in accord with my own observations.
- Gee (1967a) noted that the geometry of the Rocky Cape Groups depositional environment was a northeast-southwest elongate basin. It can be suggested that this correlates with the elongate northeast-southwest orientation of the Burnie and Oonah Formations, although the orientation of all three units may partly be attributed to subsequent deformation.
- The 1200 Ma detrital zircon age for the Rocky Cape Group (Black *et al.* 1997) provides a poorly constrained maximum age for sedimentation. The minimum age of the Rocky Cape Group is defined by the *ca.* 600 Ma dolerite dyke swarm that intrudes the group (Adams *et al.* 1985). This 1200 – 600 Ma window

encompasses the possible depositional age range of the Burnie and Oonah Formations, which is poorly defined by the K-Ar obtained 725 ± 35 Ma minimum age from magmatic biotite in the syn-sedimentary Cooee Dolerite (Crook 1979).

- Gee (1967a) observed that regionally both the Rocky Cape Group and the Burnie Formation young to the east, suggesting a similar structural history.

1.6.2 "eastern" and "western" Ahrberg, and Togari Groups and the Success Creek Group-Crimson Creek Formation

Several lines of evidence support correlation between the Ahrberg Group (western margin of southern Arthur Lineament) and Togari Group (Smithton Trough), and the Success Creek Group-Crimson Creek Formation (Dundas Trough).

- The volcanic units of the "western" Ahrberg Group (Bernafai and Tunnelrace Volcanics), "eastern" Ahrberg Group (Lucy and Nancy Formations) Togari Group (Kanunnah Subgroup), and the Crimson Creek Formation all have rift tholeiitic chemistry (Brown 1989, Turner 1992, Crawford 1992).
- The carbon isotope stratigraphy of the Savage Dolomite ("western" Ahrberg Group) and Black River Dolomite (Togari Group) is very similar (Calver 1996).
- The stratigraphy of the "eastern" and "western" Ahrberg and Togari Groups and the Success Creek Group-Crimson Creek Formation is very similar. The units have a common basal conglomerate interbedded with siliclastics, overlain by carbonates, shales and cherts, rift tholeiites and associated volcaniclastics. (Spry 1964, Brown 1989, Turner 1992, Everard *et al.* 1996, Calver 1998).
- The conglomeratic basal units of both the "western" Ahrberg and Togari Groups unconformably overlie the Rocky Cape Group (Spry 1964, Turner 1992). According to Brown (1986) the basal conglomerate of the Success Creek Group unconformably overlies the Oonah Formation, although the only known exposure of this surface, along the Pieman River, was flooded by the development of the Lower Pieman Dam. Elsewhere the contacts are faulted (Seymour & Calver 1995).

1.7 Methods of Study

1.7.1 Field methods

The fieldwork was designed to cover the areas of best exposure, which were also expected to yield the most useful structural and metamorphic data across the Arthur Lineament. Given the dense vegetation cover in northwestern Tasmania, tracks, creeks and small rivers that predominantly trend perpendicular to the strike of the lineament were targeted. Numerous traverses were carried out across the lineament, resulting in a degree of overlap between the sections mapped. Mapping was carried out using enlarged 1:25000, and 1:5000 scale topographic base maps. In some cases mapping at a greater level of detail (1:250 scale) was warranted.

The southern part of the Arthur Lineament was the primary focus of the study area, due to accessibility, logistic support, and less extensive cover sequences. Traverses of the northwest- and west- coast exposures of the Arthur Lineament and the surrounding areas were also carried out.

1.7.2 Analytical methods

Analytical work was carried out to determine:

- Mineral compositions (metamorphic grade),
- Whole rock chemical compositions (environment of extrusion),
- Strain levels across the Arthur Lineament.

These data are necessary to constrain the tectonic setting, metamorphic and structural history of the Arthur Lineament and surrounds.

Mineral Analysis

Constituent minerals of rocks were analysed using a CAMECA SX50 electron microprobe at the Central Science Laboratory (CSL), University of Tasmania, Hobart. The regulated electron beam current was set at 25 na at an accelerating voltage of 15 kV, for routine mineral analyses, with a nominal incident beam size of 5μm diameter. Standard procedures of the CSL were followed, using the calibrations provided by Dr. D.A. Steele. A full description of analysing conditions and standards is provided in Appendix 1.

Whole-rock Analysis

Whole-rock analyses were carried out on intrusive mafic rocks to obtain their chemical compositions. The aim of the analysis was to determine the tectonic setting of the various intrusives occurring within the Arthur Lineament and in the surrounding units, in order to help in the reconstruction of the structural history of the Arthur Lineament. The samples were carefully selected to avoid rocks containing (i) abundant amygdale minerals, (ii) extensive mesoscopic, near-monomineralic domains of secondary minerals and alteration products, such as albite, epidote, and chlorite, (iii) quartz, epidote or calcite veins or patches totalling >5 modal %, as these may lead to incorrect results, and thus cause misleading interpretation of the tectonic setting. Some 37 samples were analysed for major elements (Si, Ti, Al, Fe, Mn, Mg, Ca, Na, K, P and ignition loss) and trace elements (Nb, Zr, Y, Ba, Xr, Rb, Pb, Th, Ni, Cr, V, Sc, La, Ce; Nd).

The selected samples were prepared for analysis by splitting hand specimens into ~ 10 mm chips, then discarding any weathered or altered material. The chips were then further crushed with a steel jaw crusher and cleaned of dust with an airhose. Approximately 40 g of the crushed material, free of weathering, alteration or veins were ground for approximately 3 minutes using a Rocklab tungsten-carbide ring mill. The analyses were carried out by an automated Philips PW 1480 X-ray fluorescence (XRF) spectrometer at the Department of Geology, University of Tasmania, with calibrations provided by Mr. P. Robinson. Fusion discs were used for major element analysis, whereas pressed powder pills were used form trace element analysis. A full description of the XRF process is provided in Appendix 2.

1.8 Classification and Terminology

1.8.1 Classification of rocks

The terminology used to describe metamorphic rocks follows Mason (1978) and Yardley (1989), with mineral identification following Deer *et al.* (1992). Rocks which are interpreted to be of sedimentary origin are termed *psammite* (sandstone), or *pelite* (mudstone). Rocks interpreted to have a sandy shale precursor are termed *psammopelite*. Rocks that have a basaltic or doleritic precursor are termed *metabasalt, metabasite* and *metadolerite*. Rocks that are interpreted to be

volcaniclastic and sedimentary in origin and are dominated by mafic minerals are termed *mafic schists*.

1.8.2 Classification and terminology of structures

Fold classification and terminology outlined by Ramsay (1967), Suppe (1985), McClay (1997) are utilised in this study. The morphological classification of cleavage is according to Powell (1979), Borradaile *et al.* (1982) and Passchier & Trouw (1996).

Fault terminology is after Hobbs *et al.* (1976). Faulted-related rock terminology is after Wise *et al.* (1984). All readings recorded and presented have been corrected to true North (declination = 12.5°). Structural measurements are presented in 'dip/dip direction' notation, as described in McClay (1997).

CHAPTER 2

STRUCTURAL HISTORY OF THE ARTHUR LINEAMENT

2.1 Introduction

This chapter is structured to best enable the reader to develop an understanding of the complex structural history of the Arthur Lineament. Following on from the background geological summary including an outline of the previous work in the region, is the detailed structural work undertaken as part of this study. In order to annotate the structural history satisfactorily, the characteristics of the different deformational episodes (cleavage, fold and faulting styles), and their overprinting relationships, are first presented in chronological order. Following on from this, the detailed mesoscopic and macroscopic field relationships for the key areas in the Arthur Lineament have been described. This allows the reader to apply the information pertaining to the characteristics of the deformational events, to the field relationships described from the different areas.

The Arthur Lineament, which is composed of meta-sedimentary and mafic meta-igneous lithologies of the "eastern" Ahrberg Group, Bowry Formation and a high strain part of the Oonah Formation, separates the Rocky Cape Group (and correlates) and "western" Ahrberg Group to its west from the relatively low strain parts of the Oonah Formation, and the correlated Burnie Formation, to its east (Figure 2.1). Early folding and thrusting, during the Middle to Late Cambrian, caused emplacement of the allochthonous Bowry Formation, which is interpreted to occur as a fault-bound slice, towards the eastern margin of the parautochthonous "eastern" Ahrberg Group metasediments. There are other fault bounded units within the Arthur Lineament, in particular east of the Bowry Formation and faulted against the high strain Oonah Formation is a block of material that is similar in appearance to the Ahrberg Group, and correlation with this unit is suggested. This block will be referred to as AGC throughout this chapter.

The lineament was multiply deformed during the Middle to Late Cambrian, Tyennan Orogeny (***Ca***D_1-***Ca***D_3) and has subsequently undergone several episodes of minor

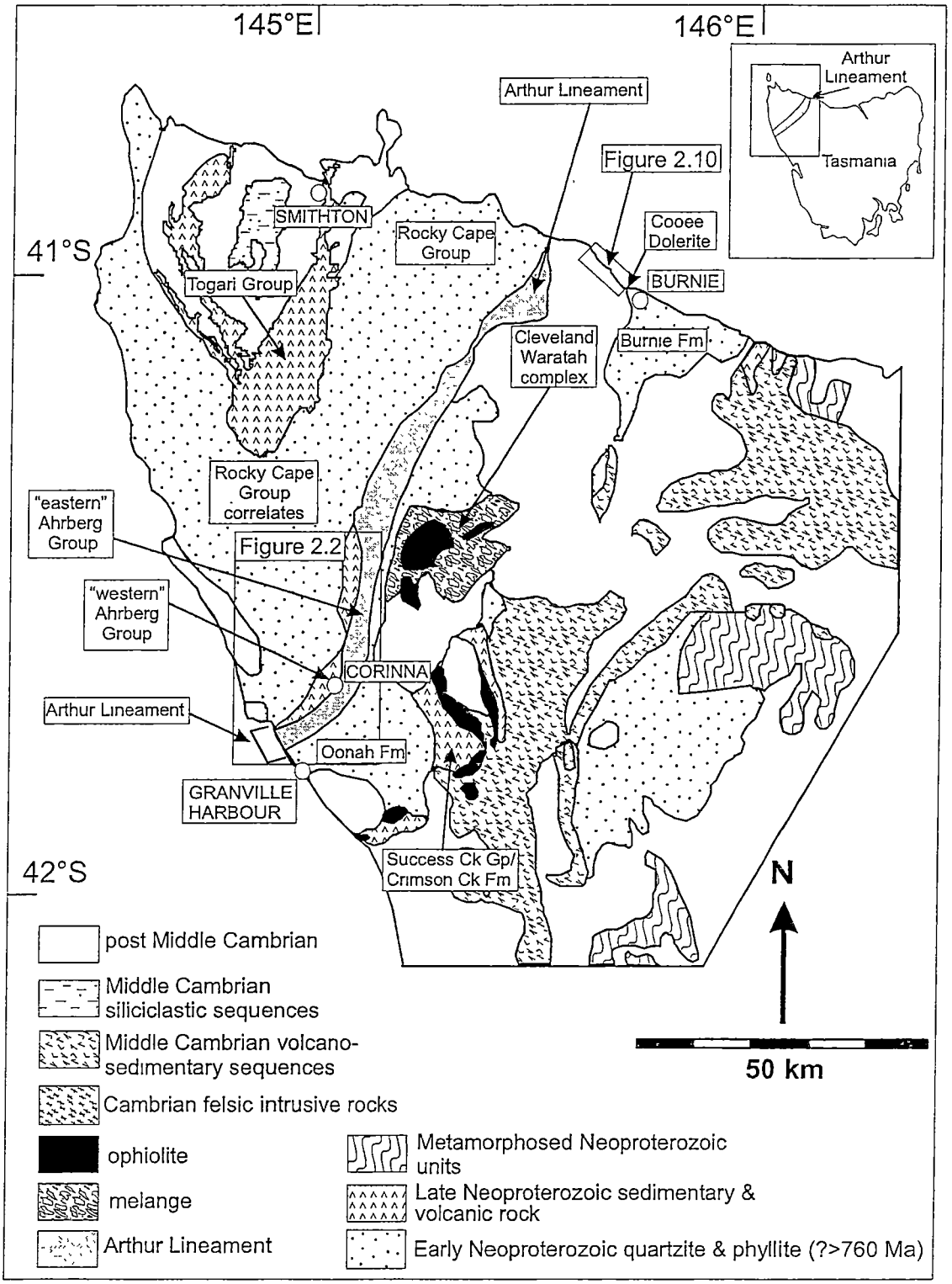

Figure 2.1. Setting of the Arthur Lineament, NW Tasmania (modified after Brown *et al.* 1995). The Arthur Lineament consists of the high strain (metamorphosed) Burnie and Oonah Formations, the "eastern" Ahrberg Group, the Bowry Formation, and other uncorrelated fault bounded units.

deformation in the Middle Devonian (***De***D_1, ***De***D_4). The aim here is to use detailed structural information from parts of the Arthur Lineament to determine the nature of Cambrian tectonism in northwestern Tasmania.

The eastern and western boundaries of the lineament were defined by Gee (1967a) as the point at which the lithologies change from being metamorphosed to unmetamorphosed. However, as yet, no one has demonstrated any change in metamorphic conditions at these boundaries possibly due to the simple mineral assemblage in the psammite-dominated packages. The boundary mapped by Gee (1967a) matches a transition from slaty cleavage in meta-sedimentary rocks to phyllitic cleavage. At the same position, early folds become tighter and quartz veining is more abundant. In recognition of the absence of any evidence for change in metamorphic grade, the boundaries are referred to here as a change in fabric intensity from low strain (slaty) to high strain (phyllitic or schistose). There may be a correlation with metamorphic grade but that remains problematic. Using these textural criteria, the position of the southeastern boundary of the Arthur Lineament as mapped by Gee (1967a), can be reproduced. On the north coast, the eastern margin of the lineament was recognised near Doctors Rocks and is not hidden under cover as suggested by Gee (1967a).

As discussed in Chapter 1, the Arthur Lineament has been the focus of several previous workers, at varying levels of detail. Gee (1967b) and Gee *et al.* (1967) carried out detailed structural mapping of the north coast of Tasmania, including the Somerset-Doctors Rocks area. Spry (1957a) and Turner *et al.* (1991) carried out regional mapping in the lower Pieman River and Corinna areas, but did not attempt a detailed structural analysis. The present work is based on regional mapping of the Arthur Lineament and surrounds, with detailed structural studies of the Somerset-Doctors Rocks area, and numerous traverses in the southern study area. These include the Savage River to Waratah road from Savage River township to 4km to the northeast, Savage River township, the Savage River to Corinna Road, the Whyte River track, the Rocky River and surrounding area, the Lower Pieman Dam Road from the Stanley River bridge to Reece Dam, the Reece Dam and spillway area, sections of the Owen Meredith, Paradise and Pieman Rivers, Lucy, Nancy, and Timbs Creek, the Mt Donaldson-Longback-Crescent Hills area, and the

southwestern-most exposure of the lineament from to the north of Granville Harbour to 4 mile beach. (Figure 2.1 and Figure 2.2(a) - (b)).

Factual and interpretive cross sections for the above areas have been compiled and presented. The approximate locations of the cross sections, presented in the relevant parts of this chapter, are illustrated in Figure 2.2(b). The coordinates of the start and end point of each section line are presented above the section line, on the cross section figure. Sections are consistently oriented 110/290, looking to the north (east to the right of the figure). However, sections constructed from mapping on the west coast are oriented 000/180 (section J" in Figure 2.22), 310/130 (section K" in Figure 2.32, and section I" in Figure 2.36(c)), and and 340/160 (sections G" and H" in Figure 2.36(c)) and viewed to the east-northeast (south to the right of the figure), due to the different trend of the Arthur Lineament in this area, as a result of Devonian refolding. The orientation of cross sections on the west coast (south to the right of the figure) is used in order to maintain orientation consistent with the other sections.

Each cross section consists of a factual data section, and an interpretive cross section aligned directly below. Due to the constant orientation of the cross sections, and the aim to keep extrapolation lengths to less than 1 km where strip-mapping has been undertaken, in some areas the cross sections are short (less than 1 km in length) and staggered. Where extrapolation has been required, the data has been extrapolated along lines at 90 degrees to the section line orientation. In these areas, some cross sections overlap (Figure 2.2(b)), in order to represent the structural style in the region satisfactorily. In some cases (such as data collected on the Lower Pieman Road), the cross sections are staggered as a result of a change in the orientation of the mapped area. On the cross section diagrams, section breaks are represented by vertical lines and identified by the notation 'SB'. On the figures with multiple sections, the cross sections are oriented with east-southeast to the right, with ongoing section lines continuing on the right of the figure (east) on the section line below. Measurements are corrected to apparent dip, using the method outlined in Appendix 2 of McClay (1987). Observations made of cleavage and fold facing changes in different deformational generations enabled the interpretation of geological structures and clarification of fold facing relationships in the complexly deformed parts of the study area. In order to clearly demonstrate these fold and cleavage

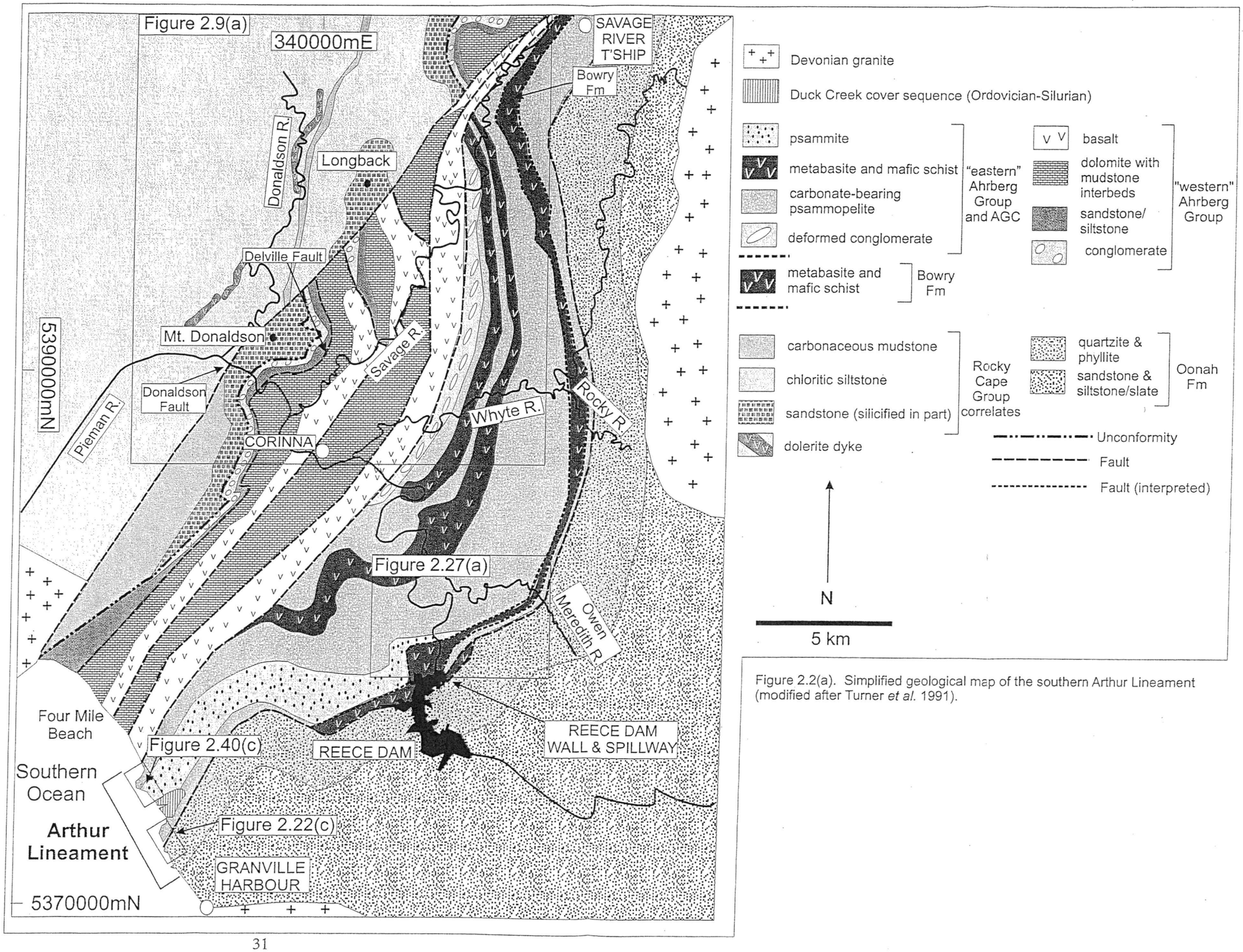

Figure 2.2(a). Simplified geological map of the southern Arthur Lineament (modified after Turner *et al.* 1991).

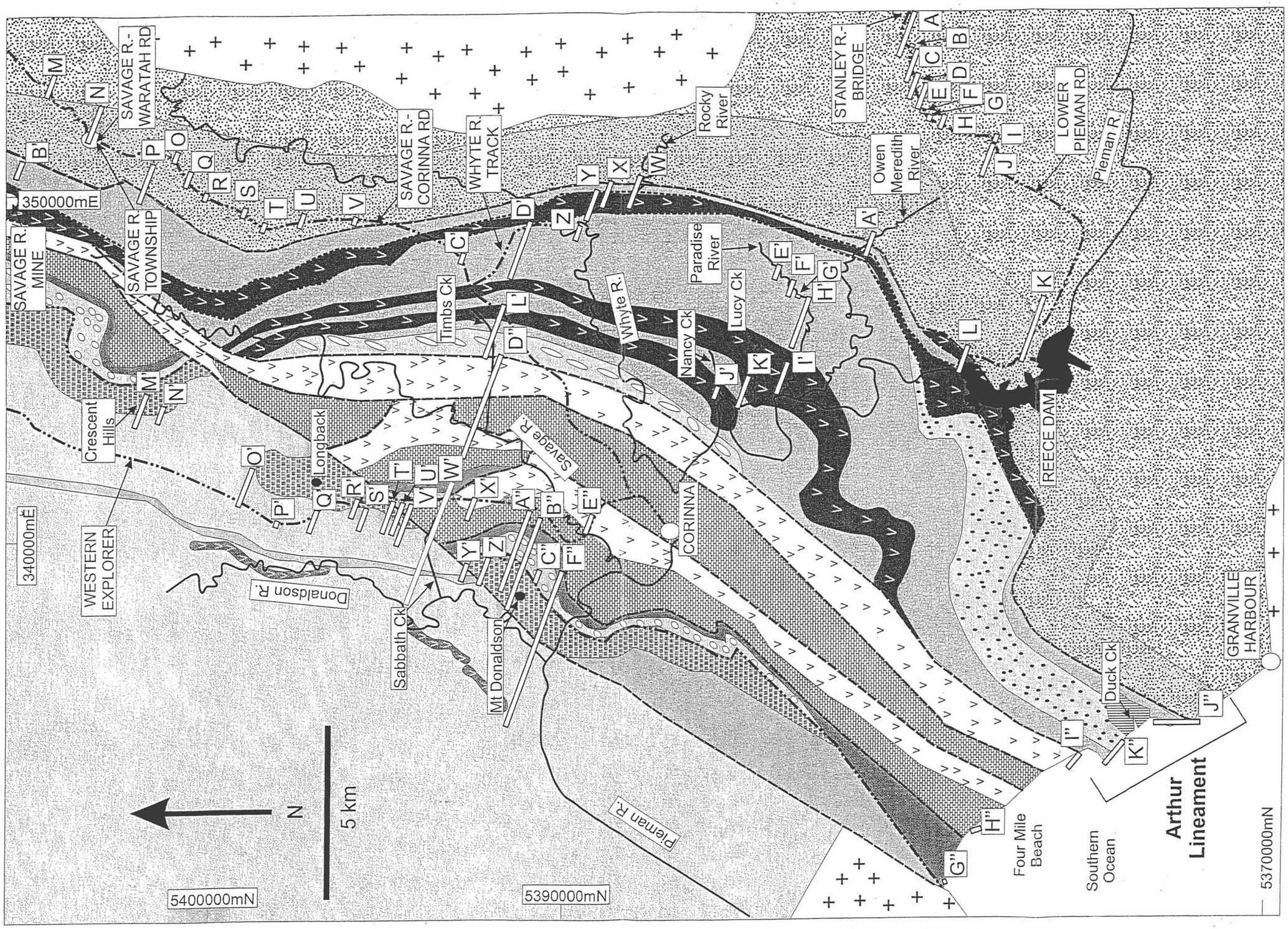

Figure 2.2(b). Simplified geological map of the Arthur Lineament (modified after Turner *et al.* 1991), with cross section locations illustrated. Cross sections are presented and discussed in the relevant area of the text. Legend for 2.2(b) is the same as Figure 2.2(a).

facing relationships in the factual cross sections, a clearly illustrated method has been employed. The scale of the cross sections is displayed at the base of the figures. In areas where a greater detail of mapping was employed, the scale accommodates the increased structural complexity.

The structural events described below are based on a synthesis of data from all these areas. Some of the results reported here have been accepted for publication (Holm & Berry *in press*).

2.2 Regional Geology

The early to middle Neoproterozoic of northwest Tasmania was dominated by deposition of shallow water siliciclastics and siltstone (Rocky Cape Group and correlates) in the west and turbidites (Burnie and Oonah Formations) in the east (Spry 1964) (Figure 2.3). An extensional phase followed in the Late Neoproterozoic *ca.* 550-650 Ma (Adams *et al.* 1985, Calver & Walter 2000). This featured widespread intrusion of tholeiitic dolerite dykes (Rocky Cape dyke swarm), extrusion of tholeiitic basalts and deposition of associated volcanogenic sediments, carbonates and shallow marine siliciclastics (Success Creek Group-Crimson Creek Formation, Togari and Ahrberg Groups) (Brown 1989, Turner 1989, Crawford & Berry 1992). The Togari and "western" Ahrberg Groups rest on a regional-scale low angle unconformity.

Deformational episodes at *ca.* 1270 Ma and 760 Ma are recognised on King Island (Figure 2.3). The 1270 Ma event was a lowest amphibolite/uppermost greenschist facies (biotite grade) regional metamorphic event (Berry *et al.* 2001), whereas the 760 Ma event (the Wickham Orogeny) featured polyphase deformation and extensive granitoid intrusion (Cox 1989, Turner *et al.* 1998). Previous workers have suggested that the Wickham Orogeny may correlate with the regional low angle unconformity beneath the late Neoproterozoic sequences of northwest Tasmania, although this is uncertain (Everard *et al.* 2000).

An arc-continent collision in the Early to Middle Cambrian initiated the Tyennan Orogeny (510 ± 10 Ma) (Berry & Crawford 1988, Crawford & Berry 1992, Turner *et*

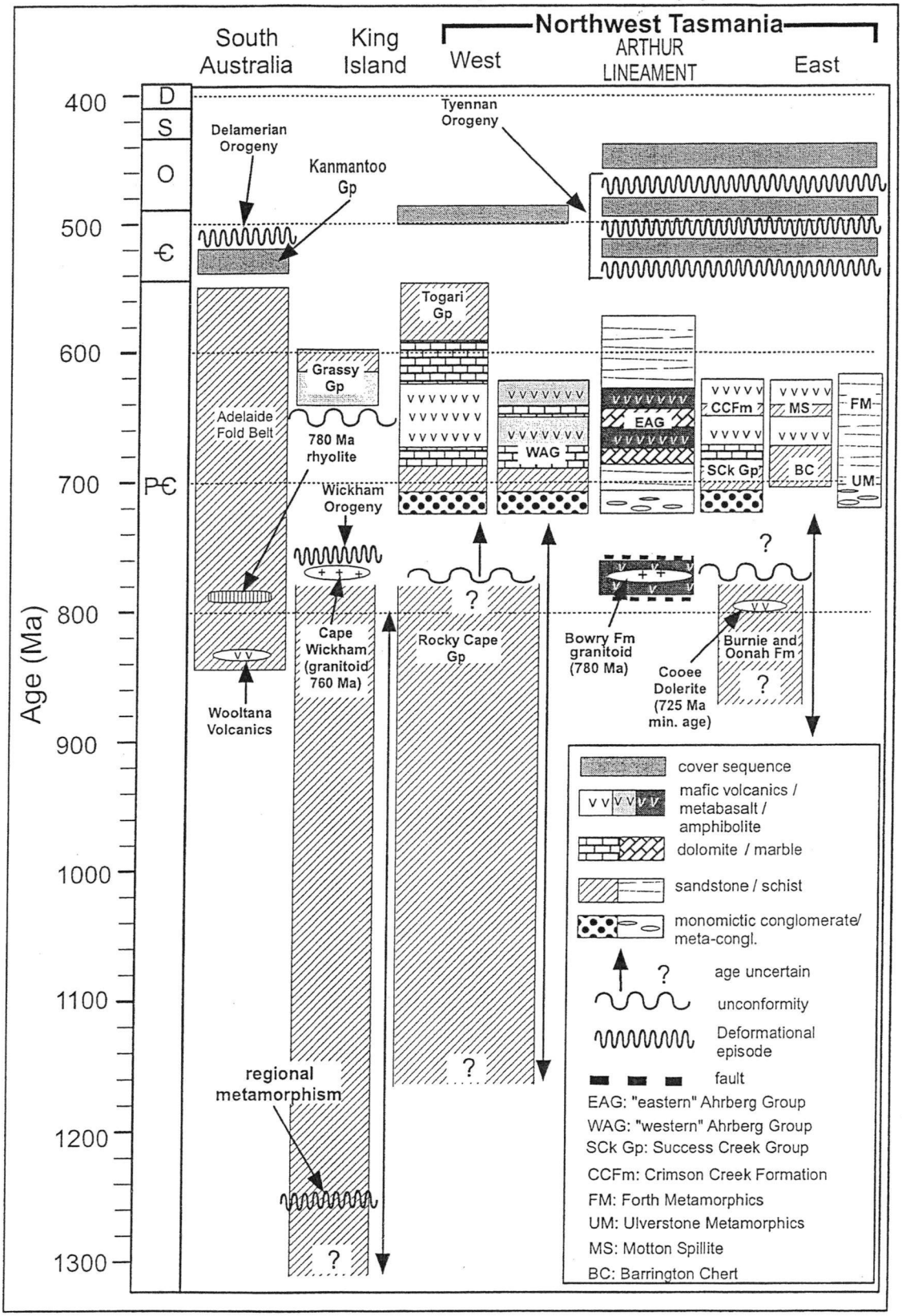

Figure 2.3. Time-space diagram for south eastern Australia from the Mid to Late Proterozoic to Devonian periods, emphasising lithological similarities and extensiveness of deformational events (modified from Calver & Walter 2000).

al. 1998). This resulted in the emplacement of allochthons, including mafic-ultramafic complexes in western and northern Tasmania (Crawford & Berry 1992, Turner *et al.* 1998). Movement indicators from the mylonitic soles of the allochthonous mafic-ultramafic complexes indicate west-directed obduction, the regional synthesis supporting the interpretation of an east-dipping subduction zone by Berry & Crawford (1988). The Arthur Lineament was formed during the early stages of the Tyennan Orogeny and predates a Middle Cambrian unconformity (Turner *et al.* 1998), but the exact process of its formation remains in doubt (Turner 1989, Berry 1994).

Subsequent deformation in the Middle Devonian as part of the Tabberabberan Orogeny (~370 Ma) resulted in further faulting and dome-and-basin style folding (Figure 2.3). This was closely followed by granitoid intrusion (332-367 Ma) (Williams *et al.* 1989).

2.3 Regional structural history of the Arthur Lineament

In both the northern and the southern areas of the Arthur Lineament, two intense, early fabrics are recognised. These fabrics decrease in intensity away from the lineament (Figure 2.4(a) and (b)). There is clear, consistent, and widespread evidence for the relative timing of the $Ca D_1$ and $Ca D_2$ events (see sections 2.3.1, 2.4.1.1). The existing data (Turner *et al.* 1998) suggests both geometric events occur very early in the Tyennan Orogeny, and they have very similar spatial distributions. There appears to be a close genetic link between these events and they can be correlated throughout the length of the lineament (see below).

A D_3 event was recognised in the northern Arthur Lineament. It has produced a weak, sub-vertical cleavage, with a north-northeast strike, in pelitic layers. F_3 macro-scale, open folds predate deformation interpreted to be Devonian in age. A D_3 event is also present in the southern parts of the Arthur Lineament. It also produced a variably developed, upright to west-dipping, north-northeast striking cleavage, of similar intensity to the S_3 fabric in the north of the Arthur Lineament. In the southern area the D_3 event is Late Cambrian in age, constrained by overprinting relationships at the Reece Dam spillway, where the D_3 refolds the earlier fabrics, and

Figure 2.4. ***Ca***S_1, ***Ca***S_2 and ***Ca***S_3, within and near the Arthur Lineament. (a) weakly developed slaty ***Ca***S_2 crenulating weakly developed ***Ca***S_1, in Burnie Formation sandstone (plane polarised light) (399790 mE, 5457060 mN); (b) weakly developed slaty ***Ca***S_2 crenulating weakly developed ***Ca***S_1, in Oonah Formation sandstone, lens cap is 50mm diameter (353830 mE, 5380140 mN); (c) strongly developed schistose ***Ca***S_2 enveloping ***Ca***S_1, basal unit of "eastern" Ahrberg Group (cross polarised light) (345240 mE, 5392040 mN); (d) strongly developed schistose ***Ca***S_2 and syn-***Ca***S_2 albite porphyroblasts with oblique ***Ca***S_1, preserved as S_i in albite, correlate of "eastern" Ahrberg Group, to the east of the Bowry Formation (cross polarised light) (350180 mE, 5388100 mN); (e) phyllitic metasiltstone, showing formation of oblique microlithons in coarse-grained layers (***Ca***S_2) (plane polarised light) (398450 mE, 5758200 mN); (f) phyllitic metasiltstone, with ***Ca***S_2 developed sub-parallel to S_0. No evidence of ***Ca***S_1 was found, "western Ahrberg Group, 300m west of boundary-fault with "eastern" Ahrberg Group (cross polarised light) (344530 mE, 5392100 mN); (g) finely spaced, S_0-parallel ***Ca***S_2, evident in mudstone beds and crenulated by spaced ***Ca***S_3, Rocky Cape Group correlate beds (plane polarised light) (343860 mE, 5401800 mN); (h) finely spaced, S_0-parallel ***Ca***S_2, crenulated by spaced ***Ca***S_3, Rocky Cape Group correlate beds (plane polarised light) (339200 mE, 5394155 mN). Symbols 'm' indicate white mica, 'a' albite, and 'q' quartz.

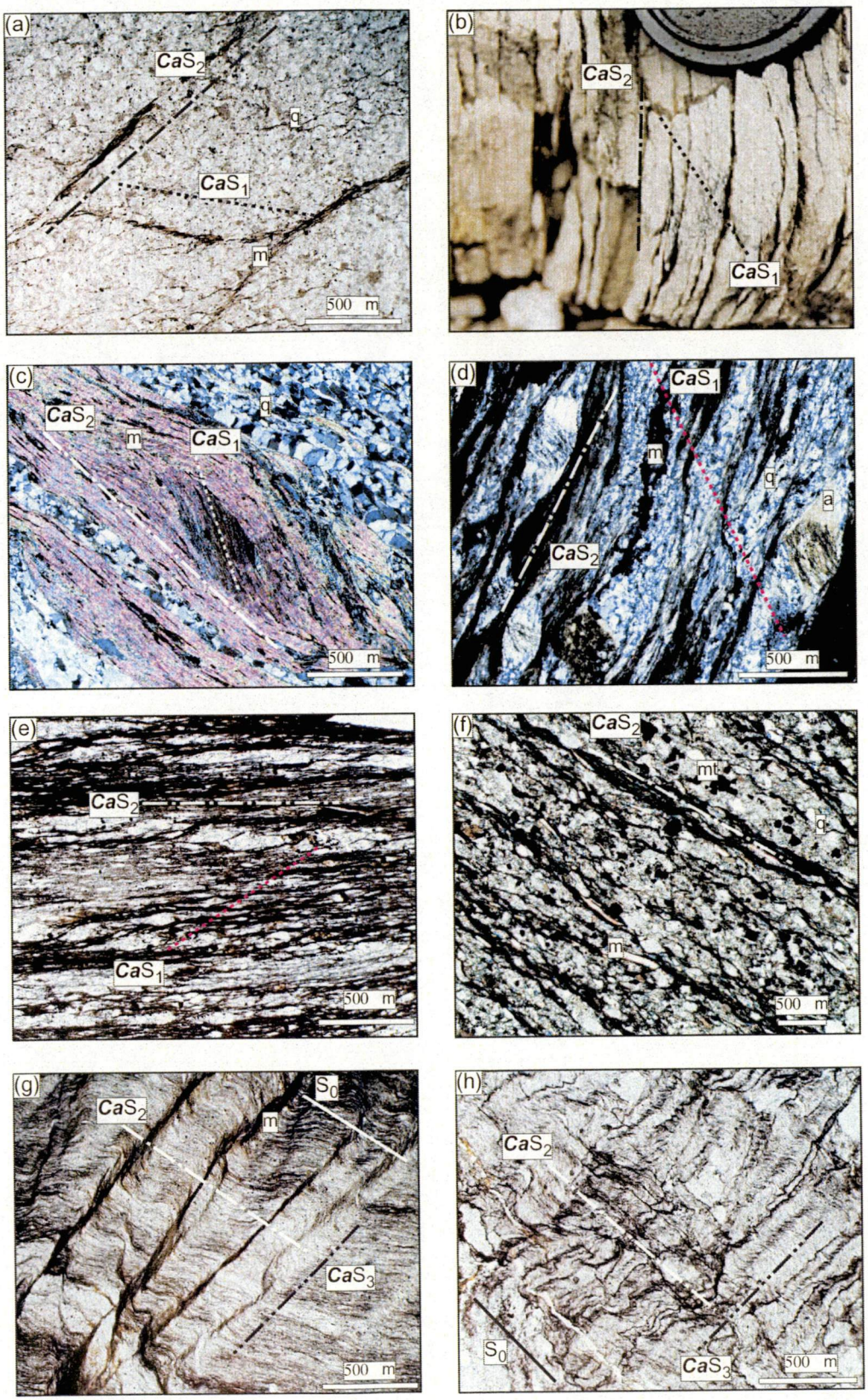
(a)
CaS2
q
CaS1
m
500 m
(b)
CaS2
CaS1
(c)
CaS2
m
CaS1
q
500 m
(d)
CaS1
m
q
a
CaS2
500 m
(e)
CaS2
CaS1
500 m
(f)
CaS2
mt
q
m
500 m
(g)
CaS2
S0
m
CaS3
500 m
(h)
CaS2
S0
CaS3
500 m

Figure 2.4(a)-(h).

on the west coast, north of Granville Harbour, where the S_3 does not penetrate the overlying Ordovician sediments. In the Balfour and Trowutta areas, to the west of the Arthur Lineament, a fabric with consistent style and orientation, related to folding interpreted here to be Late Cambrian in age, is widely developed (Everard *et al.* 1996). On these grounds, the D_3 event in both areas is considered to be the same event.

A brief overview of the structural variations is given below in sections 2.3.1 to 2.3.4. This provides a background for the more detailed discussion that follows. The supporting evidence for these summaries is given in section 2.4.

2.3.1 Deformation *Ca*D_1

A ***Ca***D_1 (***Cambrian*** D_1) event was observed throughout the lineament. It is a well developed event, however it is commonly overprinted by ***Ca***D_2. ***Ca***D_1 was detectable several kilometres to the east of the lineament's eastern boundary, although it does not extend as far to the east as ***Ca***D_2. To the west of the lineament however, the ***Ca***D_1 event weakens markedly over a short distance, and was rarely noted to the west of the lineament's western boundary.

CaD_1 produced mesoscopic to macroscopic, gently inclined to recumbent, isoclinal folds (***Ca***F_1). However, ***Ca***F_1 folds were not observed in the low strain domains. In contrast, in areas of high strain, they are interpreted to have been widely developed, although they are only preserved in zones of weak ***Ca***D_2, due to the intense overprinting and obliteration by the later event. ***Ca***F_1 folds have strongly attenuated limbs, and are frequently associated with ***Ca***$D_{1/2}$-related shear zones, which are most often observed close to lithological boundaries between units of contrasting competency. The shear zones are bedding parallel, and occur on the limbs of ***Ca***F_1 isoclinal folds, as a consequence of the competency contrast between psammite and psammopelite layers. The change in competency at the lithological boundaries results in strain partitioning, which leads to shearing.

CaD_1 has produced a finely spaced to schistose, S_0-parallel axial planar foliation (***Ca***S_1), that varies in its pervasiveness. In zones of low strain, it is a moderately well

developed cleavage, but it does not widely penetrate coarse grained layers. In these low $Ca D_1$ strain zones to the east of the lineament, $Ca S_1$ is finely spaced to phyllitic. The cleavage is a smooth, 0.5 mm spaced, parallel cleavage, with discrete cleavage domains and microlithons. In the southern study area, in the low strain zone 3-7 km east of the lineament, the $Ca S_1$ foliation dips steeply to the northwest, whereas $Ca L_{01}$ intersection lineations plunge moderately to steeply to the northeast (Figure 2.5). 0-3 km east of the lineament, where the strain levels are slightly higher (zones of phyllitic $Ca S_1$ are dominant) the $Ca S_1$ foliation dips moderately to the northeast, whereas $Ca L_{01}$ intersection lineations plunge gently to moderately to the northeast (Figure 2.5).

However in zones of high $Ca D_1$ strain, $Ca S_1$ is a pervasive schistosity, although it is commonly strongly overprinted by the $Ca S_2$ foliation and $Ca F_2$. In outcrops where $Ca D_1$ is not obliterated by $Ca D_2$, the $Ca S_1$ foliation is the dominant form surface. $Ca S_1$ is a smooth, zonal schistosity with finely spaced parallel cleavage domains (0.02-0.2 mm wide microlithons), and discrete transitions between cleavage domains and microlithons. Within the lineament, in psammopelitic lithologies, $Ca S_1$ is preserved in $Ca S_2$ microlithons of mica and chlorite (Figure 2.4(c)). Within syn-$Ca D_2$ albite porphyroblasts, inclusion trails (S_i) interpreted to be relict $Ca S_1$ are preserved (Figure 2.4(d)). The inclusion trails are aligned with the $Ca S_1$ foliation preserved in the $Ca S_2$ microlithons. $Ca D_1$ high strain zones feature intensely developed $Ca S_1$ and are dominated by $Ca F_1$ folds and S_0-parallel, syn-$Ca D_1$ thrust faults. In these areas $Ca S_1$-parallel quartz boudins are common, although they are commonly isoclinally folded by $Ca F_2$ (Figure 2.6(a) and (b)), which is also recognised by $Ca S_2$-parallel quartz segregations defining the $Ca S_2$ schistosity planes. $Ca L_{01}$ intersection lineations and $Ca L_1$ stretching lineations are common and plunge moderately to the south-southwest.

2.3.2 Deformation $Ca D_2$

Throughout the Arthur Lineament, strain levels are high for both the $Ca D_1$ and $Ca D_2$ (***Cambrian*** D_2) events, although locally the intensity of $Ca D_1$ and $Ca D_2$ vary. However, $Ca D_2$ structures are pervasively developed throughout the lineament. The $Ca D_2$ event is the dominant deformational episode within the Arthur Lineament.

Figure 2.5. Stereographic projections for the $Ca D_1$ and $Ca D_2$ structures in the southern Arthur Lineament and surrounding area. Planes (S_0, $Ca S_1$ and $Ca S_2$) are presented as poles. Intersection lineations between S_0, and $Ca S_1$ are annotated as $Ca L_{01}$. Intersection lineations between S_0, and $Ca S_2$ are annotated as $Ca L_{01}$. Intersection lineations between $Ca S_1$ and $Ca S_2$ are annotated as $Ca L_{12}$. The study area is divided into four main structural domains, with the High strain zone and Moderate-High strain zone subdivided to account for exposure on the west coast that has been re-oriented during Devonian deformation. Roman numerals correspond to areas illustrated in Figure 2.15. WAG, EAG and AGC are abbreviations for "western" Ahrberg Group, "eastern" Ahrberg Group and Ahrberg Group correlates, respectively. ELS1 and ELS2 are western and eastern subdivisions, respectively, of the Eastern low strain zone.

WESTERN LOW STRAIN ZONE	HIGH STRAIN ZONE	MODERATE-HIGH STRAIN ZONE		HIGH STRAIN ZONE		MODERATE-HIGH STRAIN ZONE			EASTERN LOW STRAIN ZONE		
i WAG-Rocky Cape Group correlates 0-10km west of A.L	iiⁱ(a) EAG (west coast-north)	ivⁱ(a) AGC (west coast-south)	Vⁱ(a) Oonah Formation (west coast-south)	iiⁱ(b) EAG	iii Bowry Formation	ivⁱ(b) AGC	Vⁱ(b) Oonah Formation within Arthur Lineament		viⁱ(a) ELS1 Oonah Formation 0-3 km east of Arthur Lineament		viⁱ(b) ELS2 Oonah Formation 3-7 km to east of Arthur Lineament
Four Mile Beach-Pieman River-Corinna-Mt Donaldson-Longback	Granville Harbour-Four Mile Beach			Timbs-Lucy-Nancy Cks-Paradise & Pieman Rs-Savage R.-Corinna Rd	Rocky River-Owen Meredith River-Lower Pieman Dam	Rocky River-Owen Meredith River-Lower Pieman Dam	Savage River-Waratah-Corinna Road	Rocky River-Owen Meredith River-Lower Pieman Dam Road	Savage River-Waratah Road	Lower Pieman Dam Road	
S_0											
N=367	N=87	N=24	N=31	N=154	N=39	N=25	N=32	N=24	N=11	N=80	N=45
CaS_1											
N=5	N=78	N=18	N=13	N=10	N=8	N=3	N=65	N=14		N=22	N=21
CaS_2											
N=9	N=46	N=23	N=18	N=64	N=50	N=23	N=65	N=22	N=11	N=33	N=13
$CaL_{01}(\cdot)/L_{12}(\cdot)$											
	N=40	N=9	N=12	N=12		N=5	N=41	N=18		N=14	N=16
CaL_{02}											
N=8	N=17	N=9	N=8	N=20	N=20	N=20	N=61	N=23	N=11	N=22	N=9

Figure 2.5

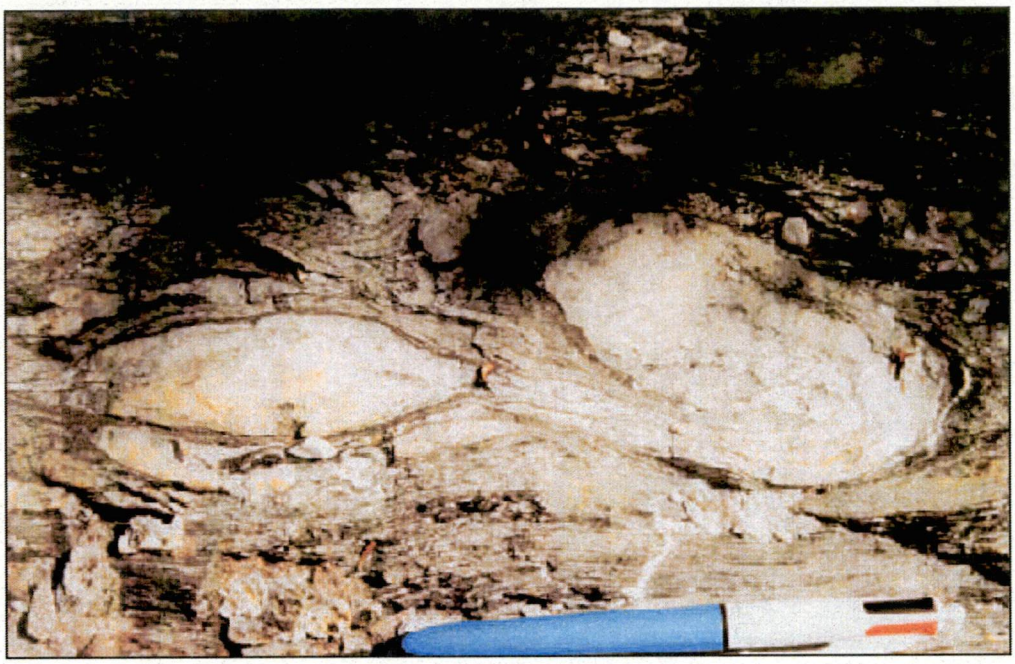

Figure 2.6(a). ***Ca***S_1 quartz boudin isoclinally refolded by ***Ca***F_2. Host lithology is quartz-mica schist. Pen is 13.5 cm in length.(349200 mE, 5396850 mN)

Figure 2.6(b). ***Ca***S_1 quartz boudin tightly refolded by ***Ca***F_2. ***Ca***S_2-parallel quartz segregations are also evident, axial planar to the ***Ca***F_2 fold. Pen is 13.5 cm in length.(349200 mE, 5396850 mN)

CaD_2 decreases in intensity gradually to the east of the lineament. In the northern and southern areas of the lineament, ***Ca***D_2 was observed up to 7 km from the lineament's eastern margin. To the west of the lineament however, ***Ca***D_2 decreases sharply in intensity over 2 km, from the lineament's western boundary, although in this region it is developed further to the west than the ***Ca***D_1 deformation. In areas where ***Ca***S_2 is strongly developed, ***Ca***F_1 and ***Ca***S_1 are overprinted and were difficult to identify. In Figure 2.6(a) and (b), the ***Ca***S_1 foliation is only clearly represented by the folded ***Ca***S_1 quartz segregrations. The ***Ca***S_1 fabric is crenulated by ***Ca***S_2, whereas the limbs of ***Ca***F_1 folds and syn-***Ca***D_1 thrust faults are tight to isoclinally folded by ***Ca***F_2.

CaD_2 produced recumbent, tight to isoclinal folds (***Ca***F_2) of varying scales (Figure 2.6(a) and (b), Figure 2.7). The mesoscopic ***Ca***F_2 folds observed in the field were predominantly asymmetrical folds, with moderately attenuated long limbs (Figure 2.7). The ***Ca***F_2 are the dominant folding event recognised in the field. They are found refolding ***Ca***F_1 folds, ***Ca***S_1 and pre-***Ca***D_2 fault surfaces. On the north coast, in low ***Ca***D_2 strain areas to the east of the lineament, ***Ca***F_2 folds plunge gently to the east and west, with axial planes dipping gently to the south. However, in the south, 3-7 km from the lineament, ***Ca***F_2 folds plunge moderately to the northeast and ***Ca***S_2 dips moderately to steeply to the east.

In areas of high and low ***Ca***D_2 strain, the axial planar ***Ca***S_2 foliation varies in intensity between the short and long limbs of the ***Ca***F_2 folds. In particular, in the low strain area on the north coast in the Somerset region, the ***Ca***S_2 foliation is better developed on the short limbs than on the long limbs, with the microlithons more finely spaced. In these low ***Ca***D_2 strain areas, the deformation produced a smooth, parallel 3-8 mm spaced axial planar cleavage in sandstones with discrete transitions between cleavage domains and microlithons (***Ca***S_2) (Figure 2.4(a) and (b)). The foliation is pervasively developed in psammopelitic and psammitic layers, and was frequently observed to be the dominant form surface in these areas (Figure 2.8).

More proximal to the lineament (1-3 km to the east of the lineament), ***Ca***S_2 is a smooth 2-3 mm spaced, parallel, phyllitic cleavage with discrete transitions between cleavage domains and microlithons (Figure 2.4(e)). Regionally, in the moderate to high strain areas, ***Ca***S_2 is the dominant foliation in both pelitic and psammitic

Figure 2.7. Gently west-pluinging ***Ca***F_2 fold in low strain Domain N1 on north coast near Somerset. Fold is tight, with well developed axial planar ***Ca***S_2 spaced cleavage. View is to the west.(400075 mE, 5456990 mN).

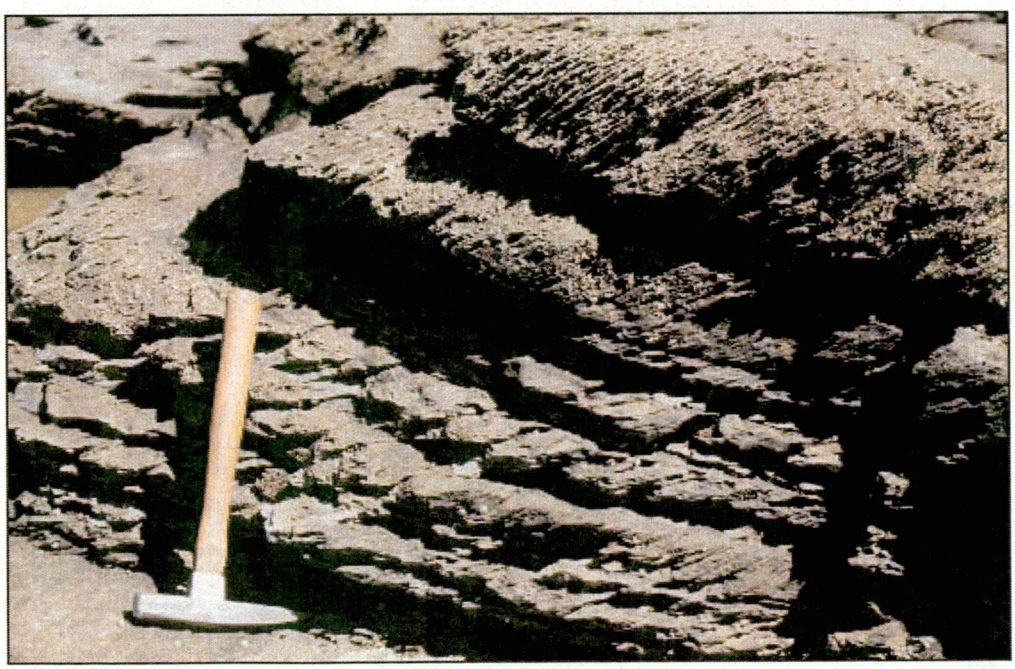

Figure 2.8. Pervasively developed, south-dipping ***Ca***S_2 axial planar cleavage in sandstone beds (Domain N1 north coast). Positioned on upper, downward-facing limb of tight, gently west-plunging ***Ca***F_2 fold. View is to the west..(400075 mE, 5456990 mN).

layering. Within the lineament, in zones of high $Ca D_2$ strain, $Ca S_2$ is a smooth, 0.5-1.5 mm spaced, parallel schistosity with discrete cleavage domains and microlithons (Figure 2.4(c) to (d)). $Ca S_2$ is sub-parallel to S_0 and axial planar to the $Ca F_2$ folds. Crenulated $Ca S_1$ is preserved within $Ca S_2$ microlithons (Figure 2.4(c) and (d)). In these high strain zones, in the south, $Ca F_2$ folds predominantly plunge gently to the south, however 1-3 km to the east of the lineament, in the Eastern Low Strain Zone (Figure 2.5), they also plunge to the north. Axial planes dip gently to steeply to the east.

At the lineament's western boundary, with the sharp decrease in intensity of $Ca D_2$, $Ca S_2$ is less well developed, as are $Ca F_2$ folds. Within the lineament, close to its western margin, $Ca S_2$ is schistose, defined by chlorite and mica planes interlayered with quartz-rich layers (Figure 2.4(c)). However, 300 m to the west of the lineament, $Ca S_2$ is a phyllitic fabric, and only penetrates pelitic phyllite layers (Figure 2.4(f)). Two kilometres to the west of the lineament's western boundary, $Ca S_2$ is a smooth, continuous, and parallel cleavage, that is best developed in mudstone interbeds. In this area $Ca S_2$ is widely crenulated by $Ca S_3$ (Figure 2.4(g) and (h)).

2.3.3 Deformation $Ca D_3$

The $Ca D_3$ (*Cambrian* D_3) deformational event is not as strongly developed, and $Ca S_3$ is not as pervasive as $Ca S_1$ and $Ca S_2$. In the study area $Ca D_3$, which featured east-west compression, is most prominent to the west of the lineament in the "western" Ahrberg Group and Rocky Cape Group correlates, and in the southern parts of the "eastern" Ahrberg Group. Minor north-south trending post-$Ca D_2$ folds with an associated weakly developed spaced cleavage in pelitic layers, in the north of the study area are attributed to this event.

In the south of the study area (Corinna area) the structural overprint of the $Ca D_3$ event is represented by gently south plunging, open to close $Ca F_3$ folds, with gently dipping, "right way up" western limbs, and steeply east-dipping to overturned eastern limbs (Figure 2.9(c) to (e)). The folds are moderately inclined with west-dipping axial planes that reflect an east-directed transport (Figure 2.9(b)). West dipping syn-$Ca D_3$ thrusts were mapped in the Rocky Cape Group correlates at the

Figure 2.9(a) simplified geology of the Corinna area (map modified after Turner *et al.* 1991), (b) stereographic projections showing effects of $Ca D_3$ deformation; (c) cross sections D", E" and F" illustrating structural data (with structural interpretation for sections immediately below) for the Corinna area, west of the Arthur Lineament, cross section start and end point coordinates are presented above the data sections, at the far left and right of the section lines. Sections are viewed to the north, (d) detailed sketch of river section in the lower most sandstone unit of the "western" Ahrberg Group, illustrating the gently west-dipping long limb and steeply east-dipping to downward facing short limb typical of the $Ca F_3$ deformation (337280 mE, 5389940 mN); (e) close up of the hinge of a $Ca F_3$ fold within the detailed sketch area, sandstone beds showing well developed axial planar $Ca S_3$ cleavage; (f) overturned (eastern, short limb of $Ca F_3$) sandstone beds in the upper most Rocky Cape Group correlates, showing $Ca D_3$–related boudinage (337160 mE, 5390000 mN); (g) sketch of (f) inset highlighting the $Ca D_3$–related boudinage; (h) close up of boudin in (g), (i) sketch of boudin closeup, illustrating mesoscopic folding ($Ca F_3$) observed in siltsone layers. Legend for 2.9 (a) is the same as for Figure 2.2(a). Area excluded from data collection ("eastern" Ahrberg Group, right side of map) is shown in pale grey Figures 4 (d) to (i) are mirror images of photographs/sketches (adjusted to match the north looking sense of the section).

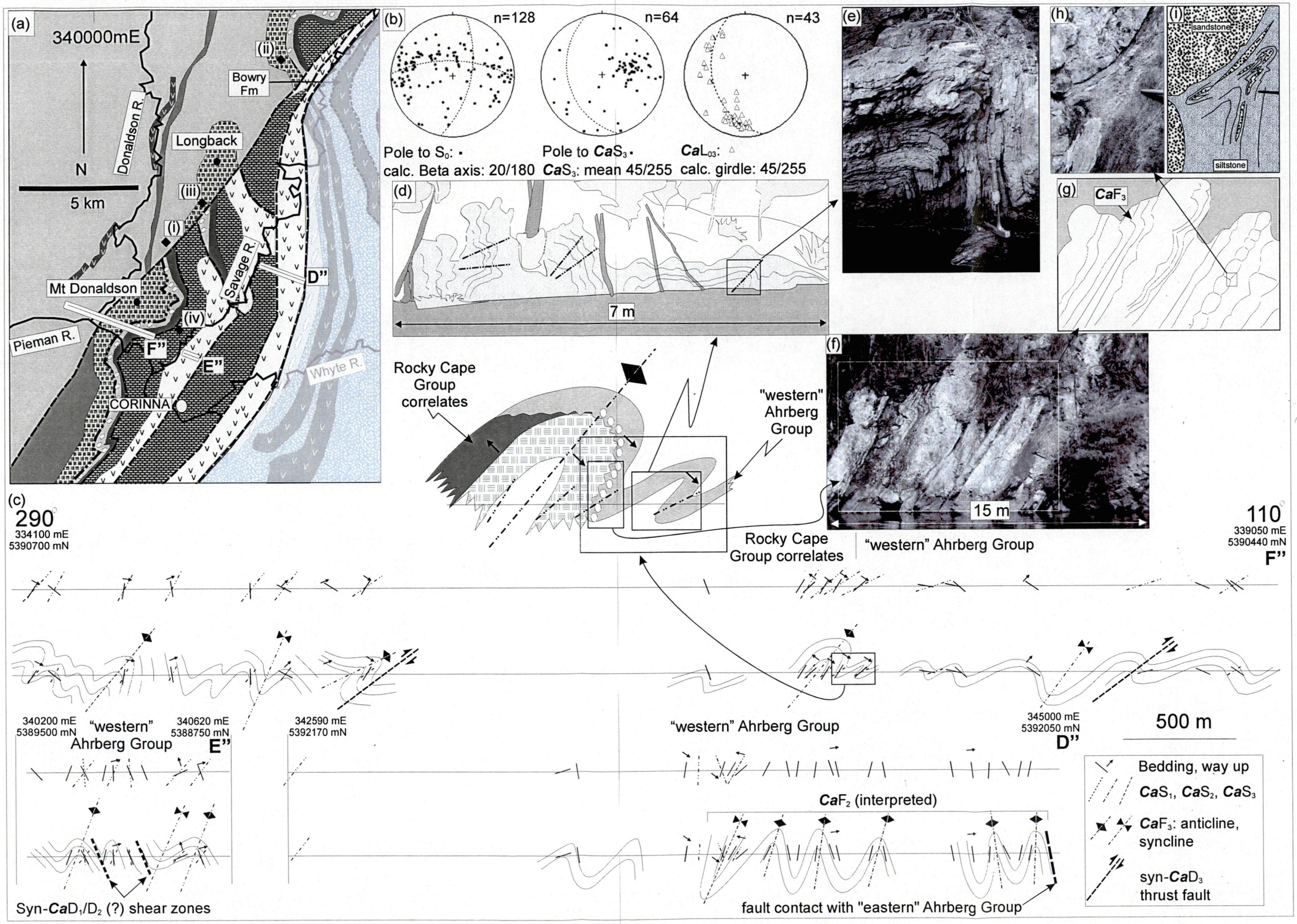

Figure 2.9 (a) to (i).

Longback Ridge (341360 mE, 5398900 mN) and at Crescent Hills (344240 mE, 5402280 mN). A major west dipping syn-***Ca***D_3 thrust is interpreted to occur in the "western" Ahrberg Group in Guthrie Ck (339980 mE, 5390980 mN) (Figure 2.2(a)). This was reported by Spry (1964) as the Delville Fault, however the author did not assign a specific age to the structure. Spry (1964) mapped a west dipping thrust fault on the Pieman River (the Donaldson Fault), associated with the main deformational event in that area, interpreted here to be ***Ca***D_3. Boudinage of competent beds commonly occurs on the limbs of the ***Ca***F_3 folds (337160 mE, 539000 mN) (Figure 2.9(f) to (i)).

In the north of the study area (Somerset-Doctors Rocks area) ***Ca***D_3 was weak. Mesoscopic symmetrical ***Ca***F_3 folds have upright axial planes and shallowly dipping limbs. Associated with ***Ca***F_3 is a smooth, 2-5 mm spaced parallel cleavage with discrete transitions between cleavage domains and microlithons (***Ca***S_3). The age of these folds on the northwest coast is poorly constrained, and they are tentatively assigned a ***Ca***D_3 age based on their relative timing post-***Ca***D_2 and pre-***De***D_1.

Although ***Ca***D_3 is not directly dated, a Late Cambrian age was inferred based on the folding of ***Ca***S_1 and ***Ca***S_2, and the absence of ***Ca***S_3 in the Ordovician Gordon Limestone on the west coast, north of Granville Harbour (334250 mE, 5372700 mN) (Figure 2.2(a)).

2.3.4 Devonian deformation

Devonian age deformation, attributed to the Tabberabberan Orogeny, is widespread throughout western Tasmania and is interpreted to predate the widespread 332-367 Ma granitoid intrusion (Williams *et al.* 1989). In the north of the study area (Somerset-Doctors Rocks area) a mild deformational event postdates the ***Ca***D_3 event. This is tentatively correlated with the Loongana/Wilmot trend (D_1 Devonian event) of Williams *et al.* (1989), referred to here as ***De***D_1. It features sub-horizontal to gently plunging upright open folds (***De***F_1), that has produced a poorly developed axial planar cleavage. The interference of the north-south trending ***Ca***F_3 and the east-west trending ***De***F_1 has resulted in dome and basin style folding (5-15 m wavelength). ***De***D_1–related faulting was not recognised in this area.

In the southern study area two deformational events corresponding to the D_4 of Williams *et al.* (1989) and known as the Zeehan/Gormanston trend overprint the Cambrian deformation. In this work the first of these is referred to as ***De***D_4, and the second is referred to as ***De***D_5. In the south of the study area, both ***De***D_4 and ***De***D_5 produced gently plunging meso- to macroscopic upright open folds (***De***F_4 and ***De***F_5). The ***De***S_4 is a smooth, 5-10 mm spaced parallel crenulation cleavage locally developed in ***De***F_4 fold hinges. The ***De***S_5 is a very weak, smooth, <10 mm spaced, parallel crenulation cleavage that is also locally developed. The interference of the E-W trending ***De***F_4 and ESE-WNW trending ***De***F_5 has resulted in dome and basin style folding (10-50 m wavelength). Faulting interpreted to be contemporaneous with ***De***D_4 and ***De***D_5 is common in the southern part of the study area.

2.4 Detailed mesoscopic and macroscopic structural relationships

Spatial variation in intensity of both all deformations (***Ca***D_1-***Ca***D_3 and ***De***D_1, ***De***D_4 and ***De***D_5) has lead to complex overprinting relationships. The aim here is to determine how the Cambrian structural elements of the Arthur Lineament were produced. Strongly deformed Burnie Formation, on the northwest coast (Somerset-Doctors Rocks area), contain a structural transition that correlates closely with the eastern margin of the Arthur Lineament in the south, and is much better exposed. The central and western portions of the Arthur Lineament are better exposed in the southern part of the study area (Reece Dam and Corinna areas). The following discussion highlights the relationships in these critical areas.

2.4.1 Northern study area: structure of the Burnie Formation

Along the northwest coast of Tasmania in the Somerset-Doctors Rocks area there is excellent exposure of the variably deformed Burnie Formation (Figure 2.1 and Figure 2.10(a)). Lithologies are composed of psammites and psammopelites with minor basaltic lavas and associated intrusives (Cooee Dolerite). On the eastern flank of the Arthur Lineament, the westernmost outcrop of Burnie Formation provides evidence for the changing fold style and progressive increase in strain approaching the lineament. The deformation in this area is more complex than previously

interpreted. The area is dominated by mesoscopic and macroscopic ***Ca***F_2 folds (Figure 2.7 and Figure 2.8). Syn-***Ca***D_1 and syn-***Ca***D_2 thrusts are common (e.g. locations (i) 400075m NE, 5456990 mN and (ii) 399750 mE, 5457100 mN on Figure 2.10(a)). Subsequent deformation (***Ca***D_3 and ***De***D_1) has resulted in dome-and-basin style folding.

Three structural domains resulting from Cambrian-age deformation can be identified in the Somerset-Doctors Rocks area based on orientation and tightness of folds, frequency of faulting and intensity of associated fabrics. The domains are:

- Eastern low-strain Domain N1 (Somerset)
- Central moderate-strain Domain N2 (west of Somerset)
- Western high-strain Domain N3 (east of Doctors Rocks).

No change in mineralogy has been detected across these three domains. While historically (Gee 1967a) the textural changes described here have been associated with increasing "metamorphism" no evidence of a change of metamorphic grade found across these zones.

2.4.1.1 Eastern low-strain Domain N1

Domain N1 is dominated by tight, gently west-plunging, south-verging downward-facing parasitic ***Ca***F_2 folds with moderately south dipping axial planes (Figure 2.7, Figure 2.10(b) and Figure 2.11(a) and (b)), however there is clear evidence of folding and thrusting prior to the dominant ***Ca***D_2 deformation (Figure 2.12(a) to (f)). At this location ((ii) on Figure 2.10(a)) (399750 mE, 5457100 mN), folding which predates ***Ca***D_2 was observed in siltstone and mudstone units. This pre-***Ca***D_2 event is interpreted to correspond to ***Ca***F_1 folding and syn-***Ca***D_1 thrusting seen elsewhere in the Arthur Lineament. At location (ii) on Figure 2.10(a), illustrated in Figure 2.12(a) to d, faulting has a low angle reverse sense, and is interpreted to indicate movement towards the southwest (Figure 2.12(a)). Proximal to the fault surface, mesoscopic ***Ca***F_1 fold limbs and axial planes are dragged into a sub-parallel orientation with the fault surface (Figure 2.12(c) and (d)). The geometry of these ***Ca***F_1 folds provides evidence for the southwest transport interpretation on the fault surface. The ***Ca***S_2 foliation overprints the fault surface, and does not show evidence of displacement due to reactivation. The pre- to syn-thrusting folds, which are interpreted to be ***Ca***F_1,

Figure 2.10. Structural overview of the Somerset-Doctors Rocks area. (a) simplified structural map of the Somerset-Doctors Rocks area with structural domain boundaries (400405 mE, 5456925 mN to 398310mE, 5458250mN) (modified after Gee 1977). Locations (i) to (vi) illustrate key structural relationships and are referred to in the text; (b) equal area stereographic projections, with block diagram illustrating the style and orientation of the dominant folding ($Ca$$F_2$) for Domain N1 (downward facing parasitic $Ca$$F_2$ fold) (modified after Gee 1977); (c) Equal area stereographic projections, with block diagram illustrating the style and orientation of the dominant folding ($Ca$$F_2$) for Domain N2 (steepening of $Ca$$F_2$ due to type 2 refolding by $Ca$$F_3$); (d) equal area stereographic projections, with block diagram illustrating the style and orientation of the dominant folding ($Ca$$F_2$) for Domain N3 (rotation of $Ca$$F_2$ due to simple shear with component of oblique shortening); (e) detailed sketch and equal area stereographic projection, illustrating the change in orientation of the dominant lineation ($Ca$$L_{02}$) at the boundary between Domains N2 and N3.

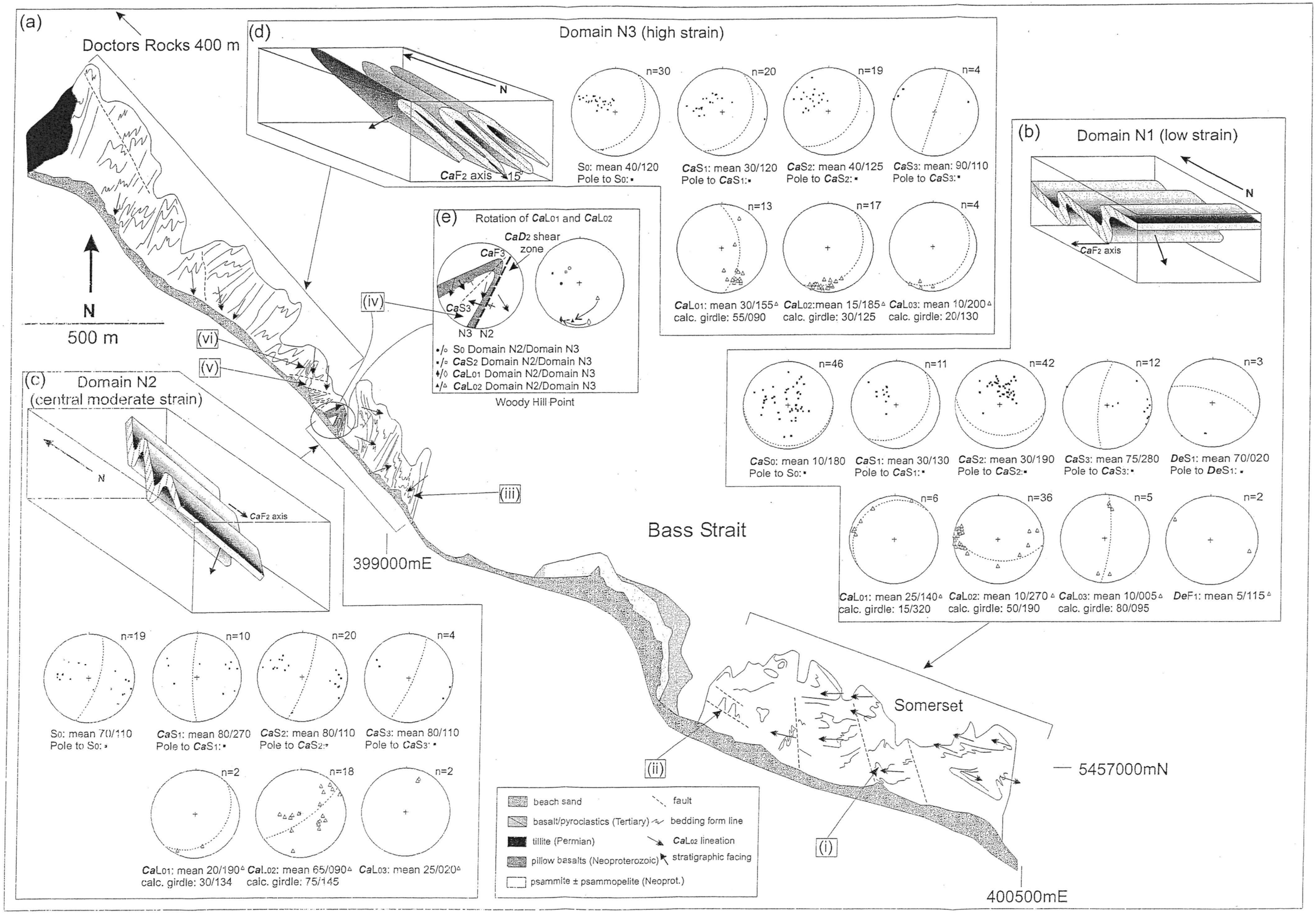
(a)
Doctors Rocks 400 m
N
500 m
(iv)
(vi)
(v)
(iii)
399000mE
Bass Strait
(ii)
(i)
Somerset
5457000mN
400500mE
(b) Domain N1 (low strain)
N
CaF2 axis
n=46
n=11
n=42
n=12
n=3
CaS0: mean 10/180
Pole to S0:▪
CaS1: mean 30/130
Pole to CaS1:▪
CaS2: mean 30/190
Pole to CaS2:▪
CaS3: mean 75/280
Pole to CaS3:▪
DeS1: mean 70/020
Pole to DeS1: ▪
n=6
n=36
n=5
n=2
CaL01: mean 25/140△
calc. girdle: 15/320
CaL02: mean 10/270△
calc. girdle: 50/190
CaL03: mean 10/005△
calc. girdle: 80/095
DeF1: mean 5/115△
(c) Domain N2
(central moderate strain)
N
CaF2 axis
n=19
n=10
n=20
n=4
S0: mean 70/110
Pole to S0: ▪
CaS1: mean 80/270
Pole to CaS1:▪
CaS2: mean 80/110
Pole to CaS2:▪
CaS3: mean 80/110
Pole to CaS3: ▪
n=2
n=18
n=2
CaL01: mean 20/190△
calc. girdle: 30/134
CaL02: mean 65/090△
calc. girdle: 75/145
CaL03: mean 25/020△
(d) Domain N3 (high strain)
N
CaF2 axis
n=30
n=20
n=19
n=4
S0: mean 40/120
Pole to S0:▪
CaS1: mean 30/120
Pole to CaS1:▪
CaS2: mean 40/125
Pole to CaS2:▪
CaS3: mean: 90/110
Pole to CaS3:▪
n=13
n=17
n=4
CaL01: mean 30/155△
calc. girdle: 55/090
CaL02:mean 15/185△
calc. girdle: 30/125
CaL03: mean 10/200△
calc. girdle: 20/130
(e) Rotation of CaL01 and CaL02
CaD2 shear zone
CaF3
CaS3
N3 N2
•/○ S0 Domain N2/Domain N3
▪/▫ CaS2 Domain N2/Domain N3
♦/◊ CaL01 Domain N2/Domain N3
▲/△ CaL02 Domain N2/Domain N3
Woody Hill Point
beach sand
basalt/pyroclastics (Tertiary)
tillite (Permian)
pillow basalts (Neoproterozoic)
psammite ± psammopelite (Neoprot.)
fault
bedding form line
CaL02 lineation
stratigraphic facing

Figure 2.10.

Figure 2.11. Cambrian deformation in Domain N1 at Somerset (400075 mE, 5456990 mN). (a) photograph of outcrop dominated by mesoscopic $Ca F_2$, with south-dipping axial plane and gentle plunge to west (view to west), hammer in foreground for scale; (b) sketch of $Ca F_2$ fold in (a), illustrating Cambrian age $Ca F_1$ fold (small fold enlarged in Figure 2.11(c)) overprinted by $Ca S_2$ at the bottom of the sketch. $Ca S_2$ cleavage is the dominant form surface; (c) closeup photograph of $Ca F_1$ fold and shear zone visible in lower part of (a) and (b); (d) sketch of $Ca F_1$ fold close up showing $Ca F_1$ fold on lower surface of syn-$Ca D_2$ shear and $Ca S_2$ transecting the $Ca F_1$ fold.

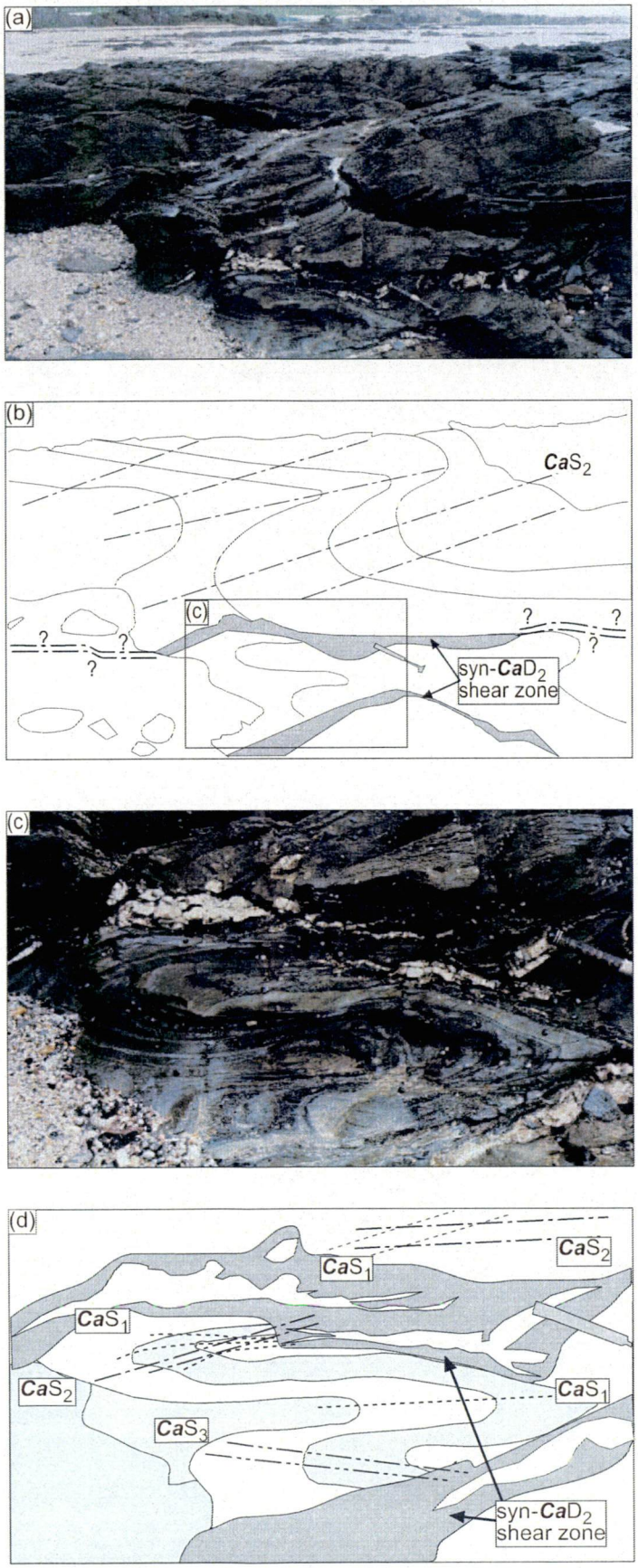

Figure 2.11(a)-(d).

Figure 2.12. Example at western end of Domain N1 (399750 mE, 5457100 mN) of syn-***Ca***D_1 thrust and ***Ca***F_1, folded by ***Ca***F_2 and overprinted by ***Ca***S_2. The syn-***Ca***D_1 and ***Ca***D_2 features are overprinted by ***Ca***D_3 (a) sketch map of overview of detailed study area; (b) photograph of detailed study area, with ***Ca***F_3 fold at lower left, ***Ca***F_1 fold at lower right, and fault surface in upper part of photo, viewed to the north; (c) and (d) close-up of thrust contact, which features ***Ca***F_1 folds being dragged along the fault, suggesting southwest transport, lens cap 50 mm diameter; (e) example of ***Ca***F_1 fold, with timing relationship to ***Ca***F_2 illustrated by transecting ***Ca***S_2 cleavage; (f) sketch of ***Ca***F_1 fold (e), illustrating the overprinting by transecting ***Ca***S_2, which is consistent on both limbs.

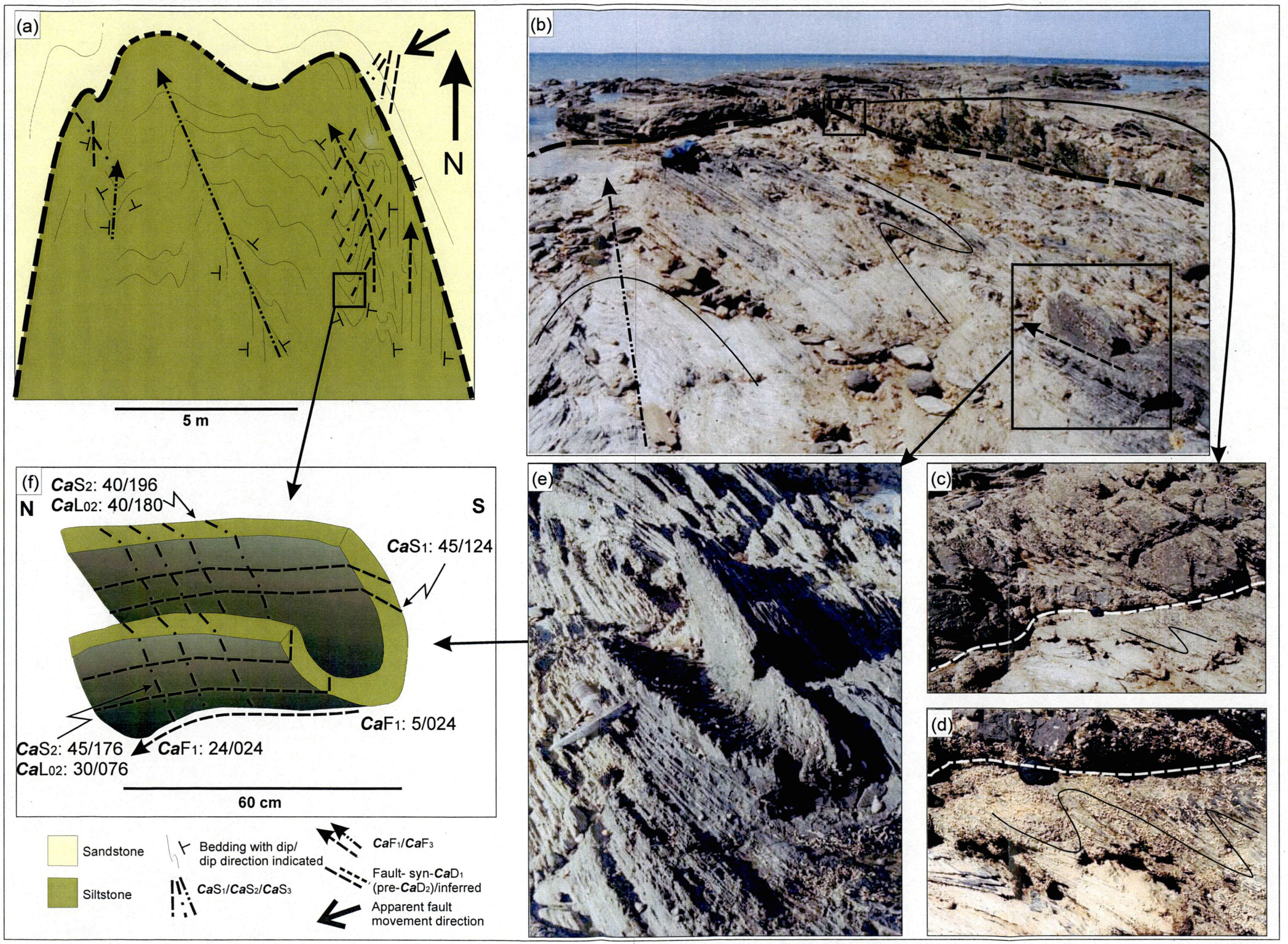

Figure 2.12(a)-(f).

are mesoscopic tight to isoclinal folds, that have variable plunges to the north-northeast (5/024 to 24/024)(Figure 2.12(f)). In this area, the associated axial planar cleavage (***Ca***S_1) dips moderately to steeply to the east-southeast (45/125). The ***Ca***S_1 axial planar fabric is spaced (1-3 mm) in sandstone layers and slaty in phyllites, although it does not penetrate the coarser grained sandstone beds very well. The ***Ca***F_1 folds are transected by the south-dipping ***Ca***S_2 foliation (40/196), which remains constant in its orientation across the ***Ca***F_1 fold hinge, illustrating the relative timing of the two events (Figure 2.12(e) and (f)). The orientation of the ***Ca***D_1 features at this location is consistent with other areas in the low strain domain, which are not strongly refolded by ***Ca***F_2.

In other areas of the low strain domain (location (ii) in Figure 2.10(a)), further examples of ***Ca***F_1 folds strongly overprinted by ***Ca***D_2 structures were observed (Figure 2.11(a) to (d)). At location (ii) (400075 mE, 5456990 mN), syn-***Ca***F_2 shearing was recognised. These shear zones are also interpreted to have been thrusts. In the overlying sandstone sequence, both ***Ca***S_1 and ***Ca***S_2 were observed. The ***Ca***S_1 foliation is a southwest-dipping spaced cleavage (25/235), that is crenulated by the more pervasive, south-dipping axial planar ***Ca***S_2 foliation (35/190). ***Ca***L_{01} lineations are present on the bedding surfaces of the sandstone units, and plunge gently to the west (10/285). The south-dipping ***Ca***S_2 is the dominant fabric here, and is the form surface in the sandstone sequence. At the base of the sandstone sequence, a shear zone infilled by quartz segregations separates the overlying unit from the silstone/mudstone sequence beneath. The sub-horizontal shear zone is not refolded by ***Ca***F_2, and is sub-parallel to the contact between the two lithological units. On this basis, it is interpreted to have occurred syn- to late-***Ca***D_2. Below the shear zone, within the mudstone sequence, a series of mesoscopic, gently west-plunging, isoclinal folds were observed. These have the opposite vergence to the overlying ***Ca***F_2 folds. Furthermore, the folds are transected by the ***Ca***S_2 foliation, which locally dips more steeply to the south (50/204) than ***Ca***S_1 (26/236) (Figure 2.11(c) and (d)). On this basis, the folds below the shear zone are interpreted to be ***Ca***F_1.

Elsewhere in Domain N1, in areas of more strongly developed ***Ca***S_1, boudinaged quartz segregations that are parallel to ***Ca***S_1 occur locally. In areas where they are

abundantly developed, they are interpreted to mark high strain zones coincident with $Ca D_1$.

Throughout Domain N1 the orientation of the $Ca D_2$ related features is consistent. $Ca D_2$ is the dominant event in this domain, and controls the outcrop pattern. The downward facing $Ca F_2$ parasitic 'Z' folds have wavelengths of 5 to 20 metres and have a 3 mm spaced to phyllitic axial planar $Ca S_2$ cleavage that commonly represents the dominant form surface (Figure 2.8). Axial planar fabric development varies on the different $Ca F_2$ fold limbs, with overturned gently-dipping limbs displaying weaker cleavage development than the 'right way up' steep limbs. $Ca S_2$ predominantly dips gently to moderately to the south (30/190). $Ca F_2$ are consistent in style, with moderate to steeply south dipping 'right way up' short limbs, and gently south dipping overturned long limbs (Figure 2.10(b) and 2.11(a)). The $Ca F_2$ hinges plunge gently to the west (10/270), however some variation in orientation occurs due to refolding by $Ca F_3$ (Figure 2.10(a)). The consistent facing of $Ca F_2$ implies the entire area is on one limb of a $Ca F_1$ fold and only small scale $Ca F_1$ folds are present.

Overprinting the $Ca D_1$ and $Ca D_2$ structures in the both the low and high-strain domains are folding events correlated with $Ca D_3$ to the west and south, and $De D_1$ (Loongana/Wilmot trend) to the east. The $Ca D_3$ event has gently north plunging open upright $Ca F_3$ folds (10/005) and a weakly developed spaced axial planar cleavage ($Ca S_3$) only observed in the minor mudstone interbeds. $Ca S_3$ dips steeply to the west (75/280) (Figure 2.10(b) and (c), Figure 2.12(a)). This generation has been folded by open east-west trending $De F_1$ (5/115) that has a steeply dipping poorly developed, spaced axial planar cleavage (70/020), that is only recognised in some pelitic layers, resulting in dome and basin interference patterns (Figure 2.10(b)).

2.4.1.2 Central moderate-strain Domain N2

$Ca D_1$ was observed in Domain N2, but in most cases was strongly overprinted by $Ca D_2$. $Ca F_1$ fold hinges are rare in this area, however where evident they are isoclinal folds that plunge gently to the south (20/190). Although $Ca F_1$ were not

frequently recognised, crosscutting relationships between bedding and the CaS$_1$ cleavage indicate changes in CaF$_1$ vergence occur in this area (eg. location (iii) 399050 mE, 5457600 mN). The CaS$_1$ foliation is a steeply west-dipping (80/270), widely developed phyllitic cleavage with 1 to 2 mm wide microlithons, and is more intensely developed than in Domain N1 (Figure 2.10(c)).

At outcrop-scale, this domain is dominated by CaD$_2$ structures, although their orientations are different to those in Domain N1. The CaD$_2$ strain level is higher in Domain N2 than in Domain N1. The axial planar CaS$_2$ cleavage is also better developed (phyllitic) and more penetrative, with the microlithons becoming more finely spaced than to the east (3 mm). CaS$_2$ dips steeply to the east-southeast (80/110) (Figure 2.10(c)).

The area is dominated by mesoscopic overturned, moderately east-dipping S$_0$ (70/110) and downward-facing, CaF$_2$ parasitic 'Z' folds, however symmetrical isoclinal CaF$_2$ fold hinges were observed. The prevailing vergence direction for CaF$_2$ in Domain N2 is consistent with Domain N1, with the area positioned on the overturned 'long limb' of a macroscopic 'Z' CaF$_2$ fold. CaL$_{02}$ (S$_0$/CaS$_2$ intersection lineation), plunge moderately to the northeast and southwest (Figure 2.10(c)). The spread in the orientation of CaL$_{02}$ reflects subsequent refolding, by CaF$_3$ and DeF$_1$.

CaS$_1$ and CaS$_2$–parallel, syn-CaD$_{1/2}$ fault zones were seen truncating S$_0$ at low angle. These syn-CaD$_{1/2}$ fault zones are widespread throughout Domain N2. However, they are more common towards the western part of the area, proximal to the boundary with the high strain Domain N3 (398790 mE, 5457875 mN, location (iv) on Figure 2.10(a) and (e)). The boundary between Domain N2 and N3 is defined by a major, north-south trending syn-CaD$_{1/2}$ fault zone. The lithologies to the east of the fault are dominated by psammopelite, with minor psammite and pelite. Here the CaS$_1$ and CaS$_2$ foliations are sub-parallel, finely spaced (<1.5 mm) and phyllitic. CaS$_1$ and CaS$_2$–parallel quartz segregations are abundant close to the boundary between Domain N2 and N3.

Within Domain N2, CaF$_3$ are gentle to open folds, and are seen folding S$_0$ and the earlier cleavages. The CaF$_3$ folds have upright axial planes (80/110), and mostly

plunge shallowly to the north in this area (25/020) (Figure 2.10(c)). The ***Ca***S_3 foliation is a weak, axial planar, subvertical to steeply west-dipping, spaced cleavage, with 5 to 10 mm wide microlithons. In Domain N2, ***De***D_1 is weak, and causes very minor, gentle refolding of the earlier foliations, resulting in minor dome and basin style folds. It has not produced a cleavage in this area, although based on the ***De***F_1 that were observed, is it is interpreted to have a consistent orientation with Domain N1.

2.4.1.3 Western high-strain Domain N3 (east of Doctors Rocks)

Lithologies in Domain N3 are more varied than in Domains N1 and N2. To the west of the boundary shear zone between Domains N3 and N2, chlorite zone metabasalts are interbedded with minor volcanogenic metasediments (Figure 2.10(a) and Figure 2.13). The pillow basalts have undergone significant flattening (Figure 2.13(a) and (b)), which is greatest towards the margins of the sequence (Figure 2.13(c)). The orientation of the flattening is consistent with ***Ca***S_1 and ***Ca***S_2, which are subparallel in this area. However, due to their high degree of weathering, further microstructural investigations were not undertaken. The metabasalts are interpreted to be the extrusive equivalent of the alkaline Cooee Dolerite, which is intruded into the Burnie Formation 6.5 km to the east, and has a minimum age of 725±35 Ma (Spry 1957a, b, Gee 1967b, Crook 1979) (see Chapter 4).

The N3 Domain is more structurally complex than the lower strain domains to the east. Mesoscopic scale ***Ca***F_1 and syn-***Ca***D_1 thrusts are more prevalent in this area, reflecting the higher levels of syn-***Ca***D_1 strain imparted on the rocks. The ***Ca***F_1 folds observed in Domain N3 are 0.5 to 1 metre wavelength isoclinal folds, and have strongly attenuated limbs (Figure 2.14(a) to (d)). In the eastern part of Domain N3, at location (v) on Figure 2.10(a) (398760 mE, 5457915 mN) the ***Ca***F_1 folds are upward facing, parasitic 'S' folds, however they are difficult to identify due to the horizontal outcrop surface and the gently dipping axial planar cleavage (Figure 2.14(a) to (d)). The ***Ca***F_1 fold hinges and ***Ca***L_{01} lineations have changed orientation relative to Domain N2, and plunge gently to moderately to the south-southeast (30/155). ***Ca***S_1 is finely spaced (1 mm) and phyllitic, although it is strongly overprinted by ***Ca***S_2. ***Ca***S_1 is axial planar, and dips gently to moderately to the

Figure 2.13(a) Photograph of deformed pillow basalts outcropping at the eastern end of Domain N3 (398790 mE, 5457875 mN). Foreground shows increasingly strained pillows, close to boundary of unit, background shows contact with psammopelitic sequence, hammer for scale in centre of image; (b) overview of strain increase in pillows, with marked change evident above hammer; (c) close up of strain increase seen in (b). Lower portion of photograph illustrates psammopelitic unit. All photos viewed to the south.

Figure 2.14(a) Mesoscopic $Ca F_1$ folds in Domain N3 (398760 mN, 5457915 mN). Folds are in interlayered psammite and psammopelite and plunge gently to the southeast. Axial planes dip to the southeast, hammer for scale centre of photograph; (b) sketch of (a), illustrating location of fold hinges and interpreted thrust faults in background; (c) closeup of $Ca F_1$ fold in lower part of (a) and (b), pen (at lower right) is 14 cm in length; (d) sketch of $Ca F_1$ fold closeup (c).


(2.13a)


(2.13b)

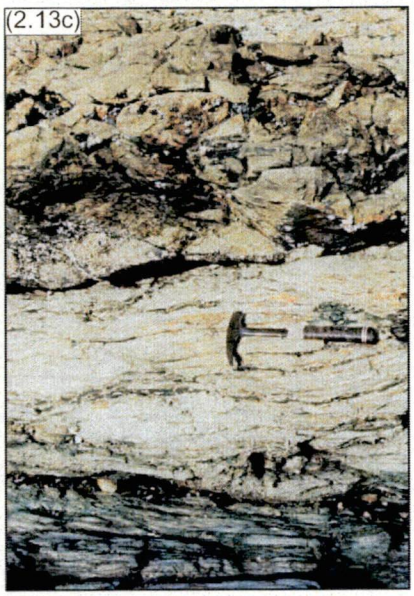
(2.13c)

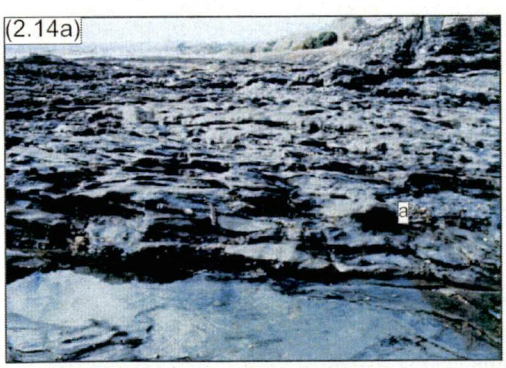
(2.14a)
a

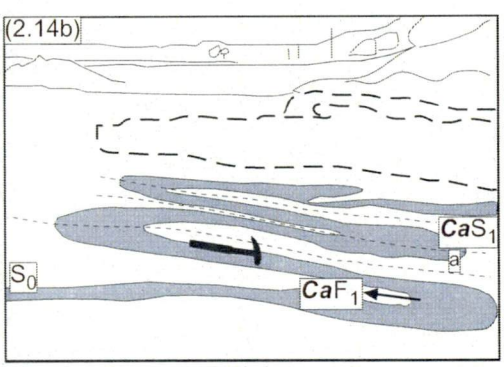
(2.14b)
CaS1
a
S0
CaF1


(2.14c)
b

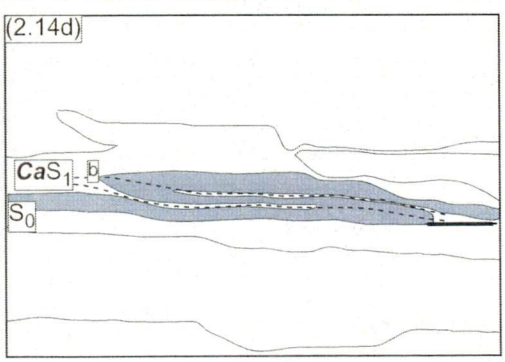
(2.14d)
CaS1
b
S0

southeast (30/120), also reflecting a change in orientation to Domain N2 (Figure 2.10(c) and (d)). Locally, boudinaged quartz segregations are found parallel to $\boldsymbol{Ca}S_1$. These are interpreted to reflect the high level of strain imparted on the rocks during $\boldsymbol{Ca}D_1$. $\boldsymbol{Ca}F_1$ fold vergence is difficult to establish in this area, due to complex faulting and folding overprinting relationships, and the closeness in orientation between $\boldsymbol{Ca}S_1$ and $\boldsymbol{Ca}S_2$.

$\boldsymbol{Ca}D_2$ is well developed in Domain N3. $\boldsymbol{Ca}F_2$ folds and the $\boldsymbol{Ca}S_2$ axial planar foliation are common, however their orientation and vergence is different to $\boldsymbol{Ca}F_2$ and $\boldsymbol{Ca}S_2$ in Domains N1 and N2. In this area, $\boldsymbol{Ca}F_2$ are mesoscopic tight to isoclinal folds, that are best exposed in the eastern part of Domain N3 at location (vi) (398775 mE, 5457940 mN)(Figure 2.10(a)). $\boldsymbol{Ca}F_2$ folds plunge to the south (15/185) (Figure 2.10(d)) and are predominantly symmetrical, reflecting the proximity to a macroscopic $\boldsymbol{Ca}F_2$ hinge. $\boldsymbol{Ca}F_2$ have larger wavelengths (5 to 10 m) than the $\boldsymbol{Ca}F_1$ folds, and have amplitudes of 20 m. In this area, they are also difficult to identify, due to the isoclinal style of folding, closeness in orientation between $\boldsymbol{Ca}S_1$ and $\boldsymbol{Ca}S_2$, and lithological uniformity. This makes the bedding-$\boldsymbol{Ca}S_2$ angle on the $\boldsymbol{Ca}F_2$ fold limbs less obvious. The axial planar $\boldsymbol{Ca}S_2$ foliation is phyllitic to schistose (Figure 2.4(e)), and dips moderately to the southeast (40/125) (Figure 2.10(d)). $\boldsymbol{Ca}S_2$ is a pervasively developed phyllitic foliation, although it has broader microlithons (2 mm) than $\boldsymbol{Ca}S_1$.

Outcrop-scale $\boldsymbol{Ca}F_3$ and $\boldsymbol{De}F_1$ are minor in Domain N3. The $\boldsymbol{Ca}D_3$ foliation is best developed in the eastern part of the area, where is has folded the pillow basalt sequence (Figure 2.10(a) and (e)). The $\boldsymbol{Ca}F_3$ exposed is a mesoscopic fold with a wavelength greater than 100 m. This open synform plunges gently to the south (10/200), and has produced a sub-vertical axial planar spaced foliation ($\boldsymbol{Ca}S_3$), that dips steeply to the east and west (90/110) (Figure 2.10(d)). $\boldsymbol{De}D_1$ does not cause any recognisable refolding of the earlier foliations, and has not produced a foliation in this area.

2.4.2 Southern study area: structure of the low strain zone to the east of the Arthur Lineament

In order to establish the deformational history of the lineament in the southern study area, structural mapping has been carried out in the moderately deformed, low strain zone to the east of the Arthur Lineament (within the Oonah Formation) in the following areas:

- to the northeast of Savage River township (along the Savage River-Waratah Road, (area vi(a))
- along the Lower Pieman Dam Road, from the Stanley River bridge to the boundary with the high strain Oonah Formation (areas vi(a) and vi(b) in Figure 2.15).

The structural style of $\boldsymbol{Ca}D_1$ and $\boldsymbol{Ca}D_2$ in these two areas is very similar, both at the eastern boundary of the Arthur Lineament, and several kilometres to the east. In both areas, a progressive increase in the intensity of Cambrian age deformation, approaching the lineament was observed. $\boldsymbol{Ca}S_1$ is not as well developed as $\boldsymbol{Ca}S_2$ to the east of the lineament, and both fabrics become relatively better developed near to the eastern boundary. On this basis, the low strain/unmetamorphosed zone to the east of the lineament, in the southern study area, will be discussed as one structural zone. However, whereas these two areas display consistent deformational styles and orientations of the $\boldsymbol{Ca}S_1$ and $\boldsymbol{Ca}S_2$ foliations, the low strain zone can be subdivided into two domains (eastern and western), reflecting the proximity to the eastern boundary of the Arthur Lineament. These will be discussed below.

Distal to the lineament (to the east), $\boldsymbol{Ca}S_1$ is not as well developed as $\boldsymbol{Ca}S_2$ (Figure 2.16). $\boldsymbol{Ca}S_1$ was only observed in mudstone layers, and was crenulated by $\boldsymbol{Ca}S_2$. Further to this, $\boldsymbol{Ca}S_1$ does not penetrate as far from the lineament as $\boldsymbol{Ca}S_2$. In some cases, where $\boldsymbol{Ca}S_1$ is evident, it is strongly overprinted by $\boldsymbol{Ca}S_2$. $\boldsymbol{Ca}S_1$ is best developed in pelitic and psammopelitic layers, where it is a finely spaced, smooth, foliation, with discrete 0.5-1 mm wide microlithons (Figure 2.16). In psammitic layers, however, the foliation is an anastamosing, more coarsely developed foliation, with 2 mm wide microlithons (Figure 2.4(b)). $\boldsymbol{Ca}F_1$ folds in the low strain zone were not observed in the field, although based on S_0-$\boldsymbol{Ca}S_1$-$\boldsymbol{Ca}S_2$ vergence relationships,

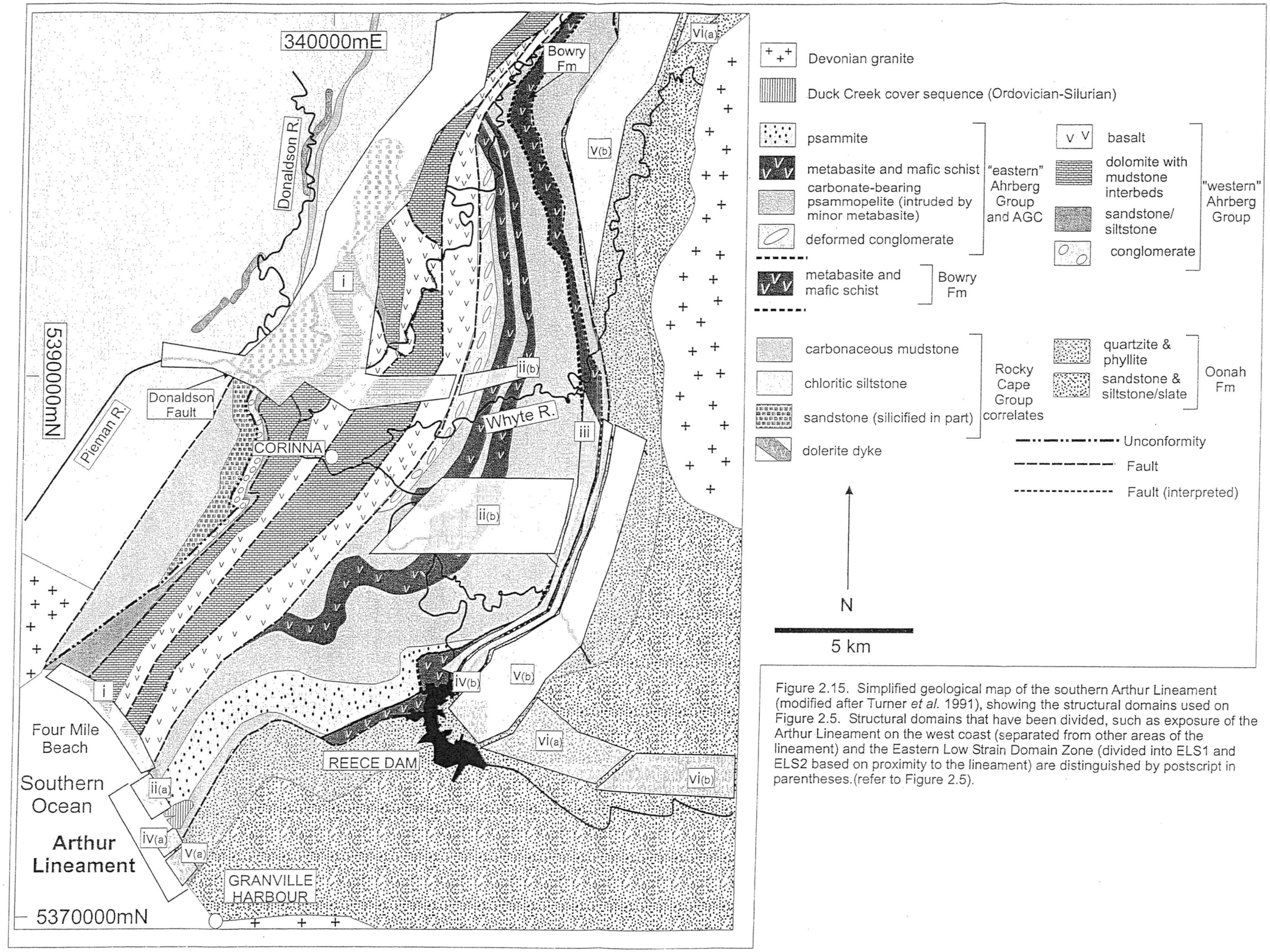

Figure 2.15. Simplified geological map of the southern Arthur Lineament (modified after Turner *et al.* 1991), showing the structural domains used on Figure 2.5. Structural domains that have been divided, such as exposure of the Arthur Lineament on the west coast (separated from other areas of the lineament) and the Eastern Low Strain Domain Zone (divided into ELS1 and ELS2 based on proximity to the lineament) are distinguished by postscript in parentheses.(refer to Figure 2.5).

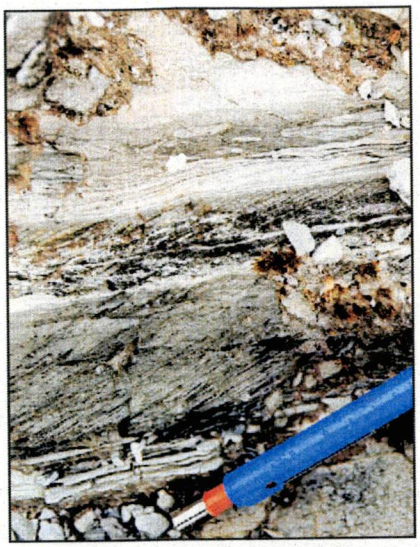

Figure 2.16. Pervasively developed, spaced ***Ca***S_2 foliation (parallel to pen), crenulating weakly developed spaced ***Ca***S_1 (dipping to the right), which is best developed in finer grained layers. Pen is 8mm in diameter. (354100 mE, 5380460 mN).

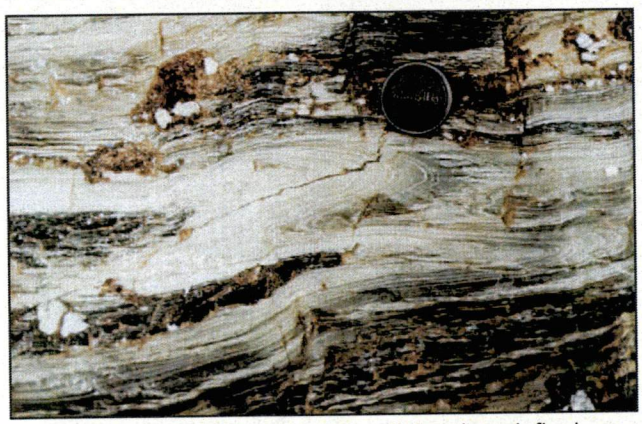

Figure 2.18. Mesoscopic, tight ***Ca***F_2 fold with well developed, finely spaced, axial planar ***Ca***S_2, crenulating ***Ca***S_1 in hinge zones (below lens cap). The ***Ca***S_2 foliation dips steeply to the east (65/095). Lens cap is 53 mm in diameter. (352200 mE, 5378700 mN).

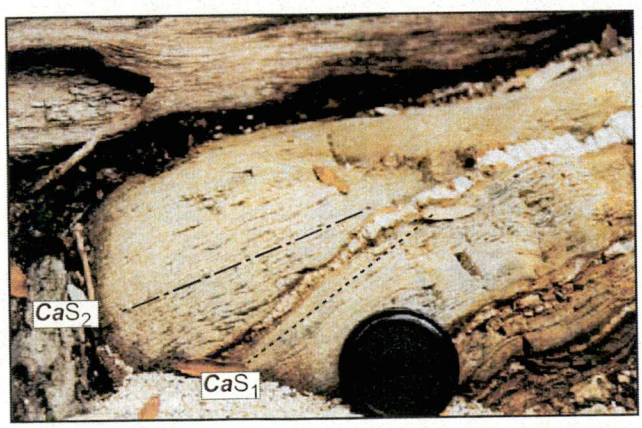

Figure 2.20. Well developed, finely spaced ***Ca***S_1 (defined by cleavage planes and ***Ca***S_1-parallel quartz segregations), overprinted by schistose ***Ca***S_2. Lithology is quartz-mica psammopelitic schist. Lens cap is 53 mm in diameter. (348540 mE, 5382440 mN) .

Figure 2.17(a). Structural cross sections A to L, of the Oonah Formation to the east of the Arthur Lineament in the southern study area. Sections are oriented 290/110, with east to the right. Data on factual sections (top of set) are corrected to apparent dip. Interpretive sections (bottom of set) take into account vergence relationships presented on factual sections. Coordinates for each section are presented at the ends of the section lines. Locations of sections are illustrated on Figure 2.2(b).

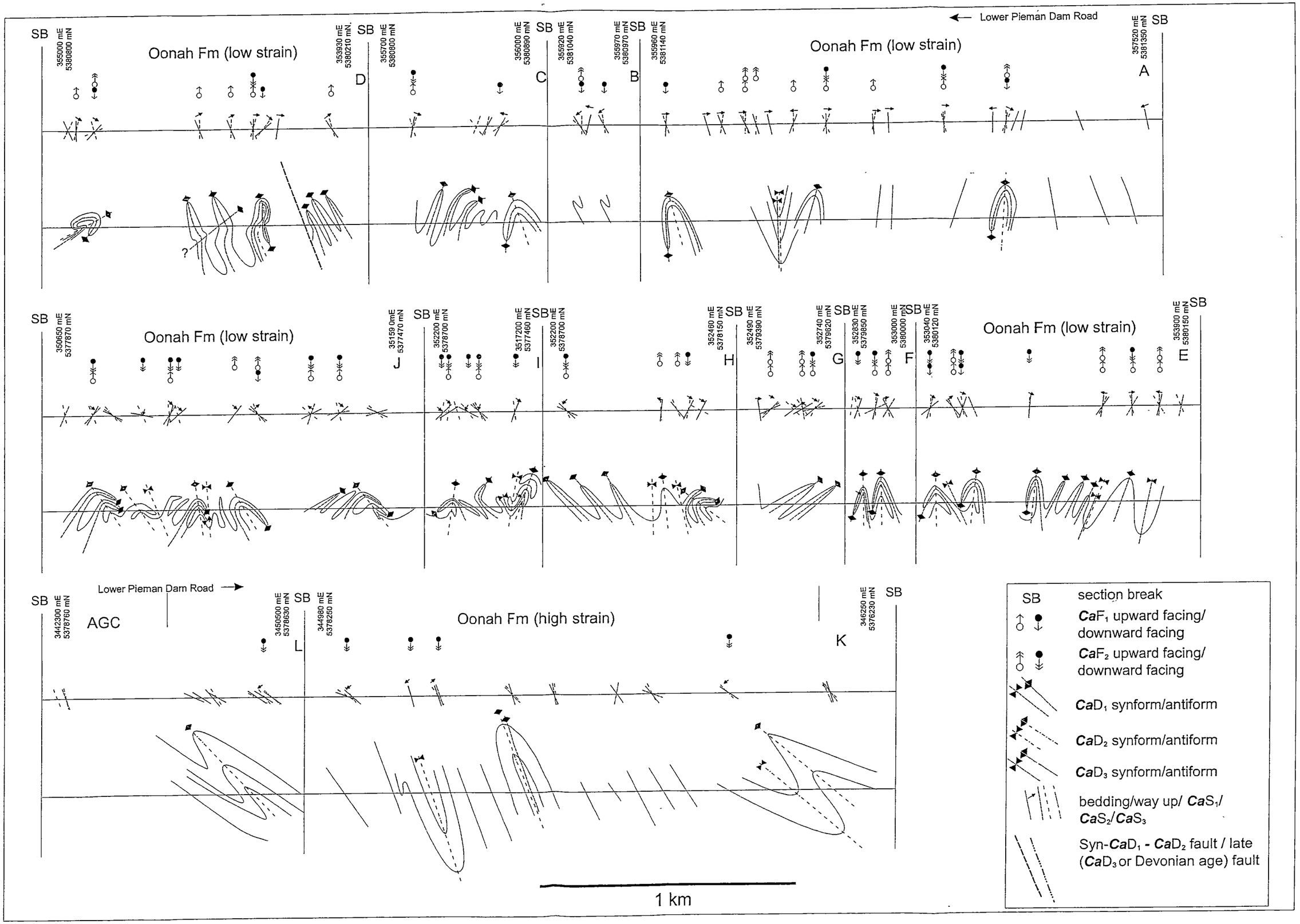
Lower Pieman Dam Road
SB
355000 mE 5380800 mN
Oonah Fm (low strain)
353930 mE 5380210 mN
D
355700 mE 5380800 mN
356000 mE 5380890 mN
C
355920 mE 5381040 mN
355970 mE 5380970 mN
B
355960 mE 5381140 mN
Oonah Fm (low strain)
357520 mE 5381350 mN
A
?
SB
350650 mE 5377870 mN
Oonah Fm (low strain)
35159 0mE 5377470 mN
J
352200 mE 5378700 mN
35172000 mE 5377460 mN
I
352200 mE 5378700 mN
352460 mE 5378150 mN
H
352490 mE 5379390 mN
352740 mE 5379620 mN
G
352830 mE 5379850 mN
353000 mE 5380000 mN
F
353040 mE 5380120 mN
Oonah Fm (low strain)
353900 mE 5380150 mN
E
Lower Pieman Dam Road
SB
3442300 mE 5378760 mN
AGC
3450500 mE 5378630 mN
L
344980 mE 5378250 mN
Oonah Fm (high strain)
346250 mE 5376230 mN
K
1 km
SB section break
CaF1 upward facing/ downward facing
CaF2 upward facing/ downward facing
CaD1 synform/antiform
CaD2 synform/antiform
CaD3 synform/antiform
bedding/way up/ CaS1/ CaS2/CaS3
Syn-CaD1 - CaD2 fault / late (CaD3 or Devonian age) fault

Figure 2.17(a)

Figure 2.17(b). Structural cross sections M to V, of the Oonah Formation in the high strain zone in the east of the Arthur Lineament in the southern study area. Sections are oriented 290/110, with east to the right. Data on factual sections (top of set) are corrected to apparent dip. Interpretive sections (bottom of set) take into account vergence relationships presented on factual sections. Coordinates for each section are presented at the ends of the section lines. Locations of sections are illustrated on Figure 2.2(b).

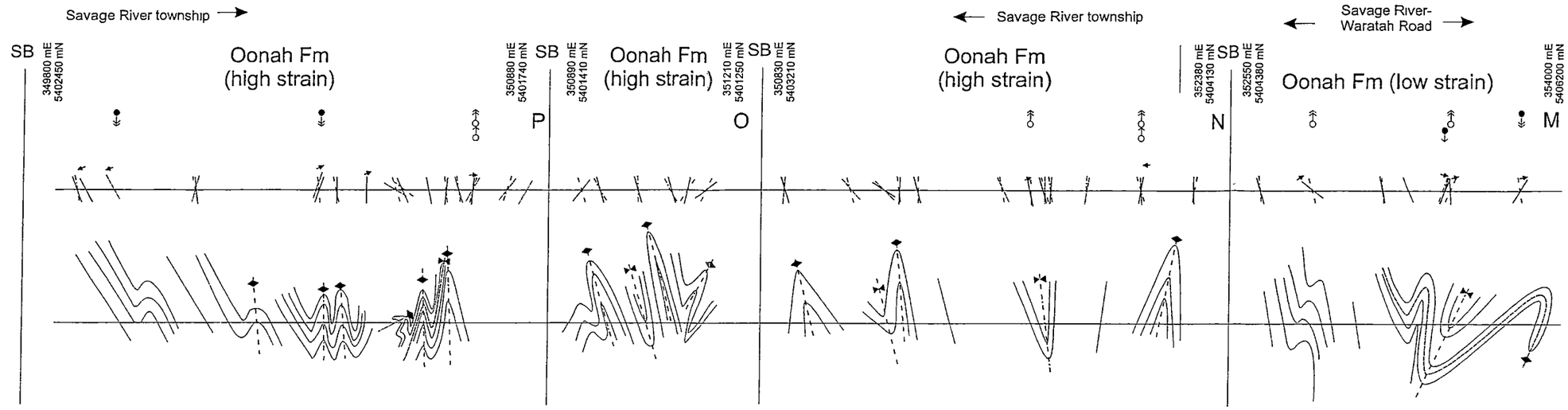
Savage River township
SB
349800 mE 5402450 mN
Oonah Fm (high strain)
350880 mE 5401740 mN
P
350890 mE 5401410 mN
Oonah Fm (high strain)
351210 mE 5401250 mN
O
350830 mE 5403210 mN
Savage River township
Oonah Fm (high strain)
352380 mE 5404130 mN
N
352550 mE 5404380 mN
Savage River-Waratah Road
Oonah Fm (low strain)
354000 mE 5406200 mN
M

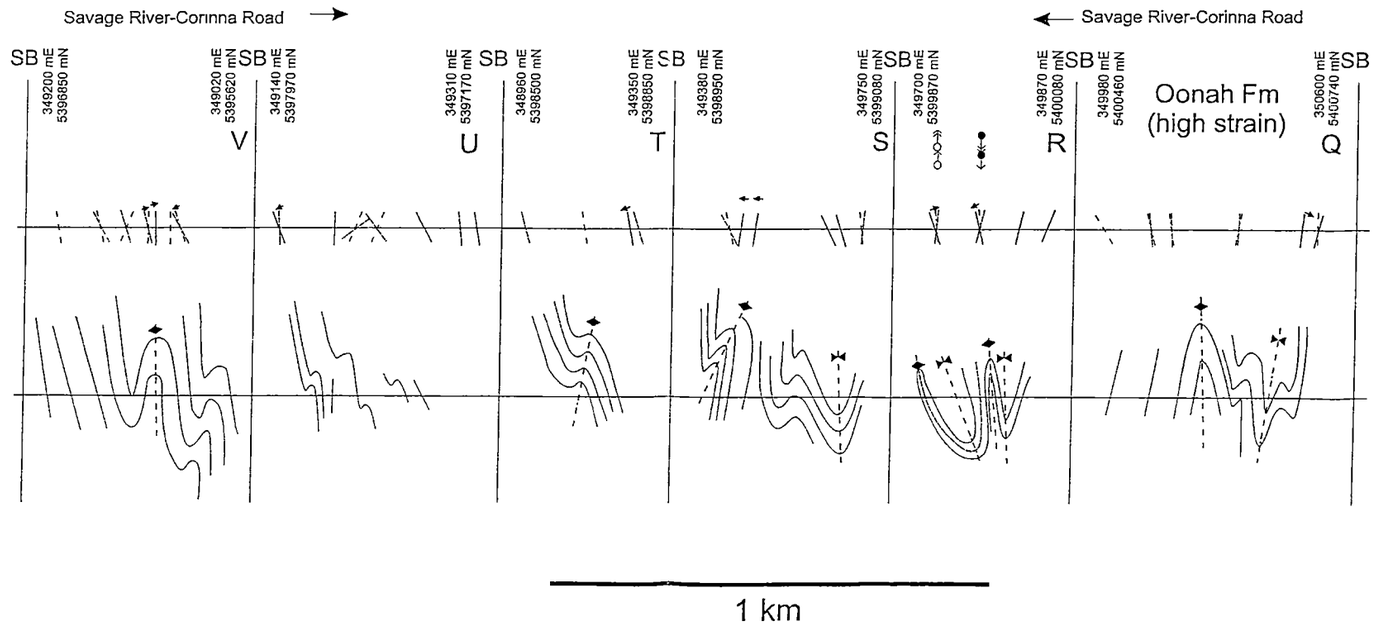
Savage River-Corinna Road
SB
349200 mE 5396850 mN
349020 mE 5395620 mN
V
349140 mE 5397970 mN
SB
349310 mE 5397170 mN
U
SB
348960 mE 5396500 mN
349350 mE 5398850 mN
T
SB
349380 mE 5398950 mN
Savage River-Corinna Road
349750 mE 5399080 mN
S
SB
349700 mE 5399870 mN
349870 mE 5400080 mN
R
SB
349980 mE 5400460 mN
Oonah Fm (high strain)
350600 mE 5400740 mN
Q
SB
1 km

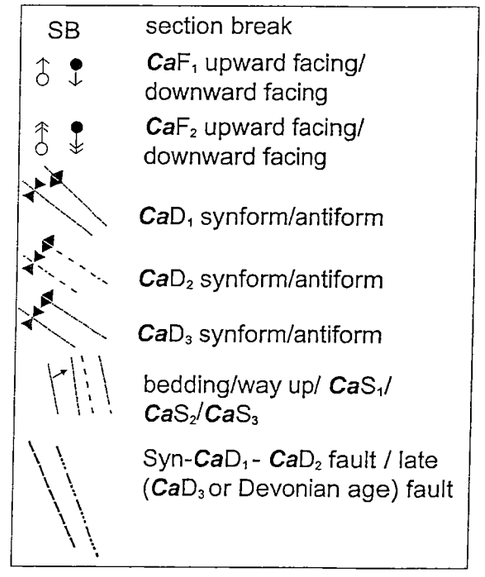
SB
section break
CaF1 upward facing/ downward facing
CaF2 upward facing/ downward facing
CaD1 synform/antiform
CaD2 synform/antiform
CaD3 synform/antiform
bedding/way up/ CaS1/ CaS2/CaS3
Syn-CaD1- CaD2 fault / late (CaD3 or Devonian age) fault

Figure 2.17(b)

the approximate location of ***Ca***F_1 fold hinges can be interpreted (sections A to J and M in Figure 2.2(b), Figure 2.17(a) and Figure 2.17(b)). ***Ca***F_1 are interpreted to be macroscopic-scale folds, with steeply east- to steeply west-dipping axial planes. The orientation of ***Ca***L_{01} intersection lineations in this area are varied, however they mainly plunge moderately to the northeast (Figure 2.5).

CaS_2 is pervasively developed in both siltstone and sandstone layers, although away from the lineament it is more evident in the finer grained layers, and towards the tops of graded beds. ***Ca***S_2 is a spaced, smooth, foliation, with microlithons that are 2-3 mm wide (wider than ***Ca***S_1), and more pervasively developed than ***Ca***S_1 (Figure 2.4(b) and Figure 2.16). Narrow ***Ca***S_2–parallel zones (3-5 m) of more intensely developed, phyllitic ***Ca***S_2 are present. Near to the lineament, these zones of phyllitic ***Ca***S_2 are more common, and at the lineament boundary are the dominant style of the ***Ca***S_2 foliation. Bedding-***Ca***S_1-***Ca***S_2 vergence relationships indicate macroscopic ***Ca***F_2 folds are common in this area (Figure 2.17(a) sections A to J and Figure 2.17(b) section M), however in the field, only small scale ***Ca***F_2 folds were evident. These parasitic ***Ca***F_2 folds, are tight, asymmetric, mostly downward facing folds with a well developed axial planar cleavage (Figure 2.18). Towards the western boundary of this domain, the frequency of ***Ca***F_2 increases, and the tightness of refolding due to ***Ca***F_2 becomes greater (Figure 2.17(a) sections A to J and Figure 2.17(b) section M).

Structural analysis has enabled this domain to be subdivided into two domains (ELS1 and ELS2, vi(a) and vi(b) respectively) (Figure 2.5 and Figure 2.15). The ELS2 (eastern domain) of the low strain zone (3 to 7 km to the east of the eastern boundary of the Arthur Lineament) is distinguished by the orientation of ***Ca***S_1 and ***Ca***S_2, and associated intersection lineations. In this domain, S_0 and ***Ca***S_1 have very similar orientations, dipping steeply to the northwest/southeast (85/150 and 80/310 respectively). The spread of data for both surfaces indicates later refolding by an event with a northeast trending fold axis. ***Ca***L_{01} intersection lineations plunge moderately to steeply to the north-northeast (65/033) (Figure 2.5). ***Ca***S_2 dips moderately to steeply to the east (60/090), and produces ***Ca***L_{02} intersection lineations that plunge moderately to the northeast (46/044) (Figure 2.5).

As can be seen from Figure 2.5, in ELS2 the orientations of $\boldsymbol{Ca}L_{01}$ and $\boldsymbol{Ca}L_{02}$ intersection lineations are variable. Stereographic analysis indicates both generations have subsequently undergone refolding, predominantly about a southeast-trending fold axis. This northeast-southwest component of the spread is largely attributed to the Devonian deformation, although it is possible the $\boldsymbol{Ca}D_3$ event has caused some interference. The $\boldsymbol{Ca}D_3$ and Devonian events will be discussed in detail in section 2.5.

In ELS1 (western domain) of the low strain zone (0-3 km to the east of the Arthur Lineament), the orientation of S_0, $\boldsymbol{Ca}S_1$, $\boldsymbol{Ca}S_2$, and the associated intersection lineations vary from that in the eastern domain (Figure 2.5). Although the orientation of S_0 is quite variable, the majority of poles to bedding form a well-defined great circle, folded about an axis plunging shallowly to the north-northeast. Poles to $\boldsymbol{Ca}S_1$ also suggest refolding about this axis. $\boldsymbol{Ca}S_2$ has a strong preferred orientation, dipping steeply to the east-southeast (74/103). Although the $\boldsymbol{Ca}L_{01}$ intersection lineations have a preferred orientation, plunging moderately to the north-northeast, these lineations are also spread about a north-northeast fold axis. The great circle of best fit for the poles to S_0, and the preferred orientation of the $\boldsymbol{Ca}L_{01}$ intersection lineations, are consistent with refolding about a gently to moderately plunging, north-northeast trending fold axis. This corresponds with refolding by the $\boldsymbol{Ca}F_2$ event in this domain, as is indicated by $\boldsymbol{Ca}L_{02}$ (30/025) (Figure 2.5).

Some variability in the orientation of S_0, $\boldsymbol{Ca}S_1$, $\boldsymbol{Ca}S_2$, and the associated intersection lineations may be attributed to localised refolding by late deformational events (of Devonian age). However, the strengthening development and clustering of $\boldsymbol{Ca}S_2$ and $\boldsymbol{Ca}L_{02}$, in addition to the well defined great circle of poles to bedding, approaching the eastern boundary of the Arthur Lineament (in the western zone) indicates the increasing dominance of the $\boldsymbol{Ca}D_2$ event.

2.4.3 Southern study area: structure of the moderate to high strain (transitional) zone of the Arthur Lineament

Structural mapping in the eastern part of the Arthur Lineament, in the metamorphosed Oonah Formation, and the AGC was carried out in the following areas:

- to the northeast of the Savage River township along the Savage River-Waratah Road,
- in the Savage River township area,
- to the south of the Savage River township on the Savage River-Corinna Road,
- on the Lower Pieman Dam Road, from the Lower Pieman Dam (Reece Dam) to the boundary with the low strain, unmetamorphosed Oonah Formation,
- in the upper reaches of the Rocky River,
- in the upper reaches of the Owen Meredith River
- and on the west coast to the north of Granville Harbour, south of the Duck Creek cover sequence.

These locations are grouped in areas iv(b) and v(b) in Figure 2.15. The mapping undertaken indicates this region is a moderate to high strain transitional zone (ie. the foliations are predominantly phyllitic in the east, becoming mostly schistose in the west), and it is within the defined eastern boundary of the Arthur Lineament (Turner *et al.* 1991). This zone is dominated by $Ca F_2$ folding (Figure 2.17(a) sections K and L, Figure 2.17(b) sections N to V)), although there are major zones of intense $Ca F_1$ development (Figure 2.19 sections W and A'). These areas are also zones of major syn-$Ca D_2$, apparently laterally continuous fault zones (corresponding shear zones observed along strike in both the Rocky and Owen Meredith Rivers), which result in changes in the $Ca F_1$ closure directions (Figure 2.19 sections W and A'), and clearly represent significant faults related to the formation of the Arthur Lineament. Metamorphic geochronology studies undertaken on samples from these zones are described in Chapter 3. Microstructural analysis of these fault zones indicate the intense overprinting of $Ca S_1$ by $Ca S_2$ (Figure 2.4(d)). Although the $Ca S_1$ and $Ca S_2$ foliations are generally better developed than in the low strain zone of the Oonah Formation, they are not as well developed as in the most strongly deformed zones (with highest strain) of the Bowry Formation and "eastern" Ahrberg Group, to the

Figure 2 19. Structural cross sections W to A', of the Oonah Formation-AGC (Ahrberg Group Correlate)-Bowry Formation-"eastern" Ahrberg Group, within the Arthur Lineament in the southern study area. Sections are oriented 290/110, with east to the right Data on factual sections (top of set) are corrected to apparent dip. Interpretive sections (bottom of set) take into account vergence relationships presented on factual sections Coordinates for each section are presented at the ends of the section lines. Locations of sections are illustrated on Figure 2 2(b).

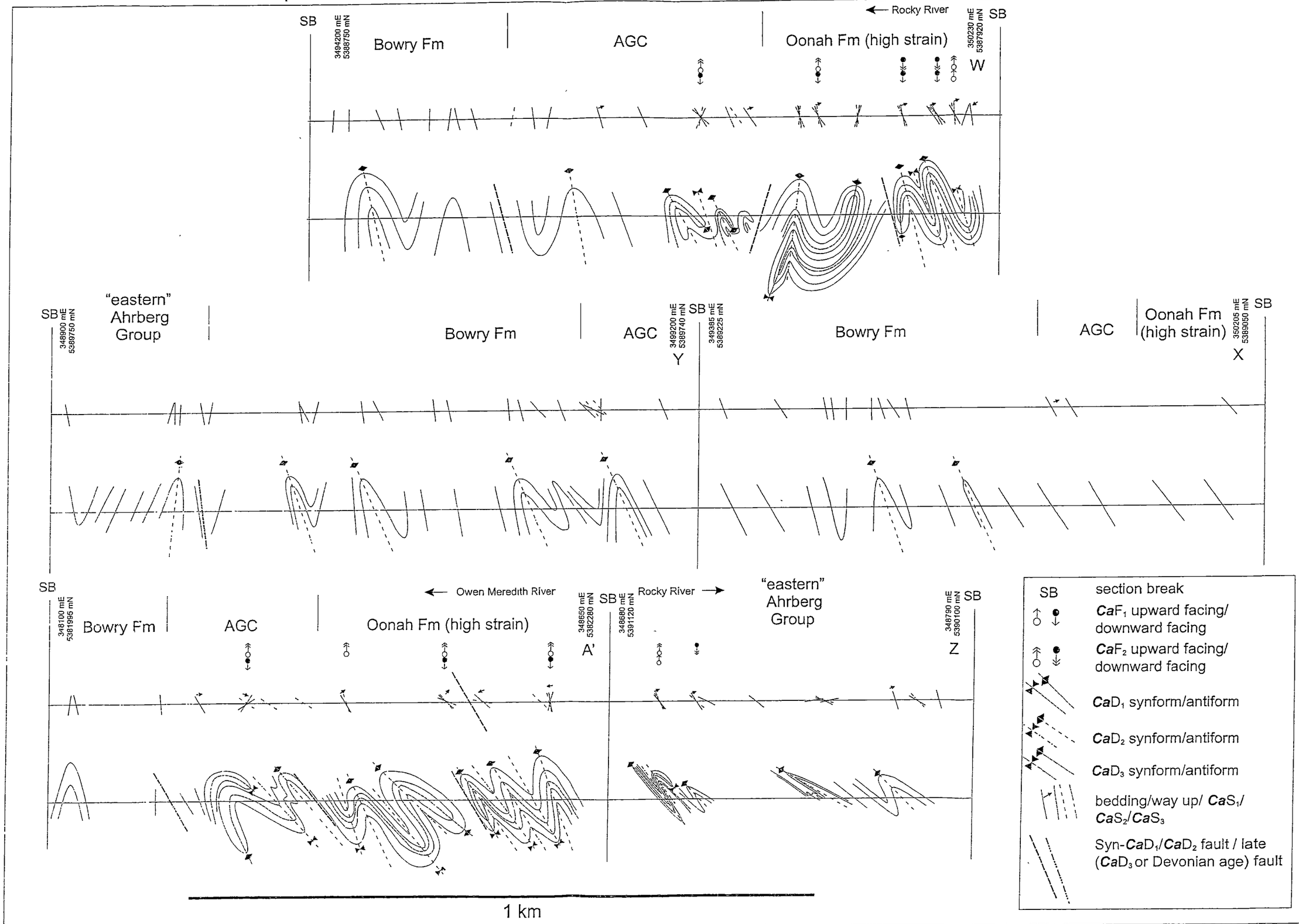
SB
3494200 mE
5388750 mN
Bowry Fm
AGC
Oonah Fm (high strain)
Rocky River
350230 mE
5387920 mN
SB
W
SB
348900 mE
5389750 mN
"eastern"
Ahrberg
Group
Bowry Fm
AGC
3499200 mE
5389740 mN
Y
SB
349385 mE
5389225 mN
Bowry Fm
AGC
Oonah Fm
(high strain)
350205 mE
5389050 mN
SB
X
SB
348100 mE
5381995 mN
Bowry Fm
AGC
Owen Meredith River
Oonah Fm (high strain)
348650 mE
5382280 mN
SB
A'
348680 mE
5391120 mN
Rocky River
"eastern"
Ahrberg
Group
348790 mE
5390100 mN
SB
Z
1 km
SB
section break
CaF1 upward facing/ downward facing
CaF2 upward facing/ downward facing
CaD1 synform/antiform
CaD2 synform/antiform
CaD3 synform/antiform
bedding/way up/ CaS1/ CaS2/CaS3
Syn-CaD1/CaD2 fault / late (CaD3 or Devonian age) fault

Figure 2.19

west. The structural style and intensity of $Ca D_1$ and $Ca D_2$, and the orientation of the related foliations and folds in these different areas within the eastern boundary of the Arthur Lineament is consistent. However the orientations on the coastal section, to the north of Granville Harbour (south of the Duck Creek cover sequence), vary due to localised refolding by later (Devonian) events (Figure 2.5). In all of the above areas, $Ca S_1$ and $Ca S_2$ are both well developed, phyllitic to schistose fabrics that increase in intensity progressively towards the western boundary of the Oonah Formation. Based on this, the Oonah Formation in the moderate to high strain/transitional zone, within the eastern boundary of the lineament, in the southern study area, will be discussed as one structural domain. The AGC, which lies to the west of the Oonah Formation and to the east of the Bowry Formation (area iv(b) on Figure 2.15), is also examined as one structural domain. Its structural history and deformation style are discussed separately, in order to independently assess the structural style of this unit, which has a faulted contact with the Oonah Formation.

2.4.3.1 Moderate to high strain zone - Oonah Formation

At the mapped eastern boundary of the Arthur Lineament, which is the transition zone between the low and the moderate to high strain (unmetamorphosed/metamorphosed) Oonah Formation (Turner *et al.* 1991), bedding features were observed. Both $Ca S_1$ and $Ca S_2$ are parallel to sub-parallel to bedding on the limbs of $Ca F_1$ and $Ca F_2$ folds (Figure 2.5). $Ca S_1$ is a predominantly phyllitic, finely spaced, smooth foliation, with 1 mm wide discrete microlithons. It is best developed in pelitic and psammopelitic layers, although is also detectable in psammites. However, towards the western boundary of the Oonah Formation (faulted contact with the AGC), bedding becomes more difficult to identify, and $Ca S_1$ is more commonly schistose. Although $Ca S_1$ is well developed, it is strongly overprinted by $Ca S_2$. In areas with intense development of $Ca D_1$, $Ca S_1$ is highlighted by $Ca S_1$-parallel quartz segregations (Figure 2.20). Strong syn-$Ca D_1$ boudinage of the quartz segregations occurs. Where small scale parasitic $Ca F_2$ were observed, the $Ca S_1$-related quartz segregations were tightly folded (Figure 2.6(a) and (b)). Outcrop scale $Ca F_1$ folds are rarely evident and difficult to identify, as they are strongly overprinted and refolded by $Ca F_2$. Where $Ca F_1$ folds were found, they were isoclinal folds mostly with steeply east-southeast dipping axial planes (85/100) and

fold axes that plunge moderately to steeply to the southeast and south (approximately 60/160) (Figure 2.5). Refolding of $Ca F_1$ by subsequent deformations, such as is seen in the area to the north of Granville Harbour, has resulted in variable orientations of the $Ca D_1$ features. However the style of $Ca F_1$ is consistent (Figure 2.5 and Figure 2.21(a) to (f)). $Ca F_1$ are distinguished from $Ca F_2$ on several grounds. The parasitic $Ca F_1$ folds are distinguished from $Ca F_2$ in the field by the different style of folding. $Ca F_1$ are isoclinal and have strongly attenuated limbs (Figure 2.21(a) to (f)), whereas $Ca F_2$ are tight and their limbs do not have the same degree of attenuation. The $Ca S_2$ cleavage transecting the $Ca F_1$ folds and S_0-$Ca S_2$ vergence relationships that conflict with $Ca F_1$ help to distinguish between the different generations (Figure 2.22(a) and (b)). Furthermore the $Ca S_2$ foliation is more broadly spaced, and more penetrative than $Ca S_1$. Parasitic $Ca F_1$ folds exposed in the field are generally smaller in scale than the $Ca F_2$. However, structural analysis indicates that based on consistent $Ca F_1$ vergence relationships over a distance of several hundred metres, the major $Ca F_1$ folds are also macroscopic-scale (Figure 2.19 sections W and A', and Figure 2.22(b) and (c)).

In the moderate to high strain zone, $Ca S_2$ is also a phyllitic, axial planar, finely spaced, smooth, parallel foliation, proximal to the eastern boundary of the Arthur Lineament, although it has broader microlithons (1-3 mm) than $Ca S_1$ (Figure 2.23). It is a more pervasive foliation than $Ca S_1$, and is well developed in pelitic, psammopelitic and psammitic layers (Figure 2.20). To the west of the eastern boundary of the Arthur Lineament, $Ca S_2$ gradually becomes schistose, over a distance of approximately two kilometres, with phyllitic zones decreasing in frequency (Figure 2.24(a) and (b)). $Ca F_2$ in this zone are macroscopic scale folds, although outcrop scale and small scale parasitic $Ca F_2$ are evident (Figure 2.17(a) sections K and L, Figure 2.17(b) sections N to V, and Figure 2.23). They are tight to isoclinal folds, with strongly attenuated limbs, and in some instances were observed to be gently inclined (Figure 2.23).

Stereographic analysis shows that throughout the moderate to high strain zone (areas iv(b) and v(b) on Figure 2.5 and Figure 2.15, Figure 2.17a sections K and L, Figure 2.17(b) sections N to V), bedding mostly dips moderately to steeply to the east-southeast (80/100), although on the west coast section, bedding predominantly dips

Figure 2 21(a) Overview of mesoscopic, tight, recumbent ***Ca***F_1 and ***Ca***F_2 folds in deformed Oonah Formation psammite, within the Moderate-High strain zone of the Arthur Lineament, on the west coast (334320 mE, 5372315 mN). *De*S_4 cleavage dips steeply to the left of photograph, hammer for scale is centre left; (b) sketch of (a), illustrating close up locations (c) and (f); (c) close up photograph ***Ca***F_1 antiformal hinge, showing attenuation of limbs, weathering of recessive layers and transecting *De*S_4 cleavage; (d) sketch of (c), showing location of close up (e); (e) detailed photograph of tight ***Ca***F_1 hinge with recessive layering (bedding) and transecting *De*S_4 cleavage; (f) close up of synformal ***Ca***F_1 hinge, pen at centre is 14 cm in length

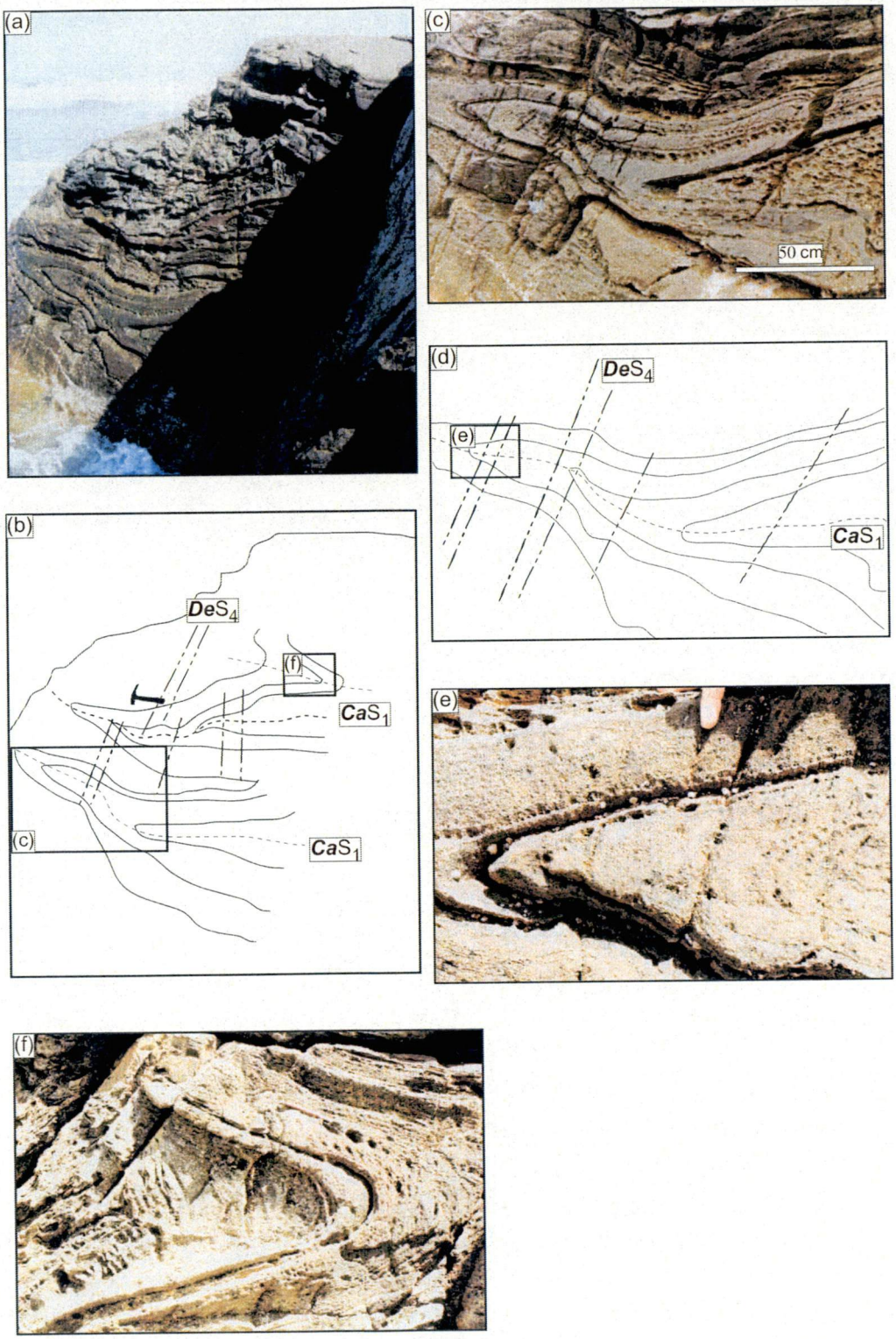

Figure 2.21(a)-(f).

Figure 2.22. Structural style of the southernmost edge of the Arthur Lineament, on the west coast of Tasmania, to the north of Granville Harbour (3349915 mE, 5371325 mN to 334300 mE, 5372610 mN). (a) cross section J", illustrating structural data for the west coast exposure of the southern Arthur Lineament; (b) interpretive cross section for the area; (c) simplified geological map of the section, (i) is location of isoclinally folded and boudinaged (***Ca***F_1) amphibolite body; (d) stereographic projections for ***Ca***L_{01} and ***Ca***L_{02} illustrating the predominantly shallow to moderate southeast plunge. Refer to Figure 2.2a and b for location.

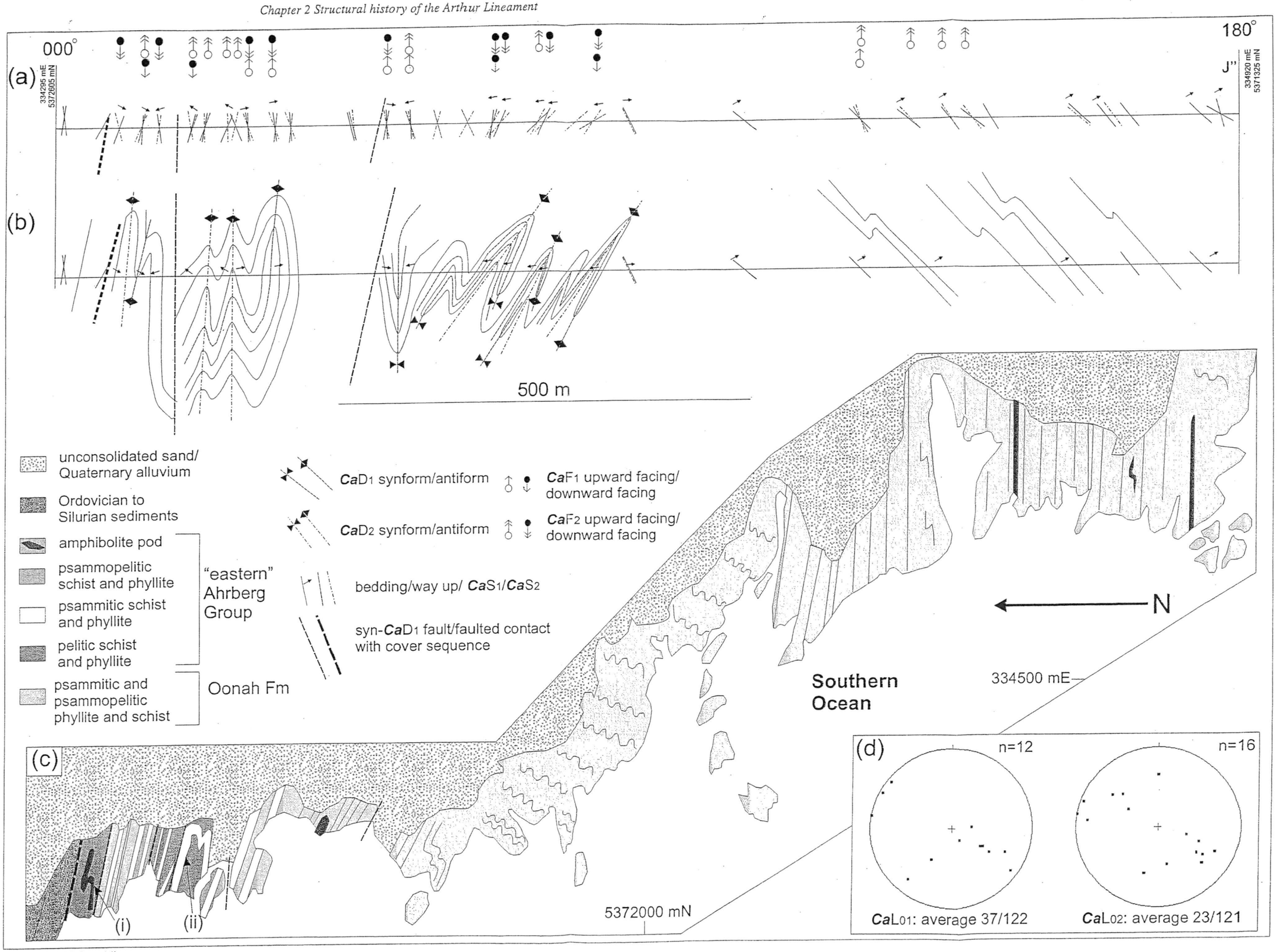

Figure 2.22(a) to (d).

Figure 2.23. Mesoscopic, gently inclined $Ca F_2$ with finely spaced (2-3 mm) to phyllitic axial planar $Ca S_2$ cleavage. Lithology is moderate-high strain Oonah Formation psammopelite-pelite, grading up to the right. Lens cap is 53 mm diameter (345050 mE, 5378690 mN).

Figure 2.24. Photomicrographs of cleavage development near to the eastern boundary of the Arthur Lineament. (a) Photomicrograph of weak, phyllitic $Ca S_2$ cleavage development in quartz-rich psammopelite, close to the eastern boundary of the Arthur Lineament (moderate-high strain Oonah Formation). Quartz grains show moderate levels of deformation and alignment of long axes horizontally. Micaceous cleavage domains also are horizontal. Weak crenulation trending perpendicular to the main foliation is evident ($De S_4$). 5X magnification, XPL (334415 mE, 5372055 mN)(sample 932). (b) Photomicrograph of developing schistose $Ca S_2$ foliation in quartz-rich psammopelite, within the eastern boundary of the Arthur Lineament. Quartz grains are more strongly aligned and flattened than in (a). Weak crenulation trending perpendicular to the main foliation is evident ($De S_4$). 5X magnification, XPL (334295 mE, 5372605 mN)(sample 923a).

Figure 2.25. Boudinaged psammite layer in psammopelite, AGC. (a) psammite layer (ps) has preserved $Ca S_1$ and is boudinaged by $Ca S_2$. In psammopelitic layer (pp) the $Ca S_1$ is represented by magnetite veinlets that crosscut bedding (mt). The $Ca S_2$ is pervasively developed in the psammopelite, and is parallel to bedding. Way up was identified by graded bedding(b) detailed sketch map of (a) (location (ii) on Figure 2.22d (334310 mE, 5372500 mN).


(2.23)

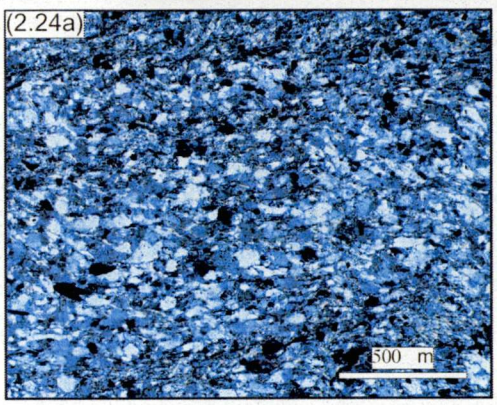
(2.24a)
500 m

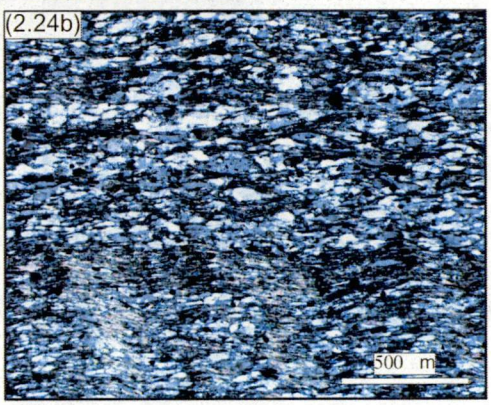
(2.24b)
500 m

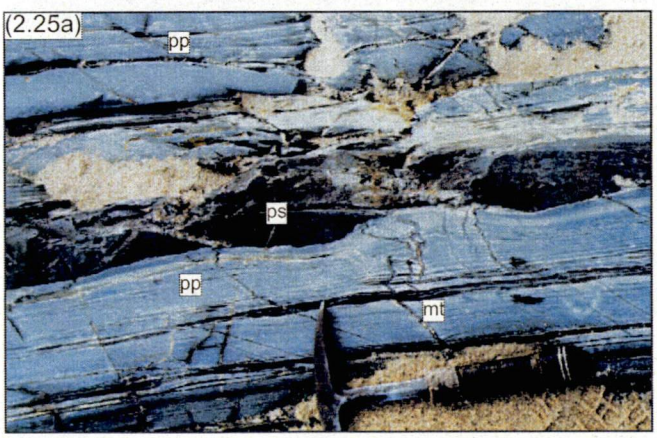
(2.25a)
pp
ps
pp
mt

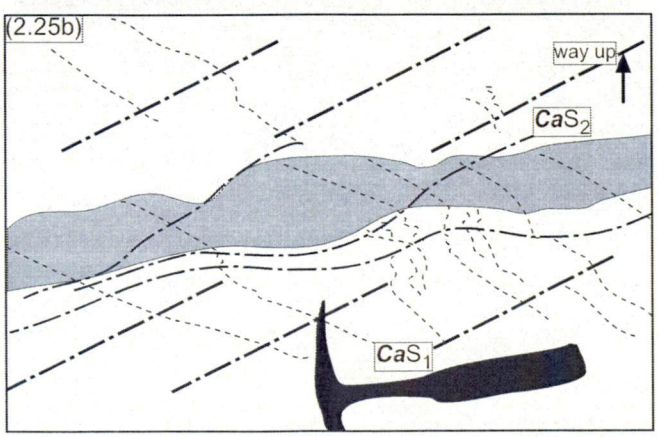
(2.25b)
way up
CaS2
CaS1

steeply to the south (82/194), due to the later Devonian refolding (areas iv(a) and v(a) on Figure 2.5 and Figure 2.15, Figure 2.22(a) and (b). The north-south spread of the poles to bedding indicates several generations of folding and refolding have occurred. The predominant, bedding-parallel, east-southeast dip of $Ca S_1$ and $Ca S_2$ reflects the tight to isoclinal style of $Ca F_1$ and $Ca F_2$, which mostly plunge moderately to steeply to the south (Figure 2.5). On the west coast section, $Ca S_1$ and $Ca S_2$ are also parallel to bedding, and dip steeply to the north and south (70/190) (Figure 2.5).

$Ca L_{01}$, $Ca L_{12}$ and $Ca L_{02}$ intersection lineations and $Ca F_1$ and $Ca F_2$ fold axes mostly plunge moderately to steeply to the south-southwest, although variation is evident, as some lineations plunge to the north-northwest and southeast (Figure 2.5 and Figure 2.22(d)). The spread of lineations and fold axes in this area is due to later refolding about an east-northeast axis.

2.4.3.2 Moderate to high strain zone – AGC ("eastern" Ahrberg Group correlate)

In the "eastern" Ahrberg Group correlate, the $Ca S_1$ and $Ca S_2$ foliations are sub-parallel to bedding on the limbs of $Ca F_1$ and $Ca F_2$ folds. Furthermore, they are more intensely developed than in the Oonah Formation, as are $Ca F_1$ and $Ca F_2$ folds, reflecting an increase in strain towards the core of the Arthur Lineament.

Compositional differences between the metasediments of the two sequences causes some contrast in the pervasiveness of the foliations. Within interbedded psammite/pelite sequences, $Ca S_1$ is preserved as a crosscutting fabric, mostly found in microlithons of $Ca S_2$ and within some $Ca S_2$ psammite boudins. In these instances, the earlier fabric is recognisable due to its slightly different orientation to $Ca S_2$, and its termination at the boundaries between intensely and weakly developed $Ca S_2$. These correspond with the boundaries between competent and incompetent layering, as $Ca S_2$ is more intensely developed in the finer grained metasediments (Figure 2.25(a) and (b)). In lithological sequences with less contrast in competency, such as psammite/psammopelite sequences, $Ca S_1$ is a more pervasive foliation, evident in layers of different competency, however it is still obliterated in areas of

intensely developed ***Ca***S_2. The ***Ca***S_2 foliation cleavage domains are parallel in psammopelitic units, and anastamosing in psammitic layers (Figure 2.26(a) and (b)). Consistent with the moderate to high strain zone in the Oonah Formation, ***Ca***F_1 folds evident in the field are smaller in scale and less common than ***Ca***F_2 (Figure 2.22(a) and (b)). However, structural mapping indicates changes in ***Ca***F_1 vergence are less frequent than ***Ca***F_2, suggesting the wavelength of macroscopic-scale ***Ca***F_1 folds are greater than ***Ca***F_2. The outcrop scale ***Ca***F_1 folds are intensely developed as is seen on the west coast, with syn-***Ca***F_1 isoclinal folding and boudinage of bedding-parallel amphibolite bodies occurring (location (i) in Figure 2.22(d)) (Figure 2.22(a) and (b)).

In the Reece Dam area, the "eastern" Ahrberg Group correlate is extensively exposed at the base of the spillway, in Stringer Creek (345120mE, 5378860mN) (Figure 2.27(b)). This provides a detailed insight into the structural style of the "eastern" Ahrberg Group correlate in this area. In addition to the outcrop of metasediments, this location features exposure of a structurally interlayered tholeiitic metagabbroic unit (Turner 1992, Crawford 1992, Turner & Crawford 1993). To the west of the "eastern" Ahrberg Group correlate, and also exposed, is the faulted contact with the Bowry Formation.

The "eastern" Ahrberg Group correlate in this area is dominated by ***Ca***S_1 and ***Ca***S_2 (Figure 2.26(a) to (c)), as well as syn-***Ca***D_1 to syn-***Ca***D_2 faults, and based on consistent ***Ca***F_2 vergence, is positioned on the downward-facing, east-dipping limb of a ***Ca***F_2 fold. The orientations of S_0, ***Ca***S_1 and ***Ca***S_2 are variable due to refolding by ***Ca***F_3, ***De***F_4 and ***De***F_5 (Figure 2.5). Late faults, possibly Devonian in age, also cut the Cambrian-age structures. The varying orientation, style and intensity of the ***Ca***D_1 and ***Ca***D_2 structures enable the area to be divided into two structural domains (Domains S1 and S2) (Figure 2.27(b)).

Domain S1 is defined as the short limb and hinge-zone of a late (***Ca***D_3 or ***De***D_5) upright southeast-plunging 'Z' fold with a wavelength of 150 metres. The domain features pervasive development of ***Ca***S_1 and ***Ca***S_2, which have consistent vergence relationships with S_0. ***Ca***F_2 are small-scale (5-15 cm wavelength) 'Z' folds that verge to the southeast. The folds feature moderately southeast-dipping overturned long limbs, steeply southeast dipping upright short limbs. ***Ca***S_2 is finely spaced (1-2

Figure 2.26. Mesoscopic ***Ca***F_2 fold from the base of the spillway at Reece Dam, in AGC. (a) Overview of asymmetric fold, illustrating moderate level of attenuation of limbs. ***Ca***S_2 is axial planar, and pervasively developed in carbonate bearing psammitic layers (orange) and graphitic psammopelitic layers (grey); (b) close up of hinge area, illustrating anastamosing ***Ca***S_2 in psammite and parallel ***Ca***S_2 in psammopelite. The ***Ca***S_1 foliation is developed in both psammitic and psammopelitic layers, and is crenulated by ***Ca***S_2; (sample 1114a) (c) photomicrograph of interlayered graphitic psammopelite and carbonate-bearing quartz psammite with schistose ***Ca***S_2 featuring more finely spaced microlithons in psammopelite-rich zones (lower left). Crosscutting crenulation cleavage (possibly Devonian in age) dips more steeply to the right (5X XPL) (sample 1114b)(345120 mN, 5378860 mN).


(a)
cm

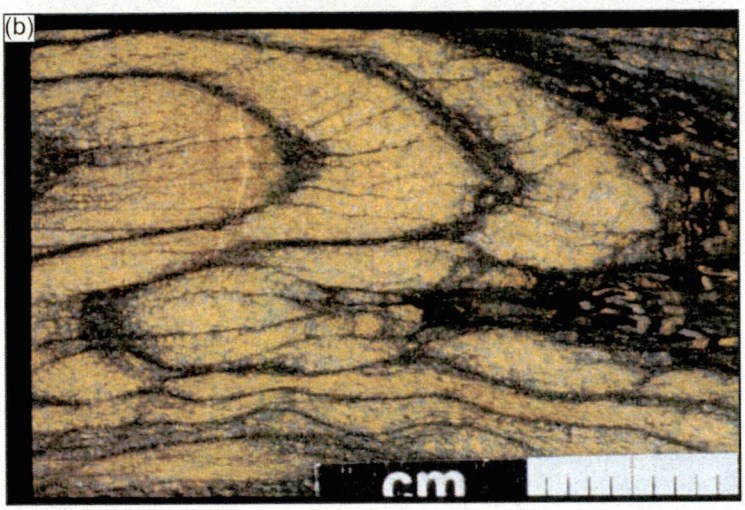
(b)
cm


(c)
500 m

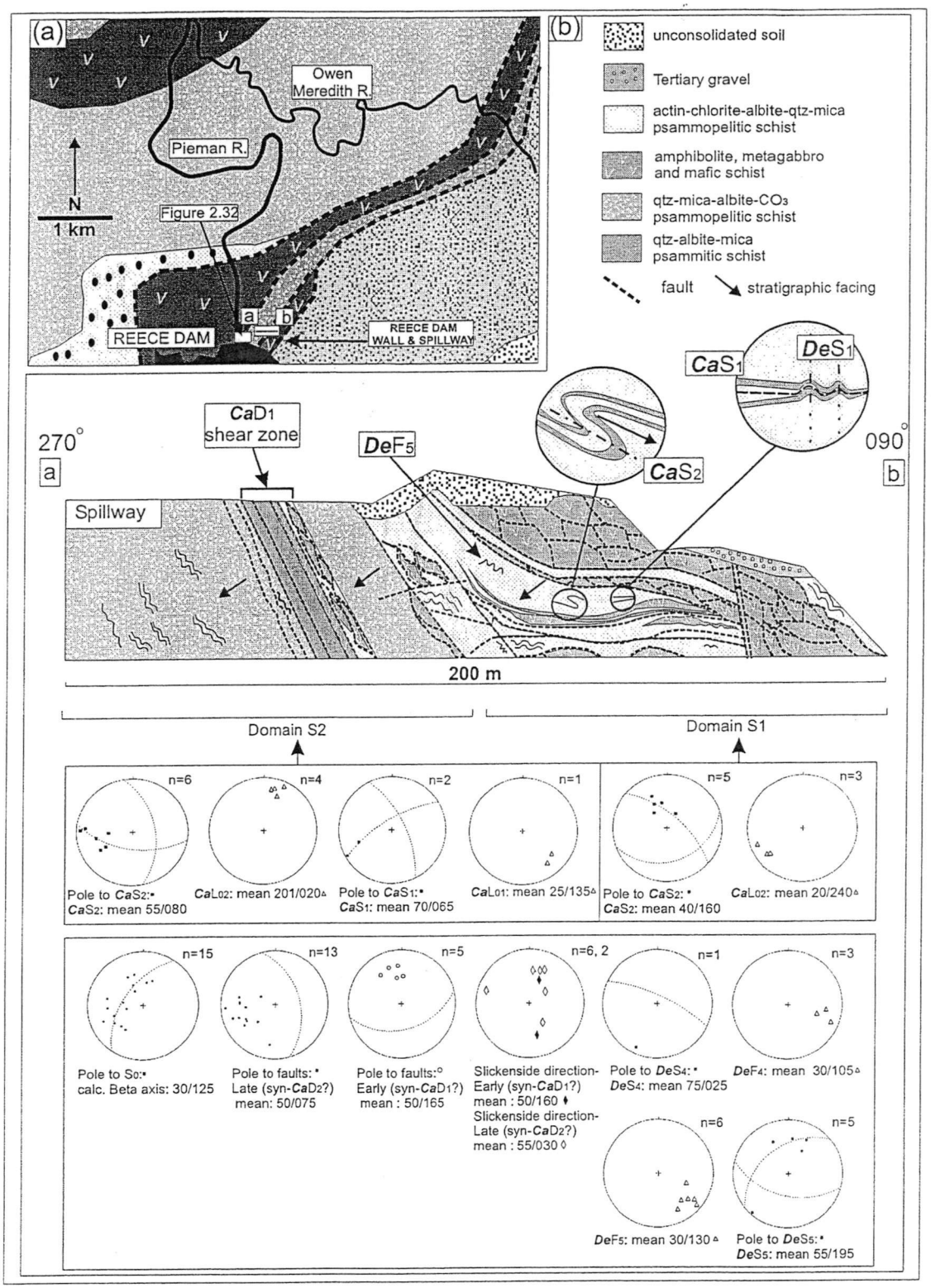

Figure 2.27 (a)-(b). Reece Dam and spillway, (a) location map (modified after Turner *et al.* 1991), with section line A-B; (b) cross section of the Reece Dam-spillway area (section A-B), with equal area stereographic projections for Domains S1 and S2 (345300 mE, 5378875 mN to 345100 mE, 5378875 mN). Legend for 2.27(a) is the same as for Figure 2.2.

mm) and phyllitic to schistose. The ***Ca***F_2 folds refold the very finely spaced (1 mm) phyllitic to schistose ***Ca***S_1 cleavage.

CaS_1- to ***Ca***S_2- parallel faulting and shearing is common (Figure 2.27(b)). These shear zones are typically planar features, within zones up to 5 metres wide, of intensely developed ***Ca***S_1 and ***Ca***S_2. The metagabbro described by Crawford (1992) and Turner & Crawford (1993) outcrops in Domain S1 as boudins that have margins penetrated (up to 1 m) by the ***Ca***S_1- to ***Ca***S_2- foliations, due to competency contrast between the metagabbro and the surrounding quartz-mica-albite-carbonate schist. The cores of the boudins are unfoliated.

Domain S2 is the moderately dipping long limb of the late (***Ca***D_3 or ***De***D_5) upright southeast-plunging 'Z' fold (Figure 2.27(b)). ***Ca***S_1 and ***Ca***S_2 are pervasively developed. ***Ca***S_1 is a finely spaced schistosity (0.5 mm) (Figure 2.26(a) to (c)), and produces a ***Ca***L_{01} intersection lineation. ***Ca***S_2 is also schistose (1-2 mm spacing), and produces a ***Ca***L_{02} intersection lineation. The syn-***Ca***D_1 and syn-***Ca***D_2 faults display a consistent reverse sense of movement and predominantly dip to the east (Figure 2.27(b)). They lack fault gouge or breccia.

Stereographic analysis of the AGC in the moderate to high strain zone was undertaken. It is evident that the orientation of bedding (45/095), ***Ca***S_1 (70/060) and ***Ca***S_2 (50/100) is broadly consistent with the moderate to high strain zone Oonah Formation, both within the Arthur Lineament in the Reece Dam-Rocky River area, and on the west coast (Figure 2.5). In the AGC, bedding, along with ***Ca***S_1 and ***Ca***S_2 predominantly dip moderately to the east-southeast, whereas intersection lineations (***Ca***L_{01} ***Ca***L_{12} and ***Ca***L_{02}) mostly plunge moderately to steeply to the south-southwest (***Ca***L_{01} and ***Ca***L_{12}: 65/220) and north-northeast (***Ca***L_{02}: 10/025). On the west coast, the foliations (S_0, ***Ca***S_1 and ***Ca***S_2) predominantly dip steeply to the north-northeast (85/020), although some surfaces dip to the south-southwest. ***Ca***F_1 and ***Ca***F_2 fold axes and intersection lineations (***Ca***L_{01} ***Ca***L_{12} and ***Ca***L_{02}) consistently plunge gently to moderately to the southeast (25/115) (Figure 2.5).

2.4.4 Southern study area: structure of the high strain zone of the Arthur Lineament

The high strain zone of the Arthur Lineament consists of the Bowry Formation in the east, and the "eastern" Ahrberg Group to its west (areas labelled ii(a), ii(b) and iii in Figure 2.5 and Figure 2.15). The Bowry Formation (iii in Figure 2.5 and Figure 2.15) is a fault-bounded unit, and is interpreted to be allochthonous due to its different early metamorphic history and the presence of a deformed *ca.* 780 Ma granitoid (Turner *et al.* 1998). The "eastern" Ahrberg Group is considered to be a correlate of the "western" Ahrberg Group based on similarities in the stratigraphy and geochemistry of mafic igneous rocks (discussed in Chapters 1 and 4) and is interpreted as a para-autochthonous unit. Structural mapping in the high strain zone of the Arthur Lineament was carried out in the following areas:

- in the Rocky River,
- in the Owen Meredith River,
- in lower Stringer Creek and around the Reece Dam power station,
- along the Savage River–Corinna Road,
- in the Paradise River,
- in Lucy, Nancy and Timbs Creeks,
- on the west coast, to the north of Granville Harbour, between the northern boundary of the Duck Creek cover sequence and the southern end of Four Mile Beach.

These areas are labelled ii(b) and ii(a) on Figure 2.15. The structural histories of the Bowry Formation and the "eastern" Ahrberg Group appear to be similar. However, whereas the style and intensity of deformation is consistent throughout the high strain zone, the orientation of the foliations ($\boldsymbol{Ca}S_1$ and $\boldsymbol{Ca}S_2$) and intersection lineations ($\boldsymbol{Ca}L_{02}$) in the two sequences is slightly different (Figure 2.5). On this basis, the deformation in the Bowry Formation and "eastern" Ahrberg Group sequences will be discussed as two separate structural domains, in order to facilitate the independent structural assessment of these units.

2.4.4.1 High strain zone – Bowry Formation

The Bowry Formation occurs to the west of the moderate to high strain "eastern" Ahrberg Group correlate (Figure 2.15). The style of deformation within the Bowry Formation, throughout the three areas which the unit has been mapped (Rocky River, Owen Meredith River and lower Stringer Creek) is consistent. Therefore the deformational history evident in these areas of the Bowry Formation will be discussed as a single structural domain. The Bowry Formation is not exposed on the west coast, and is interpreted to be covered by the Duck Creek sequence (Eldon Group) (Figure 2.2a).

Bedding is not always visible within the Bowry Formation. The metasediments which comprise the unit are mostly fine grained, and uniform in composition. The protolith of these fine grained metasediments is interpreted to be volcanic-derived siltstone, with little evidence for sedimentary structures. However, where bedding is evident, it is slightly different in orientation to $\boldsymbol{Ca}S_1$, and is sub-parallel to $\boldsymbol{Ca}S_2$, mostly trending steeply towards the east (70/095). The closeness in orientation is interpreted to be a result of the tight to isoclinal style of $\boldsymbol{Ca}F_2$. The style of $\boldsymbol{Ca}S_2$ and $\boldsymbol{Ca}F_2$ will be discussed in greater detail below.

The transition in deformational style and intensity from the AGC (moderate to high strain zone) to the Bowry Formation (high strain zone) is sharp, with the frequency of faulting increasing and the $\boldsymbol{Ca}S_1$ and $\boldsymbol{Ca}S_2$ foliations developed as schistosities. Eventhough $\boldsymbol{Ca}S_1$ and $\boldsymbol{Ca}S_2$ are both schistose foliations, the intense development of $\boldsymbol{Ca}S_2$ within the Bowry Formation has caused the common obliteration of early ($\boldsymbol{Ca}S_1$) textures. As a result, on a microscopic scale, $\boldsymbol{Ca}S_1$ is preserved in microlithons of $\boldsymbol{Ca}S_2$ (Figure 2.28(a)). Where $\boldsymbol{Ca}S_1$ is preserved, in zones of weakly developed $\boldsymbol{Ca}S_2$, it is a pervasively developed schistosity, with very finely spaced (0.5-1 mm wide), parallel, smooth microlithons and discrete cleavage domains. However, in some areas of less intense deformation, the foliation is phyllitic. As in other areas of high strain, commonly associated with, and parallel to $\boldsymbol{Ca}S_1$, are quartz segregations, which highlight the orientation of the foliation (Figure 2.28(b) to (d)). In some cases the quartz segregations were observed being folded $\boldsymbol{Ca}F_2$ (Figure 2.28(c) and (d)). $\boldsymbol{Ca}S_1$ commonly dips steeply to the northeast (70/040) (Figure 2.5).

Figure 2.28(a) Photomicrograph of quartz-chlorite-opaque schist from the Bowry Formation, showing the preservation of $Ca S_1$ (dipping to the right) in microlithons of $Ca S_2$ (horizontal). The $Ca S_2$ schistosity crenulates $Ca S_1$ (sample DDH1 Rocky River, 210.3 m) (349800 mE, 5389800 mN); (b) $Ca S_1$ quartz segregation boudinaged by $Ca S_2$ (trending up to the right) in chloritic schist interlayered with laminated magnetite (grey) (349610 mE, 5388610 mN); (c) mesoscopic $Ca F_2$ refolding $Ca S_1$-parallel quartz segregation in chloritic psammopelitic schist. $Ca S_2$ schistosity is defined by quartz-rich domains, axial planar to the fold. White area of pen is 7 cm in length (349480 mE, 5388820 mN); (d) abundant $Ca S_1$ quartz segregations in chloritic schist, intensely folded by $Ca F_2$, pen at centre is 14 cm in length (349885 mE, 5388250 mN); (e) photomicrograph of psammopelite from the Bowry Formation, showing intense development of $Ca S_2$ schistosity. Quartz grains are fully recrystallised, and are intergrown with carbonate (sample 809) (344700 mE, 5379130 mN); (f) photomicrograph of strongly foliated amphibolite in the Bowry Formation. Dominant foliation (horizontal) is $Ca S_2$. Albite porphyroblasts are syn-$Ca D_2$. Foliation is defined by chlorite (olive green) and actinolitic amphibole (blue green). Opaques are magnetite. (sample 667) (349570 mE, 5388650 mN).

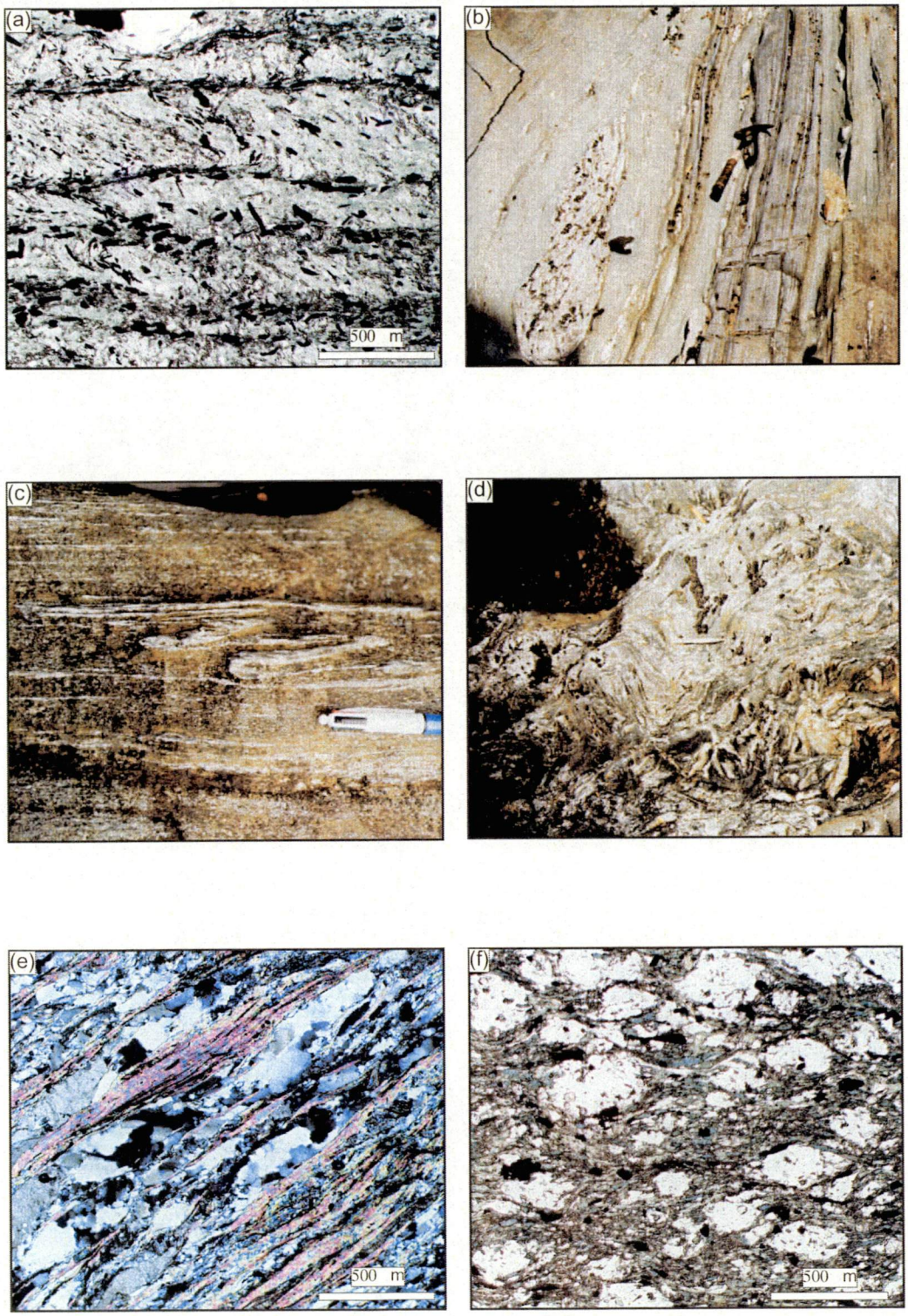

Figure 2.28(a)-(f).

The $Ca S_2$ foliation is much more pervasive than $Ca S_1$. It is an intensely developed, schistose foliation, and has finely spaced cleavage domains (0.5-2 mm) (Figure 2.28(e)), with more broadly spaced cleavage domains in psammitic layers. The foliation penetrates the margins of amphibolite bodies, causing syn-deformational mineral growth, and metamorphic mineral alignment (Figure 2.28(f)). The $Ca S_2$ foliation mostly dips to the east-southeast (60/105), however due to subsequent refolding, there is a spread in the orientation of $Ca S_2$ (Figure 2.5).

Syn-$Ca D_1$ and $Ca D_2$ boudinage of competent layers is common in the Bowry Formation. Boudinaged $Ca S_{1-2}$-parallel quartz segregations are common within psammopelite (Figure 2.28(b)). $Ca F_1$ were not found in the Bowry Formation and $Ca F_2$ were minor (Figure 2.19 sections W to Y and A'). The $Ca F_2$ folds observed were mostly small scale, parasitic tight to isoclinal folds, refolding syn-$Ca S_1$ quartz segregations (Figure 2.28(c)). Stretching lineations related to $Ca D_1$ and $Ca D_2$ were not observed. As a result of the intense overprinting of $Ca S_1$ by $Ca S_2$, intersection lineations between $Ca S_1$ and other surfaces were difficult to detect. However, $Ca L_{02}$ intersection lineations are common, and mostly plunge gently to the south (5/185), but they also plunge gently to the north, as a result of refolding in some areas (Figure 2.5).

Although $Ca F_1$ and $Ca F_2$ folding in the Bowry Formation was not frequently observed, syn-$Ca D_1$ to $Ca D_2$ faulting is common, and based on detailed mapping in the lower Stringer Creek-Reece Dam powerstation area (Figure 2.29(a)), appears to be the main style of deformation in this unit (Figure 2.29(b) and (c), Figure 2.30). Faults are $Ca S_1$- and $Ca S_2$-parallel planar features, with quartz segregations common on the margins of the fault plane. The faults are narrow zones and do not have associated fault gouge or brecciation.

The mapped eastern boundary of the Bowry Formation (faulted contact with the AGC) is exposed to the west of the spillway at Reece Dam, in lower Stringer Creek (Turner *et al.* 1991). Approaching this boundary from the east, the geology becomes more complex, in the vicinity of lower Stringer Creek and the Reece Dam power station. Mafic schist and amphibolite bodies become common and syn-$Ca D_{1-2}$ faults are more frequent. Furthermore, structural repetition and the interlayering of units of

Figure 2.29(a) overview map of geology in the vicinity of the Reece Dam area, and the location of cross sections; (b) cross section (viewed to the north) of AGC outcrop along lower Stringer Creek. The area is dominated by $Ca F_2$ and syn-$Ca D_2$ faulting, with minor overprinting by $Ca D_3$ structures. Sketch is mirror image in order to keep consistent orientation with Figure 2.33. (345140 mE, 5379190 mN) (points A and B in Figure 2.29b are along strike, on opposite banks of Stringer Creek. Outcrop is lithologically varied, with moderately deformed amphibolite and metasedimentary schists outcropping. $Ca F_2$ vergence is consistent on both sides of creek. Section is viewed to the north (344730 mE, 5379090 mN); (c) cross section immediately downstream of tunnel outlets on the Pieman River, within Bowry Formation. Area is fault dominated, with reverse sense of movement apparent on most fault surfaces, which are steeply east dipping. Amphibolite is crossitic, indicative of high metamorphic conditions. Bedding and $Ca S_2$ predominantly dip steeply to the southeast, however $Ca S_1$ dips steeply to the north. (344720 mE, 5379210 mN).

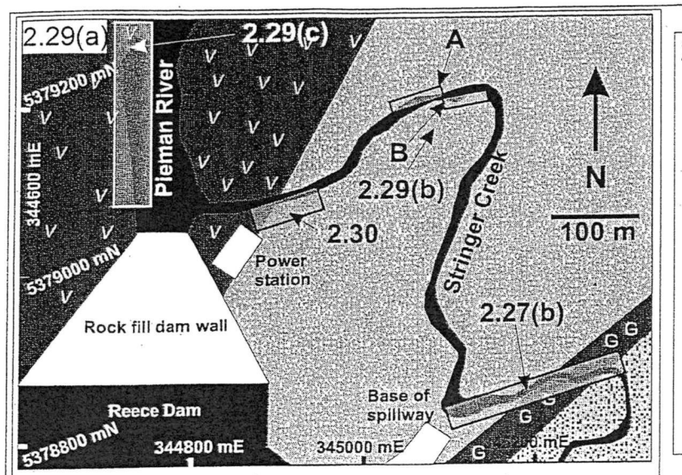

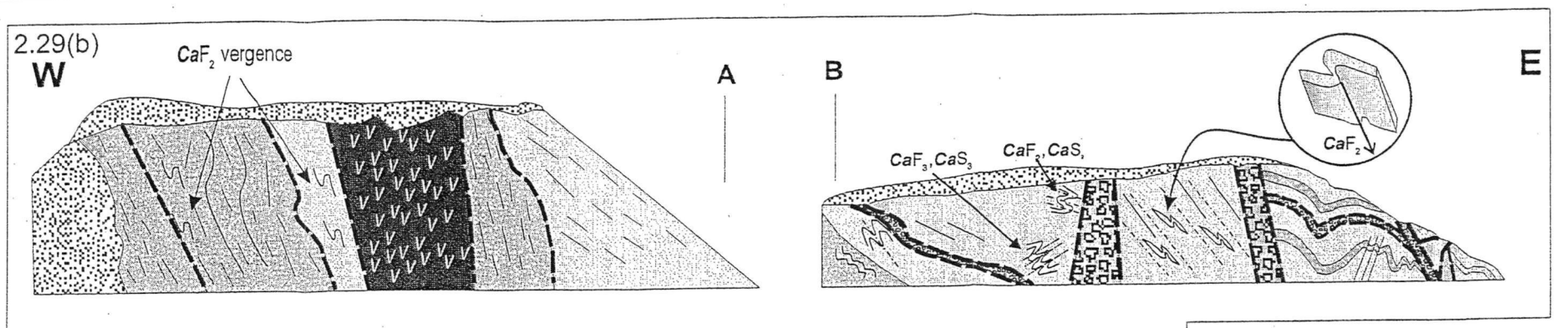

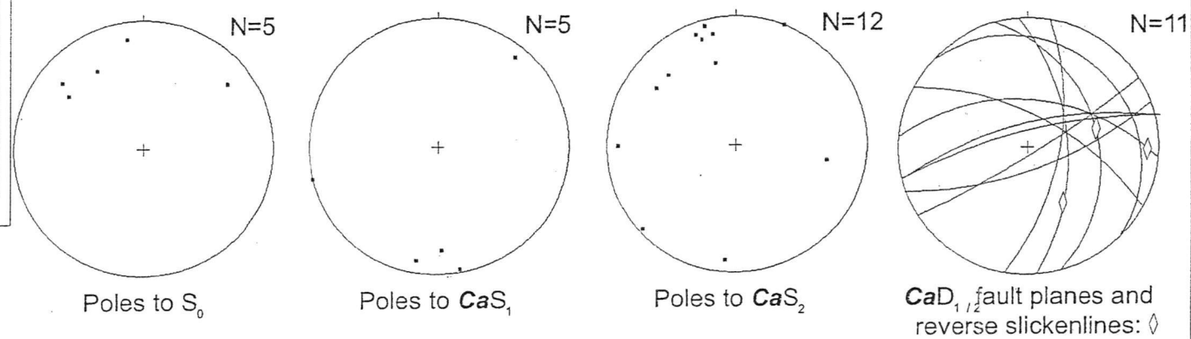

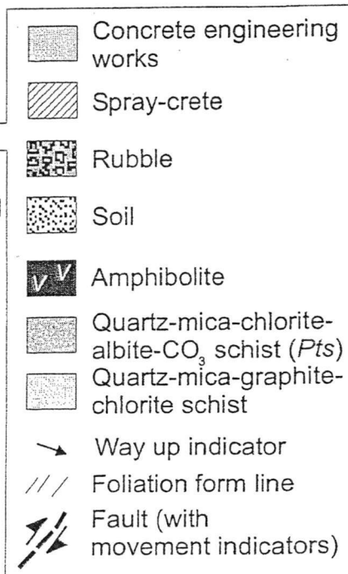

2.29(c)

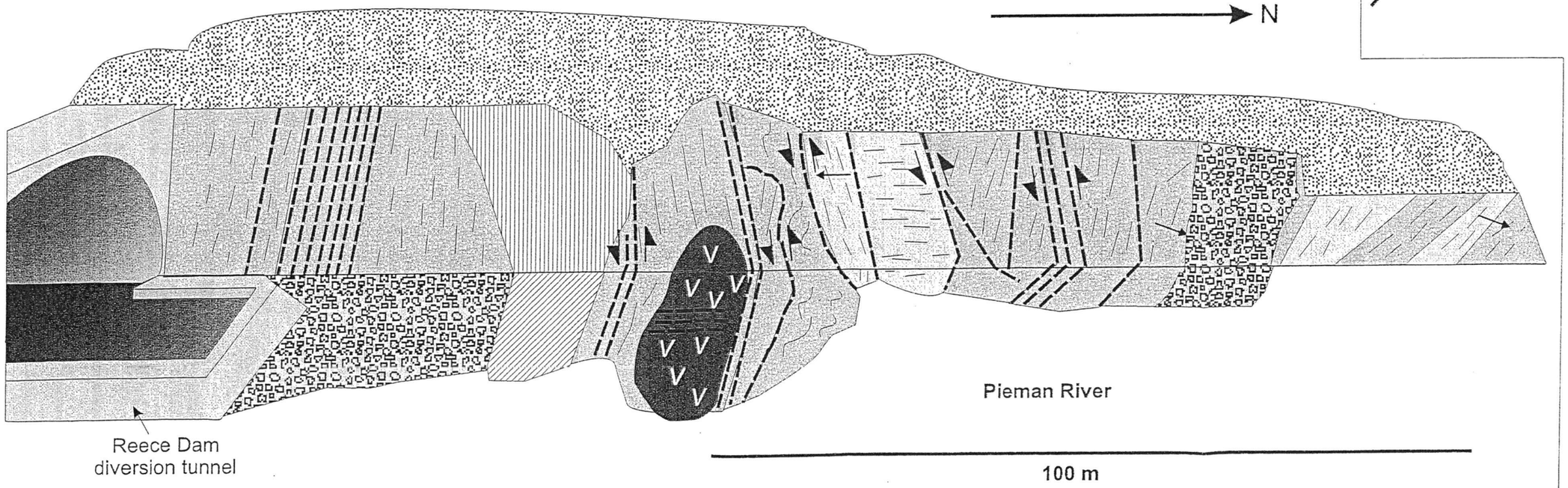

Figure 2.29(a) to (c).

Figure 2.30. Detailed geological map and photographic collage (oblique view) of the same area (lettering A,B and C correspond) from the mouth of Stringer Creek, near Reece Dam power station (344900 mE, 5379100 mN). The intense faulting (visible as east dipping surfaces in the photograph) has resulted in the stacking of slices of differing composition and metamorphic grade. Measured fault planes with movement indicators are illustrated in the stereographic projection.

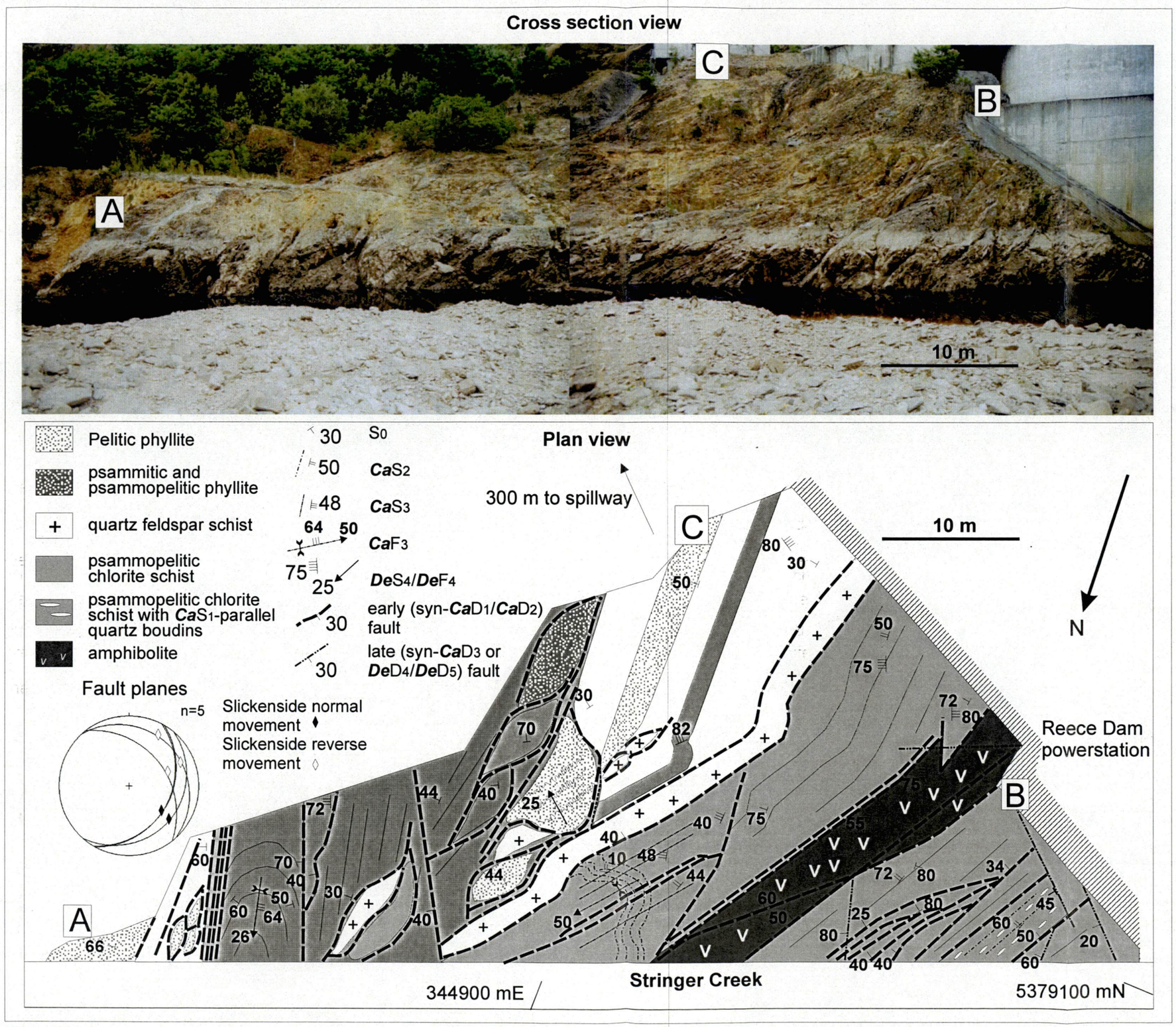
Cross section view
A
C
B
10 m
Pelitic phyllite
psammitic and psammopelitic phyllite
quartz feldspar schist
psammopelitic chlorite schist
psammopelitic chlorite schist with CaS1-parallel quartz boudins
amphibolite
30 S0
50 CaS2
48 CaS3
64 50 CaF3
75 25 DeS4/DeF4
30 early (syn-CaD1/CaD2) fault
30 late (syn-CaD3 or DeD4/DeD5) fault
Fault planes
n=5
Slickenside normal movement
Slickenside reverse movement
Plan view
300 m to spillway
C
10 m
N
Reece Dam powerstation
B
A
Stringer Creek
344900 mE
5379100 mN

Figure 2.30

different metamorphic grade is observed. The increase in the frequency of early faulting (syn-***Ca***D_1 and syn-***Ca***D_2) at the spillway and dam (Figure 2.27(c) and 2.30) is interpreted to represent the style of deformation within the most strongly deformed parts of the Arthur Lineament. Individual syn-***Ca***D_{1-2}-related fault bounded slices are typically 5 to 10 m thick, with strongly foliated to sheared margins demonstrating well developed S-C fabrics. These zones are dominated by small scale faults (Figures 2.29(b) to (d) and Figure 2.30). The faults have resulted in the stacking of slices of different composition and different metamorphic grade, including graphitic phyllite, pelitic and psammopelitic schist, chlorite and mafic schist, amphibolite and minor quartz-feldspar schist (344900 mE, 5379075 mN), and are critical to the understanding of this high strain zone of the Arthur Lineament.

These contrasting styles of deformation are widespread, and are interpreted to occur on a mesoscopic scale, and on a macroscopic scale (eg. Figures 2.27(c), 2.29(b) to (d) and Figure 2.30). They are interpreted to have produced stacks of regionally mappable fault bounded slices of contrasting metamorphic grades, such as the allochthonous Bowry Formation.

2.4.4.2 High strain zone – "eastern" Ahrberg Group

The high strain "eastern" Ahrberg Group is faulted against the Bowry Formation to the east, and the "western" Ahrberg Group to the west. It is the largest tectono-stratigraphic unit of the Arthur Lineament, and is compositionally varied, with psammopelite, psammite, carbonate-bearing metasediments, mafic metasediments and amphibolites (see Chapter 1 and 4).

The structural style in the "eastern" Ahrberg Group" is consistent in the different areas in which the sequence was mapped (Rocky River, Savage River-Corinna Road, Paradise River, Lucy, Nancy, Timbs Creek and on the west coast, to the north of the Duck Creek cover sequence). However, the orientation of bedding and the ***Ca***D_1 and ***Ca***D_2 deformational features in the "eastern" Ahrberg Group on the west coast differs from other areas of the southern Arthur Lineament (Figure 2.5). This is interpreted to be the result of subsequent refolding by Devonian deformation, discussed in detail in Section 2.5. On the basis of the similar structural style and

orientation (prior to the Devonian deformation) in the above mentioned areas, the "eastern" Ahrberg Group will be discussed as one structural domain.

Within the "eastern" Ahrberg Group, bedding is mostly detectable in the field and in hand specimen, due to the predominantly interbedded nature of the precursor sediments (Figure 2.31(a) and (b)). S_0 predominantly dips steeply to the east-southeast (70/100), however due to subsequent refolding, the poles to bedding define a great circle reflecting folding about a north plunging axis. On the west coast the orientation of S_0 differs from elsewhere in the "eastern" Ahrberg Group, and mostly dips steeply to the southeast (60/140) (Figure 2.5). Bedding is commonly parallel to sub-parallel to ***Ca***S_1 and ***Ca***S_2, due to the tight to isoclinal style of folding. However, in ***Ca***F_1 and ***Ca***F_2 hinge zones, the respective foliations are at a high angle to bedding.

CaS_1 is a very finely spaced (less than 0.5 mm) schistosity, with mostly parallel, smooth cleavage domains and discrete microlithons. In some cases, the foliation is phyllitic. In coarser grained, psammitic metasediments, the spacing of the cleavage domains increases (1 mm), although the foliation does not penetrate these layers as pervasively as in the pelitic and psammopelitic layers. As in the other moderate to high strain zones, where ***Ca***D_2 is intensely developed, ***Ca***S_1 is strongly overprinted by ***Ca***S_2. In most areas, ***Ca***S_1 is only preserved in microlithons of the ***Ca***S_2 foliation, and as inclusions in late syn to post-***Ca***D_1 and syn-***Ca***D_2 porphyroblasts (Figure 2.4(c) and (d)). In the majority of the high strain "eastern" Ahrberg Group, ***Ca***S_1 varies slightly in orientation from bedding, and dips steeply to the southeast (80/075), although the data set is small. However on the west coast, in the zone of intensely developed ***Ca***D_1, ***Ca***S_1 is closer in orientation to bedding (70/150) (Figure 2.5).

CaS_2 is finely spaced (1-2 mm) and schistose, with parallel, smooth cleavage domains and discrete microlithons (Figure 2.31(b) and (c)). Rarely was the foliation observed to be phyllitic. It is the dominant foliation in the majority of the "eastern" Ahrberg Group, and is pervasive. In the high strain zone ***Ca***S_2 is well developed in pelitic, psammopelitic and psammitic lithologies. ***Ca***S_2 also penetrates amphibolite bodies much more extensively than ***Ca***S_1 (Figure 2.31(d)). The foliation is sub-

Figure 2.31(a) interbedded psammitic and psammopelitic schist from the "eastern" Ahrberg Group, in the Paradise River area. Bedding grades up to the left. ***Ca***S_1 is represented by ***Ca***S_1-parallel quartz segregations (top left of frame), that has been asymmetrically folded by ***Ca***F_2. ***Ca***S_2 is the dominant foliation, and dips steeply to the left, crosscutting both S_0 and ***Ca***S_1. Image is 10 cm wide (347150 mE, 5383690 mN); (b) interbedded psammitic and psammopelitic metasediment in the "eastern" Ahrberg Group, on the west coast. Bedding dips steeply to the left, and is weakly overprinted by finely spaced ***Ca***S_1 (dipping gently to the right), evident only in finer grained layers. The schistose ***Ca***S_2 foliation is pervasive, and dips gently to the left. It is best developed in the psammitic layers. Pen is 13.5 cm in length (333410 mE, 5374605 mN); (c) photomicrograph of psammopelitic schist in the high strain "eastern" Ahrberg Group, Paradise River area. ***Ca***S_2 is the dominant schistosity and trends up to the right. Microlithons are finely spaced. Albite porphyroblasts (lower left and upper right) are syn-***Ca***D_2 (5X XPL) (sample 608a) (344380 mE, 5383800 mN); (d) photomicrograph of strongly foliated amphibolite in the "eastern" Ahrberg Group, Paradise River area. The dominant ***Ca***S_2 schistosity is defined by chlorite (pale green) and sphene aggregates (dark brown) (sample 32) (347150 mE, 5383700 mN); (e) interbedded psammite (orange) and psammopelite (pale grey) in the "eastern" Ahrberg Group, west coast sub domain. The psammite layers are intensely boudinaged by ***Ca***D_1 (plunging 52/204) consistent with the orientation of ***Ca***F_1 in this area (see Figure 2.5). Hammer for scale is centre right; (f) psammite clasts in psammopelitic matrix, in the "eastern" Ahrberg Group, west coast sub domain. The psammite clasts have undergone stretching during the ***Ca***D_1 event, and are consistent in their orientation with ***Ca***F_1 in this area (50/152) (see Figure 2.5). Lens cap is 53 mm diameter.

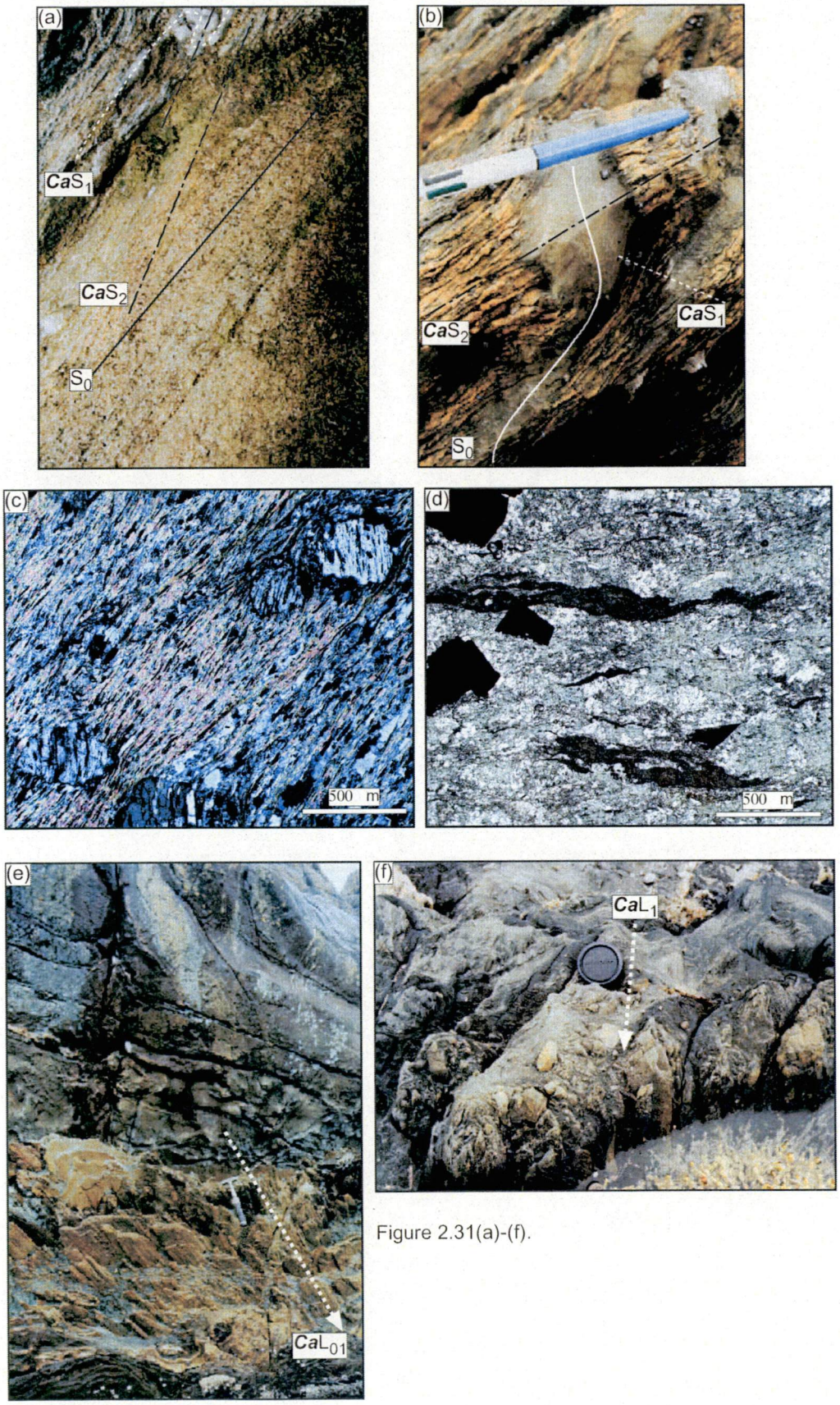

Figure 2.31(a)-(f).

parallel to bedding (65/130) on the west coast, and is parallel to bedding in the other areas of the "eastern" Ahrberg Group (70/100).

CaF_1 are not commonly observed throughout the high strain zone, as a result of the pervasive overprinting and obliteration by ***Ca***S_2 and ***Ca***F_2. However, in areas of the western part of the "eastern" Ahrberg Group, ***Ca***D_1 is intensely developed and is not as pervasively overprinted by ***Ca***D_2 as in other areas (eg. 333740 mE, 5374220 mN) (Figure 2.32). In this sub-domain of intense ***Ca***D_1, ***Ca***F_1 folds are clearly discernable. They are mesoscopic scale isoclinal folds, with strongly attenuated limbs and wavelengths of 5 to 10 m. On the west coast ***Ca***F_1 fold axes and ***Ca***L_{01} and ***Ca***L_{12} intersection lineations plunge moderately to the south-southwest (50/190), whereas in other areas of the "eastern" Ahrberg Group, they plunge gently to the south and south-southeast (5/165). Within the west coast sub-domain (area ii(a) on Figure 2.15), syn-***Ca***D_1 boudinage of psammitic layers and stretching of pebble sized psammite clasts in psammopelite is common, producing lineations consistent in orientation with ***Ca***F_1 (locations (i) and (ii) on Figure 2.32(d), corresponding to Figure 2.31(e) and (f) respectively). Elsewhere in the western part of the "eastern" Ahrberg Group, close to the western boundary of the Arthur Lineament, in Timbs Creek (345350 mE, 5392080 mN), stretching lineations are also observed. Here deformed clasts in conglomeratic layers show evidence of south-plunging stretching lineations (Figure 2.33(a) to (d)).

Coincident with ***Ca***F_1, ***Ca***F_2 folds and ***Ca***L_{02} intersection lineations also plunge moderately to the south-southwest (45/190) on the west coast (Figure 2.5). In other parts of the "eastern" Ahrberg Group high strain zone in the southern Arthur Lineament, they plunge gently to the south (5/185), although some variation due to later refolding is evident (Figure 2.5). Structural analysis incorporating S_0-***Ca***S_1-***Ca***S_2 vergence relationships indicates that ***Ca***F_2 are predominantly large folds with wavelengths of greater than 50 m, however outcrop scale parasitic limb and hinge folds with wavelengths ranging between 0.5 and 5 m are common (Figure 2.32(a) and (b), and Figure 2.33(e) and (f) (location (iii) on Figure 2.32(d))). They are tight to isoclinal folds with attenuated limbs which, in conjunction with the sub-parallel orientations of ***Ca***S_1 and ***Ca***S_2 reflects the coaxial style of refolding present in the Arthur Lineament. In regions of the "eastern" Ahrberg Group in the study area,

Figure 2.32. Structural style of the core of the Arthur Lineament, on the west coast of Tasmania, to the north of Granville Harbour (333925 mE, 5374120 mN to 333515 mE, 5375000 mN). (a) cross section K", illustrating structural data for the core of the Arthur Lineament, west coast section; (b) interpretive cross section for the area; (c) simplified geological map of the section, (i) is boudinaged psammite bed location (pictured in Figure 2.31(e), (ii) is stretched pebble location (pictured in Figure 2.31(f)), (iii) is location of parasitic $Ca F_2$ limb folds (pictured in Figure 2.33(e) and (f)), (iv) and (v) are locations of well developed Devonian deformation (pictured in Figure 2.40 and Figure 2.41(a) and (b), respectively); (d) stereographic projections of $Ca L_{01}$ and $Ca L_{02}$ lineations for the area, showing their predominantly moderate plunge to the south. Refer to Figure 2.2(a) and (b) for location.

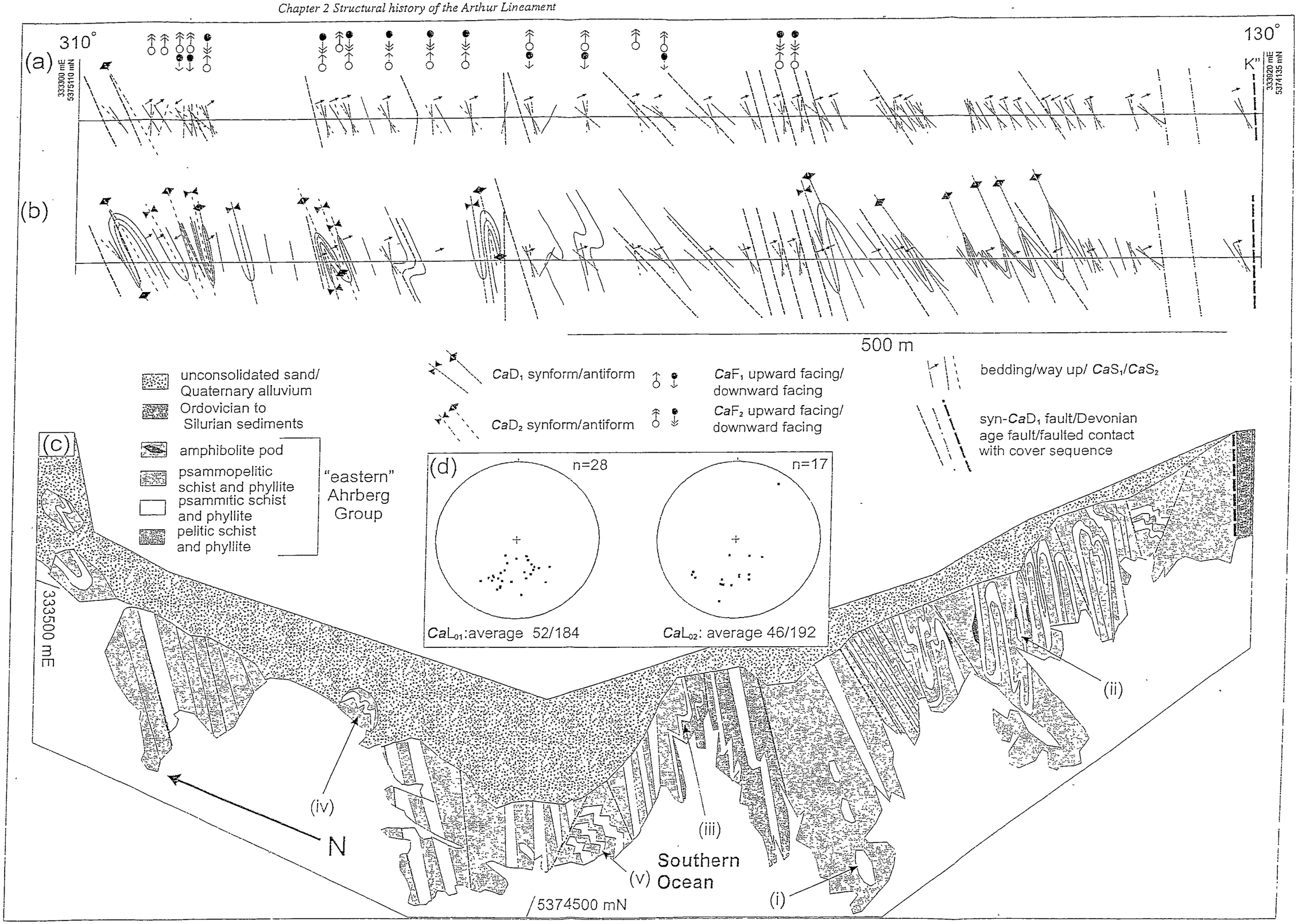

Figure 2.32 (a) to (d).

Figure 2 33(a) syn-CaD_1-CaD_2 shear zone in basal conglomerate unit of the "eastern" Ahrberg Group, in Timbs Creek. Quartzite clasts have undergone high levels of flattening and stretching, with stretching lineations gently plunging to the south (left of photograph); (b) close up of flattened clast, with south plunging fibres visible; (c) syn-CaD_1-CaD_2 sheared quartz segregations interlayered with quartzite clasts, south is up, (d) sheared quartz segregations implying dextral shear sense, south is up. Segregations are interpreted to be CaD_1-, deformed during CaD_2 Pen is 16 cm in length (345350 mE, 5392080 mN), (e) mesoscopic, parasitic isoclinal CaF_2 folds in psammite, in the "eastern" Ahrberg Group, west coast sub-domain. Folds plunge moderately to the south (52/174)(location (iii) on Figure 2.32(d)); (f) close up of CaF_2 hinge, axial plane dips steeply to the southeast (75/120). CaL_{01} intersection lineations plunge steeply to the southwest (70/214) (location (iii) in Figure 2.32d)(333550 mE, 5374460 mN).

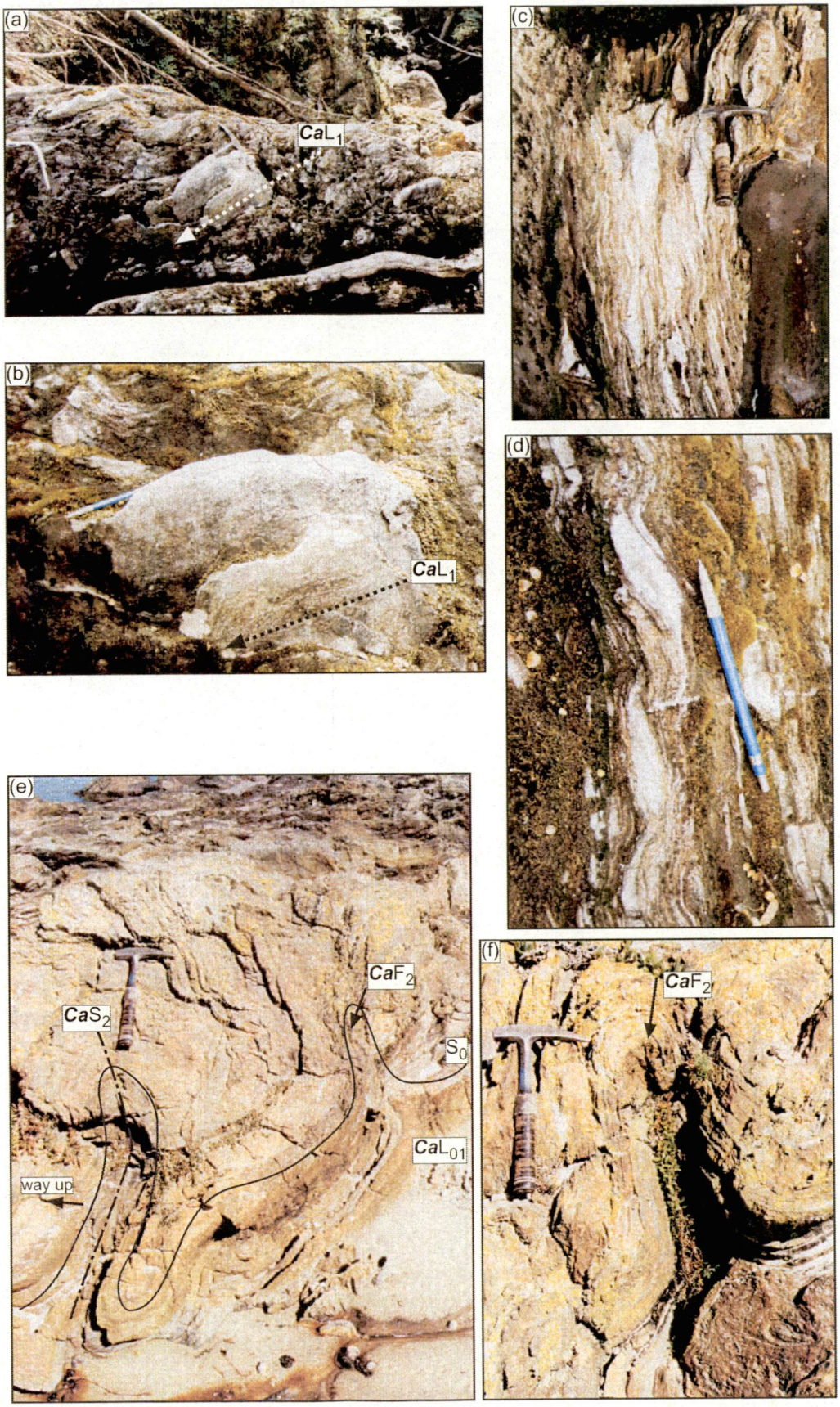

Figure 2.33(a)-(f).

Figure 2.34. Structural cross sections B' to L', of the "eastern" Ahrberg Group in the high strain zone of the Arthur Lineament, in the southern study area. Sections are oriented 290/110, with east to the right. Data on factual sections (top of set) are corrected to apparent dip. Interpretive sections (bottom of set) take into account vergence relationships presented on factual sections. Coordinates for each section are presented at the ends of the section lines. Locations of sections are illustrated on Figure 2 2(b).

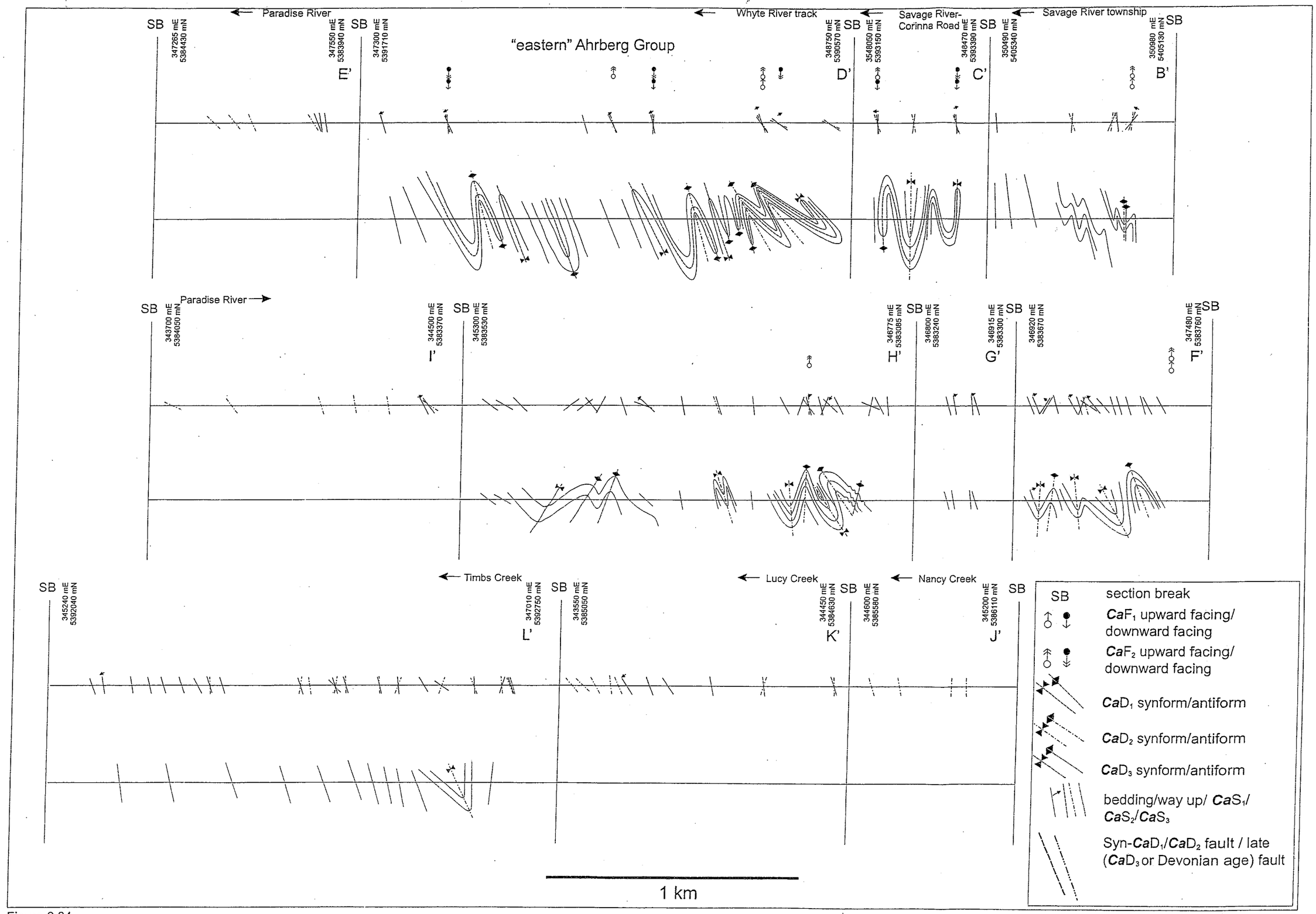
Paradise River
Whyte River track
Savage River-Corinna Road
Savage River township
"eastern" Ahrberg Group
SB
347265 mE 5384430 mN
347550 mE 5383940 mN
347300 mE 5391710 mN
348750 mE 5390570 mN
3548050 mE 5393150 mN
348470 mE 5393390 mN
350490 mE 5405340 mN
350980 mE 5405130 mN
E'
D'
C'
B'
Paradise River
343700 mE 5384050 mN
344500 mE 5383370 mN
345300 mE 5383530 mN
346775 mE 5383085 mN
346800 mE 5383240 mN
346915 mE 5383300 mN
346920 mE 5383670 mN
347480 mE 5383760 mN
I'
H'
G'
F'
Timbs Creek
Lucy Creek
Nancy Creek
345240 mE 5392040 mN
347010 mE 5392750 mN
343550 mE 5385050 mN
344450 mE 5384630 mN
344600 mE 5385580 mN
345200 mE 5386110 mN
L'
K'
J'
1 km
section break
CaF1 upward facing/ downward facing
CaF2 upward facing/ downward facing
CaD1 synform/antiform
CaD2 synform/antiform
CaD3 synform/antiform
bedding/way up/ CaS1/ CaS2/CaS3
Syn-CaD1/CaD2 fault / late (CaD3 or Devonian age) fault

Figure 2.34

where outcrop was limited, macroscopic scale $Ca F_1$ and $Ca F_2$ folds can be interpreted from vergence relationships observed in the field (Figure 2.34)

As in the Bowry Formation, the "eastern" Ahrberg Group features multiple $Ca S_1$ and $Ca S_2$-parallel faults. These are interpreted to be early structures, and reflect the strong shearing associated with the early deformation in the high strain zones of the Arthur Lineament. In areas of extensive outcrop, such as near the Reece Dam powerstation (see section 2.4.4.1) and on the west coast, to the north of the Duck Creek cover sequence, the style, and frequency of faulting can be elucidated (Figure 2.32(a) and (b)). In the "eastern" Ahrberg Group, as can be seen on the west coast, syn-$Ca D_{1-2}$ faults are common. However, in Timbs, Lucy and Nancy Creeks, and the Paradise and Whyte River areas (Figure 2.34), syn-$Ca D_{1-2}$ faulting was not observed, most likely as a result of the limited outcrop. On the west coast (Figure 2.32), syn-$Ca D_{1-2}$ faults parallel the respective foliations and cause structural repetition of lithologies. Although the $Ca D_{1-2}$ dislocation surfaces are narrow, planar features, zones of up to 5 m, either side of the faults consist of abundant $Ca S_{1-2}$–parallel quartz segregations. In some instances, the segregations are sigmoidal, implying dextral movement, and taking into consideration the stratigraphic way up, suggest transport to the south (Figure 2.33(a) to (d)). Field observations indicate that within these zones, the $Ca S_1$ and $Ca S_2$ foliations are intensely developed, with cleavage domains becoming narrower and microlithons becoming more pronounced.

2.4.5 Southern study area: structure of the western low strain zone ("western" Ahrberg Group and Rocky Cape Group correlates)

To the west of the Arthur Lineament, structural mapping has been carried out in the "western" Ahrberg Group and Rocky Cape Group correlates. As described in Chapter 1, the "western" Ahrberg Group is faulted against the "eastern" Ahrberg Group, forming the western boundary of the Arthur Lineament. The "western" Ahrberg Group sequence unconformably overlies the Rocky Cape Group correlates, at a low angle. Both of these units are interpreted to be *in situ* (Figure 2.9(c)).

Mapping in the "western" Ahrberg Group and Rocky Cape Group correlates was carried out in the following areas:

- Mt Donaldson and numerous un-named tributaries flowing off its slopes,
- Guthrie and Sabbath Creeks,
- the Western Explorer Road from the junction with the Savage River-Corinna Road to north of the Longback (341660 mE, 5402320 mN),
- the Longback and Crescent Hills,
- outcrop along the Pieman River from Corinna to west of the mouth of the Donaldson River (334100 mE, 5390700 mN),
- outcrop on Four Mile Beach, on the west coast.

The geographical features are illustrated in Figure 2.2(b), and a summary of the areas mapped is presented in Figure 2.15 (area i). In the study area, the Rocky Cape Group correlates have not been strongly deformed prior to deposition of the "western" Ahrberg Group. However, the contact between the two units is a low angle (0-15°) unconformity. Outside the study area, other workers have suggested the unconformity reflects a major structural break, during which the Rocky Cape Group and correlates were strongly deformed (E. Williams and P.W. Baillie, in Turner 1989). Alternatively, Gee (1967a,b) interpreted the unconformity (also outside the study area) to be unrelated to folding, and a result of the depositional angle of the basal unit of the overlying sequence. The earliest deformation observed in this study, in both sequences, corresponds with $\boldsymbol{Ca}D_1$, however this event is not widely developed. On this basis, the structural history of the Rocky Cape Group correlates and the "western" Ahrberg Group will be discussed together. Further to this, the orientation and style of the different deformational events throughout the areas examined in this region are consistent (across both units), and therefore will be examined and discussed as a single entity.

Within the western low strain zone, bedding orientations vary, and predominantly lie on a great circle which suggests folding about a south plunging axis (Figure 2.5). Deformation relating to $\boldsymbol{Ca}D_1$ and $\boldsymbol{Ca}D_2$ are evident in the eastern parts of the Rocky Cape Group correlates and the "western" Ahrberg Group, however they are not strongly represented. $\boldsymbol{Ca}D_3$ is the most strongly developed deformation in this

region, and is interpreted to largely control the orientation of S_0. As ***Ca***D_3 is not related to the high strain deformation which has formed the Arthur Lineament, the ***Ca***D_3 event will be discussed separately, in section 2.5.

CaD_1 rapidly decreases in intensity outside the lineament. ***Ca***S_1 is only observed as a weak, finely spaced S_0-parallel foliation, defined by muscovite. It dips steeply to the east-northeast (80/065) (Figure 2.5). ***Ca***F_1 are not observed. ***Ca***D_2, while being substantially weaker than within the lineament, was recognised up to 2.5 km to the west of the lineaments western boundary. In rare instances, the ***Ca***S_1 and ***Ca***S_2 foliation were observed in pelitic layers, several kilometres to the west of the lineament (Figure 2.9(a), locations (i) to (iv)). Where ***Ca***S_2 is evident, it is a weakly developed differentiation cleavage, with 1-2 mm wide cleavage domains and parallel microlithons (Figure 2.4(g) and (h)). ***Ca***S_2 also dips steeply to the east-northeast (75/080) (Figure 2.5). ***Ca***F_2 are close to tight folds, visible on a microscopic scale, and inferred in cross section (Figure 2.9(c), Figure 2.35). ***Ca***L_{02} intersection lineations are uncommon, and plunge gently to the north and south, with an average direction of 1/000 (Figure 2.5). In the Rocky Cape Group correlates, key examples of the overprinting relationships between ***Ca***S_1, ***Ca***S_2 and ***Ca***S_3 are seen at (i) Sabbath Ck (339200 mE, 5394155 mN), (ii) Crescent Hills (343860 mE, 5401800 mN) and on the Longback Ridge (iii) (340600 mE, 5395280 mN). Less well preserved examples are seen in the "western" Ahrberg Group at (iv) Elizabeth Ridge (340530 mE, 5388750 mN) (Figure 2.9(a)).

2.5 ***Ca***D_3 and Devonian deformation

Throughout the study area, deformation relating to ***Ca***D_3 has been recorded, but it is patchy in its development. To the west of the Arthur Lineament, in the Rocky Cape Group correlates and the "western" Ahrberg Group, ***Ca***D_3 is pervasive, and it is the dominant deformational event. However, within the lineament, ***Ca***D_3 is sporadically developed, and to the east of the lineament, it is uncommon, with most areas examined showing little or no evidence of this deformation. As a consequence of this, the following section concentrates on the Rocky Cape Group correlates and the "western" Ahrberg Group, where these deformational events are best developed.

Figure 2.35. Microscopic ***Ca***F_2 fold in graphitic (black) and micaceous (light grey) mudstone (view along fold axis). Very finely spaced ***Ca***S_2 is axial planar to the fold, dips to the right. Fine to medium spaced ***Ca***S_3 dislocates and crenulates the CaS_2 foliation, and dips to the left. Sample OHH1019 (343860 mN, 5401800 mN).

Within the Rocky Cape Group and the "western" Ahrberg Group, $Ca F_3$ have west-dipping axial planes, with steeply east-dipping to overturned eastern limbs and gently west-dipping, 'right way up' western limbs (Figure 2.9(a) and (c), and Figure 2.36(a) to (c)). Both mesoscopic and macroscopic $Ca F_3$ folds were observed (Figure 2.9(e) and (c), Figure 2.36(a) to (c)). The $Ca F_3$ hinges plunge gently to steeply to the south (Figure 2.9(b) and Figure 2.37), but show some variation in orientation due to subsequent refolding by the Devonian deformation. Quartzite on the overturned eastern limbs is commonly strongly boudinaged (Figure 2.9(f) and (g)), and has the same plunge and plunge azimuth as the $Ca F_3$ fold hinges.

In some examples from within the "eastern" Ahrberg Group, where $Ca D_3$ is locally developed, south-plunging $Ca F_3$ are observed with east-dipping axial planes (Figure 2.38(a)), however the mesoscopic development of $Ca D_3$ in these areas is rare. Furthermore, $Ca S_3$ is most commonly west-dipping (Figure 2.36(a) to (c) and Figure 2.37). At this location in the Paradise River (Figure 2.38(a) and (b)), the $Ca S_3$ foliation is well developed, and crenulates the $Ca S_2$ schistosity. The east dip of $Ca S_3$ at this outcrop is interpreted to be the result of subsequent Devonian refolding.

Throughout the "western" Ahrberg Group and Rocky Cape Group correlates, the west-dipping $Ca S_3$ cleavage is pervasive, and it is the dominant foliation (Figure 2.36(a) to (c)). $Ca S_3$ is developed in most lithologies, although it is strongest in siltstone and mudstone units (Figure 2.38(c) to (e)). It is a spaced (3-5 mm) cleavage, with parallel cleavage domains and discrete microlithons and dips towards the west (40/265)(Figure 2.4(g) and (h), Figure 2.9(d) and (e), and Figure 2.36(a) to (c) and Figure 2.37). In the Rocky Cape Group correlates and the "western" Ahrberg Group, $Ca S_3$ is observed crenulating $Ca S_2$, and cutting S_0 at a high angle (Figure 2.4(g) and (h)). However, most examples of this overprinting relationship were observed to the west of the Arthur Lineament, in areas where $Ca S_3$ is well developed.

Along the Pieman River, the outcropping contact between the Rocky Cape Group correlates and the "western" Ahrberg Group displays critical field relationships, typifying the $Ca D_3$ event in this region, to the west of the Arthur Lineament (Figure 2.9). At this location, the contact between the Rocky Cape Group correlates and the

Figure 2.36(a) Structural cross sections M' to V', in the Crescent Hills and Longback range areas; (b) structural cross sections W' to A", in the Mt Donaldson area; (c) structural cross sections G' to I", in the Mt Donaldson and Four Mile Beach areas. Lithological sequences include the Rocky Cape Group correlates and the "western" Ahrberg Group in the western low strain zone (see Figure 2.5 and Figure 2.15); (b), to the west of the Arthur Lineament in the southern study area. Sections are oriented 290/110, with east to the right. Data on factual sections (top of set) are corrected to apparent dip. Interpretive sections (bottom of set) take into account vergence relationships presented on factual sections. Coordinates for each section are presented at the ends of the section lines. Locations of sections are illustrated on Figure 2.2(b).

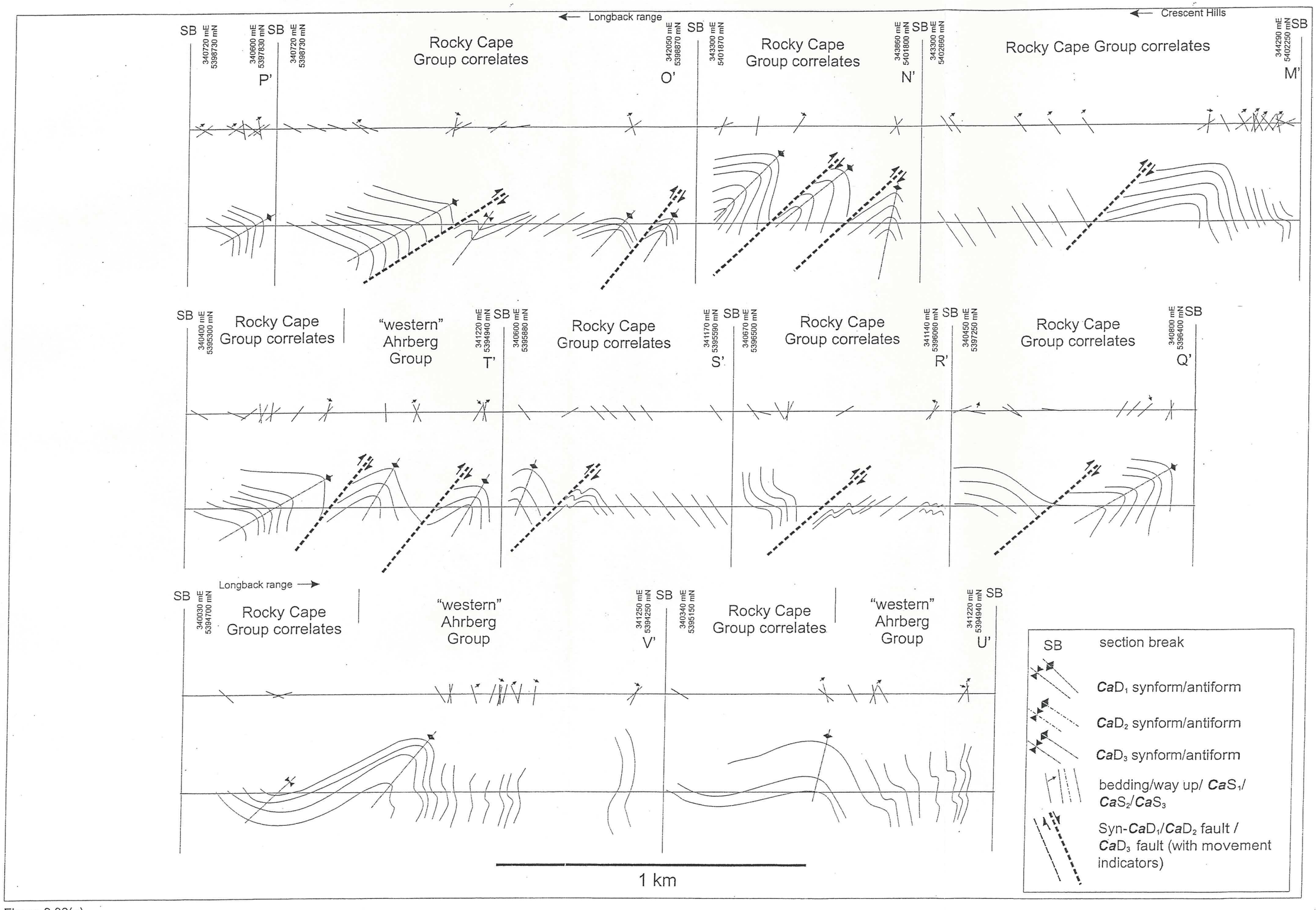
Longback range
Crescent Hills
SB
340720 mE 5398730 mN
340600 mE 5397830 mN
340720 mE 5398730 mN
342050 mE 5396870 mN
343300 mE 5401870 mN
343860 mE 5401800 mN
343300 mE 5402660 mN
344290 mE 5402250 mN
P'
O'
N'
M'
Rocky Cape Group correlates
340400 mE 5395300 mN
341220 mE 5394940 mN
340600 mE 5395880 mN
341170 mE 5395590 mN
340670 mE 5396500 mN
341140 mE 5396060 mN
340450 mE 5397250 mN
340800 mE 5396400 mN
"western" Ahrberg Group
T'
S'
R'
Q'
340030 mE 5394700 mN
341250 mE 5394250 mN
340340 mE 5395150 mN
341220 mE 5394940 mN
V'
U'
1 km
section break
CaD1 synform/antiform
CaD2 synform/antiform
CaD3 synform/antiform
bedding/way up/ CaS1/ CaS2/CaS3
Syn-CaD1/CaD2 fault / CaD3 fault (with movement indicators)

Figure 2.36(a)

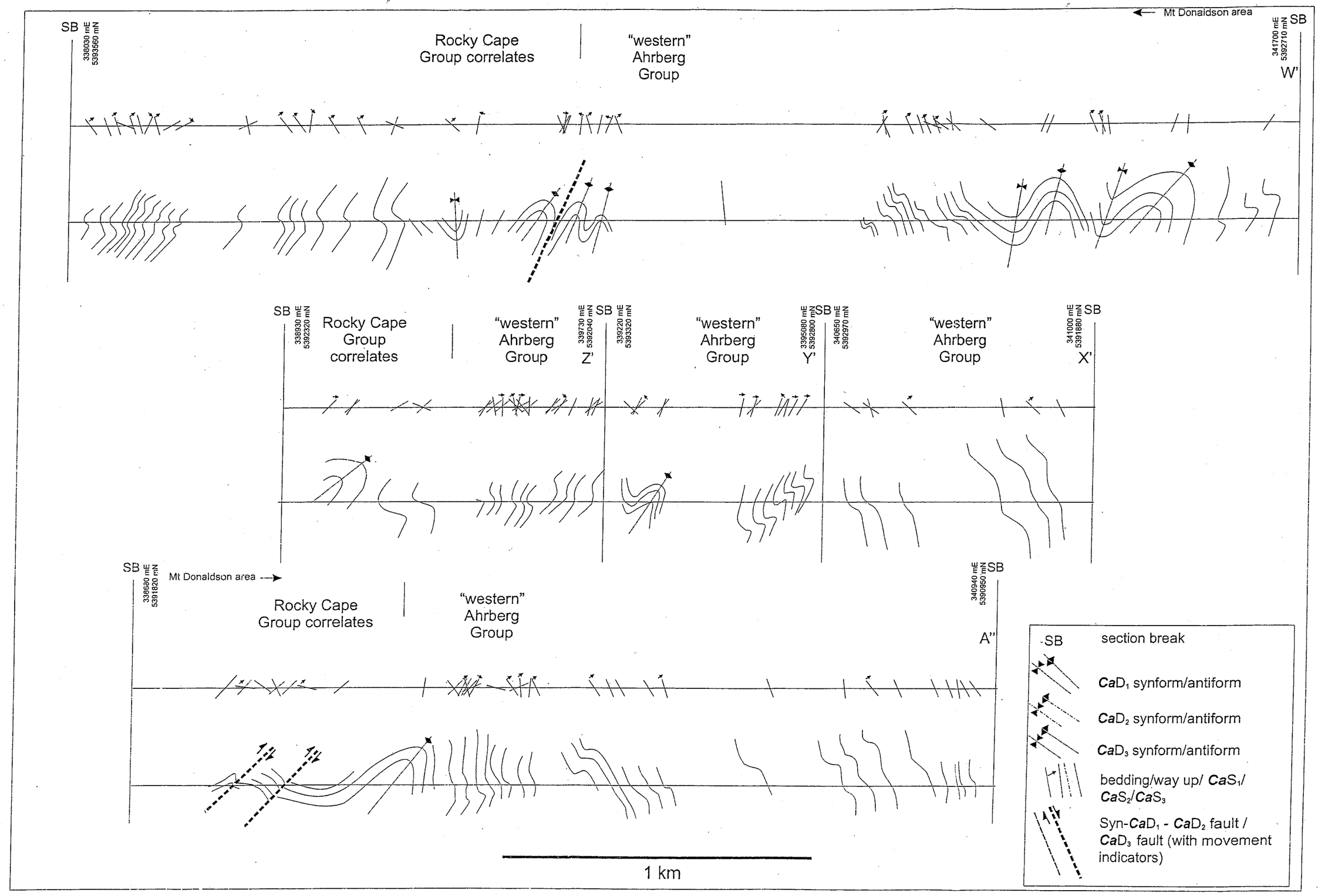
SB
338030 mE
5393560 mN
Rocky Cape
Group correlates
"western"
Ahrberg
Group
Mt Donaldson area
341700 mE
5392710 mN
SB
W'
SB
338930 mE
5392320 mN
Rocky Cape
Group
correlates
"western"
Ahrberg
Group
339730 mE
5392040 mN
Z'
SB
339220 mE
5393320 mN
"western"
Ahrberg
Group
3395080 mE
5392800 mN
Y'
SB
340650 mE
5392970 mN
"western"
Ahrberg
Group
341000 mE
5391880 mN
SB
X'
SB
336630 mE
5391920 mN
Mt Donaldson area
Rocky Cape
Group correlates
"western"
Ahrberg
Group
340940 mE
5390950 mN
SB
A"
1 km
SB
section break
CaD1 synform/antiform
CaD2 synform/antiform
CaD3 synform/antiform
bedding/way up/ CaS1/ CaS2/CaS3
Syn-CaD1 - CaD2 fault / CaD3 fault (with movement indicators)

Figure 2.36(b)

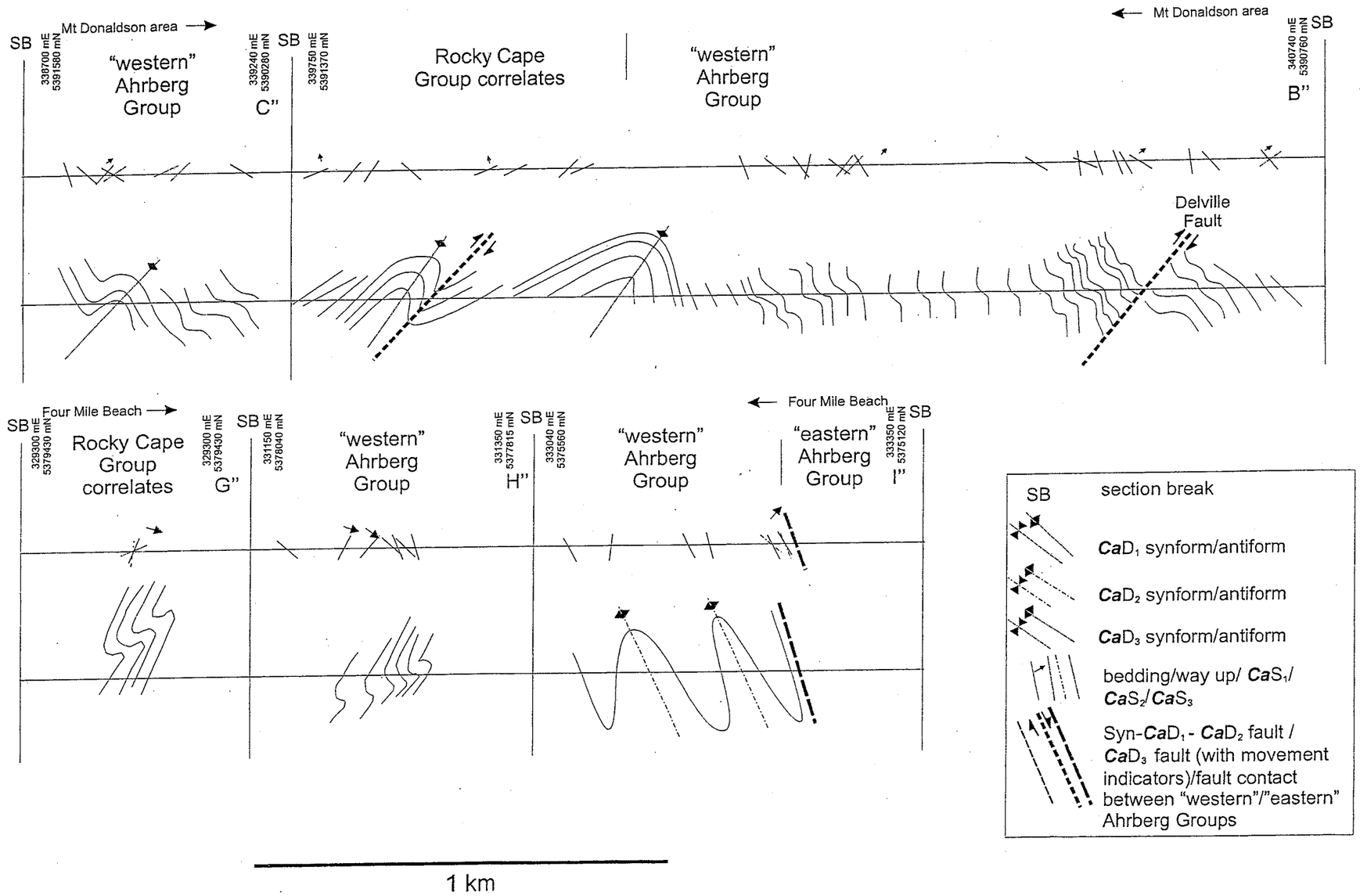
SB
338700 mE
5391580 mN
Mt Donaldson area
"western" Ahrberg Group
SB
338240 mE
5390280 mN
C"
SB
339750 mE
5391370 mN
Rocky Cape Group correlates
"western" Ahrberg Group
Mt Donaldson area
SB
340740 mE
5390760 mN
B"
Delville Fault
SB
329300 mE
5379430 mN
Four Mile Beach
Rocky Cape Group correlates
SB
329300 mE
5379430 mN
G"
SB
331150 mE
5378040 mN
"western" Ahrberg Group
SB
331350 mE
5377815 mN
H"
SB
333040 mE
5375560 mN
"western" Ahrberg Group
Four Mile Beach
"eastern" Ahrberg Group
SB
333350 mE
5375120 mN
I"
1 km
SB
section break
CaD1 synform/antiform
CaD2 synform/antiform
CaD3 synform/antiform
bedding/way up/ CaS1/ CaS2/CaS3
Syn-CaD1 - CaD2 fault / CaD3 fault (with movement indicators)/fault contact between "western"/"eastern" Ahrberg Groups

Figure 2.36(c)

Figure 2.37. Stereographic projections for the $Ca D_3$, $De D_4$ and $De D_5$ events in the southern Arthur Lineament and surrounding area. Planes ($Ca S_3$, $De S_4$ and $De S_5$) are presented as poles. As these later deformational events are do not show strong local variability, the study area is considered as a single structural domain.

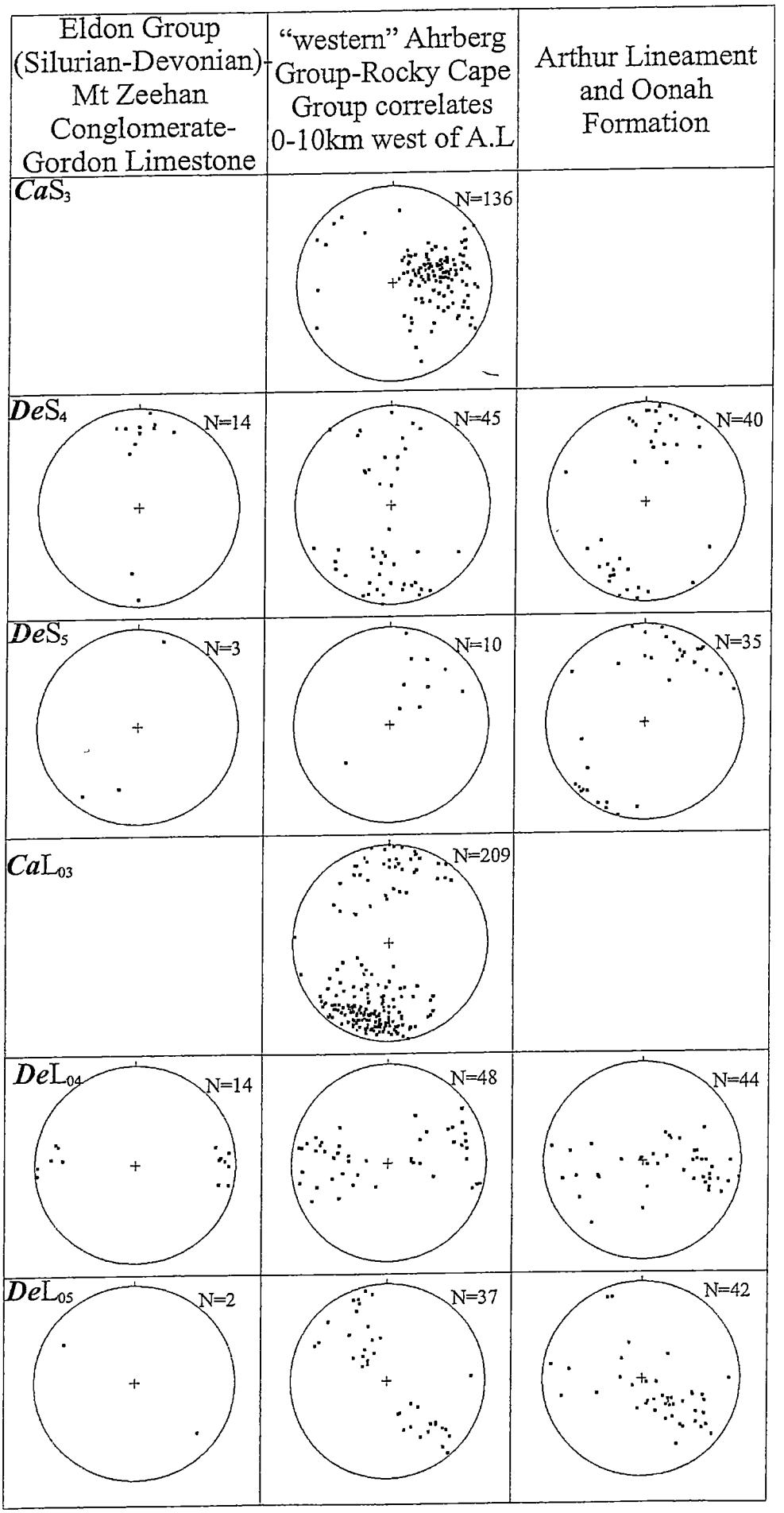
Eldon Group (Silurian-Devonian)- Mt Zeehan Conglomerate-Gordon Limestone
"western" Ahrberg Group-Rocky Cape Group correlates 0-10km west of A.L
Arthur Lineament and Oonah Formation
CaS3
N=136
DeS4
N=14
N=45
N=40
DeS5
N=3
N=10
N=35
CaL03
N=209
DeL04
N=14
N=48
N=44
DeL05
N=2
N=37
N=42

Figure 2.37

Figure 2.38(a) mesoscopic $\boldsymbol{Ca}F_3$ in psammopelitic schist, in the Paradise River area. Bedding was observed, and is overturned, younging to the left. The axial planar $\boldsymbol{Ca}S_3$ spaced foliation is visible, and crenulates earlier surfaces. Fold axis trends 34/193, axial plane trends 47/103; (b) photomicrograph of psammopelite in (a) (sample 73). The $\boldsymbol{Ca}S_3$ axial planar foliation (dipping to the left) crenulates the dominant $\boldsymbol{Ca}S_2$ schistosity, which features syn-$\boldsymbol{Ca}D_2$ albite porphyroblasts and dips to the right (346460 mE, 5383020 mN); (c) $\boldsymbol{Ca}S_3$ foliation (30/305) is penetrative in siltstone layers, but is not developed in quartzite interbeds, positioned on the right way up, gently west dipping long limb of a $\boldsymbol{Ca}F_3$ fold, Longback range area in the Rocky Cape Group correlates, to the west of the Arthur Lineament (western low strain zone) (341480 mE, 5398920 mN); (d) mesoscopic $\boldsymbol{Ca}F_3$ fold with axial planar $\boldsymbol{Ca}S_3$ cleavage development, dipping to the west (right), and weakly overprinted by Devonian age cleavage $\boldsymbol{De}S_4$, Crescent Hills area in the Rocky Cape Group correlates. Pen is 13.5 cm in length, (344230 mE, 5402310 mN); (e) pervasive $\boldsymbol{Ca}S_3$ spaced cleavage developed in silstone beds (dark grey) grading up from thin sandstone layers (light grey), Crescent Hills area in the Rocky Cape Group correlates (344160 mE, 5402260 mN).

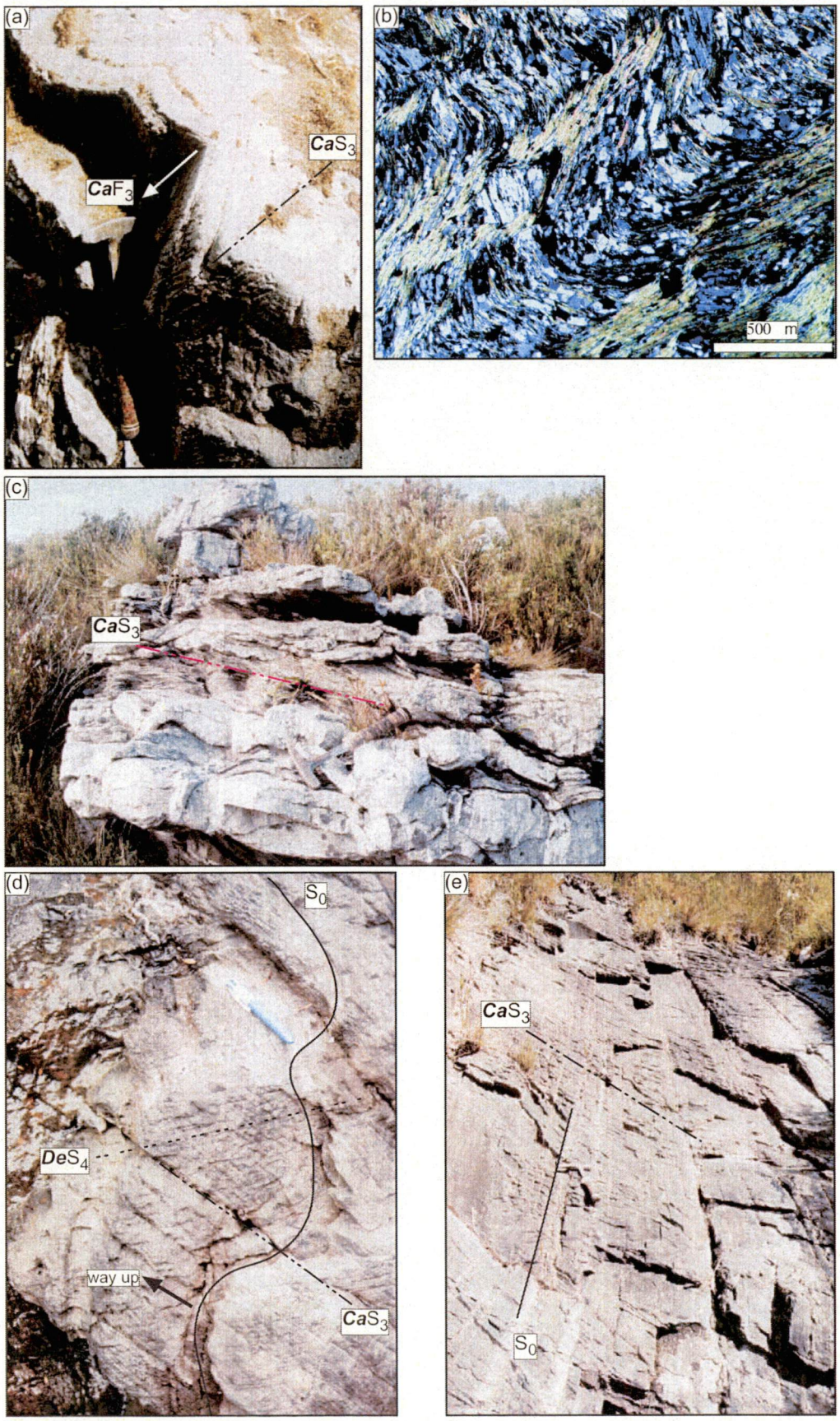

Figure 2.38(a)-(e).

"western" Ahrberg Group is positioned on the steeply west-dipping, overturned eastern limb of a macroscopic ***Ca***F_3 fold (Figure 2.39(a)). As a result of this structural position, the younger "western" Ahrberg Group is structurally underneath the older Rocky Cape Group correlates. Other examples of the overturned limb position are the mesoscopic, downward facing parasitic ***Ca***F_3 folds within siltstone layers interbedded with boudinaged quartzite (Figure 2.9(f) to (i)). Although the ***Ca***S_3 axial planar cleavage does not penetrate the boudinaged quartzite beds, it is well developed in the surrounding sandstone layers that have a silty matrix (Figure 2.9(h) and (i)). Elswhere in the region, where the boundary between the two units is not positioned on the hinge of a macroscopic ***Ca***F_3, the "western" Ahrberg Group unconformably overlies the Rocky Cape Group correlates at low angle (0-15°) (339060 mE, 5392080 mN).

The pervasiveness of the ***Ca***D_3 event to the west of the Arthur Lineament is evident in the topography of the Mt Donaldson-Longback-Crescent Hills area. This area corresponds to the boundary between the Rocky Cape Group correlates and the "western" Ahrberg Group, and is controlled by ***Ca***D_3-related strike ridges (Figure 2.39(b)). The ridges are produced by the weathering-resistant quartzite sequence (the uppermost unit of the Rocky Cape Group correlates in this region) and conglomerate-dominated sequence (the basal unit of the "western" Ahrberg Group in this region), which outcrop in this area, and are located on the steeply east-dipping short limbs of macroscopic ***Ca***F_3. In addition to the contact of the two weathering-resistant sequences, the region coincides with the hinge zone of a regional ***Ca***F_3 antiform. The north-south trending valleys that separate the strike ridges correspond with recessive siltstone and mudstone sequences, and west-dipping, syn-***Ca***D_3 thrust faults. The easternmost ridge in the Crescent Hills area, which is along strike of the Longback, is also composed of a series of asymmetric ***Ca***F_3 antiforms, with syn-***Ca***D_3 thrust faults separating the steeply east-dipping to overturned eastern limbs from the gently west dipping western limbs (Figure 2.36(a), Sections M'and N').

Folding attributed to the Devonian deformation was also observed in this region, however it is patchy in its development. In the south of the study area, two Devonian deformations were recorded. These have been interpreted to represent D_4 and D_5 of the Devonian deformational episode (herein ***De***D_4 and ***De***D_5), based on

Figure 2.39(a). Overturned basal conglomerate of the western Ahrberg Group, positioned on short limb of macroscopic ***Ca***F_3 fold, in the Pieman River area. The axial planar ***Ca***S_3 cleavage dips less steeply, in the same direction as bedding. To the right of the picture Rocky Cape Group correlates overly the younger western Ahrberg Group sequence. Photograph is 50 m across. (337200 mE, 5389975 mN);

Figure 2.39(b). Looking to the south along ***Ca***F_3-related, strike controlled ridges in the Rocky Cape Group correlates, Crescent Hills area. Ridges are coincident with steeply east dipping, short limbs of macroscopic ***Ca***F_3 folds, and are dominated by quartzite beds. Valleys correspond to recessive beds (photograph taken at 343300 mE, 5402660 mN).

previous work (see section 2.3.4). In most areas, ***De***F_4 folds are minor, weakly developed, mesoscopic scale (1 metre wavelength) folds and rarely produce an axial planar fabric. However well developed ***De***F_4 and ***De***S_4 were observed (Figure 2.40). In addition, some localised areas feature zones of intense deformation attributed to ***De***D_4. These areas are dominated by ***De***D_4 related folding and faulting (Figure 2.41(a) and (b)). The ***De***F_4 folds are open, and mostly plunge gently to the east. ***De***D_4 related faulting is brittle in style, and occurs in localised zones of intense deformation (Figure 2.41(a) and (b)).

In the Rocky Cape Group correlates and the "western" Ahrberg Group, only ***De***S_5 was observed. It is mostly finely spaced foliation (1-5 mm) with cleavage domains varying between parallel and anastamosing, and weakly crenulates earlier foliations. The cleavage typically dips steeply to the north and south, and produces variably oriented intersection lineations (Figure 2.37). There are minor examples of ***De***S_5-parallel extensional quartz veins, which occur in the hinge zones of the ***De***F_5 folds.

Open ***De***F_5 folds overprint ***De***F_4 and produce dome-and-basin interference patterns. The best developed examples of ***De***F_5-***De***F_4 dome-and-basin style folding is near the Devonian granitoids in the vicinity of Granville Harbour (Figure 2.2(a)).

In the Reece Dam area the ***Ca***D_2-related features change orientation from Domain S1 to S2 (Figure 2.27(c)). Unlike the changes in orientation of the ***Ca***D_1 and ***Ca***D_2–related features between Domains N1, N2 and N3 due to shear-related rotation, stereonet analysis indicates the change in orientation from Domain S1 to S2 is the result of refolding by the ***Ca***D_3, ***De***D_4 and ***De***D_5 events. Rotation of the eastern domain ***Ca***S_2 and ***Ca***L_{02} about the ***De***F_5 axis (30°/130°) 50° in an anticlockwise direction (looking down plunge), changes the ***Ca***S_2 orientation from 45°/150° to 55°/090° and the ***Ca***L_{02} orientation from 25°/230° to 15°/020°. This angle corresponds to the refolding caused by the ***De***F_5 event. ***Ca***D_1- and ***Ca***D_2-related faulting and shearing in Domain S2 are ***Ca***S_1- and ***Ca***S_2-parallel respectively, and also differ in orientation between Domains S1 and S2 due to rotation caused by subsequent refolding.

Figure 2.40. Mesoscopic ***De***F_4 (plunging 44/080), developed psammopelite and pelite interbeds in the "eastern" Ahrberg Group, west coast area. Broad, kink style axial planar cleavage (***De***S_4) is visible, trending 88/210 (location (iv) on Figure 2.32(d)) (333485 mE, 5374685 mN).

Figure 2.41. Zone of intense ***De***D_4 deformation in the "eastern" Ahrberg Group, west coast area (location (v) on Figure 2.32(d)). (a) open, kink style ***De***F_4 folds plunge gently to the east (44/082) and have axial planes dipping steeply to the south (75/170), although axial planar cleavage is poorly developed foreground is 10 m wide. Syn- ***De***D_4 fault planes bound the area, and have apparent dextral offsets. Locations of bounding faults area labelled A to E; (b) sketch map of the area, indicating plunge direction of folding and apparent movement along fault planes, fault labels correspond with (a) (333885 mE, 5374180 mN)

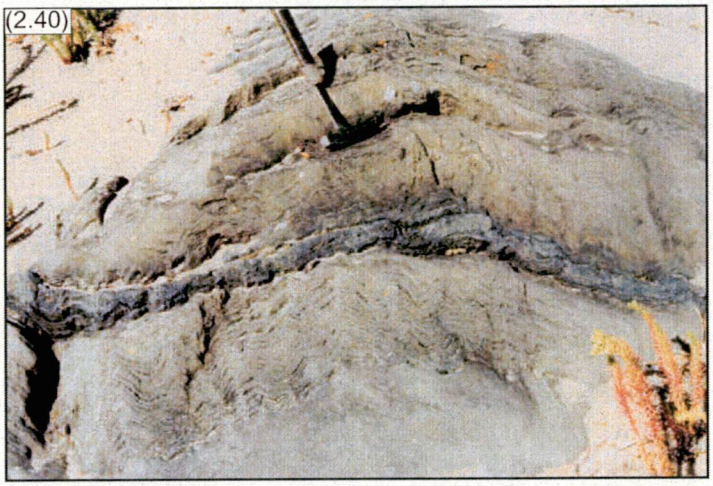
(2.40)

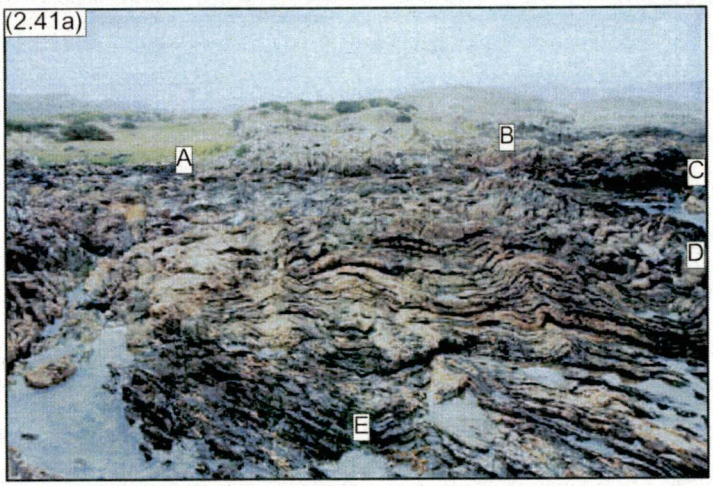
(2.41a)
A
B
C
D
E

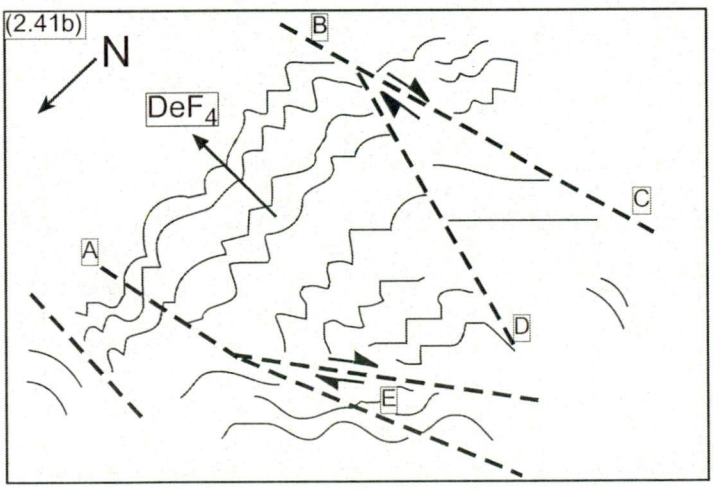
(2.41b)
N
B
DeF4
C
A
D
E

2.6 Discussion

Despite a distance of 60 km separating the outcrop studied in the north (Somerset-Doctors Rocks area) and south (Reece Dam and Corinna areas) of the Arthur Lineament, there is strong evidence supporting the correlation of deformational events between these areas. Evidence for the Cambrian age deformations (***Ca***D_1-***Ca***D_3) being widespread regional events is supported by mapping in the southern Arthur Lineament, where the fabric associated with these deformations have been mapped over a 40 x 10 km area. The ***Ca***D_1 and ***Ca***D_2 events in the Somerset-Doctors Rocks area are correlated with those in the south of the Arthur Lineament (Reece Dam and surrounding area), based on the consistent style of ***Ca***D_1 and ***Ca***D_2 features, orientations, and the interference relationships. In both areas the ***Ca***S_1 and ***Ca***S_2 foliations increase in intensity from a spaced cleavage to a schistosity approaching the lineament from the east. Widespread interference between the strongly developed high strain ***Ca***D_1 and ***Ca***D_2 events, followed by overprinting of the less intense third Cambrian deformation (***Ca***D_3) and subsequent multiple Devonian age deformations (***De***D_1, ***De***D_4, ***De***D_5) has resulted in complex, outcrop patterns. The orientations of the dominant, early structures are regionally consistent, but show local evidence of refolding.

In the Somerset-Doctors Rocks area, the ***Ca***D_1 and ***Ca***D_2 structures change orientation from east to west. The ***Ca***D_1 event is interpreted to be a major deformational event, but overprinting by the intensely developed ***Ca***D_2 event obscures many of the ***Ca***D_1 structures. Within Domains N1 and N2 recognisable ***Ca***D_1 structures are rare. Throughout Domains N1 to N3 the orientation of the ***Ca***D_1 structures is dependent on the intensity of ***Ca***D_2 and the ***Ca***F_2 fold position. Several ***Ca***D_1 thrust faults, folded by ***Ca***F_2 and transected by ***Ca***S_2, are present along the attenuated ***Ca***F_1 limbs.

The most significant change in orientation of ***Ca***L_{01} and ***Ca***L_{02} occurs at the boundary between Domains N2 (low strain) and N3 (high strain) (Figure 2.10(e))(398780mE, 5457890mN). This location also corresponds with a major early shear zone, interpreted to be Cambrian in age (***Ca***D_2). In Domain N2, on the overturned ***Ca***F_2 limbs, ***Ca***L_{01} and ***Ca***L_{02} plunge to the east-southeast. Close to the

shear zone, the orientation of $\boldsymbol{Ca}L_{01}$ and $\boldsymbol{Ca}L_{02}$ rotates. On the predominantly high strain western side of the shear zone (Domain N3), the lineations plunge towards the south-southwest.

The change in plunge and plunge azimuth of $\boldsymbol{Ca}L_{01}$ and $\boldsymbol{Ca}L_{02}$ from the low strain zone to the east of the lineament, to the high strain zone within the lineament is consistent both in the north of the study area, and in the south. In the Savage River to Reece Dam region (southern study area), outside the lineament (Eastern Low Strain Zone) and close to its eastern margin (Moderate-High Strain Zone), areas with steeply plunging $\boldsymbol{Ca}L_{01}$ and $\boldsymbol{Ca}L_{02}$ are present (Figures 2.5 and 2.15). However, within the lineament, in the high strain Oonah Formation and the "eastern" Ahrberg Group, $\boldsymbol{Ca}L_{01}$ and $\boldsymbol{Ca}L_{02}$ have consistent shallow plunges to the south, or locally, shallowly to the north.

Further to this, outcrop on the west coast, between Granville Harbour and Ahrberg Bay shows a similar change in structural style and $\boldsymbol{Ca}L_{01}$ and $\boldsymbol{Ca}L_{02}$ lineation direction to the Savage River-Reece Dam area. The coastal exposure of the southern Arthur Lineament is divided into southern and northern areas, separated by the weakly deformed Ordovician Duck Creek sequence (Figures 2.22 and 2.32). The two areas have distinctive differences in structural style, reflecting different strain intensities. The southern area exposes the moderate to high strain transition zone of the eastern boundary of the Arthur Lineament, with deformed Oonah Formation and "eastern" Ahrberg Group correlates outcropping. This area is dominated by $\boldsymbol{Ca}F_1$ and $\boldsymbol{Ca}F_2$ folding, with infrequent faulting observed (Figure 2.22). $\boldsymbol{Ca}L_{01}$ and $\boldsymbol{Ca}L_{02}$ lineations plunge moderately to steeply to the northwest and southeast. In contrast, the northern area exposes the high-strain zone well within the Arthur Lineament. The lithologies are more strongly deformed, and while $\boldsymbol{Ca}F_1$ and $\boldsymbol{Ca}F_2$ folding is common, thrust faults causing repetition of units are much more frequent (Figure 2.32). Here the $\boldsymbol{Ca}L_{01}$ and $\boldsymbol{Ca}L_{02}$ lineations on average plunge moderately to the south. The increase in faulting and strain from the southern area to the northern area is accompanied by a change in orientation of $\boldsymbol{Ca}F_1$ and $\boldsymbol{Ca}F_2$, into alignment with the lineaments dominant north-south stretching direction.

The uniform change in orientation of $\boldsymbol{Ca}L_{01}$ and $\boldsymbol{Ca}L_{02}$ from the low strain domain to the high strain domain, over the length of the southern study area (45 km) (Figure 2.5), is considered to be a result of syn-$\boldsymbol{Ca}D_2$ rotation due to increasing strain. Based on similarities with examples of shear-related rotation discussed by Ridley & Casey (1989) and Dewey *et al.* (1998), it is suggested that the change in orientation associated with $\boldsymbol{Ca}D_2$ described above is the result of a strongly rotational shear component with a north-south stretching direction in the high strain zone at the core of the Arthur Lineament.

The east-west trend of the $\boldsymbol{Ca}F_2$ hinges and fold vergence in Domain N1 can be interpreted to reflect south-directed transport, provided the overturning occurred during $\boldsymbol{Ca}D_2$. The alternative possibility is that the $\boldsymbol{Ca}F_2$ are downward facing because of a pre-existing $\boldsymbol{Ca}F_1$ overturned limb. This is considered to be unlikely based on the evidence that the rotational high strain history cannot predate $\boldsymbol{Ca}D_2$. Both $\boldsymbol{Ca}F_1$ and $\boldsymbol{Ca}F_2$ are rotated into the Arthur Lineament high strain zone by the same amount and at the same position. Thus the rotational strain must have formed during $\boldsymbol{Ca}D_2$. The regional scale of the overturned limb (more than 60 Km by 7 km) and its close spatial relationship to the Arthur Lineament argues for a close genetic link of the overturned limb to the most intense event within the lineament.

The Corinna area to the west of the Arthur Lineament is dominated by the $\boldsymbol{Ca}D_3$ event. Although this study only includes the "western" Ahrberg Group and Rocky Cape Group to the west of the southern Arthur Lineament, work by Everard *et al.* (1996) indicates this event is also prominent in the Trowutta area to the west of the Arthur Lineament further north. In the Corinna area the style and orientation of the $\boldsymbol{Ca}F_3$ folding indicates east-west compression and a west-over-east transport direction. This suggests a change in the structural regime probably during the Late Cambrian.

The Devonian deformation is interpeted to have caused localised changes in orientation of the earlier structures. On a regional scale (Figure 2.2(a)), changes in orientation of surfaces are evident. The trend of bedding, Cambrian age structural foliations and fold axes on the west coast are notably different to other parts of the southern study area (iv(a) and v(a) on Figure 2.5). This is interpreted to result from

the refolding of the east-dipping lineament, about a gently southeast plunging fold axis of a regional scale, as can be suggested from the change in orientation evident in Figure 2.2(b).

2.7 Conclusion

Gee (1967a) and Gee (1977) interpreted the main deformation in northwestern Tasmania (***Ca***D_2 in this work) as the earliest event, during which the Rocky Cape Group and the Burnie Formation were transported to the southeast and deformed against the Precambrian Tyennan Nucleus. Further to this Gee (1967a) concluded that this event produced shallow plunging folds trending northeast-southwest (***Ca***F_3 in this work) and recumbent folds (***Ca***F_2 in this work) in conjunction with the metamorphism defining the Arthur Lineament.

The ***Ca***D_1 event (not described by Gee 1967a, Gee 1967b, and Gee 1977) is interpreted to represent major shearing producing isoclinal folds and bedding-parallel thrust faults (Figure 2.42(a)). ***Ca***D_2 produced widespread areas of low and high strain. The change in style and orientation of ***Ca***F_2 from areas of low to high ***Ca***D_2 strain suggests the change is the result of rotational strain (Figure 2.42(a) and (b)). The rotation of ***Ca***F_2 into the Arthur Lineament is interpreted to result from north-south extension along a shallowly dipping detachment, with some evidence supporting south-southwest-directed transport. This resulted in the juxtaposition of the allochthonous Bowry Formation and parautochthonous "eastern" Ahrberg Group with the "western" Ahrberg Group and Oonah Formation.

The early stages of formation of the Arthur Lineament involved two folding events. The first deformation (***Ca***D_1) produced a schistose axial planar fabric and isoclinal folds synchronous with thrusting (Figure 2.42(a)). The second deformation (***Ca***D_2) produced a coarser schistosity and tight to isoclinal folds (Figure 2.42(a) and (b)). South-plunging, north-south stretching lineations, top to the south shear sense indicators, and south-verging, downward facing folds in the Arthur Lineament suggest south-directed transport. However at the base of ophiolite sheets elsewhere in western Tasmania, also emplaced in the Cambrian, hornblende mylonites indicate a more westerly transport direction. ***Ca***F_1 and ***Ca***F_2 were rotated to a north-south

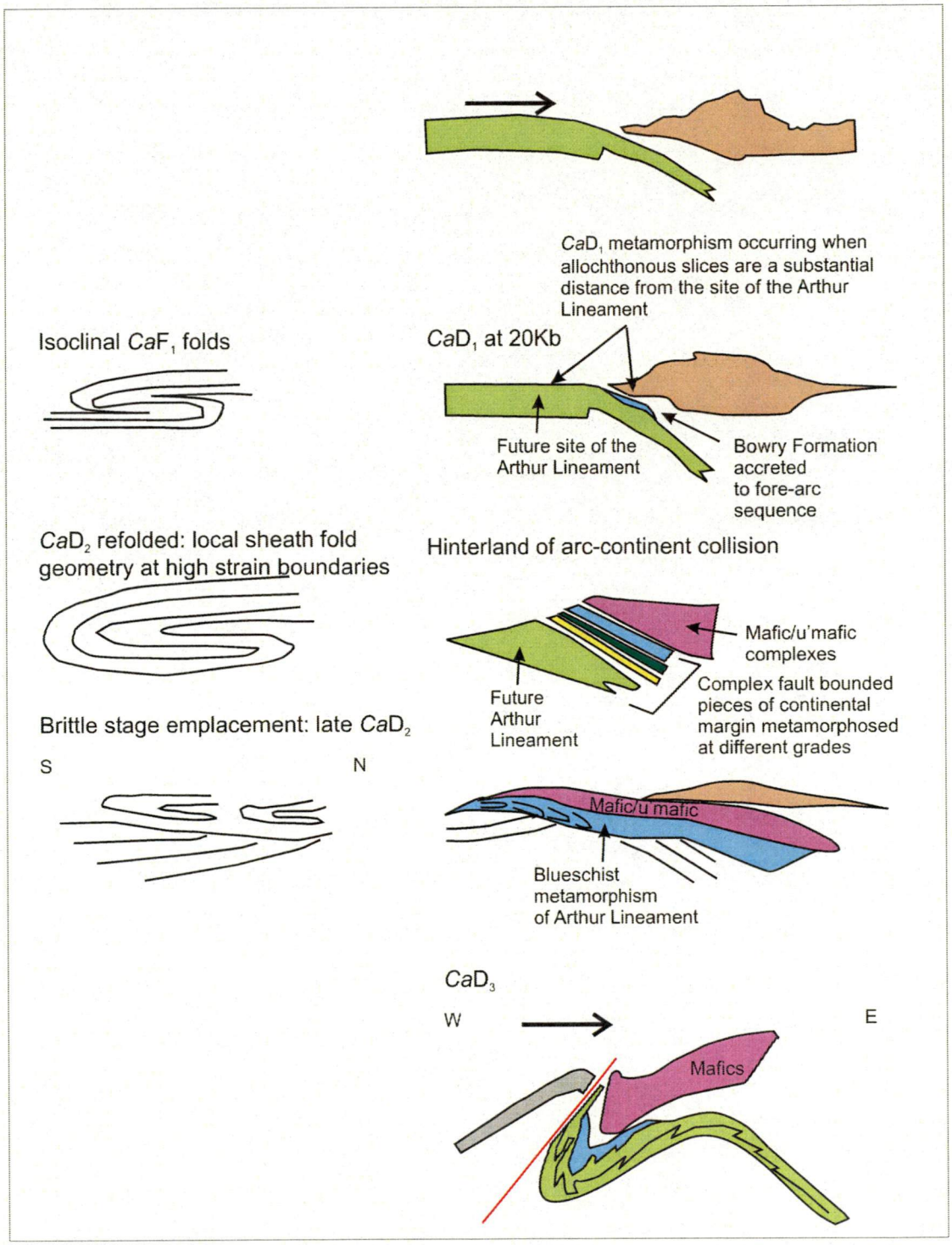

Figure 2.42(a) . Stages of the Cambrian arc-continent collision resulting in formation of the Arthur Lineament.

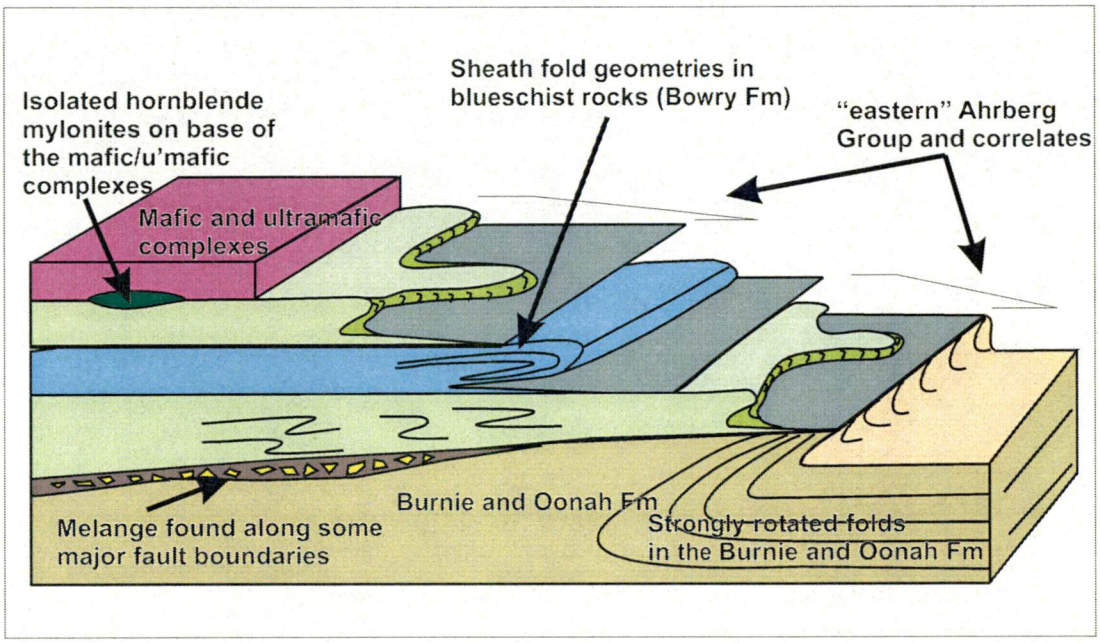

Figure 2.42(b).Schematic diagram emphasising the stacking of variable type sheets (not always in order).

trend in zones of high strain during the ***Ca***D_2 event. ***Ca***D_3, later in the Cambrian, folded the earlier foliations in the Arthur Lineament and produced west dipping steep thrusts, creating the linear expression of the structure (Figure 2.42(a)). Subsequent open folding during the Devonian has caused localised variability.

At the conclusion of the ***Ca***D_2 event, the lineament is interpreted to have been a sub-horizontal feature, with the various slices being vertically stacked. The interpretation of a shallowly dipping detachment is largely based on the Somerset-Doctors Rocks area. Where ***Ca***D_3 is weak (Domains N1 and N3), ***Ca***D_2 structures are sub-horizontal. In this area, ***Ca***S_2 dips gently to the south and southeast, and ***Ca***F_2 fold axes have gently plunges, to the east and west (in Domain N1) and to the south (in Domain N3). There is no evidence for a later structure that could have rotated this foliation from an original steep dip. However where ***Ca***D_3 is more strongly developed (Domain N2, and the southern Arthur Lineament), the ***Ca***D_2 features are moderately to steeply dipping. The transition from a sub-horizontal structure to an east-dipping structure along most of the Arthur Lineament, probably occurred as a result of the folding and thrusting during ***Ca***D_3, resulting in the present linear expression of the structure (Figure 2.43(a) and (b)). During the Middle Devonian, further folding resulted in localised dome-and-basin style folds and additional variability in the trend of the Arthur Lineament.

The detailed structural studies within the Arthur Lineament indicate a strong north-south extension on the detachments during the Cambrian. A similar stretching direction occurs in the allochthonous high strain rocks of the Ulverstone Metamorphic Complex, 20km to the east. Reed (2001) has recognised evidence for very early (syn-D_1) thrusting to the SE in the Badger Head Complex. Meffre *et al.* (2001) have reported Cambrian south directed transport on mylonites in the Port Davey Metamorphic Complex. All these structures have been correlated with arc-continent collision and ophiolite subduction (Berry 1994). The hornblende mylonites exposed within metres of the base of the ophiolite sheets show a west to southwest-directed transport direction when reoriented to a pre-Devonian orientation (Berry 1989). These hornblende mylonites formed at a high temperature (>700°C) based on the mineral chemistry. In contrast the structures in the Arthur Lineament

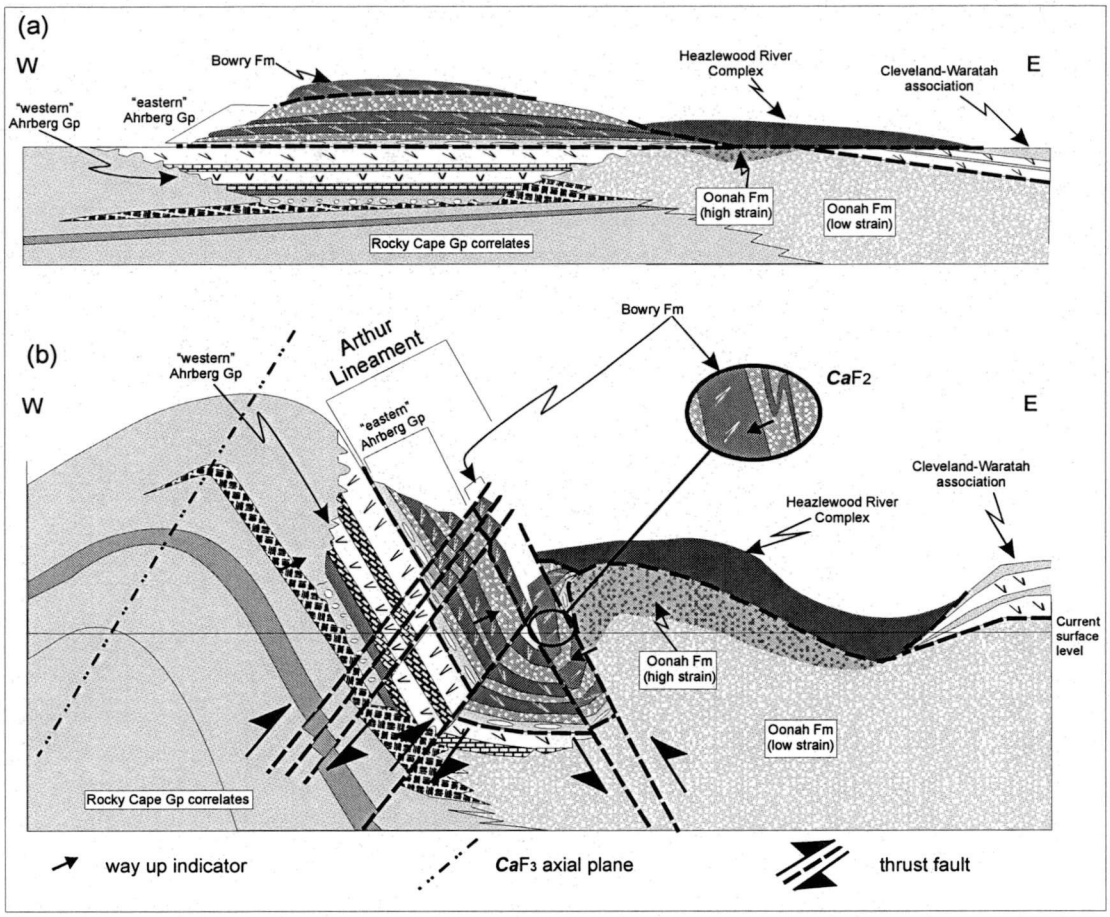

Figure 2.43(a) and (b). Schematic sections showing the formation of the southern Arthur Lineament. (a) emplacement of allochthonous and parautochthonous slices over sub-horizontal Neoproterozoic stratigraphy during the ***Ca***D_1 and ***Ca***D_2 events; (b) intense folding and faulting (***Ca***D_3) leading to the present linear expression of the Arthur Lineament. Lineament. Refer to Figure 2.2 for legend. Heazlewood River Complex is an allochthonous ultramafic complex. Cleveland-Waratah association consists of tholeiitic basalts, and marine sediments and is interpreted to be part of an oceanic melange unit associated with emplacement that was obducted onto western Tasmania in the late Early or early Middle Cambrian (Berry & Crawford 1988, Brown & Jenner 1988, Seymour & Calver 1995). West dipping faults in 2.43(b) are interpreted to be syn-***Ca***D_3, east-dipping thrust faults are late, age uncertain.

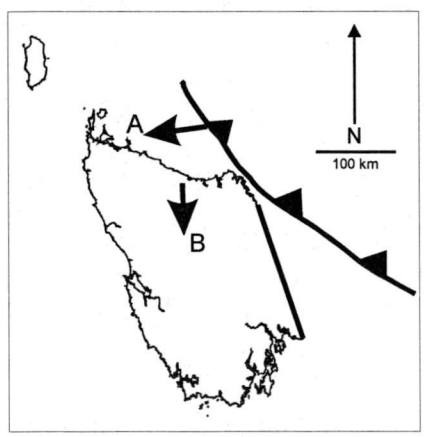

Figure 2.44. Schematic diagram of Tasmania during the west-directed obduction of oceanic fore-arc in the late Early or early Middle Cambrian. A. Transport direction based on hornblende mylonite at the base of the ophiolite bodies (Berry 1989). B. Transport direction inferred from the Arthur Lineament and Port Davey Metamorphic Complex.

formed at greenschist to low amphibolite facies conditions. The difference in these directions is interpreted to represent a change in ophiolite transport direction (Figure 2.44) from an early vector towards the west to a south directed transport in the later stages of the emplacement onto Tasmania.

CHAPTER 3

METAMORPHISM OF THE ARTHUR LINEAMENT

3.1 Introduction

Northwestern Tasmania has been affected by several orogenic events during the Mesoproterozoic to Cambrian. Holm *et al.* (2001) have shown that metasediments on King Island underwent metamorphism at around 1250 Ma, and were intruded by syn-deformational, 760 ± 12 Ma granitoids, as part of the Wickham Orogeny (Cox 1973, Turner *et al.* 1998). A deformed granitoid dated at 777 ± 7 Ma (Turner *et al.* 1998) occurs within the allochthonous Bowry Formation of the Arthur Lineament. The Bowry Formation granitoid is thought to be similar in origin to the 760 ± 12 Ma Cape Wickham granitoid on King Island (Turner *et al.* 1998). The geochemical similarity of the granitoids is discussed in Chapter 4.

The subsequent Tyennan Orogeny commenced around 510 Ma, in the early part of the Middle Cambrian. It is correlated with the Delamerian Orogeny in South Australia. The Tyennan Orogeny is widely represented in western Tasmania, and featured crustal collision with associated emplacement of ultramafic-bearing allochthons and high P, low T metamorphism (Turner *et al.* 1998). The medium to high strain deformation and low to medium grade metamorphism in the Arthur Lineament is a result of the Tyennan Orogeny (Turner *et al.* 1998) (Figure 3.1). The early structural events in the lineaments deformational history were accompanied by varying levels of metamorphism, with variation in peak conditions evident between the Bowry Formation and other units of the lineament (Figure 3.2(a)). However, contention exists over whether the metamorphic boundaries are gradational and lithological boundaries are conformable, or whether the lineament represents a series of faulted slices of different composition and metamorphic grade.

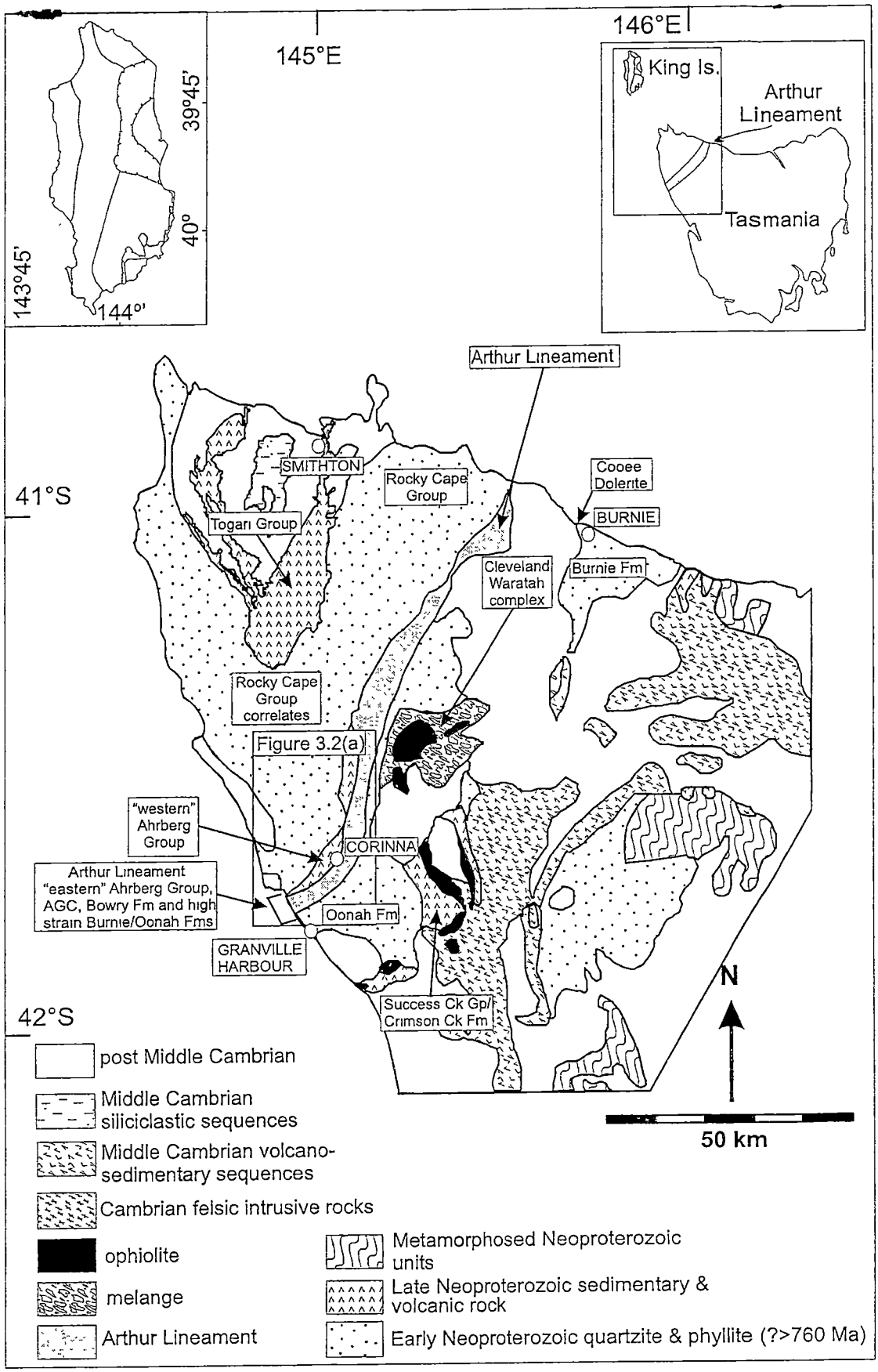

Figure 3.1. Setting of the Arthur Lineament, NW Tasmania (modified after Brown *et al.* 1995). The Arthur Lineament consists of the high strain (metamorphosed) Burnie and Oonah Formations, the "eastern" Ahrberg Group, the Bowry Formation, and the AGC. King Island geological detail is provided on Figure 3.40.

The Arthur Lineament is comprised of:

- The "eastern" Ahrberg Group and correlates, consisting of a deformed Late Neoproterozoic rift sequence, including psammitic and psammopelitic metasediments, tholeiitic metabasites and metadolerites
- The Bowry Formation, consisting of deformed metadolerites, metabasites, massive and banded magnetite layers, deformed granitoids and mafic metasediments
- The Burnie and Oonah Formations, consisting of strongly deformed metasedimentary lithologies.

The moderately deformed Burnie and Oonah Formations occur to the east of the lineament (Figure 3.1 and Figure 3.2(a)). To the west of the lineament, in the southern study area, the low strain, weakly deformed "western" Ahrberg Group is faulted against the lineament's western boundary. This unit unconformably overlies the weakly deformed correlates of the Rocky Cape Group, which crop out to the north and west of the "western" Ahrberg Group (Figure 3.2(a)).

The aim of this study into the metamorphic history of the Arthur Lineament and surrounding area is to define the distribution and nature of the different metamorphic events. An additional aim is to use the characteristics and age of metamorphic monazites found in the study area to investigate the timing of deformation in different regions.

In order to achieve these outcomes, an approach integrating field mapping and sampling, petrographic observations of strategically located samples (Figures 3.2(a) and (b)), microprobe analysis, and geothermobarometric techniques has been used.

3.2 Geothermobarometric techniques

In order to calculate the conditions of metamorphism (discussed in section 3.3, 3.4 and 3.5), the mineral stoichiometry and the activity of end-members were calculated using the AX (Activity Composition) program of Holland & Powell (1998). The AX program accepts raw microprobe data in the form of oxide weight percents and performs standard mineral recalculations, with attempts at ferric iron estimation. The

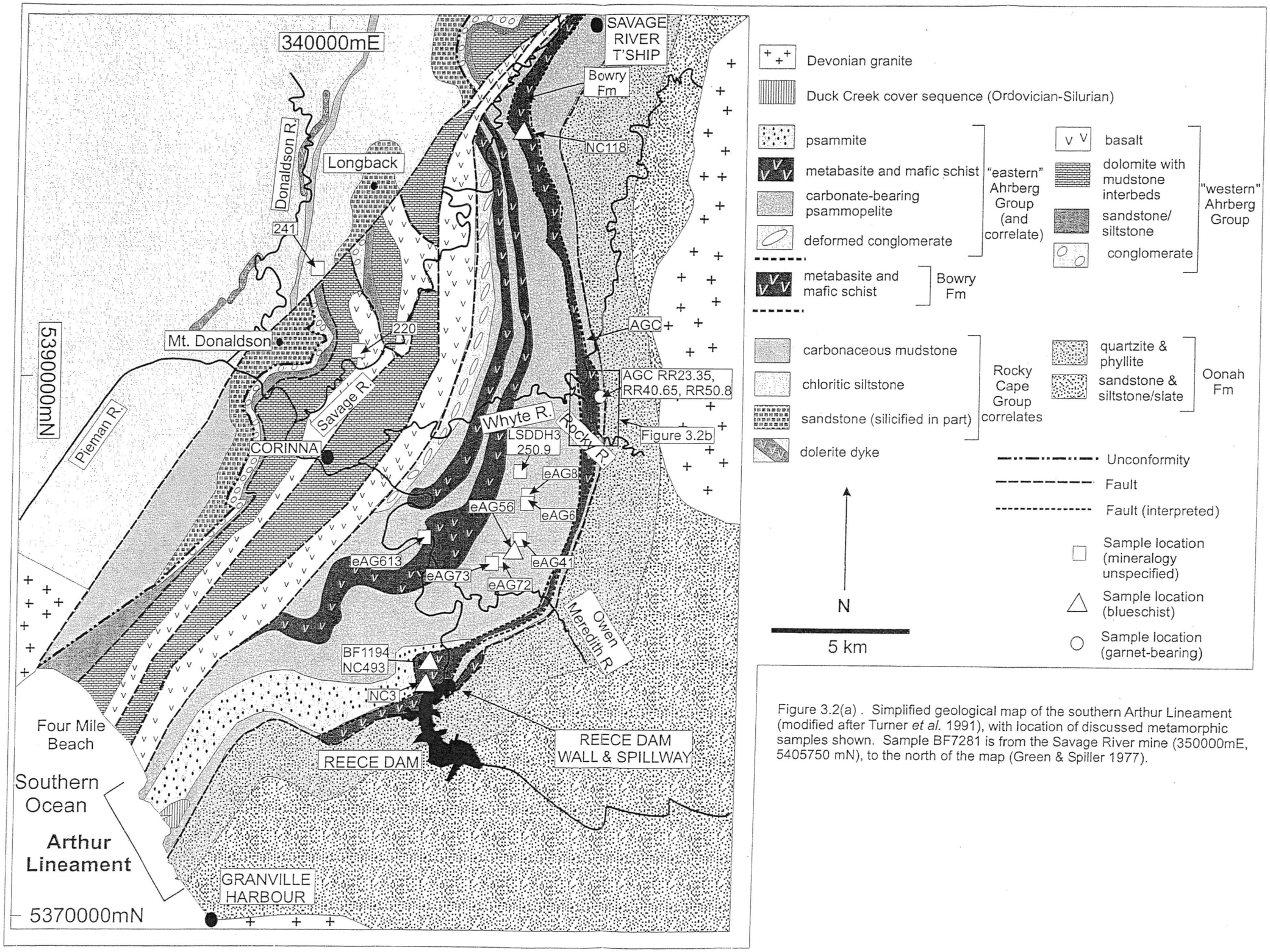

Figure 3.2(a) . Simplified geological map of the southern Arthur Lineament (modified after Turner *et al.* 1991), with location of discussed metamorphic samples shown. Sample BF7281 is from the Savage River mine (350000mE, 5405750 mN), to the north of the map (Green & Spiller 1977).

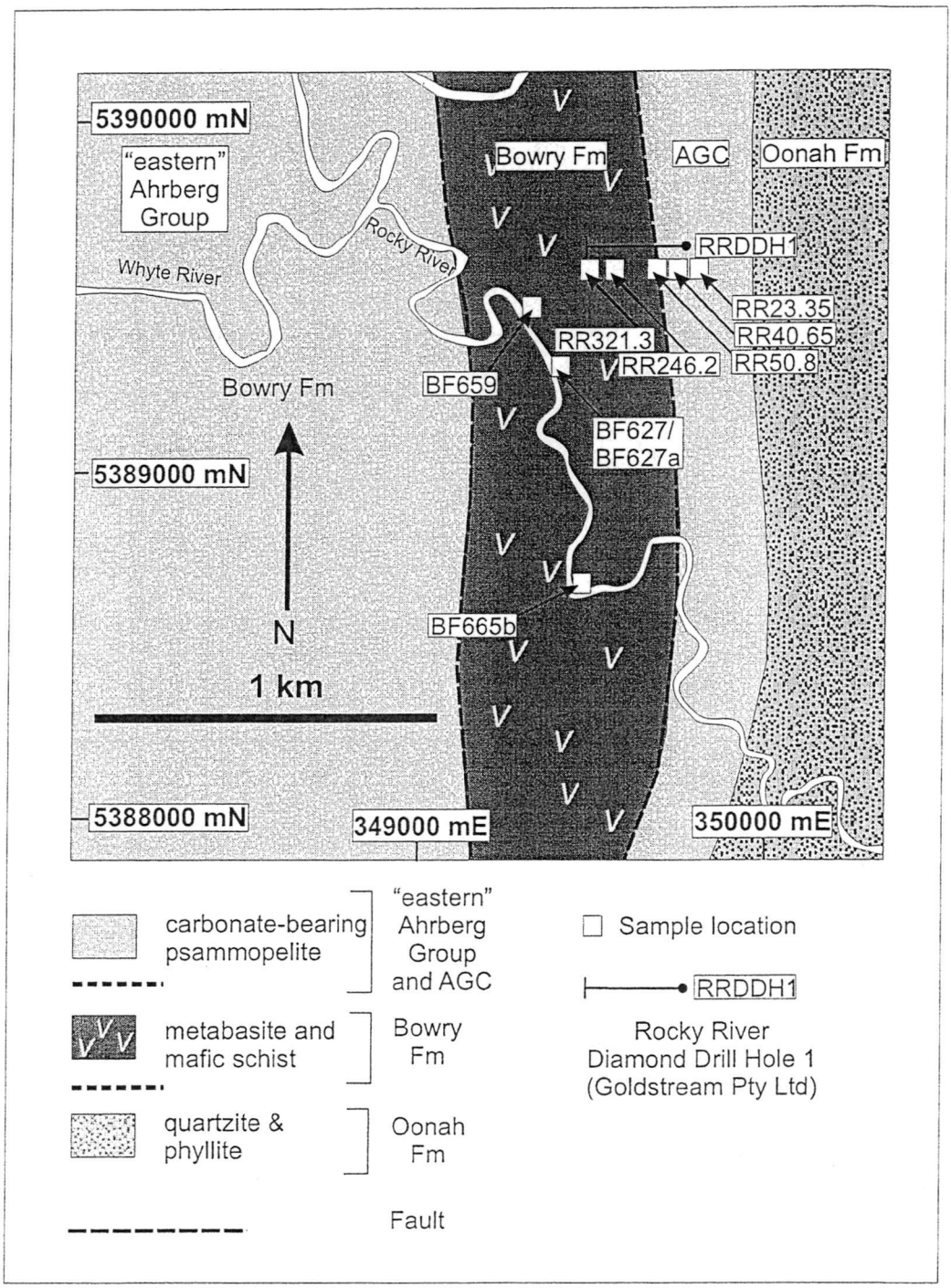

Figure 3.2(b). Location of metamorphic samples analysed (with electron microprobe) in the Rocky River area (modified after Turner *et al.* 1991).

program calculates activities for end-members that can then be used for rock calculations in THERMOCALC (Powell & Holland 1998, 2000). However, critical mineral assemblages were only present in a few samples. The results of geothermobarometric calculations using THERMOCALC (Powell & Holland 1998, 2000) are presented in Appendix 3.28.

Temperature estimates have been calculated using THERMOCALC (Powell & Holland 1998, 2000). For most samples pressure estimates are based on amphibole composition and the amount of Na allocated to the M4 site in the structural formula of amphiboles (Brown 1974, 1977). The amount of Na in the M4 site (expressed as Na^B) defines whether amphiboles are classified as calcic, sodic-calcic, or sodic (Leake *et al.* 1997). Brown (1974, 1977) presented the following buffering reaction, relating glaucophane of the blueschist facies and Ca-amphiboles of the greenschist facies:

glaucophane + epidote + H_2O = Ca-amphibole + albite + chlorite + iron oxide

The mineral assemblages in metabasites and mafic metasediments throughout the Arthur Lineament are broadly similar to the assemblages in the reaction of Brown (1974, 1977), and therefore support the use of the reaction as a geobarometer. However, Brown (1974, 1977) indicated that the pressures derived from the reaction have a moderate degree of accuracy, and they are used here as a relative indicator of pressure stability for the different amphibole compositions and mineral assemblages.

3.3 Metamorphism of the "eastern" Ahrberg Group and Ahrberg Group correlate

Within the "eastern" Ahrberg Group and Ahrberg Group correlate (AGC), metabasites and metadolerites are interlayered with the metasedimentary lithologies. Although the metasediments are more voluminous than the meta-igneous lithologies, the relatively simple mineral assemblage of the metasediments is not suitable for detailed geothermobarometric investigations. The mineral assemblages and mineral chemistry of the mafic meta-igneous lithologies is more useful. Therefore they have been examined in greater detail, and will be discussed first.

3.3.1 Metabasites

Mafic meta-igneous rocks are common in the "eastern" Ahrberg Group, and are mostly fine to medium grained. Rare coarse grained bodies were observed. The whole rock geochemistry of the meta-basic rocks is discussed in Chapter 4. The samples analysed were largely recrystallised, and primary igneous textures are rare. The level of strain of the rocks is varied, and within single bodies, contrasting levels of strain, relating to the proximity to the margin of the body, are apparent. However, most samples examined have a structural fabric. The meta-igneous rocks are composed of metamorphic minerals indicative of polyphase metamorphism, with upper greenschist facies assemblages dominating. They consist of quartz-albite-chlorite-epidote-amphibole-sphene ± (magnetite, titanomagnetite, rutile, carbonate, white mica, green biotite and/or tourmaline).

Petrography

In the metabasites, albite occurs as subhedral porphyroblasts (Figure 3.3(a)). They have inclusions of epidote and amphibole (Figure 3.3(b)). Quartz is polycrystalline and occurs interstitially with epidote, chlorite and sphene. The quartz grains have wavy extinction, indicative of deformation syn- to post-recrystallisation. Amphibole is blue green, brown green and pale blue-lavender in appearance (Figures 3.3(c) to (e)). It occurs as both fine grained, crystals, and as porphyroblasts, which are the dominant form. Epidote occurs as stubby to elongate, colourless to pale green crystals, that are subhedral to euhedral (Figure 3.3(f)). Chlorite is pale green, and wraps around the porphyroblast phases. In rare cases, it is intergrown with fine grained green biotite, which is also aligned with the dominant $\boldsymbol{Ca}S_2$ foliation (Figure 3.3(g)). Sphene was observed as very fine grained aggregates, that are intermixed with epidote. In addition, sphene occurs as overgrowths on titanomagnetite, which is the dominant opaque phase. In samples that are foliated, the dominant foliation ($\boldsymbol{Ca}S_2$) is defined by elongate aggregates of sphene, chlorite and actinolitic needles (Figure 3.3(h)). Garnet which has grown syn-$\boldsymbol{Ca}D_2$ occurs in some AGC metabasites

Figure 3.3(a) to (h) photomicrographs of metamorphic mineral assemblages in of the "eastern" Ahrberg Group and AGC. (a) albite porphyroblast, with minor inclusions of epidote and occurring within actinolite, quartz and chlorite, metabasalt sample 613; (b) albite porphyroblast with epidote inclusions, occurring with interstitial epidote, quartz and chlorite, metabasalt sample 72; (c) hornblende with actinolite rim, occurring with epidote, magnetite and chlorite, metabasalt sample 613; (d) randomly oriented hornblende occurring with chlorite in weakly foliated metabasalt, sample 8; (e) glaucophane with albite and quartz in unfoliated metadolerite, sample 56; (f) aligned epidote grains in foliated metabasalt, occurring with chlorite, metabasalt sample 32; (g) chlorite intergrown with green biotite, actinolite, sphene and albite, metabasalt sample 72; (h) wispy sphene aggregates interlayered with chlorite (defining the CaS_2 foliation) and occurring with magnetite, metabasalt sample 72.

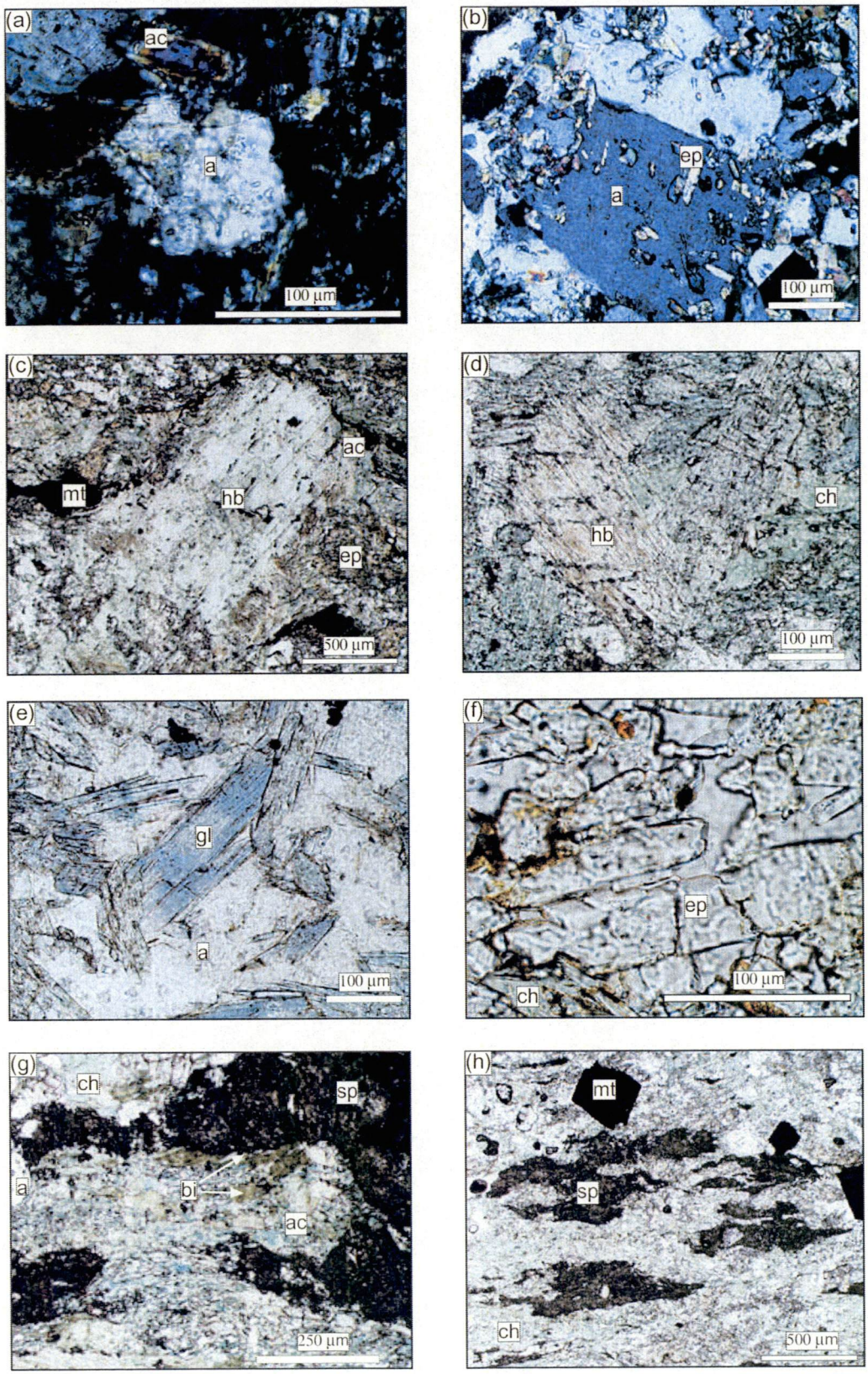

Figure 3.3(a) to (h).

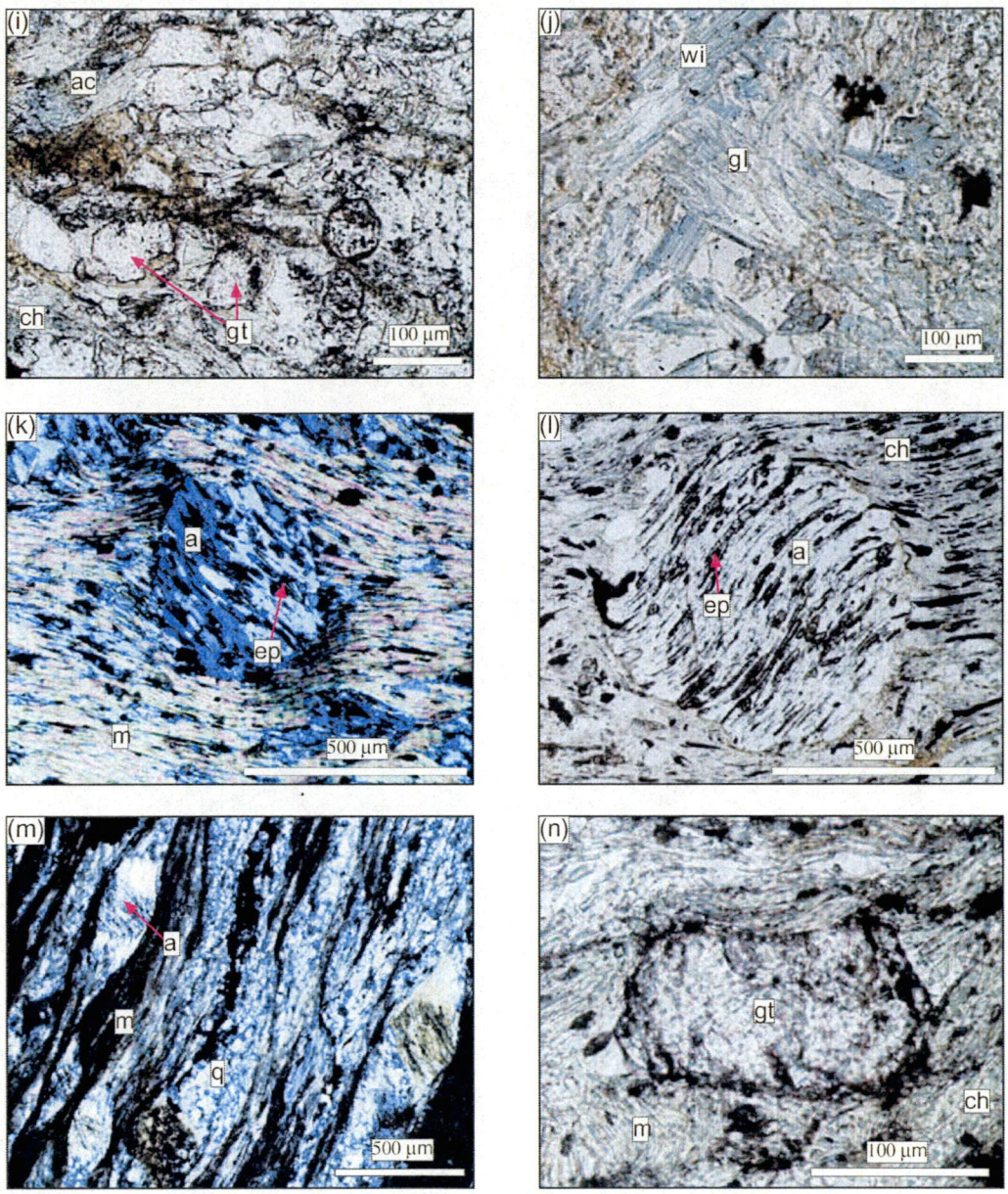

Figure 3.3. (i) to (n) photomicrographs of mineral assemblages in mafic meta-igneous rocks and metasedimentary schists of the eastern Ahrberg Group and AGC. (i) garnet porphyroblasts occurring with chlorite and retrogtrade actinolite in metadolerite of the AGC, sample RR40.65; (j) randomly oriented glaucophane and winchite occurring in unfoliated metadolerite, sample 56; (k) syn-CaD_2 albite porphyroblast heavily included by straight, CaS_2-aligned epidote, in white mica-rich domain, sample 73; (l) albite porphyroblast with CaS_2-aligned epidotes that are rotated at the margins of the albite porphyroblast, sample 608a; (m) albite porphyroblasts in quartz-albite-mica schist, with inclusions (S_i) that preserve the orientation of earlier deformation (CaS_1). S_i are rotated close to margins, (syn-CaD_2); (n) garnet porphyroblast aligned with CaS_2 and interpreted to be syn-CaD_2, interlayered with chlorite and white mica. a: albite, ch: chlorite, q: quartz, ep: epidote, m: white mica. bi: biotite, mt: magnetite, sp: sphene, gt: garnet, ac: actinolite, hb: hornblende, gl: glaucophane, wi: winchite.

and metadolerites (Figure 3.3(i)). The garnets are small, colourless, subhedral to euhedral grains, in some cases as inclusions in albite porphyroblasts.

The coarser grained metadolerites and metagabbros are uncommon, and in some cases preserve relict igneous textures. These are commonly unfoliated to very weakly foliated (Figure 3.3(j)), and have no preferred orientation of amphibole grains.

Mineralogy

Albite

Plagioclase feldspar was present in all of the metabasite and metadolerite samples that were studied (Appendix 3.1). Iron was calculated as Fe^{3+}. All plagioclase feldspar in the psammites and psammopelites of the "eastern" Ahrberg Group are albite (An_{0-2}) (Appendix 3.2).

Amphibole

Amphibole was present in all metabasites and metadolerites that were analysed. In the majority of samples, the amphibole has completely replaced pyroxene, and relict primary igneous textures were not observed. Relict igneous pyroxene has been reported from a metagabbro from the spillway of Reece Dam (Turner & Crawford 1993), however this was not confirmed. Amphiboles (Appendix 3.3) varied in composition, according to the Leake *et al.* (1994), across the range of calcic, sodic-calcic, and sodic classifications (Figures 3.4(a) to (c)). The majority of amphiboles from the "eastern" Ahrberg Group are calcic amphibole (Figure 3.4(a)). The individual samples have small ranges in XMg and Si, and plot in the magnesiohornblende and actinolite fields. However, an overall a trend reflecting positive correlation between XMg and Si in the structural formula is evident.

Some analyses from 4 rocks have $0.5>Na_B<1.5$, and plot in the sodic-calcic group (Figure 3.4(b)). Sodic-calcic amphiboles are minor in comparison to the number of analyses in the calcic field. The analyses all plot in the winchite field, but show some variation in XMg values.

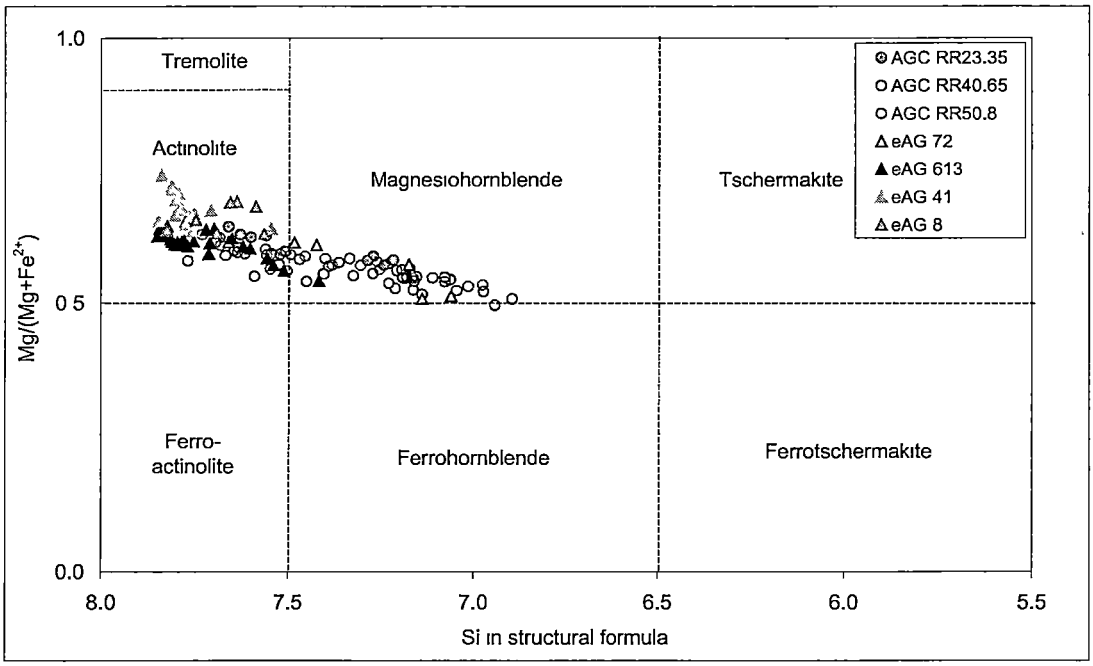

Figure 3.4(a). Calcic amphiboles of the "eastern" Ahrberg Group, plotted on the XMg vs Si diagram, from Leake *et al.* (1997). When $(Ca + Na)_{B\ site} \geq 1.00$ and $Na_{B\ site} < 0.50$ then amphiboles are part of the *calcic group* (Leake *et al.* 1997). Structural formula and cation calculations are presented in Appendix 3.3.

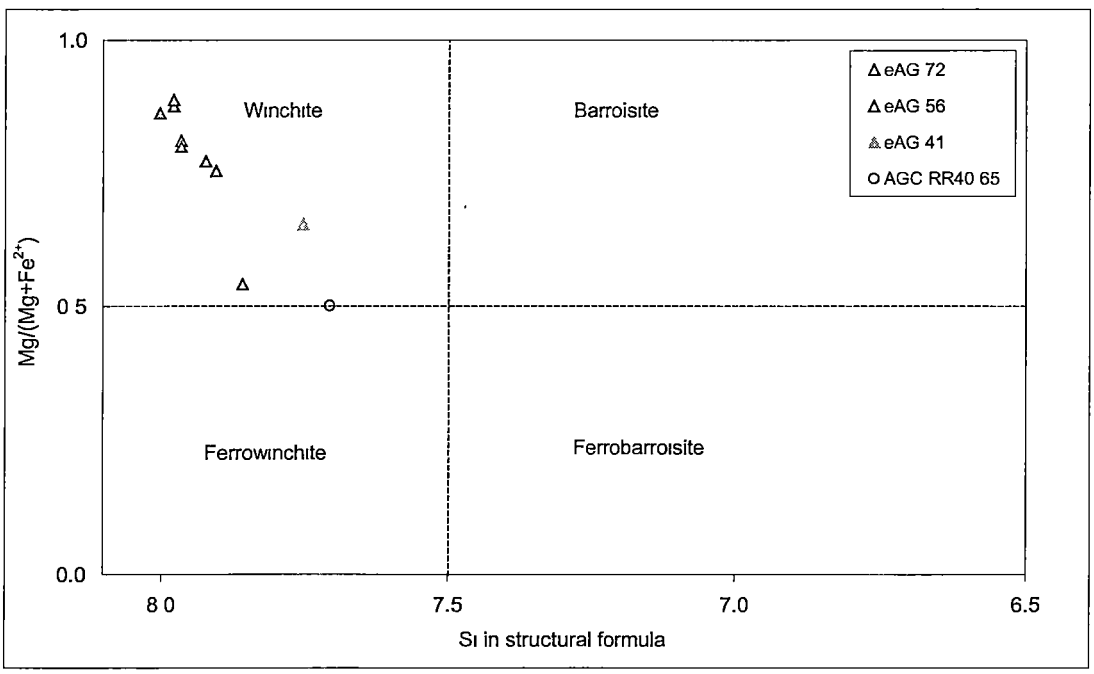

Figure 3.4(b). Sodic-calcic amphiboles of the "eastern" Ahrberg Group, plotted on the XMg vs Si diagram, from Leake *et al.* (1997). When $(Ca + Na)_{B\ site} \geq 1\ 00$ and $Na_{B\ site}$ 0.50 to 1.50 then amphiboles are part of the *sodic-calcic group* (Leake *et al.* 1997). Structural formula and cation calculations are presented in Appendix 3 3.

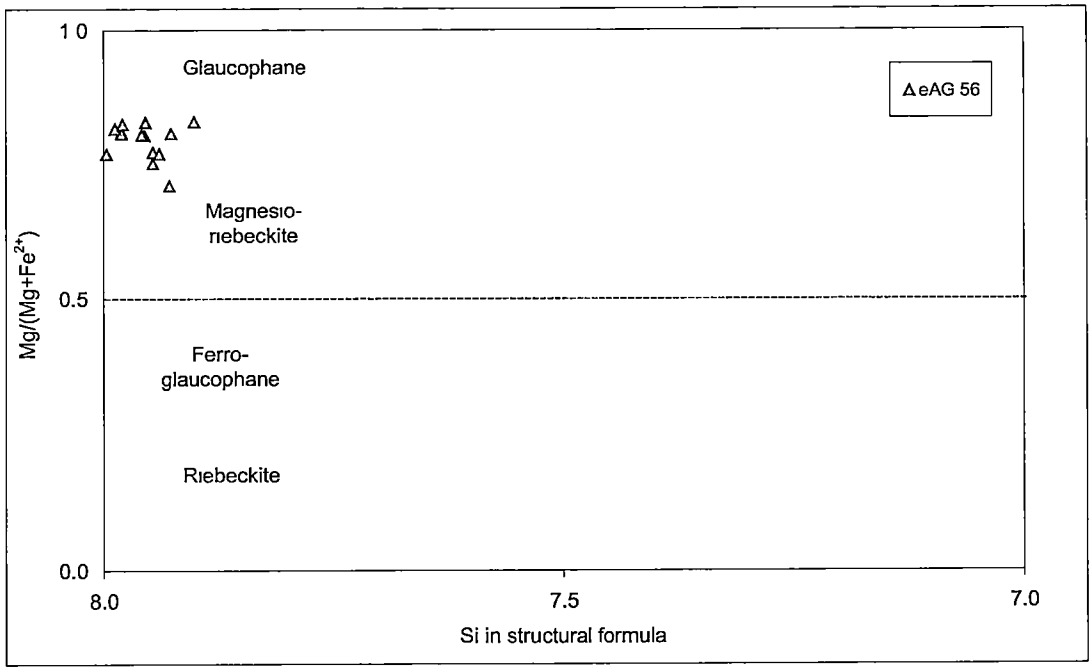

Figure 3.4(c). Sodic amphiboles of the "eastern" Ahrberg Group, plotted on the XMg vs Si in structural formula diagram, from Leake *et al.* (1997). When $Na_{B\ site} \geq 1.50$ then amphiboles are part of the *sodic group* (Leake *et al.* 1997). Structural formula and cation calculations leading to subdivision is presented in Appendix 3.3.

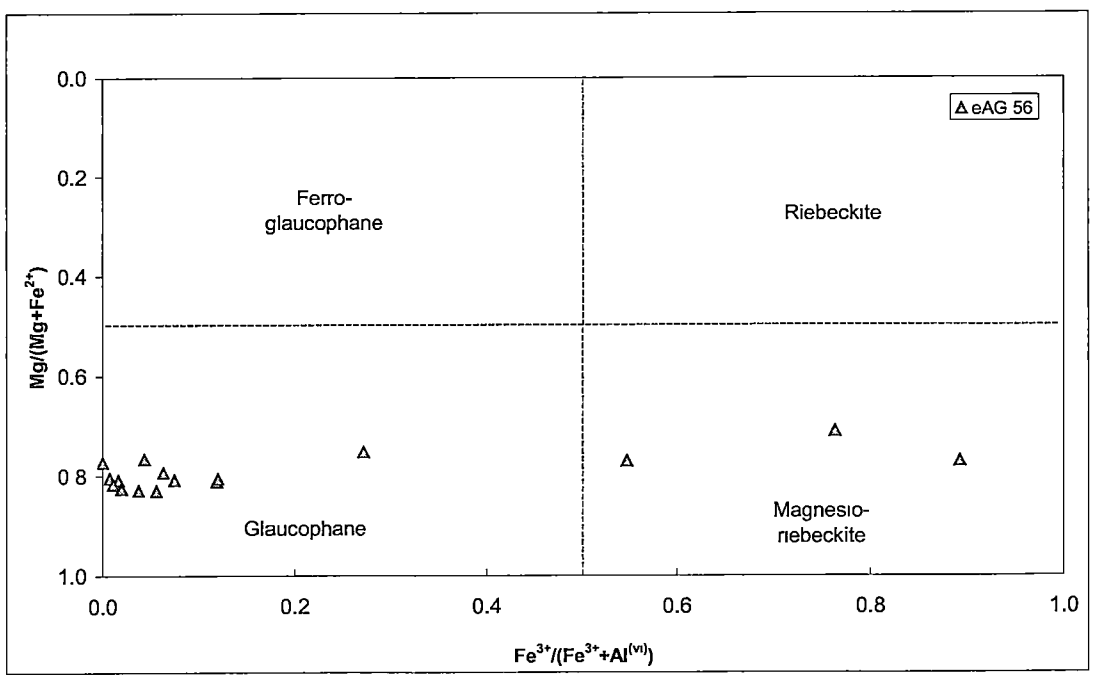

Figure 3.4(d). Sodic amphiboles of the "eastern" Ahrberg Group, plotted on the XMg vs $Fe^{3+}/(Fe^{3+}+Al^{(IV)})$ diagram, from Leake *et al.* (1997). Structural formula and cation calculations leading to subdivision is presented in Appendix 3.3.

Analyses from a single sample (eAG 56) have Na_B>1.5, and plot in the sodic field (Figure 3.4(c)). This sample is texturally distinct from the other samples analysed. It is doleritic in its texture, and unfoliated. The grains are mostly glaucophane with minor magnesioriebeckite (Figure 3.4(d)). They are anomalous in comparison to the majority of the "eastern" Ahrberg Group, and are interpreted to reflect a previously unidentified fault block. The implications of their different compositions will be discussed in Section 3.3.

Chlorite

Chlorite was observed in all of the metasediments analysed (Appendix 3.1). The chlorites (Appendix 3.4) have a small range in values of Fe^{2+} (3.14-4.94), although the Mg range is large (3.73-6.23). The range in XMg is limited (0.48-0.67) (Figure 3.5(a)). The chlorite has Al^{iv} values ranging between 2.15 and 2.57.

Epidote

Colourless to pale green epidote was observed in 94% of the metabasites analysed (Appendix 3.1). The chemistry of the analysed epidotes was calculated on the basis of 12.5 oxygens, and assuming all iron as Fe^{3+}. The chemical variation in the epidotes from the "eastern" Ahrberg Group is small, with Al_2O_3, Fe_2O_3 and CaO all displaying a small chemical range (Appendix 3.5). The pistacite content ($Ca_2FeAl_2Si_3O_{12}(OH)$) varies from 0.14 to 0.30, with a modal value of approximately 0.22, (Ps_{22}) (Figure 3.6(a)). A clear trend in Ps content from core to rim of the epidote grains was not observed, however four grains had a small decrease in Ps content in the rims relative to the cores, whereas a single grain had an increase in Ps content towards the rim of the grain, (Ps_{23} in core to Ps_{27} in rim) (Appendix 3.5). The grains with decreasing Ps towards the rims may imply a slight increase in metamorphic grade accompanied the growth of the epidote grains.

Biotite

Green biotite is a minor component in some of the metabasites of the "eastern" Ahrberg Group and AGC. It was found to be present in 3 of the samples analysed (Appendix 3.1). The biotites are notably more aluminous than those of the Bowry Formation (section 3.4.1). They have lower Fe contents (Appendix 3.6)(Figure

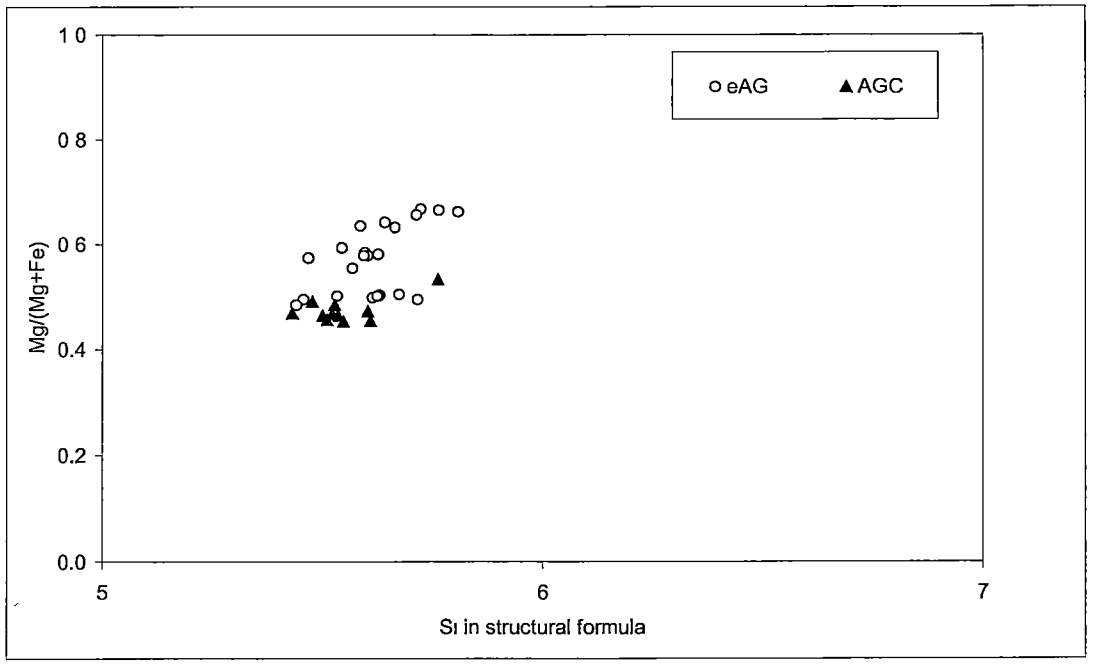

Figure 3.5(a). Plot of XMg vs Si in structural formula for chlorites in the "eastern" Ahrberg Group (eAG) and the AGC mafic meta-igneous rocks. Chlorite compositions are presented in Appendix 3.4.

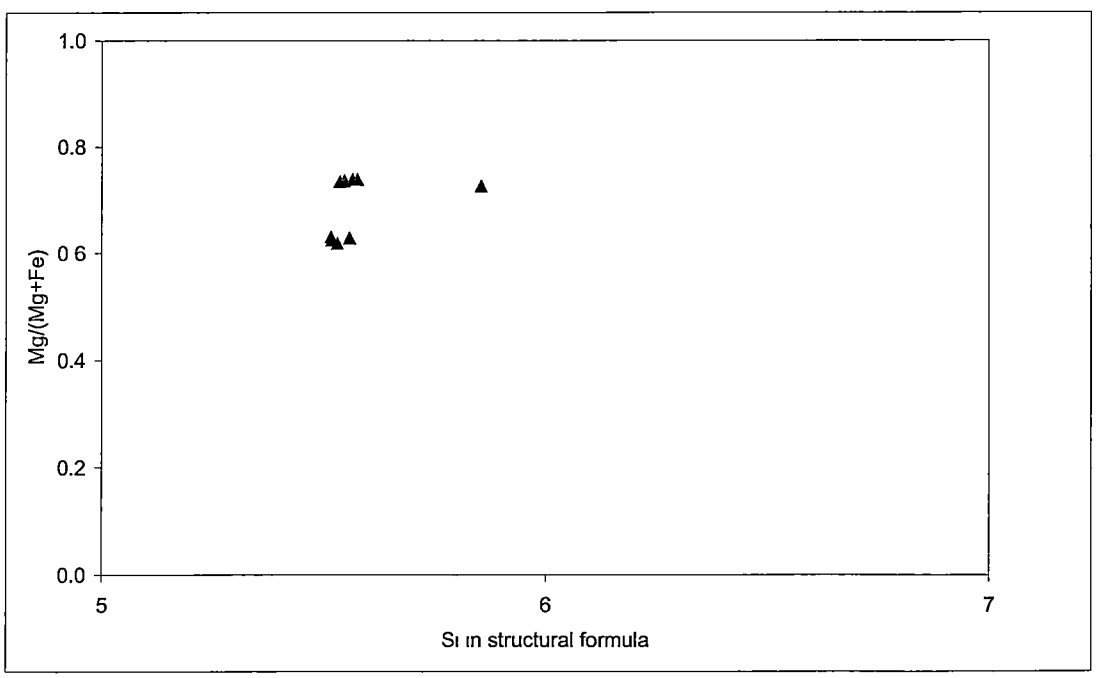

Figure 3.5(b). Plot of XMg vs Si in structural formula for chlorites in the "eastern" Ahrberg Group (eAG) metasedimentary rocks. Chlorite compositions are presented in Appendix 3.4.

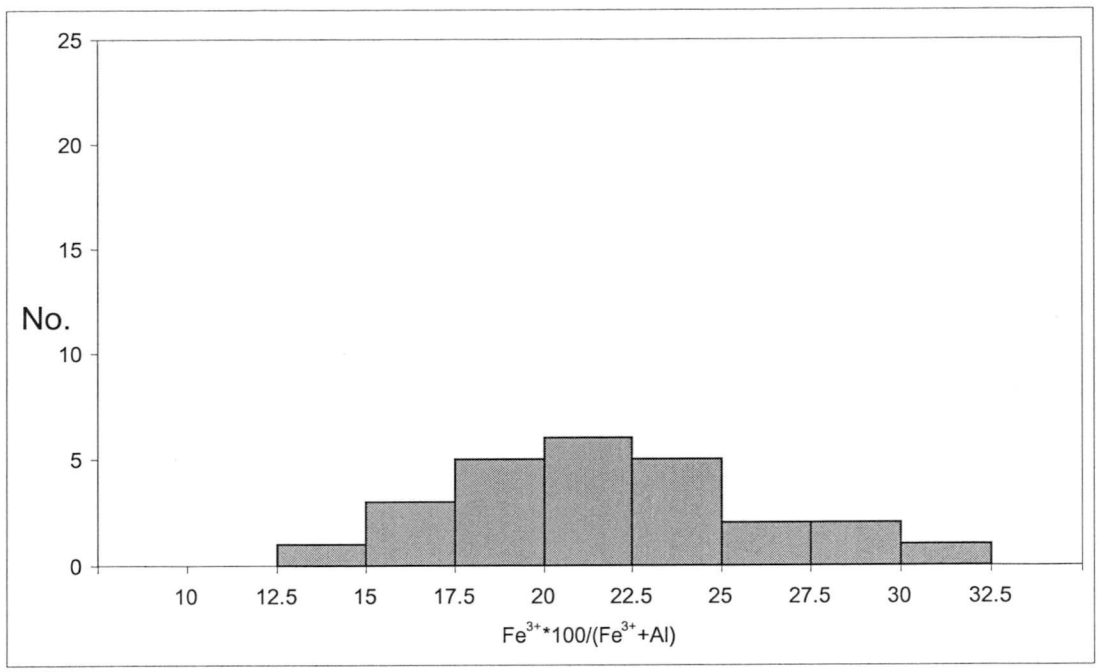

Figure 3.6(a). Histogram of pistacite content of epidotes from metabasites of the "eastern" Ahrberg Group. Pistacite is calculated as $Fe^{3+}*100/(Fe^{3+}+Al)$.

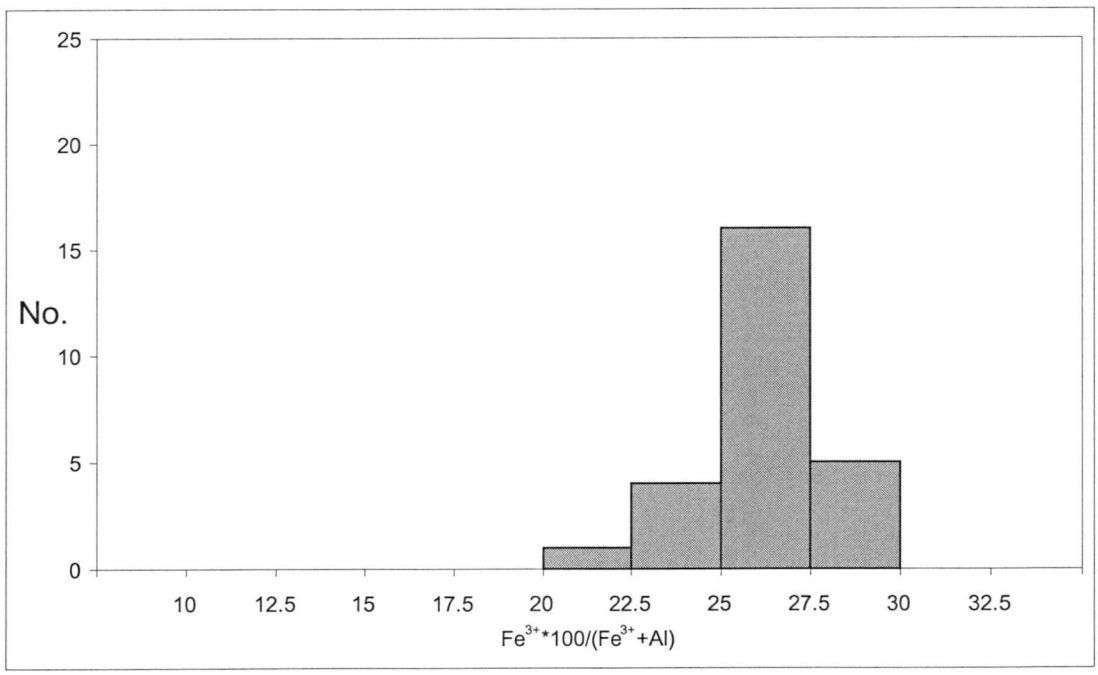

Figure 3.6(b). Histogram of pistacite content of epidotes from metasedimentary rocks of the "eastern" Ahrberg Group. Pistacite is calculated as $Fe^{3+}*100/(Fe^{3+}+Al)$.

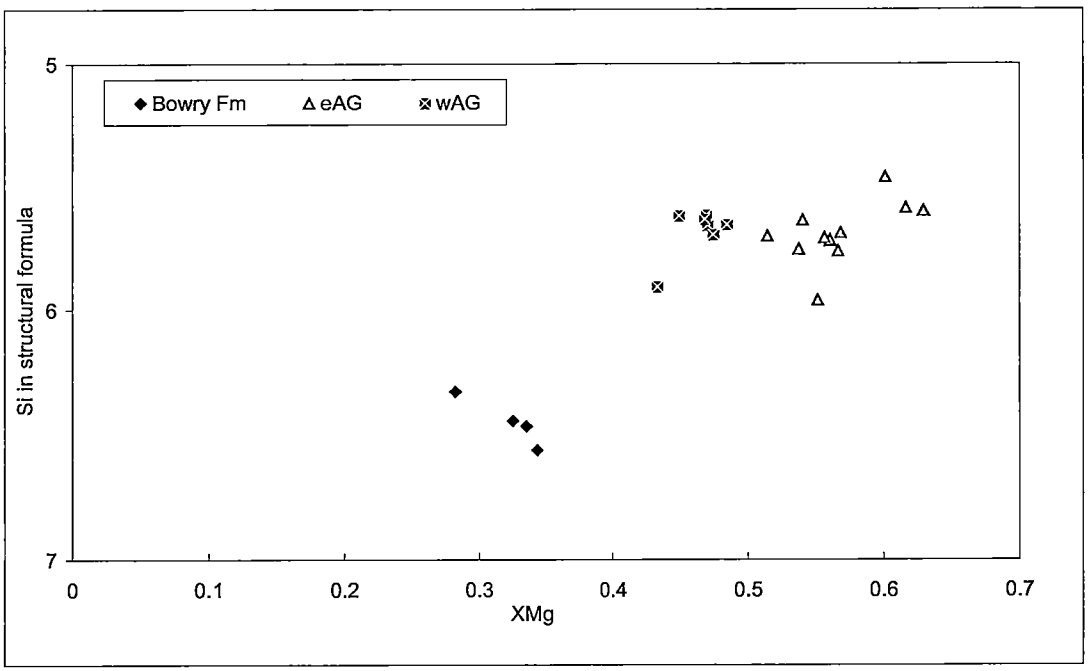

Figure 3.7. Biotite compositions of the Bowry Formation, "eastern" Ahrberg Group (eAG) and "western" Ahrberg Group (wAG) plotted on the XMg ($Mg/(Mg+Fe^{2+})$) vs Si in structural formula diagram. High XMg values of the eAG and wAG is due to fluorine substitution on Fe^{2+}.

3.7), which is interpreted to be due to substantial fluorine substitution (Appendix 3.6) and the Fe avoidance effect (Zhu & Sverjensky 1991).

Garnet

Garnet is a rare mineral in the Arthur Metamorphic Complex, and was only found in 3 samples from the AGC, and in the Bowry Formation. Garnet was not found in samples from the "eastern" Ahrberg Group. Within the AGC, garnet occurs close to the boundary with the Bowry Formation. The compositions show little variation (Appendix 3.7), although garnets from sample RRDDH1 40.65 have consistently lower XMg levels than garnets from RRDDH1 50.8. Garnets in the AGC samples analysed have pyrope contents ranging between 1.6 and 3.5, almandine contents of between 35.5 and 54.9 (with a median of 43.5), spessartine of between 10.4 and 30.4 (with a median of 23.0), and grossular contents ranging between 27.7 and 36.3 (Figures 3.8(a) to (d)). The lower pyrope reflects formation under low temperatures (Appendix 3.7), whereas higher grossular contents suggests growth under high pressure conditions (see section 3.3.3).

3.3.2 Psammites and Psammopelites

Psammopelites are the dominant precursor lithology within the "eastern" Ahrberg Group, however psammites were also observed. In addition, volcaniclastic metasediments, associated with metabasites are also present, although these are minor. The psammopelites and psammites are mineralogically similar, differing in the proportions of constituent minerals. The psammites and psammopelites have a lower greenschist facies mineral assemblage, consisting of quartz-albite-white mica-epidote-chlorite, with carbonate, opaques and green biotite present in some samples (Appendix 3.1). In the AGC, close to the boundary with the Bowry Formation and interlayered with garnet-bearing metadolerites, some quartz-mica schists are garnet-bearing (Figure 3.2(b)).

Petrography

Throughout the high strain "eastern" Ahrberg Group and Ahrberg Group Correlate (AGC), the metasediments are texturally similar, with the well developed $\boldsymbol{Ca}S_2$ schistosity occurring as the dominant foliation. Grains of white mica have grown

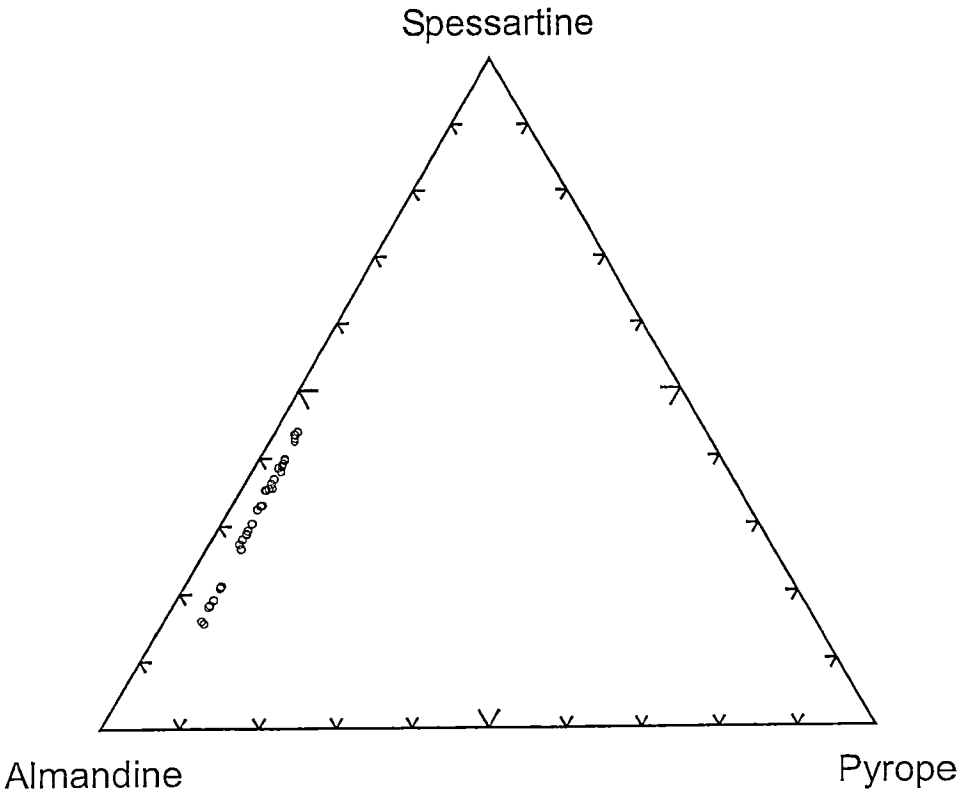

Figure 3.8(a). Almandine-Spessartine-Pyrope diagram for garnets from the AGC (sample RRDDH1 50.8).

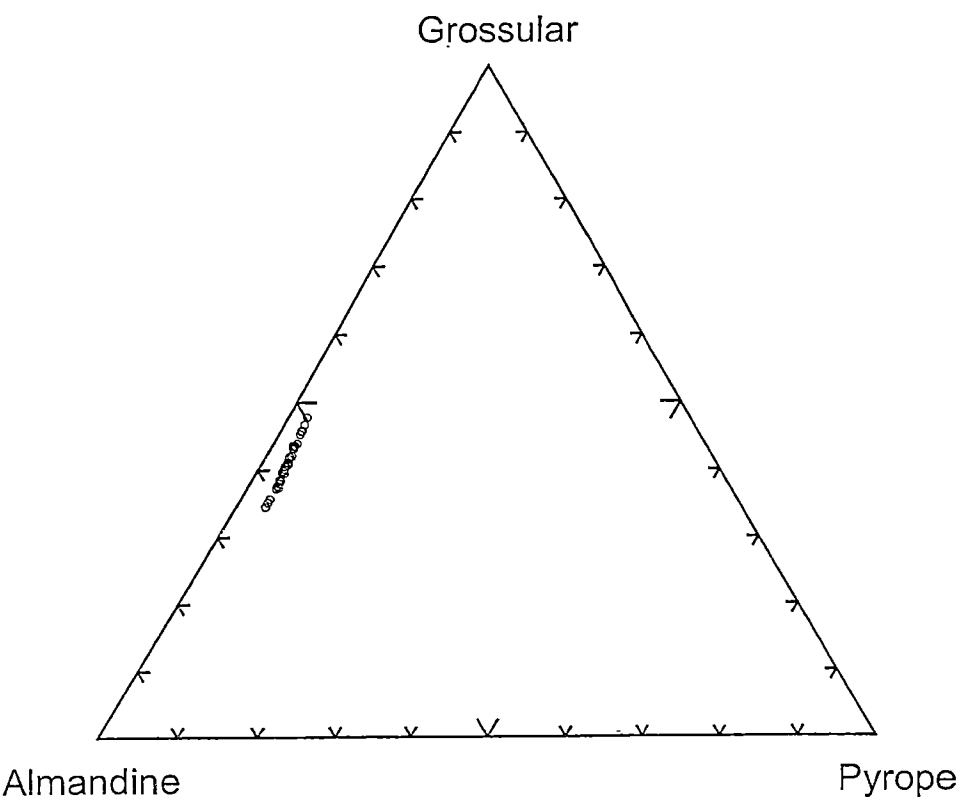

Figure 3.8(b). Almandine-Grossular-Pyrope diagram for garnets from the AGC (sample RRDDH1 50.8).

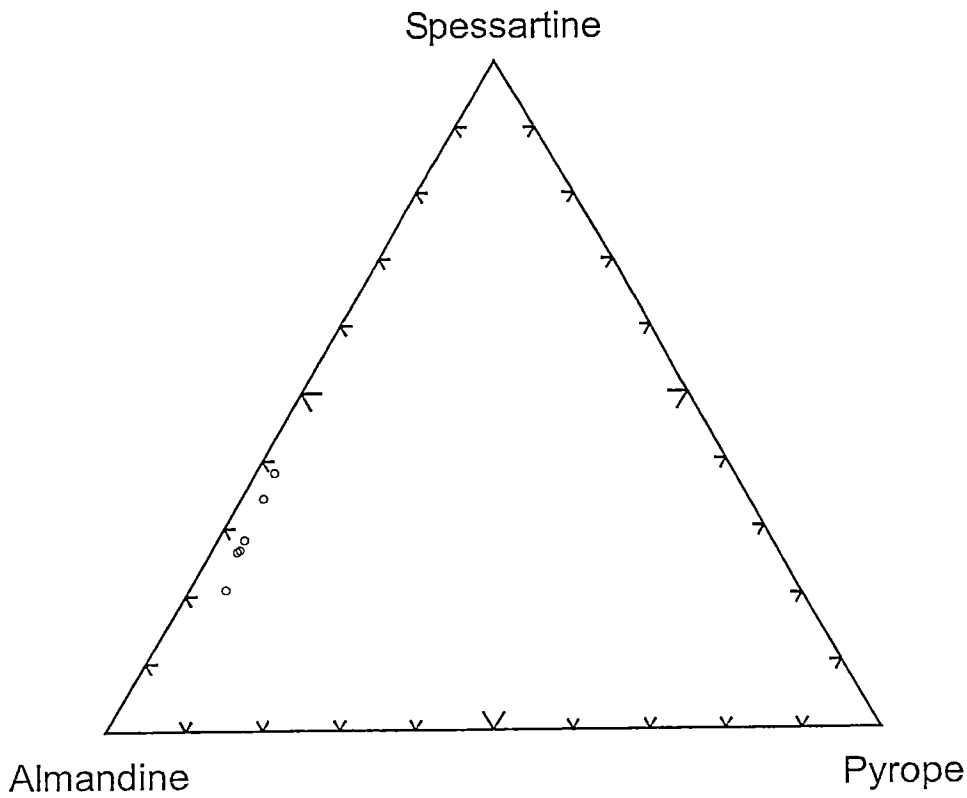

Figure 3.8(c). Almandine-Spessartine-Pyrope diagram for garnets from the AGC (sample RRDDH1 40.65).

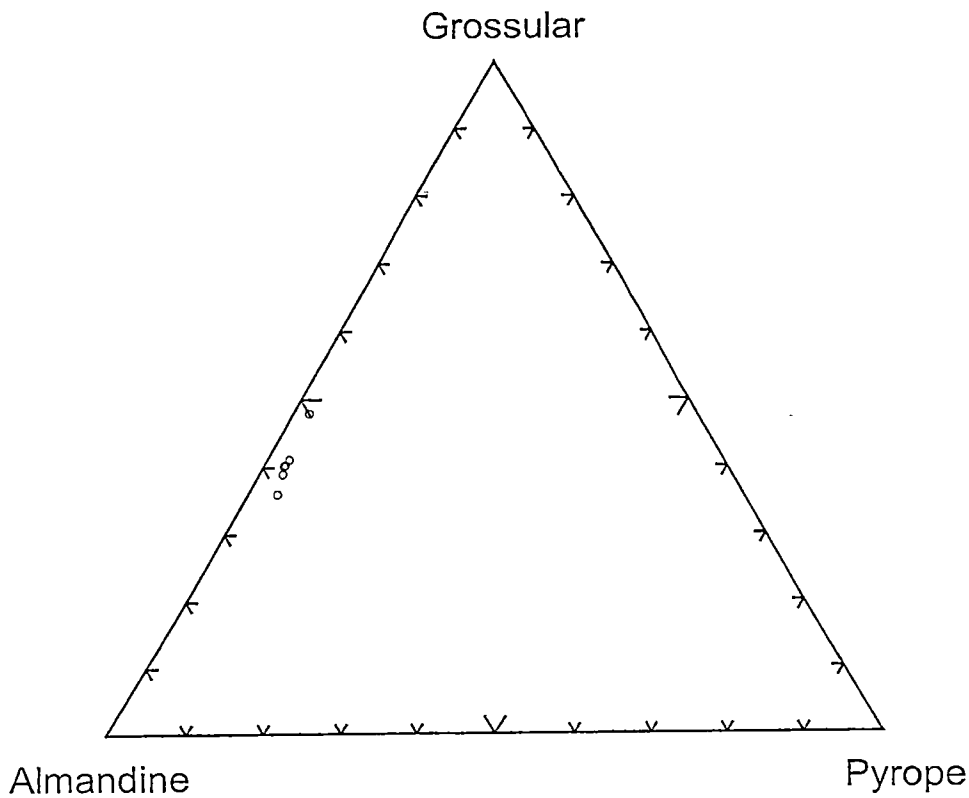

Figure 3 8(d). Almandine-Grossular-Pyrope diagram for garnets from the AGC (sample RRDDH1 40.65).

during this event, and define the schistosity. They are interlayered with variably strained, polycrystalline quartz, syn-$\boldsymbol{Ca}D_2$ albite porphyroblasts, chlorite and epidote. Both polygonal and elongate albite porphyroblasts were observed. Equigranular albite grains have an S_i that is straight, indicating a lack of deformation during growth (Figure 3.3(k)), whereas the elongate albites, display clear evidence of having undergone rotation contemporaneous with their growth (Figures 3.3(l) and (m)). These syn-rotational albites have S_i that are straight in the core of the porphyroblasts, but curved towards the rim, indicative of progressive porphyroblast growth during deformation.

Epidote grains are common to abundant, and range between stubby and elongate in shape. They are commonly found as inclusions in albite and as matrix grains aligned with the $\boldsymbol{Ca}S_2$ foliation. Chlorite is intergrown with white mica. In the garnet-bearing quartz-mica schists of the AGC (Appendix 3.1), the garnet occurs as small, colourless, euhedral grains, predominantly in mica-rich domains. The garnets have grown post-$\boldsymbol{Ca}D_1$, and are most likely syn-$\boldsymbol{Ca}D_2$ (Figure 3.3(n)).

Mineralogy

Albite

Plagioclase feldspar was found in 65% of the metasedimentary samples that were studied petrographically (Appendix 3.1). Iron was calculated as Fe^{3+}. All plagioclase feldspar in the psammites and psammopelites of the "eastern" Ahrberg Group are albite (An_{0-2}) (Appendix 3.2).

White mica

White mica was present in 97% of metasedimentary samples that were studied (Appendix 3.1). It is a prominent mineral component of the psammitic and psammopelitic schists, occurring as thin grains aligned with the dominant foliation. 50 % of total iron was assumed to be Fe^{3+}. This correction has been suggested as an acceptable first order approximation for pelitic schists (Guidotti *et al.* 1994). The XMg ($Mg/(Mg + Fe^{2+})$) content of the white mica ranges between 0.47 and 0.60 (Appendix 3.8). The celadonite component ($K(Mg, Fe)AlSi_4O_{10}(OH)_2$) of the mica, expressed as Mg + Fe, is between 0.72 and 1.25 (Figure 3.9(a)). The paragonite component of the micas, expressed as Na/(Na + K), is small (ranging between 0.03

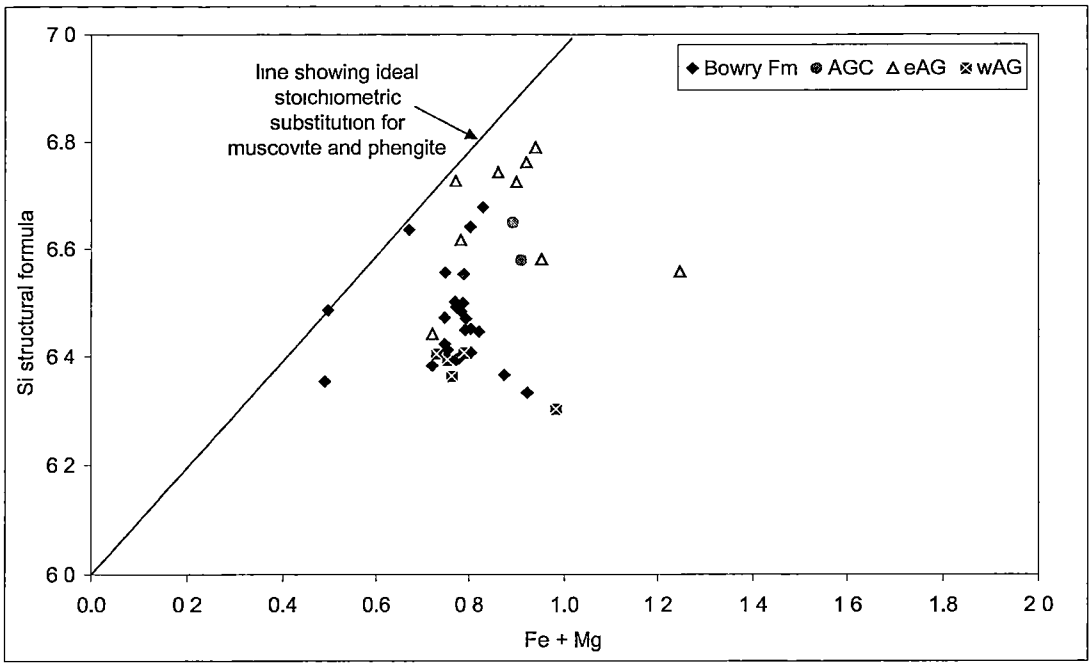

Figure 3.9(a). Diagram illustrating the celadonite component of white micas (expressed as Fe+Mg) of the Bowry Formation, AGC, "eastern" Ahrberg Group (eAG) and "western" Ahrberg Group (wAG), plotted against Si in structural formula. Diagram assumes ½ Fe is Fe^{3+}.

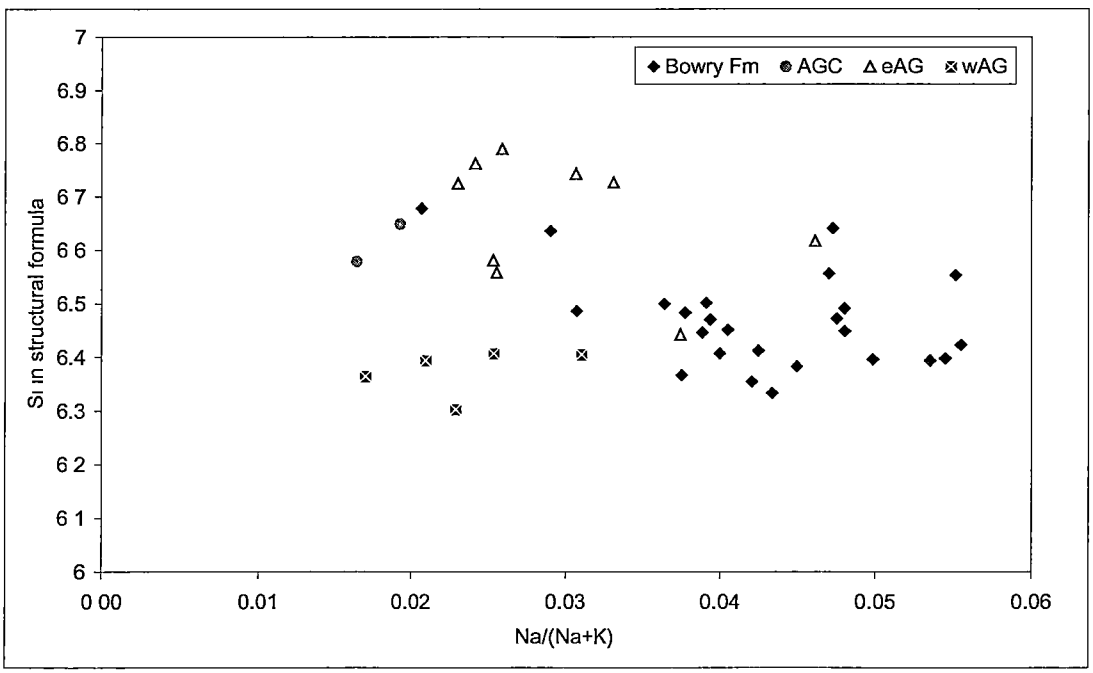

Figure 3.9(b). Diagram illustrating the paragonite component of white micas (expressed as Na/(Na+K)) of the Bowry Formation, AGC, "eastern" Ahrberg Group (eAG) and "western" Ahrberg Group (wAG), plotted against Si in structural formula.

and 0.08), although a noticeable difference between different samples (possibly reflecting the subsequent alteration of some samples) was observed (Figure 3.9(b)). The variation in paragonite content within individual samples is also small (Appendix 3.8).

Chlorite

Chlorite was observed in 83% of the metasediments analysed (Appendix 3.1). The chlorites (Appendix 3.4) have a small range in values of Fe^{2+} (2.46-3.51) and Mg (5.63-6.96). The range in XMg is small (0.62-0.74)(Figure 3.5(b)). The analyses have Al^{IV} values ranging between 2.43 and 2.49.

Epidote

Colourless to pale green epidote was observed in 43% of the metasediments analysed (Appendix 3.1). The chemical variation in the epidotes from the "eastern" Ahrberg Group is small, (Appendix 3.5). The pistacite content ($Ca_2FeAl_2Si_3O_{12}(OH)$), varies from 0.22 to 0.28, with a modal value of approximately 0.28, (Ps_{28}) (Figure 3.6(b)). A clear trend in Ps content from core to rim of the epidote grains was not observed (Appendix 3.5). The pistacite content of the epidotes in the metasediments is consistently higher than in the metabasites (Figure 3.6(b)). This is attributed to bulk rock composition, as both rock types have undergone the same metamorphic history.

Biotite

Green biotite is a minor component in several of the metasediments that were analysed. It was found in 14% of the samples analysed (Appendix 3.1). Just as with the biotite in the metabasites, the biotite in the metasedimentary rocks are notably more aluminous than those of the Bowry Formation, and have lower Fe contents (Appendix 3.6) (Figure 3.7). This is interpreted to be due to the Fe-avoidance effect of the substantial fluorine substitution for OH (Appendix 3.6).

Other Minerals

Carbonate was observed in approximately half of the samples observed petrographically. The composition of the carbonate was not investigated. Minor sphene, tourmaline, magnetite, hematite, rutile and ilmenite were also detected, however these were not investigated in detail.

3.3.3 Conditions of metamorphism of the "eastern" Ahrberg Group and AGC

The "eastern" Ahrberg Group metasediments and metabasites have mostly experienced the same metamorphic history. Throughout the unit albite, epidote, chlorite and carbonate are stable. However some metabasites have a range of amphibole compositions, indicative of changing metamorphic conditions during early metamorphism. Actinolite is widely stable during later metamorphism (discussed in detail below). The AGC metabasites and metadolerites that were investigated have also experienced different early metamorphic conditions to the "eastern" Ahrberg Group (Figures 3.2(a) and (b)).

The "eastern" Ahrberg Group metasediments have uniform metamorphic mineral assemblages for $\boldsymbol{Ca}D_2$, predominantly consisting of quartz-albite-white mica-epidote-chlorite-carbonate (Appendix 3.1), whereas the majority of the metabasites consist of quartz-albite-chlorite-epidote-actinolite-sphene-magnetite.

Hornblende cores of amphiboles are also present in some samples (Appendix 3.1), although most analyses were actinolitic (Figure 3.10(a)). Most amphibole cores plot in the Na^B-rich area of the actinolite field. By comparison with the calibrations, of Brown (1977), the cores grew at approximately 500 MPa. Single core analyses from samples eAG 72 and eAG 41 plot in the winchite field, however these are still close to the 500 MPa isobar. The rims of the grains (late $\boldsymbol{Ca}D_2$) are also actinolitic, and cluster around the 300 MPa isobar. Analyses from sample eAG 72 are mostly hornblendes, although this composition is rare in the "eastern" Ahrberg Group samples. Both amphibole cores and rims from this sample grew at approximately 500 MPa.

The amphibole compositions are compared with other regional metamorphic provinces on Figure 3.11(a). Amphibole compositions from medium pressure (Dalradian) and medium to high pressure environments (Sanbagawa and Franciscan terranes, and the Hazens Notch Fm from north Vermont) are shown (Laird & Albee 1981b). The calcic and sodic-calcic amphiboles of the "eastern" Ahrberg Group

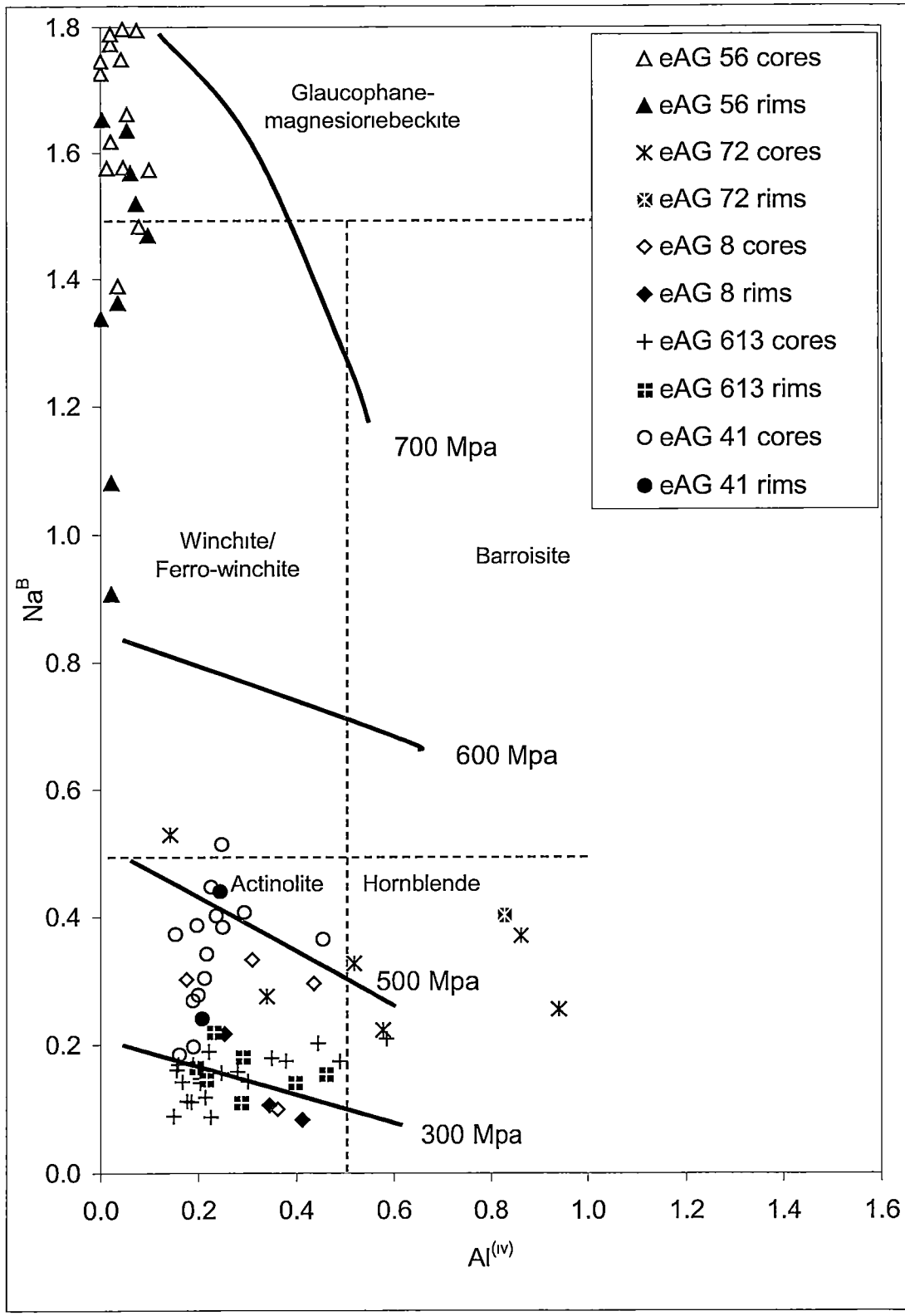

Figure 3.10(a). Amphibole compositions from the "eastern" Ahrberg Group, plotted on the $Na^{(B\ site)}$ vs $Al^{(iv\ site)}$ diagram. Compositional fields from Leake *et al.* (1997), isobars from Brown (1977).

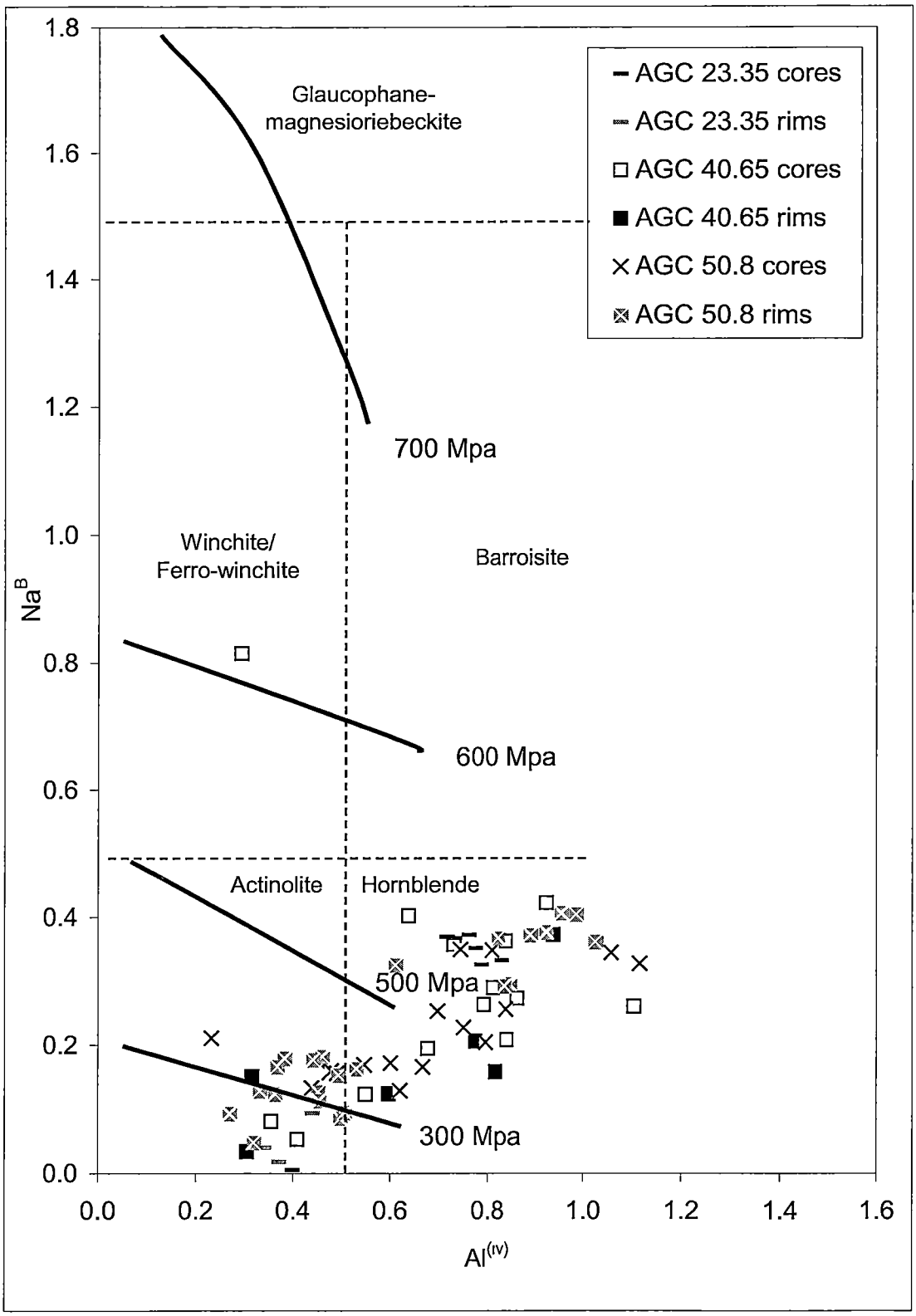

Figure 3.10(b). Amphibole compositions from the AGC, plotted on the $Na^{(B\ site)}$ vs $Al^{(IV\ site)}$ diagram. Compositional fields from Leake *et al.* (1997), isobars from Brown (1977).

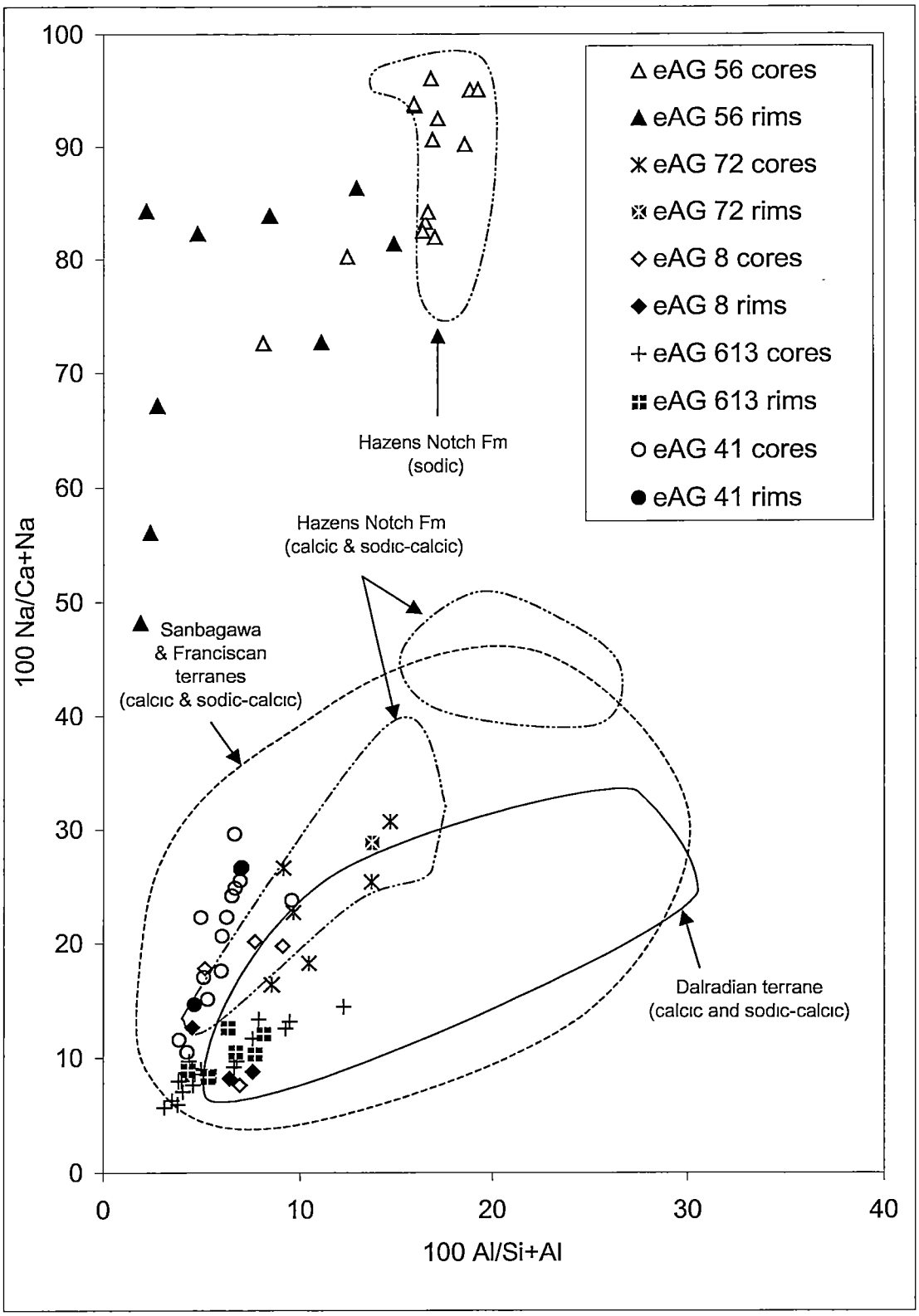

Figure 3.11(a). Amphibole compositions of the "eastern" Ahrberg Group, plotted on the 100 Na/(Ca+Na) vs 100 Al/(Si+Al) diagram. Calcic, sodic-calcic and sodic fields for other high (Sanbagawa, Franciscan terranes and Hazens Notch Fm) and medium (Dalradian) pressure terranes are from Laird & Albee (1981b).

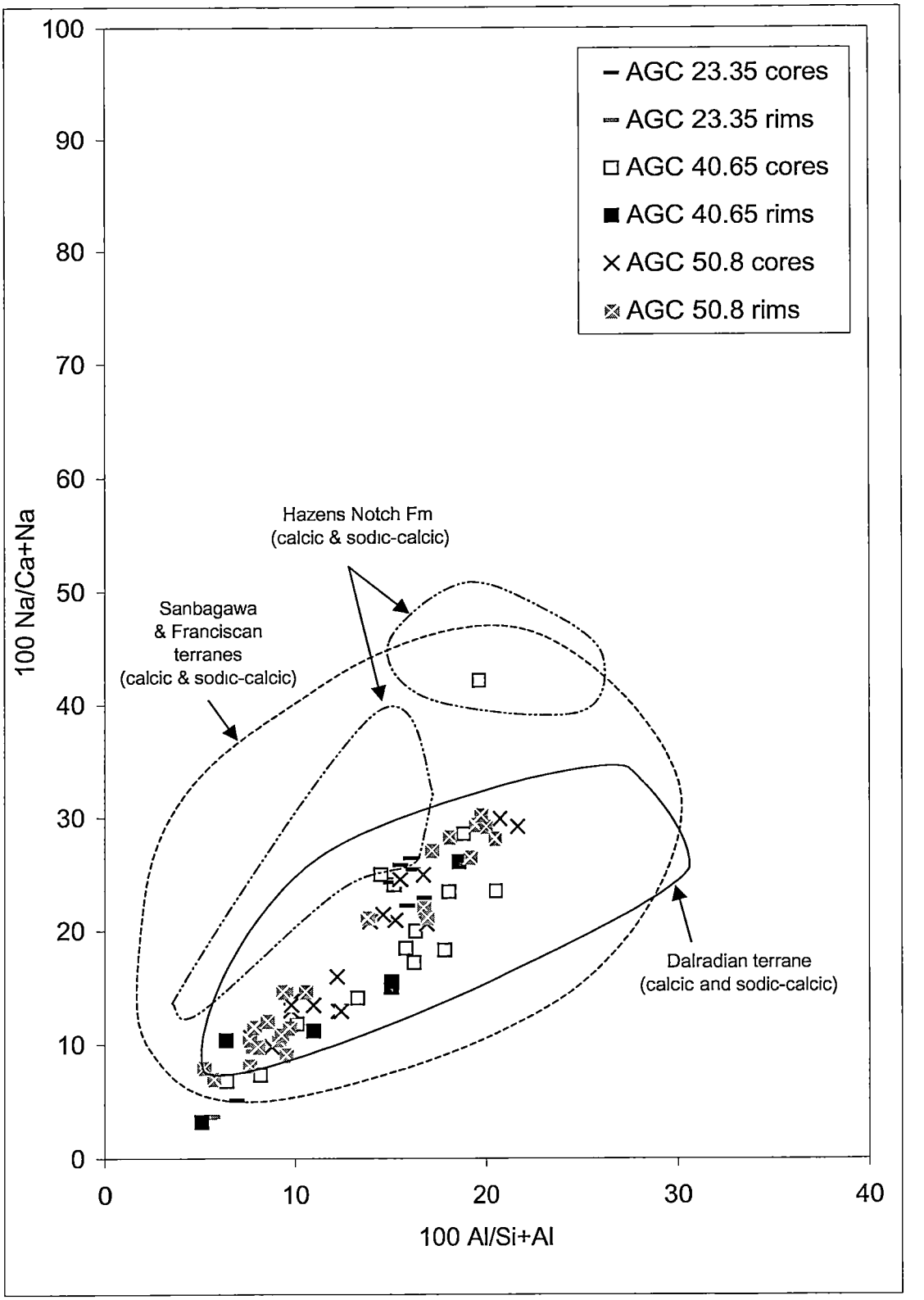

Figure 3.11(b) Amphibole compositions of the AGC, plotted on the 100 Na/(Ca+Na) vs 100 Al/(Si+Al) diagram. Calcic, and sodic-calcic fields for other high (Sanbagawa, Franciscan terranes and Hazens Notch Fm) and medium (Dalradian) pressure terranes are from Laird & Albee (1981b).

display a steep trend, that is consistent with medium pressures, and low temperatures, similar to those of the Sanbagawa and Franciscan terranes, and the Hazens Notch Fm. Given the metamorphic assemblage of the metasediments and metabasites, and the absence of garnet, the mineral assemblage is interpreted to be in equilibrium at 400-450°C.

Amphiboles compositions from sample eAG 56 are anomalous. They show a well defined compositional trend from glaucophane-rich cores to winchite-rich rims (Figure 3.10(a)). This transition from sodic to sodic-calcic amphibole corresponds to decreasing pressure with growth, however the conditions are very different to the majority of the "eastern" Ahrberg Group amphiboles. According to the isobaric contours defined by Brown (1977), amphibole cores from sample eAG 56 grew at close to 700 MPa, whereas rims show a decrease in pressure, to above 600 MPa (Figure 3.10(a)). Again these pressures can only be used as a guide to the metamorphic conditions. The eAG 56 amphiboles were also plotted on the Na/(Ca+Na) vs Al/(Si+Al) diagram (Figure 3.11(a)), and overlap with the field defined by amphiboles from the Hazens Notch Fm of north Vermont (high P). The variation in amphibole composition in sample eAG 56 compared to other "eastern" Ahrberg Group samples (Figure 3.11(a)) suggests sample eAG 56 has undergone early metamorphism (at higher pressures) some distance from the rest of the group. It may be part of an allochthonous block.

The mineral assemblages of the meta-igneous mafic and metasedimentary rocks of the AGC differ to those of the "eastern" Ahrberg Group, with garnet present in both psammitic and basic rock types (see section 3.3.1) (Appendix 3.1). The common mineral assemblage of the mafic metasediments and meta-igneous rocks consists of quartz-albite-amphibole-epidote-chlorite-garnet, with green biotite present in some samples (Appendix 3.1).

Amphibole compositions in the AGC have a consistent, linear trend, ranging from hornblende to actinolite (Figure 3.10(b)), and thus differ from the "eastern" Ahrberg Group amphiboles, which are mostly actinolitic. Cores are predominantly hornblende, reflecting higher temperatures and according to the isobars defined by Brown (1977), developed at approximately 500 to 550 MPa. Rims are mostly

actinolite and are stable at pressures of around 300 MPa, however hornblende-rich rims (stable at higher pressures) were also observed. A single core analysis plots in the winchite field, and may represent a relict grain of an early metamorphic event, contemporaneous with the metamorphic conditions that produced sodic-calcic amphiboles in the "eastern" Ahrberg Group. However, the majority of analyses from this sample plot in the calcic amphibole area ($Na^B<0.5$). The AGC samples were also plotted on a Na/(Ca+Na) vs Al/(Si+Al) diagram (Figure 3.11(b)). As can be seen, the trend of the slope is more gentle than the amphiboles of the "eastern" Ahrberg Group, further supporting the interpretation of higher temperatures during metamorphism, similar to the Dalradian trend.

The presence of syn-$\boldsymbol{Ca}D_2$ garnet in these samples also indicates the $\boldsymbol{Ca}D_2$ metamorphic conditions in the AGC were higher in temperature than the "eastern" Ahrberg Group. In comparison to the "eastern" Ahrberg Group, AGC epidotes that were analysed have anomalously low modal pistacite contents ($Ps_{17.5}$) (Figure 3.12), reflecting the lower levels of Fe^{3+} present in the samples. Magnetite is absent in the analysed samples, indicative of the lack of available Fe^{3+}. In addition, the chlorites from the AGC that were analysed have lower XMg than the "eastern" Ahrberg Group chlorites, indicative of higher levels of Fe^{2+} (Figure 3.5(a)). These characteristics of high levels of Fe^{2+} are indicative of less oxidised compositions.

Geothermobarometric calculations have been attempted using THERMOCALC (Powell & Holland 1998, 2000). However, errors in the pressure and temperature calculations of the AGC assemblages are large, and confidence is less than 95%. Despite this, THERMOCALC calculated metamorphic conditions of 720 ± 240 MPa and 466 ± 45°C for sample RR40.65, and 620 ± 280 MPa and 463 ± 41°C form sample RR50.8 (Figure 3.13, Appendix 3.28). This is in contrast to samples from the "eastern" Ahrberg Group, which did not reach the greenschist-amphibolite facies transition zone and was below the garnet stability field. Based on the THERMOCALC results for sample 613, from within the centre of the "eastern" Ahrberg Group, the unit underwent metamorphism at about 450°C at a pressure of 337 ± 160 MPa (Figure 3.13, Appendix 3.28). The implications of these results will be discussed in section 3.6.

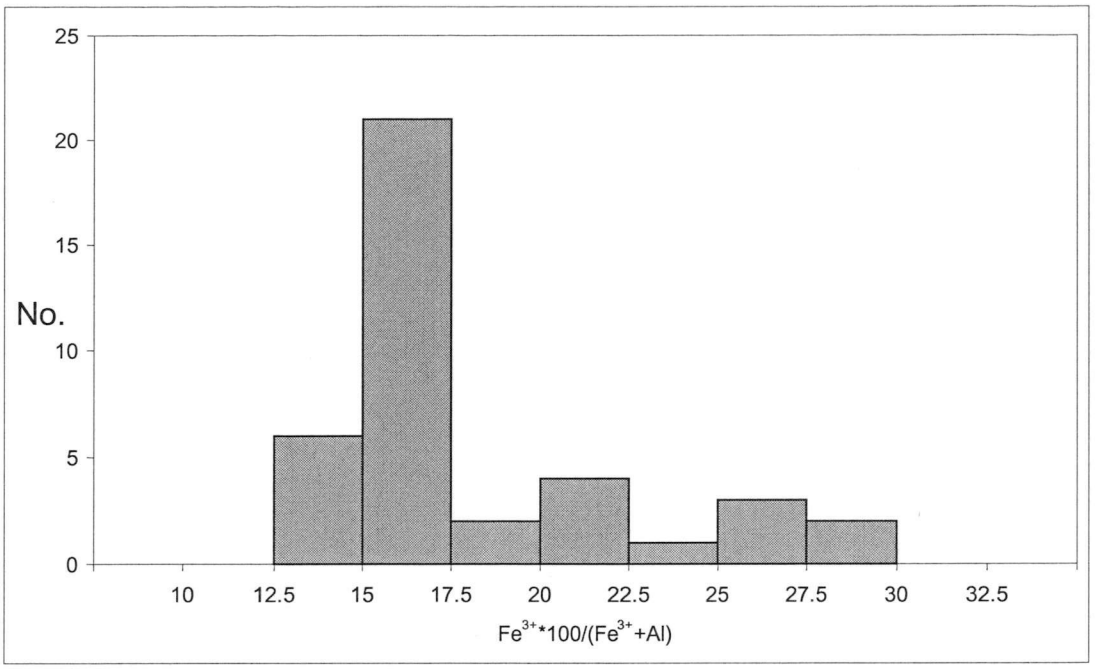

Figure 3.12. Histogram of pistacite content of epidotes from mafic meta-igneous rocks of the AGC. Pistacite is calculated as $Fe^{3+}*100/(Fe^{3+}+Al)$.

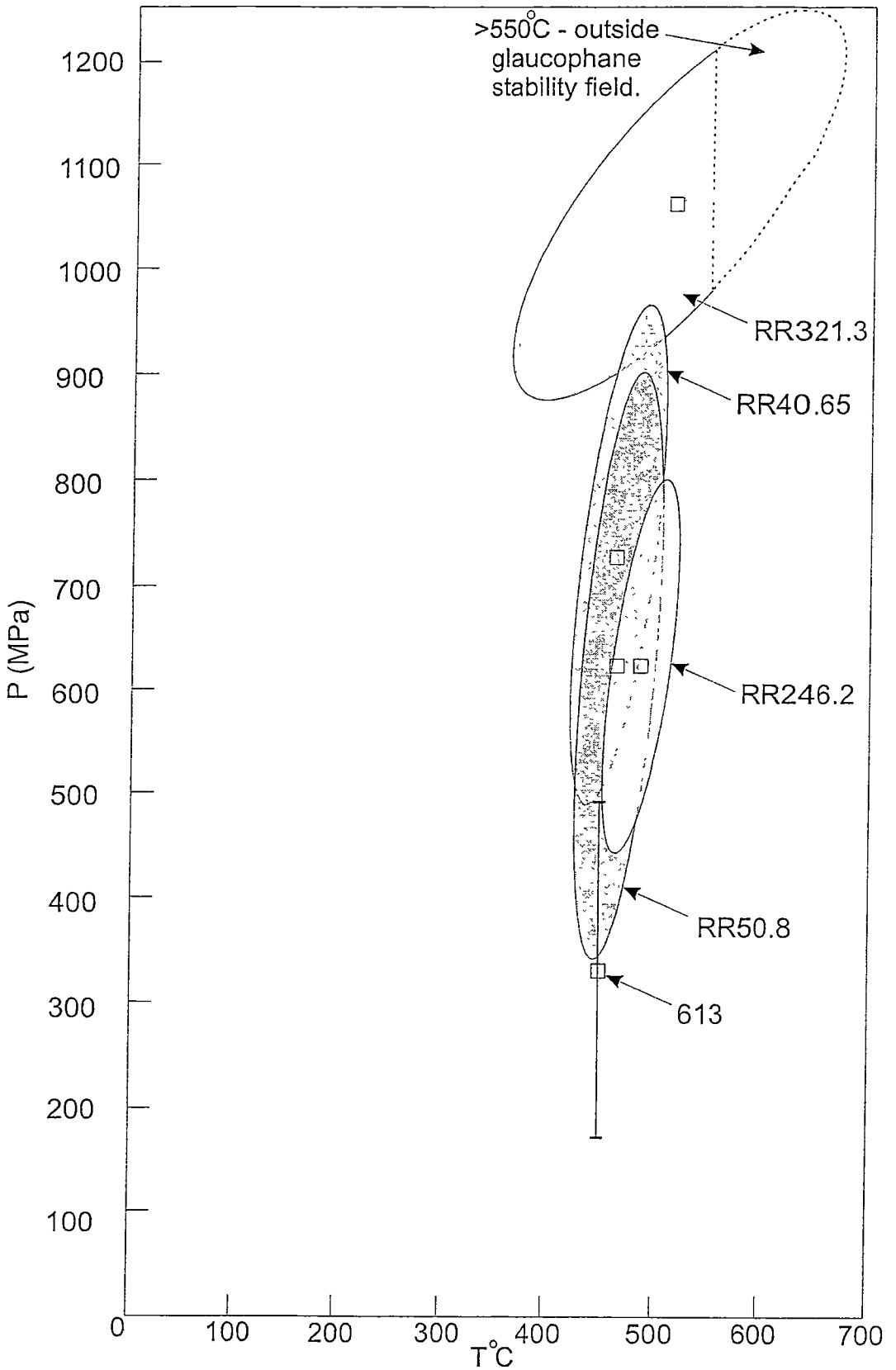

Figure 3.13. Pressure-temperature diagram for mineral assemblages of samples, calculated using THERMOCALC (Powell & Holland 1998, 2000). Sample 613 is from the "eastern" Ahrberg Group, samples RR40.65 and RR50.8 are from the AGC, samples RR246.2 and RR321.3 are from the Bowry Formation. The pressure of sample 613 is calculated at 450°C. Calculations are presented in Appendix 3.28.

3.4 Metamorphism of the Bowry Formation

The Bowry Formation consists of metasediments and meta-igneous rocks that vary in composition and metamorphic grade. The unit predominantly consists of metabasites metadolerites, metagabbros, and associated mafic metasedimentary schists. There are also carbonate- and albite-rich metasediments, garnet-bearing schists and minor metamorphosed granitoids. The garnet-bearing schists are restricted to the eastern part of the Bowry Formation, whereas granitoids are restricted to the western part of the unit.

Greenschist, blueschist and lower amphibolite facies assemblages were observed in the Bowry Formation. Various authors (Spry 1964, Spiller 1974, Green & Spiller 1977, Turner & Bottrill 2001) have described blue amphiboles from within the unit, but later upper greenschist to lower amphibolite facies mineral assemblages are dominant. The amphibolites are predominantly magnetite-bearing, and have been derived from tholeiitic magmas (see Chapter 4).

3.4.1 Mafic and felsic meta-igneous lithologies

Petrography

The mafic meta-igneous lithologies are primarily composed of syn-kinematic albite porphyroblasts (syn-$\boldsymbol{Ca}D_2$), amphibole, epidote, chlorite, quartz, magnetite and sphene (Appendix 3.9). The albite porphyroblasts commonly have inclusions of epidote, tourmaline, and amphibole and minor garnet. In some samples, the inclusions are aligned with the $\boldsymbol{Ca}S_2$ foliation, however randomly oriented inclusions are common. Amphibole occurs intergrown with minor green biotite, garnet, carbonate, pyrite and tourmaline both in coarse- and fine-grained samples (Appendix 3.9).

In the metabasites (which are now mostly foliated) amphibole occurs as porphyroblasts aligned with the dominant foliation, that are predominantly bluish green to green brown pleochroic. These amphiboles commonly have some variation in optical properties between the cores and rims of grains, indicative of compositional variation.

In metadoleritic and metagabbroic samples, the amphiboles are randomly oriented to weakly aligned, depending on the strength of foliation present in the sample (usually weak). In the coarser grained samples, patches completely dominated by amphibole were observed (Figure 3.14(a)), although these are rare. Amphiboles in these coarse grained samples range in pleochroism from green-brown, to blue-green and colourless-mauve blue (Figure 3.14(a) to (c)), although they predominantly contain amphiboles that are bluish in colour. The bluish amphiboles are interpreted to represent earlier ($Ca D_1$) metamorphism, preserved in samples that did not feature strong tectonism (and hence lack a strong foliation) during $Ca D_2$.

In both coarse- and fine-grained samples, epidote occurs in the matrix, and as inclusions in albite. The grains are commonly colourless to pale green, and are much smaller than the amphiboles. In some coarse-grained samples the epidotes occur in concentrated zones, perhaps reflecting the breakdown of primary, igneous magnetite (Figure 3.14(d)). Chlorite is present in most metadolerites and metagabbros, and also defines any foliation present. Quartz is also in the matrix. Quartz crystals mostly have undulose, wavy extinction. Sphene is a common phase, and also parallels the weak foliation in the rocks. It occurs as subhedral grains and as grubby, altered aggregates, that are intergrown with the other minerals present. Biotite, where present, occurs as small grains, aligned and intergrown with chlorite, and as matrix grains. Garnet occurs as subhedral to euhedral porphyroblasts that are small and colourless to pale pink. In some examples they are included, and are also found in association with green biotite (Figure 3.14(e)). Primary magnetite and titanomagnetite grains have been deformed and pseudomorphed by sphene and fine-grained epidote.

Felsic meta-igneous rocks in the Bowry Formation are granitoids and microgranitoids. While some samples are transitional towards leucogabbros and the coarser grained mafic meta-igneous rocks described above, the whole rock chemistry of the granitoids and leucogabbros are quite distinct (see Chapter 4). In thin section, the granitoids are medium grained, and feature holocrystalline intergrowths of albite and microcline with pronounced subgrain development, recrystallised sugary quartz, bluish green amphibole, minor chlorite, carbonate and sphene. Rare zircons are also

Figure 3.14(a) to (h) photomicrographs of metamorphic mineral assemblages in the Bowry Formation rocktypes. (a) amphibole (winchite) in amphibole-rich zone of metadolerite, sample 659; (b) early glaucophane with actinolite rims in weakly foliated metadolerite, sample 1193; (c) hornblende porphyroblast with actinolite rim, occurring with quartz, albite and epidote, metadolerite sample RRDDH1 138.35; (d) epidote-rich patch in metadolerite, possibly replacing primary phase, occurring with chlorite and hornblende, metadolerite sample RRDDH1 138.35; (e) garnet porphyroblast occurring with chlorite and green biotite, metabasalt sample 664b; (f) early syn-$\boldsymbol{Ca}D_2$ garnet porphyroblast preserving the crenulated $\boldsymbol{Ca}S_1$ foliation (defined by quartz inclusions), occurs with chlorite, quartz and late white mica, metasedimentary schist sample RRDDH1 246.2; (g) albite porphyroblast with inclusions of epidote, in chlorite matrix, metasedimentary schist sample RRDDH1 224.55; (h) glaucophane inclusions preserved in albite porphyroblast, note curved inclusion trains towards margins of porphyroblast, metasedimentary schist sample RRDDH1 321.3.

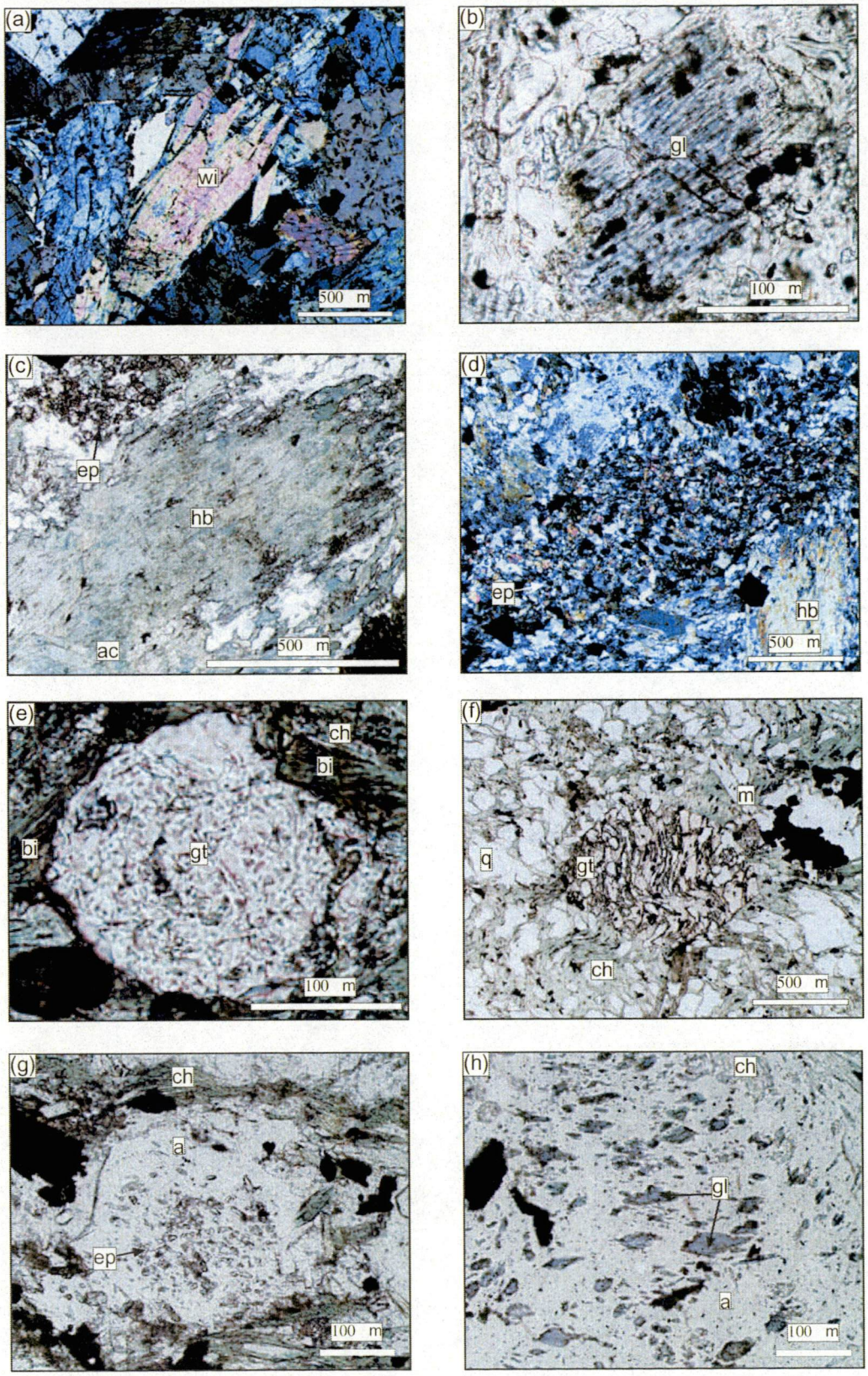

Figure 3.14(a)-(h).

present. The feldspars commonly display deformation twins. A weak foliation, defined by amphibole and chlorite was observed.

Mineralogy

Albite

Feldspar is present in 98% of the mafic meta-igneous rocks investigated. Compositionally, the feldspar is albite, with all analyses ranging between An_0 and $An_{4.5}$ (Appendix 3.10). The majority of analyses have An_1 values. Microcline is present in the granitoids in the Bowry Formation but no microprobe analyses of microcline were undertaken.

Amphibole

Amphibole was present in all metabasites and metadolerites of the Bowry Formation that were studied. Other than amphibole pseudomorphing and replacing pyroxene in some metagabbroic samples, no primary igneous textures were preserved. Using the classification scheme of Leake *et al.* (1994), the amphiboles can be grouped into the calcic, sodic-calcic, and sodic compositions (Figures 3.15(a) to (c)). The majority of amphiboles from the Bowry Formation plot in the calcic group (Figure 3.15(a)). Amphiboles in individual samples have small ranges in XMg, and slightly larger ranges in Si. Most analyses plot in the magnesiohornblende and actinolite fields, although several analyses plot in the tremolite and ferrohornblende fields (Appendix 3.11). Overall a trend reflecting positive correlation between XMg and Si in the structural formula is evident in the analyses that plot in the calcic amphibole field.

Analyses with $Na^B>0.5$, sodic-calcic amphiboles (Figure 3.15(b)) plot in the winchite, barroisite and ferrobarroisite fields. Like calcic amphiboles, these analyses have small ranges in XMg, but larger ranges in Si content. Sodic-calcic amphiboles are not as common as those in the calcic group. Most of the samples analysed have amphiboles with both calcic and sodic-calcic compositions. This is interpreted as evidence of the polyphase metamorphic history of the rocks, with the different amphibole compositions reflecting different metamorphic conditions.

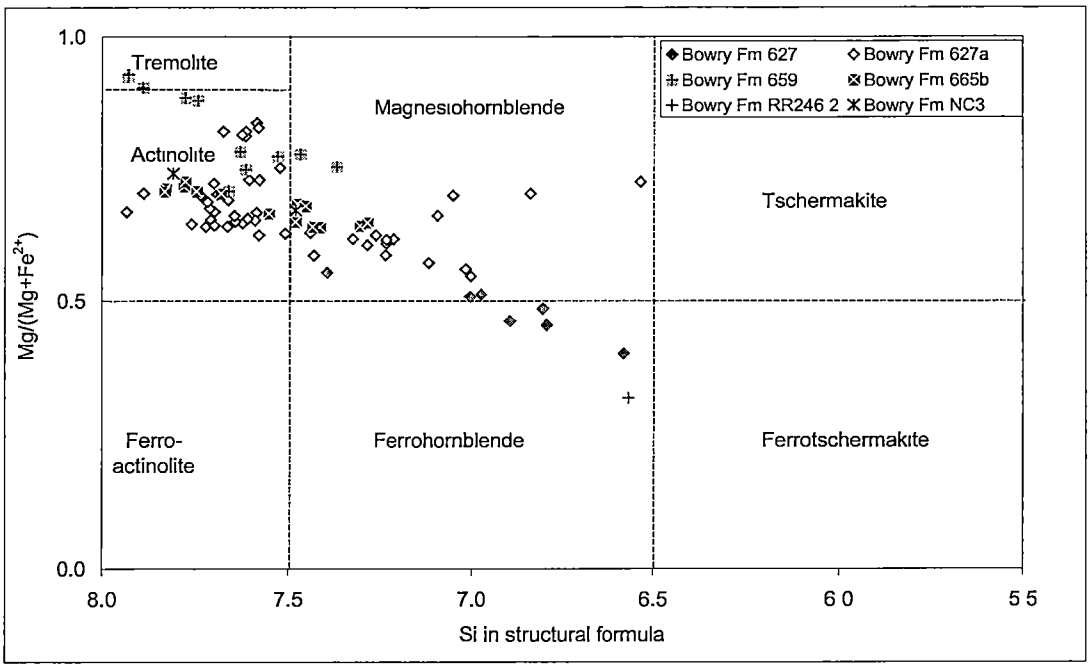

Figure 3.15(a). Calcic amphiboles of the Bowry Formation, plotted on the XMg vs Si in structural formula diagram, from Leake et al. (1997). Structural formula and cation calculations leading to subdivision is presented in Appendix 3.11.

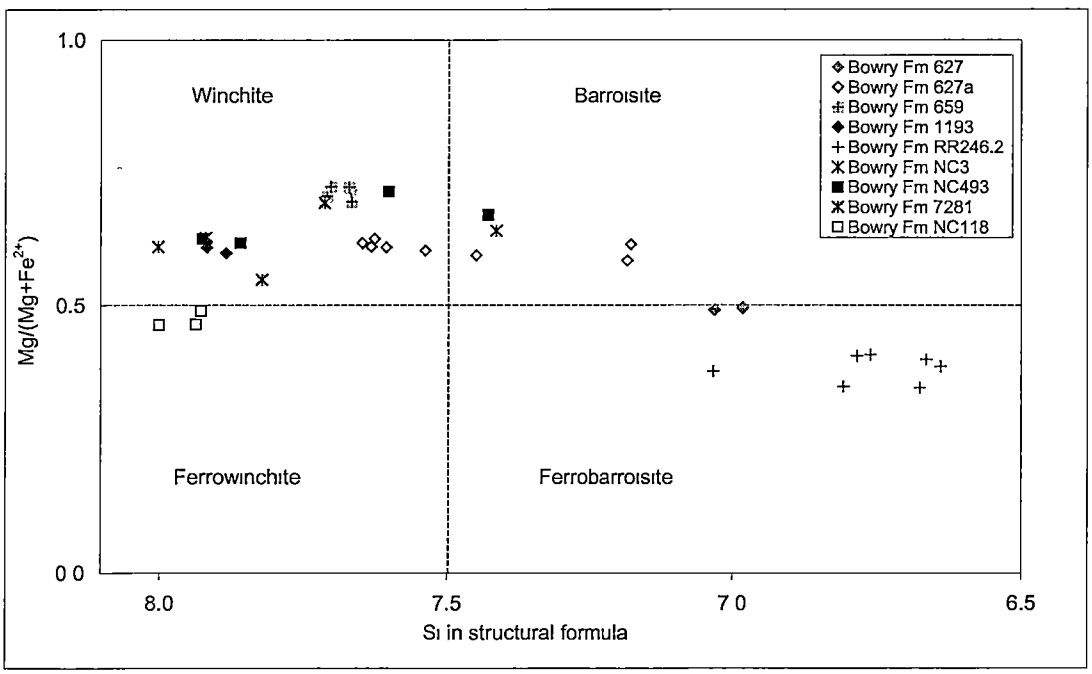

Figure 3.15(b). Sodic-calcic amphiboles of the Bowry Formation, plotted on the XMg vs Si in structural formula diagram, from Leake et al. (1997). Structural formula and cation calculations leading to subdivision is presented in Appendix 3.11.

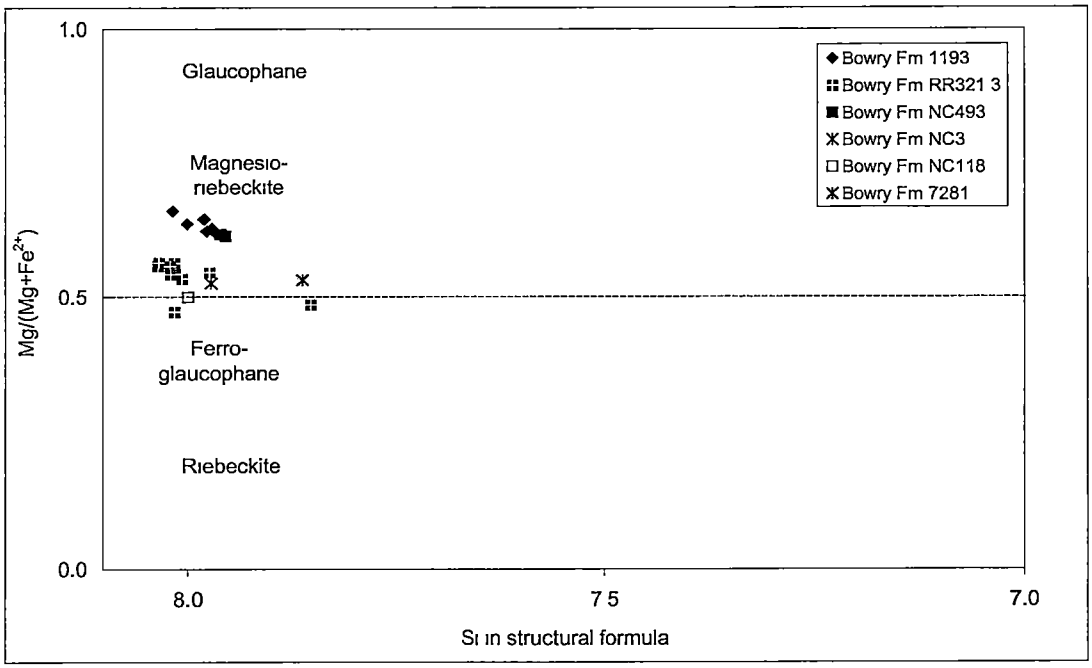

Figure 3.15(c). Sodic amphiboles of the Bowry Formation, plotted on the XMg vs Si in structural formula diagram, from Leake *et al.* (1997). Structural formula and cation calculations are presented in Appendix 3.11.

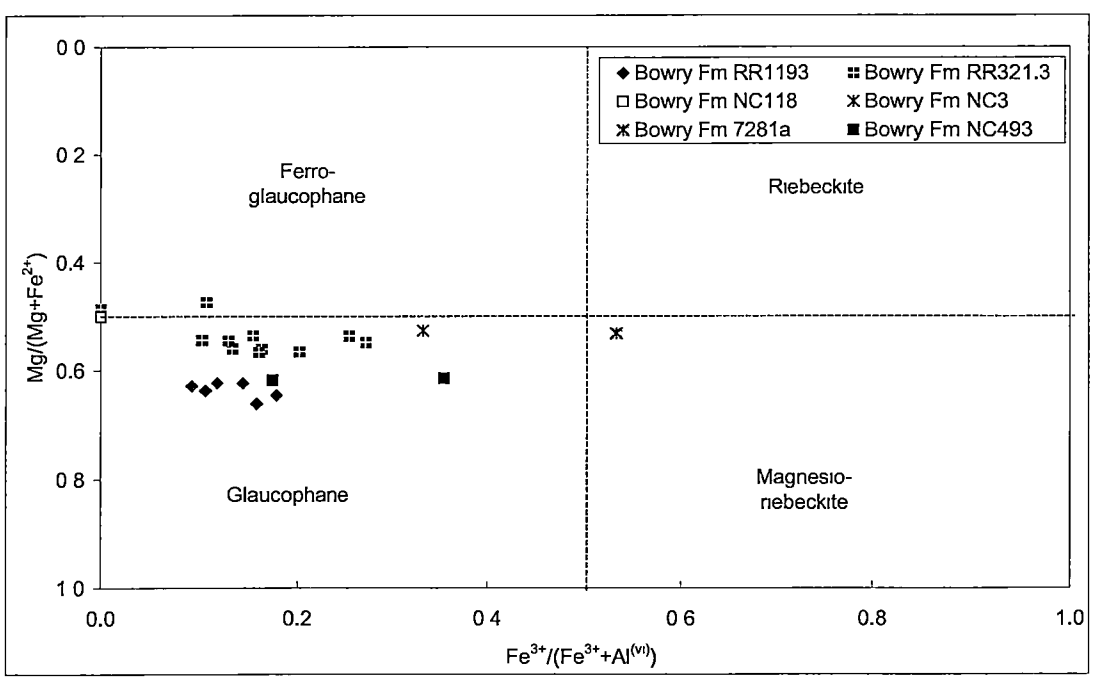

Figure 3.15(d). Sodic amphiboles of the Bowry Formation, plotted on the XMg vs $Fe^{3+}/(Fe^{3+}+Al^{(IV)})$ diagram, from Leake *et al.* (1997). Structural formula and cation calculations leading to subdivision is presented in Appendix 3.11.

Amphiboles from six samples of the Bowry Formation have compositions that plot in the sodic amphibole field (Figures 3.15(a) to (d)). Sample RRDDH1 321.2 and NC118 are metasedimentary schists, and will be discussed in section 3.4.2. Sample 1193 is a holocrystalline metadolerite, and does not display a foliation. The amphiboles from this sample have XMg values greater than 0.5 (Figure 3.15(c)), and based on the Fe^{3+} to $Al^{(vi)}$ ratio, are classified as glaucophane (Figure 3.15(d)).

Chlorite

Chlorite was observed in 83% of the mafic meta-igneous rocks analysed (Appendix 3.9). Samples free of chlorite were all coarse grained. The chlorites (Appendix 3.12) have a small range in values of Fe^{2+} (2.84-4.81) and Mg (4.42-6.18). The range in XMg is also small (0.48-0.68) (Figure 3.16). The chlorites have Al^{iv} values ranging between 2.19 and 2.55.

Epidote

Colourless to pale green epidote was observed in 93% of the metabasites and coarse grained mafic meta-igneous rocks analysed (Appendix 3.9). The chemical variation in epidotes from the Bowry Formation is small, with Al_2O_3, Fe_2O_3 and CaO all displaying a small range (Appendix 3.13). The pistacite content ($Ca_2FeAl_2Si_3O_{12}(OH)$), which determines the Fe to Al ratio (expressed as $Fe^{3+}/(Fe^{3+}+Al)$, varies from 0.16 to 0.32, with a modal value of approximately 0.23, (Ps_{23}) (Figure 3.17). The majority of samples analysed displayed an increase in Ps content from core to rim (Ps_{20} to Ps_{25}) (Appendix 3.13).

Biotite

Green biotite is a minor component in some of the mafic meta-igneous rocks of the Bowry Formation, and in the granitoids. It was found in 10% of the mafic samples (Appendix 3.9). The biotites observed were petrographically similar to those in mafic schists of the Bowry Formation (see section 3.4.2), however biotite compositions in the meta-igneous rock types were not investigated.

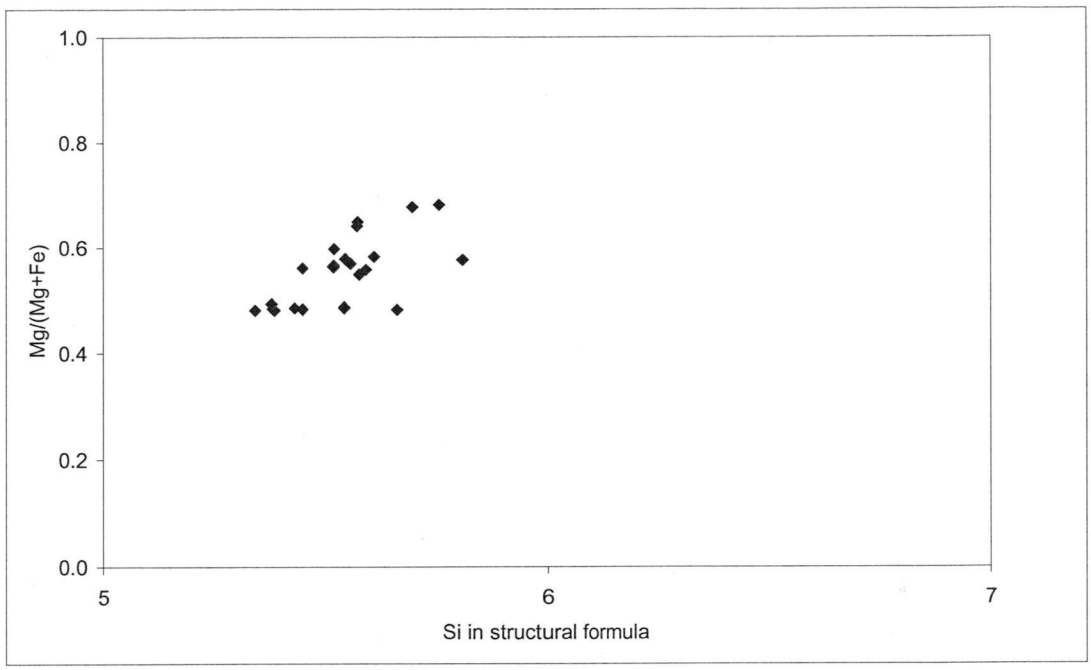

Figure 3.16. Plot of XMg vs Si in structural formula for chlorites in the Bowry Fm rocks. Chlorite compositions are from Appendix 3.12.

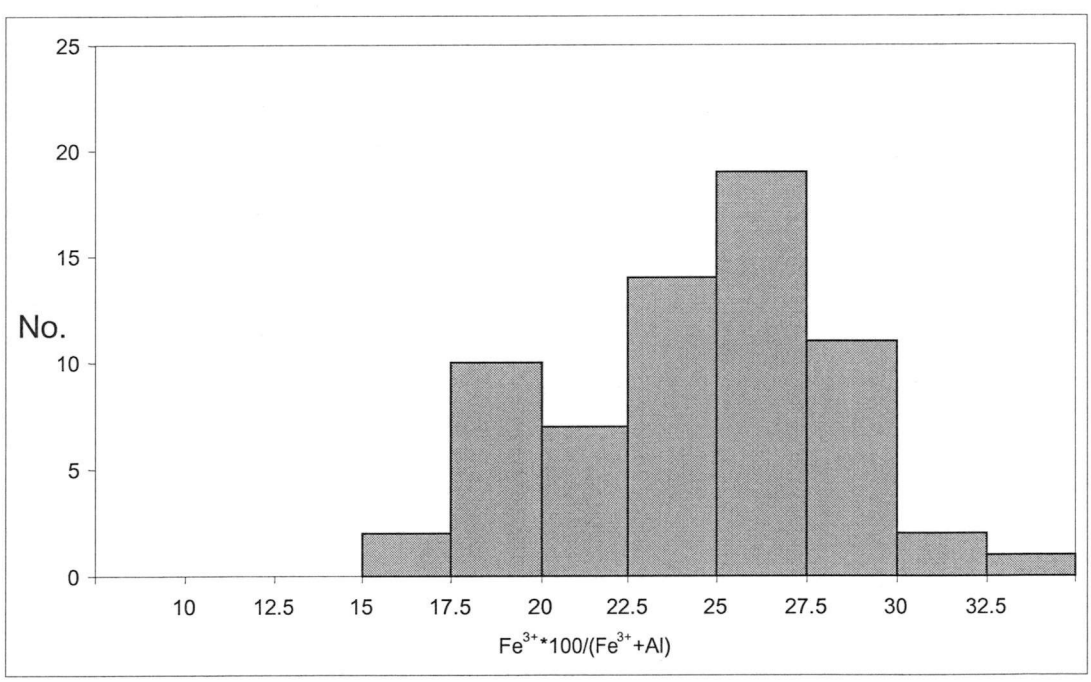

Figure 3.17. Histogram of pistacite content of epidotes from rocks of the Bowry Formation. Pistacite is calculated as $Fe^{3+}*100/(Fe^{3+}+Al)$.

Garnet

Garnet is present in the eastern Bowry Formation, in the Rocky River area (Figure 3.18(a) and (b)). It was observed in 50% of the meta-igneous rocks in the eastern Bowry Formation that were analysed, however mineralogical investigations were not undertaken. Garnet was also observed in several metasedimentary schists of the Bowry Formation, and these will be discussed in section 3.4.2

3.4.2 Psammites and psammopelites

Within the Bowry Formation, metasediments of varying composition are present. Chloritic psammopelites are dominant, however carbonate-rich psammopelites, quartz-mica-garnet schists, and quartz-albite schists were also observed. In some cases, it was difficult to establish whether the precursors to the schists were igneous or sedimentary, due to the strong degree of recrystallisation. However, in some of these cases textural styles and mineralogical abundances were found to be more consistent with a metasedimentary precursor. Other minerals present in the metasedimentary schists include amphibole, feldspar, epidote, sphene, tourmaline, magnetite, minor biotite and detrital zircon

Petrography

Garnet-bearing schists are restricted to the eastern part of the Bowry Formation, as well as the westernmost AGC, probably reflecting local metamorphic conditions. In most cases, the garnet occurs in a matrix of chlorite, with polycrystalline quartz, albite porphyroblasts, carbonate and magnetite also present. White mica was observed in these metasediments, and occurs as large post-kinematic blades that are weakly aligned with the $\boldsymbol{Ca}S_2$ foliation. Less common examples also feature green biotite, amphibole, hematite, pyrite and ilmenite. The garnets are pink in colour, and in some samples are much larger than the garnets found in the western part of the AGC. Furthermore, they have crenulated $\boldsymbol{Ca}S_1$ inclusion trails of quartz that are continuous with the foliation in the matrix of the sample (Figure 3.14(f)). The garnets are interpreted to have overgrown the $\boldsymbol{Ca}S_1$ foliation after it was crenulated by $\boldsymbol{Ca}S_2$. The samples with coarse grained garnet are not rich in albite.

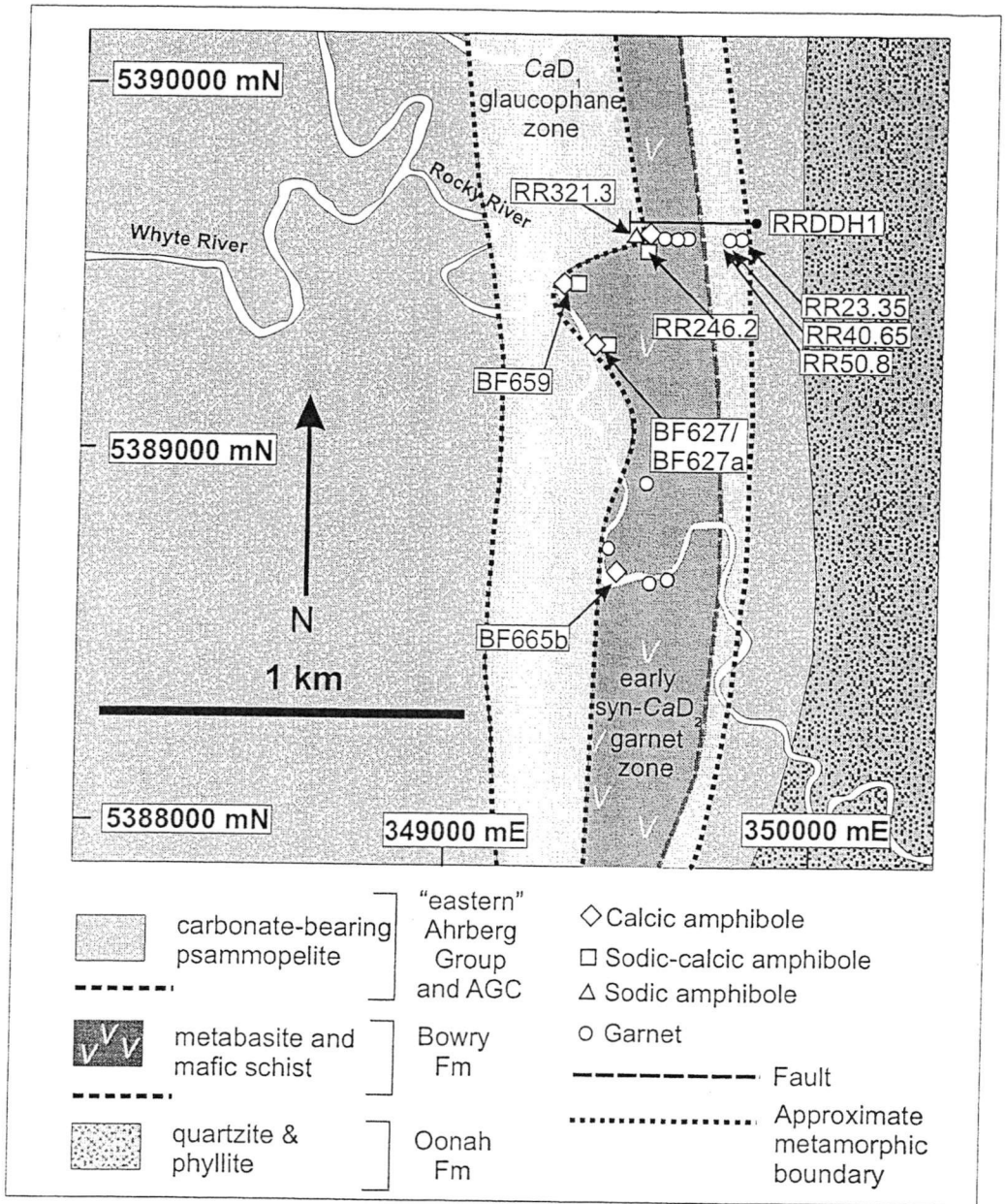

Figure 3.18(a). Location of indicator metamorphic mineral occurrences in the Bowry Formation and AGC . (modified after Turner *et al.* 1991).

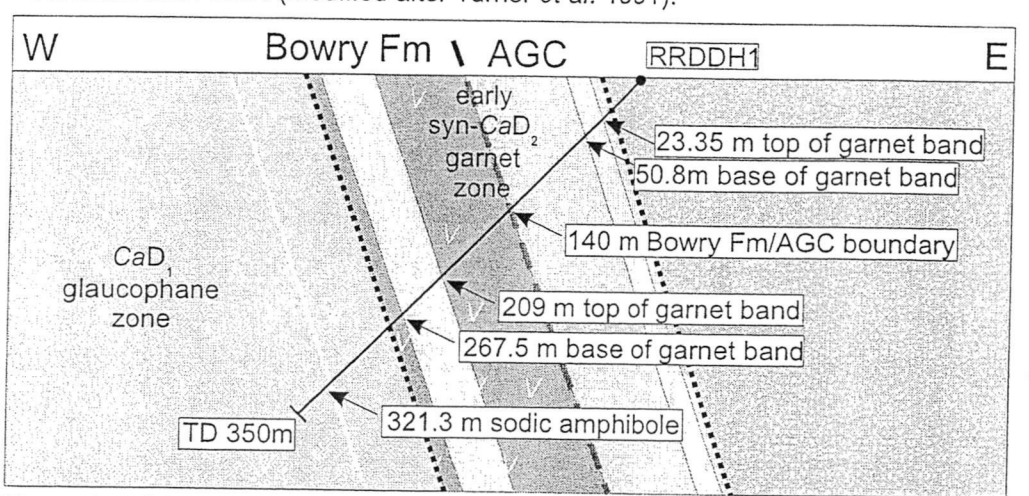

Figure 3.18(b). Location of garnet and sodic amphibole occurrences in the Bowry Formation and AGC in Rocky River DDH1. Note scale in (b) is different to (a). RRDDH1 courtesy of Goldstream Pty Ltd. Total Depth of hole (TD) = 350m

In finer grained garnet-bearing samples, garnet is colourless to pale pink, fine grained and euhedral, and does not have inclusions of other minerals. In this rock type, the anhedral albite porphyroblasts are commonly included by epidote (Figure 3.14(g)). Chlorite defines the $\boldsymbol{Ca}S_2$ foliation.

Garnet-absent metasedimentary schists in the Bowry Formation are broadly similar. They feature common syn-$\boldsymbol{Ca}D_2$ albite porphyroblasts in a strongly foliated, chlorite-dominated matrix. The amount of chlorite present is variable, with amphibole present in some of the samples analysed. Euhedral amphibole was observed in the matrix, and as inclusions in albite. Amphibole ranges in colour from green brown to lavender blue (Figure 3.14(h)). Carbonate is present in 60% of the metasediments analysed. Petrographic observations suggest the carbonate is ankerite, however its mineral chemistry was not investigated.

Mineralogy

Albite

Feldspar is present in 52% of the metasedimentary schists investigated. Compositionally, the feldspar is albite, with all analyses ranging between An_1 and $An_{6.5}$ (Appendix 3.10). The majority of analyses have An_1 values.

Amphibole

Amphibole was found to be present in 32% of the metasedimentary schists of the Bowry Formation that were analysed. Amphiboles in the metasedimentary schists are varied in composition (Appendix 3.11). Using the classification scheme of Leake *et al.* (1994), the amphiboles from metasediments (samples RR246.2, RR321.3 and NC118) can be grouped into the calcic, sodic-calcic, and sodic compositions (Figures 3.15(a) to (c)). All analyses from sample RR321.3 are sodic amphiboles, and plot in the glaucophane field (Figures 3.15(c) and (d)). Analyses from RR246.2 are calcic and sodic-calcic amphiboles (ferrohornblende and ferrobarroisite), whereas analyses from NC118 are sodic-calcic and sodic (ferrowinchite and ferroglaucophane/ glaucophane) (Figures 3.15(c) and (d)).

Chlorite

Chlorite was observed in 89% of the mafic metasedimentary schists analysed (Appendix 3.9). The analysed chlorites (Appendix 3.12) display a small range in values of Fe^{2+} (3.31-4.74) and Mg (4.37-6.12). The range in XMg is small (0.48-0.65) (Figure 3.16). The analyses have Al^{IV} values ranging between 2.43 and 2.66.

Epidote

Colourless to pale green epidote was observed in 52% of the metasediments (Appendix 3.9). The chemical variation in the epidotes from the Bowry Formation is small (Appendix 3.13). The pistacite content varies from 0.26 to 0.33, with a modal value of approximately 0.27, (Ps_{27}) (Figure 3.17).

Biotite

Green biotite occurs in 16% of the metasedimentary schists that were analysed (Appendix 3.9). The biotites observed were petrographically similar to those in other units of the Arthur Metamorphic Complex. The biotites have consistent XMg and Si levels (Figure 3.7), and despite their petrographic similarities to biotites in the "eastern" Ahrberg Group and AGC, the Bowry Formation biotites have significantly lower XMg, Si, Ti and F levels (Appendix 3.14).

Garnet

Garnet occurs in the metasediments of the eastern Bowry Formation, in the Rocky River area (Figure 3.18(a) and (b)). It was observed in 25% of the metasedimentary schists in the eastern Bowry Formation that were analysed. All of these were in the Rocky River area. The compositions show variation (Appendix 3.15), with pyrope contents ranging between 1.3 and 3.2, almandine contents of between 39.7 and 58.2 (with a median of 55.9), spessartine of between 21.1 and 42.0 (with a median of 24.5), and grossular contents ranging between 14.8 and 18.4 (Figures 3.19(a) and (b)). In comparison to the garnet compositions of the AGC samples, the Bowry Formation garnets are more almandine-rich, and grossular-poor. The two groups have similar spessartine contents.

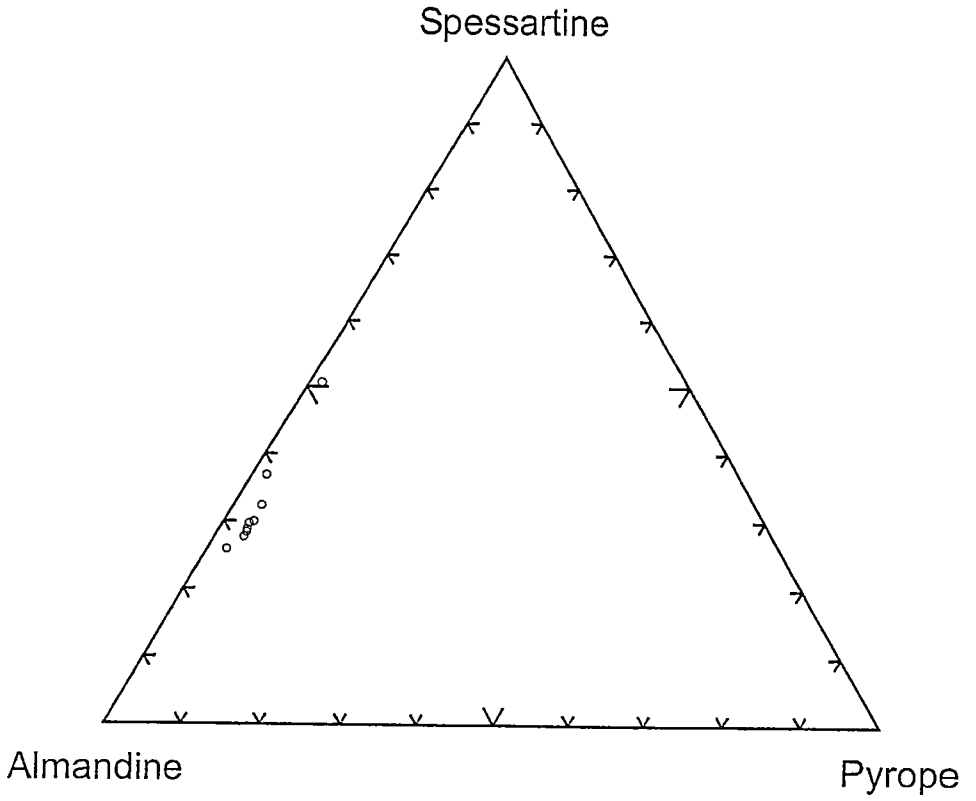

Figure 3.19(a). Almandine-Spessartine-Pyrope diagram for garnets from the Bowry Formation (sample RRDDH1 246.2).

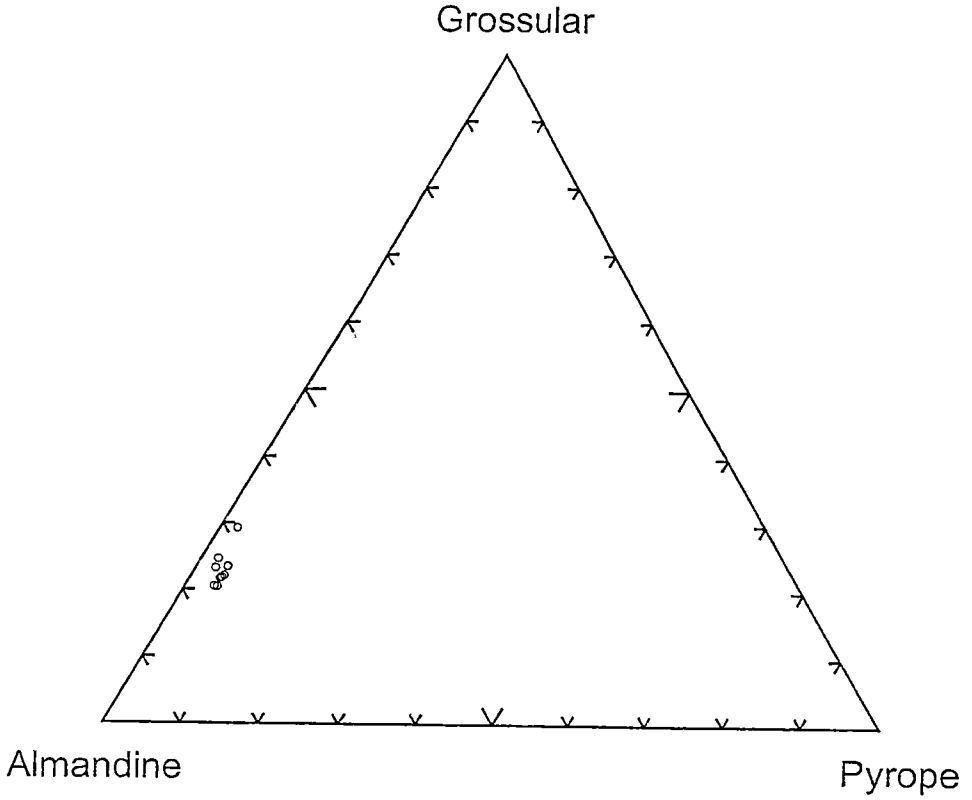

Figure 3.19(b). Almandine-Grossular-Pyrope diagram for garnets from the Bowry Formation (sample RRDDH1 246.2).

3.4.3 Conditions of metamorphism of the Bowry Formation

The Bowry Formation lithologies have undergone metamorphism at a range of conditions. In the Rocky River area, metabasites and metasediments containing garnet or glaucophane are restricted to the eastern part of the Bowry Formation. In the Reece Dam area however, glaucophane is present in the central, and western parts of the unit.

As was discussed in section 3.4.2, amphiboles in the Bowry Formation are varied in composition. Several groups of amphiboles were recognised in the Bowry Formation, reflecting different stages in the metamorphic history, and the spatial distribution of samples. The majority of samples are calcic and sodic-calcic in composition, indicative of the pervasive early $\boldsymbol{Ca}D_2$ event (Figure 3.20(a)). The composition of the cores are mostly sodic-calcic, whereas the rims are calcic, although the trend is only weakly defined (Figure 3.20(b)). This suggests the cores formed under higher temperatures and pressures than the rims. While the isobars defined by Brown (1977) are approximate, Figures 3.20(a) and (b) suggest that most cores grew with pressures in the order of 500 to 600 MPa, whereas rims are stable at lower pressures of around 300 to 400 MPa. The large range in $Al^{(iv)}$ content indicates that metamorphic temperatures were varied, and were highest in the eastern part of the Bowry Formation (samples 627, 627a and RR246.2) (Figure 3.18(a) and (b), Figure 3.20(a) and (b)). The distinct characteristics of the different samples, and the different metamorphic events is emphasised in the Na/(Ca+Na) vs Al/(Si+Al) diagram (Figure 3.21(a). Although the samples are distinct in terms of their chemistry, and therefore the metamorphic conditions under which they were formed, the calcic and sodic-calcic amphiboles lie on a uniform trend that is similar to amphiboles from subduction related environments such as the Sanbagawa and Franciscan terranes, and the Hazens Notch Formation from northern Vermont (Figure 3.21(b)). While the range of amphibole compositions overlaps with the Dalradian field, the Dalradian does not have the high sodic compositional range of the Bowry Formation

Amphiboles that are sodic in composition, from the Reece Dam, Rocky River and Savage River mine areas are interpreted to have formed in an early high pressure

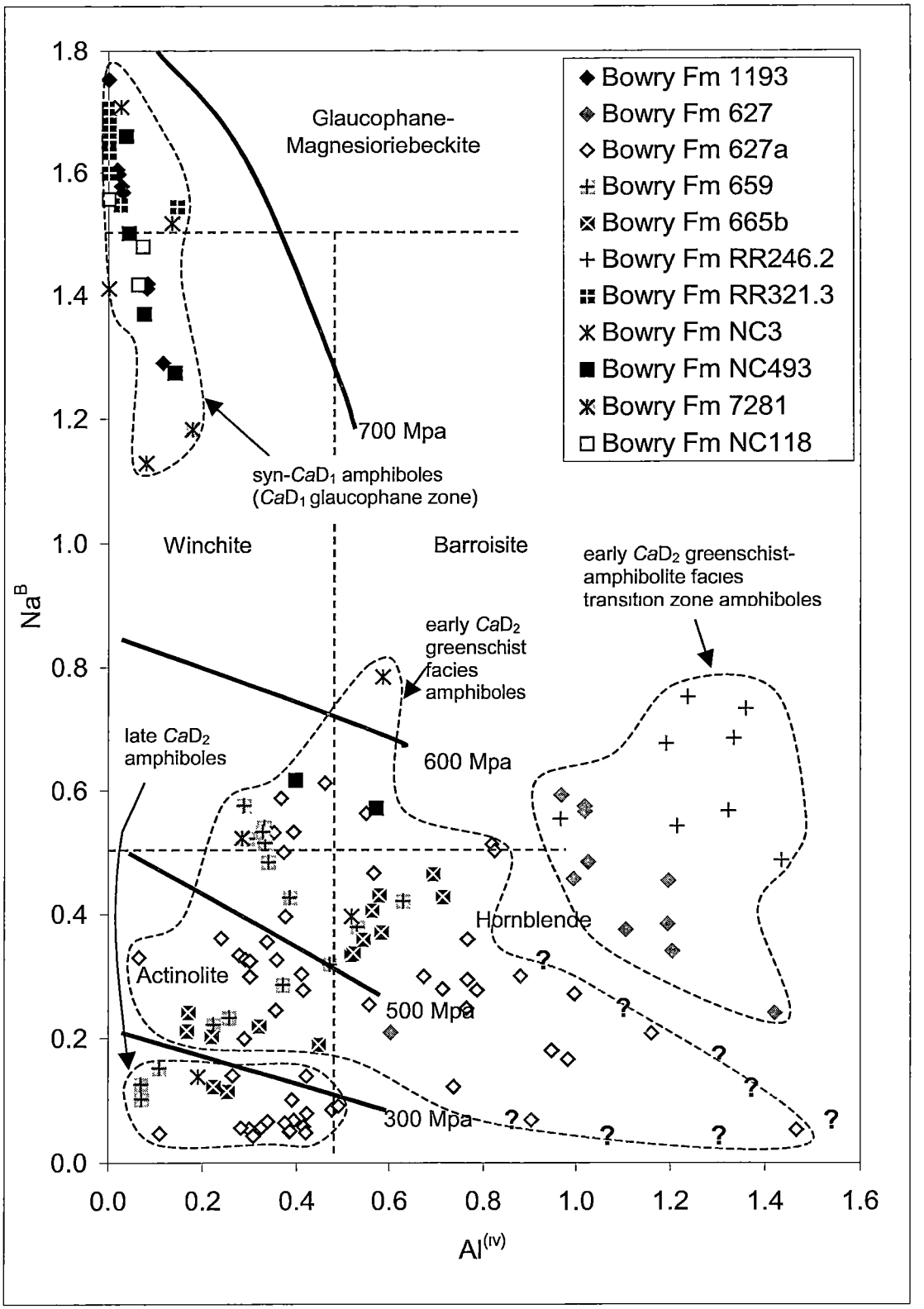

Figure 3.20(a). Amphibole compositions of the Bowry Formation plotted on the $Na^{(B\ site)}$ vs $Al^{(iv\ site)}$ diagram. The amphibole compositions reflect the spatial and temporal distribution of the samples. A tentative division is suggested, based on the individual sample compositions. Compositional fields from Leake *et al.* (1997), isobars from Brown (1977).

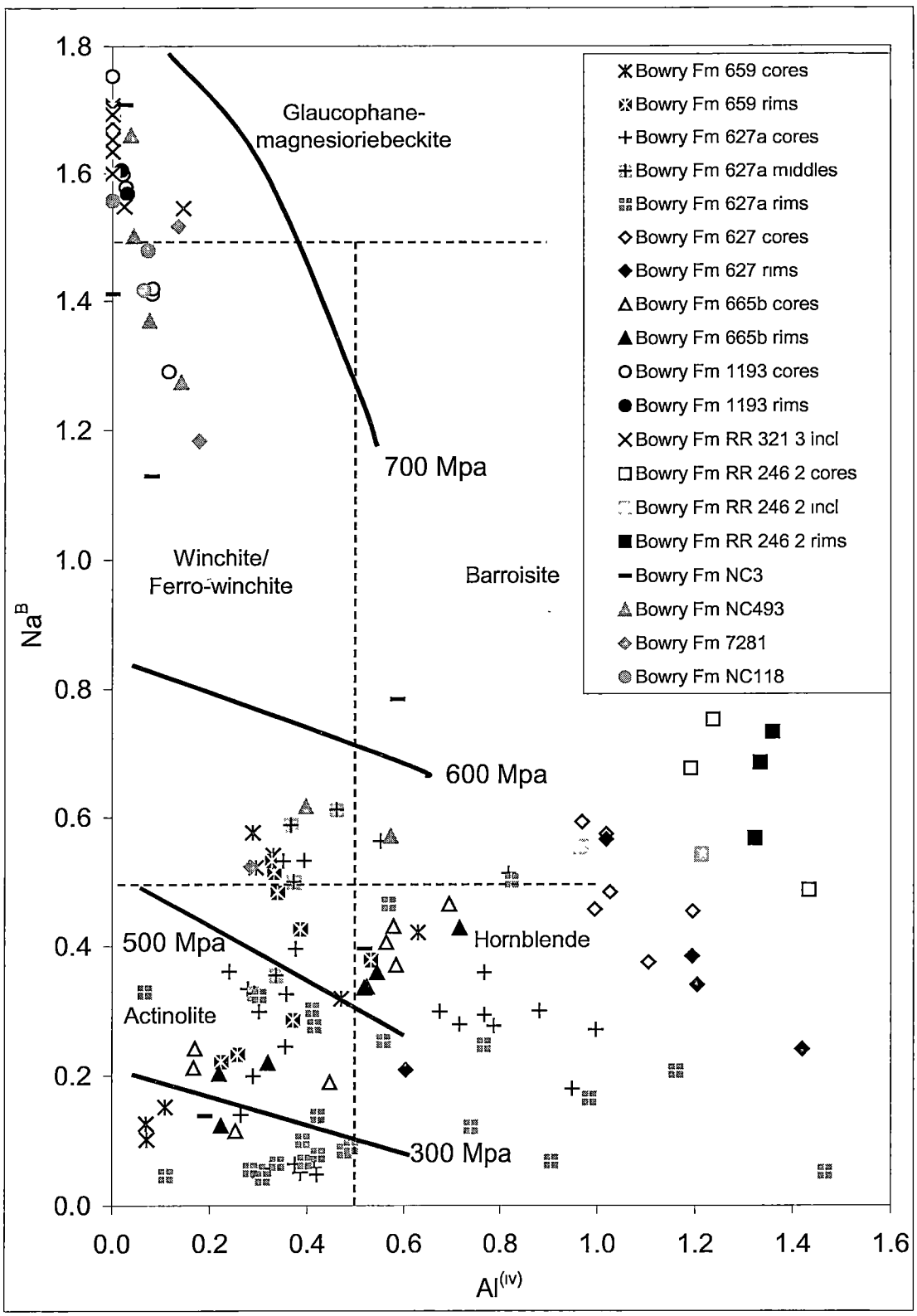

Figure 3.20(b). Amphibole compositions from the Bowry Formation, plotted on the $Na^{(B\ site)}$ vs $Al^{(IV\ site)}$ diagram. Compositional fields from Leake *et al.* (1997), isobars from Brown (1977).

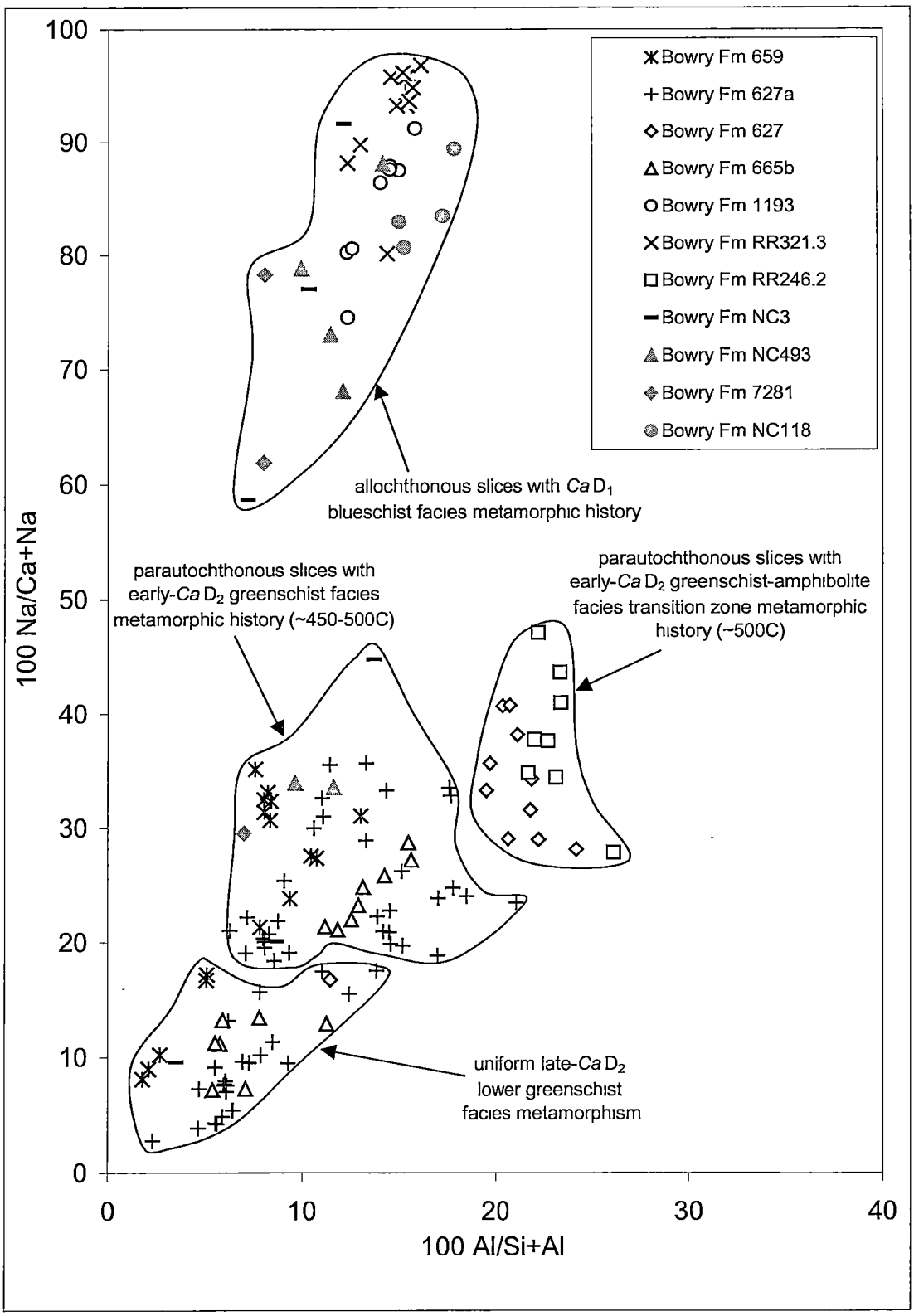

Figure 3.21(a). Amphibole compositions of Bowry Formation, plotted on the 100 Na/(Ca+Na) vs 100 Al/(Si+Al) diagram. The amphiboles lie in distinct groups, reflecting their temporal and spatial distribution.

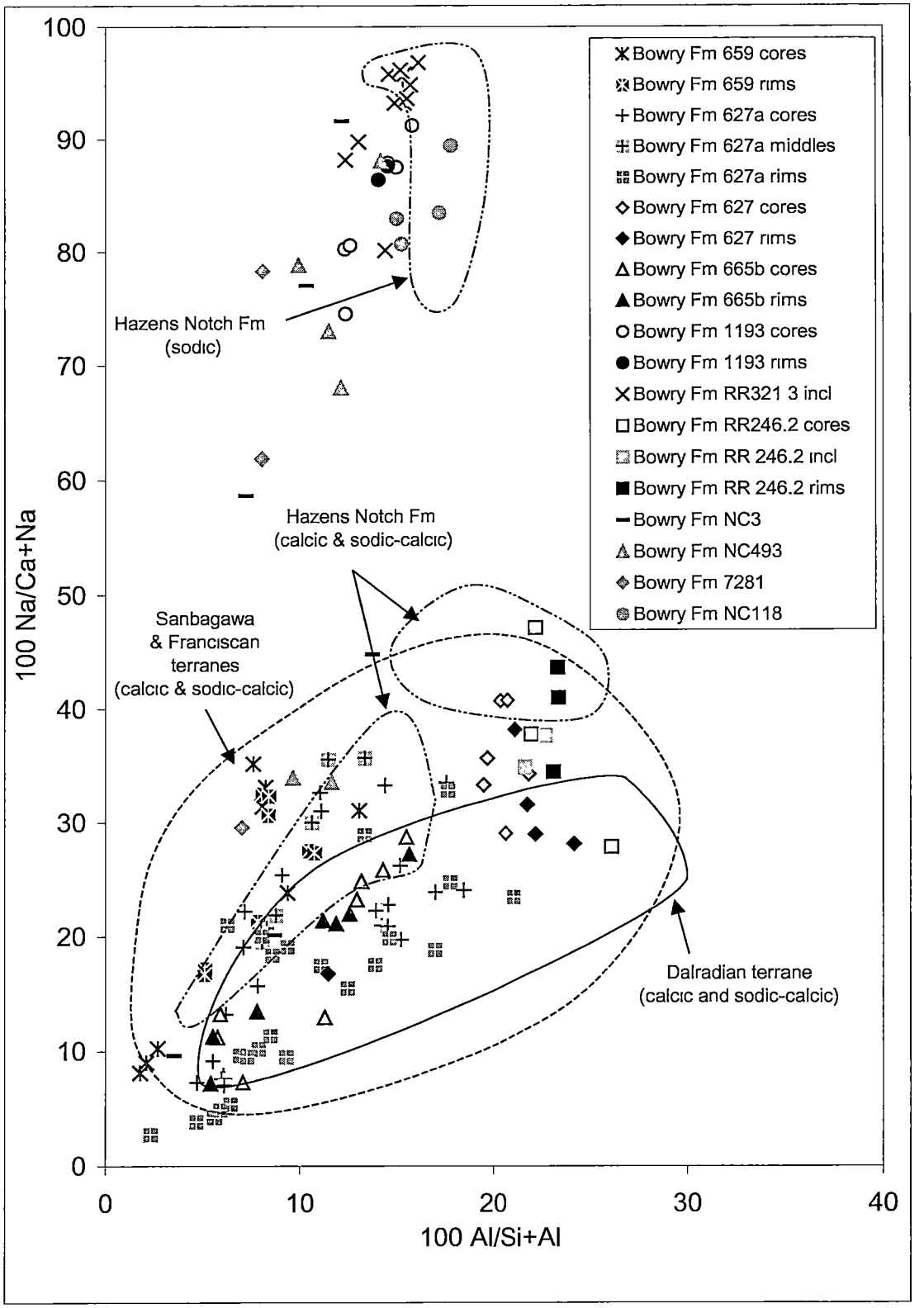

Figure 3.21(b). Amphibole compositions of Bowry Formation, plotted on the 100 Na/(Ca+Na) vs 100 Al/(Si+Al) diagram. Calcic, sodic-calcic and sodic fields for other high (Sanbagawa, Franciscan terranes and Hazens Notch Fm) and medium (Dalradian) pressure terranes are from Laird & Albee (1981b).

metamorphic event (see Section 3.6). The sodic amphiboles plot close to the 700 MPa isobar defined by Brown (1977). Based on similar metamorphic conditions in other areas (eg. Hazens Notch Formation) pressures of up to 900 MPa may have existed (Laird & Albee 1981a). Glaucophane has been shown to be unstable above 550°C (Maresch 1977), and the associated mineral assemblage (and rare occurrence of garnet) suggests temperatures during the high pressure event were considerably lower than this, probably around 450°C. Several of these samples (NC3, NC118, NC493, 1193, 7281) have a range of medium to high pressure amphibole compositions, from sodic to sodic calcic (with $Na^B \geq 1.1$) (Figure 3.20(a)). These amphiboles display a linear trend, with cores having higher Na^B contents than rims, reflecting the decreasing pressure conditions during metamorphism. The sub-vertical decompressional trend of the high pressure amphiboles (ie. constant, low $Al^{(iv)}$ content) suggests their decompressional pathway was isothermal.

Samples NC493 and NC3 also have amphibole compositions with $Na^B \leq 0.8$ (Figure 3.20(a)). The absence of calcic and sodic-calcic amphibole (with $Na^B \leq 0.8$) analyses in the other samples may be due to the complete destruction of their early mineral chemistry; or the concentration of analyses on prograde areas of the grains. Alternatively, these samples may represent faulted slices within the Bowry Formation, that have a different early metamorphic history. As can be seen in Figure 3.21(b)), the sodic amphiboles cluster around the sodic amphibole field defined by the Hazens Notch Formation samples (Laird & Albee 1981a).

Garnet (syn-$\boldsymbol{Ca}D_2$) was only observed in the eastern parts of the Bowry Formation (Figures 3.18(a) and (b)). The garnets analysed (Appendix 3.15 and Figures 3.19(a) and (b)) are slightly more almandine-rich than garnets of the AGC. The garnet-bearing sample that was analysed (RR246.2) also contains biotite. The biotite analyses are notably lower in XMg and higher in Si than the "eastern" Ahrberg Group and "western" Ahrberg Group biotites (Figure 3.7). The Bowry Formation biotites have lower F contents that the others, and may be closer to the normal biotite stability field than the "eastern" and "western" Ahrberg Groups.

Epidote compositions of the Bowry Formation are comparable to those of the "eastern" Ahrberg Group. The meta-igneous rocks from both units have lower

pistacite contents than the metasediments, suggestive of less available Fe^{3+} in the metabasites. While the chlorites from the Bowry Formation that were analysed have similar levels of XMg to the "eastern" Ahrberg Group chlorites, (*cf.* Figures 3.5(a) and (b)), the mica compositions are distinctive. The analyses from the different units form a reasonably well defined trend that, with increasing paragonite content, could be interpreted to correlate to increasing grade of metamorphism (Figure 3.9(b)).

Geothermobarometric calculations for sample RR246.2 and RR321.3 have been attempted using THERMOCALC (Powell & Holland 1998, 2000). Sample RR246.2 consists of quartz-albite-biotite-chlorite-amphibole-epidote-garnet and was considered to have a useful metamorphic assemblage. Using THERMOCALC, the calculated metamorphic conditions were 620 ± 180 MPa and 490 ± 36°C (Figure 3.13). The errors on pressure and temperatures calculated by THERMOCALC were small, and confidence in the results is greater than 95%. This pressure and temperature is comparable to samples RR40.65 and RR50.8 from the AGC. In contrast, sample RR321.3 is a glaucophane-albite-epidote schist. Using the pressure estimates of Brown (1977), the glaucophane composition implies metamorphic pressures of around 700 MPa (Figure 3.20). However, using THERMOCALC (Powell & Holland 1998), the mineral assemblage in this glaucophane-bearing rock implies metamorphic pressures were significantly higher than the garnet-bearing assemblages, at 1060 ± 190 MPa. The temperature is comparable, despite a large error (520 ± 154°C), although temperatures above 550°C are unrealistic (Figure 3.13). These results indicate that parts of the Bowry Formation have distinctly different metamorphic histories, and that it is not a coherent unit, but it is made up of a complex of blocks. The significance of this will be discussed in Section 3.6.

3.5 Metamorphism of the surrounding units

3.5.1 The "western" Ahrberg Group metasediments, metabasites and associated dolerite

The contact between the "western" Ahrberg Group and the "eastern" Ahrberg Group is faulted. The "western" Ahrberg Group unconformably overlies the Rocky Cape Group, exposed at its western boundary. The lithologies of the "western" Ahrberg Group are very similar to the "eastern" Ahrberg Group, although they are less

intensely deformed. The two units have been correlated on the basis of stratigraphic and geochemical similarities (see Chapters 1 and 4). During the Cambrian Tyennan Orogeny, in which the Arthur Lineament formed, the "western" Ahrberg Group is interpreted to have been the weakly deformed, *in situ* footwall, whereas the para-autochthonous "eastern" Ahrberg Group is interpreted to have been the more strongly deformed hangingwall. Field observations of the "western" Ahrberg Group indicate that the lithologies in this unit have experienced approximate lower greenschist facies peak metamorphic conditions, as is reflected in the chlorite dominant mineralogy of the Bernafai and Tunnelrace Volcanics, and the slaty to phyllitic textures of the interlayered metasediments. There is evidence of five episodes of ductile deformation, and at least one episode of brittle deformation (discussed in Chapter 2).

As a result of the low grade of metamorphism, and simple precursor mineralogy, the metasediments in the "western" Ahrberg Group have limited scope for metamorphic assemblage studies. Investigations into their mineral chemistry were not undertaken, although a petrographic study of the metasediments was carried out. The mineral chemistry of the mafic meta-igneous rocks of the "western" Ahrberg Group (Bernafai and Tunnelrace Volcanics) was investigated, in order to gain a better understanding of the pressures and temperatures experienced during peak metamorphism.

Petrography of metasediments

Metasedimentary rock types in the "western" Ahrberg Group include quartzites, metasiltstones, weakly deformed slates and carbonates (see Chapter 1). Metasiltstones within the Bernafai and Tunnelrace volcanics are distinguishable from siltstones in the "western" Ahrberg Group due to the presence of chlorite and magnetite.

Quartzites of the "western" Ahrberg Group consist of quartz ± mica-tourmaline (Appendix 3.16). They are fine grained, well sorted and have a grain size of 0.2-0.4 mm. Quartz grains are angular, and weakly aligned. They show slightly undulose, randomly oriented extinction. Textural evidence for recrystallisation of quartz was not observed (Figure 3.22(a)).

Figure 3.22(a) to (g) photomicrographs of metamorphic mineral assemblages in the "western" Ahrberg Group rocktypes. (a) weakly aligned, unstrained quartz grains in quartzite, no evidence of recrystallisation, sample 96; (b) moderately well foliated metasiltstone, quartz grains display straight extinction, intergrown with white mica and graphite, sample 127; (c) well foliated metasiltstone, quartz grains strongly deformed with straight extinction, intergrown with white mica and graphite, sample 151; (d) chlorite aggregate , occurring with quartz and magnetite in volcanigenic siltstone, sample 186b; (e) actinolite aggregate, possibly pseudomorphing pyroxene, in chlorite matrix, metabasalt sample 220; (f) epidote (possibly due to pre-deformational hydrothermal alteration) in actinolite, quartz and chlorite matrix, metabasalt sample 756b; (g) margin of epidote clot, with late generation epidote growing on margin of alteration-related clot, sample 756b. q: quartz, m: white mica, ch: chlorite, mt: magnetite, ac: actinolite, $ep^{(e)}$: epidote (early), $ep^{(l)}$: epidote (late).

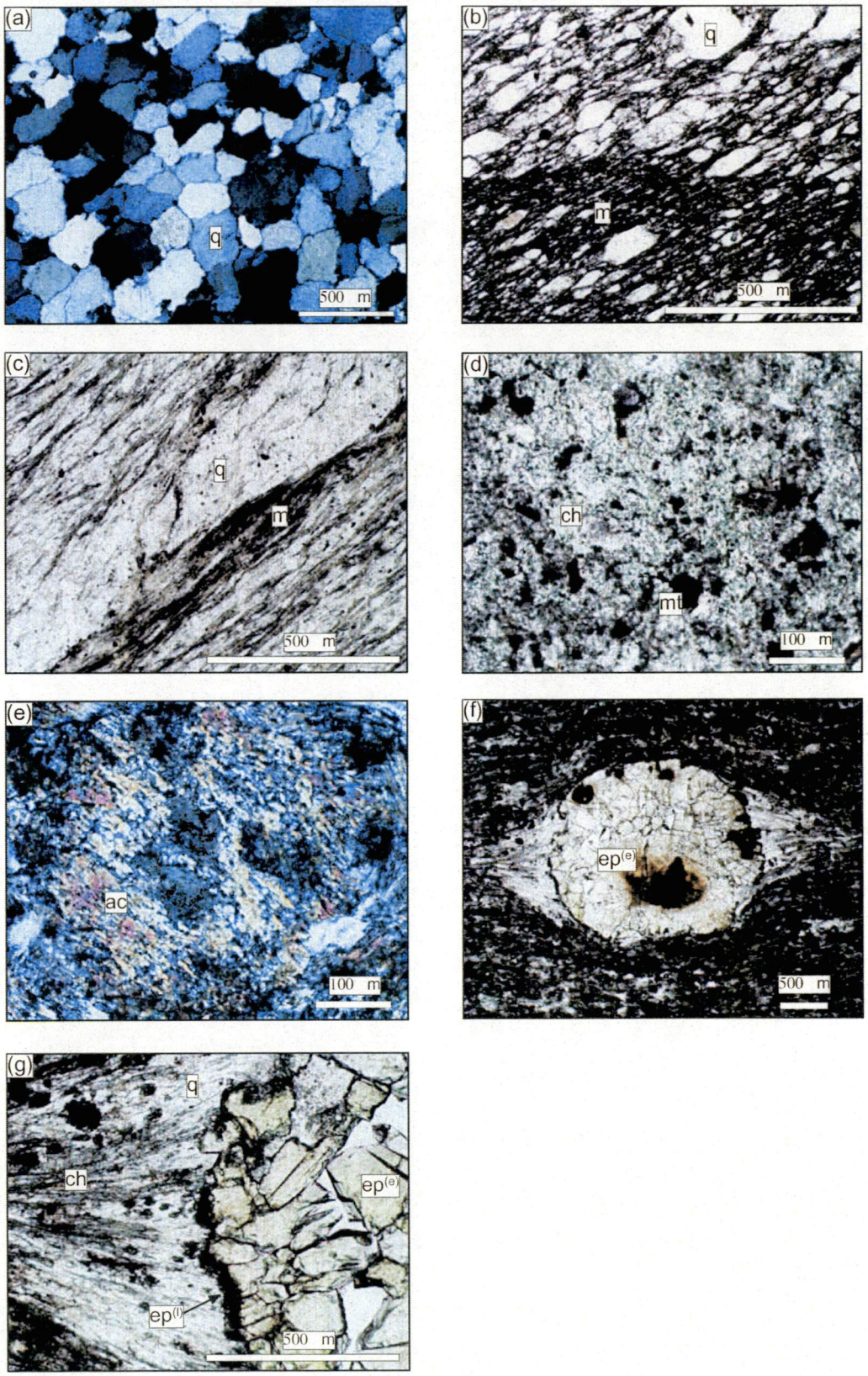

Figure 3.22(a)-(g).

The metasiltstones and slates of the "western" Ahrberg Group consist of quartz-mica-graphite ± pyrite-tourmaline-zircon-monazite-opaques, with foliations defined by white mica (Appendix 3.16). The intensity of foliation development is variable. The metasiltstones and slates are more foliated than the quartzites, and display several foliations (see Chapter 2). The units closer to the western boundary of the Arthur Lineament display more intense development of the $\boldsymbol{Ca}S_2$ foliation than those further west (*cf.* Figures 3.22(b) and (c)). The increasing intensity of $\boldsymbol{Ca}S_2$ is represented by more pronounced alignment of white mica and quartz grains. In the more strongly deformed samples, segregation of quartz and mica was observed, as part of the formation of a spaced cleavage (Figure 3.22(c)).

Within the Bernafai and Tunnelrace Volcanics, metasediments are predominantly fine grained, volcanigenic metasiltstones. They consist of quartz-chlorite-white mica-magnetite ± plagioclase-graphite-pyrite-tourmaline-carbonate-epidote (Appendix 3.16). Foliations are defined by mica and chlorite, although chlorite also occurs as clots, consisting of aggregates of randomly oriented grains (Figure 3.22(d)).

Petrography of metabasites and related dolerites

Metabasites of the Bernafai and Tunnelrace volcanics are fine grained and unfoliated to weakly foliated. Dolerite dykes which intrude the Rocky Cape Group correlates and interpreted to be related to the volcanic sequence (see Chapter 3) and are included in this section. The dolerite is slightly coarser grained than the metabasalt, and weakly foliated. A single dyke from within the Rocky Cape Group, close to the unconformity with the "eastern" Ahrberg Group (sample 241) was investigated.

The metabasites are composed of actinolite-albite-chlorite-epidote ± quartz-carbonate-sphene-magnetite-ilmenite (Appendix 3.16). In weakly foliated samples, chlorite and actinolite define the foliation. Fine grained epidote is common, and occurs as stringy aggregates aligned with the foliation. In unfoliated samples, randomly oriented actinolite was observed replacing pyroxene (Figure 3.22(e)). Several samples feature large (2 mm diameter) clots of randomly oriented yellow-green epidote, suggestive of hydrothermal alteration (Figure 3.22(f)). The epidote aggregates are interpreted to be pre-$\boldsymbol{Ca}D_2$ features. The $\boldsymbol{Ca}S_2$ foliation which is

defined by needles of actinolite and chlorite, wraps around the epidote aggregates. At the margins of the epidote aggregates, fine grained epidote that is consistent with epidote in the matrix, in terms of texture and colour, was observed (Figure 3.22(g)).

The dolerite dyke, consists of chlorite-green biotite-sphene white mica-magnetite and is strongly altered (Appendix 3.16). No primary pyroxene or metamorphic amphibole was observed. These are interpreted to have been replaced by biotite and chlorite.

Mineralogy

Amphibole

Amphibole was found to be present in 90% of the metabasites of the "western" Ahrberg Group that were analysed. Amphiboles analysed are all from a single sample (sample 220) (Appendix 3.17). Using the classification scheme of Leake *et al.* (1994), the amphiboles analysed all plot in the actinolite field of the calcic amphibole group (Figure 3.23 and Figure 3.24).

Chlorite

Chlorite was observed in all of the metabasites and metadolerites that were analysed (Appendix 3.16). The chlorites from sample 220 that were analysed (Appendix 3.18) display a small range in XMg (0.70-0.73) but a large range in Si (Figure 3.25). The analyses have Al^{IV} values ranging between 1.92 and 2.36. In contrast, sample 241 (which is altered) has higher Fe^{2+} (4.45) and Al^{IV} (2.66), and lower Mg (4.91) and XMg (0.53).

Epidote

Colourless to pale green epidote was observed in 90% of the metasediments analysed (Appendix 3.16), however only epidotes from sample 220 were analysed. The chemical variation in the epidotes from sample 220 is large (Appendix 3.19). The epidotes are aluminous relative to analyses in the other units, and the pistacite content varies from 0.13 to 0.20, with a modal value of approximately 0.20, (Ps_{20}) (Figure 3.26).

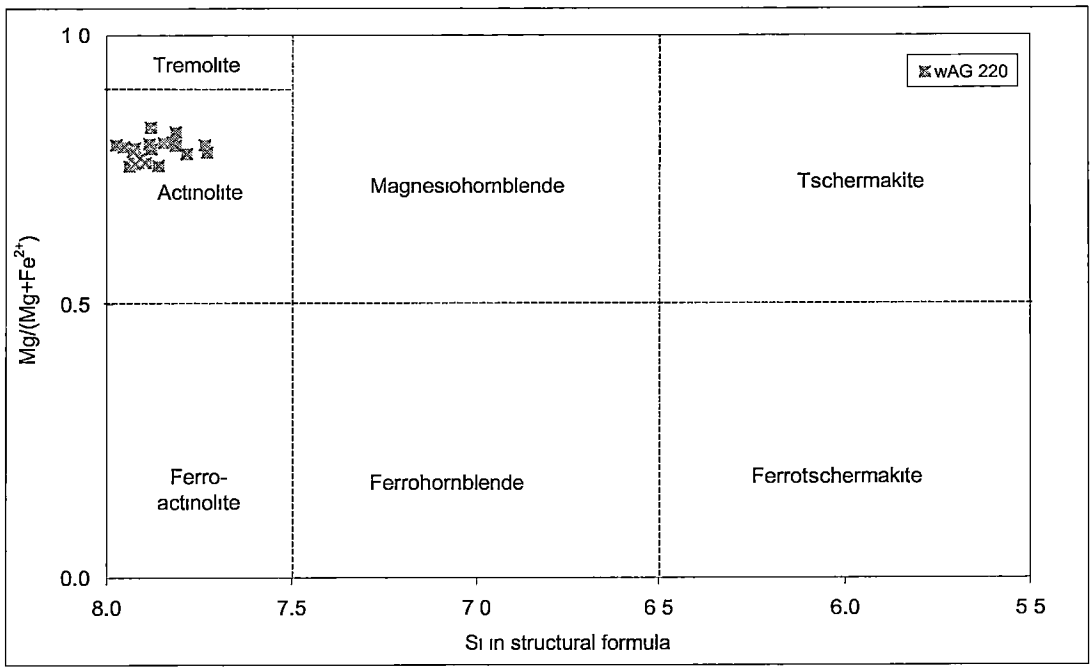

Figure 3.23. Calcic amphiboles of the "western" Ahrberg Group, plotted on the XMg vs Si in structural formula diagram, from Leake *et al.* (1997). Structural formula and cation calculations leading to subdivision is presented in Appendix 3.17.

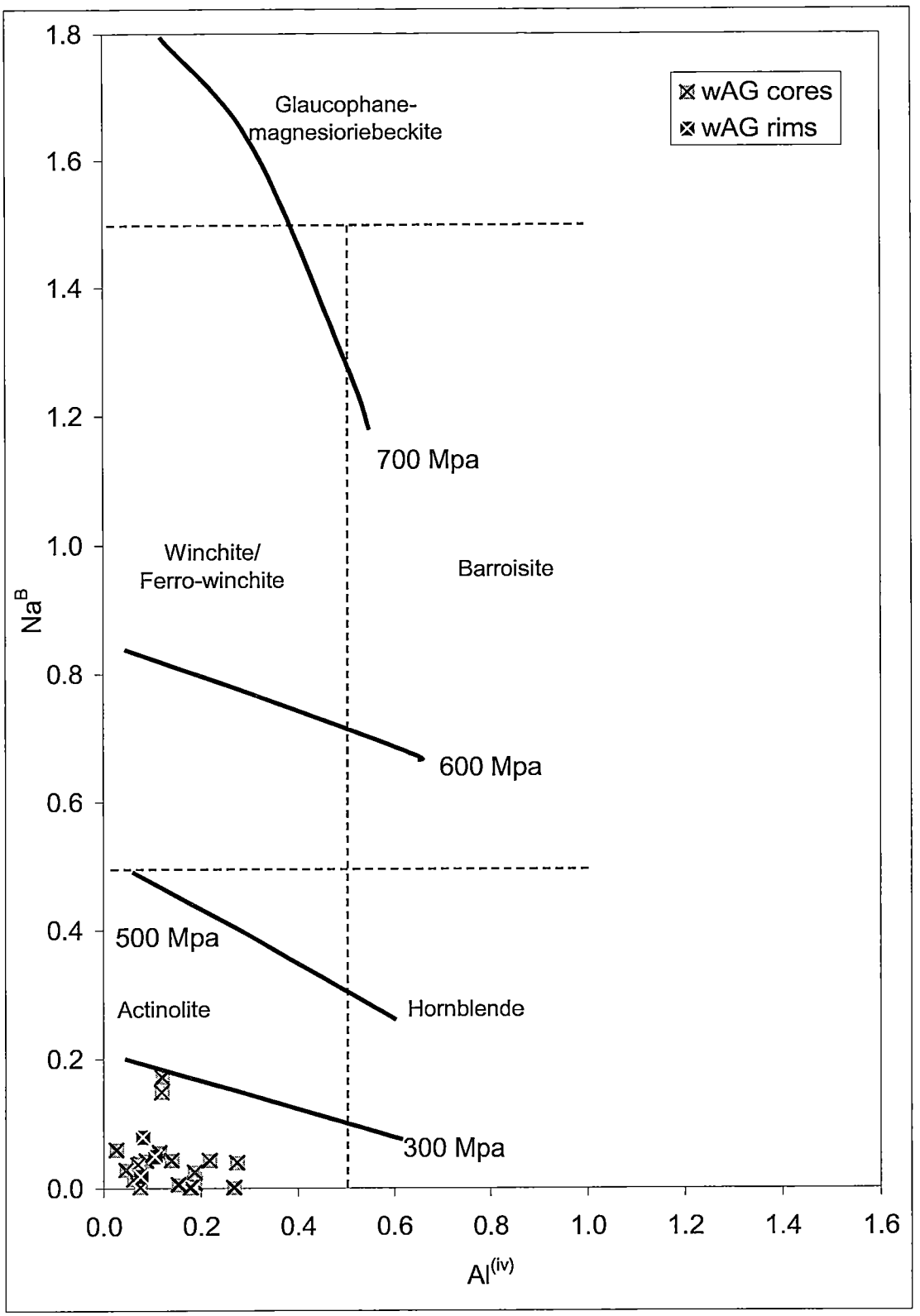

Figure 3.24. Amphibole compositions from the "western" Ahrberg Group, plotted on the $Na^{(B\ site)}$ vs $Al^{(iv\ site)}$ diagram. Compositional fields from Leake *et al.* (1997), isobars from Brown (1977).

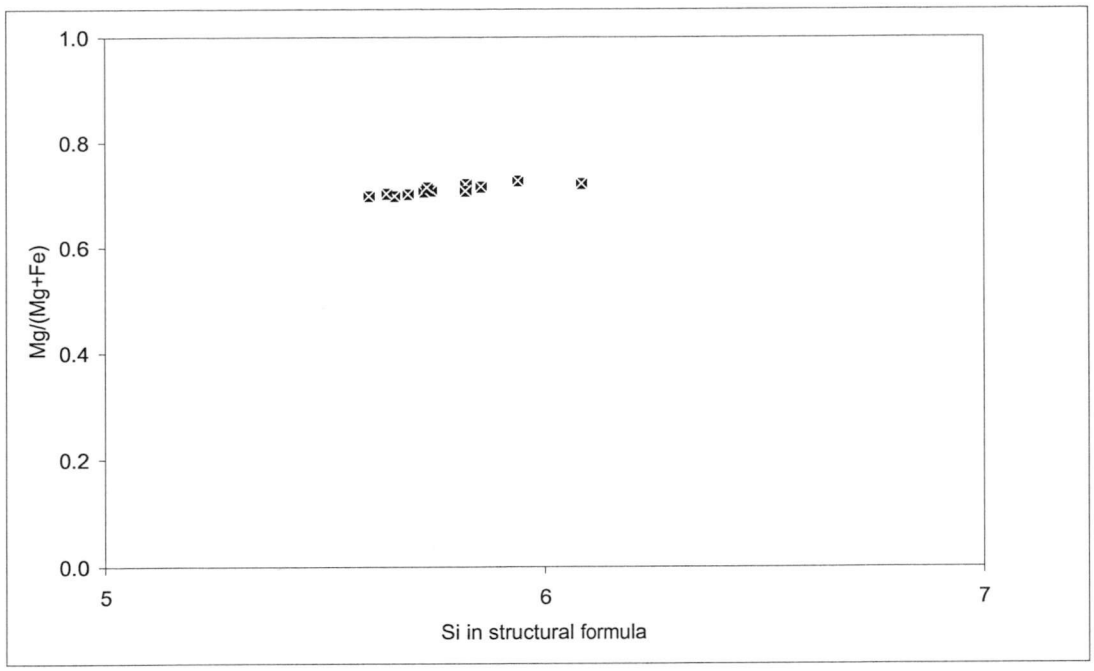

Figure 3.25. Plot of XMg vs Si in structural formula for chlorites in the "western" Ahrberg Group (wAG) metasedimentary rocks. Chlorite compositions are presented in Appendix 3.18.

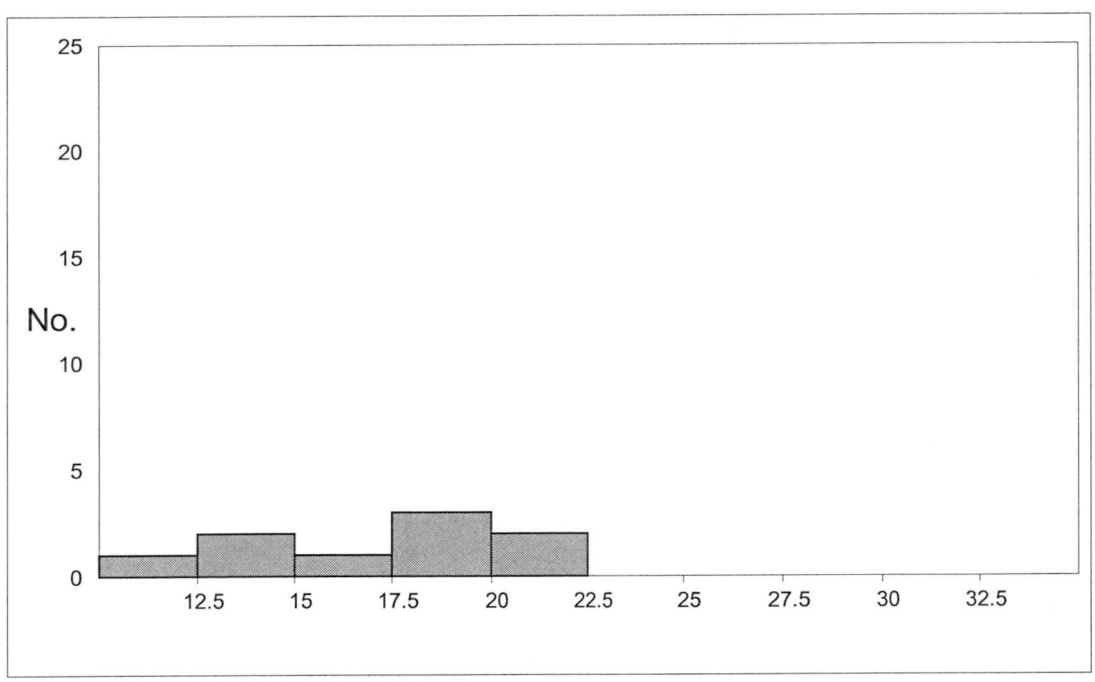

Figure 3.26. Histogram of pistacite content of epidotes from mafic meta-igneous rocks of the "western" Ahrberg Group. Pistacite is calculated as $Fe^{3+}*100/(Fe^{3+}+Al)$.

Biotite

Green biotite was only observed in the metadolerite sample 241 (Appendix 3.16). The biotites observed were petrographically similar to those evident in the "eastern" Ahrberg Group. They have consistent XMg and Si levels (Figure 3.7), and are chemically similar to biotites in the "eastern" Ahrberg Group and AGC. The levels of XMg are also interpreted to be a result of the Fe-avoidance in high-fluorine biotites (Appendix 3.20).

White mica

White mica was only present in sample 241 (Appendix 3.16). The small grains are aligned with the weakly developed foliations. 50 % of iron was assumed to be Fe^{3+}. Chemically, the XMg ($Mg/(Mg + Fe^{2+})$) content of the white mica ranges between 0.35 and 0.37 (Appendix 3.21). The celadonite component ($K(Mg, Fe)AlSi_4O_{10}(OH)_2$) of the mica, expressed as $Mg + Fe^{2+}$, is between 0.73 and 0.99 (Figure 3.9(a)). The range in Si:Al ratios is between 1.36 and 1.38. The paragonite component of the micas, expressed as $Na/(Na + K)$, is small (ranging between 0.02 and 0.03), reflecting the low metamorphic grade of the sample (Appendix 3.21 and Figure 3.9(b)).

3.5.2 Rocky Cape Group correlates

The sedimentary lithologies of the Rocky Cape Group correlates, which crop out to the west of the "western" Ahrberg Group, are weakly deformed, and display similar foliation development (see Chapter 2) and low grade metamorphic minerals to the "western" Ahrberg Group. The unit is composed of quartzites, chloritic metasiltstones and graphitic slates (see Chapter 1).

Petrographic investigations of the Rocky Cape Group correlates were undertaken. Samples from the unit were analysed for monazites (see section 3.63), however mineral chemistry studies were not carried out.

Petrography

Quartzites

Quartzites of the Rocky Cape Group correlates consist of quartz–mica ± tourmaline (Appendix 3.16). They are fine grained, poorly sorted and have a grain size of 0.2-1.0 mm. Quartz grains are angular, and weakly aligned. They show slightly undulose, randomly oriented extinction. White mica wraps around the quartz grains, and defines the weakly developed foliations (Figure 3.27(a)).

The metasiltstones and slates of the Rocky Cape Group correlates consist of quartz-mica ± chlorite-graphite-tourmaline- -zircon-monazite-pyrite, with foliations defined by white mica grains and graphite (Appendix 3.16). The intensity of foliation development is variable, however in general the metasiltstones and slates are more foliated than the quartzites. The increasing intensity of $\boldsymbol{Ca}S_2$, towards the western boundary of the Arthur Lineament is represented by more pronounced alignment of white mica and quartz grains (Figure 3.27(b)).

3.5.3 The Burnie and Oonah Formations

The low strain Burnie and Oonah Formations, to the east of the Arthur Lineament, are increasingly deformed closer to the lineament (see Chapter 2). The metasediments undergo a transition in strain from a quartzwacke, interlayered with sparsely-chloritic pelitic siltstone and mudstone to a high strain, quartz-mica schist. Due to the simple mineral assemblage of the Burnie and Oonah Formations, petrographic studies were carried out, but mineralogical investigations were not undertaken.

Petrography

The metasiltstones are mineralogically similar, consisting of quartz-mica-graphite ± chlorite-tourmaline-plagioclase (Appendix 3.16). Within the Burnie and Oonah Formations, the modal proportions of the mineral phases is variable. Whereas the intensity of the Cambrian age foliations increases westwards towards the lineament (see Chapter 2), new metamorphic mineral assemblages have not developed. However, recrystallisation of mica and quartz has occurred in the high strain Burnie and Oonah Formations, inside the lineaments eastern boundary. The size of white mica grains increases towards the lineament, with the $\boldsymbol{Ca}S_1$ and $\boldsymbol{Ca}S_2$ foliations becoming increasingly well defined. Several kilometres to the east of the lineament,

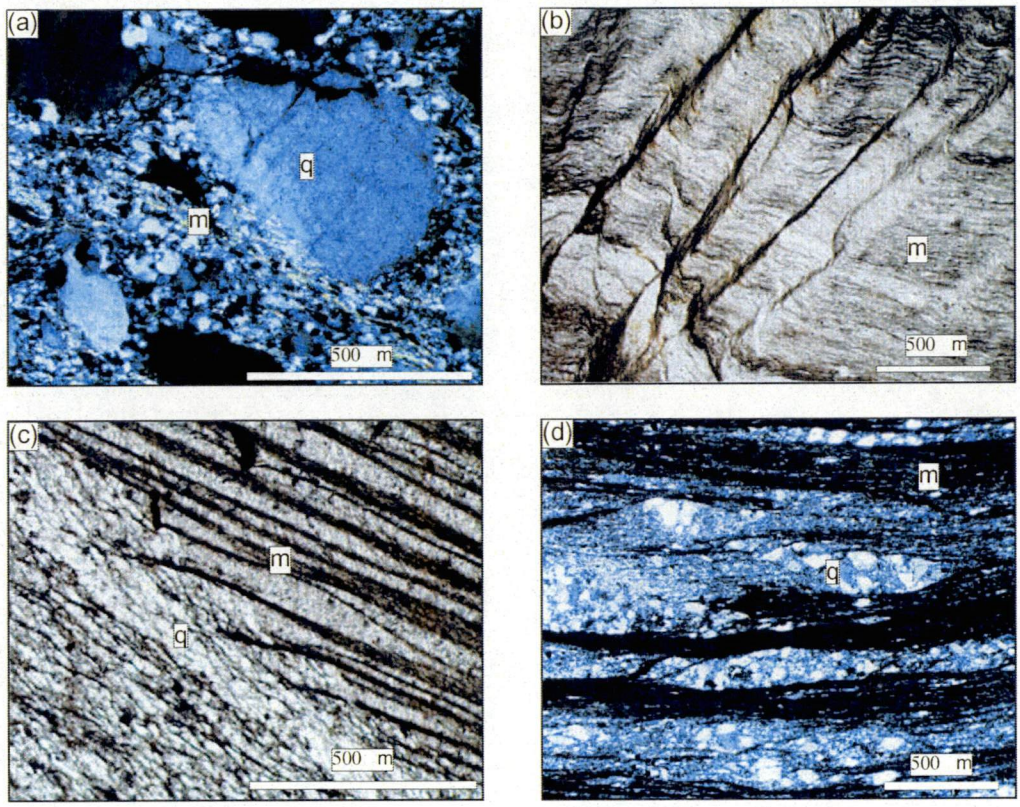

Figure 3.27.(a) to (d) photomicrographs of metamorphic mineral assemblages in metasedimentary rocks of the units surrounding the Arthur Lineament. (a) quartzite with minor white mica, quartz grains randomly oriented, Rocky Cape Group correlate, sample 181b; (b) foliated white mica-graphite-quartz metasiltstone, Rocky Cape Group correlate, sample 1019; (c) foliated quartz-white mica-graphite metasiltstone interlayered with slate, quartz grains display uniform extinction, Oonah Formation, sample 1082; (d) quartz-white mica phyllite, quartz has undergone partial recrystallisation and displays uniform extinction, Burnie Formation, sample 33309. m: white mica, q: quartz.

Figure 3.27(a) to (d).

mica grains are 0.05 mm in length, and the $Ca S_2$ foliation is a spaced cleavage (Figure 3.27(c)). Close to the lineaments eastern boundary, the mica becomes coarser grained due to recrystallisation, with grains reaching 0.2 mm in length. Here the dominant foliation is phyllitic (Figure 3.27(d)).

3.5.4 Conditions of metamorphism

Metamorphic grade decreases over a short distance to the east and west of the Arthur Lineament, coincident with the weakening development of structural fabrics associated with the lineaments formation. As is discussed in sections 3.5.1 to 3.5.3, the mineral chemistry in the units surrounding the lineament were not investigated in great detail. However, from petrographic observations, and the limited investigations into mineral compositions, the conditions of metamorphism in the "western" Ahrberg Group, Rocky Cape Group correlates, and Burnie and Oonah Formations can be approximated.

The metamorphic assemblage of actinolite-chlorite-albite-epidote (Ps_{17-22}) in the metabasites of the "western" Ahrberg Group indicates the unit is stable in greenschist facies conditions, at approximately 400°C and 300-500 MPa. The actinolitic amphiboles have Na^B contents of <0.2, and $Al^{(iv)}$ of <0.3, indicative of relatively low pressures and temperatures. The mineral assemblage is attributed to the $Ca D_2$ event. The absence of minerals stable in the zeolite and prehnite-pumpellyite facies, and the presence of actinolite in the metabasites indicates the metamorphic stability field is greenschist facies (Spear 1993, Bucher & Frey 1994). The weak development of the $Ca D_1$ event in the "western" Ahrberg Group has prevented any assessment of the metamorphic conditions during this event.

The exact metamorphic grades of the Burnie and Oonah Formations, and the Rocky Cape Group correlates were not resolved, however based on textural evidence far from the lineament, the metamorphic grade is close to the transition between the prehnite-pumpellyite facies and the greenschist facies. Close to the lineament's boundary, and within the lineament in the high strain Burnie and Oonah Formations, the metamorphic grade is interpreted to be lower to middle greenschist facies, based on the texture and mineralogy.

3.6 Discussion of metamorphism

The mineral chemistry and mineral assemblages of samples in the "eastern" and "western" Ahrberg Groups, the Bowry Formation, and the AGC illustrate that during the Cambrian deformation that produced the Arthur Lineament, metamorphic conditions, varied spatially and temporally. As a result, several different metamorphic zones within the lineament are present (Figure 3.2(a), Figure 3.18(a) and (b), Figure 3.28(a)). These zones do not directly correspond to the tectonostratigraphic divisions that are in place. The following discussion considers the metamorphic zonation across the lineament, and how this relates to the tectonostratigraphy. This will enable a better understanding of the process of emplacement of the allochthonous and parautochthonous slices within the lineament, and the timing of metamorphic events.

The extent of metamorphic recrystallisation attributed to $\boldsymbol{Ca}D_1$ in the metasediments and metabasites within the Arthur Lineament is uncertain. White mica was observed defining the $\boldsymbol{Ca}S_1$ foliation in the metasediments, however the $\boldsymbol{Ca}S_1$ foliation is not as intensely developed as $\boldsymbol{Ca}S_2$ (see Chapter 2), and it was not observed penetrating the meta-igneous rocks. Therefore, in most rocks it is not possible to confidently attribute particular mineral assemblages, and mineral compositions to the $\boldsymbol{Ca}D_1$ event. Further to this, the $\boldsymbol{Ca}D_2$ event was pervasive, and strongly overprints the earlier foliation.

In some central and eastern areas of the southern Arthur Lineament (discussed in sections 3.3. and 3.4) the $\boldsymbol{Ca}D_1$ metamorphic event is represented by sodic amphiboles, indicative of blueschist facies metamorphism (Figure 3.28(a)). Glaucophane occurs as inclusions in albite in sample RR321.3 (Figure 3.20(a)). Importantly, in this sample the long axes of the glaucophane inclusions are oriented at 55° to the dominant, $\boldsymbol{Ca}S_2$ foliation (Figure 3.29(a)). This strongly suggests that the glaucophane predates $\boldsymbol{Ca}D_2$, and represents the $\boldsymbol{Ca}D_1$ event. The glaucophane is aligned with more clinozoisite-rich epidotes, which are concentrated in the cores of albite porphyroblasts (Figure 3.29(b)).

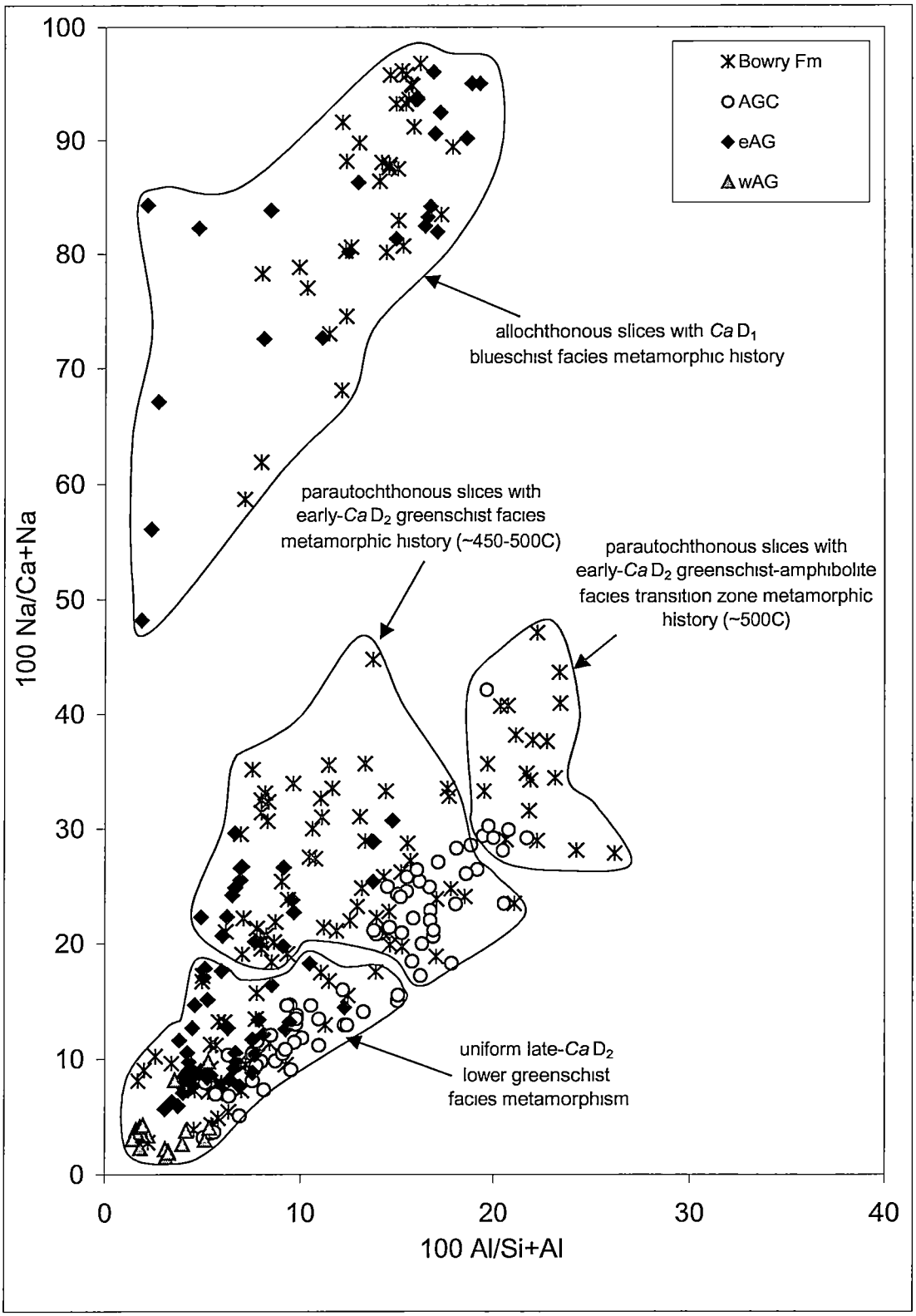

Figure 3.28(a). Amphibole compositions of the "eastern" Ahrberg Group, AGC, Bowry Formation and "western" Ahrberg Group, plotted on the 100 Na/(Ca+Na) vs 100 Al/(Si+Al) diagram. The $Al^{(IV)}$ content of the amphiboles (reflecting metamorphic temperatures) is represented by the x-axis (100 Al/Si + Al). The amphiboles can be subdivided into 4 categories, based on timing relationships and their composition. Some amphibole analyses from the allochthonous slices (with the blueschist facies history) are sodic-calcic in composition (lower value on y-axis), reflecting the isothermal decompression during CaD_2.

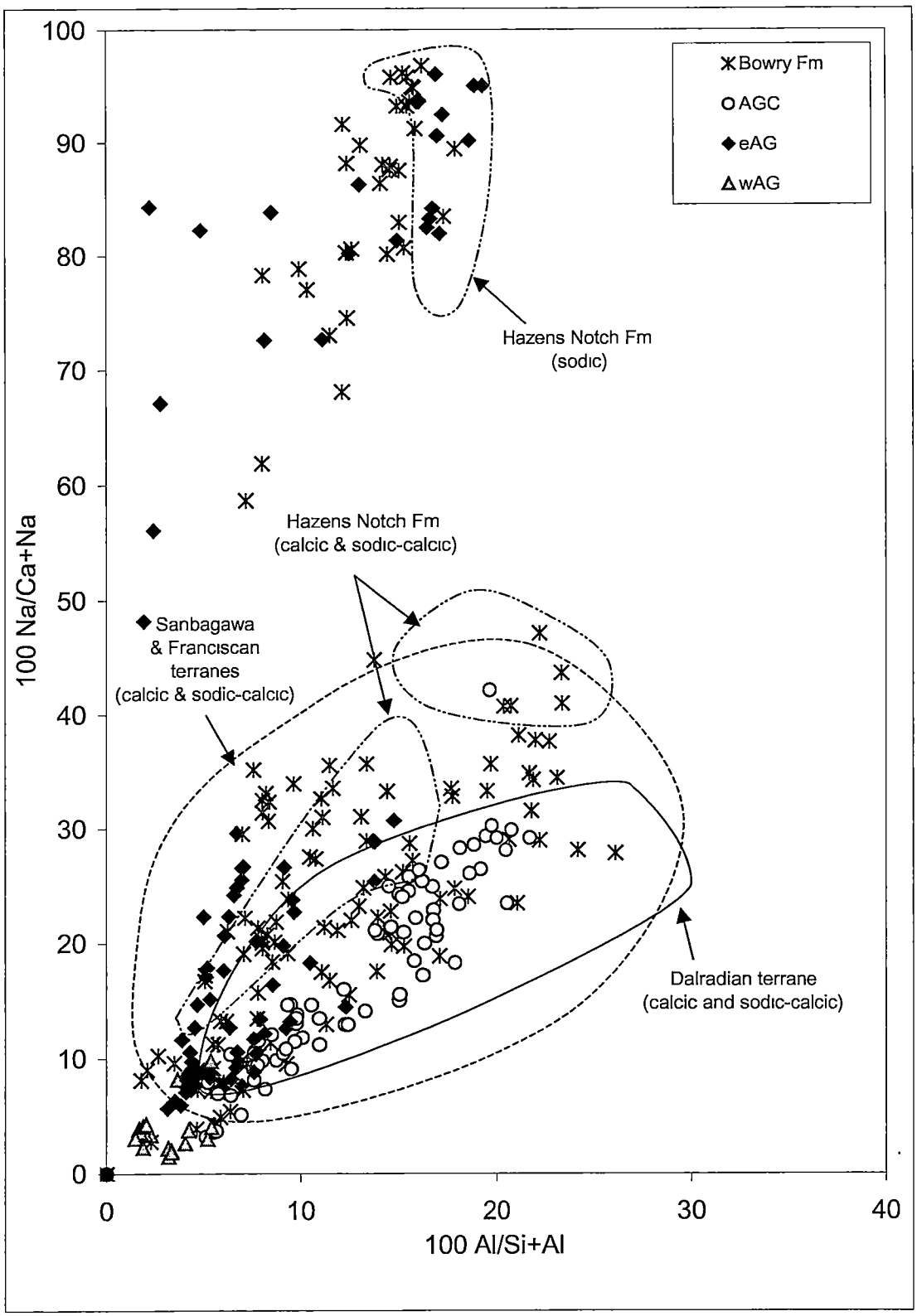

Figure 3.28(b). Amphibole compositions of the "eastern" Ahrberg Group, AGC, Bowry Formation and "western" Ahrberg Group, plotted on the 100 Na/(Ca+Na) vs 100 Al/(Si+Al) diagram. Calcic, sodic-calcic and sodic fields for other high (Sanbagawa, Franciscan terranes and Hazens Notch Fm) and medium (Dalradian) pressure terranes are from Laird & Albee (1981b)

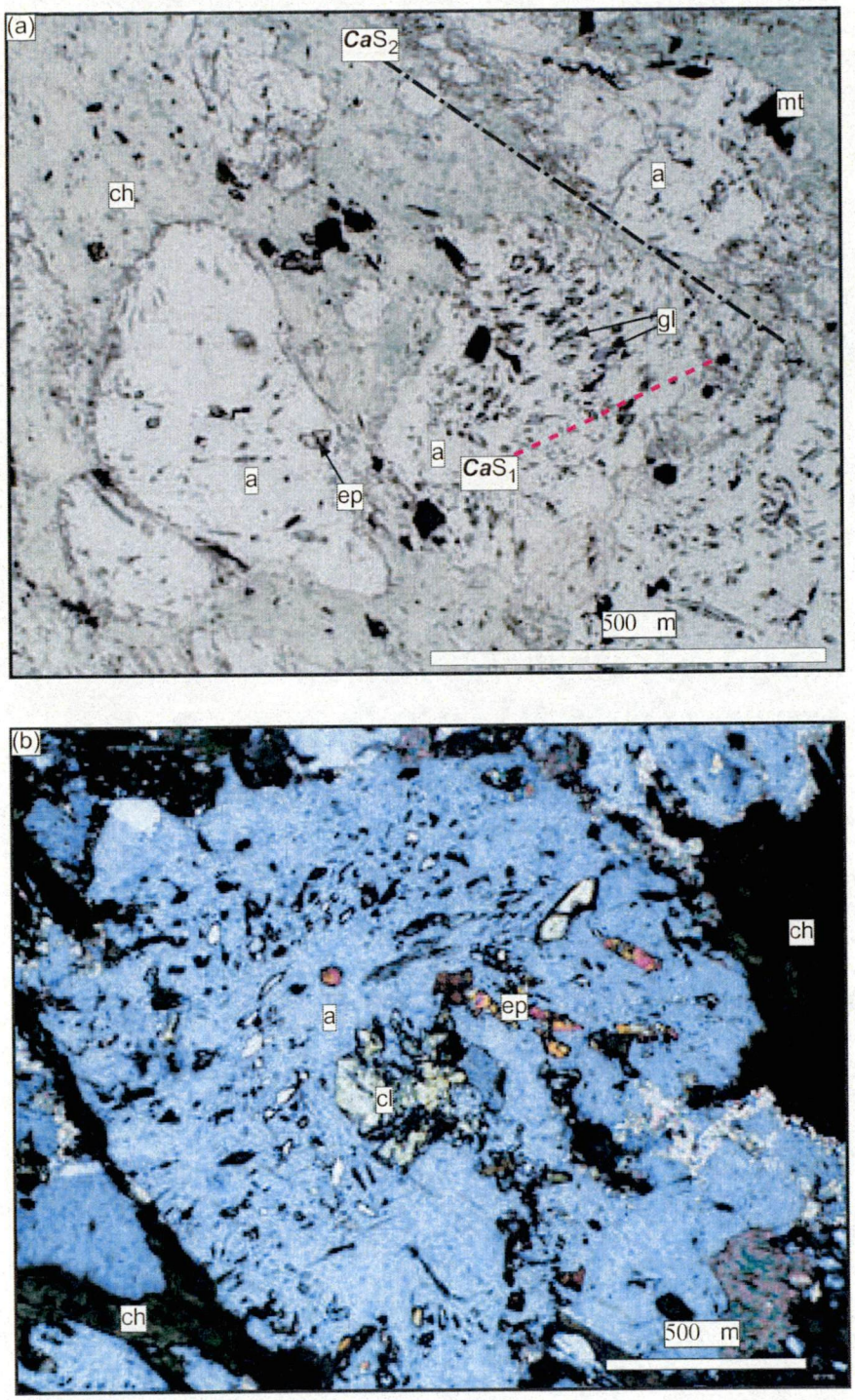

Figure 3.29(a). photomicrograph illustrating the preserved orientation of glaucophane inclusions in an albite porphyroblast, oblique (55¡) to the ***Ca***S_2 foliation defined by chlorite, metasedimentary schist sample RRDDH1 321.3; (b) photomicrograph of albite porphyroblast with zoned inclusions of clinozoisite and epidote, metasedimentary schist sample RRDDH1 321.3. ch: chlorite, a: albite: gl: glaucophane, ep: epidote, mt: magnetite, cl: clinozoisite.

The sodic amphibole analyses, which include sample eAG 56 of the "eastern" Ahrberg Group, and several other samples from the eastern part of the Bowry Formation (1193, NC3, NC118, NC493, 7281) all have consistently low $Al^{(iv)}$ contents (and therefore low Al/(Si+Al) levels), reflecting low temperature metamorphic conditions (Figure 3.28(a)). This implies that these rocks had an isothermal decompression pathway, following the ***Ca***D_1 event. Most of these samples have a range of Na^B content in the amphibole structural formula ($0.91 < Na^B < 1.80$). The amphiboles are predominantly sodic (with $Na^B > 1.5$), however several samples have amphibole compositions that are sodic-calcic (with $0.5 < Na^B < 1.5$), which are interpreted to represent a later stage of metamorphism, possibly the early ***Ca***D_2 event. In some samples, the range in Na^B content of the amphiboles corresponds to zonation from core to rim, with cores having higher levels of Na^B (more glaucophane-rich) than some rim analyses (eg. sample 1193).

The chemical affinity between the amphiboles of the different blueschist facies samples suggests a common early metamorphic history. The blocks that contain the blueschist material are interpreted to be allochthonous, as there is no evidence of this metamorphic grade in the "western" Ahrberg Group, Rocky Cape Group correlates, or Burnie and Oonah Formations (autochthonous blocks), or the "eastern" Ahrberg Group and the AGC (parautochthonous blocks). The allochthonous blocks are interpreted to have undergone rapid burial and exhumation, in a subduction zone setting, in order to have produced the blueschist facies mineral assemblages, which indicate metamorphic recrystallisation at pressures of approximately 700 to 1200 MPa, and temperatures of 450 to 500°C (Figure 3.13).

In some eastern parts of the lineament, close to the boundary between the AGC and the Bowry Formation, the early phase of the ***Ca***D_2 event is represented by metamorphism in the greenschist-amphibolite facies transition zone, with metamorphic conditions just reaching the garnet stability field (Figure 3.18(a) and (b)) (Spear 1993). The amphiboles in the samples from this area are hornblende and winchite, and post-date the ***Ca***D_1 event (Figure 3.28(a)). However, they clearly predate the development of actinolite, which is a late ***Ca***D_2 event. As the development of the Arthur Lineament is interpreted to have featured a progressive style of deformation, the higher temperature calcic and sodic-calcic amphiboles are

thought to represent the early phase of the ***Ca***D_2 event. The garnets vary slightly in composition, with the westernmost garnets (from the Bowry Formation) having a larger almandine component, and less spessartine and grossular (Appendices 3.7 and 3.15, Figures 3.8(a) to (d) and Figures 3.19(a) and (b)). As the some samples with garnets occur in equilibrium with sodic-calcic amphiboles that have high $Al^{(iv)}$ contents (indicative of higher temperatures), the eastern part of the Bowry Formation is considered to have been marginally hotter than the western part of the AGC during the early part of the ***Ca***D_2 event (Figure 3.13). To the west of the boundary zone between the Bowry Formation and the AGC, temperatures during the early ***Ca***D_2 metamorphism were lower, in the lower greenschist facies (Figure 3.28(a)). The calcic and sodic-calcic amphiboles and the absence of garnet in the western parts of the lineament are indicative of a lower thermal gradient during this event. Both groups of early ***Ca***D_2 amphiboles are consistent with the medium pressure amphibole compositions from the defined terranes in subduction-related settings (Figure 3.28(b)) (Laird & Albee 1981b).

The late-***Ca***D_2 mineral assemblage represents the lowest grade of metamorphism in the Arthur Lineament, and is consistent in the "eastern" and "western" Ahrberg Groups, the AGC and the Bowry Formation. The amphiboles are actinolite, indicative of greenschist facies metamorphism at pressures of around 300 MPa (Figure 3.28(a)). A change in amphibole composition from core to rim in the metabasites of the "eastern" Ahrberg Group and AGC is discernible, and implies a decrease in temperature and pressure from early to late ***Ca***D_2 (Figures 3.10(a) and (b), Figures 3.11(a) and (b)). In contrast, in the Bowry Formation, the trend in amphibole compositions from core to rim was not as well developed (Figure 3.20(b) and Figure 3.21(b)).

The spatial and temporal variations in amphibole chemistry and mineral assemblages are critical in establishing the timing and mechanism of deformation in northwestern Tasmania, and the formation of the Arthur Lineament. The ***Ca***D_1 event was observed in all units of the lineament, however the blueschist facies metamorphism associated with ***Ca***D_1 is only present in a few blocks. As discussed above, these blocks are interpreted to be allochthonous, as the surrounding autochthonous, and parautochthonous blocks show no evidence of these metamorphic conditions, and are

thought to have experienced substantially lower pressures during $Ca D_1$ metamorphism. Incorporating the structural style and orientation of the $Ca F_1$ and $Ca F_2$ folds, as well as the implied south-directed transport during the $Ca D_1$ and $Ca D_2$ events, the blueschist-forming event (rapid burial and exhumation) is interpreted to have occurred in a subduction zone some distance from the current positions of the allochthons. The results of this work suggest this subduction zone was to the north-northeast of the Arthur Lineament.

The two stages of the $Ca D_2$ event are significant, as the metamorphic grade during the two events differs. The metamorphism attributed to the early stage of $Ca D_2$ is spatially varied in its intensity. During this stage, the autochthonous "western" Ahrberg Group, Rocky Cape Group correlates and the Burnie and Oonah Formations were weakly metamorphosed in comparison to the "eastern" Ahrberg Group, AGC and Bowry Formation.

Furthermore, metamorphic grade during the early stage of the $Ca D_2$ event varied between the "eastern" Ahrberg Group, AGC and Bowry Formation. The parts of the AGC and Bowry Formation that reached greenschist-amphibolite grade (producing garnet in some samples) are also interpreted to have originated some distance from their present positions. Although their metamorphic grade during the early stage of the $Ca D_2$ event is similar to that of the "eastern" Ahrberg Group, the AGC and Bowry Formation experienced higher temperatures. The origin of the rocks of the AGC and Bowry Formation that experienced greenschist-amphibolite facies metamorphism is interpreted to have been closer to their current position than the origin of the blueschist facies slices. As the Bowry Formation consists of some rocks that experienced blueschist facies metamorphism, followed by lower greenschist facies metamorphism; and other rocks that experienced greenschist-amphibolite grade followed by lower greenschist grade metamorphism, it is apparent that the unit is composed of blocks with different $Ca D_1$ to early $Ca D_2$ metamorphic histories. This is of critical importance, as it demonstrates that the Bowry Formation is a complex of blocks, rather than a coherent unit. In contrast to the differing $Ca D_1$ to early $Ca D_2$ metamorphic histories, the blocks have similar late-$Ca D_2$ metamorphic histories. The AGC also consists of blocks with different $Ca D_1$ to early $Ca D_2$ metamorphic histories, but which also have similar late-$Ca D_2$ metamorphic histories.

The western part of the AGC is composed of rocks that experienced greenschist-amphibolite facies, followed by lower greenschist facies metamorphism, whereas in the eastern part of the AGC (like in the "eastern" Ahrberg Group), the rocks did not experience an early, high temperature (greenschist-amphibolite facies) metamorphic event. These lower grade areas experienced middle greenschist facies conditions in early $\boldsymbol{Ca}D_2$, and lower greenschist facies conditions in late $\boldsymbol{Ca}D_2$. This suggests that the AGC, like the Bowry Formation, is a complex of blocks, with different early metamorphic histories.

From the spatial and temporal associations outlined above, it can be suggested that whereas the differing metamorphic conditions during $\boldsymbol{Ca}D_1$ and early $\boldsymbol{Ca}D_2$, indicate the blocks were distributed at various distances from their current positions, by late $\boldsymbol{Ca}D_2$ there had been substantial rearrangements. The uniform metamorphic grade throughout the lineament during the late $\boldsymbol{Ca}D_2$ event implies that by this stage, the different blocks that comprise the Arthur Lineament could have been adjacent to each other, and 'stacked' in their current position. At this stage, prior to the uplifting and tilting associated with the $\boldsymbol{Ca}D_3$ event (see Chapter 2), the lineament is interpreted to have still been a sub-horizontal feature. Metamorphism during the $\boldsymbol{Ca}D_3$ event is interpreted to have been significantly weaker than the $\boldsymbol{Ca}D_1$ and $\boldsymbol{Ca}D_2$, events, and did not result in significant metamorphic recrystallisation.

3.7 Geochronology and mineral chemistry of metamorphic monazites in northwest Tasmania

3.7.1 Introduction and analytical technique

U-Th-Pb dating is used in geology to determine the age of the minerals, which contain significant amounts of U and Th, such as zircon and monazite. Numerous studies of isotopic systems have shown that the amount of Pb in these minerals is directly proportional to the amount of Th and U and the length of time lapsed since the mineral was formed (Rollinson 1993). Monazite is a light rare-earth element phosphate ((Ce, La, Th, Nd) PO_4), common in continental metamorphic rocks and granites. It contains much greater amounts of Th (up to 18 %) and U (up to 5%) than zircons but is more susceptible to alteration and weathering and is commonly reset by recrystallisation rather than by solid state Pb diffusion.

Monazite grains are known to grow in mudstones as a result of low grade metamorphism but these are very small and cannot be dated using conventional U-Pb methods (Kingsbury *et al.* 1993). Traditionally U, Th and Pb have been measured using mass spectrometers, however the minimum spot size (area to be analysed) is ~10 μm. This type of measurement is unsuitable for measuring single crystals or zones within single crystals, due to the small spot size that is required. Recent advances in electron microprobe technology have pushed the detection limits for Pb, U and Th down to a level where they could be measured in monazite crystals (Montel *et al.* 1996). The electron microprobe can be used for routine analysis of very small areas on minerals (down to 5 μm in diameter).

Monazite occurs widely as an accessory mineral in variably metamorphosed pelites (Overstreet 1967, Parrish 1990). Monazites have been shown to form in sub-greenschist to granulite facies conditions, being evident in slates, schists and upper amphibolite to granulite facies rocks of pelitic composition (Overstreet 1967, Bons 1988, Parrish 1990). They are also found in felsic igneous intrusives, as subhedral to euhedral crystals that are commonly 40-100 μm in diameter. Igneous monazites are often found to have higher thorium levels than metamorphic monazites, and show evidence of concentric and irregular zonation.

The abundance of metamorphic monazite increases with progressive metamorphism (Overstreet 1967, Smith & Barreiro 1990). As a result, monazites are being increasingly used to date metamorphic events (Eusden & Barreiro 1988, Smith & Barreiro 1990). Monazites are thought to have lower closure temperatures than zircon and therefore are useful thermochronometers of medium to high temperature metamorphic events (Kingsbury *et al.* 1993). In comparison to zircon though, they are still relatively under-utilised in U-Pb geochronological studies. As monazites do not incorporate appreciable common lead during growth, the Pb present is radiogenic, having been derived from the decay of Th and U (eg. Scherrer *et al.* 2000).

Whilst certain micro-analytical methods (eg. ion microprobe, LA-ICP-MS) allow dating of relatively young monazites (<200 Ma), the electron microprobe (EMP) enables the dating of older monazites relatively easily and cheaply (Scherrer *et al.* 2000). The grains can be quickly located (using a back scattered electron detector) and analysed (by EMP) in thin section. By using this thin section technique as opposed to the mineral separate technique, the monazites are kept in a microstructural context, thereby enabling the significance of each deformational event to be established. The EMP has the additional advantages that small grains 10-50μm in diameter can be analysed non-destructively (and hence repeatedly), unlike with the ion microprobe and by LA-ICP-MS.

The errors quoted in this work represent only the error associated with counting statistics. They do not include any systematic errors associated with calibration, or the errors in decay constants. The calibration is continually checked against SHRIMP analysed standards and reproduces the SHRIMP ages to within error. We conclude the sum of these calibration errors is less than 1% in the age except where Pb contents are less than 3000 ppm. All samples have been adjusted to a single calibration based on long term analysis of the in-house standard MF584. This shifts the estimated age up by about 10 Myrs. For most of the rock samples the analyses are consistent with a single age population in which most (>75%) of the variability is explained by the counting statistics. For these samples a weighted mean was calculated assuming normally distributed data and that the counting statistics are an

accurate reflection of the error. For individual grain analysis the error quoted is the 1σ error. For the weighted mean age, a 2 σ error is used.

The EMP monazite dating technique described above has been utilised in this study to analyse numerous samples from northwest Tasmania (Figure 3.30). The aim of this work is to aid the resolution of several contentious aspects of the Mesoproterozoic to Devonian geological history of Tasmania. These include the age and significance of the deformational events, and by comparison with other regions, will aid in determining the proximity of Tasmania to the Australian mainland during this period. Whilst these issues have been partly resolved by recent workers (Berry *et al.* 1997, Black *et al.* 1997, Turner *et al.* 1998, Calver 1998, Calver & Walter 2000, Meffre *et al.* 2001), their findings leave many questions unanswered. There are some striking similarities between the depositional and deformational history of the Tasmanian mainland, King Island and southeast Australia from the Neoproterozoic onwards. These include stratigraphic correlation of the segments of the rift-related sedimentation in the Neoproterozoic, and the Middle Cambrian Tyennan/Delamerian Orogeny.

Importantly though, there are major differences between the different regions during and prior to the major Neoproterozoic sedimentation represented by the Adelaide Rift Complex in South Australia, the Grassy Group on King Island and the Ahrberg and Togari Groups in Tasmania. Intermixed with the Neoproterozoic rift sediments on King Island and in northwest Tasmania are large volumes of rift-related basalts, unseen in the Adelaide Rift Complex. Large amounts of 760-780 Ma granitoid together with associated amphibolite facies metamorphism and multiple folding events are present on King Island. In northwest Tasmania, a thin discontinuous unit of 780 Ma granitoid is present in an allochthonous slice of the Arthur Lineament. Other than a low angle unconformity, no significant deformation is thought to represent the 760-780 event in Tasmania. In southeast Australia, the only igneous event of this age is the occurrence of a 780 Ma rhyolite below the base of the Burra Group (Preiss 2000).

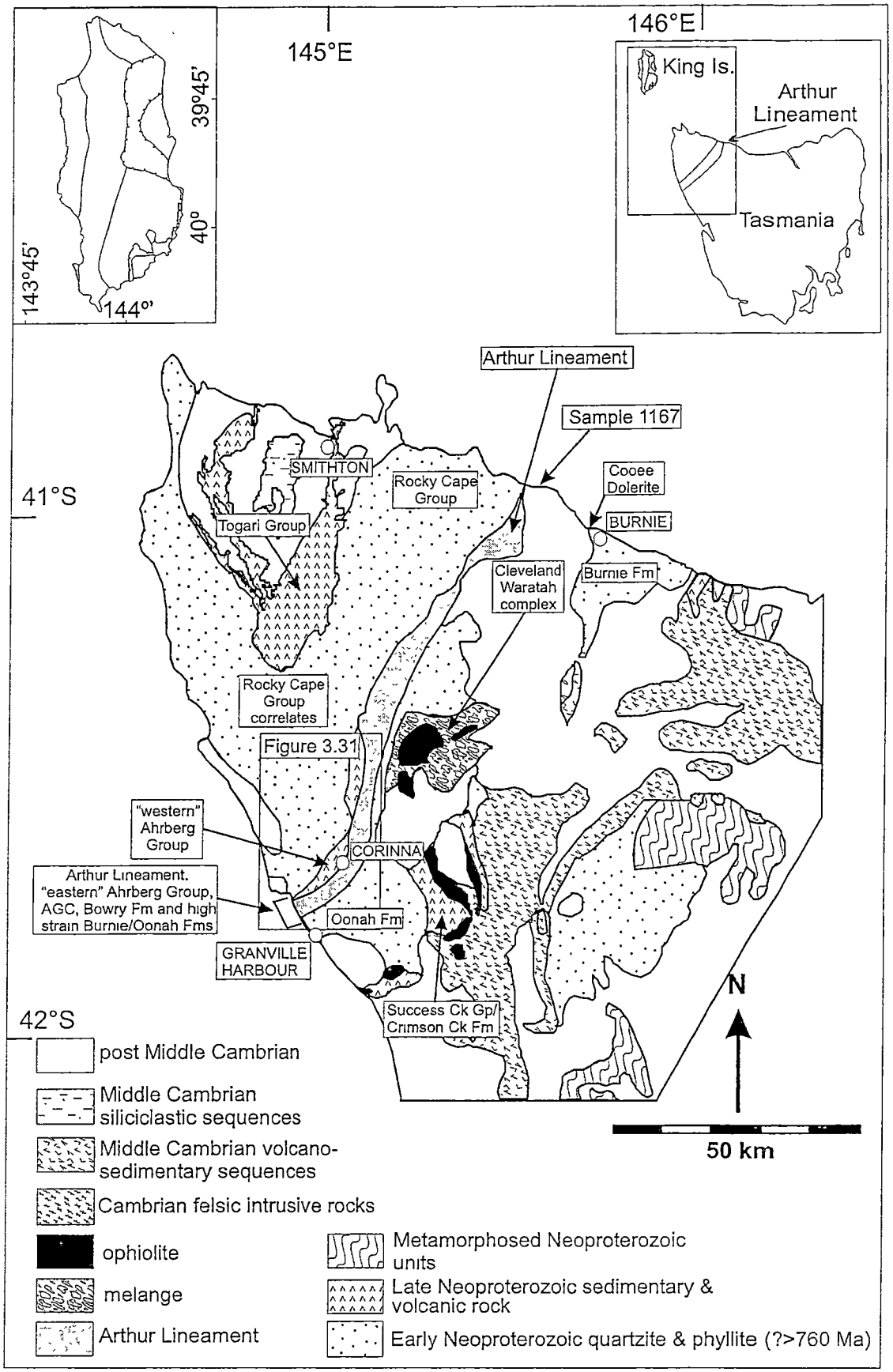

Figure 3 30. Setting of the Arthur Lineament, NW Tasmania (modified after Brown *et al.* 1995). The Arthur Lineament consists of the high strain (metamorphosed) Burnie and Oonah Formations, the "eastern" Ahrberg Group, the Bowry Formation, and the AGC. King Island geological detail is provided on Figure 3.40.

Small monazites (5-80μm in diameter), interpreted to be metamorphic in origin occur in lower greenschist to lower amphibolite facies mudstones over a wide area in northwestern Tasmania, and are also present in metasediments and granitoids on King Island. By analysing these grains using the EMP technique it is possible to distinguish Neoproterozoic events from those of Cambrian age across Tasmania. This will help in defining the regional extent of different deformational events, and has major implications for Tasmania's position at the time of break-up of Rodinia.

3.7.2 The Arthur Lineament

Areas of northwest and western Tasmania have previously been shown to have undergone metamorphism at around 510 Ma (Turner *et al.* 1998). Metamorphic grades during this event reached as high as eclogite facies in western Tasmania, in the Franklin Metamorphic Complex (FMC). Zircons from the FMC gave U-Pb ages of 511 ± 8 Ma, as recalculated by Black *et al.* (1997), and 502 ± 8 Ma (Turner *et al.* 1998), whereas hornblendes and micas derived from an amphibolite in the Forth Metamorphic Complex have given a minimum K-Ar age of 493 ± 13 Ma (McDougall & Leggo 1965). Zircon from a garnet amphibolite in the Forth Metamorphic Complex produced U-Pb ages of 514 ± 5 Ma (Black *et al.* 1997). K-Ar ages of around 510 ± 10 Ma were derived from prograde hornblendes from three Bowry Formation amphibolites (Turner 1993, Turner *et al.* 1998). However, no metamorphic ages have been reported from other units of the Arthur Lineament, or the surrounding lithological units.

The aim of this work is to determine how pervasive the Cambrian metamorphic overprint is, by utilising metamorphic monazites found in fine grained metasediments within the lineament, and the surrounding area. Samples from within the defined boundaries of the Arthur Lineament are discussed here, and samples from the surrounding units are discussed in the following section (3.7.3).

Three fine grained, psammopelitic to psammitic metasediments from the eastern parts of the Arthur Lineament, analysed for metamorphic monazites, were found to contain grains varying in size from 5 to 130 μm in diameter (samples 1114, 1036c and 1194). Sample 1194 is a foliated, pyritic metasiltstone from within the Bowry

Formation. Sample 1114 is a strongly foliated, quartz-mica-graphite-carbonate schist from within the AGC, at the base of the Reece Dam spillway. Sample 1036c is from a 20 m wide, sub-vertical shear zone in the high strain Oonah Formation, to the east of the other sample locations. These samples will be individually discussed below.

Sample 1114 (345120 mE, 5378860 mN)

This sample, from within the AGC, was collected from a psammopelite dominated sequence, at the base of the spillway to Reece Dam (Figure 3.31). The sample is schistose, with intense development of $Ca S_2$ (Figure 3.32(a)). Minor relicts of $Ca S_1$ were observed, however the early foliation was predominantly obliterated during the $Ca D_2$ event. Thin microlithons and cleavage domains within microlithons of $Ca S_2$, display mineral alignment that is at a low angle to the main $Ca S_2$ foliation. These are interpreted to represent the $Ca S_1$ foliation. A late, moderately well developed crenulation cleavage is evident, cross cutting $Ca S_2$ at a high angle. The cleavage domains of the schistose $Ca S_2$ foliation are defined by white mica and graphite, whereas the microlithons consist of recrystallised carbonate and quartz. No albite porphyroblasts were observed in the sample, reflecting a compositionally different precursor rock type to other AGC lithologies.

Monazites are present in the sample but are not as abundant as in other samples from the high strain zone. Several elongate grains, with irregular, embayed grain boundaries were observed. Three grains were analysed. The monazites are 15 to 20 μm wide, and 30 to 50 μm long, and consistently oriented with their long axis aligned with the main $Ca S_2$ foliation. Low Sm, Gd and Dy levels in comparison with other monazites of the same age within the Arthur Lineament are interpreted to reflect different bulk rock compositions (Appendix 3.22 and Figure 3.33(a)), whereas a negative correlation between age and La evident in Figure 3.33(b) may be an indication of hydrothermal alteration.

Despite the difference in mineral chemistry of the monazites in sample 1114, including lower levels of Th and Pb, in comparison to other samples from within the Arthur Lineament (samples 1036c and 1194), the Th-Pb ratios are relatively consistent with other samples, and therefore produce consistent individual grain ages

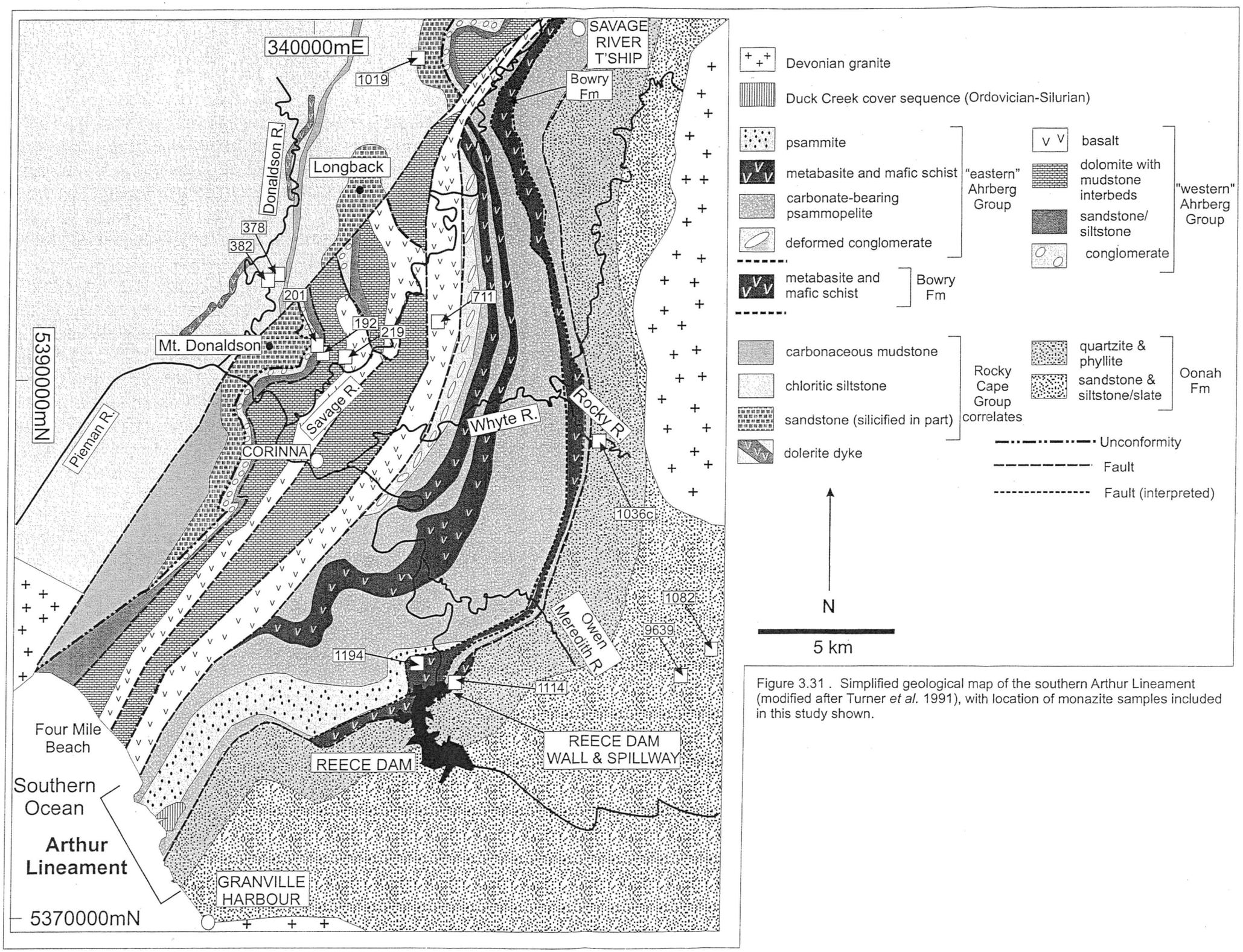

Figure 3.31 . Simplified geological map of the southern Arthur Lineament (modified after Turner *et al.* 1991), with location of monazite samples included in this study shown.

Figure 3.32(a) photomicrograph of monazite-bearing metasedimentary schist, with $Ca S_2$ foliation defined by quartz, white mica and graphite, AGC sample 1114; (b) photomicrograph of monazite-bearing, quartz-albite-white mica schist, $Ca S_2$ is the dominant foliation, AGC metasedimentary schist sample 1036c; (c) photomicrograph of albite porphyroblast, S_i in cores of albite porphyroblasts reflect the orientation of $Ca S_1$, AGC metasedimentary schist sample 1036c; (d) SEM image of elongate monazite grain, aligned with the $Ca S_2$ foliation, blades of white mica (dull grey) and chlorite (light grey) can be seen defining the matrix, AGC sample 1036c; (e) close up SEM image of elongate, embayed monazite from AGC metasedimentary schist, sample 1036c; (f) photomicrograph of multiply deformed, intensely foliated graphite-white mica-quartz mudstone, Burnie Formation sample 1167; (g) photomicrograph of multiply deformed metasiltstone from the Rocky Cape Group correlate, axial planar foliation is $Ca S_2$, spaced cleavage is $Ca S_3$, sample 1019; (h) SEM image of elongate monazite, aligned with the $Ca S_2$ foliation, from Rocky Cape Group correlate metasiltstone sample 1019. q: quartz, m: white mica, g: graphite, ch: chlorite, mo: monazite, a: albite.

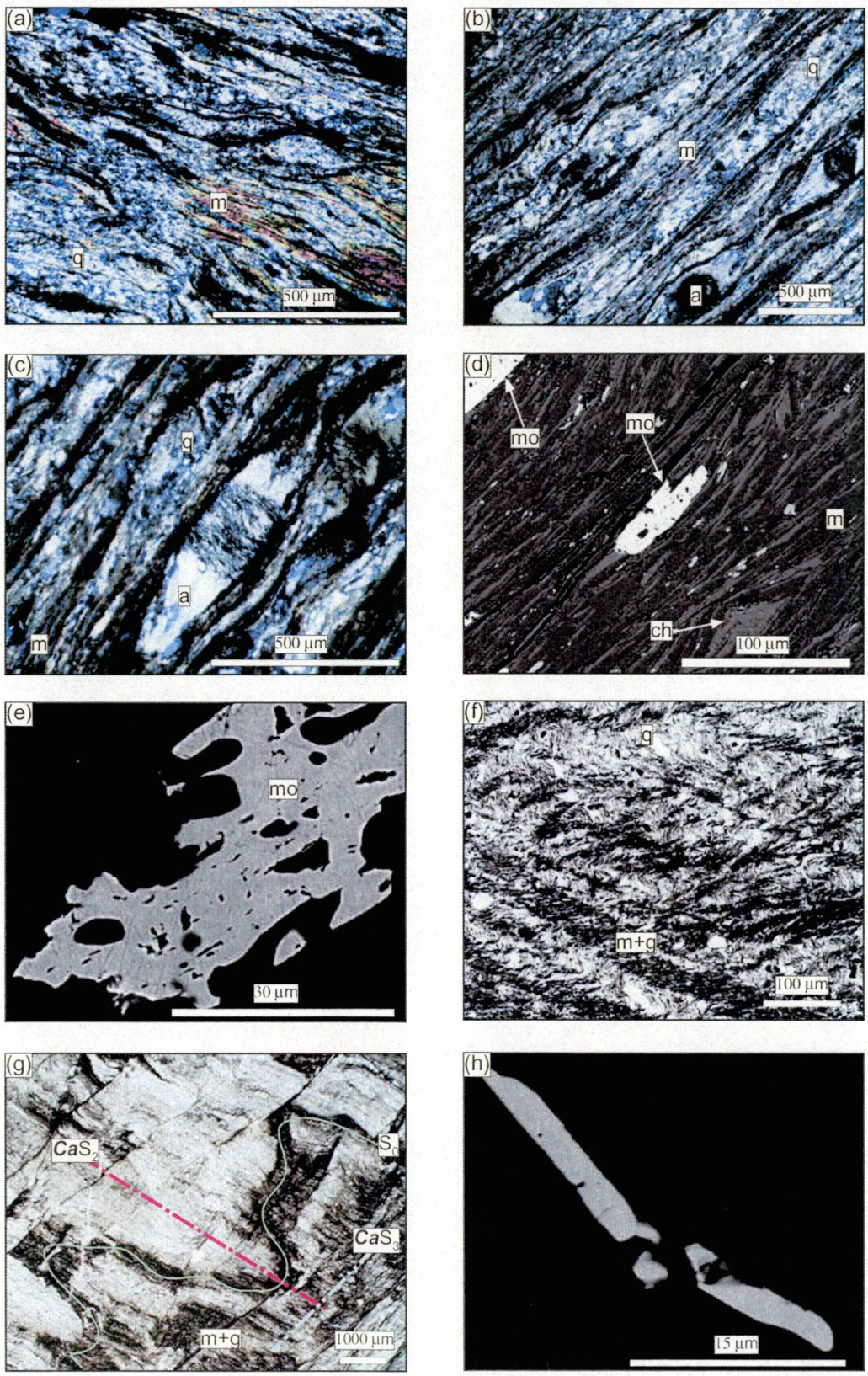

Figure 3.32(a) to (h).

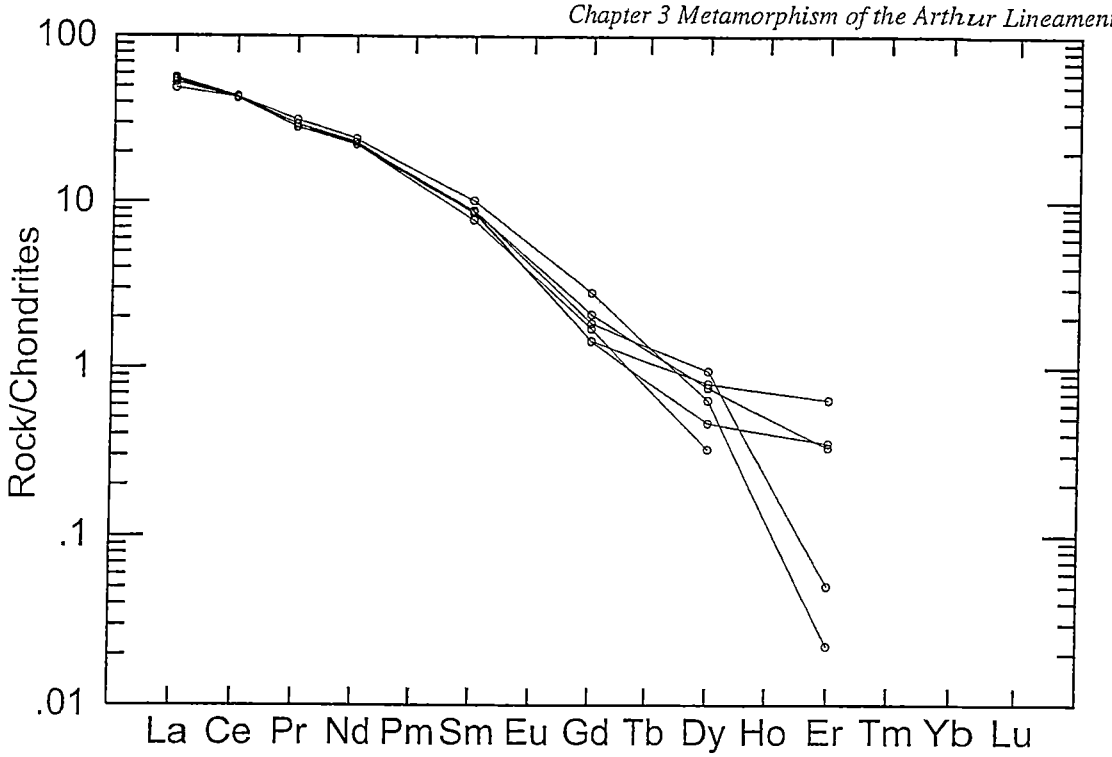

Figure 3.33(a). Rare earth element data for sample 1114 monazite analyses. Data is normalised to chondrite using values of Sun & McDonough (1989). Gd levels are significantly lower than analyses in sample 1036c. The spread in Er values is interpreted to be due to analytical error.

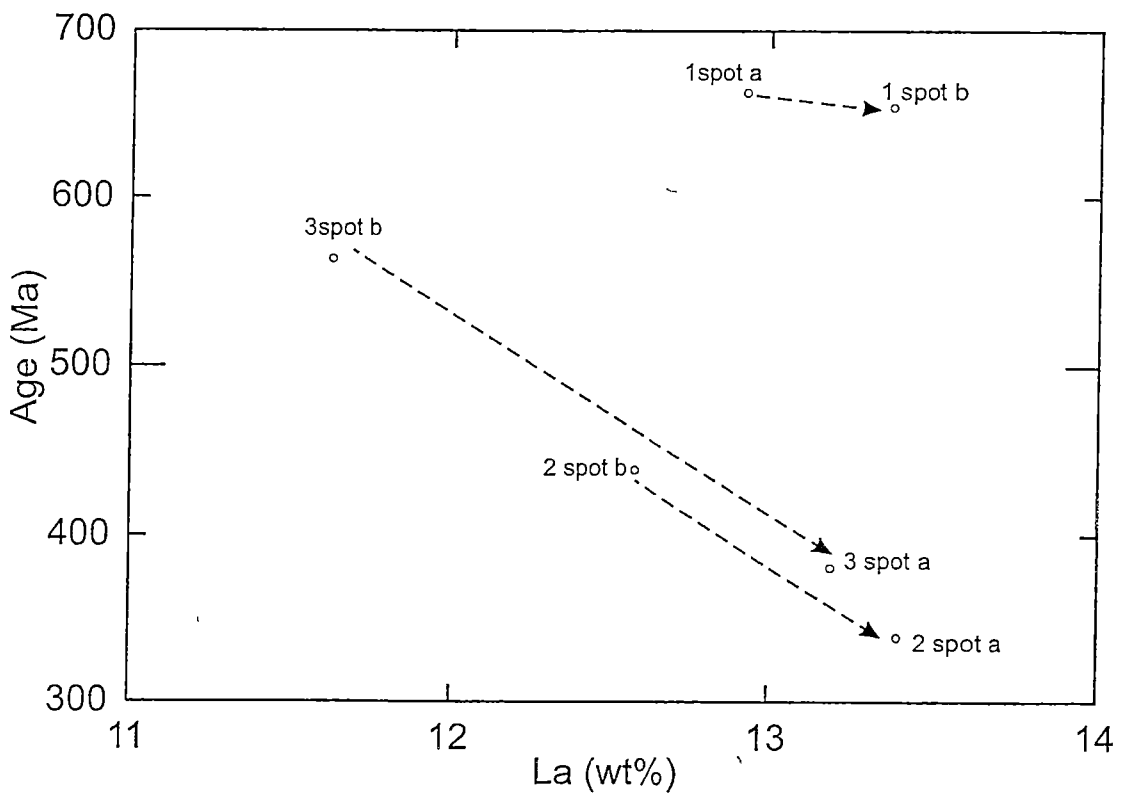

Figure 3.33(b). Age (Ma) vs La (wt %) plot for monazite analyses from sample 1114. A consistent trend of decreasing age and increasing La levels is evident, prehaps reflecting hydrothermal alteration.

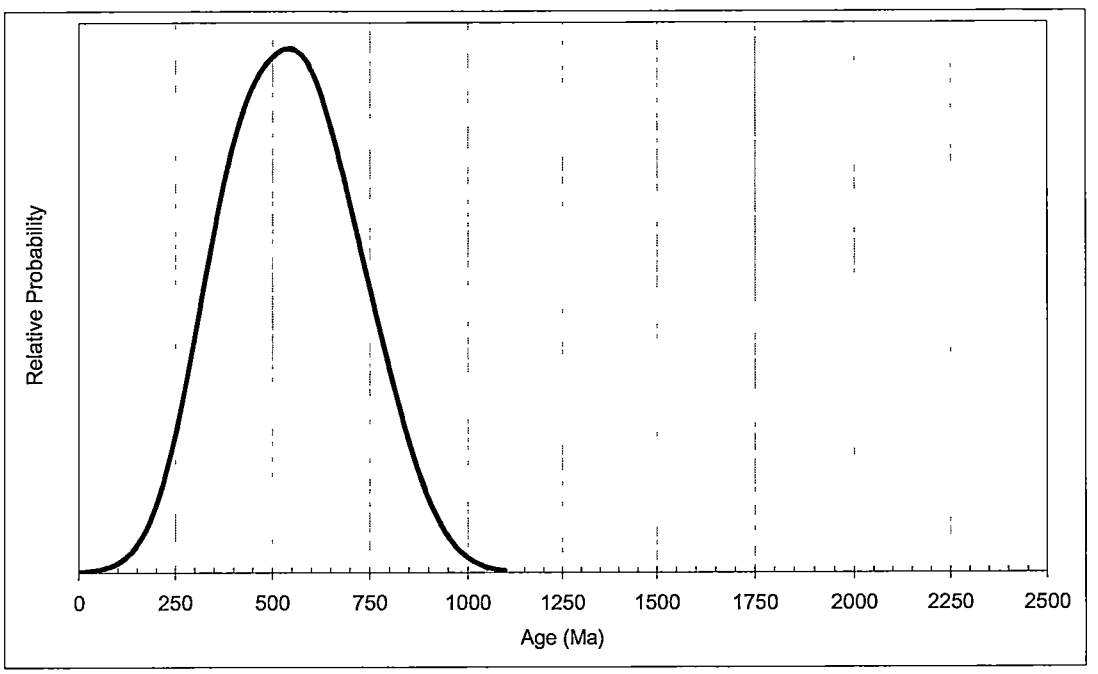

Figure 3.33(c). Relative probability plot for sample 1114. Number of analyses 6. There is no evidence of inherited grains, either due to their absence, or the complete resetting of older grains. The main metamorphic peak is at 534 ± 44 Ma. Two analyses with ages of 376 ± 104 Ma and 428 ± 128 Ma probably representing Devonian deformation, are included. Due to their large sigma 1 errors, a single peak occurs.

(Figure 3.33(c)). The six analyses have a weighted mean age of 495 ± 41 Ma, which is within σ 2 error of the monazite ages in samples 1036c and 1194.

Sample 1036c (350180 mE, 5388100 mN)

This sample is from a 25 metre wide, $\boldsymbol{Ca}D_2$ shear zone with cataclastic features and strong development of S-C fabrics, which is proximal to the boundary between the AGC and the Oonah Formation (*map*). This location corresponds to a major change in vergence of $\boldsymbol{Ca}F_1$, that is most likely a result of a fault-related change in facing direction of a macroscopic $\boldsymbol{Ca}F_1$ fold (Chapter 2).

The 1036c sample is a fine grained, quartz-graphite-mica-albite-schist (Figure 3.32(b)). The main foliation ($\boldsymbol{Ca}S_2$) is an intensely developed schistosity. Quartz is recrystallised and is developed in schistose $\boldsymbol{Ca}S_2$ microlithons. The cleavage domains are defined by aligned white mica and graphite. Albite occurs as porphyroblasts that have strained, elongate ellipsoidal grain shapes, and long axes that are aligned with the dominant $\boldsymbol{Ca}S_2$ foliation (Figure 3.32(c)). However the cores of the albite porphyroblasts are subhedral to euhedral, and are interpreted to represent pre-$\boldsymbol{Ca}D_2$ (or possibly early syn-$\boldsymbol{Ca}D_2$) development. The cores are distinguished from the rims by varying extinction angles, and concentrations of dark inclusions (in transmitted light), that pseudomorph the rectangular grain shape of the earlier generation of albite. In addition, the alignment of inclusions (S_i) in the cores of the albites is oblique to the dominant $\boldsymbol{Ca}S_2$ foliation. The S_i in the albite cores are interpreted to represent the $\boldsymbol{Ca}S_1$ foliation, which is only preserved in the albite porphyroblasts. In the outer zone of the albite porphyroblasts (Figure 3.32(b) and (c)), the S_i is rotated into alignment with $\boldsymbol{Ca}S_2$, indicative of dextral movement in this thin section.

Monazite grains were found in this sample. They have irregular, embayed margins, however they are consistently elongate and are aligned with the $\boldsymbol{Ca}S_2$ foliation (Figure 3.32(d) and (e)). Five monazites in the sample were analysed. Due to their large size (commonly 60 to 120 μm long and 30 to 50 μm wide), multiple analyses were carried out on individual grains. The mineral chemistry of the monazites in sample 1036c is largely consistent (Appendix 3.22), however two analyses (3spot1

and 3spot2) have notably lower Nd, Sm, Gd and Th levels (Figure 3.34(a)). This depletion in middle REE, reflects growth during different equilibrium conditions, and coincides with distinctly different ages of monazite growth. In addition, analysis 3spot1 has extremely high Fe levels (5.21 wt %) and 3spot2 has elevated La (15.98 wt %). These inconsistencies, again reflected in the difference in age between the 3spot1 and 3spot2 analyses (Figure 3.34(b)), are indicative of contrasting equilibrium conditions during the growth of these two areas of the monazite grain. Analyses 3spot3 and 3spot4, again from overgrowths of the same grain, are elevated in Nd and Sm, and sample 3spot3 has significantly higher Y levels (1.63 wt %). These higher than average levels may be due to enrichment as a result of element transfer from the original monazite nucleii (analyses 3spot1 and 3spot2). However, whereas analysis 3spot2 has abnormally high La levels, 3spot3 and 3spot4 have lower than average La levels (10.71 and 10.03 wt % respectively) (Figure 3.34(b)). This may be indicative of metamorphic conditions affecting La mobility, but not Nd, Sm and Gd.

On the basis of predominantly consistent levels of U, Th and Pb (apart from samples 3spot1 and 3spot2), the monazite analyses can be interpreted to have broadly uniform ages (Figure 3.34(c)). Utilising the individual age calculation method (outlined in Methodology), this is found to be an accurate assumption, with analyses having a weighted mean age of 531 ± 10 Ma. This age is a composite of results from analyses prior to, and subsequent to re-calibration for Ce. This is significant, as it conclusively demonstrates the shear zone is related to the Tyennan Orogeny, and that the $\boldsymbol{Ca}S_2$ foliation is Cambrian in age.

Analysis 3spot1 has an age of 2121 ± 141 Ma, whereas analysis 3spot2 has an age of 1038 ± 35 Ma (Figure 3.34(b)). These analyses represent detrital monazite grains that are from much older metamorphic or igneous events. The age of these analyses may shed light on the provenance of detrital material deposited in this metasedimentary sequence.

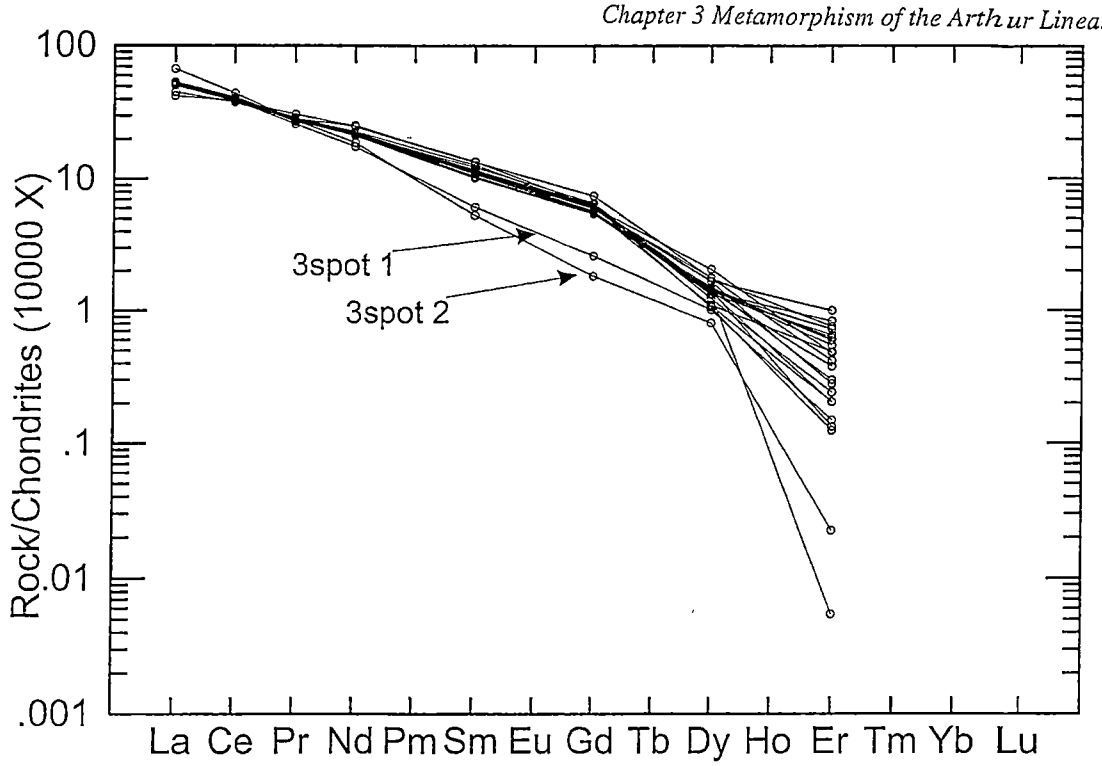

Figure 3.34(a) . Rare earth element data for 1036c monazite analyses. Data is normalised to chondrite using values of Sun & McDonough (1989). Analyses 3spot 1 and 3spot 2, with depleted MREE are indicated. The spread in Er values is interpreted to be a result of analysis near the detection limit.

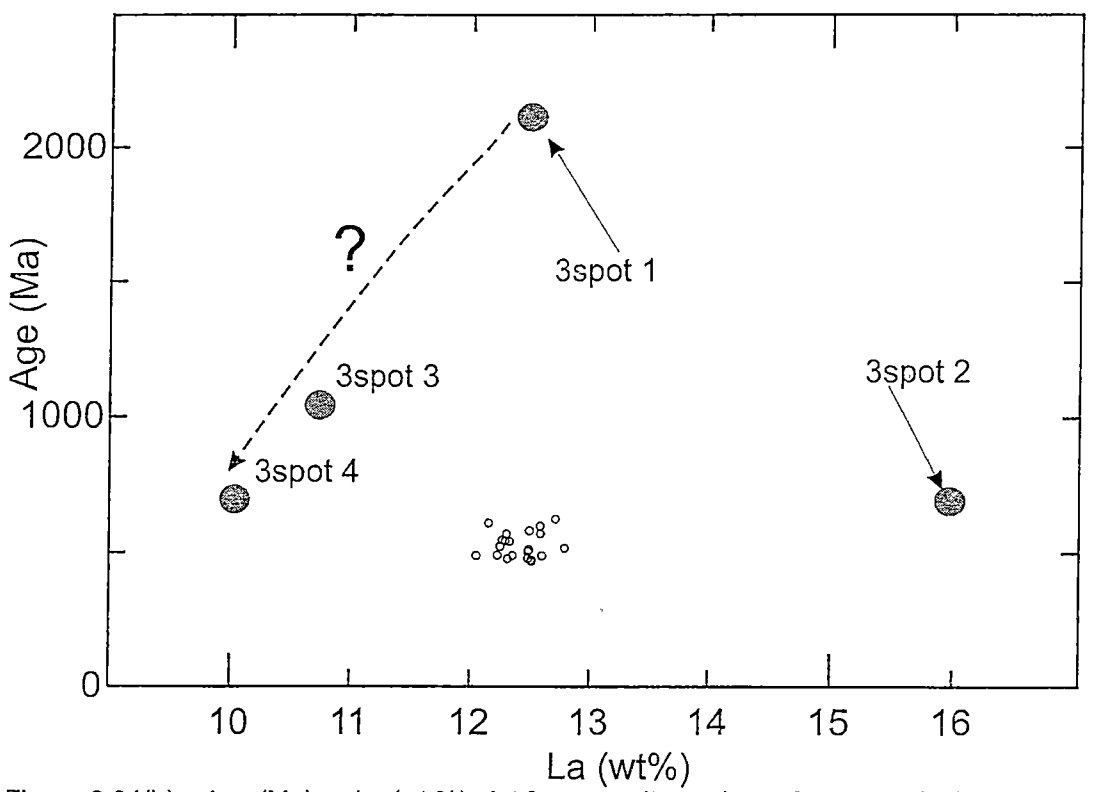

Figure 3.34(b) . Age (Ma) vs La (wt %) plot for monazite analyses from sample 1036c. The variation in La values for analyses 3spot 1 to 3spot 4, and the relationship to age is indicated. Notably, the majority of analyses, with consistent ages have similar La values

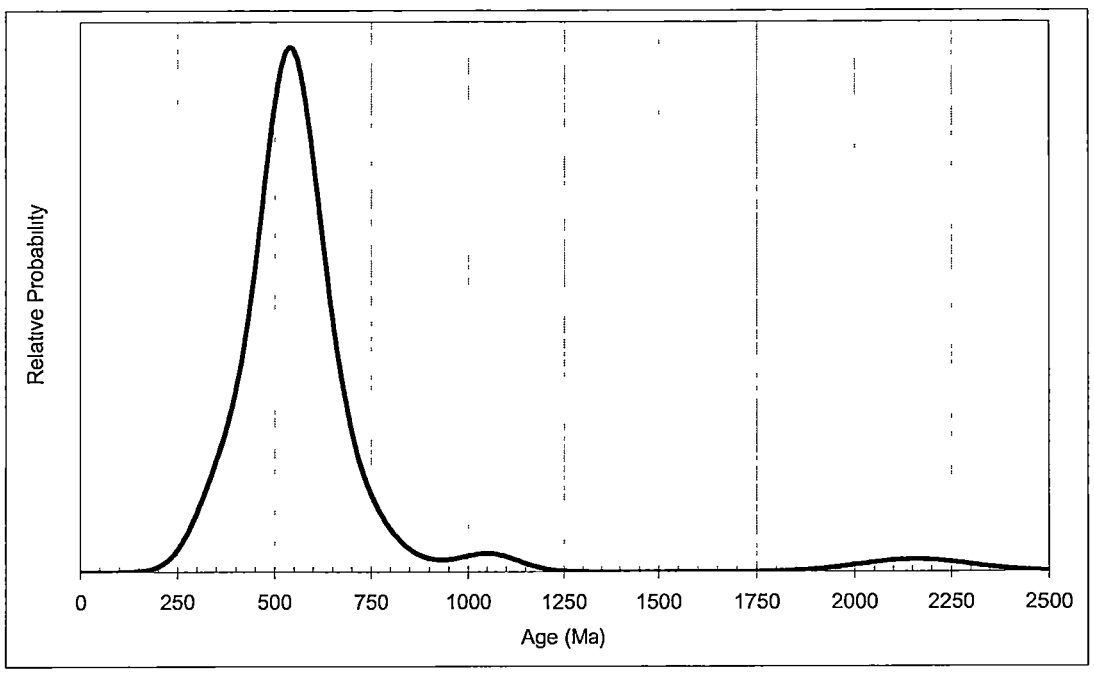

Figure 3.34(c). Relative probability plot for sample 1036c. Number of analyses 46. There is evidence of older, inherited grains, (at 1058 ± 77 Ma and 2158 ± 143 Ma) which are interpreted to be detrital. The age of the shear zone that sample 1036c is derived from, is conclusively Cambrian (531 ± 10 Ma), and supports the microstructural interpretation of ***Ca***S_2 being the dominant foliation.

Sample 1194 (343430 mE, 5379520 mN)

Sample 1194, located 5 metres from a glaucophane-bearing metadolerite in the Bowry Formation, is a strongly foliated, carbonaceous, pyritic psammopelite. The contact between the metadolerite and the metasediment is interpreted to be intrusive. The uniform mineralogy of the sample has prevented the development of mineralogically distinct cleavage domains and microlithons, however a phyllitic foliation is visible in hand specimen and from petrographic observations. The foliation is defined by alignment of elongate quartz grains, graphite, minor white mica and pyrite. Due to the predominantly graphitic composition (and hence opacity) of the sample, petrographic observations were not fruitful. The preservation of glaucophane in the proximal metadolerite (which corresponds to pre-kinematic deformation that is pre-, or early syn-$\boldsymbol{Ca}D_2$ deformation elsewhere in the Bowry Formation), and the preservation of a finely spaced foliation that has not been strongly overprinted, may infer that $\boldsymbol{Ca}D_2$ was weak in this area, and that the main foliation is $\boldsymbol{Ca}S_1$. However, this is not a conclusive argument, as no direct overprinting relationship between $\boldsymbol{Ca}S_1$ and $\boldsymbol{Ca}S_2$ was observed.

When analysed using the back scattered electron detector, monazites were found to be common in the sample. Seven monazite grains were analysed. They are irregular in shape, but more equidimensional than the monazites in samples 1114 and 1036c (commonly 10 to 15 μm in diameter). This is interpreted to reflect the relatively low strain deformational history of the sample. The monazites were found to have consistently higher Ca than monazites in samples 1114 and 1036c, whereas they have lower Fe, Nd (Appendix 3.22).

They have a small range in Pb, Th and U values (Figure 3.35(a)). The monazite analyses display a small range of elemental variation (Figure 3.35(b)). The consistent ages of the individual analyses, and their similar elemental abundances, are both indicative of constant metamorphic conditions during the growth of the different monazites. The monazite has a weighted mean CHIME age of 546 ± 15 Ma (2σ error), whereas the individual analyses have average σ 1 errors of 55 Ma.

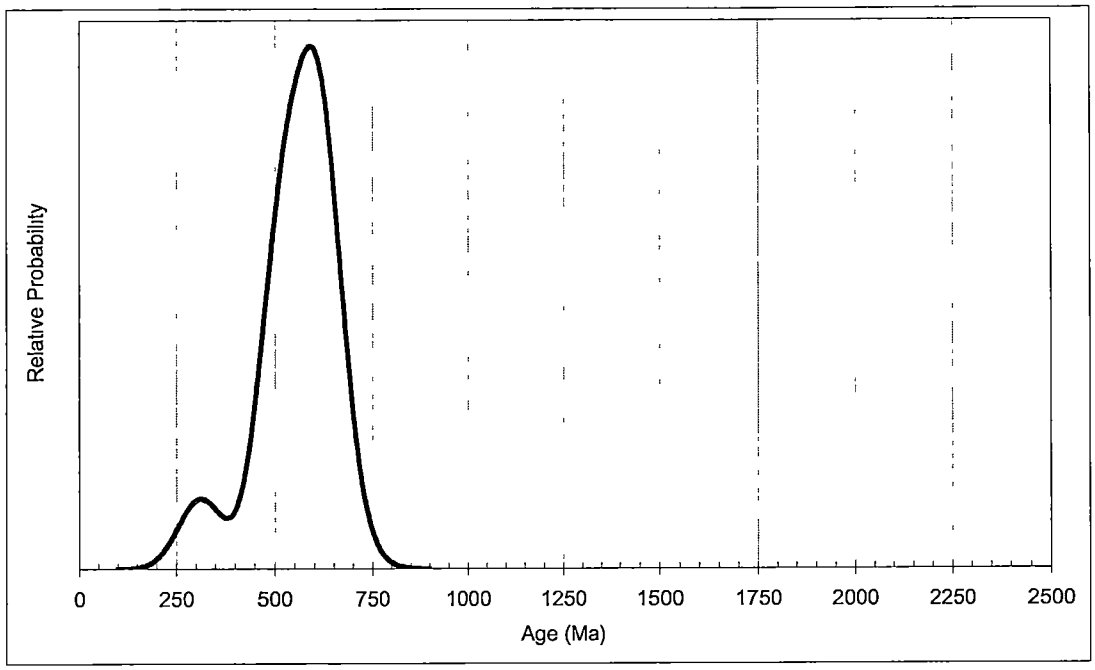

Figure 3.35(a). Relative probability plot for sample 1194. Number of analyses 13. The dominant peak occurs at 546.2 ± 15 1 Ma and is interpreted to correspond to the ***Ca***D_2 deformation. There is no evidence of inherited grains, either due to their absence, or the complete resetting of older grains. A small peak at 294.5 ± 53.6 Ma may represent monazite growth during the Devonian deformation, that has suffered from partial Pb loss.

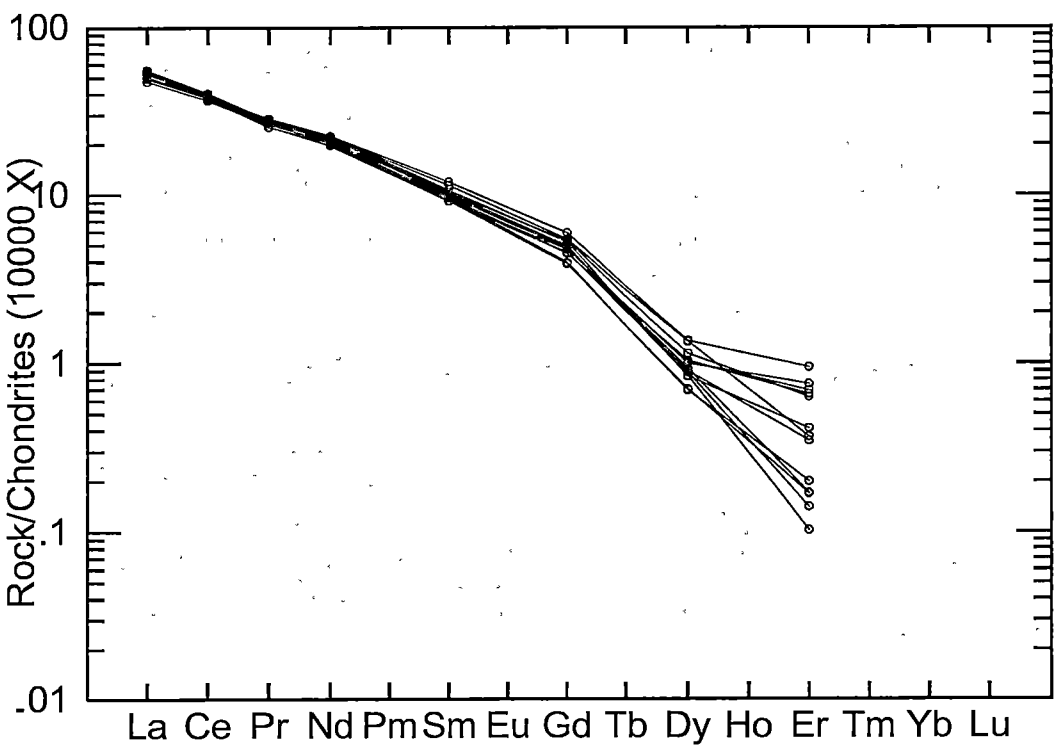

Figure 3.35(b). Rare earth element data for 1194 monazite analyses. Data is normalised to chondrite using values of Sun & McDonough (1989). The similar chemistry of analyses (corresponding to similar ages) is evident. The spread in Er values is interpreted to be due analytical error.

3.7.3 Surrounding areas

To the east and west of the Arthur Lineament, the lithologies have been variably deformed by $\boldsymbol{Ca}D_1$ and $\boldsymbol{Ca}D_2$, with the intensity of the these deformations gradually decreasing away from the lineament. The structural overprint of the $\boldsymbol{Ca}D_1$ and $\boldsymbol{Ca}D_2$ events has been shown to extend up to 7 kilometres to the east of the lineaments eastern boundary, and up to 3 kilometres to the west of the lineaments faulted western boundary (Chapter 2). However, metamorphism associated with these deformational events is confined to within the lineament, and the immediately surrounding areas. To the east of the lineament, subsequent deformation ($\boldsymbol{Ca}D_3$, $\boldsymbol{De}D_4$ and $\boldsymbol{De}D_5$) is weakly developed in the low strain Oonah Formation, and has not resulted in metamorphic overprints. Immediately to the west of the lineament, the "western" Ahrberg Group and Rocky Cape Group correlates have undergone metamorphism associated with the $\boldsymbol{Ca}D_2$ event, but do not show evidence of earlier metamorphism.

Samples from the low strain Burnie Formation (sample 1167), Oonah Formation (sample 1082 and 96-39), "western" Ahrberg Group (samples 192, 201, 219 and 711) and Rocky Cape Group correlates (sample 382, 378 and 1019) were analysed for monazites using the technique outlined above (Figure 3.30 and Figure 3.31).

Burnie Formation sample 1167 (398980 mE, 5457655 mN)

Sample 1167, collected to the east of the Arthur Lineament, on the north coast is a multiply deformed mica-graphite mudstone, with late quartz veining crosscutting bedding (Figure 3.32(f)). The age of the Burnie Formation is indirectly understood to be older than 725 Ma, based on the minimum age of the Cooee Dolerite, which intrudes the Burnie Formation in the Cooee area on the northwest coast. The earliest foliation, interpreted to be $\boldsymbol{Ca}S_1$, is a continuous foliation, defined by the growth of mica and graphite. This foliation is crenulated by a pervasive, very finely spaced cleavage with 0.025 mm wide microlithons, and interpreted to be $\boldsymbol{Ca}S_2$. No mica was observed aligned with $\boldsymbol{Ca}S_2$. The third cleavage, interpreted to be $\boldsymbol{Ca}S_3$, crenulates the earlier foliations. It is a finely spaced cleavage, with 0.1 to 0.2 mm wide microlithons. Its development is not as pervasive as the earlier two cleavages.

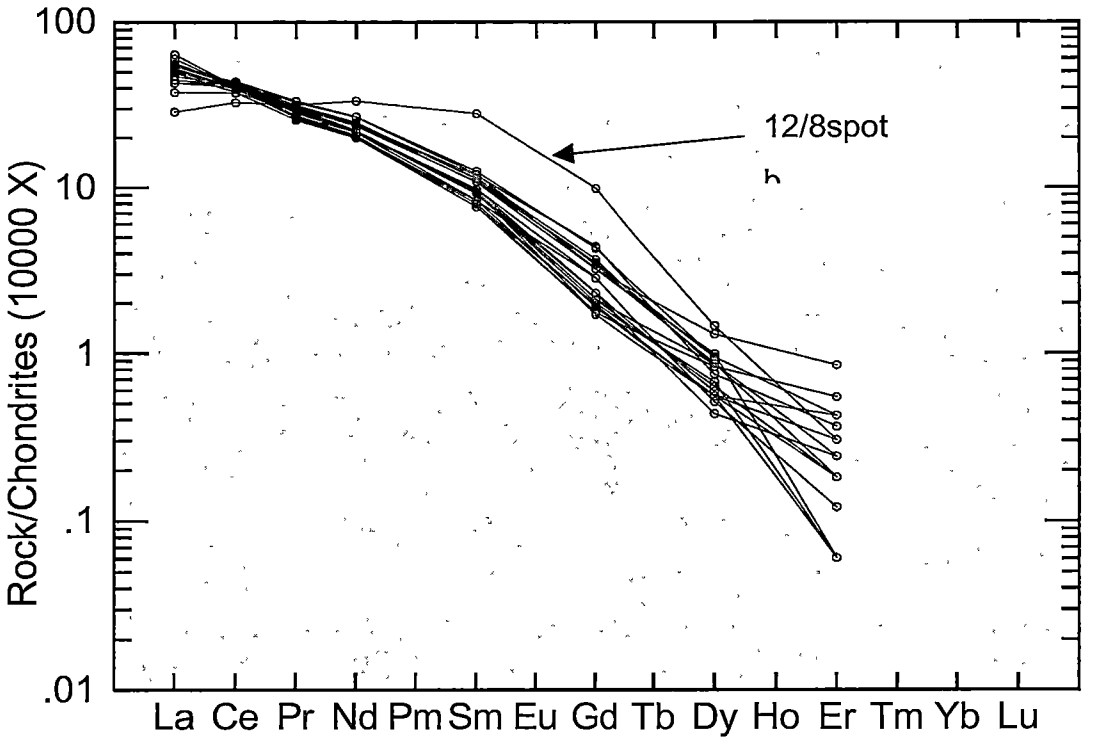

Figure 3.36(a). Rare earth element data for 1167 monazite analyses. Data is normalised to chondrite using values of Sun & McDonough (1989). Despite the variation in ages, the majority of analyses have similar chemistry, however analysis 12/8spotb has anomalously high Nd, Sm and Gd. The spread in Er values is a result of analytical error.

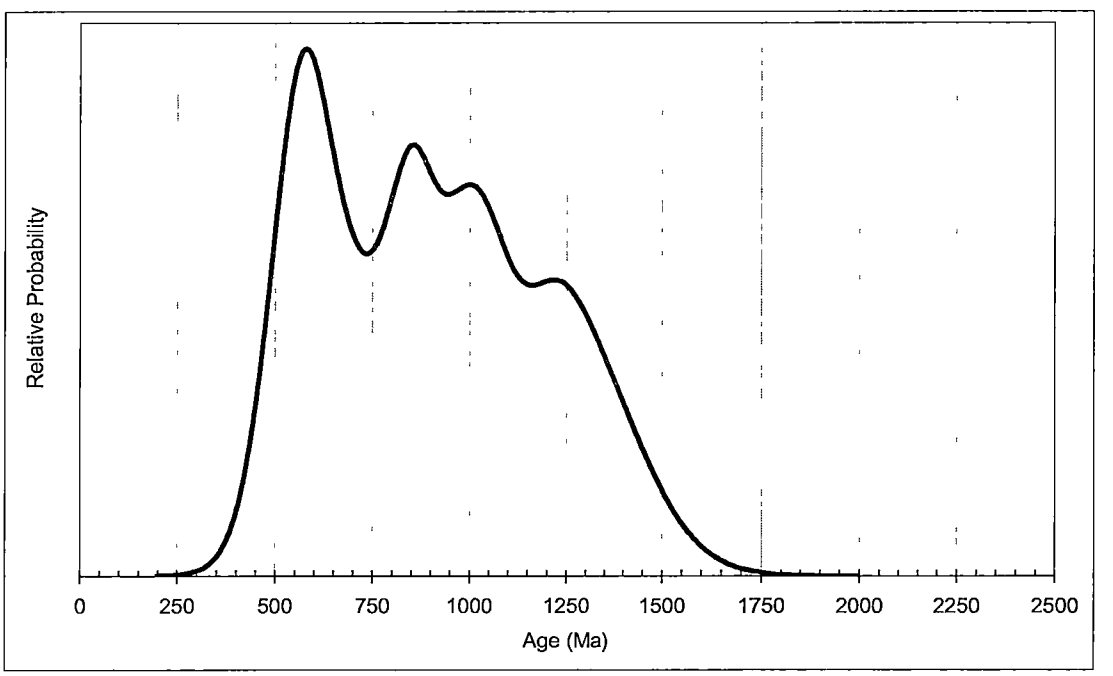

Figure 3.36(b). Relative probability plot for sample 1167. Number of analyses 26. A strong peak at 580 ± 26 Ma represents the main Cambrian deformation, however the intensity of deformation at the sample site was not great enough to reset older grains, and multiple peaks, reflecting different sources of inherited grains can be seen. The peak at around 800 Ma may represent a diagenetic phase of monazite growth (given this is the approximate age of deposition of the sediment), however this is uncertain.

Monazites are common in this sample. They have irregular shapes, with elongate, stubby, and rounded grains observed. The monazites range in size from 10 to 80 μm in length and 5 to 20 μm in width. This diversity in grain shape is reflected in the range of compositions and ages of the monazites (Appendix 3.23).
Multiple analyses on individual grains show significant variation in age (grain 12/12 spots a and b), and in some examples this corresponds to distinctly different chemistry (grain 12/8 spots a and b) (Appendix 3.23 and Figure 3.36(a)). This interpreted to reflect the contrasting equilibrium conditions at the time of monazite growth.

The individual ages of the analyses demonstrate the influence of a Cambrian metamorphic event. These analyses have a well constrained weighted average age of 542 Ma, with a 1 sigma error of 28 Ma. However, the level of intensity of the Cambrian deformation has not caused the complete resetting of inherited grains, and individual grain ages with peaks at approximately 775 Ma, 980 Ma and 1260 Ma are present (Figure 3.36(b)). Given the interpreted age of the Burnie Formation, the 775 ± 29 Ma weighted average age may reflect monazite growth during diagenesis, or the Wickham Orogeny. However, the older peaks are interpreted to be inherited ages, from detrital monazite populations.

Oonah Formation samples 1082 (353650 mE, 5380240 mN) and 9639 (352500 mE, 5379315 mN)

Sample 1082, from approximately 2.5 km to the east of the eastern boundary of the Arthur Lineament, is a laminated to thinly bedded mudstone/siltstone unit. The mudstone layers are dominated by white mica, with a minor quartz component (<10 modal %). The siltstone layers are comprised of intermixed quartz and white mica, with roughly equal modal proportions. The mica, in both mudstone and siltstone layers, is consistently aligned, representing the earliest fabric that has developed. This foliation, which cross cuts bedding at a 15 degree angle, is interpreted to be $\boldsymbol{Ca}S_1$. The mica is crenulated by a pervasively developed finely spaced cleavage, that cross cuts bedding at a similar angle, but in the opposite sense to the early foliation. This later foliation is interpreted to be $\boldsymbol{Ca}S_2$. Although the $\boldsymbol{Ca}S_2$ is a pervasive crenulation cleavage, it has caused minor growth of white mica, and in this

sample the $\boldsymbol{Ca}D_2$ event has not caused significant development of metamorphic minerals.

Monazites are present in sample 1082. The monazites observed were irregular in shape, with embayed margins, however they are consistently elongate, and between 15 and 40 μm wide and 30 to 80 μm long. In addition, they are aligned with the $\boldsymbol{Ca}S_2$ crenulation cleavage. The mineral chemistry of the analysed monazites is broadly consistent with monazites analysed in other samples (Appendix 3.24 *min chem* and Figure 3.37(a)).

Pb, Th and U levels have a small range, and this is reflected in the consistent ages of the monazite analyses, which have a weighted average age of 574 ± 24 Ma. However, a single analysis (1spot3) has similar Th levels (2.7 wt %) but anomalously high Pb levels (0.34 wt %), which reflect an old age (2278 ± 83 Ma).

Sample 9639, unlike the other samples analysed, is a grain mount of monazite from a heavy mineral separate, derived from a fine grained siltstone unit, approximately 2 km to the east of the eastern boundary of the Arthur Lineament (R. Berry *pers. comm.*2001). The monazites in this sample were prepared differently to monazites in all other samples, as they were acid-leached in order to remove any iron oxide coating. The monazite data for this sample has been included in this study.

The monazite chemistry in sample 9639 is notably different to the other samples analysed, and may be a result of the acid-leaching (Figure 3.37(b)). The monazites analysed have anomalously low La, but significantly elevated Pr, Nd, Sm, and Gd. Some internal variation is evident in the monazite chemistry of sample 9639. This is interpreted to be an indication of a mixed population, and may reflect partial resetting of the monazites, some of which must have a detrital origin.

The Pb, Th and U levels are mostly consistent, although analyses 9639_15 and 9639_5 have anomalously elevated Th levels (12.86 and 8.17 wt % respectively). However, as the Th-Pb ratios of these analyses are consistent with other analyses in this sample and sample 1082, a similar age of the monazites is indicated (Appendix

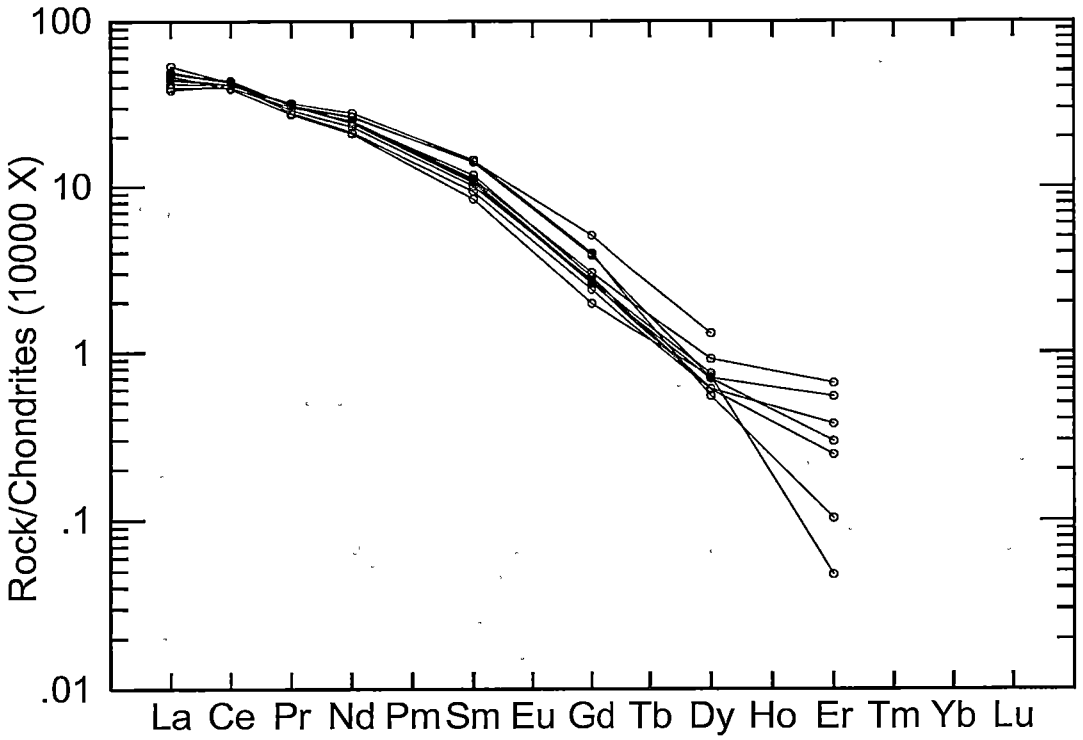

Figure 3.37(a). Rare earth element data for 1082 monazite analyses. Data is normalised to chondrite using values of Sun & McDonough (1989). The analyses have do not display large variations in their chemistry. The spread in Er values is a result of analysis near the detection limit

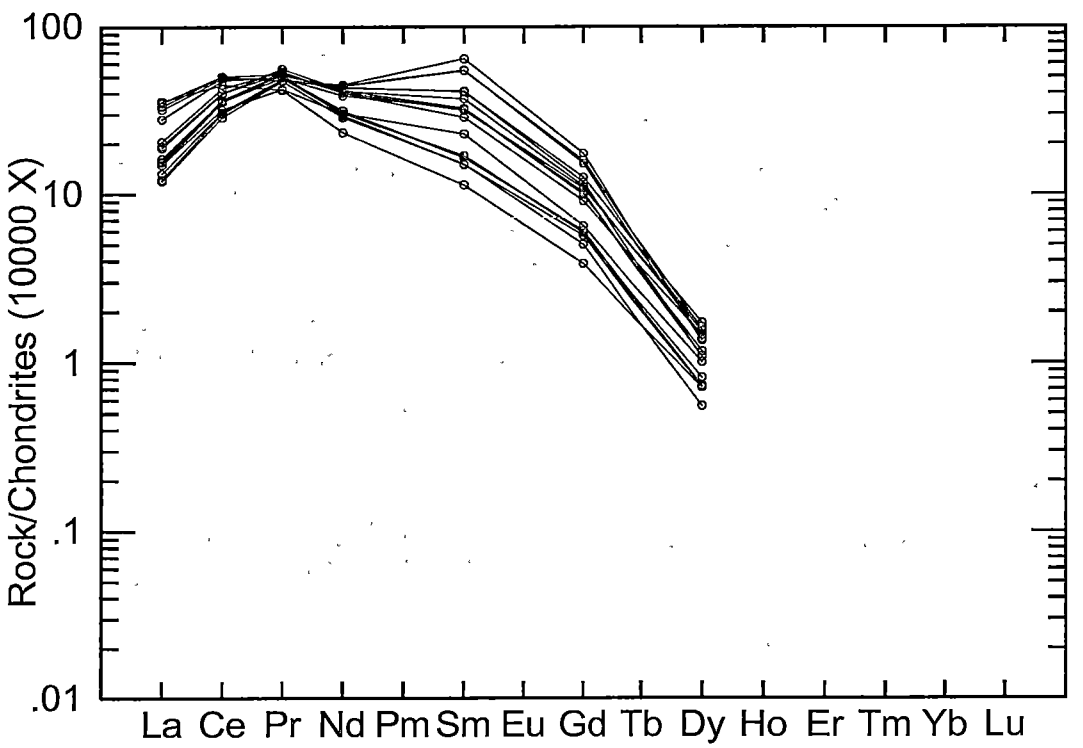

Figure 3.37(b). Rare earth element data for 9639 monazite analyses (mineral separate). Data is normalised to chondrite using values of Sun & McDonough (1989). In comparison to sample 1082 analyses (and others) the grains analysed have anomalously low LREE, and high MREE. This may be a feature of hydrothermal alteration (corresponding to similar ages).

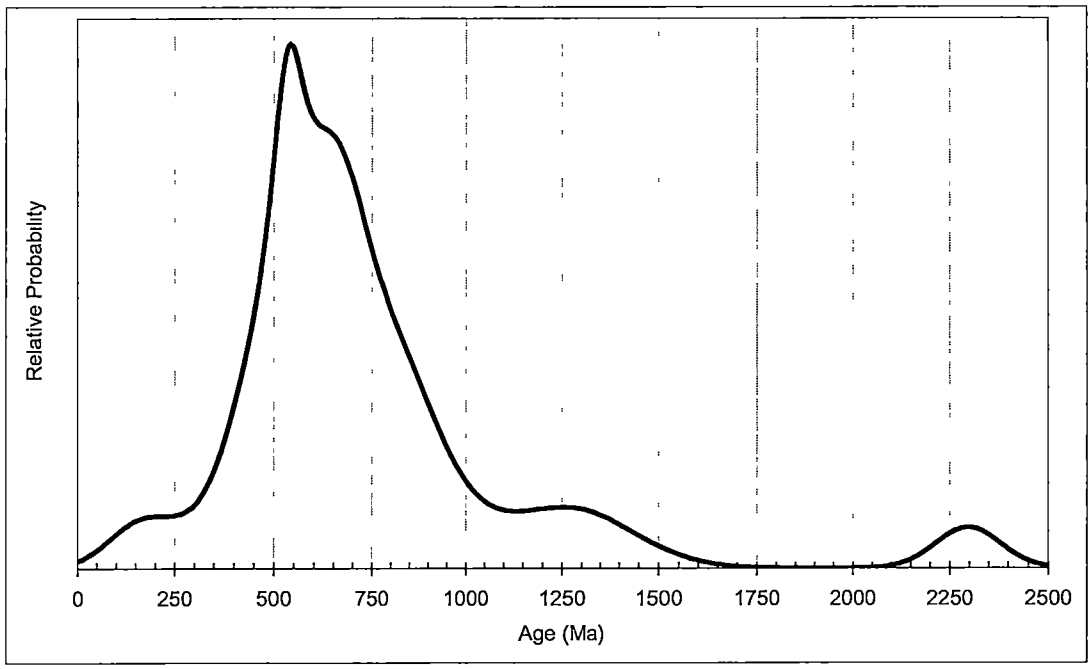

Figure 3.37(c). Combined relative probability plot for samples 1082 and 9639. Number of analyses 26. The prominent peak at 559 ± 15 Ma clearly represents the main Cambrian deformation (***Ca***D_2). Inherited ages at 1249 ± 171 Ma, 1300 ± 151 Ma and 2297 ± 84 Ma are thought be due to detrital grains, as the age of the Oonah Formation is interpreted to be around 750 Ma.

3.24 and Figure 3.37(c)). Due to the high Th levels, the sigma 1 error of these analyses is very small. Samples 9639_10 and 9639_6 have similar ages (1212 ± 166 Ma and 1268 ± 147 Ma respectively). These analyses have ages that are within error, and they are anomalous in comparison to the other grains analysed in this sample (Appendix 3.24), implying a detrital origin. However, a lack of similarity between their mineral chemistry is evident, with notably different levels of La, Ce, Nd, Sm and Gd (Appendix 3.24). This suggests that while they have a similar provenance (and hence are derived from rocks that have undergone deformation/crystallisation at a broadly concurrent age), they are probably derived from different host lithologies, with different bulk rock chemistries.

"western" Ahrberg Group samples 192 (340280 mE, 5390920 mN), 201 (340200 mE, 5390980 mN), 219 (340820 mE, 5390840 mN) and 711 (344530 mE, 5392100 mN)

The "western" Ahrberg Group samples that were analysed for monazites were collected from 0.5 km, and between 3.5 and 4.5 km to the west of the Arthur Lineament's western boundary. They are very low grade variably graphitic quartz-mica siltstones, with rare fine grained sandy layers, and micaceous mudstones. All of these samples show development of the $Ca S_2$ and $Ca S_3$ foliations, but the $Ca S_1$ foliation was not observed. The $Ca S_2$ is a finely spaced foliation, with white mica growing in alignment with the cleavage planes. The $Ca S_3$ foliation is more broadly spaced, and has not caused the growth of metamorphic minerals. It crenulates the $Ca S_2$ cleavage. The opacity of samples 192 and 201, due to the high levels of graphite, made petrographic observations difficult. Sample 711, from 0.5 km to the west of the lineament, had the largest white mica development, with blades 0.1 mm in length common. This is interpreted to reflect the samples proximity to the lineament's western boundary.

The samples were analysed for monazite, but due to the lower metamorphic grade, monazites present were smaller than in other samples investigated. The grains were not as elongate as in the more deformed samples from within the Arthur Lineament, and near its eastern boundary, and did not demonstrate a preferred alignment with the dominant foliation. Furthermore, some grains were rounded, and found in coarser

grained layers. These grains are interpreted to be of detrital origin and range in age from approximately 800 Ma to 1450 Ma (Appendix 3.25).

The monazites analysed in the "western" Ahrberg Group range in age from Cretaceous (eg sample 201) to Mesoproterozoic (eg. sample 711), as is indicated by the variation in Pb-Th ratios. In sample 711, the variety in monazite composition is best illustrated by the range in La, Nd, Sm, and Gd values. The Mesozoic monazite peak in sample 201 is well defined (Appendix 3.25). No deformation was observed in the area that can be attributed to this event, however the samples proximity to the ***Ca***D_3-age Delville Fault (see Chapter 2) may suggest that reactivation of this structure has occurred. Significantly, the mylonite zone on the west coast of King Island (see section 3.7.4 sample 63254) also has undergone reactivation in the Mesozoic, possibly as a result of the same event. An alternative explanation of the Mesozoic age monazites is the coincidence in age with the widespread intrusion of Jurassic dolerite. However, despite the significance of this thermal event in other areas of Tasmania, there is no evidence of Jurassic dolerite in this region.

In samples with consistent monazite ages, there is a small range in Pb and Th values (eg. samples 192 and 219) (Appendix 3.25), and the Pb-Th ratios are comparable. However, the monazite compositions are varied, probably reflecting the different bulk chemistry of the source rocks from which the monazites were derived (Appendix 3.25).

In samples 192, 201 and 711, some analyses have uniform Pb-Th ratios, resulting in ages of approximately 540 Ma (eg. 192-spot2 and 3, 201-spot3 and 5, and 711-10spot4). Monazite analyses from sample 219 show little variation in composition and Pb-Th levels. As a result, the Pb-Th ratios are consistent and analyses have broadly similar ages, with a weighted mean of 872 ± 88 Ma (Appendix 3.25 and Figure 3.38).

The mixed populations of monazites present in the "western" Ahrberg Group is well illustrated in the relative probability plot (Figure 3.38). Clearly, as the "western" Ahrberg Group is a well constrained correlate of the Togari Group, which has a maximum age of around 750 Ma, the maximum age of the "western" Ahrberg Group

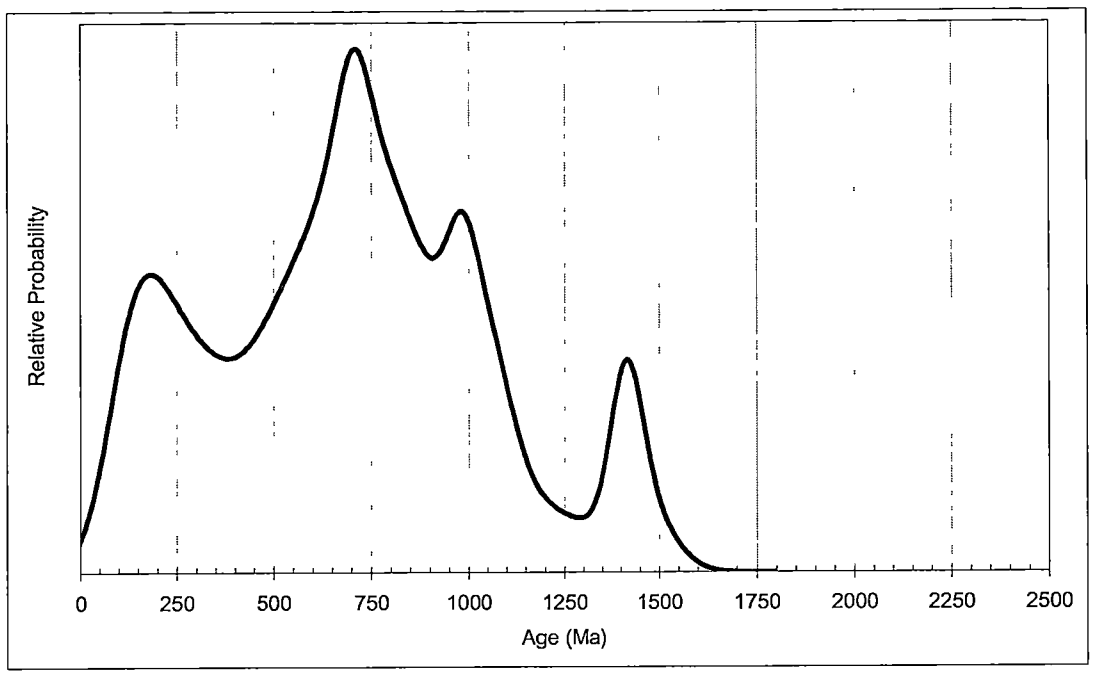

Figure 3.38. Combined relative probability plot for "western" Ahrberg Group samples 192, 201, 219 and 711. Number of analyses 35. Whereas Cambrian age monazite growth has occurred in this sequence, the effect of the deformation was minor, and hence monazites of older ages (approximately 700 Ma) are more evident and may represent diagenesis. Peaks at 980 Ma and around 1400 are considered to be inherited ages, from detrital grains that have not been reset during the Cambrian deformation. An age peak between 100 and 250 Ma is evident in sample 201. This may be a related to continental break-up. Similar age peaks are evident in the Surprise Point mylonite zone on King Island (section 3.7.4).

cannot exceed 750 Ma. Therefore, analyses with ages that are older than this must have a detrital source. As individual monazites are found have mixed ages (eg. Sample 711), partial resetting due to low levels of metamorphism can be suggested.

Rocky Cape Group correlates samples 378 (338700 mE, 5393950 mN), 382 (338250 mE, 5393630 mN) and 1019 (343860 mE, 5401800 mN)

Samples 378 and 382 from the Rocky Cape Group correlates, are fine grained quartz-graphite-mica siltstones. The samples are from 6.5 km and 6.75 km to the west of the Arthur Lineament's western boundary. They both show pervasive development of a finely spaced cleavage, with 0.2 mm wide microlithons and cleavage domains that are parallel to anastomosing. This is interpreted to be $\boldsymbol{Ca}S_3$, based on cleavage morphology and field evidence. $\boldsymbol{Ca}S_1$ and $\boldsymbol{Ca}S_2$ were not observed in this sample.

Monazites are rare in these samples. As can be seen from their chemistry (Appendix 3.26), the two grains analysed in sample 378 are similar. They have comparable compositions, and their ages (interpreted to be metamorphic) are within error. The age of the single analysis in sample 382 (1181 ± 55 Ma) suggests this grain is detrital. It has a distinctly different composition to the grains analysed in sample 378, in particular levels of La, Ce, Nd and Sm.

In contrast to samples 378 and 382, sample 1019 is from approximately 1.8 km to the west of the lineaments western boundary. The sample is a micaceous mudstone, that has several well developed foliations. The earliest foliation (interpreted to be $\boldsymbol{Ca}S_2$) is a continuous cleavage, defined by white mica grains. This cleavage is crenulated by a spaced, parallel to anastomosing cleavage, interpreted to be $\boldsymbol{Ca}S_3$ (Figure 3.32(g)).

The sample 1019 was analysed for monazites, and was found to have common, elongate, partly embayed grains that were 15 to 20 μm long and 5 to 10 μm wide (Figure 3.32(h)). The monazites were consistently aligned with the $\boldsymbol{Ca}S_2$ foliation, which occurs as the axial planar foliation to micro-folds in the sample (Figure 3.32(g)). The mineral chemistry of the monazites is mostly consistent, however several analyses (B2spot2, B3spot1, B4spot1 and B5spot1) have relatively depleted

La levels. These analyses also have elevated MREE (Figure 3.39(a)), with anomalously high Nd, Sm and Gd levels. Variation is also evident in the Th levels, however the Pb-Th ratios are consistent, other than analysis 8spot3 which, as indicated by its Pb-Th ratio, is significantly older than the other analyses (1816 ± 76 Ma). This is interpreted to a detrital age, that has not been completely reset during the Cambrian metamorphism. The weighted average age for the metamorphic monazites in the sample (543 ± 11 Ma) indicates monazite growth has occurred as part of the main Cambrian deformation ($\boldsymbol{Ca}D_2$) (Figure 3.39(b)).

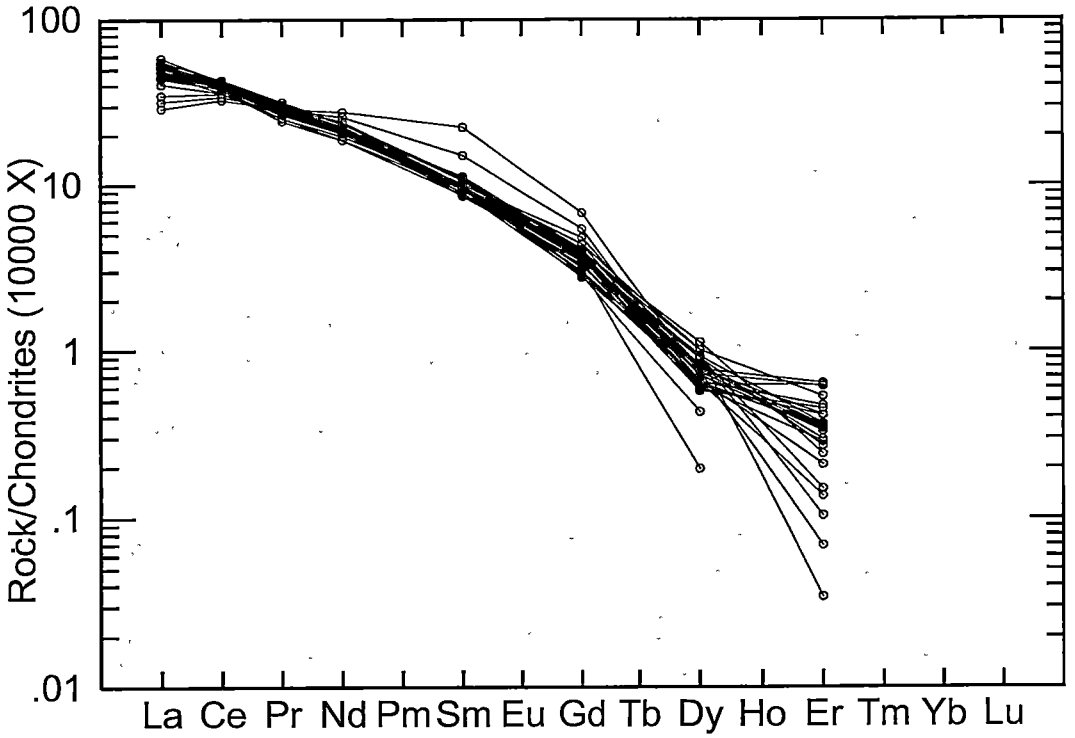

Figure 3.39(a). Rare earth element data for 1019 monazite analyses. Data is normalised to chondrite using values of Sun & McDonough (1989). The majority of analyses have similar chemistry (corresponding to similar ages), however two analyses (with comparable ages), B2spot2 and B5spot1 have elevated Nd, Sm and Gd. The spread in Er values is a result of analysis near the detection limit.

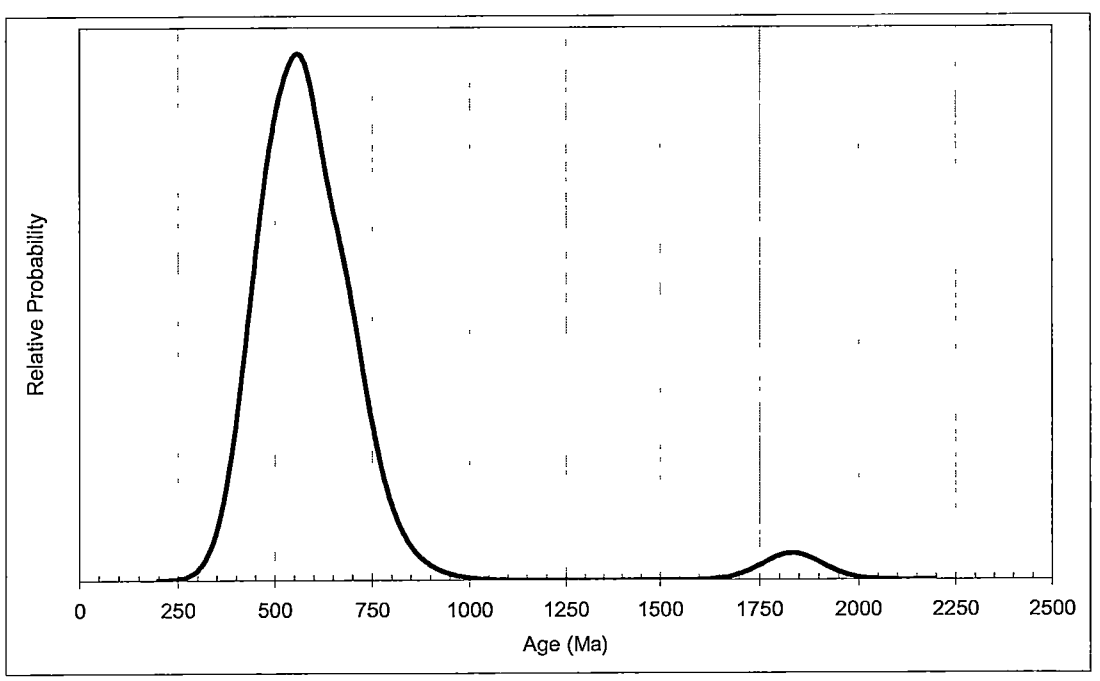

Figure 3.39(b). Relative probability plot for sample 1019. Number of analyses 32. A strong, Cambrian age peak occurs at 560 ± 11 Ma. Microstructural evidence indicates these monazites have grown parallel to $\boldsymbol{Ca}S_2$. There is evidence of an older, inherited grain, (at 1833 ± 76 Ma) which is interpreted to be detrital.

3.7.4 King Island metasediments and igneous intrusives

Regional Geology

King Island, located to the north of the northwest Tasmanian mainland, is composed of several different (meta-) sedimentary and igneous sequences, of different ages (Figure 3.40). The western half of the island is dominated by metasediments that are interlayered with minor mafic extrusives (Blackney 1982). The metasedimentary sequence comprises in excess of 1000 m of dominantly quartzofeldspathic schist with minor quartzite, micaceous quartzite, pelitic schist, and rare thin calcareous lenses. The typical mineral assemblage in the schists is quartz+muscovite+biotite (+plagioclase). Pelite may locally contain garnet and minor potash feldspar and andalusite occurs in alumina-rich rocks.

The mafic intrusives are amphibolites and have compositions similar to tholeiitic basalt (Blackney 1982) (see Chapter 4). These have been intruded in several locations, by syn-deformational granitoids, associated with the 760 Ma Wickham Orogeny (Cox 1973, Turner *et al.* 1998). The dominant granitic intrusive phase is an K-feldspar porphyritic biotite adamellite (Turner 1989). The syn-intrusional deformation was considered to be the D_2 event in the Cape Wickham region by Cox (1973). McDougall & Leggo (1965) produced age determinations for the granitoid that are significantly younger than 760 ± 12 Ma (Turner *et al.* 1998). Using the isotopic constants of Steiger & Jäger (1977), the data of McDougall & Leggo (1965) results in ages of 416 Ma (K-Ar biotite), 575 Ma (K-Ar muscovite) and 728 Ma (Rb-Sr muscovite) (Turner *et al.* 1998). Turner *et al.* (1998) concluded these ages were consistent with thermal events (such as the intrusion of Devonian to Carboniferous granitoids) having partially reset all of the mica ages.

Polyphase deformation of the Precambrian metasediments was in part broadly synchronous with the period of Precambrian granitic intrusive activity and metamorphism to amphibolite facies. The first major deformation phase (D_1) produced large, tight to isoclinal folds, associated minor folds, and a penetrative axial surface cleavage. Prograde metamorphism appears to have commenced during D_1, and S_1 microfabrics are defined by amphibolite facies mineral assemblages. Cross-cutting relationships at the margin of the pluton indicate that at the presently exposed

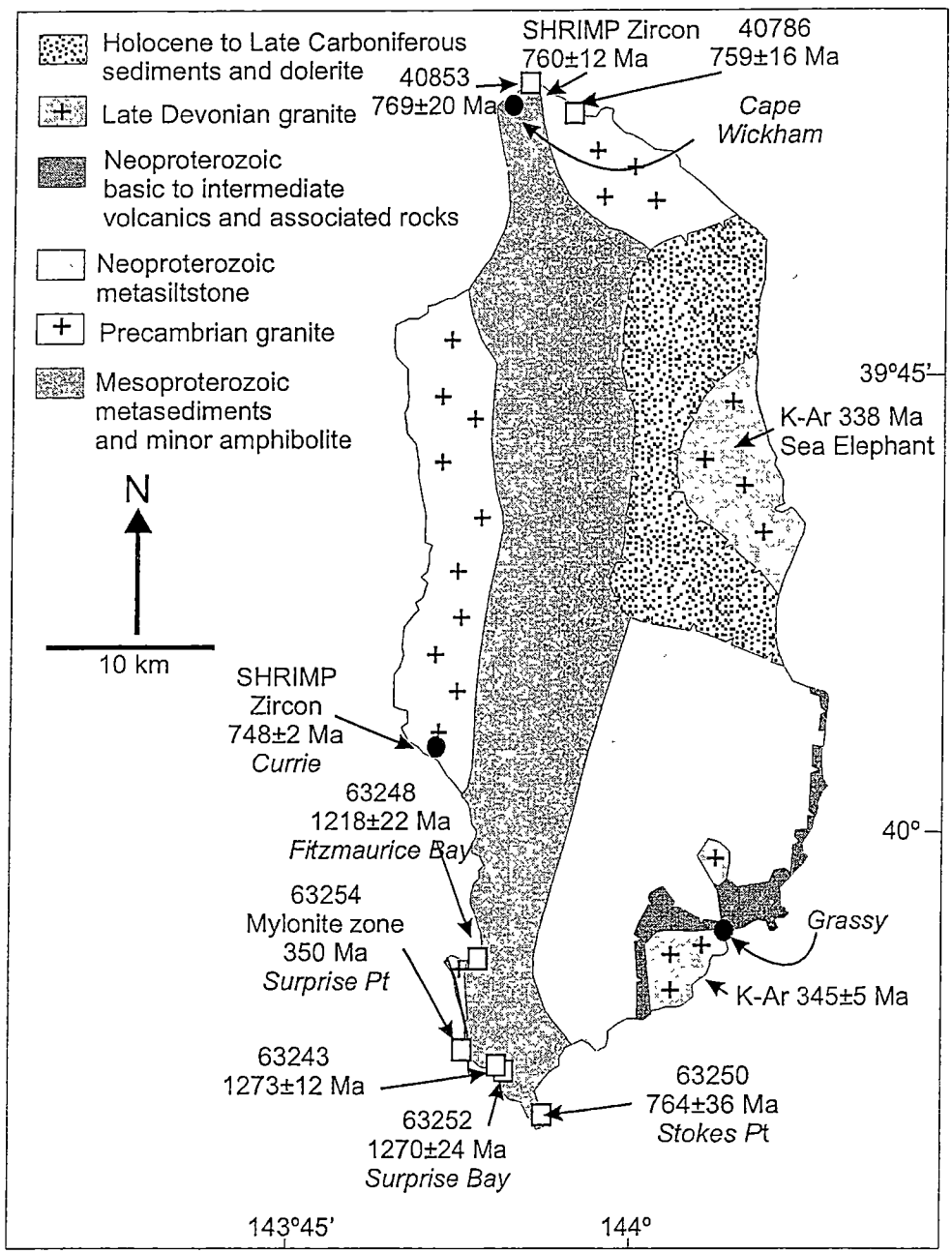

Figure 3.40. Geological map of King Island (from Calver *et al.* 1995). Sample numbers and locations with ages (from this study) are indicated. Ages from previous work (and age calculation method) are also presented.

structural level, major granitic intrusive activity post-dates D_1 folding, and probably did not commence prior to D_2.

Second generation (D_2) structures have deformed the metamorphic assemblages as well as many of the granitic rocks. However, minor granitic intrusive activity and veining post-dates D_2 folding. Within the granitic pluton D_2 has deformed xenoliths, produced a foliation in some of the granitic rocks, and produced some mylonite zones. Small scale D_2 folds in the western aureole are open to tight structures which fold the penetrative S_1 cleavage. Third generation folds, which are also cut by minor granitic sheets and veins, are moderately to gently inclined, open structures.

Upright D_4 folds post-date all granitic intrusive activity, but are apparently cut by dykes of tholeiitic dolerite which form part of an extensive and dominantly north-south trending dyke swarm in the Cape Wickham area. These extensively altered dolerites are probably related to the Neoproterozoic mafic extrusives on the east coast of King Island.

The granitoid mass which outcrops at Cape Wickham extends down the west coast of the island to south of Currie and reappears again farther south at Cataraqui Point (Gresham 1972, Turner 1989). Its boundaries trend parallel to the northerly strike of the country rocks which display metamorphism comparable with the sequence at Cape Wickham along the eastern or inland boundary of the pluton. A small belt of country rock west of the granitoid mass near Currie contains pale- and dark-grey, interbedded siltstone of low metamorphic rank, thus indicating that the western granite contact is a major fault.

South of Currie only the eastern boundary of the granitoid mass is present and the adjacent meta-sedimentary lithologies are much like those at Cape Wickham, comprising mainly quartzofeldspathic and pelitic schists and phyllites with mafic rocks and very minor carbonate (Blackney 1982). Garnet-biotite geothermometry indicates temperatures of 470–580°C and the presence of andalusite and rare phengite suggest low pressures of 100–300 MPa. Mafic rocks include intrusive and possibly, extrusive tholeiitic types with subordinate intrusives of alkali basaltic character (see Chapter 4). Throughout the granitoid mass the rocks are deformed,

exhibiting common shear surfaces and cataclastic microtextures (McDougall & Leggo, 1965, Streit & Cox 1998).

Exposure in the eastern half of King Island is dominated by a relatively unmetamorphosed siltstone and sandstone sequence. The relationship of this unit to the western sequence of schists is poorly understood. Gresham (1972) suggested the unmetamorphosed sequence unconformably overlies the schists, but this argument is inconclusive, as the contact between the two is not exposed. Calver & Walter (2000) suggested the correlation of the unmetamorphosed sequence with part of the Rocky Cape Group, whereas Turner *et al.* (1998) suggested its correlation with the Burnie and Oonah Formations of northwest Tasmania. On the east coast, this sequence is overlain by mafic volcanics and sedimentary sequences, that are Late Neoproterozoic in age, and known as the Grassy Group (Calver & Walter 2000). The Grassy Group has been correlated with parts of the late Neoproterozoic rift sequences (the Togari Group) in northwest Tasmania (Calver & Walter 2000).

This work, however, is focused on the metasediments found in the far south (Stokes Point), southwest (Surprise and Fitzmaurice Bays, Cataraqui Point) and north (Cape Wickham granitoid and contact aureole) of King Island (Figure 3.40). The King Island data presented here is part of a combined research initiative, and is currently being compiled as a manuscript for publication (Berry *et al.* in prep).

Summary of Results

Seven samples from King Island were analysed using the CHIME method. These included five samples from southwest King Island of pelitic schist far from the Neoproterozoic granitoids (63252, 63243, 63248, 63250, 63254). Two samples were included from northwest King Island to show the effect of the granitoids and the contact aureole (40853, 40786). Four other samples of schist were considered but these were dominated by xenotime rather than monazite or contained monazite with very low Th unsuitable for the application of this technique.

For six of the seven samples analysed, 20 analyses were obtained on about 10 separate grains and usually 90% of these passed compositional screens which identify inclusions and grain margins which may compromise the analyses. For the

more complex sample 63254, 36 spots were successfully analysed. The analyses are shown in Appendix 3.27.

Samples 63252 (236200 mE, 5553700 mN) 63243 (mE, mN) (Surprise Bay) and 63248 (233900 mE, 5560600 mN) (Fitzmaurice Bay)

Samples 63252 and 63243 are petrographically very similar. They are fine grained, quartz-white mica-biotite-garnet-feldspar ± sericite schists, with minor very fine grained opaque phases. The samples have moderately well foliations, defined by quartz- and mica-rich domains, however the individual white mica and red-brown biotite blades are multiply oriented, and reflect polyphase deformation and mineral growth. The quartz grains are stubby and have not been subjected to high strain levels. Garnet occurs as euhedral, mostly large (1 mm diameter) porphyroblasts in comparison to the groundmass. They are partly corroded, as are the feldspar grains (Figure 3.41(a)), due to retrograde events accompanying the sericite alteration.

Sample 63248 is a fine grained, quartz-white mica ± green biotite-tourmaline-sericite-chlorite-opaque schist. It is moderately well foliated and, as with samples 63252 and 63243, polyphase deformation is evident due to the multiply oriented white mica grains. The white mica has predominantly grown in two orientations, however a weaker, third orientation was observed. Quartz grains are mostly stubby, and have not undergone high levels of strain.

Of the five schistose samples from SW King Island, three samples have a consistent CHIME age in monazite. Samples 63252 and 63243 from Surprise Bay (Figure 3.40) both contain small 10-30 μm grains of monazite aligned in S_1 (Figure 3.41(b) and (c)). They have a CHIME age of 1273 ±12 Ma and 1270 ±24 Ma, and similar chemistries (Appendix 3.27, Figures 3.42(a) and (b), Figures 3.43(a) and (b)). These samples show evidence of equilibrium D_1 textures. The samples are both more than 1 km from the granite and garnet is part of the prograde metamorphic assemblage. Sample 63248 from Fitzmaurice Bay comes from much closer to granitoid. It is from 200m E of the visibly spotted hornfels zone and 500m E of the granite contact (Figure 3.40). The monazite from this sample has late halo-like overgrowths, and is distinguishable from the other Surprise Bay samples (Figure 3.41(d)). There is no

Figure 3.41(a) to (h) photomicrograph and SEM images of metasedimentary schists from Mesoproterozoic succession on King Island. (a) photomicrograph illustrating well defined schistosity, with aligned feldspar porphyroblast (corroded), white mica, biotite, garnet and quartz, Surprise Bay sample 63252; (b) SEM image of embayed monazite aligned with dominant foliation (S_1), Surprise Bay sample 63252; (b) SEM image of embayed elongate monazite aligned with dominant foliation (S_1), Surprise Bay sample 63243; (d) SEM image of subhedral monazite with overgrowth (dull grey), Fitzmaurice Bay sample 63248; (e) SEM image of large, poikiloblastic monazite, Stokes Point sample 63250; (f) SEM image of small, poikiloblastic textured monazite, from the mylonite zone, Surprise Point sample 63254; (g) SEM image of monazite with vermicular cracks, from contact aureole of Cape Wickham granitoid, sample 40853; (h) SEM image of irregular shaped monazite and ?zircon (zoned), Cape Wickham granitoid sample 40786. m: white mica, fsp: feldspar, q: quartz.

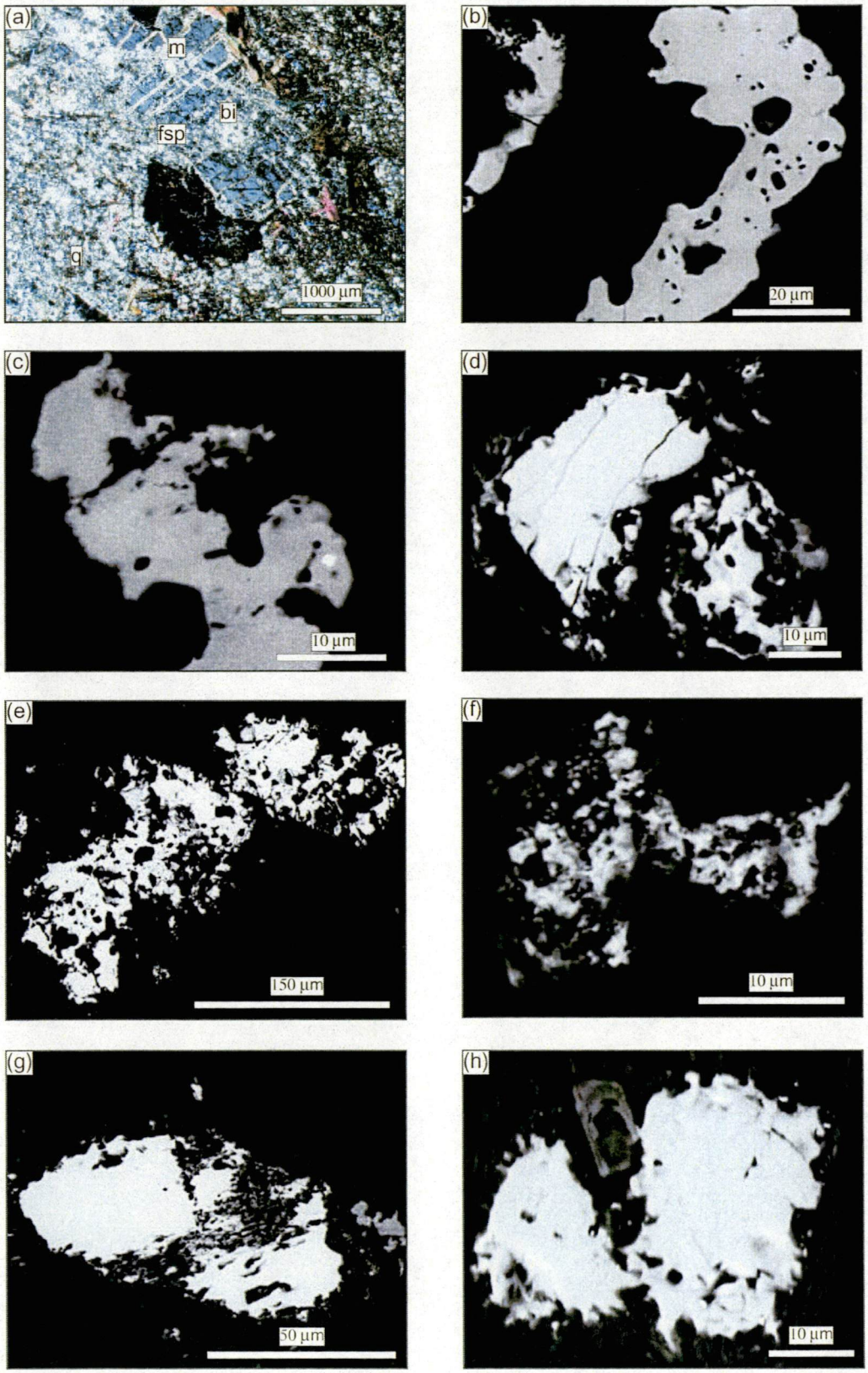

Figure 3.41(a) to (h).

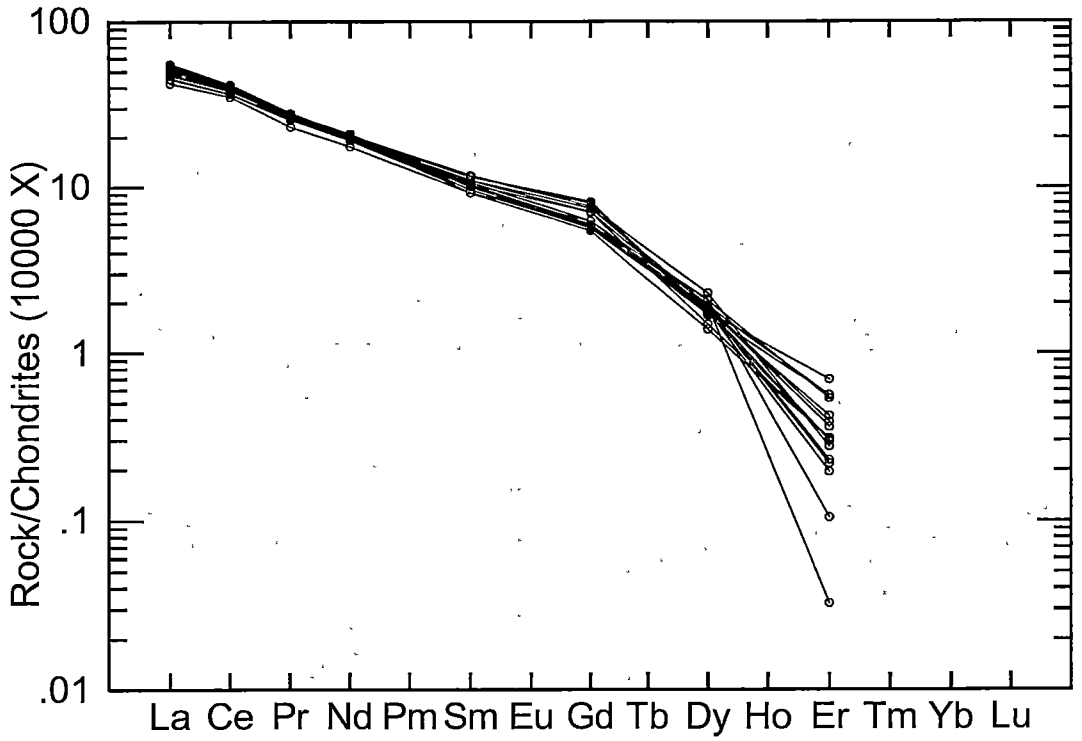

Figure 3.42(a). Rare earth element data for 63252 (Surprise Bay) monazite analyses. Data is normalised to chondrite using values of Sun & McDonough (1989). The analyses have similar chemistry (corresponding to similar ages). The spread in Er is a result of analysis near the detection limit.

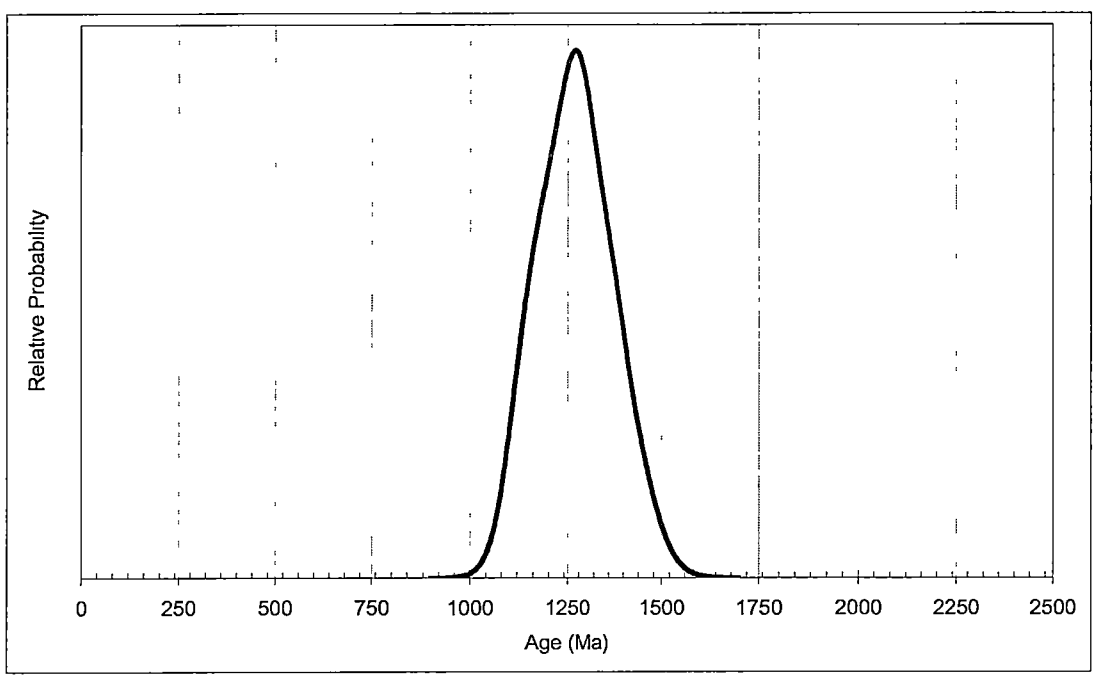

Figure 3.42(b). Relative probability plot for sample 63252. Number of analyses 18. A strong, Grenvillean-age metamorphic event occurs at 1273 ± 12 Ma. There is no evidence of a Wickham orogenic event (760-780 Ma), or other subsequent metamorphic events.

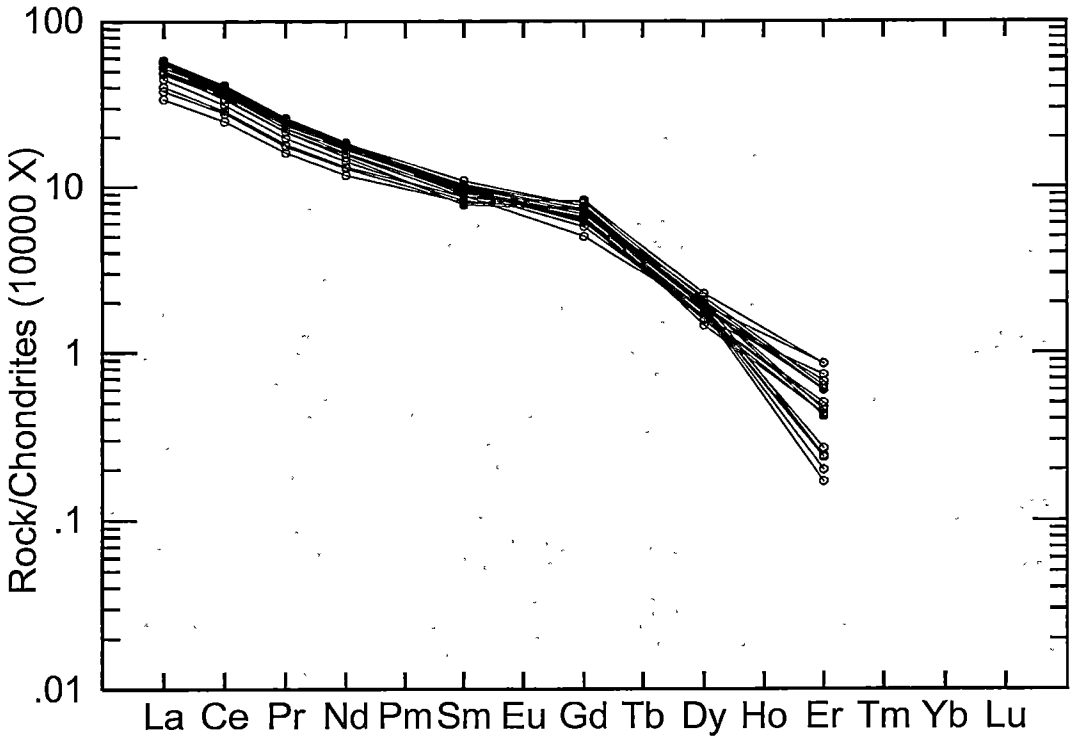

Figure 3.43(a). Rare earth element data for 63243 (Surprise Bay) monazite analyses. Data is normalised to chondrite using values of Sun & McDonough (1989). The analyses have a notable depletion in MREE relative to sample 63252, despite the similar ages. The spread in Er values is due to analytical error.

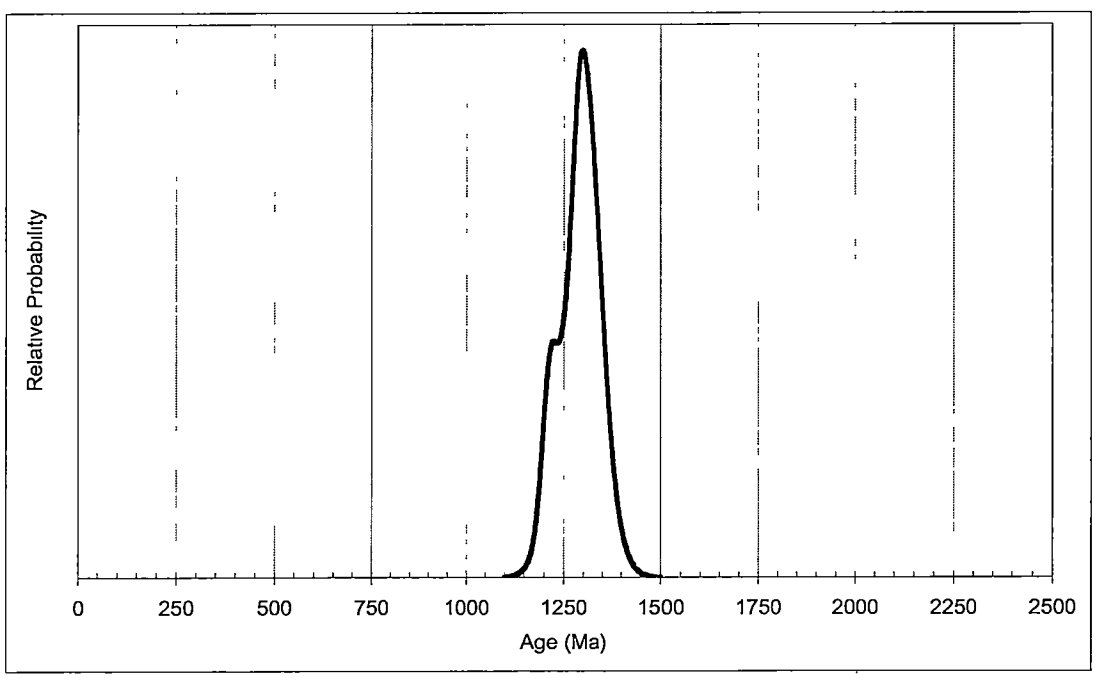

Figure 3.43(b). Relative probability plot for sample 63243. Number of analyses 20. A strong, Grenvillean-age metamorphic event occurs at 1270 ± 24 Ma. There is no evidence of a Wickham orogenic event (760-780 Ma), or other subsequent metamorphic events.

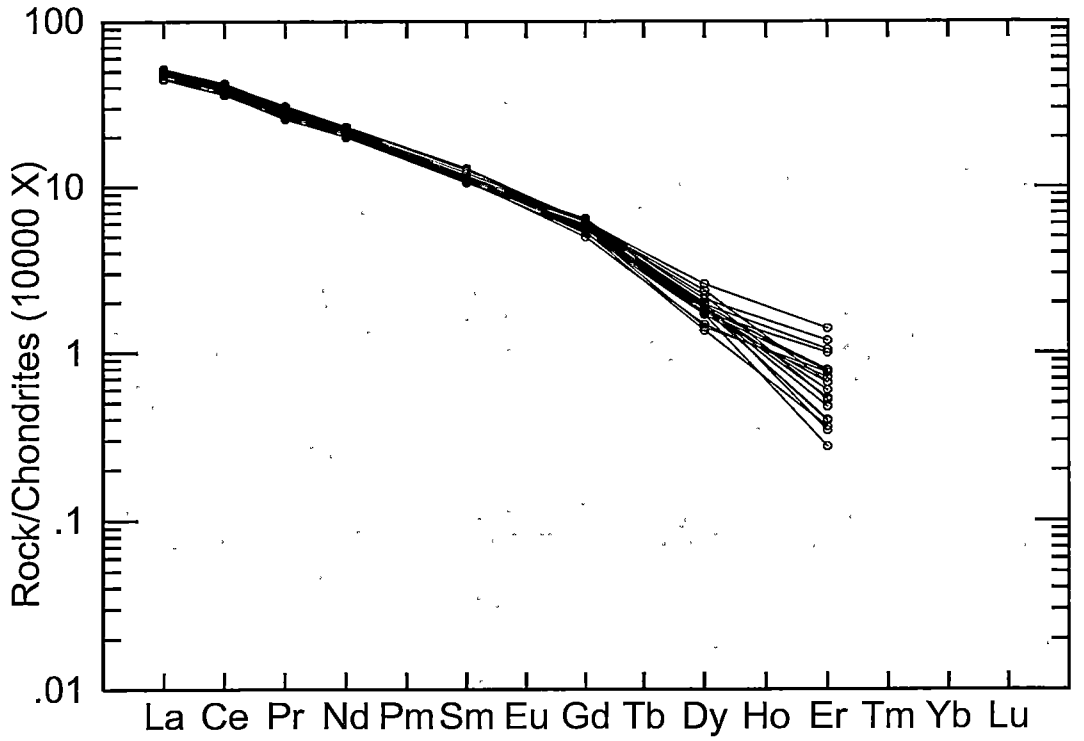

Figure 3.44(a). Rare earth element data for 63248 (Fitzmaurice Bay) monazite analyses. Data is normalised to chondrite using values of Sun & McDonough (1989). The analyses have similar chemistry (corresponding to similar ages). The spread in Er values is due to analytical error.

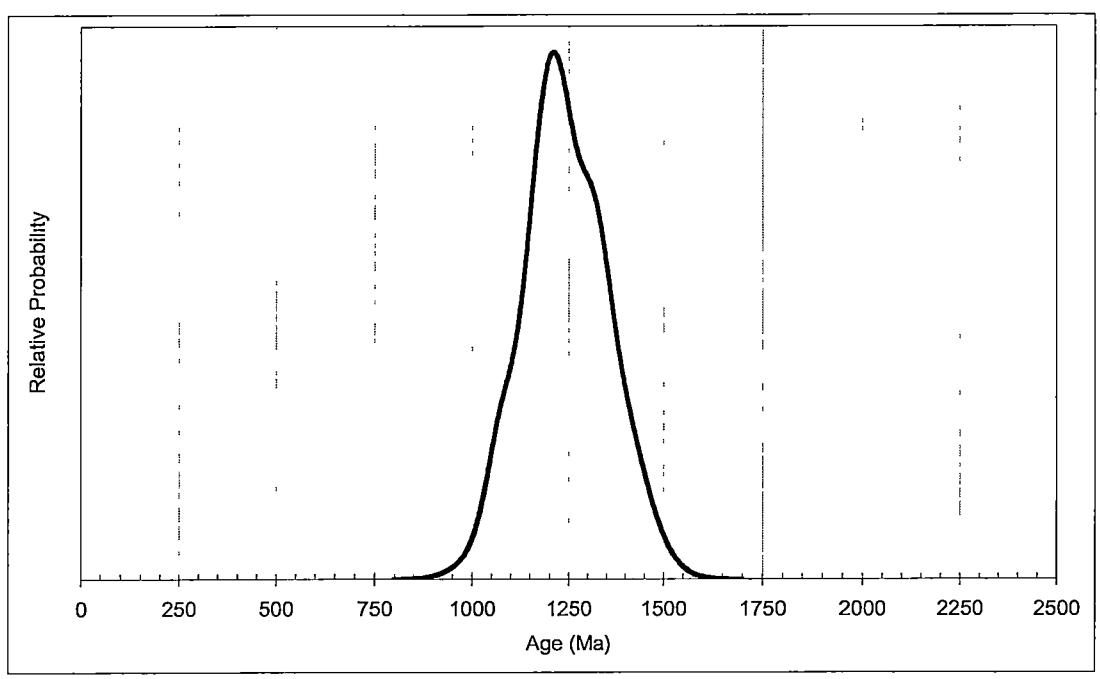

Figure 3.44(b). Relative probability plot for sample 63248. Number of analyses 20. A strong, Grenvillean age event occurs at 1218 ± 22 Ma. Several slightly older grains, at around 1380 Ma were analysed, and cause the irregularity of the upper age slope. However, as these are within error of some of the younger grains, a single peak is defined.

evidence of a mixed population in the monazite ages but the weighted mean age is 1218 ±22 Ma (Figures 3.44(a) and (b)). This is significantly younger than the two samples from Surprise Bay and may reflect a small amount of Pb loss associated with the contact metamorphism near the granitoid on Cataraqui Point.

Sample 63250 (238100 mE, 5550300 mN) (Stokes Point)

Sample 63250 is an intensely foliated, quartz-white mica ± red brown biotite-garnet schist, with minor retrograde chlorite and sericite phases. The sample exhibits a single strong foliation (the main schistosity), and has been weakly crenulated by a poorly developed cleavage at a high angle to the schistosity. The quartz grains are elongate, having undergone a high degree of flattening. The biotite is aligned with the schistosity, consistent with syntectonic growth.

The Stokes Point sample (Figure 3.40, Appendix 3.27) contains monazites that are distinct from other samples. The grains occur as large 100 μm poikiloblastic to sieve texture grains (Figure 3.41(e)). These grains have relatively low Th (1-3 %) which means the individual grain ages have very large errors. Despite this age population is compatible with a single age of 764 ± 36 Ma, and the monazites are similar in their chemistry (Figures 3.45(a) and (b)). The rock is strongly chlorite altered but otherwise does not appear to have any evidence of contact metamorphism. The age recorded matches the age of the Cape Wickham granite and the textural evidence for recrystallisation is taken here to indicate this rock has been subject to hydrothermal alteration associated with granitoids of this age. This alteration has completely reset the CHIME monazite age.

Sample 63254 (233700 mE, 5554400 mN) (Surprise Point mylonite zone)

Sample 63254 is a fine grained quartz-white mica-biotite ± tourmaline schist. It is strongly foliated, and has preserved evidence of polyphase deformation. The micas are predominantly uniformly aligned with the main schistosity, however two less well developed orientations, at a moderate angles to the main foliation, were observed.

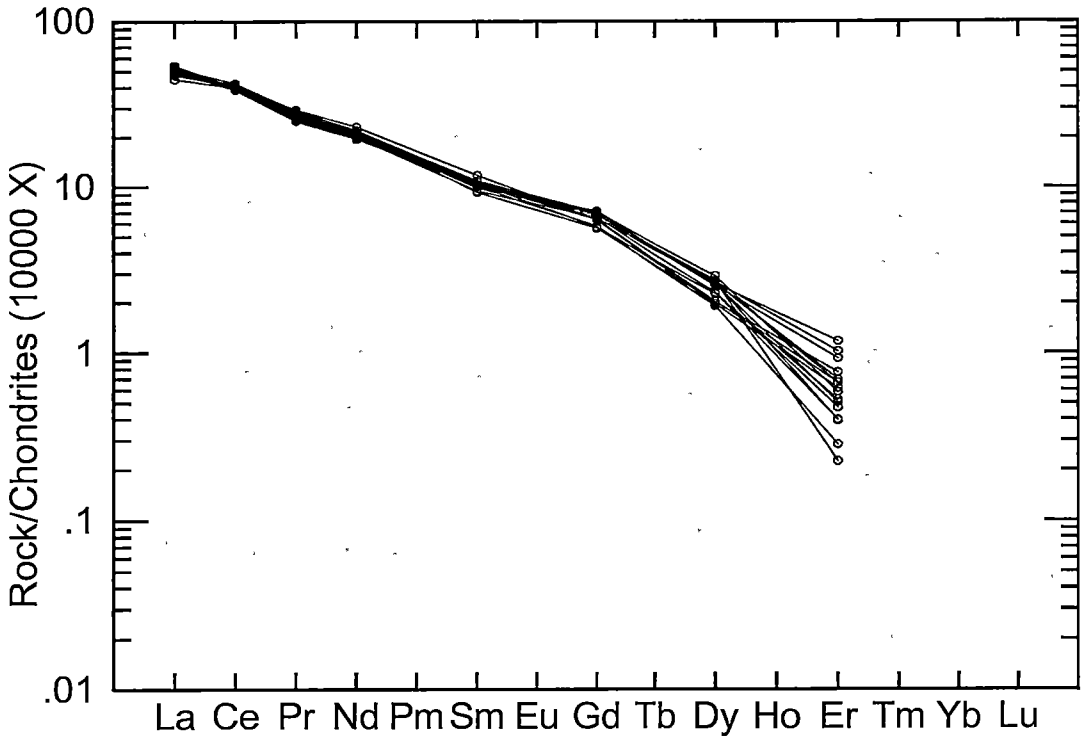

Figure 3.45(a). Rare earth element data for 63250 (Stokes Point) monazite analyses. Data is normalised to chondrite using values of Sun & McDonough (1989). The analyses have similar chemistry (corresponding to similar ages). The spread in Er values is due to analytical error.

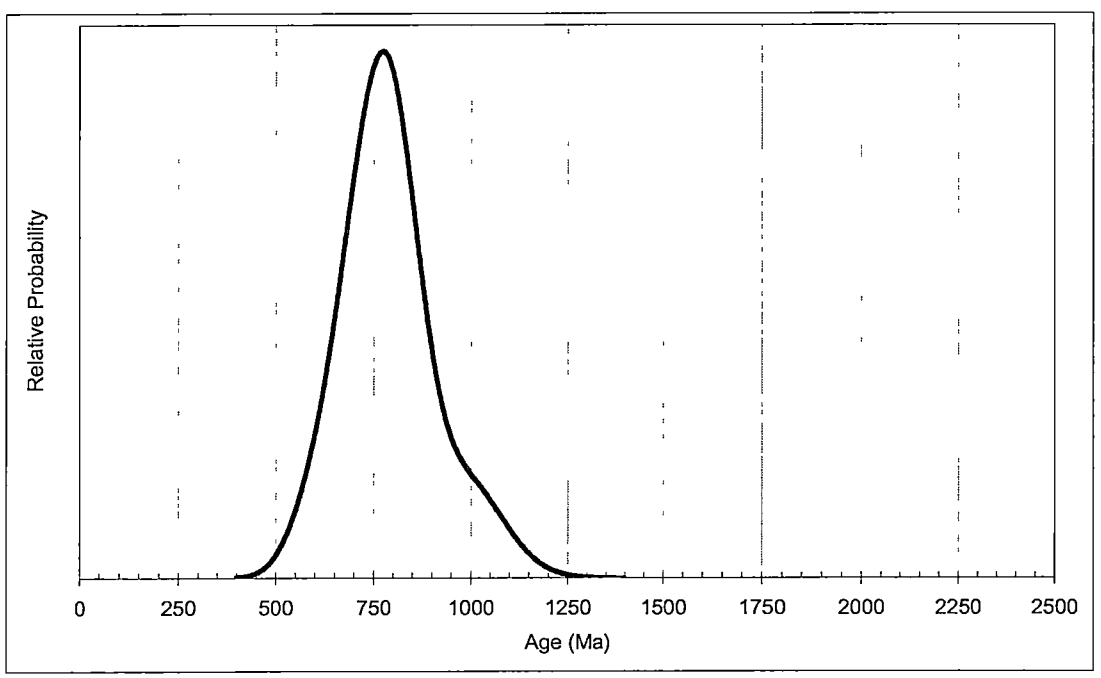

Figure 3.45(b). Relative probability plot for sample 63250. Number of analyses 16. A pronounced peak occurs at 764 ± 36 Ma, and is attributed to the Wickham Orogeny. Because of the large errors, the population at 977 ± 18 Ma (see Appendix 3.27) is not evident in the age profile.

The sample, from the margin of a large-scale mylonite zone at Surprise Point (Figure 3.40) contains monazite that have complex chemistry and age patterns. A few grains are large 30 μm and euhedral with overgrowths, and have ages similar to the Stokes Point sample (764 ± 36 Ma) (Appendix 3.27). They have low Th contents (<3%) and steep REE patterns similar to other samples from the schists (Figure 3.46(a)). Most grains are small 10-15 μm with rounded to euhedral shapes, although irregular, poikiloblastic grains were also observed (Figure 3.41(f)). These grains have a more complex age distribution but have a median age around 350 Ma implying a late Palaeozoic age (Figure 3.46(b)). These grains have 2-3.6 % Th and a flatter REE pattern indicating a substantial change in environment possible relate to the influx of fluids along the shear zone. There are a small number of grains with much higher Th content. These grains occurs as small high-Th zones in or on spongy low-Th monazite. In one case there is a close association with a late crosscutting vein. The high Th grains have very young ages and we interpret these grains as evidence of late reactivation of the mylonite zone during Gondwana break-up. The history for the mylonite zone is complex with a number of reactivation events including Neoproterozoic, late Palaeozoic and Cretaceous-Tertiary.

Sample 40853 (238000 mE, 5613900 mN) (Cape Wickham granitoid contact aureole)

Sample 40853 is a coarse grained, schistose metasediment, consisting of quartz-red brown biotite-white mica-sericite and minor chlorite. The sample is intensely folded (D_2) and has preserved evidence of polyphase deformation. Biotite has grown during several events. The early generation of biotite is in equilibrium with white mica, whereas late biotite appears to be a retrograde feature, related to sericite alteration. The sericitic alteration was observed surrounding the blades of white mica, corroding the margins.

The contact aureole of the Cape Wickham granitoid is a broad zone of intense D_2 deformation and coarse schistose texture dominated by contact mineralogy. The sample 40853 from the aureole has a strong D_2 crenulation cleavage, and most monazite from this zone appears to be in equilibrium with this metamorphic assemblage. The grains are 20-50 μm across and aligned in S_2. A few grains appear

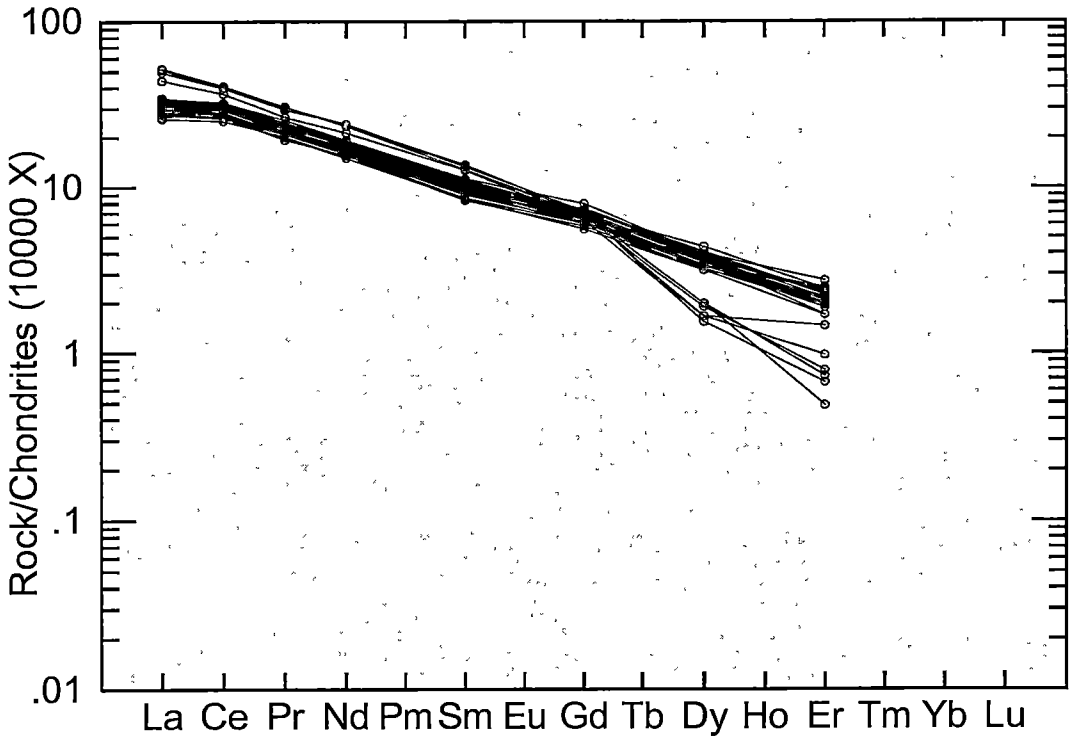

Figure 3.46(a). Rare earth element data for sample 63254 (Cataraqui Point mylonite zone) monazite analyses. Data is normalised to chondrite using values of Sun & McDonough (1989). The analyses have similar chemistry (corresponding to similar ages). The notable depletion of HREE in certain analyses corresponds to the older monazites analysed, and is interpreted to reflect monazites that have grown in equilibrium with garnet, which is known to cause HREE depletion in monazites. The spread in Er values is interpreted to be due to analytical error.

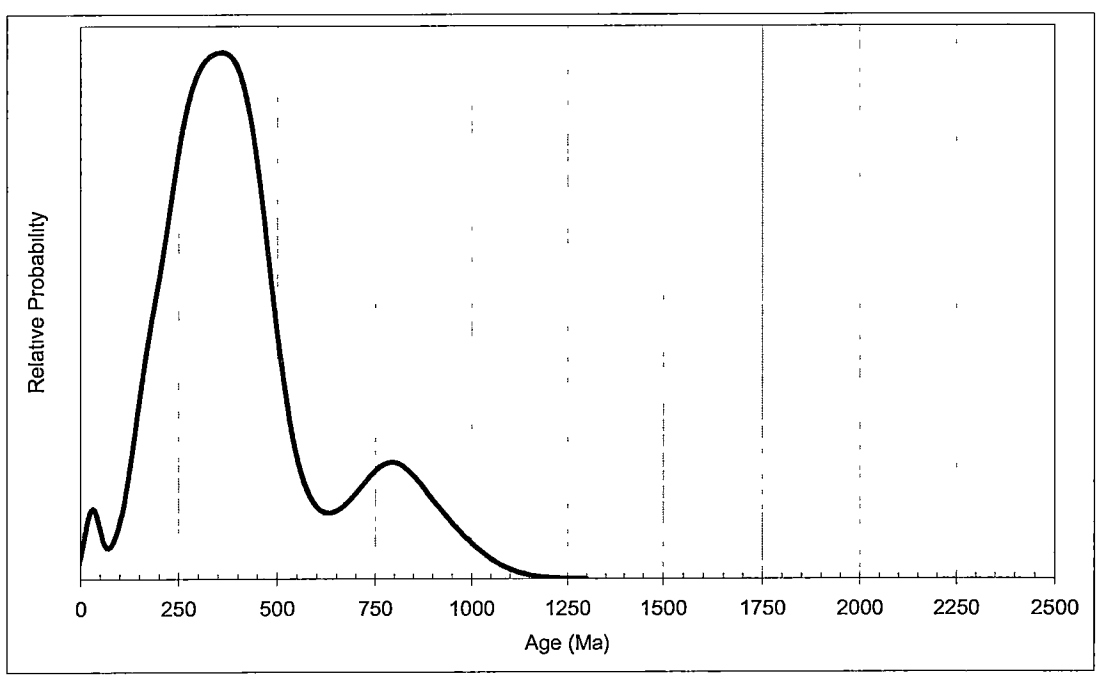

Figure 3.46(b). Relative probability plot for sample 63254. Number of analyses 36. The mylonite zone from which the sample is derived has undergone several periods of activation. A peak is evident at around 800 Ma, and is interpreted to represent monazites that have grown during the Wickham Orogeny. The main deformation has occurred at approximately 380 Ma, however reactivation has continued in the Mesozoic and Tertiary.

cracked with vermicular infilling of the cracks (Figure 3.41(g)). Despite this suggestion of textural disequilibrium, the CHIME monazite age on individual spots have a simple distribution and the weighted mean age is 769 ±20 Ma (Appendix 3.27 and Figure 3.47(a)). This is within error of the granitoid age and contrast sharply with most of the CHIME monazite dates from garnet schist outside the contact aureole. The chemistry of the analysed monazites shows little variation (Figure 3.47(b)).

Sample 40786 (239700 mE, 5612900 mN) (Cape Wickham granitoid)

Sample 40786 is a weakly foliated, medium grained granitoid. It consists of multiply twinned plagioclase, microcline, quartz, red brown- and minor green- biotite, white mica and sericite. The red brown biotite (early) is heavily included with radiogenic minerals and has abundant pleochroic haloes. It and the white mica define the foliation.

The Cape Wickham granitoid (Figure 3.40) has previously been dated by SHRIMP zircon as 760 ±12 Ma (Turner *et al.* 1998) and 762 Ma ±14 Black *et al.* (1997). A similar granite from south of Currie was dated at 748 ±2 Ma (Black *et al.* 1997). As a measure of the consistency of the CHIME monazite method with SHRIMP dating a sample of the Cape Wickham granite was included in this study. Sample 40786 has 20-50 μm irregular monazite grains (Figure 3.41(h)). The monazite has a simple age population in which the counting statistics explain the variability of the individual analyses (Appendix 3.27). No significant inheritance was found unlike the zircons. The weighted mean age of 759 ±16 Ma is indistinguishable from the zircon age of the same pluton (Figure 3.48(a)). The chemistry of the analysed monazites shows little variation (Figure 3.48(b)).

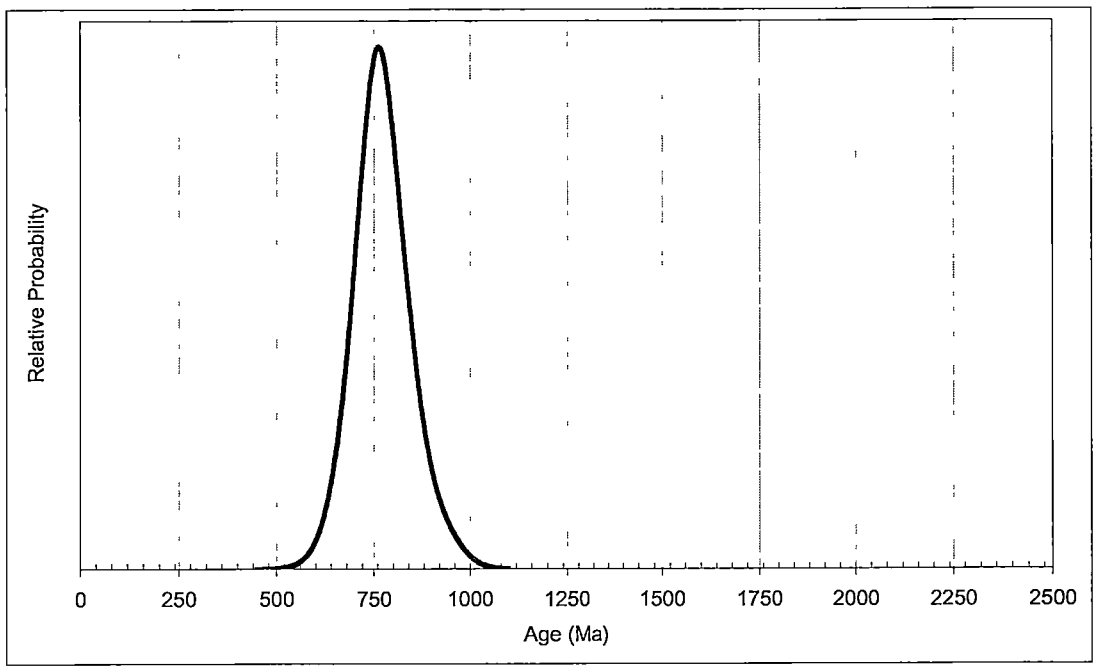

Figure 3.47(a). Relative probability plot for sample 40853, from the contact aureole of the Cape Wickham granitoid. Number of analyses 19. A pronounced peak, attributed to the thermal event of granitoid emplacement (Wickham Orogeny) occurs at 769 ± 20 Ma.

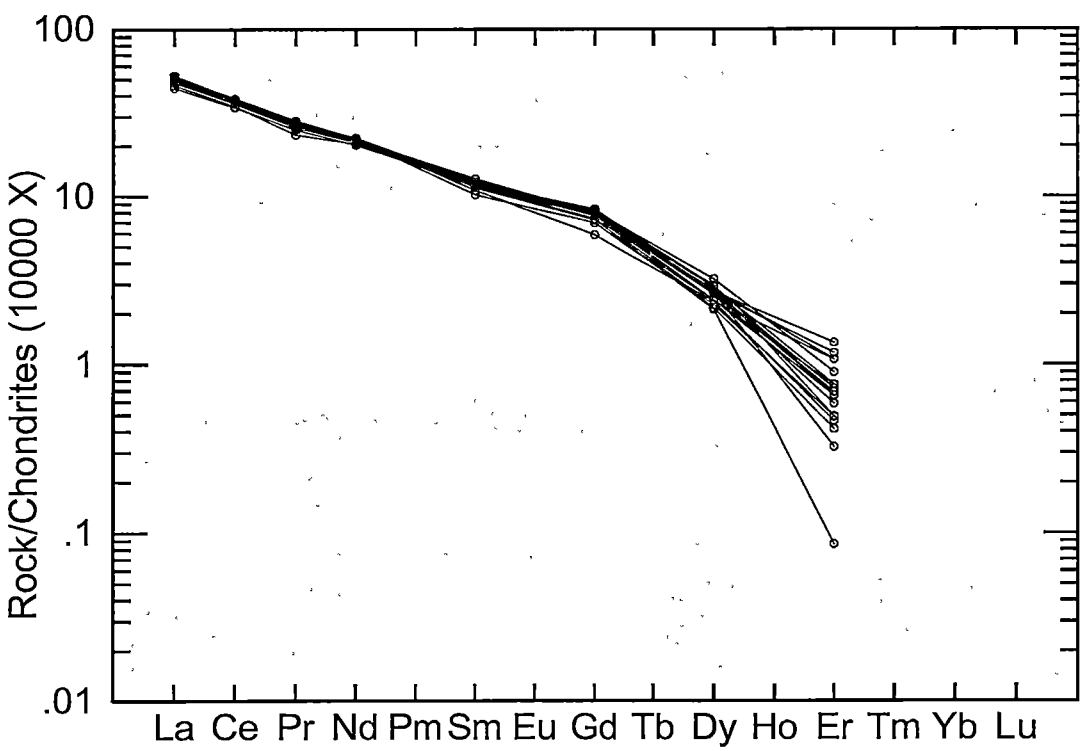

Figure 3.47(b). Rare earth element data for 40853 (Cape Wickham granitoid contact aureole) monazite analyses. Data is normalised to chondrite using values of Sun & McDonough (1989). The analyses have similar chemistry (corresponding to similar ages). The spread in Er values is due to analytical error.

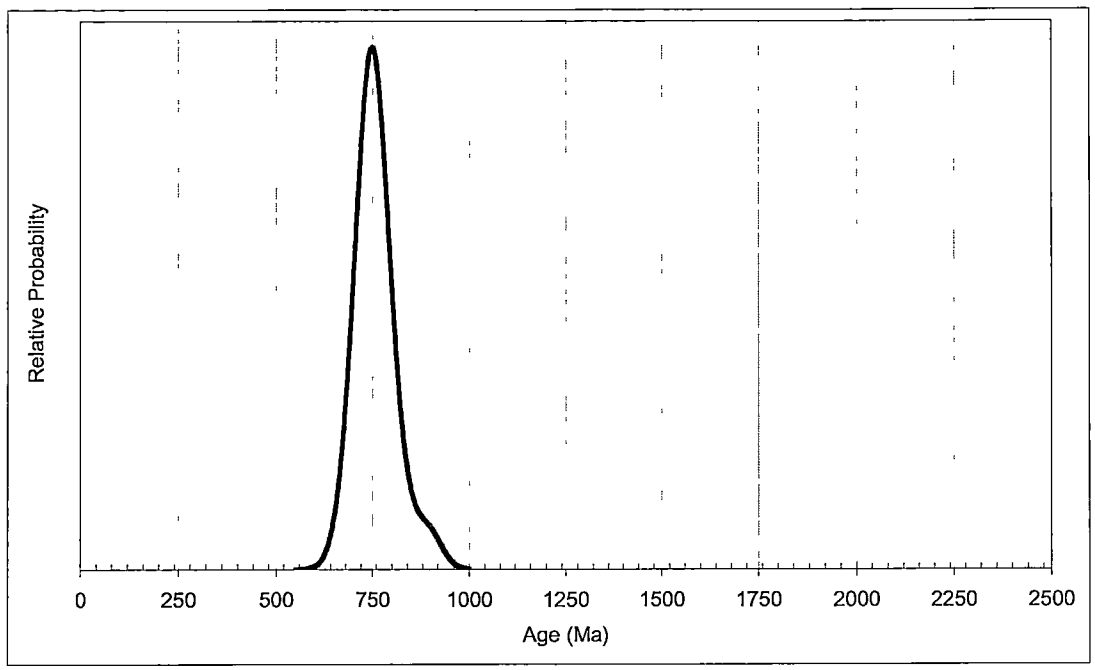

Figure 3 48(a). Relative probability plot for sample 40786. Number of analyses 20. A pronounced peak occurs at 759 ± 16 Ma, and is attributed to the Wickham Orogeny. A single analysis has an age of 896 ± 34 Ma, which may reflect partial resetting of the ~1270 Ma event.

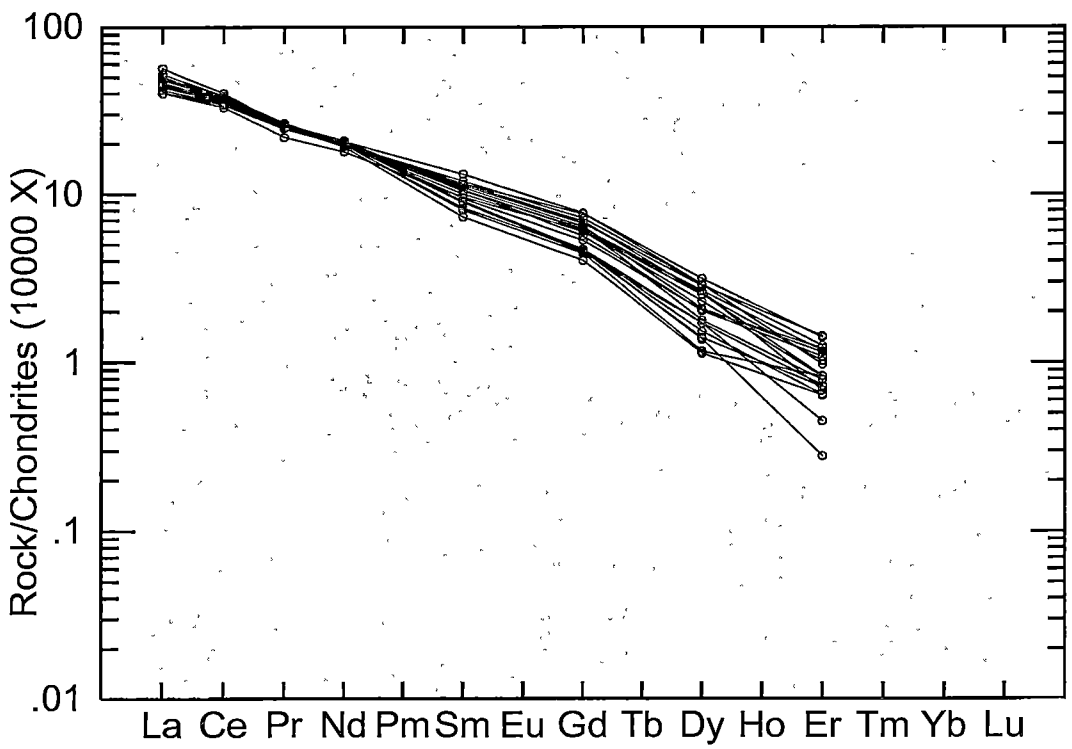

Figure 3.48(b). Rare earth element data for 40786 (Cape Wickham granitoid) monazite analyses. Data is normalised to chondrite using values of Sun & McDonough (1989). The analyses have similar chemistry (corresponding to similar ages). The spread in Er values is interpreted to be due to analytical error.

3.7.5 Discussion

The geological relationship between northwest Tasmania and King Island, prior to the Cambrian, has been a contentious issue for some time. The maximum age of the metasediments in the western areas of King Island, and the age of the regional metamorphism has been open to speculation. In addition, the timing and extent of metamorphic events in the northwest of mainland Tasmania has also been open to debate. As can be seen from the results in sections 3.7.2 to 3.7.4, northwest Tasmania and King Island have significantly different deformational histories.

There is no widespread evidence of metamorphism attributed to the Wickham Orogeny in northwest Tasmania. Monazites analysed in sample 1167 include ages that may correspond to the Wickham Orogeny (Appendix 3.23), however the representation of this age population in this sample is not dominant. Significantly older grains, as well as Cambrian age grains are common. This suggests the analyses with *ca.* 780–800 Ma ages represent an event that was not strong enough in metamorphic grade to reset older grains. This event may represent the Wickham Orogeny, or alternatively may be a diagenetic age, given the possible depositional age of the Burnie and Oonah Formations. The Cambrian event is the most pronounced peak, and reflects the samples proximity to the eastern boundary of the Arthur Lineament (Figure 3.36(b)).

The Rocky Cape Group correlates are only weakly deformed, and do not show evidence of having undergone metamorphism prior to the Tyennan Orogeny. The Wickham Orogeny may be responsible for the low angle unconformity separating the Rocky Cape Group correlates from the overlying cover sequence, although this event did not cause the growth of metamorphic monazite. Rare detrital grains, reflecting the provenance of the Rocky Cape Group correlates, were observed, however these do not have implications for the deformational history of the unit. The most strongly deformed units of the Rocky Cape Group correlates occur close the western boundary with the Arthur Lineament (sample 1019), and these have a conclusive metamorphic age of *ca.* 560 Ma (Figure 3.39(b)).

The Arthur Lineament is undoubtedly Cambrian in age, as is demonstrated by monazite ages in samples 1036c, 1094 and 1114. The main deformation, interpreted to be $\boldsymbol{Ca}D_2$ has caused significant syn-deformational growth of monazite in strongly deformed rocks of the lineament (Figure 3.32(d) and (e)). Several older grains are interpreted to be detrital grains that have not been completely reset. These have Cambrian age overgrowths. The affect of the Cambrian deformation dissipates abruptly to the west of the lineament. As a consequence, metasediments in the "western" Ahrberg Group have mixed populations, indicative of multiple sources for detrital material. A Cambrian age population was observed, however this is not dominant (*cf.* Appendix 3.25 and Figure 3.38).

Low grade metasediments to the east of the lineament show evidence of the same metamorphic event, although in this region the event was weaker. As a result, older grains were not completely reset (Figure 3.37(c)). The *ca.* 1250 Ma grains are interpreted to be detrital in origin, whereas the 780-800 Ma grains may be diagenetic or alternatively may have grown during the Wickham Orogeny. However, there is no structural evidence to support this interpretation, as the earliest deformational event observed in the rocks is attributed to the Tyennan Orogeny ($\boldsymbol{Ca}D_1$).

In the King Island monazites, a strong correlation is evident between Y content and age (Figure 3.49). Furthermore, the low Y levels occur in the garnet-bearing metasediments, that have been shown to have undergone biotite grade lower amphibolite facies metamorphism. Previous workers have shown that monazites growing with garnet are depleted in yttrium (as well as other HREE), due to its favourable site allocation in the structural formula of garnet (Zhu & O'Nions 1999). The Y depletion seen in the metasediments of western King Island is attributed to the equilibrium state of the monazite and garnet in these rocks.

The data presented shows that the earliest deformation observed to occur in the region was only experienced by the metasediments of western King Island. This event, dated using the CHIME technique, occurred at 1273 ± 12 Ma. The age of this event is contemporaneous with the widely developed Grenville Orogeny, and its development on King Island has important implications for the extensiveness of this significant deformational event. Deformation of this age has been reported in

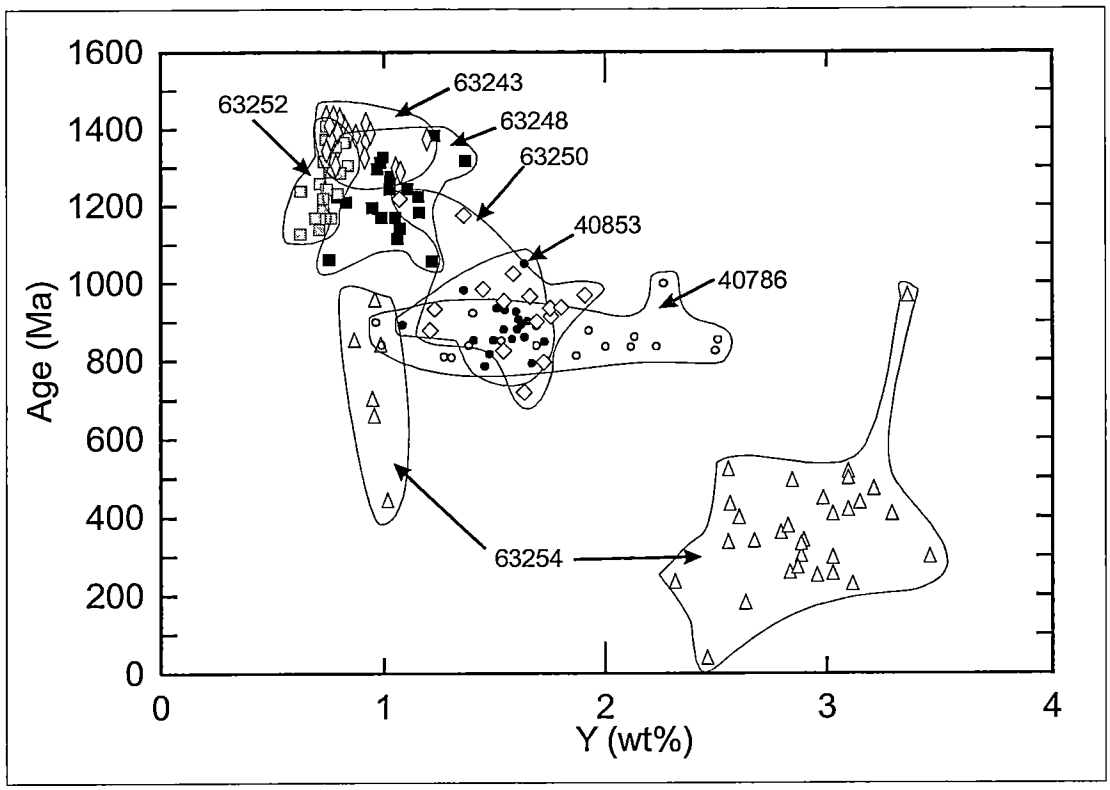

Figure 3.49. Age (Ma) vs Y (wt %) diagram for King Island analyses. The Surprise Bay (63252 and 63243) and Fitzmaurice Bay (63248) samples have similar Y values and ages. Sample 63250 (Stokes Point), has preserved monazites from the regional metamorphism affecting samples 63252 and 63248, as well as having an overprint attributed to contact metamorphism due to an unexposed (probably offshore) granitoid probably related to the Wickham Orogeny. Samples 40853 (Cape Wickham contact aureole) and 40876 (Cape Wickham granitoid) have similar ages, but the chemistry of 40853 is closer to other metasediments, in particular the 63250, possibly reflecting metamorphic conditions as well as bulk rock chemistry. Analyses from 63254 show a large range in age values, due to the multiple reactivation of the mylonite zone, and varying Y levels in the different fluids affecting the metasediments.

western Australia (Albany-Fraser Province), in central Australia (Musgrave Block) and in areas of Antarctica (Windmill Islands and Bunger Hills) (Sheraton *et al.* 1996). Metamorphism of this age on King Island suggests that the deformational event may have been laterally continuous, including these other areas and King Island. In addition, there is now evidence to suggest that King Island may correspond to the poorly exposed, unexplored coastline of Antarctica in the Commonwealth Bay-Adelie Land region, in Gondwana reconstructions (Figure 3.50).

The *ca.* 1270 Ma metamorphic age of King Island has important implications in Rodinia reconstructions. Many previous workers have placed north America adjacent to Australia in the reconstructions of Rodinia, however an accurate match up between the two continents has not been attempted (e.g. Bell & Jefferson 1987, Borg & DePaolo 1994, Brookfield 1993, Dalziel 1991, Hoffman 1991, Idnurm & Giddings 1995, Li *et al.* 1995, Moores 1991, Young 1992).

Burrett & Berry (2000) contributed to the debate over the best fit solution between Australia and Rodinia, suggesting King Island and Tasmania matched up with the Sierra Madre Oriental terrane (in Mexico), which underwent cratonisation between 1100 and 1700 Ma (Figure 3.51). This was based on the interpreted depositional age of King Island and Tasmania, thought to be between 1100 and 1500 Ma. The metamorphic age of western King Island discussed here refines this argument, and provides strength to the correlation between King Island/Tasmania and the Sierra Madre Oriental terrane, thus supporting the AUSWUS reconstruction (Figure 3.51).

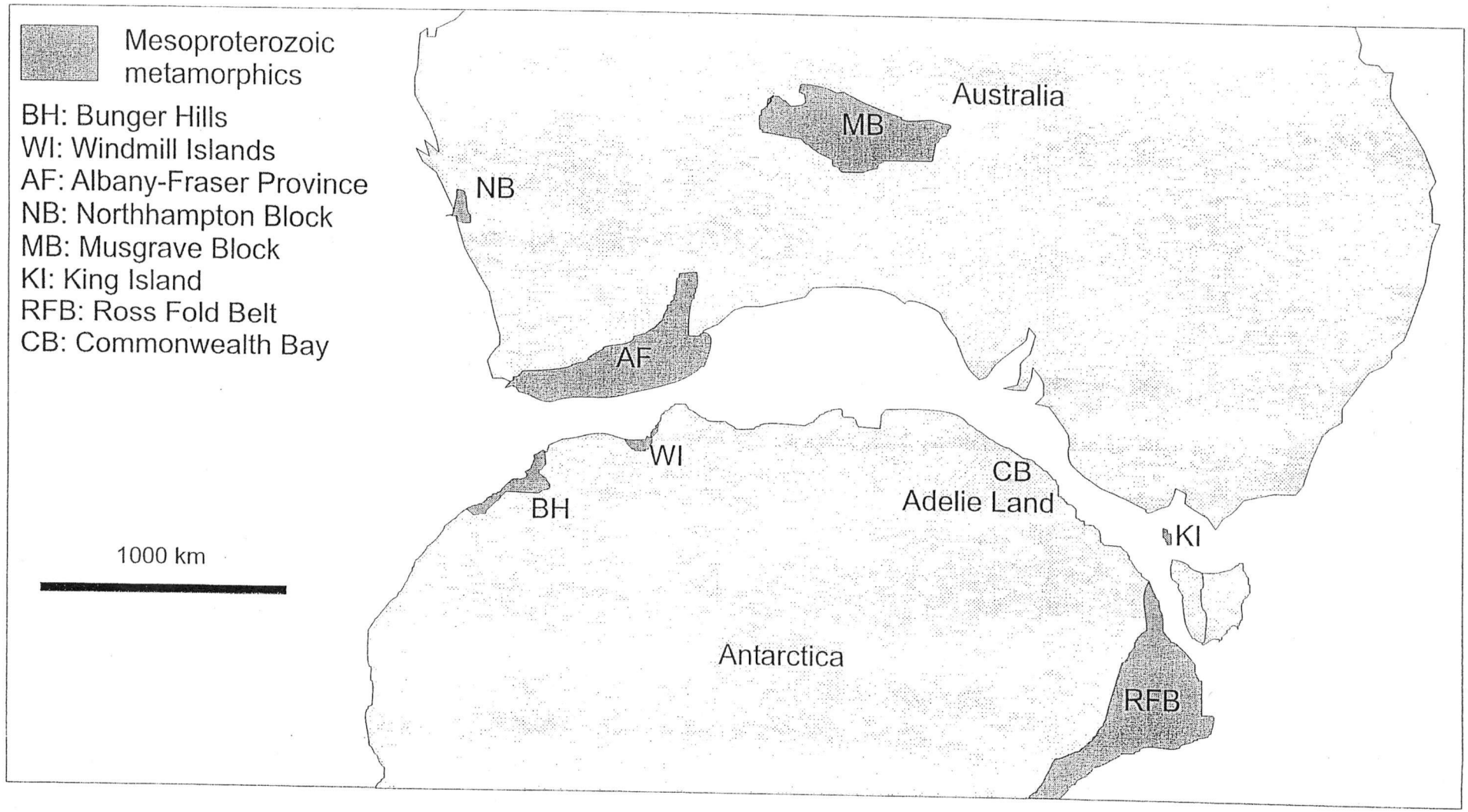

Figure 3.50. Reconstruction of Australia and Antarctica showing their relative positions at 160 Ma, prior to the break-up of Gondwana (from Sheraton et al. 1996). The diagram shows Mesoproterozoic age metamorphic terranes

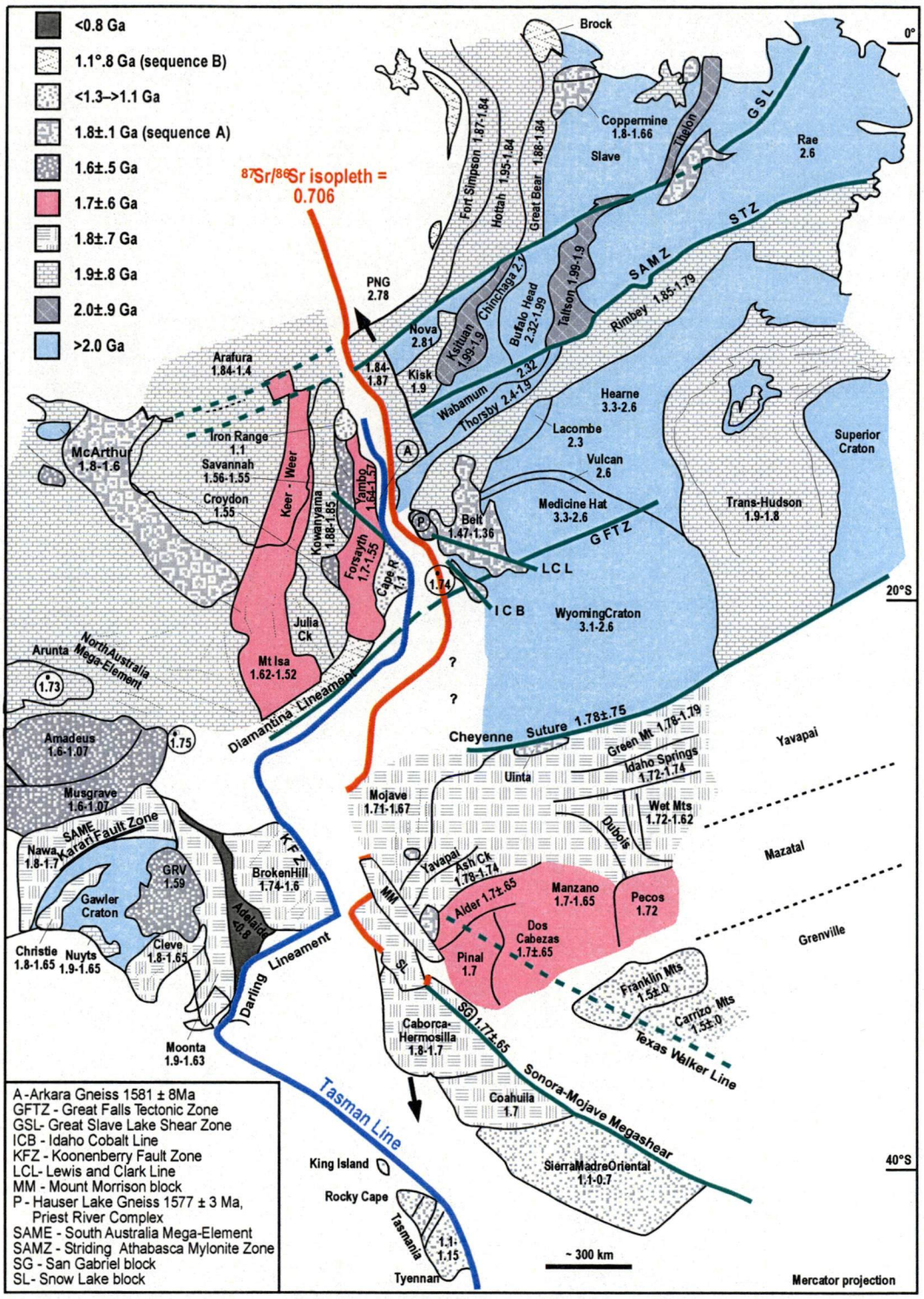

Figure 3.51. Best fit solution of Laurentia against Australia (Australia-Western U.S (AUSWUS)) (from Burrett & Berry 2000). Laurentia rotated to Australia in present coordinates about Euler pole at 50.5°N,111.6°E, Rotation = 111.6°.Terranes, ages and lineaments are based on numerous sources (mainly Bain & Draper, 1997; Condie, 1992; Doughty *et al.*, 1998; Hoffman, 1988; Reed *et al.*, 1993; Ross, 1991; Shaw *et al.*, 1996). Light dashes indicate main structural trends. Colors are chosen to depict dominant cratonization age or, for epicratonic sequences and Tasmania, major age range of deposition. (dates in Ga.). Sequence A = epicratonic sedimentary sequences between 1.8 and 1.1 Ga, sequence B = epicratonic sedimentary sequences between Ga and 800 Ma (Young, 1992). Black arrows indicate possible source areas for detrital zircons: Papua New Guinea (PNG) 2.78 Ga zircons (Baldwin & Ireland, 1995) sourced from Nova domain, Canada (2.81 Ga) and Tasmanian zircons (Black *et al.*, 1997) sourced from southern Laurentian terranes. Belt-Purcell basin zircons (Ross *et al.*, 1992) were possibly derived from northern Queensland terranes (Blewett *et al.*, 1998). Numbers in circles are granite intrusion dates from central Australia.

3.8 Summary of metamorphism

Within the Arthur Lineament, the mineral assemblages in the "eastern" Ahrberg Group, Bowry Formation and AGC provide evidence of two main metamorphic events. However the second event ($\boldsymbol{Ca}D_2$) can be subdivided into two stages. The $\boldsymbol{Ca}D_2$ event is extensively developed in comparison to the first ($\boldsymbol{Ca}D_1$), and pervasively overprints it. The events are separated on the basis of microstructural evidence, and mineral chemistry.

The $\boldsymbol{Ca}D_1$ event, where evident, was a high pressure, low temperature event. Temperatures are interpreted to have been in the vicinity of 400-450°C. The absence of lawsonite and garnet, and presence of glaucophane and epidote indicates $\boldsymbol{Ca}D_1$ metamorphism was in the higher grade blueschist facies, with pressures ranging between 700 and 1000 MPa (Bucher & Frey 1994). This event was characterised by moderate to high strain levels, resulting in a structural foliation ($\boldsymbol{Ca}S_1$) that did not penetrate igneous rocks. In contrast, the glaucophane is best preserved in these more competent, igneous rocktypes.

In different parts of the lineament, early $\boldsymbol{Ca}D_2$ varied in its intensity and metamorphic grade. In some parts of the "eastern" Ahrberg Group, metamorphic conditions reached upper greenschist facies, whereas in other areas, in the boundary zone between the Bowry Formation and the AGC, maximum metamorphic conditions reached the greenschist-amphibolite facies transition, based on the mineral assemblages present, and pressure-temperature estimates from THERMOCALC (Bucher & Frey 1994, Powell & Holland 1998, 2000). In the "eastern" Ahrberg Group, during the early $\boldsymbol{Ca}D_2$ event, the absence of garnet indicates the metamorphic grade did not reach the garnet stability field, and probably experienced temperatures of 400-450°C and pressures of around 500 MPa. In the AGC however, metamorphism during early $\boldsymbol{Ca}D_2$ reached the garnet stability field, and temperatures were approximately 460 ± 40°C. The moderately low spessartine content of the garnets indicates their growth is not attributed to high levels of Mn in the rocks. The presence of albite + garnet + chlorite + epidote + hornblende indicates that conditions did not reach amphibolite facies. The minimal anorthite component in feldspars indicates maximum temperatures did not exceed 500°C.

Pressures were in the order of 600-700 MPa. The Bowry Formation is interpreted to have experienced similar conditions to the AGC in the early ***Ca***D_2 event, as is indicated by mineralogical similarities (garnet and amphibole). During the event, pressures of 620 ± 180 MPa and temperatures of 490 ± 36°C prevailed.

Late ***Ca***D_2 was a more uniform metamorphic event. It produced a pervasive structural foliation (***Ca***S_2), and associated greenschist facies metamorphism, across the Arthur Lineament, as is shown by the widespread assemblage of actinolite + albite + chlorite +epidote + quartz in the mafic rocks. The absence of pumpellyite indicates that conditions were above sub-greenschist facies, with temperatures of approximately 350-400°C, and pressures of 300-400 MPa (Bucher & Frey 1994, Powell & Holland 1998, 2000). The strong alignment of minerals such as chlorite and actinolite with the ***Ca***S_2 foliation demonstrates the high strain that prevailed during the late ***Ca***D_2 event. In the "western" Ahrberg Group, the presence of actinolite + albite + epidote + chlorite + quartz in the metabasites indicates peak metamorphism was at lower greenschist facies. Microstructural evidence suggests this assemblage is attributed to the ***Ca***D_2 event. The common late ***Ca***D_2 assemblage and metamorphic grade in all the units of the lineament suggest that at this stage, the present 'stack' of tectonstratigraphic units had been assembled, whereas during the ***Ca***D_1 and early ***Ca***D_2 events, the various blocks were under different, metamorphic conditions, and were separate of each other.

CHAPTER 4

GEOCHEMISTRY AND TECTONIC SETTINGS OF MAFIC IGNEOUS ROCKS IN THE ARTHUR LINEAMENT AND SURROUNDING AREA

4.1 Introduction

The mafic igneous and meta-igneous lithologies within the Arthur Lineament and surrounding area of the Rocky Cape block are distributed in several main lithostratigraphic units. These are the parautochthonous "eastern" and "western" Ahrberg Groups, the Togari Group, and the Success Creek Group-Crimson Creek Formation. Several other Neoproterozoic mafic igneous series are also present, including the Rocky Cape dyke swarm, Cooee Dolerite, Montana Melaphyre and Sulphur Creek basalts (Figure 4.1).

4.1.1 The Bowry Formation

To the east of the Paradise psammite is the fault-bounded Bowry Formation, which consists of mafic schists, amphibolite, metagabbro, massive and laminated magnetite, and minor deformed granitoid. The Bowry Formation is considered to be allochthonous due to its notably different metamorphic grade, and the presence of the ~780 Ma granitoid. To the east of the Bowry Formation is the Reece psammopelite, which is interpreted to be a correlate of the metasediments within the "eastern" Ahrberg Group. This psammopelite-dominated unit contains minor amphibolites, and metagabbros (discussed herein as the Reece amphibolite and Reece gabbro). The unit is fault-bounded by the deformed Oonah Formation to its east. Included within the Bowry Formation are massive and banded magnetite and minor deformed granitoids.

4.1.2 The "eastern" Ahrberg Group

The parautochthonous "eastern" Ahrberg Group comprises the majority of the Arthur Lineament, and outcrops at several localities in the southern Arthur Lineament. It is exposed to the east and northeast of Corinna, and on the west coast, north of

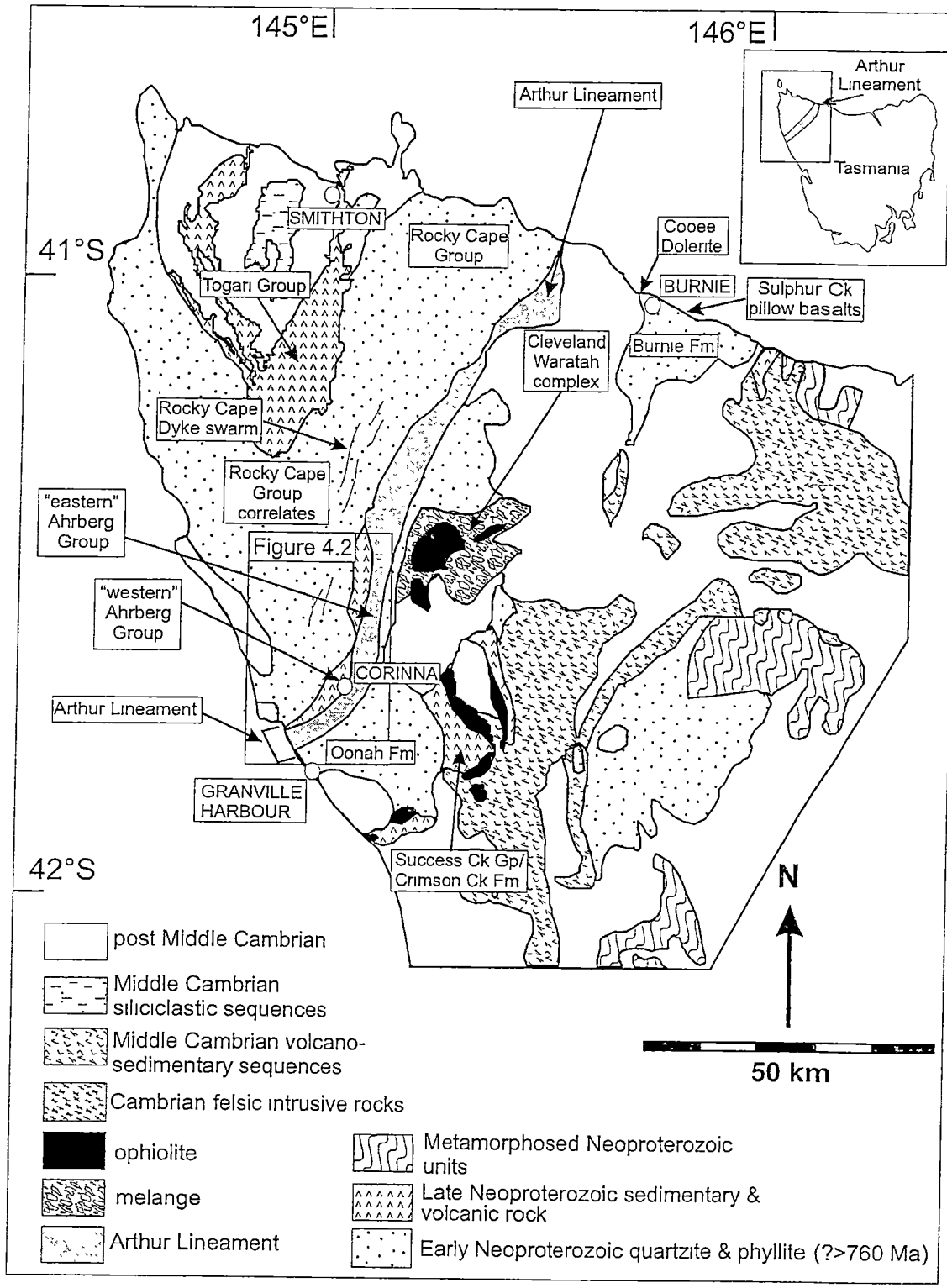

Figure 4.1. Setting of the Arthur Lineament, NW Tasmania (modified after Brown *et al.* 1995). The Arthur Lineament consists of the high strain (metamorphosed) Burnie and Oonah Formations, the "eastern" Ahrberg Group, the Bowry Formation, and other uncorrelated fault bounded units.

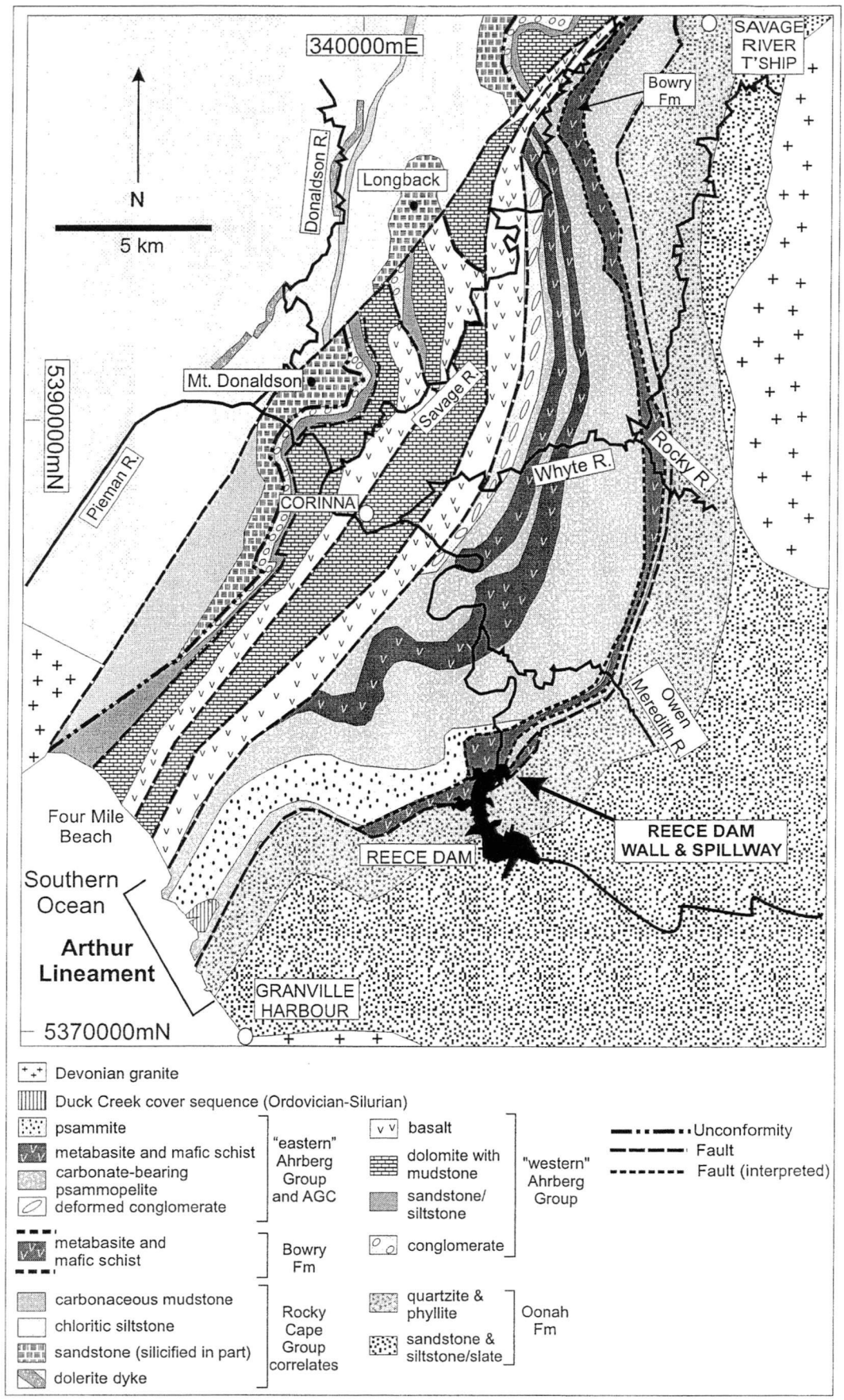

Figure 4.2. Simplified geology of the southern Arthur Lineament (from Turner *et al.* 1991).

Granville Harbour (Figure 4.2). In the Corinna area, the basal unit of the parautochthonous "eastern" Ahrberg Group is a metasedimentary unit, consisting of a deformed quartzite clast-dominated conglomerate, overlain by psammitic and psammopelitic schists. These metasediments are, inturn, overlain by the lowermost amphibolite-dominated unit, the Nancy Formation. A metasedimentary package (the Frenchman psammopelite) consisting of carbonate-bearing psammopelite and minor amphibolites (discussed herein as the Frenchman amphibolite) separates the Nancy Formation from the Lucy Formation, which is the upper amphibolite-dominated unit. Above the Lucy Formation, within the "eastern" Ahrberg Group sequence, is the metasediment-dominated Paradise psammite, which is predominantly carbonate-bearing psammite, but contains minor amphibolite bodies (discussed herein as the Paradise amphibolite).

Outcropping on the west coast, north of Granville Harbour, an extensive across-strike sequence of the "eastern" Ahrberg Group is exposed, although its contact with the "eastern" Ahrberg Group to the east of Corinna does not crop out. The sequence is mostly metasedimentary, with strongly deformed psammites and psammopelites dominant. However, several thin amphibolite-dominated packages are intercalated within the metasediments. The lowermost amphibolite sequence on the west coast is informally named here as the Hoyle amphibolite. To the south of the Hoyle amphibolite, and interpreted to be stratigraphically higher within the "eastern" Ahrberg Group, is the informally named Farm Track amphibolite. This outcrops to the south of the unconformably overlying, Ordovician to Silurian Duck Creek cover sequence. To the southeast, at Gourlays Creek, close to the boundary with the Oonah Formation, several amphibolite bodies occur (Norris 1985), informally named here as the Gourlays Creek amphibolite.

The meta-igneous rocks within the "eastern" Ahrberg Group are interpreted to have been magmatically emplaced into the host sediments, as sills and dykes. Whereas the depositional age of the "eastern" Ahrberg Group is uncertain, the age of the main deformation affecting the "eastern" Ahrberg Group has been directly dated at 510 ± 10 Ma (Turner 1993).

4.1.3 The "western" Ahrberg Group

The "western" Ahrberg Group, which lies to the southwest of the "eastern" Ahrberg Group, consists of two moderately deformed mafic meta-igneous-dominated units, the Bernafai and Tunnelrace Volcanics (Figure 4.2). These units include intercalated mafic meta-igneous rocks and chloritic metasediments (Crawford 1992, Turner and Crawford 1993) and are interlayered with siliciclastic and carbonate-rich meta-sedimentary units. The Tunnelrace Volcanics is the uppermost unit of the Ahrberg Group and is faulted against the "eastern" Ahrberg Group to its east. Due to its proximity to the fault zone, it is more strongly deformed than the Bernafai Volcanics, and commonly shows phyllitic textures. The age of the Ahrberg Group is uncertain, although based on regional correlations (see below) Calver (1998) proposed that it was deposited between 650-580 Ma. At the western margin of the Ahrberg Group, a low angle unconformity separates it from the older, underlying siliciclastic Mesoproterozoic Rocky Cape Group (Figure 4.2). The Rocky Cape Group is intruded by an extensive series of northeast-trending dolerite dykes, the Rocky Cape dyke swarm, (Crawford & Berry 1992), which have given a K-Ar age of approximately 600 Ma (Adams *et al.* 1985).

4.1.4 Igneous rocks within the Burnie and Oonah Formations

To the east of the Arthur Lineament, both extrusive (Montana Melaphyre and Sulphur Creek pillow basalts) and intrusive (Cooee Dolerite) mafic igneous rocks occur within the mid-Neoproterozoic turbiditic Burnie and Oonah Formations, and in their strongly deformed equivalents. Some of these (the Cooee Dolerite) have been intruded into wet sediment (Crook 1979). In contrast to the majority of the mafic lithologies in northwest Tasmania, these intraplate rocks have alkaline affinities (Crawford & Berry 1992). The Cooee Dolerite intrudes the Burnie Formation at Cooee and has a revised K-Ar age of 725 ± 35 Ma. This is interpreted to represent the approximate depositional age of the sediments (Crook 1979).

4.1.5 The Togari Group and Success Creek Group-Crimson Creek Formation

To the northwest of the Arthur Lineament and Ahrberg Group lies the Neoproterozoic Togari Group (Figure 4.1). This sequence, like the Ahrberg Group,

unconformably overlies the Rocky Cape Group at low angle (Brown 1989). The lower Togari Group consists of the Kanunnah Subgroup, which includes quartzite, conglomerate and carbonate (Black River Dolomite), overlain by mafic volcanics. The Black River Dolomite was deposited between 750-650 Ma, whereas the Kanunnah Subgroup was deposited between 650-580 Ma (Calver 1998).

The Success Creek Group-Crimson Creek Formation crops out to the east of the Arthur Lineament in the south and consists of siliciclastics overlain by basaltic lavas and volcaniclastics. Brown (1986) reported that in the middle Pieman River, the basal rocks of the Success Creek Group unconformably overlie the Oonah Formation, although this exposure is no longer accessible due to the flooding of the Pieman River by the Hydro Electricity Commission of Tasmania. All other known exposures of the contact are faulted (ref).

4.1.6 Aims and methodology

The aim of this study is to further define the magmatic affinities and correlations of the mafic igneous rocks in the study area, and hence determine the tectonic setting during their emplacement. To achieve this a geochemical approach has been used. The samples analysed were collected from the different units within the "eastern" and "western" Ahrberg Group, and compared with the existing database of Neoproterozoic mafic igneous rocks in western and northwestern Tasmania (Brown 1986, Crawford & Berry 1992, Turner & Crawford 1993, Turner & Botrill 1993). Crawford (1992) has shown that the tectonic setting of northwestern Tasmania in the Neoproterozoic was transitional from a pre-rifting, intraplate setting to a mature rift setting. This study further develops the work of Crawford (1992), by incorporating the geochemical study of the "eastern" and "western" Ahrberg Groups with their structural and metamorphic history, thereby enabling a better understanding of the spatial distribution of the lithologies and their tectonic setting prior to the Cambrian deformation.

4.2 Mafic meta-igneous rocks of the "eastern" Ahrberg Group

Eighteen representative samples of the "eastern" Ahrberg Group, and thirteen from the Bowry Formation have been analysed for major and some trace elements by XRF

spectrometry (see Chapter 1 for analytical specifications). Another sixteen samples from different units of the "eastern" Ahrberg Group and seventeen from the Bowry Formation have been analysed by previous workers (Norris 1985, Wilson 1991, Turner & Botrill 1992, Turner & Crawford 1993). As the Bowry Formation is considered to be allochthonous based on its notably different metamorphic history (Chapter 3), the geochemistry of the meta-igneous rocks in the Bowry Formation is discussed separately (Section 4.3).

The "eastern" Ahrberg Group samples analysed by previous workers lie on the same magmatic trend as those analysed in this study, and are thus believed to constitute a compositionally coherent suite. The identical geochemical affinities of the "eastern" Ahrberg Group samples from the different workers are illustrated in the TiO_2 vs Zr diagram (Figure 4.3).

4.2.1 Occurrence and petrography

The "eastern" Ahrberg Group occurs as a northeast-trending belt (Figure 4.1) of interlayered meta-volcanic and metasedimentary rocks and constitutes the majority of the Arthur Lineament. The samples analysed are all from the southern part of the lineament. The "eastern" Ahrberg Group is structurally complex, and strongly deformed throughout, with schistose textures. The contact relationships between the "eastern" Ahrberg Group and the Ahrberg Group in the west and the Oonah Formation in the east are interpreted to be faults.

Despite primary igneous textures being uncommon due to the regional metamorphism experienced by the amphibolites, the samples are interpreted to be igneous in origin. This is based on several lines of evidence. In the field, the mafic bodies are discontinuous and have contrasting textures to the surrounding metasediments. Although the metasediments are uniformly well foliated, with schistose textures, the mafic units have a variably developed foliation. The intensity of foliation is dependent on the position relative to the margin of the meta-igneous body. Samples from within 1 m of the margin are strongly foliated, whereas samples from greater than 1 m from the margin are weakly foliated to unfoliated. The meta-igneous bodies are commonly boudinaged due to a competency contrast with the

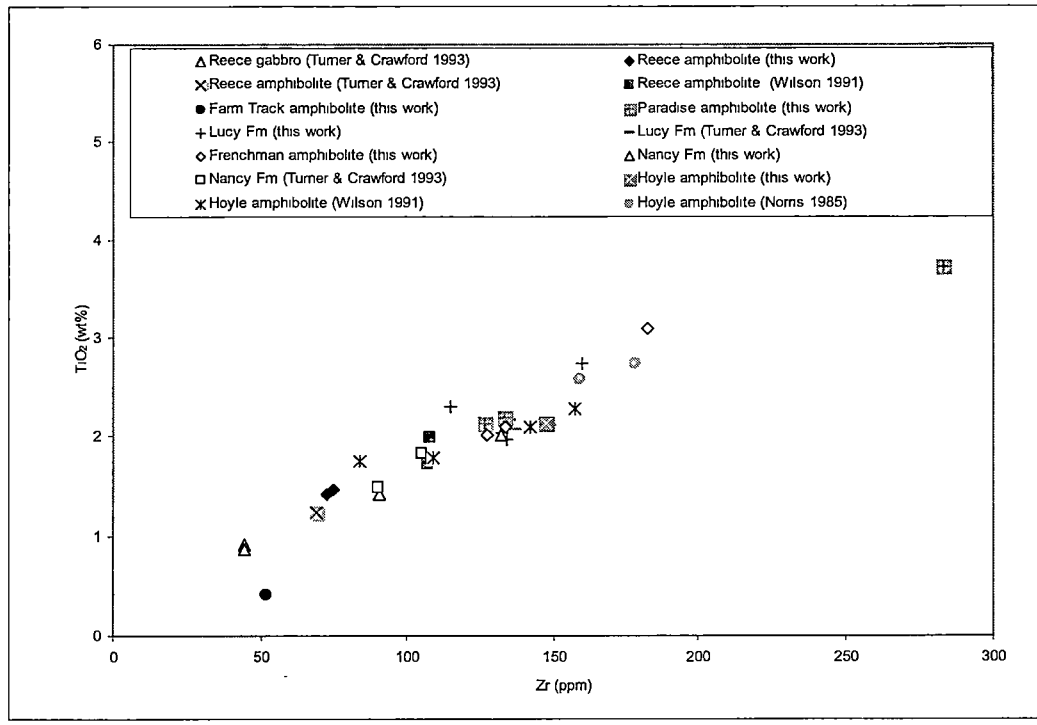

Figure 4.3. TiO_2 vs Zr variation diagram, showing analyses of mafic meta-igneous rocks from the "eastern" Ahrberg Group, from different workers. All samples analysed are interpreted to be igneous in origin. Symbols used in this diagram represent the different authors.

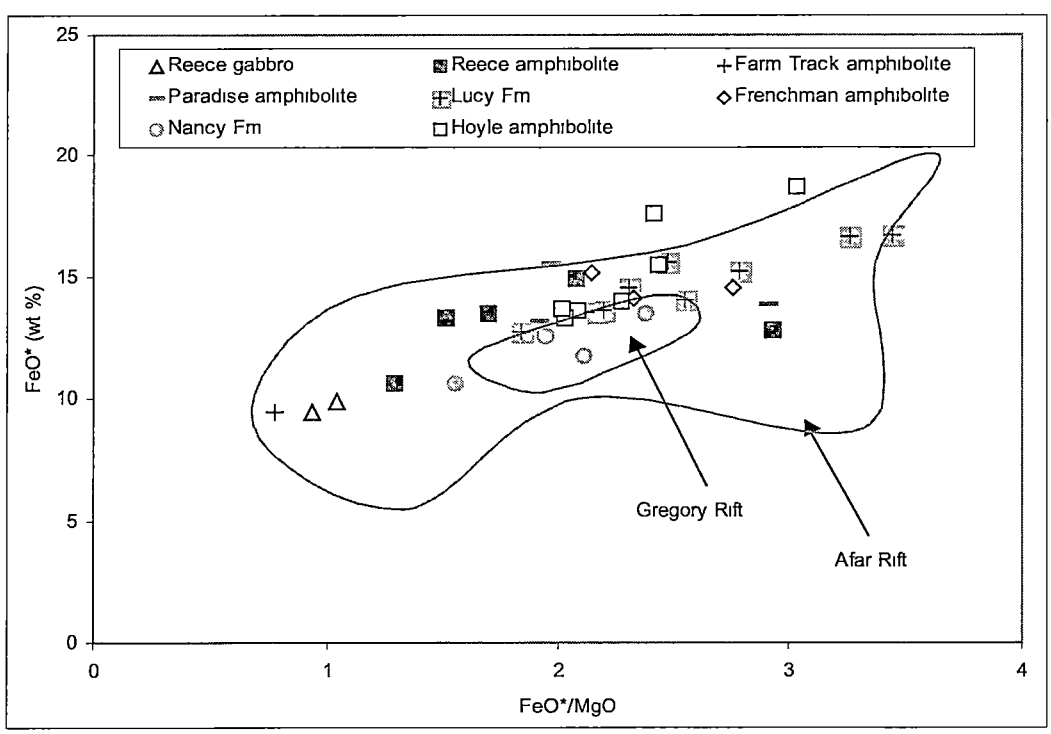

Figure 4 4(a). FeO*/MgO vs FeO* variation diagram after Miyashiro & Shido (1975). Compositional fields are also shown for representative lava suites from the Gregory Rift (12 samples) (Baker *et al.* 1977) and Afar Rift (48 samples) (Deniel *et al.* 1994) in eastern Africa Reece amphibolite: samples RRDDH1-65.5, RRDDH1-40.65, RRDDH1-36.4; Farm Track amphibolite: sample OH919; Paradise amphibolite: OH 72, OH41, OH 8; Lucy Fm: samples OH606B, OH705, OH723, OH613, OH612, OH605; Frenchman amphibolite: samples OH619B, OH951, OH944; Nancy Fm: samples OH739, OH733; Hoyle amphibolite· sample OH886B

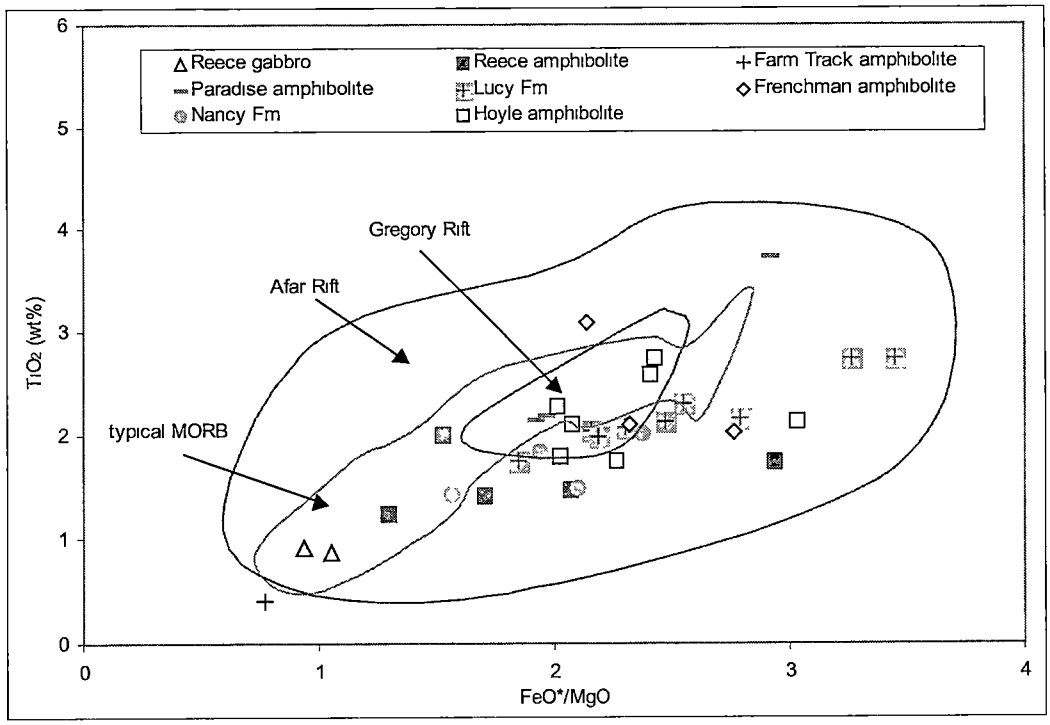

Figure 4.4(b). FeO*/MgO vs TiO_2 variation diagram after Miyashiro & Shido (1975). Compositional fields are also shown for representative lava suites from the Gregory (Baker *et al.* 1977) and Afar (Deniel *et al.* 1994) Rifts in eastern Africa. The typical MORB field (271 samples) is derived from Pacific, Southern and Indian Oceans (Danyushevsky 2001, *pers. comm.*)

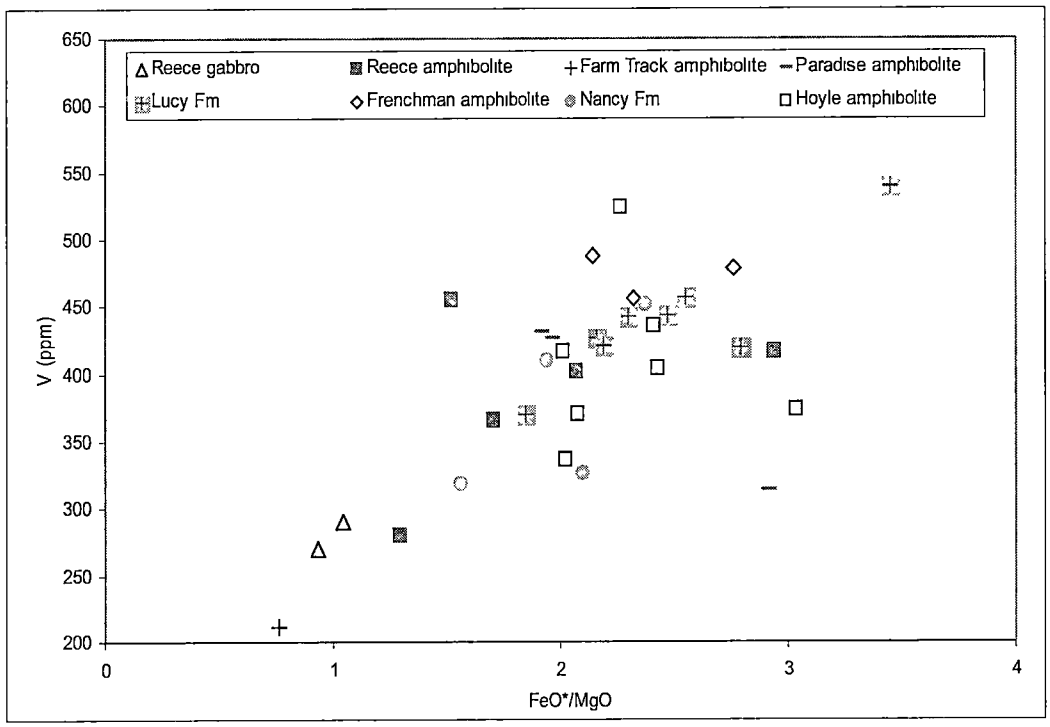

Figure 4.4(c). FeO*/MgO vs V variation diagram for "eastern" Ahrberg Group metabasalts after Miyashiro & Shido (1975).

surrounding metasediments. The mafic mineralogy and whole rock geochemistry of the samples further supports the igneous interpretation of these samples.

4.2.2 Alteration affects and element mobility

Petrographic studies indicate that the rocks of the "eastern" Ahrberg Group have undergone upper greenschist facies metamorphism (Chapter 3). Previous workers have emphasised the importance of using immobile major elements (Fe, Mg), REE and some high field strength elements (Ti, Zr, Y, Nb) as opposed to those considered to be mobile (alkalis, Ca and related trace elements such as Ba, Rb, Sr) in the classification of metamorphosed and altered mafic igneous rocks (Floyd & Winchester 1978, Pearce 1983, Rollinson 1993). Further to this, some transition metals (Sc, Ni, V, and Cr) are also considered to be immobile and thus useful in the discrimination of altered rocks (Rollinson 1993). On this basis, only immobile elements have been considered in the classification of the meta-igneous rocks in the study area.

4.2.3 Geochemical affinities and tectonic setting

The major element chemistry of the thirty one analysed samples from the "eastern" Ahrberg Group indicates that they are mostly basaltic in composition (Table 4.1). This is indicated by relatively high FeO* (total iron as FeO) (9.4-18.7 %) and MgO (4.4-12.3 %) abundances. Despite the potential mobility of SiO_2 due to the regional metamorphism experienced by the "eastern" Ahrberg Group, the analysed samples are mostly within the range of basalts (47.2-51.9 %), although several samples have values of basaltic andesites (52.2-56.9 %). The majority of samples are further characterised by moderate to high levels of TiO_2 (1.2-3.7 %), although several have notably low concentrations (0.4-0.9 %). All samples have moderate to high levels of V (212-540 ppm).

In order to illustrate the geochemical affinities of the amphibolites of the "eastern" Ahrberg Group, and to aid in the interpretation of the tectonic environment in which the basalt protoliths formed, the fields for modern day tectonic settings (emerging rifts and MORB) have been plotted. Geochemical examples of basalts from the east African rift system (Gregory and Afar Rifts), and MORB (Pacific, Southern and

Indian Oceans) have been included (Baker *et al.* 1977, Deniel *et al.* 1994, Danyushevsky 2001 *pers. comm.*).

The "eastern" Ahrberg Group samples have been plotted on a series of binary diagrams of various immobile elements against the fractionation index FeO*/MgO (Figures 4.4(a) to (c). The "eastern" Ahrberg Group shows an increase in FeO*, TiO_2, and V with increasing FeO*/MgO. The trend has a positive slope and does not pass a maximum point, indicating the suite had not commenced significant fractional crystallisation of titanomagnetite (Miyashiro and Shido 1975). This is consistent with fractionation of a tholeiitic magma under relatively low oxygen fugacity conditions, where Fe and Ti remain in the magma due to the delayed crystallisation of titanomagnetite. This notable Fe-enrichment excludes the possibility that the samples have calc-alkaline affinities. When plotted on the P_20_5 vs Zr discrimination diagram, the samples are shown to be predominantly tholeiitic, although several samples plot in the alkali basalt field close to the boundary (DOM 894846, DOM 895860, DOM 894852, OH72) (Figure 4.5). The alkali basalt affinity of OH72 is confirmed when plotted on the Ti/1000 vs V discrimination diagram, where it lies within the alkali basalt field with a Ti/V value of 70 (Figure 4.6). In contrast, the majority of the "eastern" Ahrberg Group has Ti/V values of 20 to 35, consistent with those of continental flood basalts (CFB), mid ocean ridge basalts (MORB) and back arc basin basalts (BABB) (Figure 4.6) (Shervais (1982)).

Moderate to high TiO_2 concentrations within the "eastern" Ahrberg Group, together with the moderate Zr levels indicates the analysed samples do not have island arc tholeiite (IAT) affinities. The absence of volcanically-derived fragmentals supports this interpretation. Samples OH919, 69101 and DOM 910532 have anomalously low Ti, Zr and V values, although they lie close to the trend of the other "eastern" Ahrberg Group analyses in the Ti vs Zr discrimination diagram (Figure 4.7). On this basis, they are interpreted to form part of the "eastern" Ahrberg Group fractionation series, and may represent more gabbroic or mafic cumulate compositions.

Oceanic-island basalts (OIB) may have either alkaline or tholeiitic affinities (Wilson 1989). It has been shown that the mafic meta-igneous rocks of the "eastern" Ahrberg Group have tholeiitic affinities, and therefore on the basis of major element

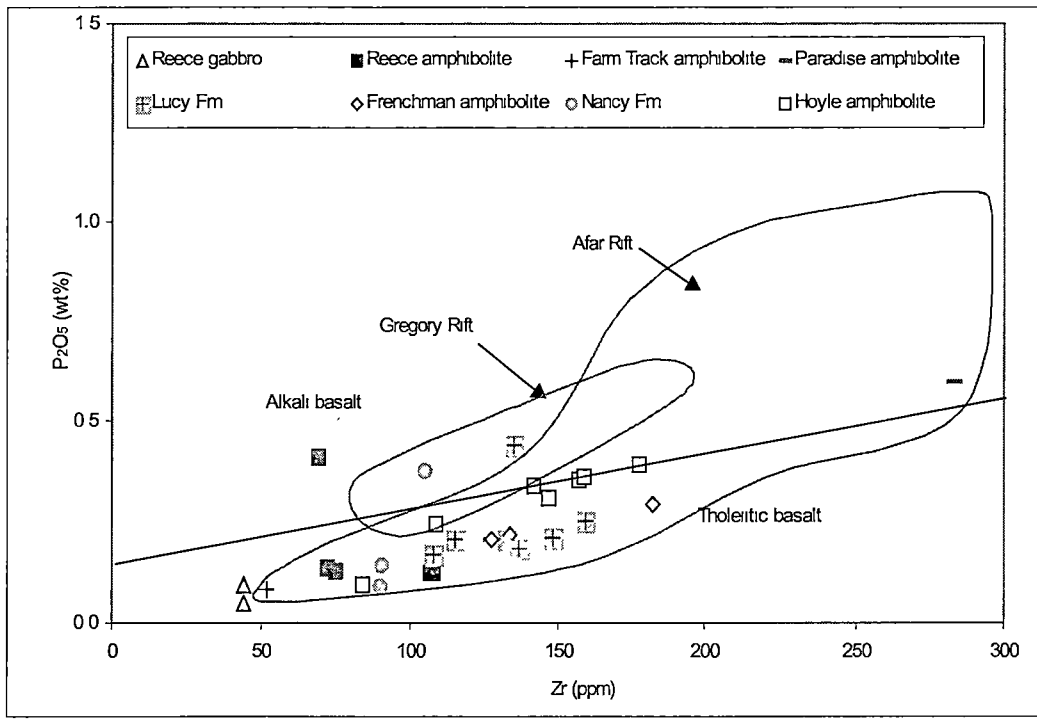

Figure 4.5. P_2O_5 vs Zr discrimination diagram after Winchester & Floyd (1976). Compositional fields are also shown for representative lava suites from the Gregory (Baker *et al.* 1977) and Afar (Deniel *et al.* 1994) Rifts in eastern Africa.

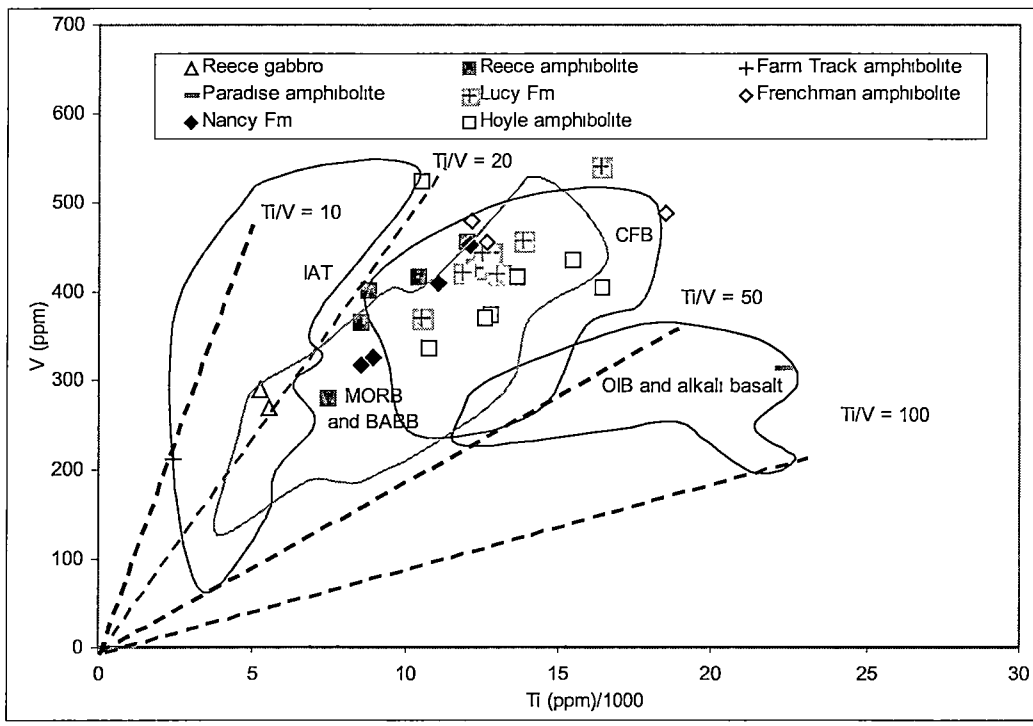

Figure 4.6. Ti/1000 vs V discrimination diagram after Shervais (1982). The majority of the "eastern" Ahrberg Group samples have Ti/V values of 20-35. Sample OHH72 (Paradise amphibolite) has an elevated Ti/V value of 70, reflecting alkali basalt affinities

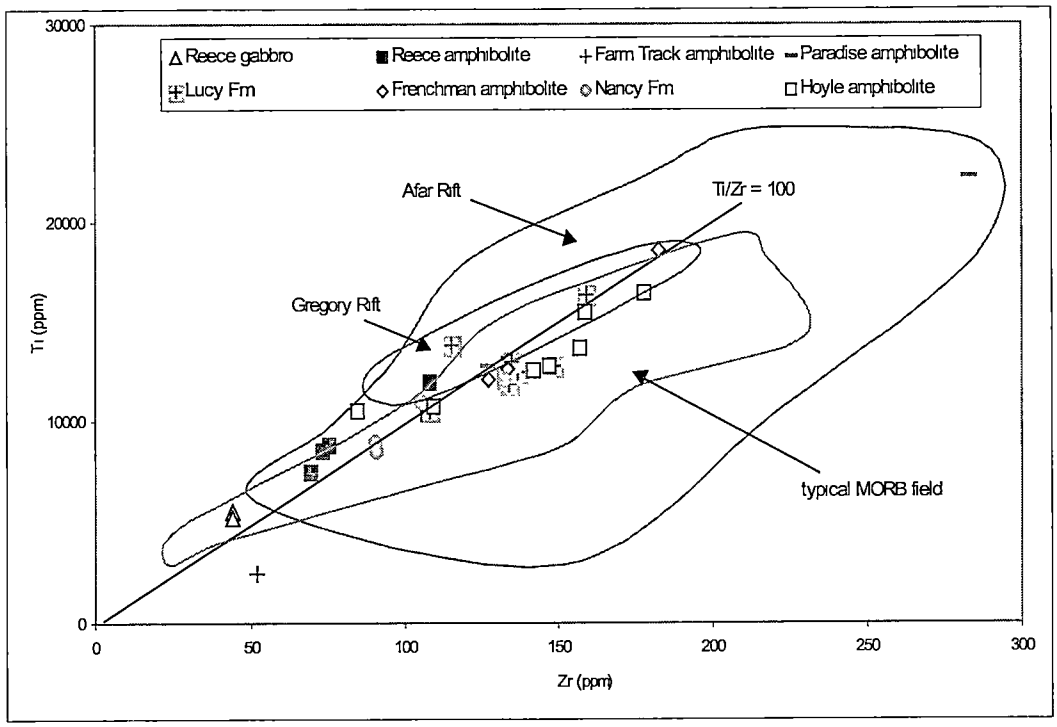

Figure 4.7. Ti vs Zr variation diagram after Pearce & Cann (1973). The Paradise amphibolite (OHH72) displays elevated Zr levels as well as elevated Ti. Compositional fields are also shown for representative lava suites from the Gregory (Baker *et al.* 1977) and Afar (Deniel *et al.* 1994) Rifts in eastern Africa, and the typical MORB field (Danyushevsky 2001, *pers. comm.*)

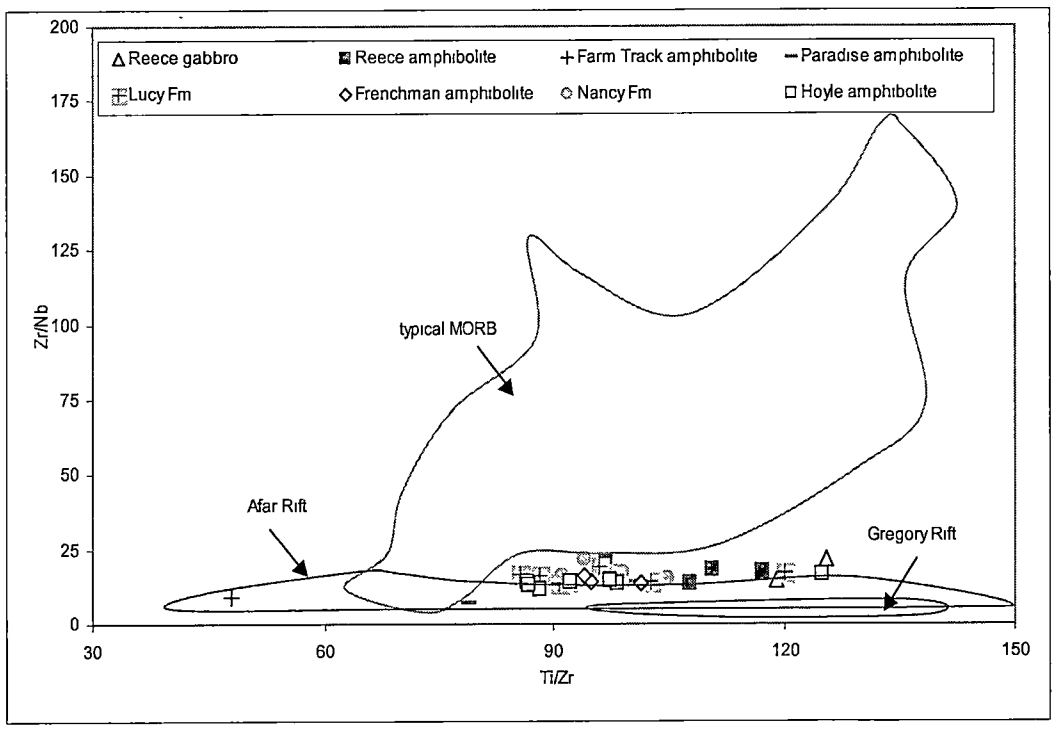

Figure 4.8. Ti/Zr vs Zr/Nb variation diagram. The "eastern" Ahrberg Group amphibolites have Zr/Nb values predominantly in the range of 12-22, outside the range for basalts with OIB affinities (<10). Compositional fields are also shown for representative lava suites from the Gregory (Baker *et al.* 1977) and Afar (Deniel *et al.* 1994) Rifts in eastern Africa, and the typical MORB field (Danyushevsky 2001, *pers. comm.*)

geochemistry alone, the possibility that they were extruded in an oceanic-island setting cannot be excluded. However, tholeiitic OIB have lower Zr/Nb values (<10) than MORB (Wilson 1989), therefore, as illustrated in the Zr/Nb vs Ti/Zr discrimination diagram (Figure 4.8), the "eastern" Ahrberg Group (with Zr/Nbvalues predominantly within the range of 11.8-22.0) do not have OIB affinities. The highly variable Nb abundances (2-39 ppm) increase with increasing fractionation. Further to this, the lithological associations within the "eastern" Ahrberg Group (carbonates, deformed conglomerates, abundant quartz-rich psammitic and psammopelitic metasediments) are not consistent with basalts erupted in an OIB setting.

Shervais (1982) noted that basaltic rocks with BABB and MORB affinities have overlapping fields on the Ti vs V discrimination diagram and hence are not distinguishable on this basis (Figure 4.6). Although the range of Zr/Nb values for BABB is large, and overlaps with the MORB field (as low as 10 for the most enriched E-MORB, to as high as 60 for the most depleted N-MORB), basalts with BABB affinities typically have Zr/Nb > 20. However distinguishing basalt affinities on this basis alone is not possible (Wilson 1989). Basalts from subduction-related settings are known to have consistently lower absolute abundances of Ti, Zr, Y and Nb relative to N-MORB (Rollinson 1993). On a N-MORB normalised element variation diagram (Figure 4.9) the "eastern" Ahrberg Group amphibolites display slightly elevated HFSE (high field strength element) levels relative to N-MORB. In addition to this, field relationships indicate that the autochthonous Ahrberg Group, to the west, rests unconformably upon stable margin, shallow marine siliciclastics. On this basis, an emerging rift is preferred. Notably the Reece gabbro (69101) is depleted in HFSE relative to N-MORB, possibly suggesting a cumulate composition.

The tectonic setting of eruption of the "eastern" Ahrberg Group can be further refined using incompatible element ratios. Zr/Nb values reflect primary magma compositions, and are unaffected by fractionation or alteration (Crawford 1992). In modern tholeiitic basalts increasing ratios represent a transition from E-MORB rift tholeiites (Zr/Nb = 10-~25) towards N-MORB (Zr/Nb = ≥30) (Crawford 1992). The range of Zr/Nb values (13.7-22.0) of the units within the "eastern" Ahrberg Group indicate E-MORB affinities. Sample OH919 has a notably low Zr/Nb ratio, as does

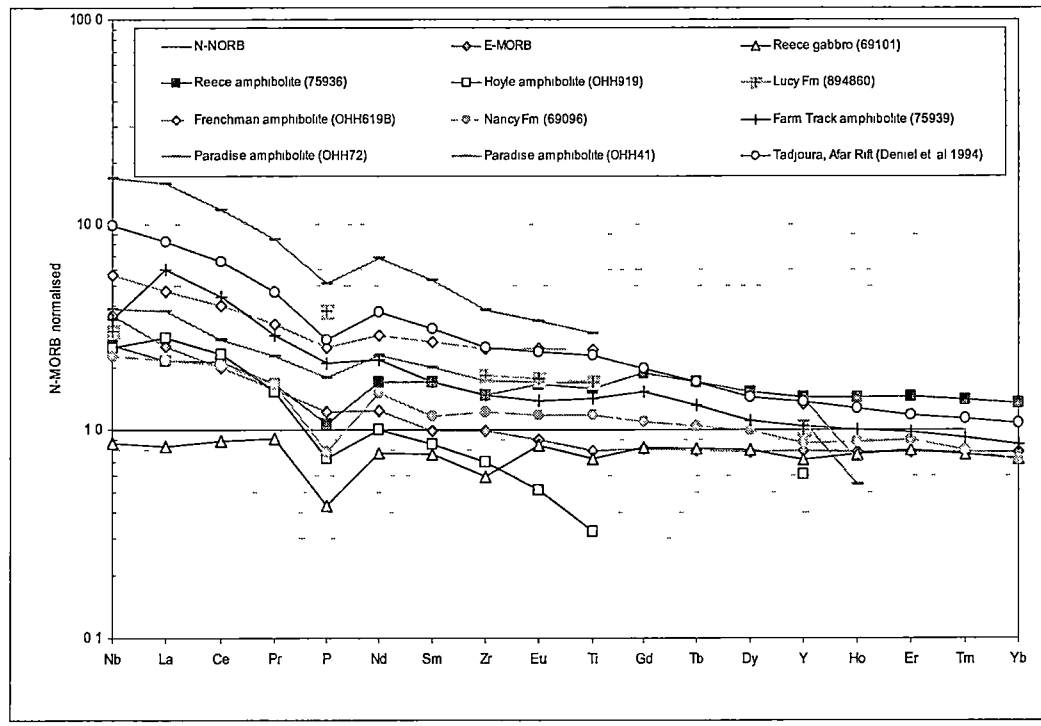

Figure 4.9. N-MORB normalised rare earth element variation diagram, showing abundances for representative analyses from the "eastern" Ahrberg Group mafic igneous lithologies Most samples show slightly elevated HFSE relative to MORB, with similar trends (but higher values) to typical E-MORB. The Paradise amphibolite sample (OHH72) has notably enriched LILE, indicative of more alkaline affinities. Values for Tb, Ho and Em are interpolated. For samples OHH919, OHH619B, OHH72 and OHH41 values for Pr, Sm and Eu are interpolated. For sample 894860 Eu is interpolated. (Normalising values and E-MORB values are from Sun & McDonough 1989).

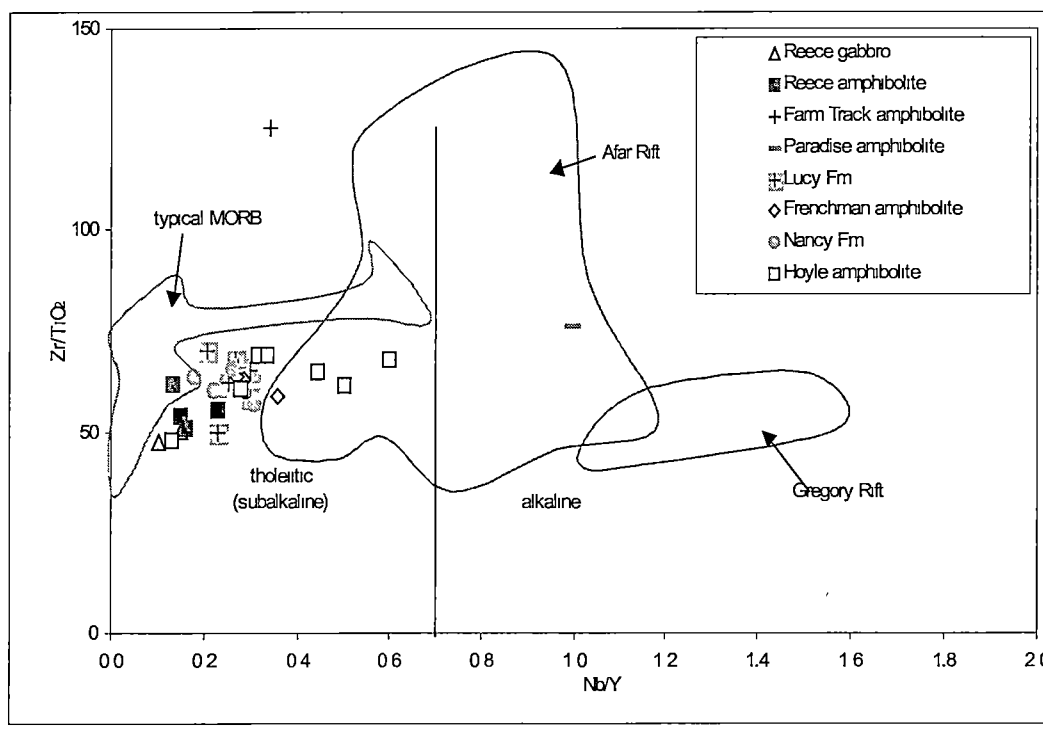

Figure 4.10. Zr/TiO_2 vs Nb/Y discrimination diagram after Winchester & Floyd (1977). The compositional variation of the different units is evident in this plot, reflecting the change in chemistry from the more alkaline at the base of the stratigraphic sequence, evolving to more tholeiitic towards the top of the "eastern" Ahrberg Group. Compositional fields are also shown for representative lava suites from the Gregory (Baker *et al.* 1977) and Afar (Deniel *et al.* 1994) Rifts in eastern Africa.

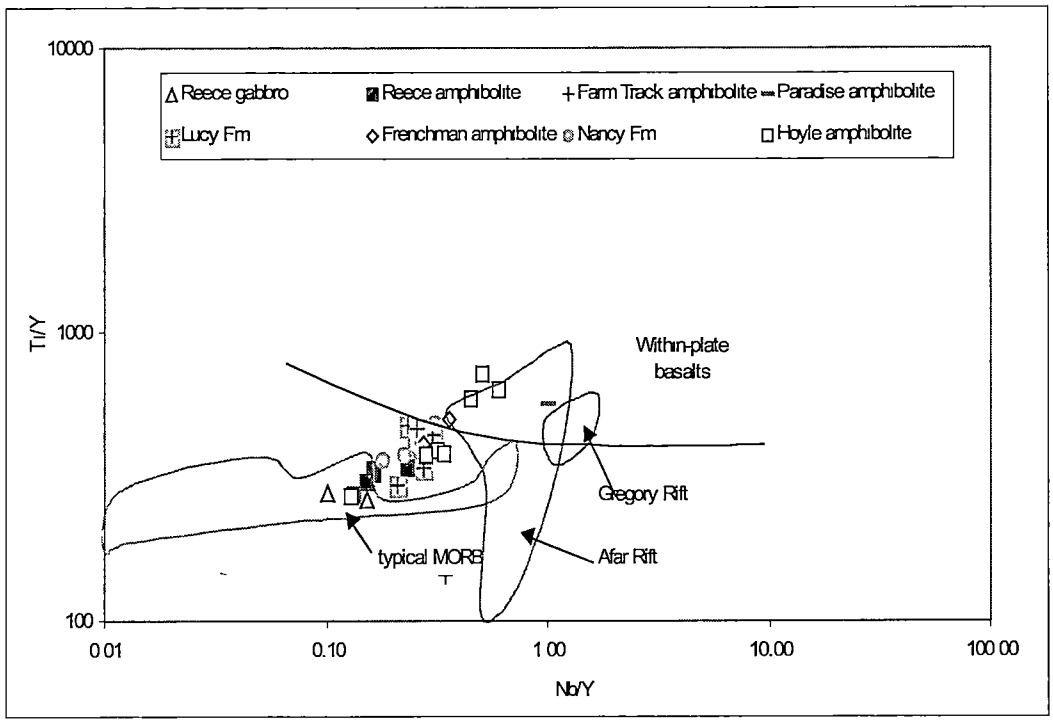

Figure 4.11. Ti/Y vs Nb/Y discrimination diagram separating MORBs from within-plate basalts. The WIB samples are tholeiitic, based on their Nb/Y values Compositional fields are also shown for representative lava suites from the Gregory (Baker *et al.* 1977) and Afar (Deniel *et al.* 1994) Rifts in eastern Africa, and the typical MORB field (Danyushevsky 2001, *pers. comm.*)

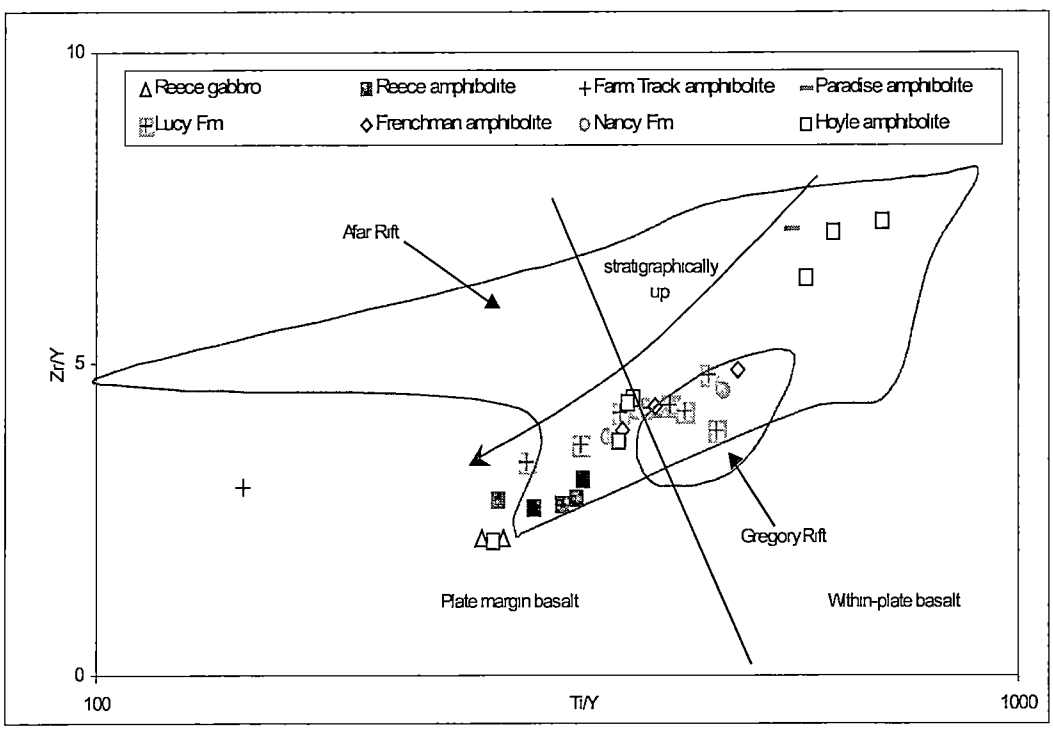

Figure 4.12. Zr/Y vs Ti/Y discrimination diagram for basalts after Pearce & Gale (1977), showing the fields of within-plate basalts and plate margin basalts. The transition in chemistry from transitional tholeiite to E-MORB, corresponding to the higher position in the stratigraphic sequence is evident Compositional fields are also shown for representative lava suites from the Gregory (Baker *et al.* 1977) and Afar (Deniel *et al.* 1994) Rifts in eastern Africa

OH72 (8.9 and 7.2 respectively) (Figure 4.8). OH72 has been shown to have transitional affinities, with a more alkaline chemistry than other "eastern" Ahrberg Group samples, whereas OH919 consistently plots on the same trend as the majority of the "eastern" Ahrberg Group, and has been shown to be sub-alkaline in the Zr/TiO_2 vs Nb/Y discrimination diagram (Figure 4.10).

The sub-alkaline geochemistry of the "eastern" Ahrberg Group, from transitional alkali basalt to E-MORB rift tholeiite is demonstrated on the Ti/Y vs Nb/Y discrimination diagram (Figure 4.11). Interestingly, the gradual change in composition, from transitional alkaline to E-MORB rift tholeiite affinities corresponds with the stratigraphic sequence of the "eastern" Ahrberg Group. This is best illustrated in the Ti/Y vs Zr/Y discrimination diagram (Fig. 4.12), which displays the compositional change from the oldest, westernmost unit of the "eastern" Ahrberg Group, with transitional alkaline affinities, to the youngest, easternmost units, which display plate margin affinities. This chemical sequence from transitional alkaline to E-MORB rift tholeiites within the "eastern" Ahrberg Group is further supported by the strong evidence supporting correlation between the lithologies of the "eastern" Ahrberg Group and the other Neoproterozoic rift-related sequences in northwestern Tasmania (Togari Group, Success Creek Group-Crimson Creek Formation) (Crawford 1992).

4.3 Meta-igneous rocks of the Bowry Formation

Twenty six mafic Bowry Formation samples have been analysed for major and trace elements by previous workers (Wilson 1991, Turner & Botrill 1992, Turner & Crawford 1993). The majority of these lie on the same fractionation trend as the thirteen samples analysed in this study, as illustrated in the FeO*/MgO vs TiO_2 discrimination diagram (Figure 4.13), and on this basis are included in this work. Several analysed Bowry Formation metagabbro samples from this study lie on a separate linear trend with the metagabbro sample 894870 of Turner & Crawford (1993), distinguished by elevated TiO_2 and low FeO*/MgO values. The deformed granitoid bodies within the Bowry Formation that have been analysed by the previous workers are also plotted on Figure 4.13, and lie on a trend that is distinct from the Bowry Formation mafics.

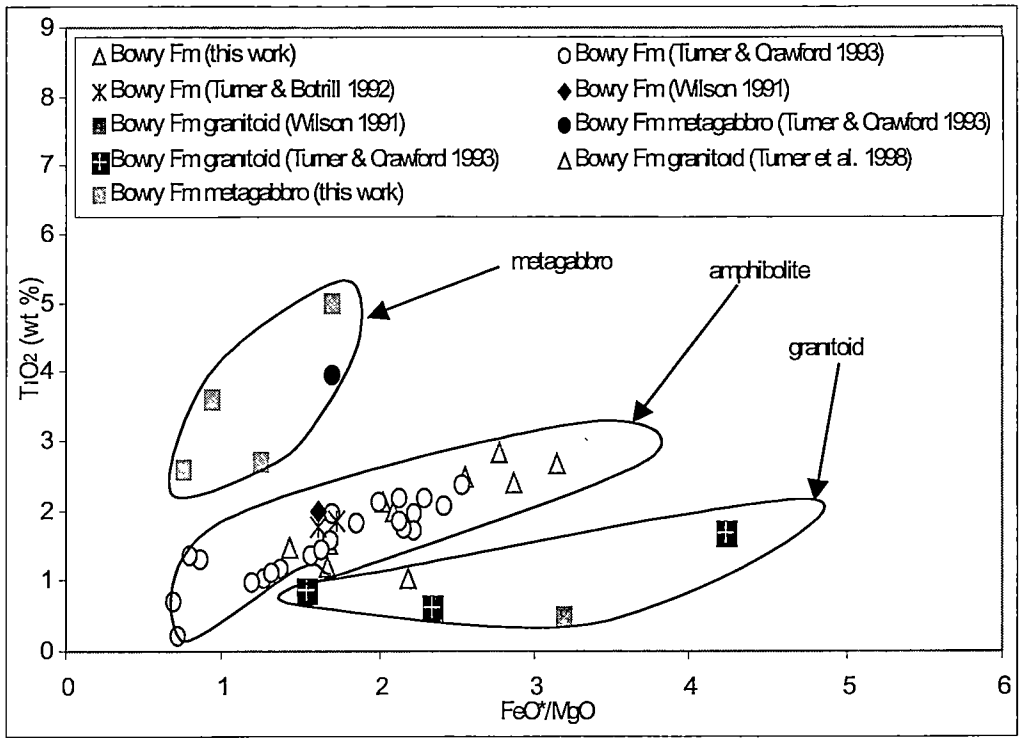

Figure 4.13 TiO_2 vs Zr variation diagram after Floyd & Winchester (1975). Shows analyses of mafic meta-igneous rocks and granitoid from the Bowry Formation, from different workers. All samples analysed are interpreted to be igneous in origin. Symbols used in this diagram represent the different authors.

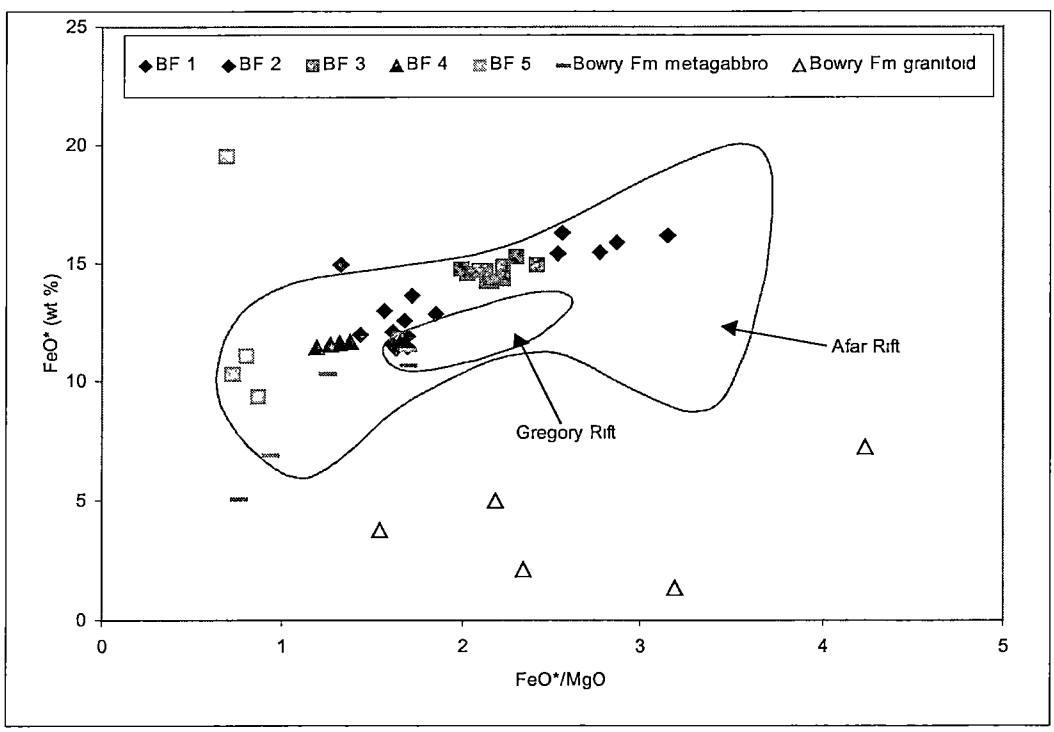

Figure 4.14(a). FeO*/MgO vs FeO* variation diagram after Miyashiro & Shido (1975). The Bowry Formation amphibolites are separated into five subgroups on the basis of chemical characteristics (BF 1-5) BF 5 contains a hydrothermally altered sample, with elevated FeO*. Compositional fields are also shown for representative lava suites from the Gregory (Baker *et al.* 1977) and Afar (Deniel *et al.* 1994) Rifts in eastern Africa. BF 1 samples: RRDDH 152 65, 75934, 69085, 69092, DOM910530, DOM910531, 894853, 894854, 894857, 840720, BF2: samples OH665A, OH667, OH664B, OH1001, 894858; BF3· samples OH689,OH675D, 69106, 69086, 69093, 69094, 69095, 69104, 894855, 840717; BF4· samples RRDDH3-283.6, 69105,69107,840721, 840723; BF5: samples 894856, 840726, 840719, 840718; Bowry Fm metagabbro· samples 894870, RRDDH3-218.4, RRDDH3-189.85, RRDDH3-138 35, RRDDH3-R133 7; Bowry Fm granitoid: samples 75960, 894869, 894871, 894872, 93220005.

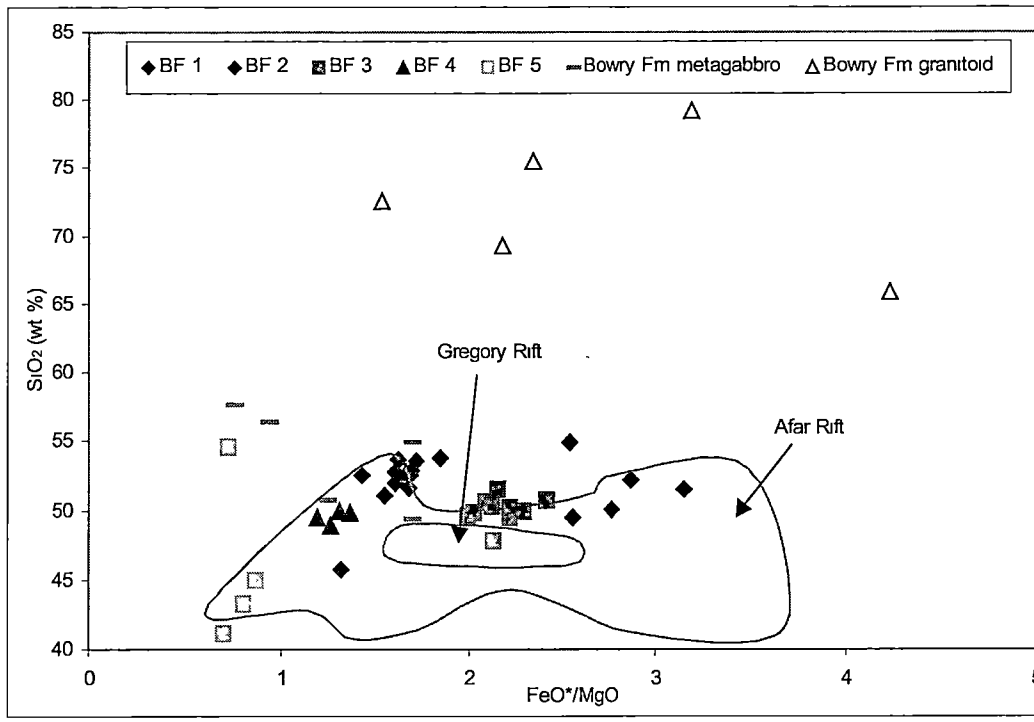

Figure 4.14(b). FeO*/MgO vs SiO_2 variation diagram after Miyashiro & Shido (1975). The granitoid samples are distinguished by their elevated SiO_2 levels. Compositional fields are also shown for representative lava suites from the Gregory (Baker *et al.* 1977) and Afar (Deniel *et al.* 1994) Rifts in eastern Africa.

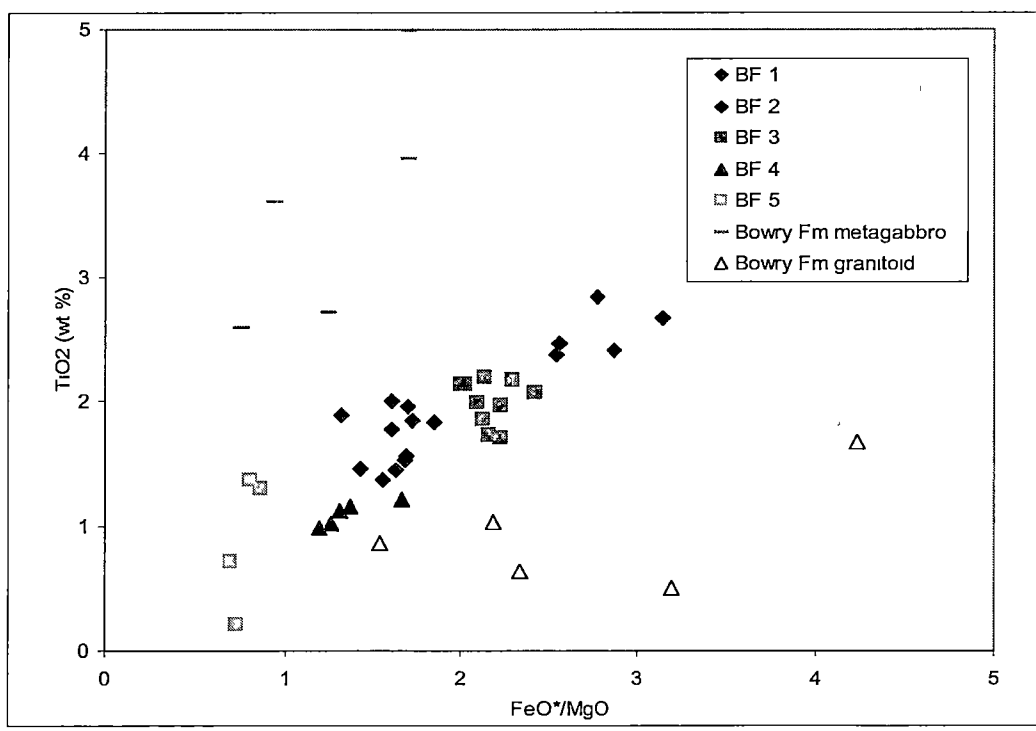

Figure 4.14(c) FeO*/MgO vs TiO_2 variation diagram after Miyashiro & Shido (1975). The Bowry Formation amphibolites and metagabbros clearly separate out into groups BF1-5.

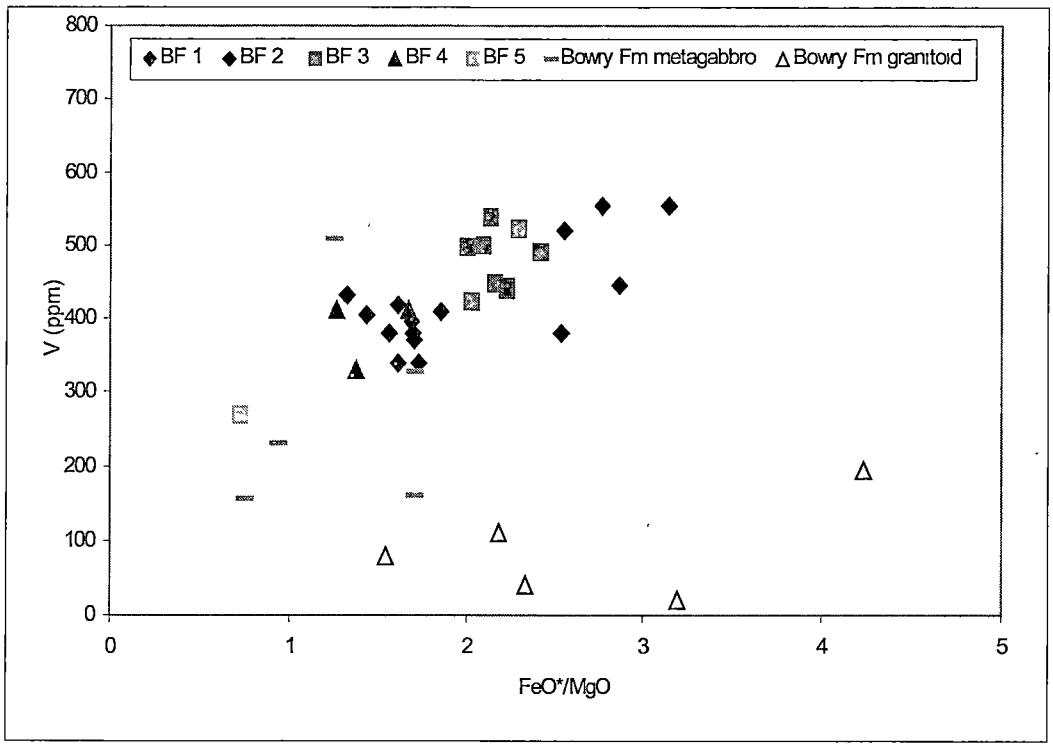

Figure 4.14(d). FeO*/MgO vs V variation diagram after Miyashiro & Shido (1975). V levels were only measured for one BF 5 sample (Turner & Crawford 1993).

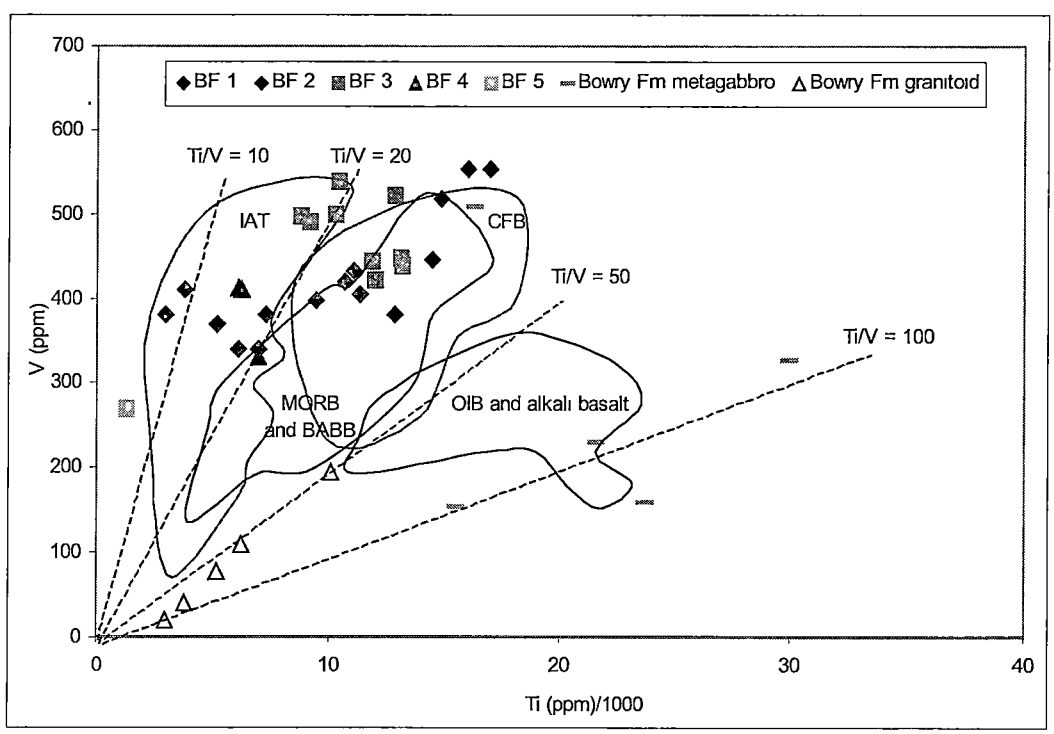

Figure 4.15. Ti/1000 vs V discrimination diagram after Shervais (1982). The majority of the Bowry Formation amphibolites have consistent Ti/V values of ~20, whereas the metagabbro samples have elevated Ti levels, causing the samples to have Ti/V values of 90.

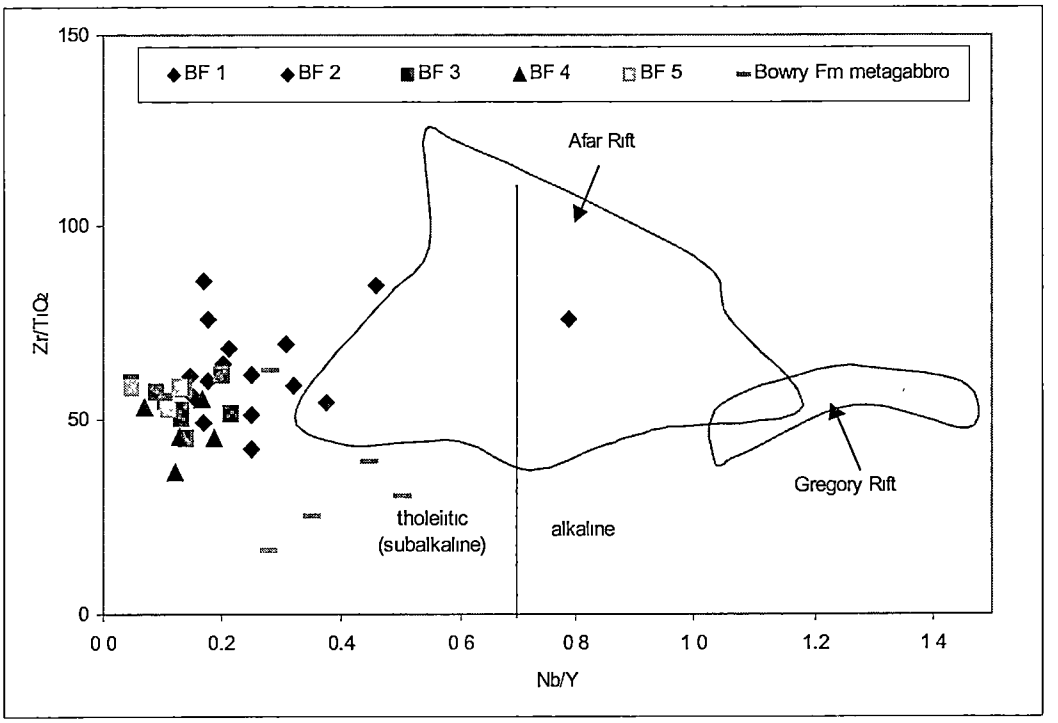

Figure 4.16. Zr/TiO_2 vs Nb/Y discrimination diagram after Winchester & Floyd (1977). The predominantly tholeiitic chemistry of the Bowry Fm is evident. Compositional fields are also shown for representative lava suites from the Gregory (Baker *et al.* 1977) and Afar (Deniel *et al.* 1994) Rifts in eastern Africa.

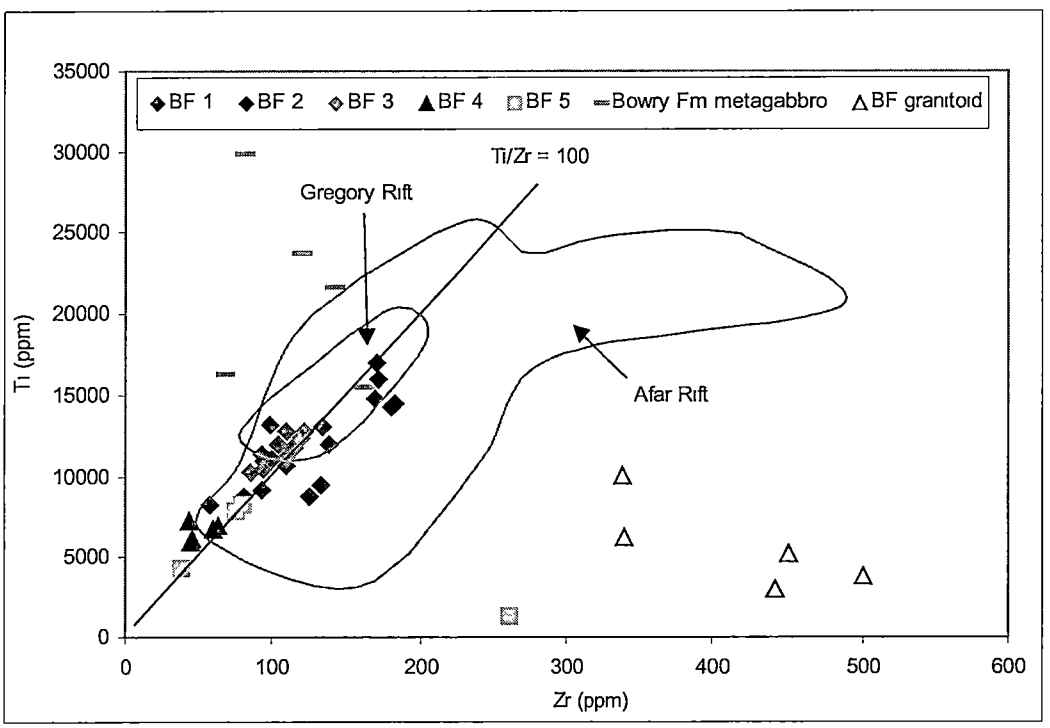

Figure 4.17. Ti vs Zr discrimination diagram with linear scale after Pearce & Cann (1973). The Bowry Fm amphibolites have consistent Ti/Zr = 100. Compositional fields are also shown for representative lava suites from the Gregory (Baker *et al.* 1977) and Afar (Deniel *et al.* 1994) Rifts in eastern Africa.

4.3.1 Occurrence and petrography

The Bowry Formation consists of magnetite-bearing amphibolite bodies, metagabbros, discontinuous massive and banded magnetite bodies (eg. Savage River mine, Long Plains, Rocky River and Owen Meredith River magnetite bodies), minor bodies of foliated granitoid, and interlayered chloritic pelite and psammopelite. The granitoid, which is interlayered with amphibolite and metagabbro, has been dated at 777 ± 7 Ma in the Rocky River (349170 mE, 5389375 mN) (Turner *et al.* 1998).

Despite the Bowry Formations complex metamorphic history (see Chapter 3), occasional examples of primary igneous textures have been retained. Like the "eastern" Ahrberg Group amphibolites, the mafics in the Bowry Formation are boudinaged. The intensity of foliation development within the mafics varies. Rims of bodies are typically strongly foliated, although the cores display only a weak foliation. The thin, elongate, discontinuous nature of the amphibolites suggests that these mafics intruded into the country rock as dykes and sills. Evidence of $\boldsymbol{Ca}S_1$ and $\boldsymbol{Ca}S_2$ overprinting the meta-igneous rocks of the "eastern" Ahrberg Group and Bowry Formation indicates they were emplaced prior to the Tyennan Orogeny.

4.3.2 Geochemical affinities and tectonic setting

Petrographic observations combined with the major element chemistry of the twenty seven analysed samples from the Bowry Formation (excluding granitoid samples) indicates that they are either mafic or intermediate in composition, with contrasting grainsize, textures, and varying levels of SiO_2, FeO* and MgO. The majority of the samples are basaltic, and can be distinguished from the intermediate samples, which have partly recrystallised coarse grained textures, and are considered to be gabbroic to leucogabbroic or dioritic in origin (Table 4.2). The basaltic composition of the Bowry Formation amphibolites is indicated by FeO* (total iron as FeO) (9.4-16.3 %) and MgO (5.1-13.9 %) abundances, although one sample (840719) has significantly higher FeO* (19.5 %) and MgO (28.1 %). This sample also has low SiO_2 (41.1 %), whereas the range of the other samples is higher (43.3-54.9 %). The majority of the amphibolites are within the range of basalts to basaltic andesites, although sample 840719 is in the range of picrobasalts. They are characterised by moderate to high

levels of TiO_2 (1.0-2.8%), V (330-554 ppm) and Nb (2-17 ppm), although samples 840719 and 894856 have lower TiO_2 (0.7 % and 0.2 %). In contrast, the intermediate composition of the gabbroic and leucogabbroic samples is indicated by low to moderate FeO* (5.1-11.3 %) and MgO (6.3-8.2 %). SiO_2 levels (49.4-57.7 %) are slightly higher than the amphibolites, as are the levels of TiO_2 (2.6-5.0 %). In contrast, the Bowry Formation granitoid has substantially higher SiO_2 values (65.9-79.3 %), lower TiO_2 (0.5-1.7 %), FeO* (1.4-7.2 %) and MgO (0.4-2.5 %).

The Bowry Formation samples have been plotted on a series of binary discrimination diagrams of FeO*/MgO vs FeO*, SiO_2, TiO_2 and V (Figure 4.14(a) to (d)). As is demonstrated in the FeO*/MgO vs TiO_2 discrimination diagram (Figure 4.14(c)), the amphibolites, intermediate metagabbros and granitoid samples plot in three distinct groups. The amphibolites have low to moderate TiO_2 and FeO*/MgO levels, and cluster along a uniform slope, reflecting a consistent fractionation trend. Although the amphibolites lie on a single fractionation trend, they can be subdivided into four groups (BF1-4) which represent different degrees of fractionation. A fifth group, BF5, includes samples from close to the magnetite ore body at the Savage River mine. Some of the BF5 samples have low TiO_2, and are interpreted to have undergone hydrothermal alteration (Turner & Crawford 1993). The metagabbros, however, have lower FeO* levels and high levels of TiO_2, reflected in the steep gradient of the trend formed by the samples. The granitoids lie on a flat trend with much lower TiO_2 values.

Based on these discrimination diagrams with immobile elements plotted against FeO*/MgO, it is clear that the positive slope of the amphibolites indicates that they have tholeiitic affinities, but did not commence significant fractional crystallisation of titanomagnetite. This interpretation is supported in both the FeO* and V vs FeO*/MgO discrimination diagram (Figure 4.14(a) and (d)). Despite the positive trend of the metagabbros in the TiO_2, FeO* and V vs FeO*/MgO discrimination diagrams, they do not consistently lie on the same fractionation trend as the amphibolites. On this basis it can be suggested that the metagabbros are part of a different fractionation series to the amphibolites.

The notable enrichment of FeO*, TiO_2 and V with advancing fractionation indicates tholeiitic affinities and excludes the possibility that these amphibolites have calc-alkaline affinities. The Bowry Formation amphibolites can be excluded from having alkali basalt affinities when plotted on the Ti/1000 vs V discrimination diagram (Figure 4.15). The amphibolites have approximate Ti/V values of 20, consistent with MORB and CFB-affinity basalts, whereas the metagabbros have significantly higher Ti/V values averaging 93. This may indicate the metagabbros are derived from a melt with a different bulk composition. However on the Nb/Y vs Zr/TiO_2 discrimination diagram (Figure 4.16), the metagabbros do not have Nb/Y values of greater than 0.5. Furthermore, they plot in the tholeiitic field, ruling out alkalic affinities.

IAT affinities for the amphibolites and intermediate metagabbros of the Bowry Formation can be excluded on the basis of the moderate to high TiO_2 and Zr concentrations of the analysed samples. IAT rarely have $TiO_2 > 1.2$ % and Zr >100 ppm (Perfit *et al.* 1980, Luff (1982). On the Ti vs Zr discrimination diagram (Figure 4.17), the amphibolites predominantly plot with Ti/Zr values typical of MORB, and separate out into the BF1-4 subdivisions reflecting fractionation. The majority of the BF5 samples lie on the same trend, although a single sample (894856) has significantly elevated Zr levels (260 ppm) and notably depleted TiO_2 (0.2 %) and may represent a late-stage highly evolved composition, co-magmatic with other amphibolites. The metagabbros have significantly higher Ti levels than the amphibolites, and display a trend which suggests the crystallisation of a TiO_2-bearing phase may have commenced as the magma evolved. The lack of volcaniclastics and the absence of volcanically-derived fragmentals is further support for the interpretation that the samples do not have IAT affinities.

The different composition of the metagabbros and the possibility that they were derived from a compositionally different melt than the parental metabasalt protoliths of the amphibolites is supported by the Zr/Nb vs Y/Nb discrimination diagram (Figure 4.18). The metagabbros form a well defined group and have lower Zr/Nb values, positioned between the Precambrian alkali basalts that intrude the Burnie and Oonah Formations in northwest Tasmania, and the Bowry Formation amphibolites. The amphibolites have higher Zr/Nb (7.7-55.0) and Y/Nb (1.3-21.5) although the

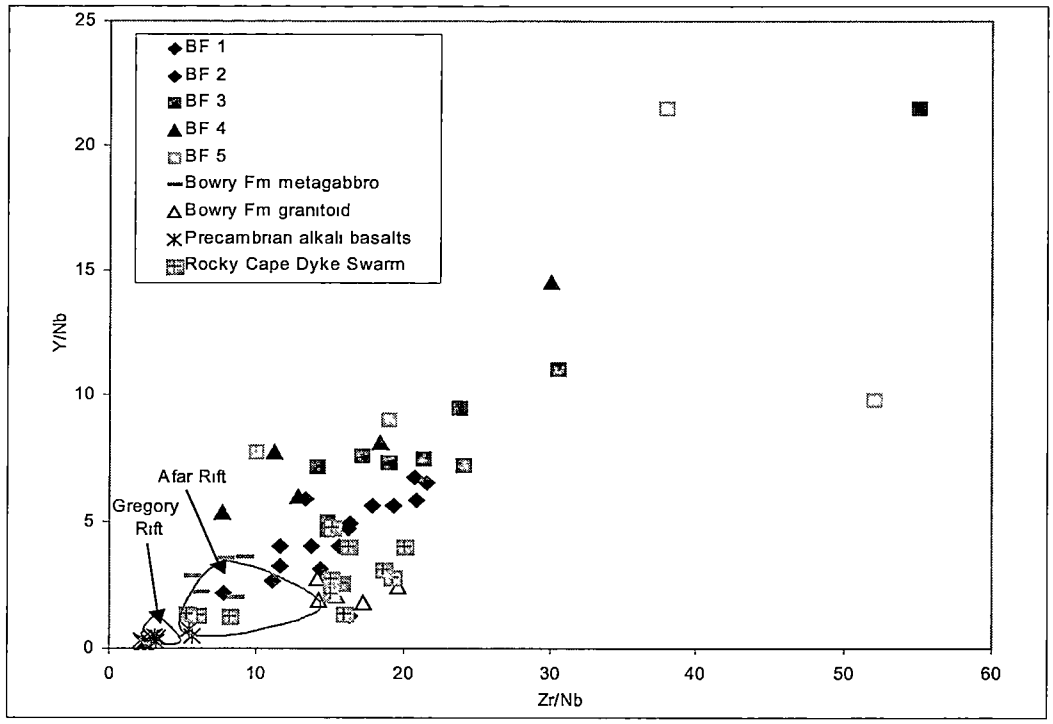

Figure 4 18 Zr/Nb vs Y/Nb variation diagram. The transitional chemistry of the Bowry Formation amphibolites is demonstrated here. The metagabbros have notably low Zr/Nb and Y/Nb values, and may be transitional towards alkaline affinities, such as the Tasmanian Precambrian alkali basalts and several Rocky Cape dyke swarm dolerites, included in the diagram OIB and BABB affinities for the amphibolites are unlikely, as the majority of the samples plot with Zr/Nb ranging between 10 and 20. Compositional fields are also shown for representative lava suites from the Gregory (Baker *et al.* 1977) and Afar (Deniel *et al.* 1994) Rifts in eastern Africa.

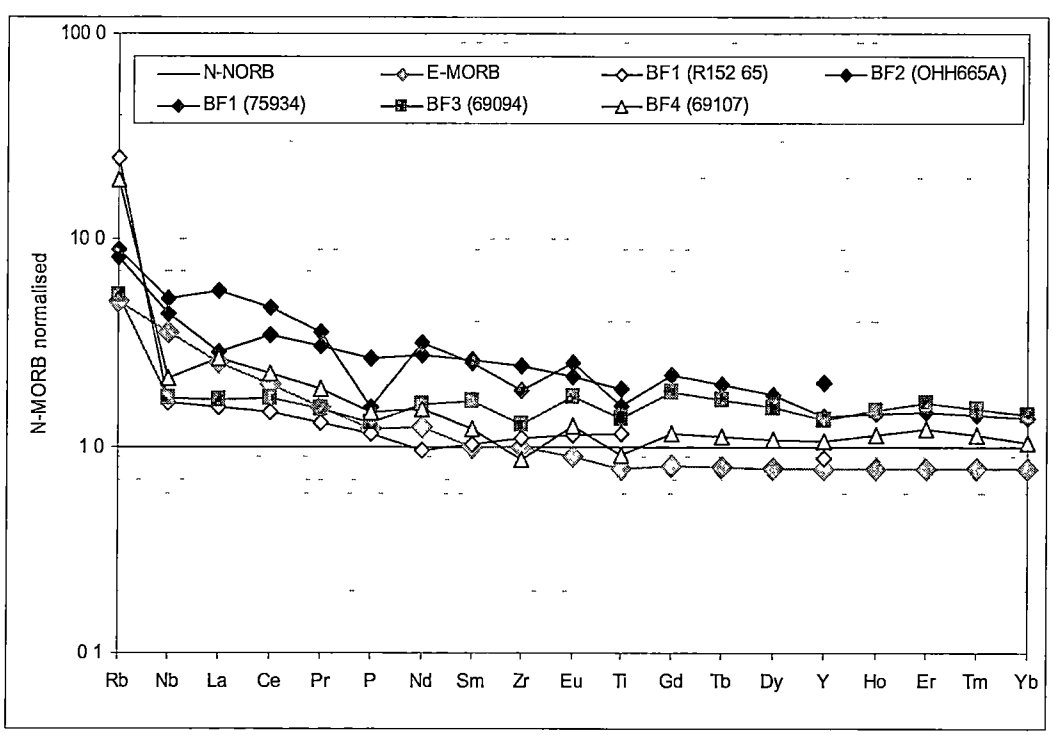

Figure 4.19. MORB normalised rare earth element variation diagram showing average abundances for the average Bowry Formation subgroup (BF 1-4) amphibolites. BF1 (R152 65) and BF4 samples have patterns broadly consistent with E-MORB. However BF1 (75934), BF3 and BF4 all display consistent patterns, with variably negative Nb, P, Zr, Ti and Y anomalies, suggesting a single source. Samples 69094, 75934, 69105 and 69107 have interpolated Tb, Ho and Tm values. Samples 894870, R218.4, OHH665A, R152 65 and 840726 have interpolated Pr, Sm and Eu. N-MORB normalising values, and typical E-MORB are from Sun & McDonough (1989).

majority of samples lie in the Zr/Nb range of 10-20 and the Y/Nb range of 5-10. Sample DOM 894858 has an anomalously low Y level (14), resulting in a low Y/Nb value (1.3). Samples in subgroup BF5 are poorly constrained on this discrimination diagram. This is thought to be due to their proximity to magnetite ore at Savage River, and is interpreted to reflect hydrothermal alteration (Turner & Crawford 1993). These Zr/Nb and Y/Nb values are consistent with E-MORB to N-MORB (Wilson 1989), and on this basis, OIB affinities for the Bowry Formation amphibolites can be discounted. The metagabbros have low Zr/Nb values (5.6-9.2) and low Y/Nb (2.0-3.6), and lie on the same magmatic trend as the amphibolites. The Zr/Nb values overlap slightly with the Precambrian alkali basalts (2.2-5.7), and they are comparable to several dolerite intrusions within the Rocky Cape dyke swarm. The metagabbros and Rocky Cape dolerite dykes with similar Zr/Nb values may reflect a transitional environment of emplacement. The Bowry Formation granitoid samples have high Zr/Nb levels but consistently low Y/Nb levels.

Due to the predominantly low Zr/Nb values and minor transitional alkali components, BABB affinities for the Bowry Formation can be excluded, as BABB have high Zr/Nb (>20) and no alkalic component. Therefore, from the discrimination diagrams it can be concluded that the amphibolites from BF4 and BF5, together with the metagabbros are the least fractionated and have transitional alkaline to E-MORB affinities, whereas the amphibolites from BF1, BF2 and BF3 are more fractionated and have E-MORB affinities.

In the N-MORB normalised rare earth element variation diagram for amphibolites from the Bowry Formation (Figure 4.19), E-MORB patterns typical of rift-type tholeiites are evident. This suggests the melt from which the samples were derived had minor alkaline affinities.

Whereas an apparent temporal transition in the chemistry of the Bowry Formation amphibolites is evident (from transitional alkaline to E-MORB rift tholeiite), as the unit is either in part, or entirely allochthonous, the tectonostratigraphy and geochemistry of the Bowry Formation in relation to the parautochthonous "eastern" Ahrberg Group is not clear. This will be discussed further in Section 4.5.

4.4 Mafics of the "western" Ahrberg Group

Six representative samples from the mafic meta-igneous units of the Ahrberg Group have been analysed for major and some trace elements by XRF spectrometry (see Chapter 1 for analytical specifications). Another eighteen samples from the Ahrberg Group have been analysed by previous workers (Turner & Crawford 1993).

The Ahrberg Group samples from Turner & Crawford (1993) lie on the same magmatic trend as those analysed in this study, as demonstrated in the FeO*/MgO vs FeO* discrimination diagram (Figure 4.20) and on this basis are included in this work.

4.4.1 Occurrence and petrography

The Ahrberg Group is a moderately deformed northeast-trending belt, consisting of metavolcanics and associated volcaniclastic metasiltstone interlayered with shallow marine sediments and dolomite (Figure 4.2). The metavolcanics are divided into two stratigraphic units, the Bernafai Volcanics and the Tunnelrace Volcanics. The Tunnelrace Volcanics are stratigraphically higher, and have experienced higher levels of strain, due to their proximity to the Arthur Lineament and the strongly deformed "eastern" Ahrberg Group.

Both units have undergone lower greenschist facies metamorphism, and are variably recrystallised. The meta-igneous rocks are fine grained, and weakly foliated. In some cases they are plagioclase-phyric, whereas primary pyroxene phenocrysts are uncommon. The samples are interpreted to be igneous in origin, based on the contrasting texture to the surrounding metasediments, and their discontinuous nature. Unlike the more strongly deformed meta-igneous rocks of the "eastern" Ahrberg Group and Bowry Formation, the metabasalts of the Ahrberg Group are not strongly boudinaged. The mafic mineralogy and whole rock geochemistry of the samples further supports the igneous interpretation of these samples.

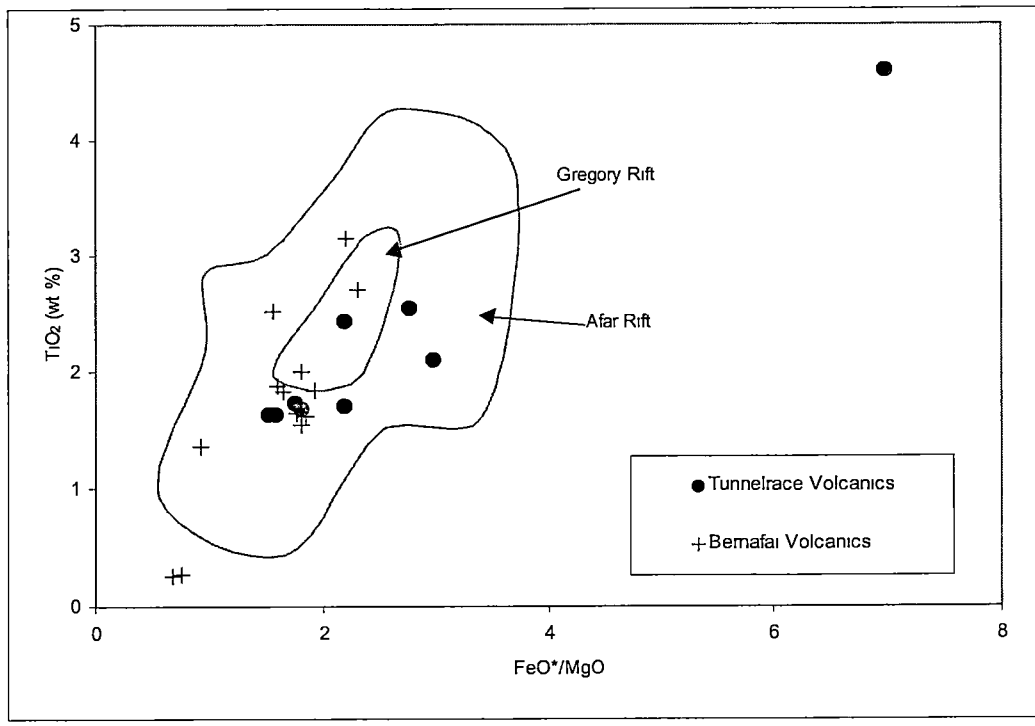

Figure 4.20. . FeO*/MgO vs FeO* variation diagram for the "western" Ahrberg Group metabasalts after Miyashiro & Shido (1975). Demonstrates the chemical similarity of the Tunnelrace and Bernafai Volcanics samples analysed by different workers. The Bernafai and Tunnelrace Volcanics samples display a tholeiitic fractionation trend.

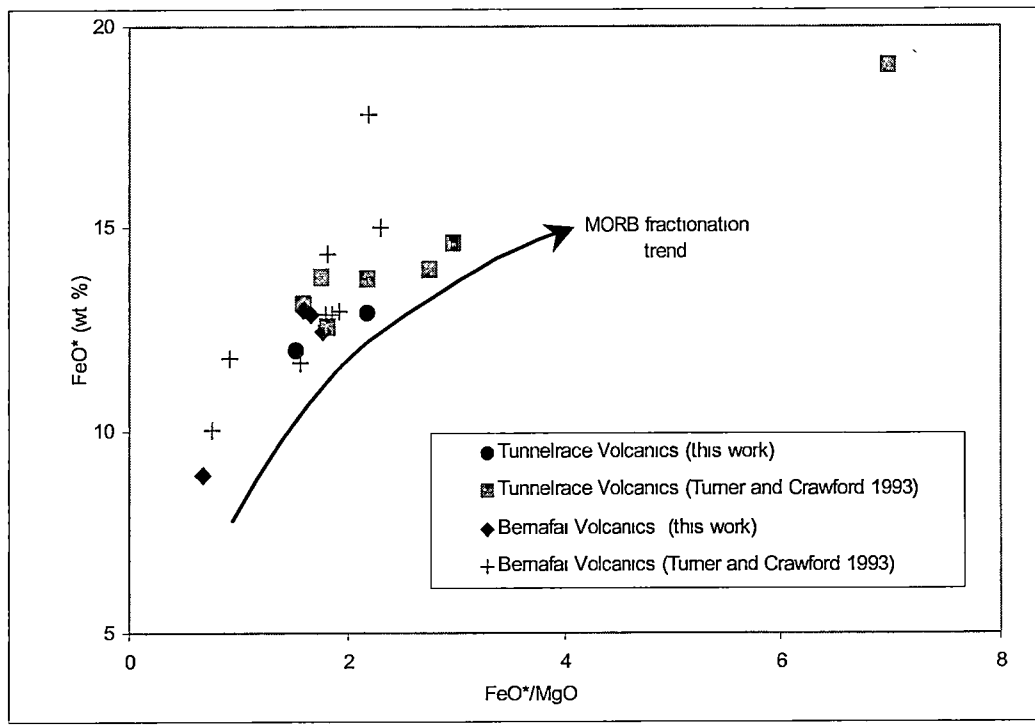

Figure 4.21(a). FeO*/MgO vs TiO_2 variation diagram for the "western" Ahrberg Group metabasalts after Miyashiro & Shido (1975). Compositional fields are also shown for representative lava suites from the Gregory (Baker *et al.* 1977) and Afar (Deniel *et al.* 1994) Rifts in eastern Africa.

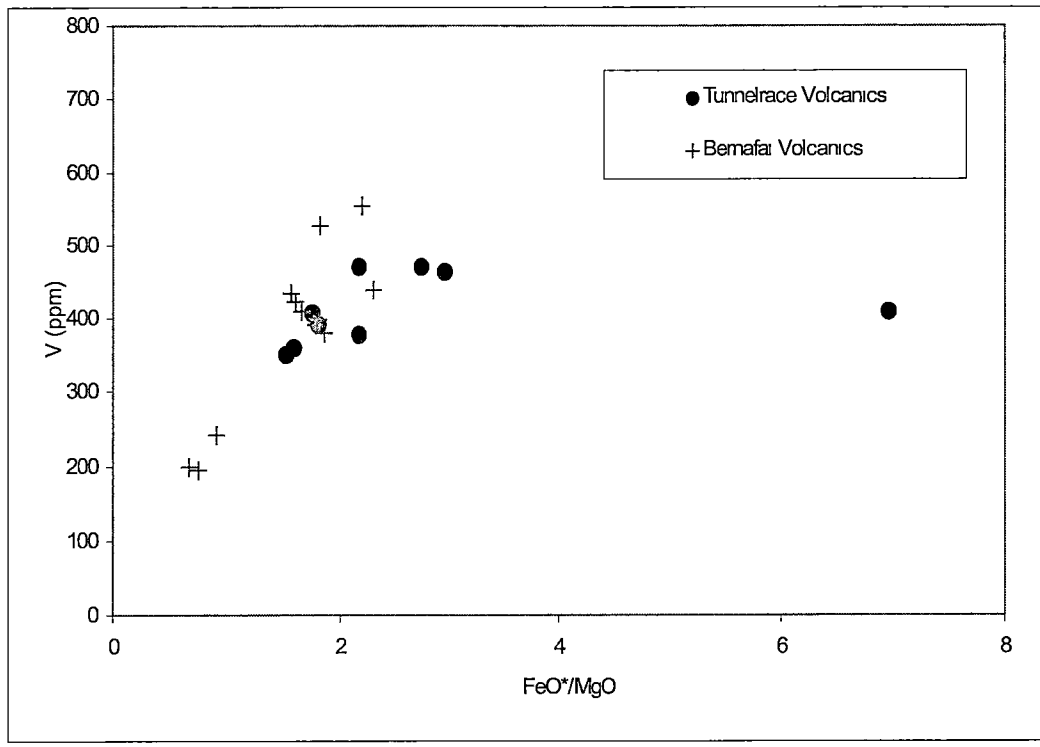

Figure 4.21(b). FeO*/MgO vs V variation diagram for the "western" Ahrberg Group metabasalts, after Miyashiro & Shido (1975).

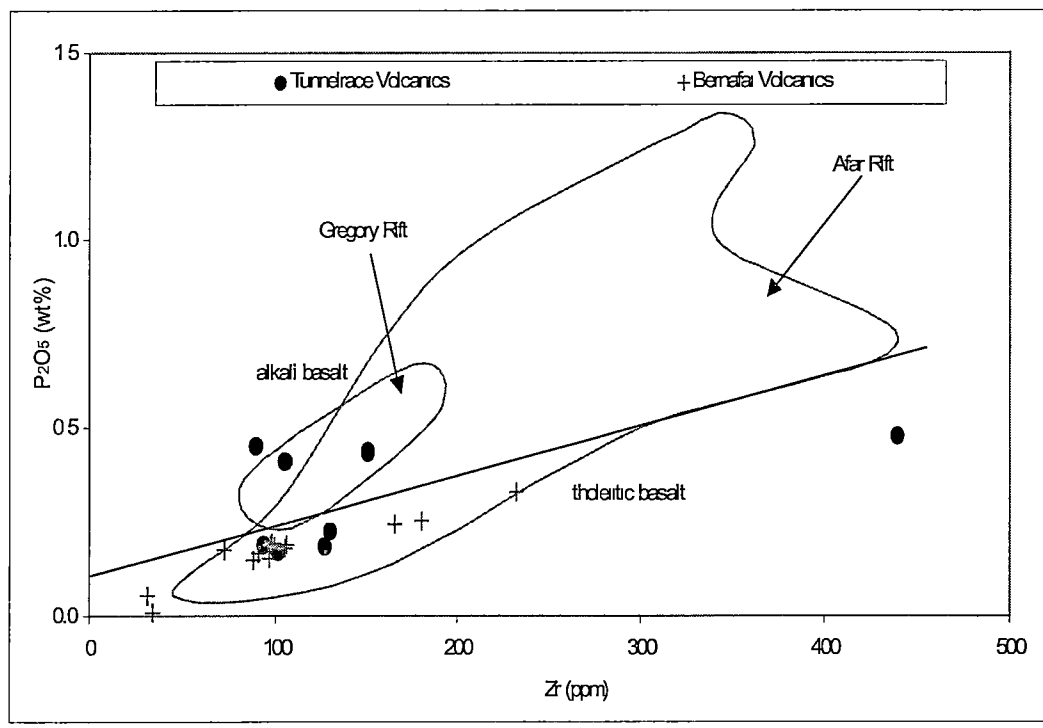

Figure 4.22. P_2O_5 vs Zr discrimination diagram for the "western" Ahrberg Group metabasalts after Winchester & Floyd (1976). Compositional fields are also shown for representative lava suites from the Gregory (Baker *et al.* 1977) and Afar (Deniel *et al.* 1994) Rifts in eastern Africa.

4.4.2 Geochemical affinities and tectonic setting

The major element chemistry of the thirty one analysed samples from the Ahrberg Group indicates that they are basaltic in composition (Table 4.3). This is indicated by relatively high FeO* (total iron as FeO) (8.9-19.0 %) and MgO (2.7-13.4 %) abundances. Despite the potential mobility of SiO_2 due to the regional metamorphism experienced by the Ahrberg Group, the analysed samples are mostly within the range of basalts (41.2-51.5 %), although several samples have values of basaltic andesites (52.1-53.2 %). The majority of samples are further characterised by moderate to high levels of TiO_2 (1.4-4.6 %), although several have notably low concentrations (0.3 %). The samples have moderate to high levels of V (199-554 ppm).

The Ahrberg Group samples have been plotted on a series of binary diagrams of various immobile elements against FeO*/MgO (Figures 4.21 (a) and (b)). The samples show an increase in FeO*, TiO_2, and V with increasing FeO*/MgO. The trend has a positive slope and does not pass a maximum point, indicating the suite had not commenced significant fractional crystallisation of titanomagnetite (Miyashiro & Shido 1975). This is consistent with fractionation of a tholeiitic magma under relatively low oxygen fugacity conditions, where Fe and Ti remain in the magma due to the delayed crystallisation of titanomagnetite. This notable FeO* enrichment excludes the possibility that the samples have calc-alkaline affinities. On the P_2O_5 vs Zr discrimination diagram, the samples are shown to be predominantly tholeiitic, although several samples from the Tunnelrace Volcanics plot in the alkali basalt field close to the boundary (Figure 4.22). On the Ti/1000 vs V discrimination diagram, both the Bernafai and Tunnelrace Volcanics plot predominantly in the CFB and MORB field, with Ti/V values of 29.8 and 31.8 respectively. One Tunnelrace Volcanics sample (DOM894848) lies within the alkali basalt and OIB field with a Ti/V value of 70 (Figure 4.23).

Moderate to high Ti concentrations within the mafics of the Ahrberg Group, together with the moderate Zr levels indicates the analysed samples do not have island arc tholeiite (IAT) affinities (Figure 4.24). The lack of volcaniclastics and the absence of volcanically-derived fragmentals supports this interpretation.

On the Zr/Nb vs Nb/Y discrimination diagram (Figure 4.25), the Bernafai and Tunnelrace Volcanics have Zr/Nb values ranging between 10.0 and 30.3, however the majority of the samples range between 10 and 17. The metabasalts have low Nb/Y (0.1-0.7). These values are both outside the typical range for OIB (Zr/Nb<10, Nb/Y>0.7) (Wilson 1989). Further to this, the lithological associations within the Bernafai and Tunnelrace Volcanics (quartzose conglomerate, quartz-rich metasediments, carbonates), are not consistent with basalts erupted in an OIB setting. BABB affinities for these metabasalts can be excluded, as they have transitional WIB to tholeiitic affinities, and the Zr/Nb values (10-17) are less than basalts with typical BABB affinities (>20).

On the N-MORB normalised rare earth element variation diagram (Figure 4.26), the "western" Ahrberg Group metabasalts display typical E-MORB rift tholeiite patterns. Although the Bernafai and Tunnelrace Volcanics samples display a broadly enriched pattern, very similar to E-MORB, samples 69087 and OH220 from the Bernafai Volcanics have a distinctive pattern, with enriched LREE, slightly depleted HREE, low Nb/La anomalies and negative Ti and P anomalies. This is interpreted to reflect crustal contamination of a melt which has N-MORB to depleted MORB affinities. Similar Ti and P-depleted patterns have been reported elsewhere in the lower Togari Group and in the uppermost Neoproterozoic Double Cove sequence on the Sorell Peninsula in western Tasmania (Griffin 1974, Crawford 1992).

It can be concluded that the evolving compositions of the Ahrberg Group reflect an emerging rift to E-MORB setting, with minor crustally contaminated N-MORB to depleted MORB basalts occurring late in the sequence due to the aborted rifting of the developing ocean basin.

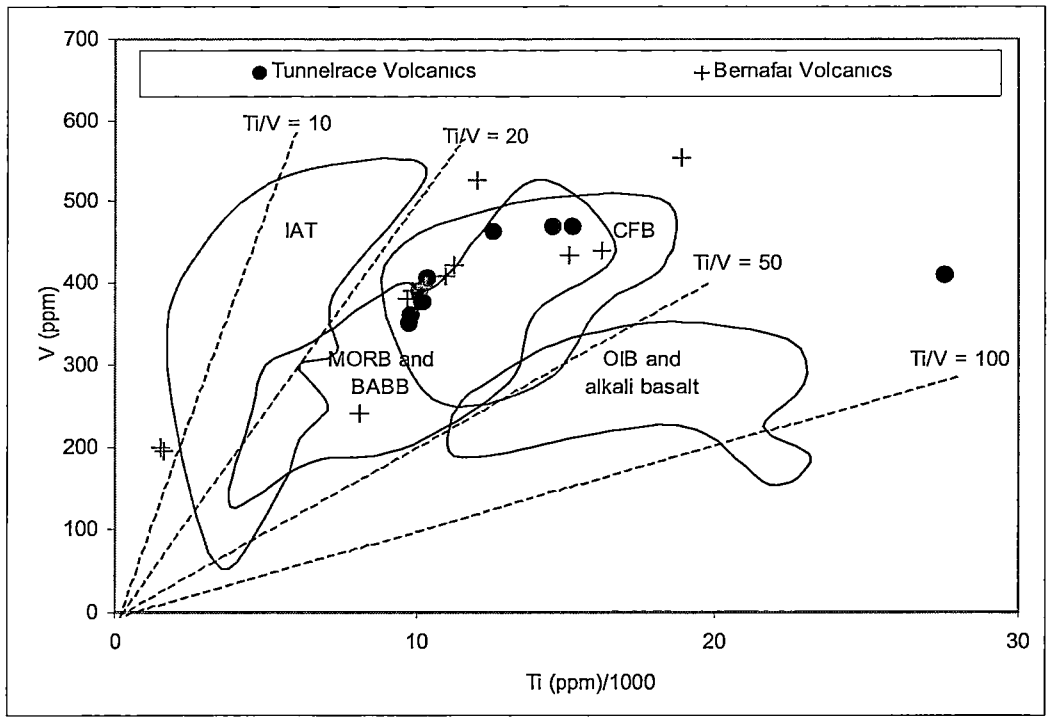

Figure 4.23. Ti/1000 vs V discrimination diagram for the "western" Ahrberg Group metabasalts after Shervais (1982). The majority of the Ahrberg Group metabasalts have consistent Ti/V values of ~30, whereas the Tunnelrace Volcanics sample DOM894848 has elevated Ti levels, indicated by the elevated Ti/V value of 70. Two samples from the Bernafai Volcanics (OH220, 69087) are notably depleted in Ti and V. These samples also have low levels of Zr and P_2O_5 in Figure 4.25.

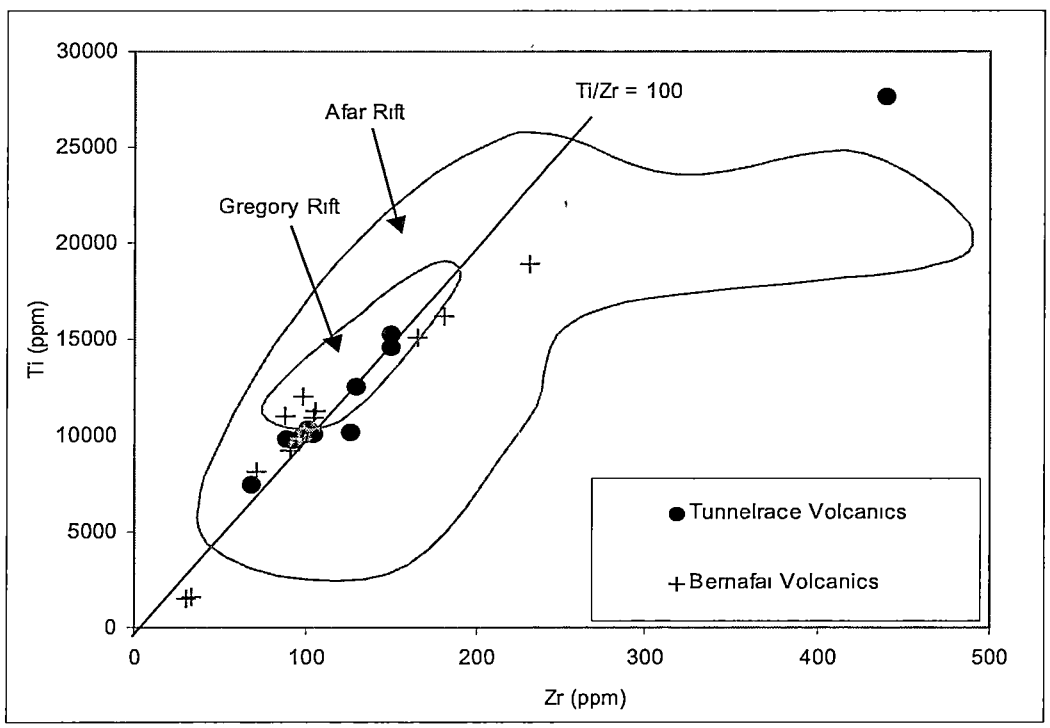

Figure 4.24. Ti vs Zr discrimination diagram for the "western" Ahrberg Group metabasalts after Pearce & Cann (1973). Note depleted values for samples OH220 and 69087, from the Bernafai Volcanics. The metabasalts have Ti/Zr levels consistent with MORB affinities. Compositional fields are also shown for representative lava suites from the Gregory (Baker *et al.* 1977) and Afar (Deniel *et al.* 1994) Rifts in eastern Africa.

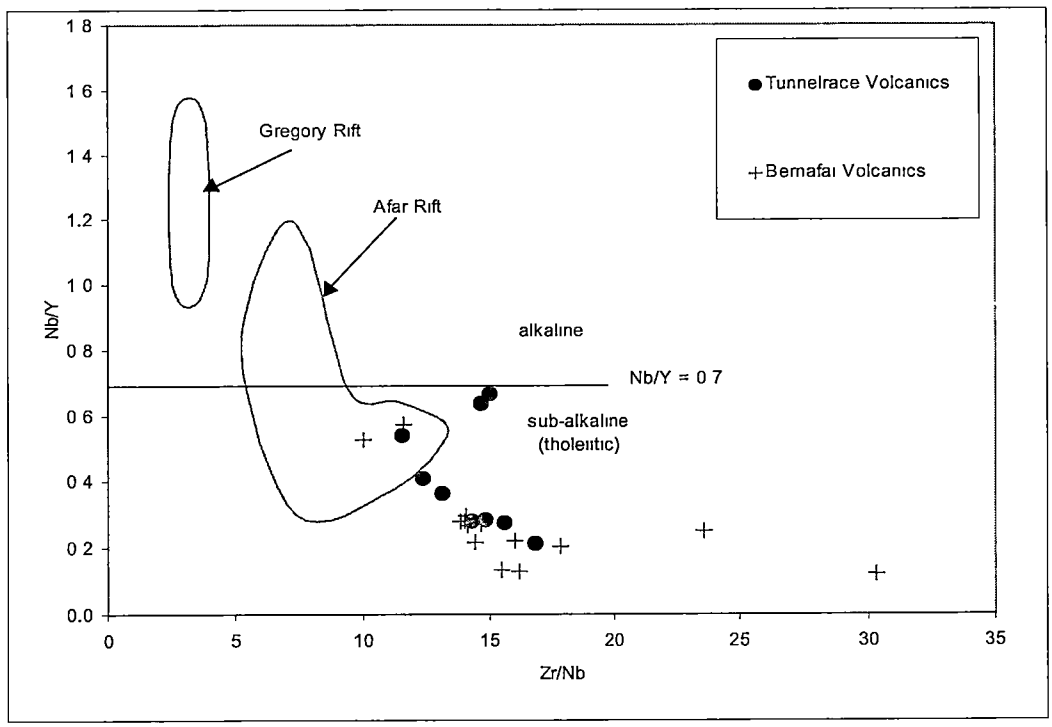

Figure 4.25. Zr/Nb vs Nb/Y discrimination diagram for the "western" Ahrberg Group metabasalts. The elevated Zr/Nb and low Nb/Y values rule out OIB affinities for the Bernafai and Tunnelrace Volcanics. Compositional fields are also shown for representative lava suites from the Gregory (Baker *et al.* 1977) and Afar (Deniel *et al.* 1994) Rifts in eastern Africa.

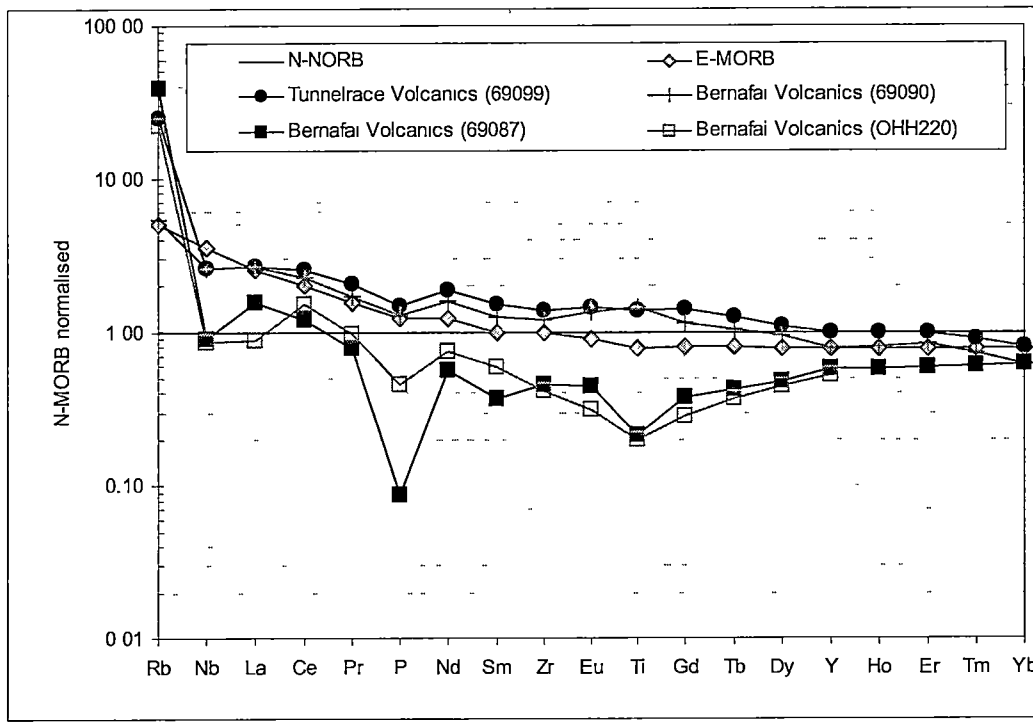

Figure 4.26. MORB normalised rare earth element variation diagram for the "western" Ahrberg Group metabasalts. The typical abundances of the Bernafai and Tunnelrace Volcanics are very similar, however samples 69087 and OHH220 depict enriched LREE and depleted HREE patterns, suggesting crustal contamination of depleted melts. Sample OH220 has interpolated Pr, Sm, Gd, Tb, and Dy values. N-MORB normalising values and E-MORB are from Sun & McDonough (1989).

4.5 Discussion

4.5.1 Introduction

In northwestern Tasmania, previous workers have correlated several different Neoproterozoic sequences (Spry 1964, Brown 1989, Turner *et al.* 1992, 1994, Calver 1998) based on stratigraphic and mafic igneous geochemical similarities. Turner *et al.* (1992) noted that the Ahrberg and Togari Groups together with the Success Creek Group-Crimson Creek Formation have broadly similar stratigraphies. These three spatially separate successions consist of dolomite units overlain by tholeiitic volcanics, together with associated volcaniclastics and other sedimentary rocks (Turner *et al.* 1992). Turner *et al.* (1992) observed that the meta-igneous rocks of the "eastern" Ahrberg Group also contain tholeiitic affinities and are likely to have formed during the same period of crustal attenuation and juvenile rifting as the other Neoproterozoic rift sequences. Previous workers (Spry 1964, Turner 1990, Turner *et al.* 1992 & 1994) also noted the common unconformable relationship between both the Togari and Ahrberg Groups with the Rocky Cape Group. Crawford & Berry (1992) and Turner *et al.* (1992) interpreted the *ca.* 600 Ma dyke swarm intruding the Rocky Cape Group to be part of the same magmatic event as the mafic volcanics of the Ahrberg Group.

My work supports these previous interpretations, and provides an increased level of detail for the regional correlations. The "eastern" Ahrberg Group has been shown to have transitional to tholeiitic, E-MORB affinities characteristic of rift tholeiites, with the increasingly tholeiitic chemistry corresponding to the stratigraphic position, with samples with depleted MORB affinities occurring highest in the sequence. The Bernafai and Tunnelrace Volcanics of the "western" Ahrberg Group have the same compositional range of metabasalts, with transitional alkaline, and E-MORB rift tholeiites occurring. Furthermore, the stratigraphy of the "western" Ahrberg Group is very similar to the "eastern" Ahrberg Group, and the two sequences have been tentatively correlated on these grounds.

The Kanunnah Subgroup, Success Creek Group-Crimson Creek Formation, Double Cove and minor basalts emplaced at the western margin of the Oonah Formation to the south of the Arthur Lineament all display tholeiitic fractionation patterns similar

to the "eastern" and "western" Ahrberg Groups, as is demonstrated on the FeO*/MgO vs TiO_2 discrimination diagram (Figure 4.27). In addition, the transition in the chemistry of the different units corresponds to that of the "eastern" and "western" Ahrberg Groups, with Ti/Zr and Zr/Nb values indicating predominantly E-MORB affinities, with transitional alkaline affinity basalts also occurring in minor proportions (Figure 4.28). However, as the detailed stratigraphy of these sequences is not known, direct correlation between individual mafic units cannot be made. The older Precambrian alkali basalts and dolerites which are intercalated within the Burnie and Oonah Formations have 2-4 % TiO_2 and very low Zr/Nb values, indicative of alkaline compositions. This is further supported by their elevated Ti/V values in the FeO*/MgO vs Ti/V discrimination diagram (Figure 4.29).

The tholeiitic MORB-type affinity of the Bowry Formation amphibolites is consistent with that of the "eastern" Ahrberg Group and the other Neoproterozoic rift sequences in northwestern Tasmania. However, the intercalation of the thin (15 – 40 m) but laterally extensive sill-like 777±7 Ma granitoid (Turner *et al.* 1998) within the westernmost Bowry Formation implies that at least part of the sequence cannot be correlated with the widespread Neoproterozoic sequences. Further to this, the presence of relict blueschist metamorphic assemblages within parts of the Bowry Formation is in contrast to the upper greenschist facies metamorphic grade of the "eastern" Ahrberg Group, and suggests that parts of the Bowry Formation are allochthonous.

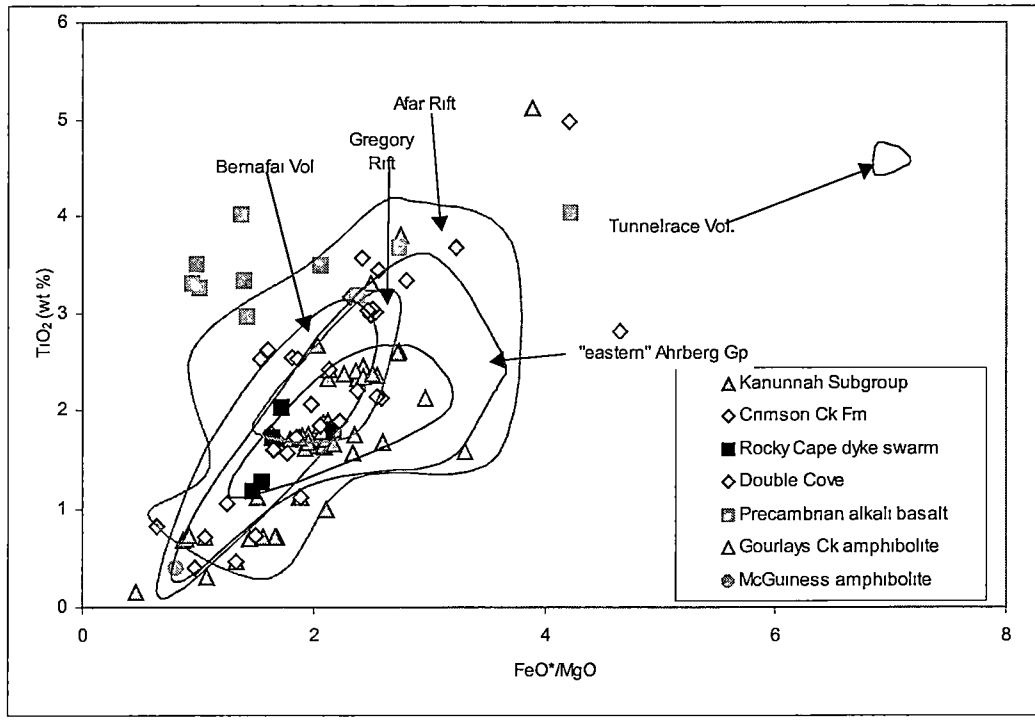

Figure 4.27. FeO*/MgO vs TiO_2 variation diagram after Miyashiro & Shido (1975). The spatially separate Neoproterozoic rift sequences display consistent tholeiitic fractionation trends, with local variation. The older Precambrian alkali basalts plot on a distinct trend. The sources for the various data are. Rocky Cape dyke swarm and Double Cove (Crawford & Berry 1992), Kanunnah Subgroup and Crimson Ck Formation (Crawford unpubl., Brown 1986 and unpubl.), Oonah Fm metabasalts from Gourlays Ck prospect (Norris 1985), Precambrian alkali basalt (Crawford & Berry 1992, Turner *et al.* 1998). Compositional fields are also shown for representative lava suites from the Gregory (Baker *et al.* 1977) and Afar (Deniel *et al.* 1994) Rifts in eastern Africa.

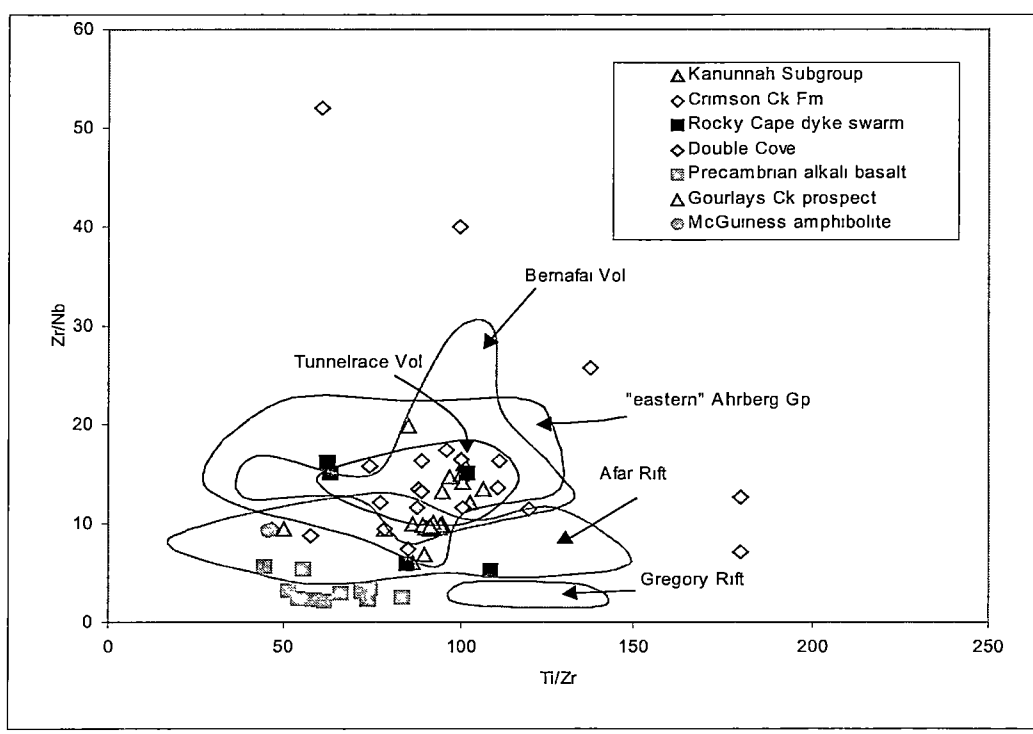

Figure 4.28 Ti/Zr vs Zr/Nb variation diagram for northwest Tasmanian mafic igneous rocks. The Ti/Zr levels and Zr/Nb levels are consistent for the different units, indicating transitional to E-MORB and minor N-MORB and D-MORB affinities. Data source as for Figure 4 34. Several Crimson Ck Fm analyses from Brown (1986) have elevated TiO_2 and depleted Nb. Compositional fields are also shown for representative lava suites from the Gregory (Baker *et al.* 1977) and Afar (Deniel *et al.* 1994) Rifts in eastern Africa

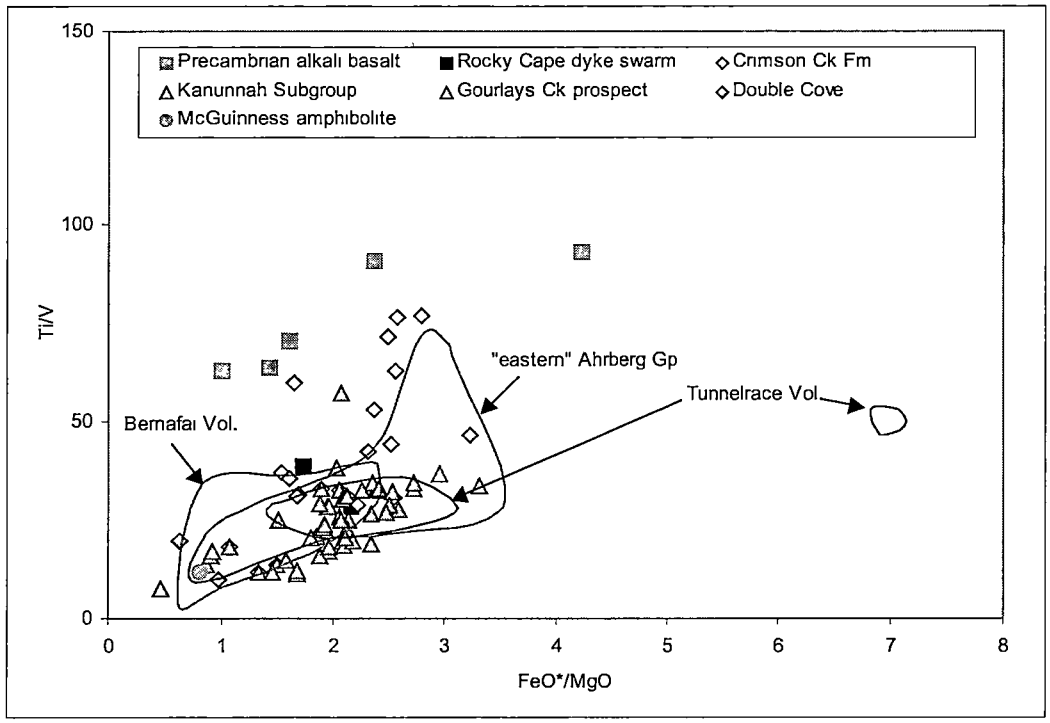

Figure 4.29. FeO*/MgO vs Ti/V variation diagram. The elevated Ti/V levels supports the alkaline affinity interpretation of the Precambrian basalts such as the Cooee Dolerite, Montana Melaphyre and Sulphur Ck pillow basalts. Notably the Crimson Ck Fm, "eastern" Ahrberg Group and Kanunnah Subgroup all have a similar range of FeO*/MgO and Ti/V levels.

Figure 4.30(a). Granitoid sill interpreted to be intruding into metabasalt and mafic schist, Owen Meredith River. The granitoid margins are parallel to the bedding and the deformational layering. (348100 mE, 5381995 mN).

Figure 4.30(b). Irregular, bedding parallel boundary between the granitoid 'intrusive' and the mafic metasedimentary schist in the Owen Meredith River. The metasediment is the pale green recessive layering, dominant towards the top. Granitoid material is pale orange, prominent layers towards the base. (348100 mE, 5381995 mN).

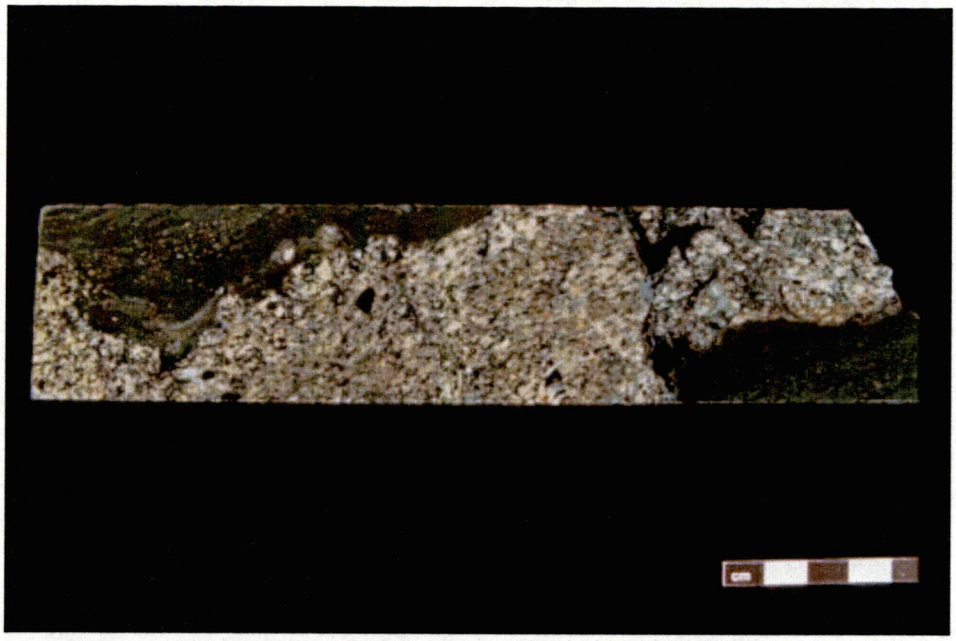

Figure 4.31(a). Photograph of granitoid-mafic schist contact in drill core. The granitoid is very weakly foliated, sub-parallel to the lithological contact and schistosity in the mafic schist. Core section 56.5-56.75m Rocky River DDH3.

Figure 4.31(b). Photomicrograph of RRDDH3 62.7 m. Granitoid/mafic schist contact, showing no evidence of chilled margins. Boundary is irregular, but parallels the dominant schistosity, which is defined by chlorite and mica blades, and syn-tectonic albite porphyroblasts (plane polarised light). Field of view 8.4 mm by 6.4 mm.

4.5.2 Relationship between mafic and felsic igneous rocks

Due to the Cambrian high strain deformation, metamorphic overprint and associated recrystallisation of the Bowry Formation, the contact relationship between the granitoid and surrounding metasedimentary schists and amphibolites is not clear. The margins of the granitoid are irregular, however over a strike length of several metres the contact is roughly planar (Figure 4.30(a) and (b)). In cases where the granitoid is in contact with amphibolite, there is no clear evidence of chilled margins within either rock-type. The amphibolite bodies are typically boudinaged, as a result of competency contrast during the subsequent deformational events. Where the granitoid is in contact with metasediment, there is also no clear evidence of chilled margins, however changes in the texture of the metasediments are evident. These may be a reflection of the competency contrast of the granitoid in comparison to the surrounding chlorite schists. The $Ca S_1$ and $Ca S_2$ schistosities typically parallel the contact between granitoid and metasediment, indicative of the isoclinal folding and associated layer parallel fabrics which characterise the $Ca D_1$ and $Ca D_2$ events (Figure 4.31(a) and (b)).

Based on structural evidence, a south-directed transport is considered to have prevailed in the region of the Arthur Lineament during the Cambrian Tyennan Orogeny (Chapter 2). Applying this interpretation to the Bowry Formation, it can be suggested the unit originated to the north of its current position, and may have a spatial relationship to King Island. As there are several Neoproterozoic intrusive and extrusive mafic suites on King Island a possible correlation between these lithologies on King Island and within the Arthur Lineament is considered below.

4.5.3 Geological setting on King Island, and its relationship to northwestern Tasmania

King Island, located to the north of northwestern Tasmania, consists of several sedimentary sequences and igneous suites, of different ages (Cox; Brown; and Turner in Burrett & Martin 1989) (Figure 4.32). Previous workers (Gresham 1972, Jennings & Cox 1978) showed that King Island is underlain by rocks and of Precambrian age. These consist of amphibolites, quartzose and minor mafic metasediments, deposited pre-760 Ma, and intruded by the 760±12 Ma granitoid

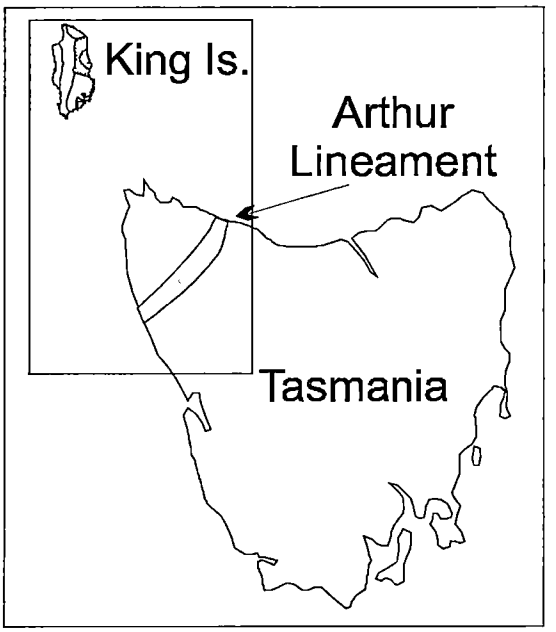

Figure 4.32. Regional map showing location of King Island relative to NW Tas.

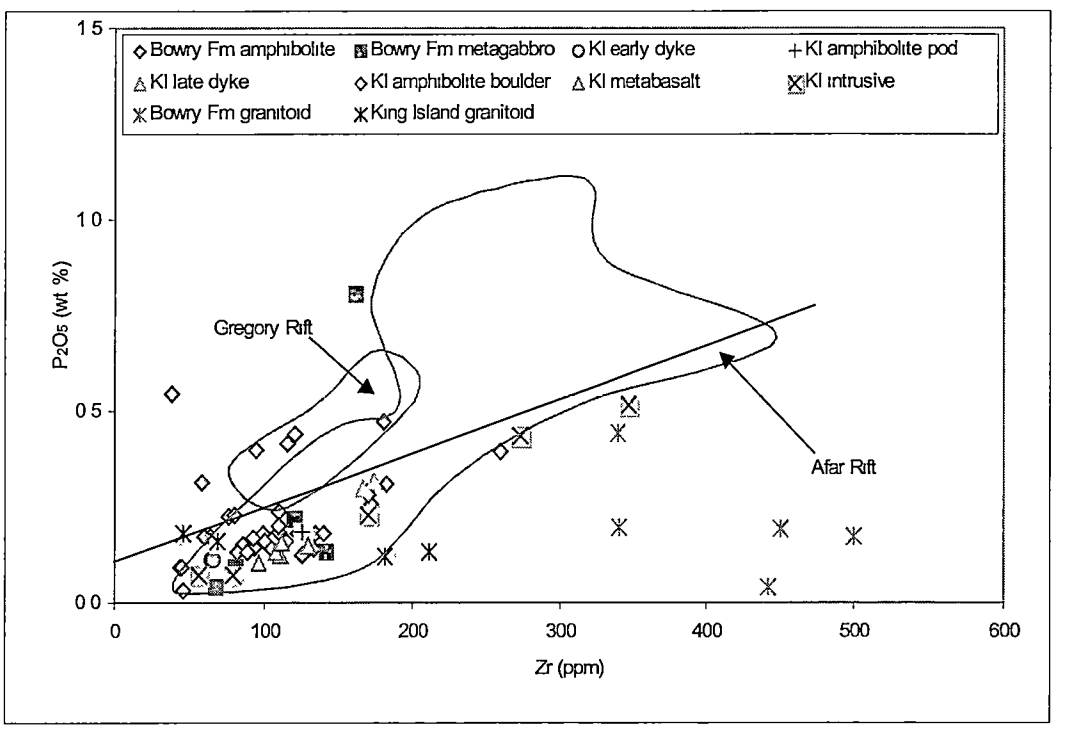

Figure 4.33. P_2O_5 vs Zr discrimination diagram after Winchester & Floyd (1976). Analyses are from this work, Blackney (1982) and Turner *et al.* (1998). Compositional fields are also shown for representative lava suites from the Gregory (Baker *et al.* 1977) and Afar (Deniel *et al.* 1994) Rifts in eastern Africa.

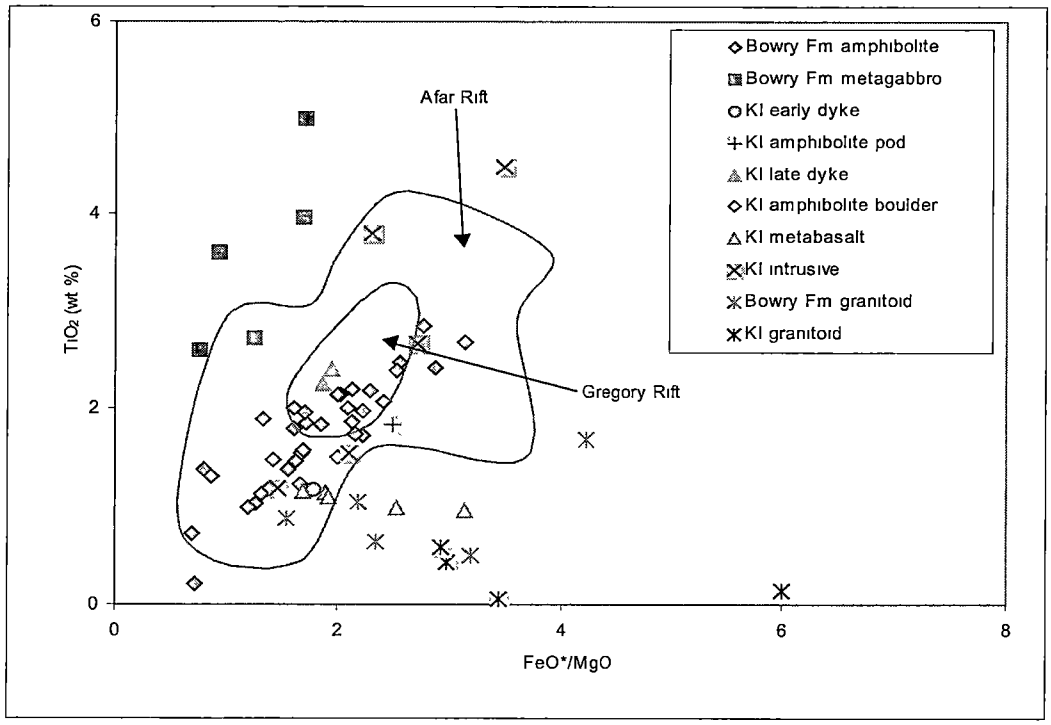

Figure 4.34(a). FeO*/MgO vs TiO_2 variation diagram after Miyashiro & Shido (1975). Compositional fields are also shown for representative lava suites from the Gregory (Baker *et al.* 1977) and Afar (Deniel *et al.* 1994) Rifts in eastern Africa.

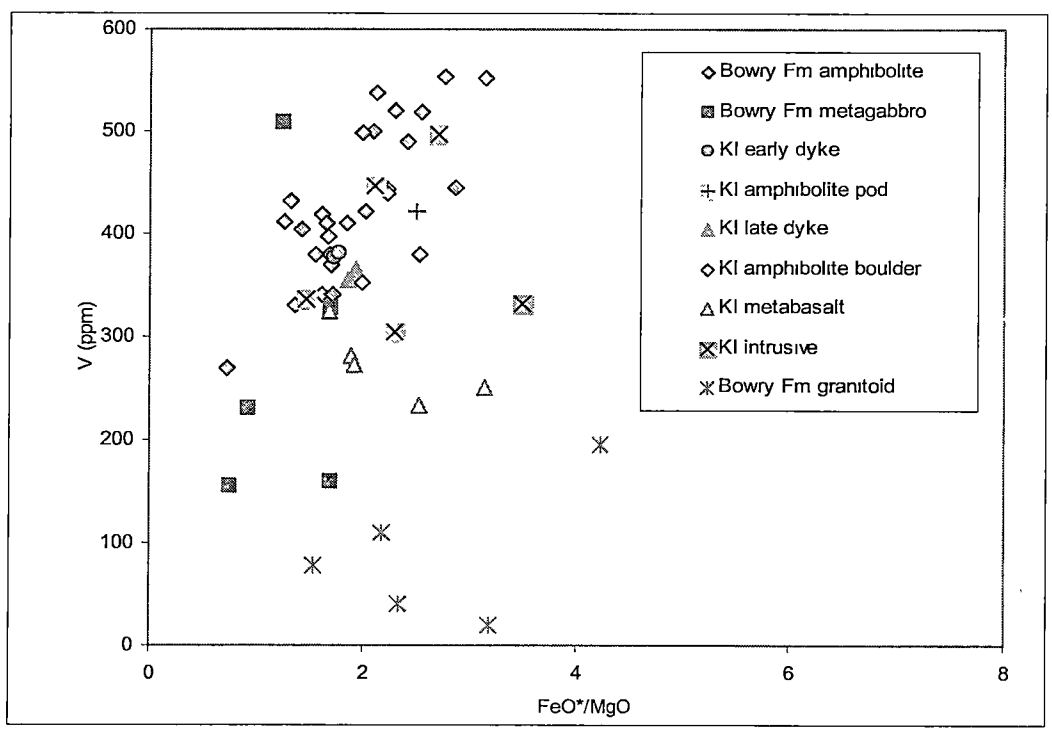

Figure 4.34(b). FeO*/MgO vs V variation diagram after Miyashiro & Shido (1975).

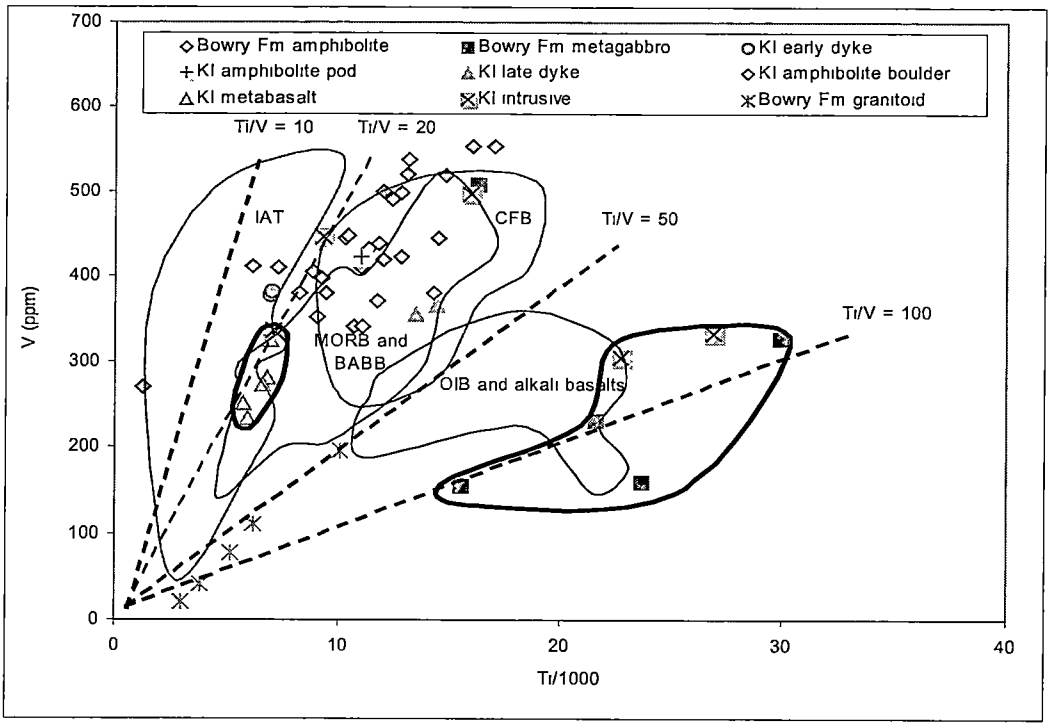

Figure 4.35. Ti/1000 vs V discrimination diagram after Shervais (1982). The King Island metabasalt samples lie on the same trend as the Bowry Fm amphibolites, whereas several King Island intrusives have similar Ti/V levels to the Bowry Fm metagabbros.

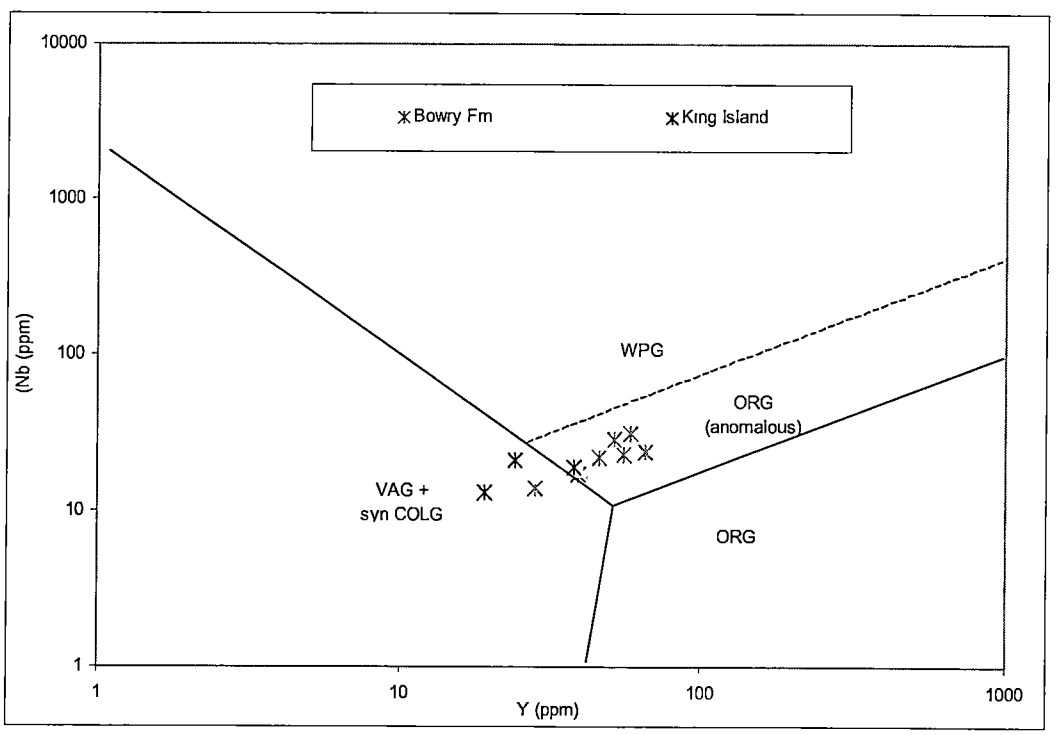

Figure 4.36. Nb vs Y discrimination diagram for granites after Pearce *et al.* (1984), showing the fields of volcanic-arc granites (VAG), syn-collisional granites (syn-COLG), within-plate granites (WPG) and ocean-ridge granites (ORG). The broken line is the field boundary for ORG from anomalous ridges.

bodies described by Cox (1973) at Cape Wickham in the north, and in the southwest of King Island (McDougall & Leggo 1965, Gresham 1972, Cox 1973, Blackney 1982, Turner *et al.* 1998). This metasedimentary sequence is laterally extensive, and also outcrops in the southwest (Blackney 1982). The southeastern part of King Island contains correlates of the Late Neoproterozoic rift sequence, evident throughout northwestern Tasmania (Brown in Burrett & Martin 1989). Several Devonian granitoids intrude the underlying Precambrian and Neoproterozoic lithologies (Turner in Burrett & Martin 1989).

The extrusive mafic igneous sequence which is intercalated with the older, Precambrian metasedimentary sequence in the southwest of King Island has tholeiitic affinities (Blackney 1982). The extrusive and intrusive mafic igneous rocks plot in the tholeiitic affinities field in the P_2O_5 vs Zr discrimination diagram (Figure 4.33), although they do not show an increase of immobile elements such as TiO_2 and V relative to FeO*/MgO (Figure 4.34(a) and (b)). However, the samples do plot on a similar trend to the Bowry Formation amphibolites in the Ti/1000 vs V discrimination diagram with Ti/V values of ~25 (Figure 4.35). The metasedimentary lithologies, which are conformable with the tholeiitic metabasalts (Blackney 1982) have been shown to have undergone amphibolite grade metamorphism at ~1270 Ma (Holm *et al.* 2001, see Chapter 3), followed by further deformation and metamorphism contemporaneous with the granitoid intrusion at ~780 Ma (Cox 1973, Blackney 1982, Turner *et al.* 1998).

As discussed, the granitoid bodies within the Bowry Formation of the Arthur Metamorphic Complex, and at Cape Wickham on King Island, have very similar emplacement ages (777±7 Ma and 760±12 Ma respectively). In addition, comparison of the Bowry Formation and Cape Wickham granitoids indicates they have similar chemical affinities, as demonstrated in the Y vs Nb discrimination diagram (Figure 4.36). The two groups overlap, lying close to the triple point formed by the WPG (within plate granite), anomalous ORG (ocean ridge granite) and VAG/syn-COLG (volcanic arc granite and syn-collisional granite) fields. This similarity is supported in the chondrite normalised element variation diagram (Figure 4.37).

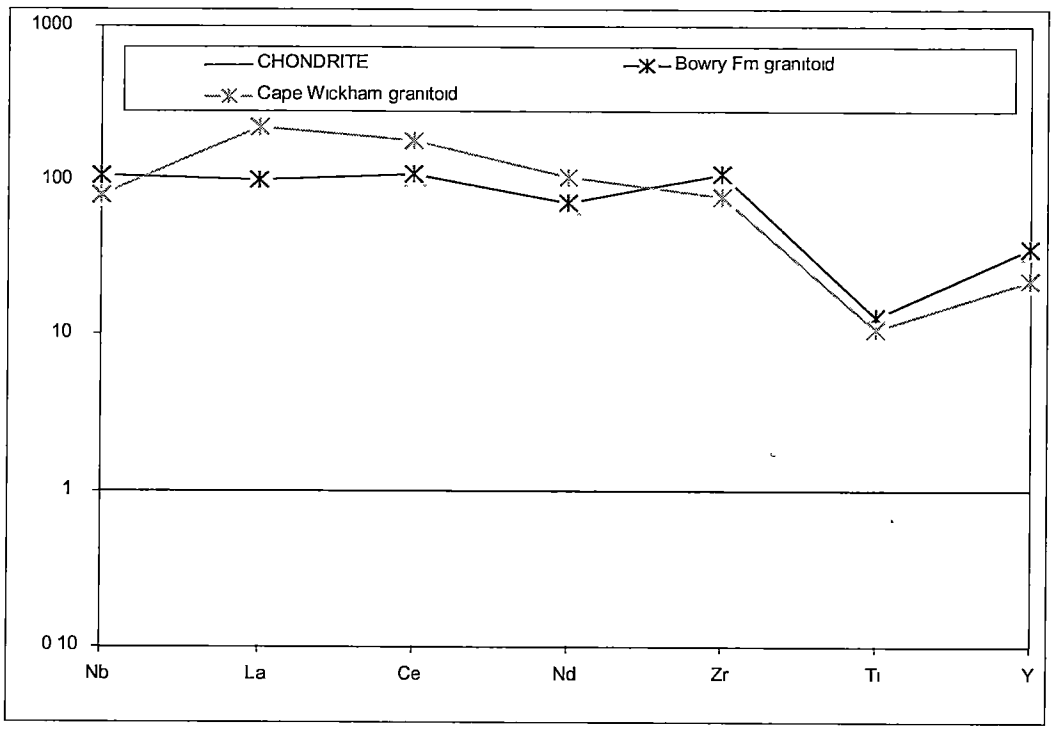

Figure 4.37. Chondrite normalised rare earth element variation diagram. The granitoid from the Bowry Fm displays similar trace element abundances to the Cape Wickham granite from King Island. Normalising values from Sun & McDonough (1989).

Therefore, several alternative correlations can be proposed:

- Considering the geochemical similarities between the Bowry Formation and King Island metabasalts and granitoids, together with the 1270 Ma metamorphic age on King Island, a correlation between the two sequences implies that parts of the Bowry Formation were deposited prior to 1270 Ma. On the basis of this correlation, these parts of the Bowry Formation cannot be related to the "eastern" Ahrberg Group and other Neoproterozoic rift lithologies in northwestern Tasmania. They represent an earlier phase of crustal extension and ocean development.

- Alternatively, another possible correlation can be made between the Bowry Formation and the late stage mafics of the ~800 Ma Willouran basic province in South Australia. This rift sequence consists of intrusive suites and volcanics with CFB, transitional and N-MORB affinities (Gairdner Dyke Swarm, Amata Suite and Wooltana Metabasalt) (Crawford & Hilyard 1990, Zhao & McCulloch 1993). The Willouran basic province was suggested to have occurred as a result of an 800 km-radius asthenospheric mantle plume, which was centred at the triple junction of an aulacogen (von der Borsch 1980, Zhao *et al.* 1994). Further to this, it was interpreted to have been located within the circumference of the mantle plume (Zhao *et al.* 1994). According to Keen (1985), an 800 km-radius plume is capable of resulting in uplift and subsidence over an area with a diameter of approximately 8000 km (Keen 1985, in Zhao *et al.* 1994). Zhao *et al.* (1994) suggested the Rook Tuff (802±10 Ma), which occurs towards the base of the Adelaidean sediments, immediately above the sequence containing the Willouran Volcanics, may be due to the rift-related magmatism. In addition, a rhyolite within the Boucaut Volcanics (777±7 Ma) (southwest of Broken Hill) is known to occur (Fanning *et al.* 1986, Preiss 2000). The Boucaut Volcanics, which are bimodal, include mafic volcanics intercalated with clastic sediments, and have been suggested to present the onset of rifting (Preiss 2000). Considering these findings, the plume located beneath the Willouran basic province may have been capable of causing uplift and magmatism (both mafic and felsic) in areas further to the southeast (such as near northwestern Tasmania).

On the above evidence, the Bowry Formation mafics and the intercalated 777±7 Ma intrusive granitoid may be a correlate of the mafic intrusives and the 760±12 Ma intrusive granitoid on King Island. On this basis, parts the Bowry Formation mafics that might correlate with the mafics on King Island must be older than the metamorphic age of 1200 Ma. However, no evidence of metamorphism that can be attributed to deformation prior to the Cambrian event was observed in the Bowry Formation. Therefore, the felsic igneous rocks on King Island and within the Bowry Formation are considered to be correlates, but the mafic units are interpreted to be unrelated.

Thus the mafic igneous rocks within the Bowry Formation are interpreted to be related to the major thermal episode and the associated ~800 Ma rifting event in central-south Australia. The Bowry Formation mafics are therefore correlated with the late stage, most evolved basalts that occur in the Willouran basic province. The granitoids on King Island and in the Bowry Formation are interpreted to have resulted from crustal melting due to the extensive heating of the mantle plume, and intruded the mafic units (in the Bowry Formation) and pre-1270 Ma metasediments and metabasalts (on King Island).

CHAPTER 5

TECTONIC IMPLICATIONS AND CONCLUSIONS

5.1 Summary of the Proterozoic and Cambrian Geological History of Northwestern Tasmania

Northwestern Tasmania and King Island underwent several changes in tectonic setting during the Proterozoic. Prior to 1270 Ma, on King Island, a passive margin to early rift setting, with transitional tholeiites existed, as is indicated by the deposition of marine sediments and the extrusion of minor sub-alkaline tholeiitic basalts (Blackney 1982)(Figure 5.1). A change in tectonic regime occurred at *ca.* 1270 Ma, possibly contemporaneous with an early phase of the Grenville Orogeny. This resulted in metamorphism of these sediments and basalts to lower amphibolite grade. This was the D_1 event in this region. Subsequent to this event, a relatively quiescent period is interpreted to have ensued until the Middle Neoproterozoic.

In the Middle Neoproterozoic, Rodinia was located to the north of Tasmania. Northwest Tasmania was in a passive margin setting, with the turbidite sequences of the Burnie and Oonah Formations being deposited to the east (seaward) of the continental shelf facies of the Rocky Cape Group and correlates (Figure 5.2). The exact age of these units and their temporal relationship is uncertain. However, they are interpreted to be contemporaneous (Spry 1962, 1964)(Figure 5.1). During deposition of the Burnie and Oonah Formations, minor alkaline intrusives (Cooee Dolerite, Montana Melaphyre) and extrusives (Sulphur Ck pillow basalts) were emplaced, indicative of an intraplate setting (Crawford & Berry 1992). Minor granitoid, dated at around 780 Ma (Turner *et al.* 1998), intruded into the basaltic sequence of the Bowry Formation, possibly as a result of the same thermal event that produced the mafic magmatism. This may be linked to the Wickham Orogeny, on King Island, which occurred from 760-780 Ma (Figure 5.1). It is represented by granitoid intrusion, with localised contact metamorphism and structural deformation. Regional, minor uplift may have also occurred as part of this event.

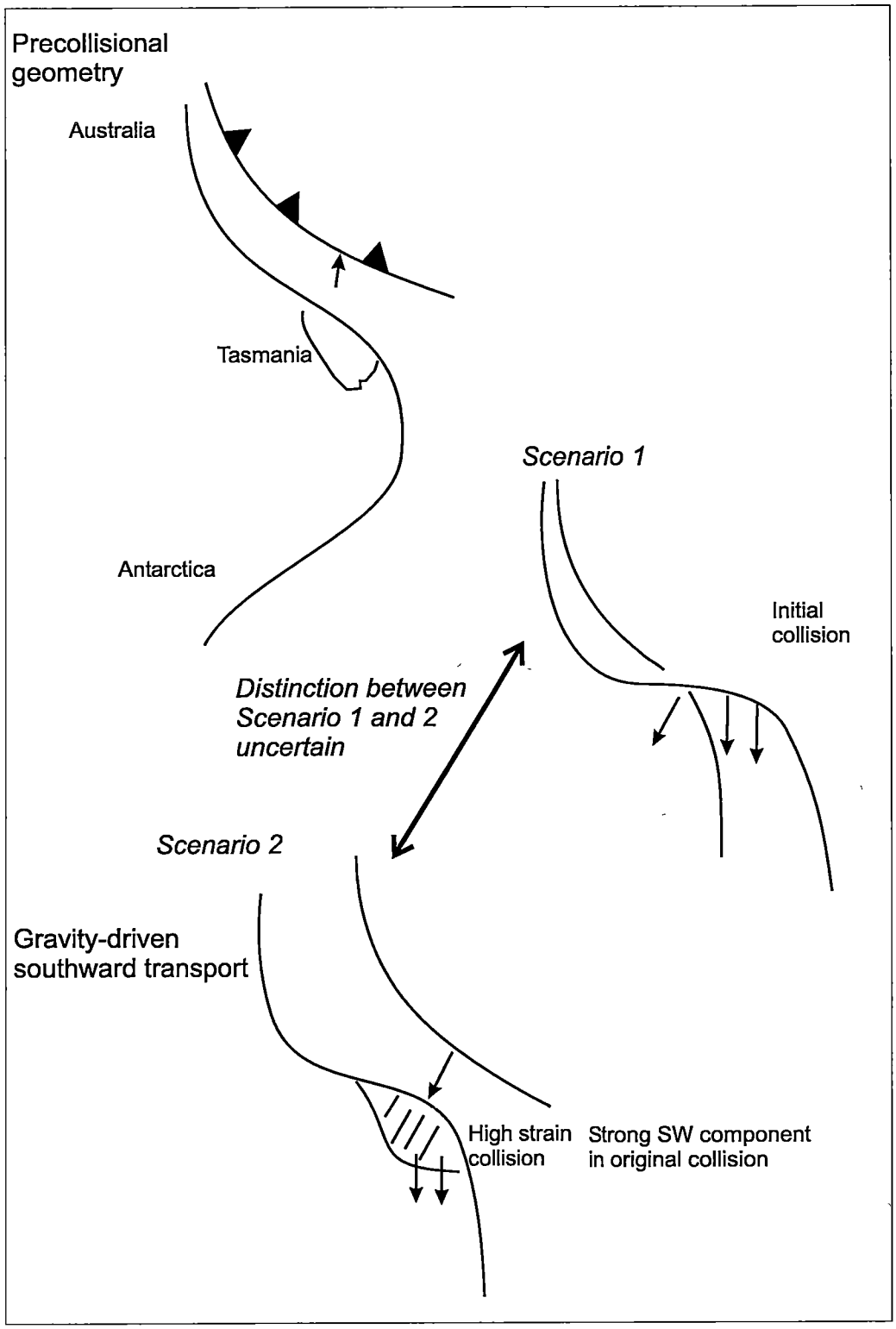

Figure 5.3. Schematic reconstruction of Cambrian arc-continent collisional event (from Meffre et al. 2000). West-directed initial transport (Berry & Crawford 1988) is interpreted to have had a localised gravity-driven southerly direction.

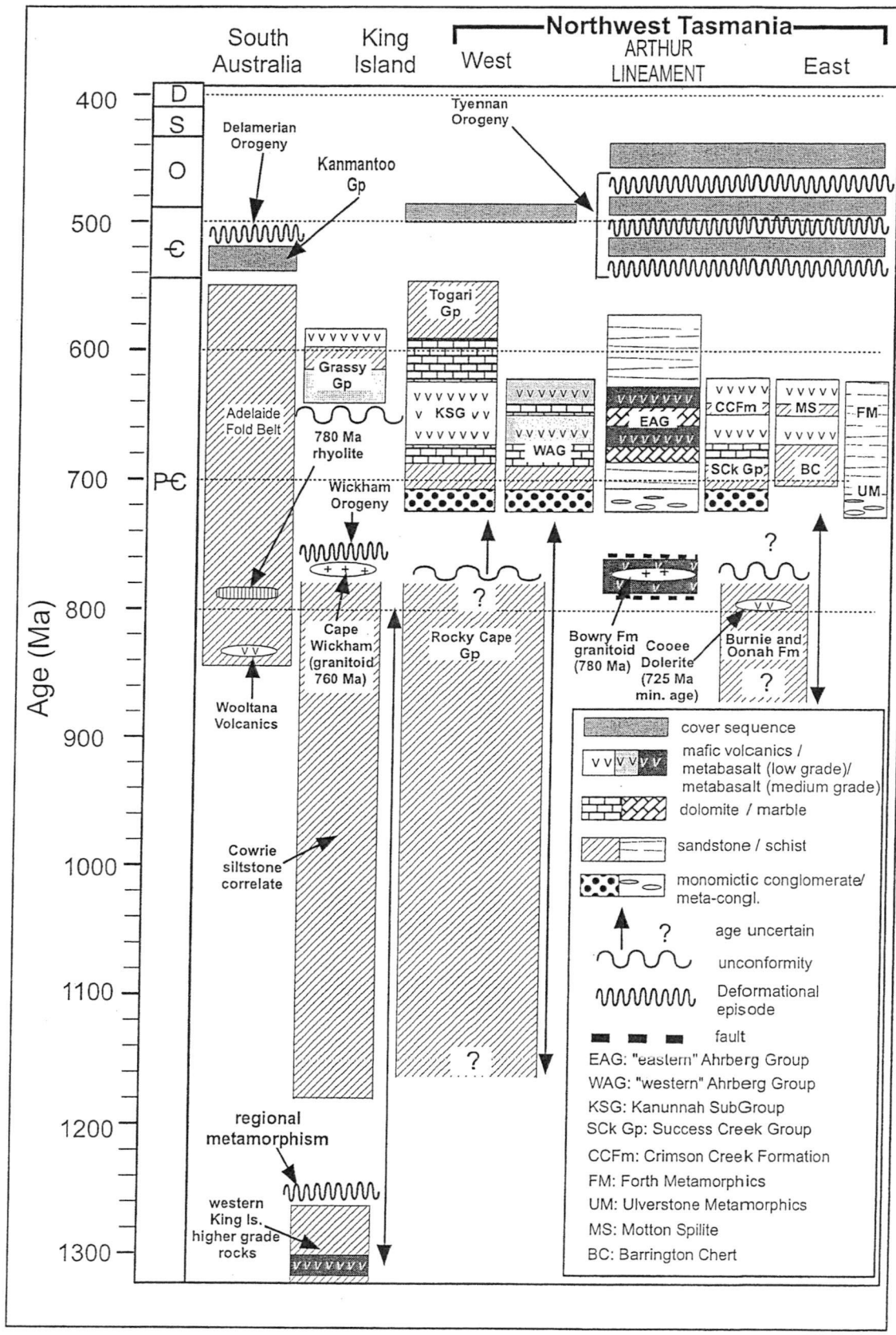

Figure 5.1. Space-time diagram displaying the contemporaneous rock packages in northwestern Tasmania, King Island and South Australia (modified from Calver & Walter 2000).

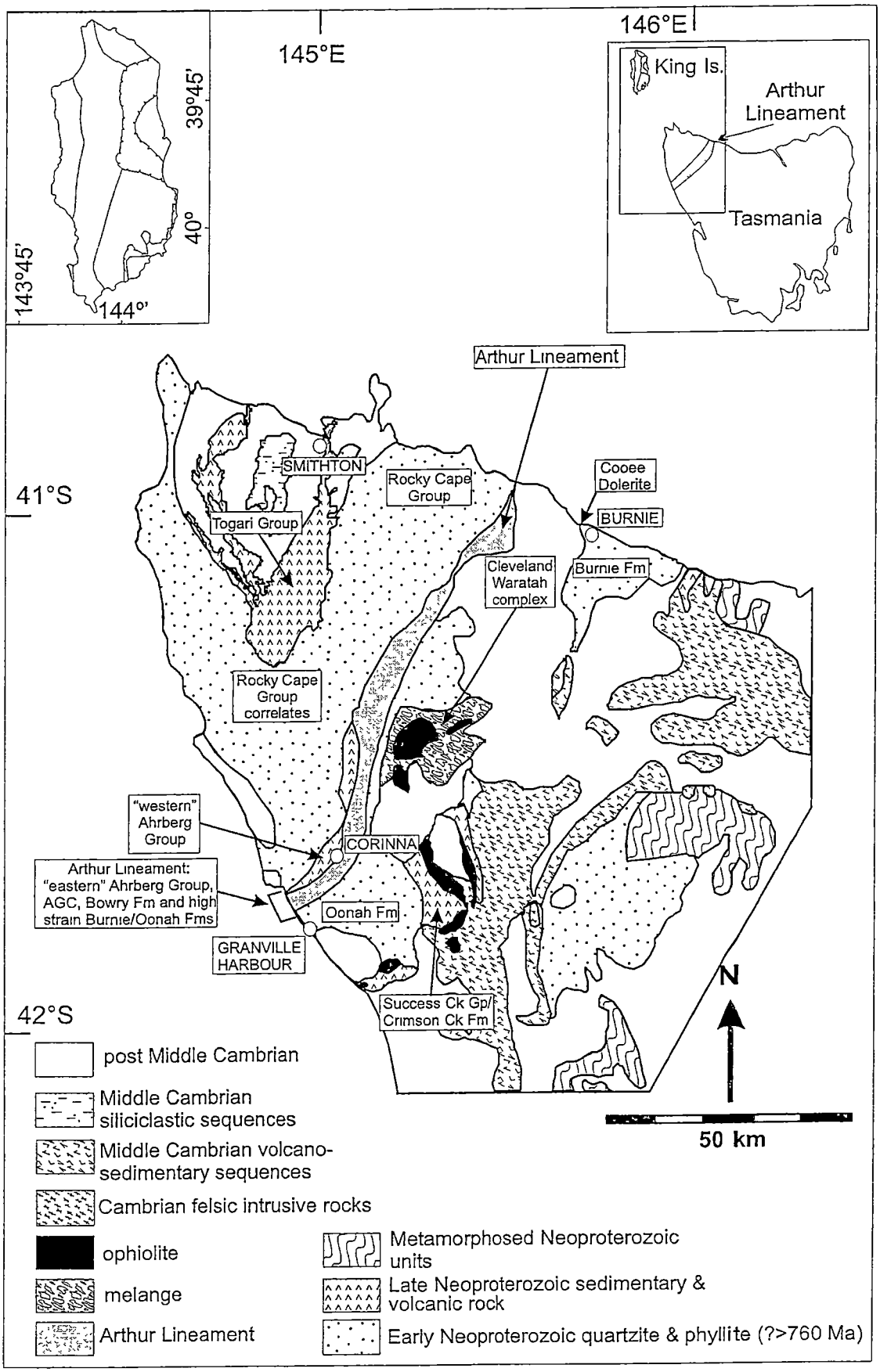

Figure 5.2. Setting of the Arthur Lineament, NW Tasmania (modified after Brown *et al.* 1995). The Arthur Lineament consists of the high strain (metamorphosed) Burnie and Oonah Formations, the "eastern" Ahrberg Group, the Bowry Formation, and the AGC.

Subsequent to the Wickham Orogeny, widespread continental rifting developed in the Late Neoproterozoic, between 750 and 580 Ma (Calver & Walter 2000), however 650 Ma is interpreted to be the likely maximum age (Calver 1998). The rift succession is widespread. The Togari Group, Ahrberg Group and Success Creek Group-Crimson Creek Formation are interpreted to be correlates, representative of the rift succession (Figure 5.1). The basal unit of the Late Neoproterozoic rift succession unconformably overlies the Rocky Cape Group at a low angle. The tholeiitic rift basalt-dominated sequence in the upper Togari Group (the Kanunnah Subgroup) has a preferred age of 650 to 600 Ma (Crawford 1992, Calver & Walter 2000). The basalts display a progression in their chemical affinities, ranging from transitional tholeiites (early) to E-MORB (late) (refer to Chapter 4). This Late Neoproterozoic rifting event, widely represented in western and northwestern Tasmania, produced voluminous rift-related basalts, interlayered with associated volcanic-derived sediments, conglomerates, sandstones, siltstones and carbonates. It is assumed to have led to the opening of an ocean basin around 600 to 580 Ma.

In the Cambrian, a major change in tectonic regime occurred (Figure 5.3). The aborted subduction of the Late Neoproterozoic passive margin, in an arc-continent collision, occurred as part of the 510±10 Ma Tyennan Orogeny, and was followed by exhumation and post-collisional re-equilibration (Berry & Crawford 1988, Crawford & Berry 1992, Turner *et al.* 1998). Associated with this crustal collision, emplacement of ultramafic-bearing allochthons occurred. In addition, multiple deformations and widespread metamorphism ranging in grade from greenschist to blueschist, and eclogite facies accompanied the orogenic event. In northwestern Tasmania, the Tyennan Orogeny also produced the high strain zone of the Arthur Lineament.

Subsequent to the Tyennan Orogeny, mild deformation accompanied granitoid intrusion in the Tabberabberan Orogeny of the Middle Devonian. In northwestern Tasmania, the folding associated with granitoid intrusion was mostly open folds with shallow plunges and sub-vertical axial planes.

5.2 Discussion

5.2.1 Overview of the geochronology and tectonostratigraphy of northwestern Tasmania

Interpretations of numerous events in the geological history of northwestern Tasmania and King Island have been contentious, and subject to ongoing revision for some time. Stratigraphic relationships, as well as the timing and significance of the different deformational events, have been the main aspects debated.

Spry (1962) suggested that the more intensely deformed and metamorphosed rocks in Tasmania belonged to an older stratigraphic unit, and had undergone a major deformational event (the Frenchman Orogeny) prior to deposition of the relatively undeformed, unmetamorphosed rocks. The older deformed sequence included the rocks of the Arthur Lineament (then known as the Whyte Schist), the Tyennan and Forth regions, and various other inliers (Turner 1989). The Penguin Movement (later called the Penguin Orogeny: Gee 1967a) was interpreted to have been a younger deformational event, in the Rocky Cape and Jubilee regions (Spry 1962).

The above interpretation was revised over time (Gee 1967a, Turner 1979, 1984, 1989), with the metamorphic terrains (including the Arthur Lineament) proposed to be part of the Penguin Orogeny, not basement (Turner 1989). The age of the Penguin Orogeny was also subject to revision. Spry (1962) and Gee (1977) suggested the minimum age of the Penguin Orogeny was defined by the intrusion of the Cooee Dolerite. Gee (1977) interpreted this dolerite as syn-deformational, whereas Crook (1979) interpreted the intrusion to be syn-depositional, with dolerite intruding into wet sediments. The occurrence of pillow basalts compositionally identical to the Cooee Dolerite at the Sulphur Creek foreshore support Crook's (1979) interpretation (Crawford & Berry (1992).

Richards (*pers. comm.*), in Crook (1979), and Turner (1989), interpreted the deformation attributed to the Penguin Orogeny to have closely followed intrusion of the dolerite, at 725 ± 35 Ma. Maximum K-Ar detrital muscovite ages of 690 ± 10 Ma from the Burnie and Oonah Formations (Adams *et al.* 1985) were interpreted to represent the third deformational event of the Penguin Orogeny, as these were not

much younger than the hornblende/biotite ages from the Cooee Dolerite (Turner 1989). Turner (1989) also proposed that the intrusion of granitoids at Cape Wickham on King Island, at around 730 Ma was due to the Penguin Orogeny.

Further revision of the tectonostratigraphic history of Tasmania was undertaken by Turner (1993) and Berry (1994). They questioned the validity of the 725 ± 35 Ma age of the Cooee Dolerite. In addition, they questioned the age of the Penguin Orogeny, on the basis of multiple 510 ± 10 Ma U-Pb zircon and K-Ar hornblende ages obtained from various metamorphic complexes in western Tasmania (Turner 1993, Black 1994, Turner *et al.* 1994). Berry (1994) also speculated that the early deformation in the Rocky Cape Group and the Burnie Formation was related to the Cape Wickham granitoid intrusion on King Island.

Turner *et al.* (1998) reconsidered the tectonostratigraphic history of Tasmania, introducing the term Wickham Orogeny to encompass granitic magmatism and the D_1 deformation on King Island. Turner *et al.* (1998) also interpreted the later deformations that deform the granitoids to be related to the Wickham Orogeny. The age of the Arthur Lineament was revised by Turner *et al.* (1998), to 500 ± 10 Ma, on the basis of the K-Ar hornblende ages from amphibolites within the lineament. These authors attributed the deformation in the lineament to the Penguin Orogeny, thereby revising the age of the orogenic event to 500 ± 10 Ma. In addition, the authors showed that the deformation in the Tyennan region, previously thought to be a product of the Precambrian Frenchman Orogeny (Spry 1962), was due to the Cambrian event. The term Tyennan Orogeny, which was originally used to account for several Middle to Late Cambrian unconformities (Carey & Banks 1954, Brown 1989, Corbett & Turner 1989, Jago & Brown 1989) was found to overlap with the 500 ± 10 Ma metamorphic event of the Penguin Orogeny (Turner *et al.* 1998). On this basis, the unifying term Tyennan Orogeny has been used in this work to describe the Cambrian deformational event, and the Penguin Orogeny has been discarded.

The Tyennan Orogeny varied in its intensity in western Tasmania. The Franklin Metamorphic Complex in western Tasmania (Figure 5.4), experienced eclogite facies metamorphism, with temperatures and pressures of 730°C and 1500 to 1700 MPa (Kamperman 1984). The Port Davey Metamorphic Complex in southwest Tasmania

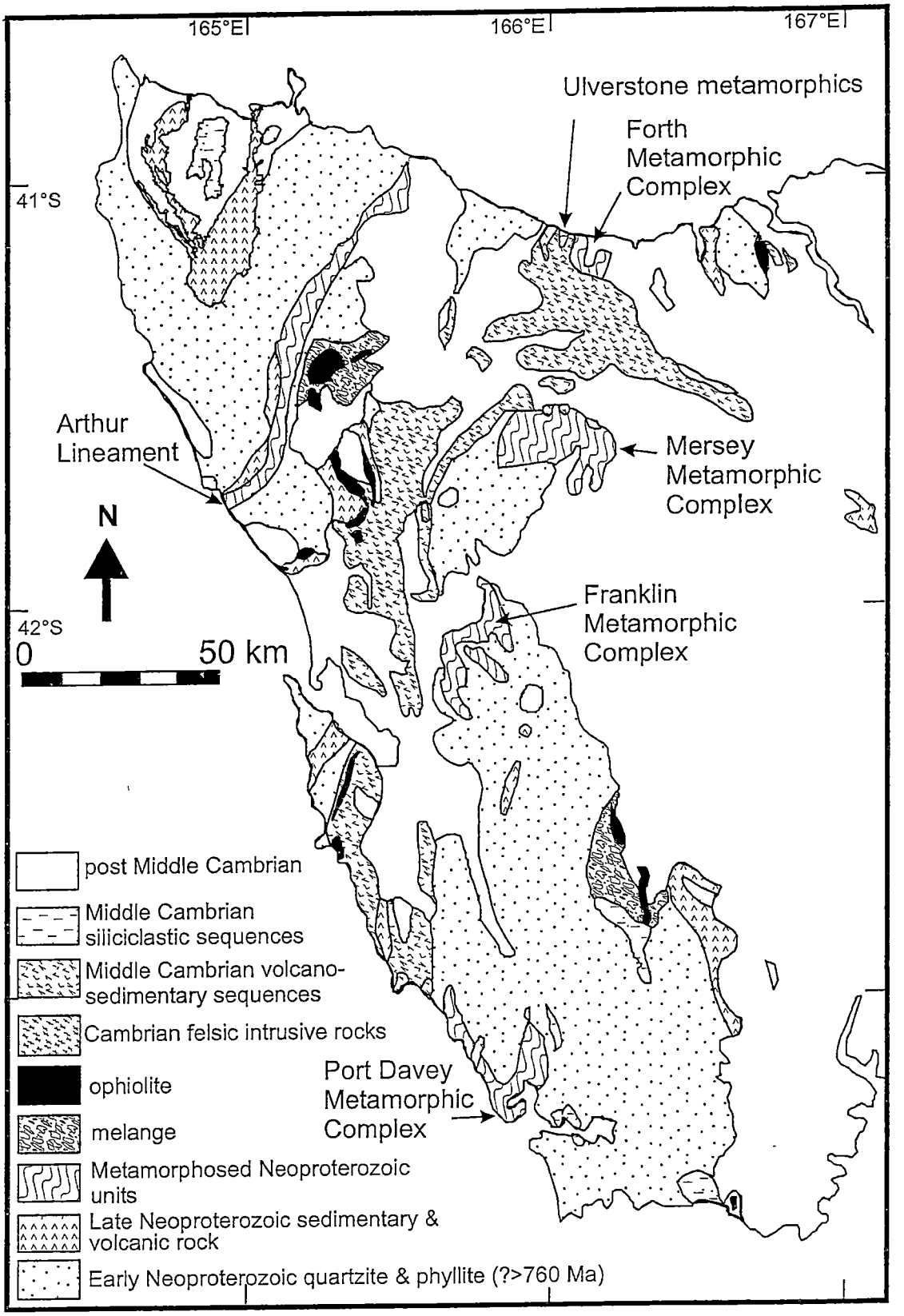

Figure 5.3. Cambrian metamorphic complexes and ultramafic slices related to the Cambrian arc-continent collision in western Tasmania. (From Meffre *et al.* 2000).

underwent metamorphism at 600°C and 750 MPa, whereas the Forth Metamorphic Complex experienced upper amphibolite facies conditions with 700-740°C at 1300-1500 MPa (Meffre *et al.* 2000, Lewis 1991) (Figure 5.4).

This work has provided further supporting evidence for Cambrian deformation being responsible for the Arthur Lineament, and the absence of any earlier major deformational events on the northwestern Tasmanian mainland. Based on the findings of the metamorphic geochronology component of this work, the ***Ca***D_2 event has been shown to be the most conducive event for monazite growth in and around the Arthur Lineament. This is interpreted to be a result of the higher temperatures associated with metamorphism, and the relatively high strain levels that coincided with this deformation. Metamorphic ages for samples from the lineament are consistent at around 540 Ma. This is older than other ages derived from the Arthur Lineament (Turner *et al.* 1998), and may be attributed to growth earlier in the ***Ca***D_2 event, or alternatively may be indicative of systematic errors as a result of calibration problems during analysis.

As a result of research undertaken as part this work (Chapter 3 and Berry *et al.* in prep), the D_1 event on King Island has been shown to have occurred at *ca.* 1270 Ma, and is not related to the Wickham Orogeny (*cf.* Turner *et al.* 1998). The D_2 to D_4 events of Cox (1973) are interpreted to be due to the *ca.* 760 Ma granitoid intrusion on King Island, as was previously suggested (Cox 1973, 1989).

5.2.2 Contentious issues of the Arthur Lineament and surrounding area

Other aspects of the tectonic evolution of northwestern Tasmania, and the Arthur Lineament in particular, have been subject to debate for many years. The main issues of contention are discussed below:

- The temporal relationships between the Rocky Cape Group and correlates, the Burnie and Oonah Formations, and the Ahrberg Group have been viewed differently by different workers. This work interprets the Burnie and Oonah Formations to represent the offshore equivalent of the Rocky Cape Group and

correlates, based on provenance research indicating similar sources for detrital material (refer to Chapter 1). This is in disagreement with the interpretation of Gee (1967a), Turner *et al.* (1992, 1998) and Turner & Bottrill (2001), who interpreted the basal units of the Togari and Ahrberg Groups as near-shore equivalents of the Burnie and Oonah Formations.

- The significance of the unconformity between the "western" Ahrberg and Togari Groups, and the Rocky Cape Group and correlates, has been debated by previous workers. The unconformity, which varies from <5° to 20° angular discordance, was observed at several locations in the study area. Turner *et al.* (1998) interpreted the unconformity to represent the Wickham Orogeny, accompanied by granitoid intrusion on King Island and in the Bowry Formation, and by the thick turbidite pile of the Burnie and Oonah Formations with the syn-depositional Cooee Dolerite and Sulphur Creek pillow basalts. Further to this these authors proposed the deposition of the basal units of the Ahrberg and Togari Groups was initiated by this instability and associated uplift.

  It is suggested in this work (refer to Section 1.6.1) that sedimentation of the Burnie and Oonah Formations and the Rocky Cape Group and correlates was a result of the Wickham Orogeny, as the detrital components of the two sequences are very similar. In contrast, the sedimentation of the lower Togari and Ahrberg Groups is interpreted to have been caused by instability due to the onset of Late Neoproterozoic rifting. This would have been contemporaneous with normal faulting, in which case deposition into a graben was likely to be accompanied by erosion of topographically upstanding blocks of Rocky Cape Group rocks. The juxtaposition of the Ahrberg and Togari Groups with different levels of the Rocky Cape Group (and correlates) stratigraphy may have occurred as a result of coincident erosion of the Rocky Cape Group during Togari Group deposition, as has been suggested by Everard *et al.* (2000). The angular unconformity between the Rocky Cape Group (and correlates) and the Ahrberg and Togari Groups might be attributed to compressional deformation. Alternatively, it may be due to uplift caused by the Wickham Orogeny, or it might also be the product of block rotation of hanging-wall strata above extensional faults. The irregular

distribution of the basal conglomerate, and the predominance of quartzite pebbles contained within the basal units, are consistent with basin compartmentalisation by normal faulting early during Ahrberg and Togari Group deposition (Everard *et al.* 2000).

- The geochemical (and temporal) relationship between the mafic meta-igneous rocks of the Bowry Formation, the "eastern" and "western" Ahrberg Groups, and the other mafic igneous rocks and volcanic sequences in Tasmania has previously not been conclusively resolved. The alkaline affinities of the Cooee Dolerite and Sulphur Creek pillow basalts (Crawford & Berry 1992) are taken here to indicate an intraplate setting at the time of magmatism. The mafic volcanics of the Ahrberg and Togari Groups have sub-alkaline affinities, indicative of an early rift setting (refer to Chapter 4). This conflicts with the interpretation of the Burnie and Oonah Formations, and the Ahrberg and Togari Groups as being contemporaneous.

  The Bowry Formation metabasalts are relatively evolved, with E-MORB to N-MORB affinities. However the Bowry Formation is interpreted to be allochthonous (based on metamorphic mineralogy and the *ca.* 780 Ma age of the granitoid). Therefore, the oceanic affinities of the mafic meta-igneous rocks in the Bowry Formation may reflect the tectonic setting and evolution of an older region, unrelated to the Late Neoproterozoic rift volcanics (Ahrberg and Togari Groups) in northwestern Tasmania.

- To the east of the Arthur Lineament, north of Savage River in the Waratah area, a possibly Lower Cambrian (Seymour & Calver 1995) presumably allochthonous oceanic-affinity succession is in structural contact with the Heazlewood River ultramafic complex (Brown 1989, Turner & Bottrill 2001). This sequence, which is informally known as the Cleveland-Waratah association (CWA), extends eastwards around an inlier of Oonah Formation correlate, near Mt Bischoff (Figure 5.2). Within the basal unit of the CWA, large rafts of material that are lithologically similar to the underlying correlate of the Oonah Formation have been reported (Brown 1989, Groves 1971, P. Williams 1989). Based on the

sedimentary relationship between the rafted blocks and the host sediments, Turner & Bottrill (2001) suggested that the two units have a common tectonic history, and that the Burnie and Oonah Formations (and correlates) are therefore also allochthonous.

Turner & Bottrill (2001) interpreted the entire assemblage (CWA and the Burnie and Oonah Formations and correlates) to be allochthonous and to have originated to the east. They proposed that these allochthonous units underwent west-directed transport, to in their present positions, away from their oceanic floor/turbidite slope-origins. This transport direction is in agreement with the west-directed transport of the mafic-ultramafic allochthons, as was suggested by Berry & Crawford (1988). Although Turner & Bottrill (2001) observed a map scale, overturned fold limb in the Burnie Formation, to the east of the Arthur Lineament's boundary on the north coast (Gee 1977), they were unable to find evidence to support west-directed transport. Gee (1977) interpreted this overturned belt of Burnie Formation to indicate north-northeast directed transport.

The findings of this study suggest in the vicinity of the Arthur Lineament, the transport direction differed from the orientation recorded for the mafic-ultramafic allochthons. On the north coast in the Somerset-Doctors Rocks area, approaching the lineament's eastern boundary, the $\boldsymbol{Ca}D_1$ and $\boldsymbol{Ca}D_2$ events increase in intensity. Accompanying the increase in intensity, $\boldsymbol{Ca}F_1$, $\boldsymbol{Ca}F_2$ and the associated axial planar cleavages change in orientation. Away from the lineament, the fold axes plunge gently to the east and west, and the axial planes dip gently to the south. Close to the boundary, and within the lineament the fold axes plunge gently to the south, and the axial planes dip gently to the southeast. This change in orientation is attributed to rotation due to increasing strain, and implies a north over south transport. In addition, in the south of the Arthur Lineament, stretching lineations that developed during the event plunge gently to the south, also suggesting north-south (as opposed to east-west) transport.

- Turner & Bottrill (2001) noted the development of two foliations in units of the Arthur Lineament, and the development of one of the foliations in the "western" Ahrberg Group. However, in contrast to the findings of this work, they proposed that the main schistosity in the lineament, and the well developed cleavage in the "western" Ahrberg Group, to be the earliest generation cleavage (***Ca***S_1), with the second generation foliation (***Ca***S_2) occurring as an intermittent crenulation cleavage. This work has found the dominant foliation in the lineament to be the ***Ca***S_2 foliation (refer to Chapter 2). Furthermore, this work found the ***Ca***S_1 foliation to have little expression in the "western" Ahrberg Group, and attributes the main foliation related to the deformation in the lineament (in the "western" Ahrberg Group), to the ***Ca***D_2 event. To the east of the lineament structural deformation attributed to the Tyennan Orogeny is well developed, and weakens in intensity over several kilometres away from the lineament's boundary. However the precise metamorphic grade at the lineament's boundary is not clear. At the western boundary of the lineament, deformation attributed to the ***Ca***D_1 and ***Ca***D_2 events dissipates abruptly. ***Ca***D_2 folding and the associated cleavage is developed up to 2.5 km to the west of the lineament, whereas ***Ca***D_1 is poorly represented. ***Ca***F_1 folds were not observed, and ***Ca***S_1 is only very weakly developed.

- Turner & Bottrill (2001) noted refolding of compositional layering, layering-parallel boudinaged quartz veins, and an early schistosity (***Ca***S_1). Based on convergence of the compositional layering, boudinaged quartz veins and the two foliations (***Ca***S_1 and ***Ca***S_2) on the limbs of second generation folds (***Ca***F_2), Turner & Bottrill (2001) interpreted the north-northeast strike and steep east-dipping orientation of ***Ca***S_2 to be its original orientation. However, these authors also suggested that the allochthonous Bowry Formation was emplaced as a sub-horizontal sheet. This work has found that the predominantly sub-parallel orientation of the two foliations (***Ca***S_1 and ***Ca***S_2) implies a consistent attitude of folding prevailed during both the ***Ca***D_1 and ***Ca***D_2 events. Therefore, as thin, laterally extensive sheets of material that are extruded from the subducted wedge in blueschist-forming, subduction-related tectonic settings are typically emplaced

as sub-horizontal nappes, the suggestion of Turner & Bottrill (2001) that the steep east-dip of $\boldsymbol{Ca}S_2$ is its original orientation is improbable.

- Gee (1967a, 1977, 1989) interpreted the lineament to have formed as a result of east-directed transport that produced east-verging, overturned folds and thrusts to the west of the northern Arthur Lineament. Furthermore, he suggested that the Rocky Cape Group and the Burnie Formation were transported to the southeast and deformed against the Precambrian Tyennan block. This east-directed folding and thrusting was reported by Everard *et al.* (1996) in the Trowutta area, who noted that the event controlled the attitude of the schistosity and lineament boundaries. I have shown here that this event is the third deformational event to have occurred in the Cambrian ($\boldsymbol{Ca}D_3$ in this work). Although $\boldsymbol{Ca}D_3$ is not responsible for the high strain deformation evident in the lineament, it has caused the steep east dip of the compositional layering and earlier foliations. The $\boldsymbol{Ca}D_3$ event was not reported by Turner & Bottrill (2001).

- Berry (1994) suggested that the Bowry Formation was allochthonous on the basis of relict blueschist metamorphic mineralogy. The presence of the 777 ± 7 Ma granitoid (Turner *et al.* 1998) in the Bowry Formation has been interpreted here to support this argument. Turner & Bottrill (2001) noted that the age of the granitoid is older than the interpreted ages for the basalt sequences in the Togari, "eastern" and "western" Ahrberg Groups, which are thought to be between 650 and 580 Ma in age (Calver 1998). In addition, Turner & Bottrill (2001) proposed several possibilities, suggesting that either:
  - only the granitoid bodies are exotic, and their contacts with the country rock are structural; or
  - the granitoid intrudes the country rock, and thus provides a minimum age of the surrounding Bowry Formation mafics (ie. older than the widespread Late Neoproterozoic rift volcanics); or
  - based on the similar chemistry between the Bowry Formation mafics and those of the Togari and Ahrberg Groups, the Proterozoic mafic volcanics in northwestern Tasmania may be substantially older (pre-777 Ma) than previously thought.

The findings of this study regarding the nature of the contact between the granitoid and the surrounding mafic meta-igneous rocks were inconclusive. However, microscopic and mesoscopic textural relationships described in Chapter 4 suggest that the granitoids are intrusive into the surrounding mafic lithologies. Furthermore, the Bowry Formation granitoid age and chemistry is comparable to the Cape Wickham granitoid on King Island, which also intrudes sub-alkaline affinity metabasalts. Given the geochemical and geochronological characteristics of the granitoids, the spatial relationship to metabasalts, and the interpreted south-directed transport of slices within the Arthur Lineament, it is suggested that the Bowry Formation originated to the north of the Tasmanian mainland, in a region that experienced limited felsic magmatism around 780 Ma. Taking into account the blueschist grade of metamorphism evident within parts of the Bowry Formation, it is likely the unit underwent this early high pressure deformation far from its current position.

- The nature of the boundaries of the Arthur Lineament has been subject to debate, with Turner & Bottrill (2001) describing the boundaries as transitions into less deformed and metamorphosed rocks. They indicated that the dips of the transitional boundaries are poorly known, and that some boundary segments are faulted. The investigations undertaken as part of this work have shown that in the south, where the lineament's western boundary is exposed, there is a sharp change in the intensity of $\boldsymbol{Ca}D_1$ and $\boldsymbol{Ca}D_2$ (refer to Chapter 2). The orientation of the $\boldsymbol{Ca}S_2$ foliation does not change across the lineaments boundary. To the west of the lineament, the intensity of deformation dissipates over several kilometres, however the most marked change is at the lineaments faulted western boundary. The eastern boundary of the lineament is far more gradational than the western boundary. Deformation attributed to the Arthur Lineament is evident 5 to 7 km to the east of the boundary. As has been shown, the $\boldsymbol{Ca}S_1$ and $\boldsymbol{Ca}S_2$ foliations have variable orientations close to the eastern margin of the lineament, however they mostly strike towards the northeast (refer to Chapter 2).

- Metamorphism attributed to the earliest event (***Ca***D_1) is not widely developed, but in allochthonous fault-bounded slices within the lineament it is represented as relict blueschist facies mineral assemblages. Metamorphic conditions during ***Ca***D_1 in the allochthonous slices are interpreted to have reached 400°C and 700 to 1000 MPa.

Early ***Ca***D_2 metamorphism is variable in its grade. Mineral assemblages indicate that different parts of the Arthur Lineament experienced metamorphic conditions ranging from upper greenschist facies (400-450°C and 500 MPa) to the greenschist-amphibolite transition zone (460 ± 40°C and 700 ± 200 MPa), in the garnet stability field (refer to Chapter 3). Late ***Ca***D_2 was more uniform and lower greenschist facies conditions (350-400°C and +300 MPa) were widely developed in the lineament. Peak metamorphism in the "western" Ahrberg Group were lower greenschist facies conditions, with actinolite stable in the metabasalts.

Turner & Bottrill (2001) interpreted widespread chlorite development in the lineament to be the result of chloritisation of biotite, based on brown biotite observed in a schist in the Rocky River area. However, in this study brown biotite was not found in any part of the Bowry Formation, "eastern" Ahrberg Group or AGC. However, green biotite was present in some samples of the "eastern" Ahrberg Group, the AGC and the Bowry Formation, indicative of upper greenschist facies conditions. Chlorite is interpreted to be prograde, as it is in equilibrium with both the ***Ca***D_1 and ***Ca***D_2 mineral assemblages. Albite porphyroblasts were found to be uniformly early- to late-***Ca***D_2 in age, in the Bowry Formation, "eastern" Ahrberg Group and the AGC. In some instances, the porphyroblasts preserve inclusion trails that are aligned with the ***Ca***S_1 foliation. However, in these cases the porphyroblasts are interpreted to have grown early in the ***Ca***D_2 event. The syn-***Ca***D_2 interpretation of the albite growth is in contrast to Turner & Bottrill (2001) who only report albite growth during the ***Ca***D_1 event.

5.3 Reconstruction and break-up of Rodinia

The findings from the metamorphic geochronology study undertaken as part of this work, in conjunction with the structural, metamorphic and igneous geochemistry investigations, contribute to a further refinement of the tectonic characteristics of northwestern Tasmania and King Island from the Mesoproterozoic to Cambrian.

The sub-alkaline, tholeiitic affinities of the pre-1270 Ma metabasalts on King Island suggest an extensional setting existed during their extrusion. At this stage, there is no age constraint on these mafic extrusives and associated sediments.

The *ca.* 1270 Ma lower amphibolite facies metamorphic event on King Island is not recorded elsewhere in Tasmania, and it is interpreted to be older than any exposed (mainland) Tasmanian basement. Metamorphism of this age has been reported in western Australia (Albany-Fraser Province), in central Australia (Musgrave Block) and in areas of Antarctica (Windmill Islands and Bunger Hills) (Sheraton *et al.* 1996). This suggests that either King Island was close to one of these areas preceding (or during the early stages of) the Grenville Orogeny (ie. King Island is not now in its *ca.* 1270 Ma position), or that a Grenville orogen extends from Bunger Hills to Wilkes Basin in Antarctica.

Several other suggestions can be made regarding the reconstruction of Rodinia, encompassing the metamorphic age on King Island, and the detrital zircon populations on King Island and on mainland Tasmania:

- King Island's position at *ca.* 1270 Ma, relative to southeastern Australia, may be only marginally different to present, and it may have been attached to the Sierra Madre Oriental terrane (in Mexico), (as suggested by Burrett & Berry 2000), which has a consistent detrital zircon population. This best fit solution is in accordance with the AUSWUS reconstruction of Karlstrom *et al.* (1999).
- Alternatively, also largely using the AUSWUS reconstruction, King Island may have been displaced relative to its current position, and located further north, close to the Musgrave Block and Amadeus Basin, as proposed by Berry *et al.* (2001).

- Berry *et al.* (2001) also present the possibility of another, 'intermediate' Rodinia reconstruction, with Australia positioned latitudinally midway between the SWEAT (Dalziel 1991) and AUSWUS best fit solutions. The SWEAT reconstruction itself is not considered viable however, as the detrital zircon populations in sandstones of British Columbia (peaks at 2400 and 1900 Ma) and Tasmania (peaks between 1600-1900 Ma and 1200-1500 Ma) are very different, inferring different source regions Berry *et al.* (2001).

On the basis of stratigraphic correlations and palaeomagnetic data, Tasmania is interpreted to have been attached to mainland Australia during the Neoproterozoic and in the Late Cambrian (Calver & Walter 2000, Li *et al.* 1997, Berry *et al.* 2001).

During the Middle Neoproterozoic, relatively stable passive margin conditions prevailed in northwestern Tasmania. During this time, the alkaline, intraplate Cooee dolerite, Sulphur Creek pillow basalts and Montana Melaphyre were emplaced into the Burnie and Oonah Formations. In addition, the continental shelf-derived Rocky Cape Group and correlates, and the turbiditic Burnie and Oonah Formations were deposited (Figure 5.5(a)).

In South Australia, at around 800 Ma, the intraplate extrusives of the Willouran basic province and the Gairdner Dyke Swarm were emplaced, as a result of a large (1600 km) diameter mantle plume (Crawford & Hilyard 1990, Zhao & McCulloch 1993, Zhao *et al.* 1994). Speculatively, the magmatism that produced the Cooee dolerite and Sulphur Creek pillow basalts, as well as the Willouran basic province and the Gairdner Dyke Swarm, are thermally related.

Felsic magmatism in southeastern Australia at around 760-800 Ma includes the granitoids on King Island (760 ± 12 Ma) and in the Bowry Formation (777 ± 7 Ma), as well as the Rook Tuff (802 ± 10 Ma) and the bimodal Boucat Volcanics (777 ± 7 Ma) (Fanning *et al.* 1986, Turner *et al.* 1998). These magmatic episodes may also be thermally related to the mantle plume, as was suggested for the Rook Tuff (Zhao *et al.* 1994). Furthermore, as rifting is often thought to commence due to arrival of a mantle plume beneath a region, it can be speculated that the mafic and minor felsic

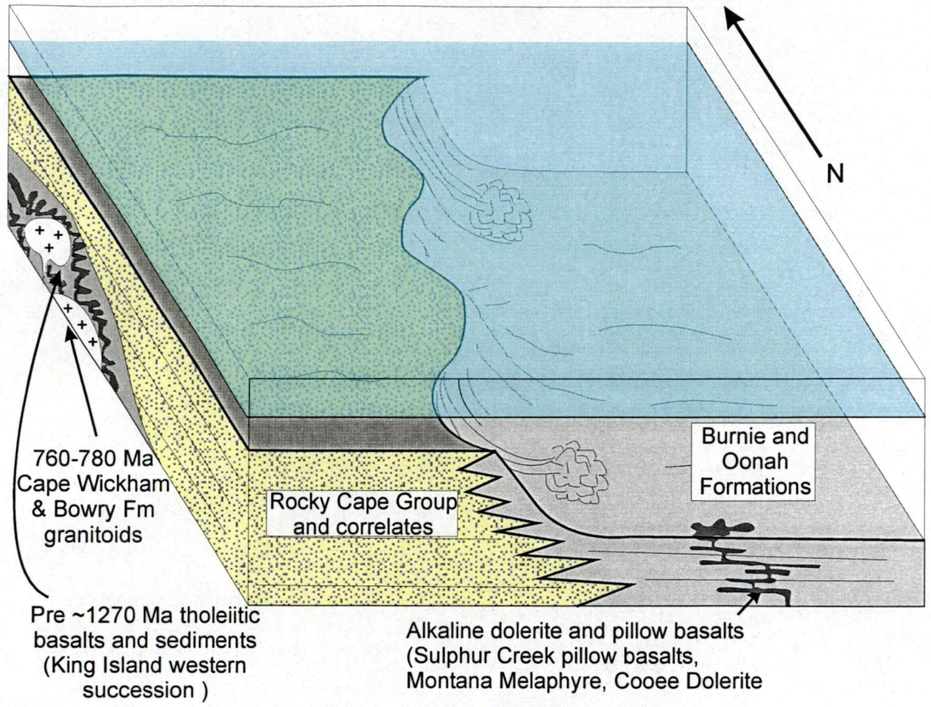

Figure 5.5(a). Passive margin setting during the Neoproterozoic (VE ~2).

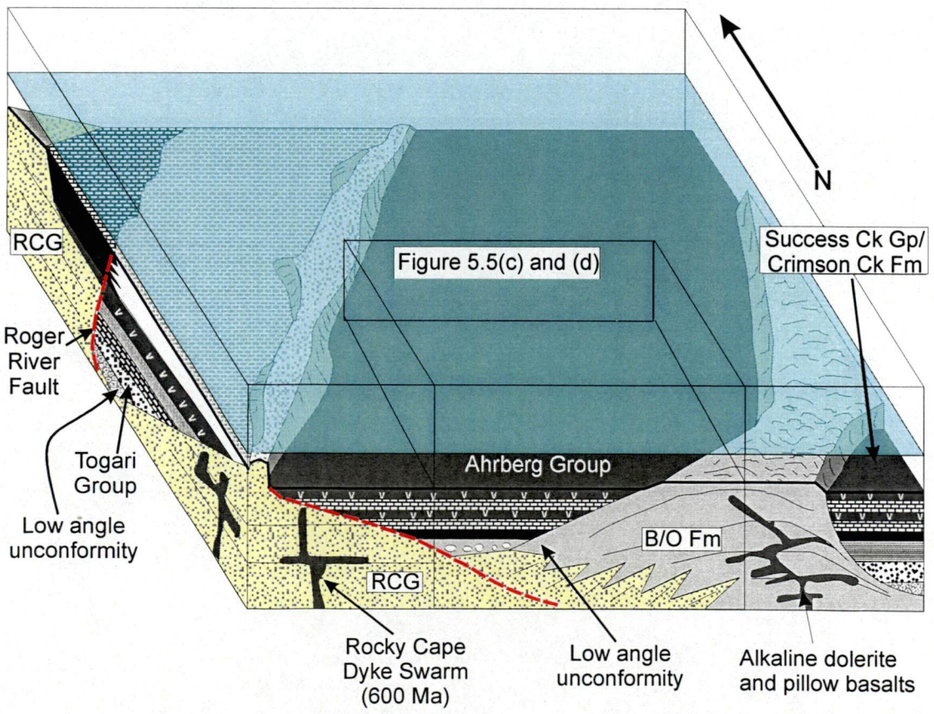

Figure 5.5(b). Extensive Late Neoproterozoic rift succession.

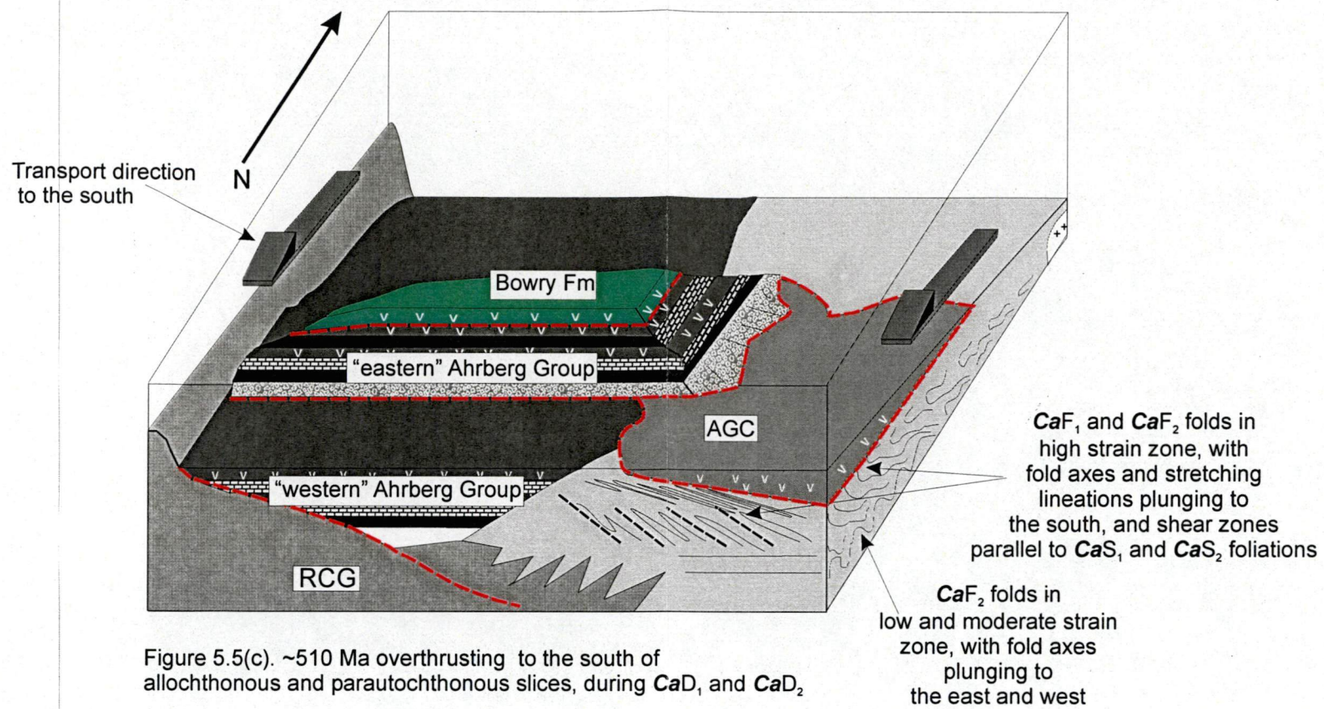

Figure 5.5(c). ~510 Ma overthrusting to the south of allochthonous and parautochthonous slices, during ***Ca***D_1 and ***Ca***D_2

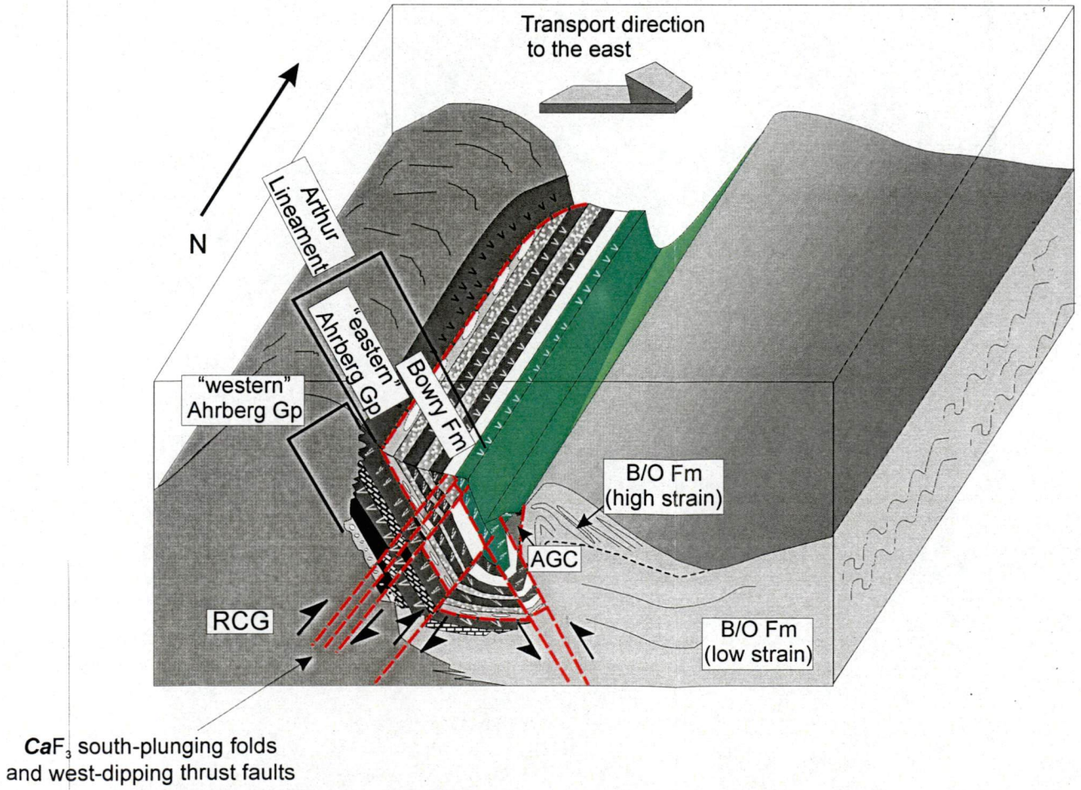

Figure 5.5(d). Latest Cambrian east-directed folding and thrusting, during the ***Ca***D_3 event. Results in the 'linear' expression of the Arthur Lineament.

volcanics and intrusives possibly represent an early rifting event at *ca.* 780 Ma (Preiss 2000). The rift-related magmatism in southeastern Australia at this time may coincide with the *ca.* 780 Ma mafic magmatism in western Laurentia (eg. the mafic dykes that intrude the Little Dal Group of the Mackenzie Mountains, Canada), which possibly represents rifting on the other edge of the rifted margin (Jefferson & Parrish 1989, Park *et al.* 1995).

Despite these possible interpretations of the significance of various events, the exact timing of the break-up of Rodinia (into Gondwana and Laurentia) is equivocal, and has been widely debated (Dalziel 1991, Moores 1991, Powell *et al.* 1993, 1994a, Crawford *et al.* 1997, Veevers *et al.* 1997, Calver & Walter 2000). Interpretations range between break-up occurring at 725-700 Ma, just after the Sturtian glaciation (Powell *et al.* 1993, 1994a), to around 600 Ma, after the Marinoan glaciation (Veevers *et al.* 1997, Crawford *et al.*, 1997). Powell *et al.* (1994a) proposed that Tasmania was involved in the earlier rift phase (725-700 Ma). However, the extensive rift-related tholeiitic magmatism in northwestern Tasmania, which includes the Ahrberg and Togari Groups, the Success Creek Group-Crimson Creek Formation, and the Neoproterozoic sequence on King Island, is interpreted to have occurred between 650-600 Ma (Crawford 1992, Calver & Walter 2000)(Figure 5.5(b)). This indicates that the most significant rifting event that took place in northwestern Tasmania was a later phase than the 725-700 Ma event.

Major rifting is interpreted to have occurred elsewhere around this time. Rift-related transitional alkaline lavas in western New South Wales, that were emplaced at *ca.* 600-585 Ma, and are also considered to represent initial rifting along the eastern margin of Australia-Antarctica (Crawford *et al.* 1997). Neoproterozoic tholeiites and associated sediments near the Weddell Sea in east Antarctica also represent rifting along this margin (Dalziel 1991, Storey *et al.* 1992). Subsequent to the break-up of Rodinia, Berry *et al.* (2001) have suggested that, based on detrital zircon age spectra, Tasmania was an isolated micro-continent or promontory, in the Palaeopacific Ocean, until its accretion back on to the Australo-Antarctic craton in the Middle to Late Cambrian. The accretion occurred as part of the Delamerian/Tyennan Orogeny (Powell *et al.* 1994b, Li *et al.* 1996, Powell 1998, Berry *et al.* 2001).

5.4 The Tyennan Orogeny and the formation of the Arthur Lineament

Upon the refinement of the metamorphic geochronology in western Tasmania, it is clear that the main period of deformation was in the Cambrian, at around 510 Ma (Turner 1993, Black 1994, Turner *et al.* 1994, Turner *et al.* 1998, Section 3.7.2). This is attributed to arc-continent collision, that involved the subduction of Late Neoproterozoic ocean floor in the Early Cambrian, and attempted subduction of the 600 Ma volcanic passive margin, as well as obduction of forearc-derived ophiolite slices, some of which crystallised at 513.6 ± 5 Ma, shortly before tectonic emplacement (Berry & Crawford 1988, Crawford & Berry 1992, Black *et al.* 1997). Meffre *et al.* (2000) noted that the arc-related geochemical affinities of the ophiolites, the high temperature amphibole mylonites on the soles of the ophiolitic detachments, the high pressure metamorphism of lithologies beneath the ophiolites, and the passive margin affinities of the underlying sequence were all characteristics typical of other arc-continent collisions. They presented other examples of more recent arc-continent collision involving ophiolite obduction, such as New Caledonia (Aitchison *et al.* 1995), the Papuan Ultramafic Belt (Davies & Jaques 1984), Newfoundland (Cawood 1991) and Oman (Alabaster *et al.* 1982, Chemenda *et al.* 1996, Hacker *et al.* 1996) as supporting evidence of their argument. Based on comparisons with other ophiolites, Meffre *et al.* (2000) interpreted the majority of the Precambrian rocks in Tasmania to have been overthrust by an ophiolite, with the metamorphic complexes being subducted to depths ranging between 10 and 50 km during the collision.

In the vicinity of the Arthur Lineament, the arc-continent collision was characterised by an overthrusting event, with a series of major décollements causing the present high-strain tectonostratigraphic pile (Figure 5.5(c)). The collision and overthrusting involved several progressive stages of structural deformation and metamorphism. These are summarised below:

- The ***Ca***D_1 event was the first stage of the arc-collision that is represented in the Arthur Lineament. During the early phase of the collision event, some distance to the north of the current high strain zone, the allochthonous slices that now

form part of the lineament were subducted, experiencing high pressure-low temperature metamorphism, and producing blueschist facies metamorphic assemblages in the metabasites. The mineral assemblage, characterised by glaucophane and epidote, indicates ***Ca***D_1 metamorphism was in the higher grade blueschist facies, with pressures ranging between 700 and 1000 MPa (Bucher & Frey 1994). Temperatures are interpreted to have been around 500°C. Despite the intensity of the ***Ca***D_1 event, the ***Ca***S_1 foliation did not pervasively penetrate the metabasites. However, the high pressures in the subducted slices caused metamorphic recrystallisation, and the glaucophane is best preserved in these more competent, meta-igneous rock types.

The exhumation and south-directed transport of the blueschist rocks was accompanied by the detatchment and transport of the greenschist facies, parautochthonous slices of the Arthur Lineament. During this process, ***Ca***D_1 was characterised by moderate to high strain levels. This resulted in a structural foliation (***Ca***S_1) that is intensely developed in the metasediments from the high strain zones of the lineament. The ***Ca***S_1 foliation is schistose in these zones, and is parallel to bedding. The ***Ca***D_1 event produced gently south-plunging isoclinal folding and stretching lineations, and associated ***Ca***S_1-parallel faulting. Shearing attributed to the ***Ca***D_1 event is common in the high strain zones, and produced quartz segregations that are also parallel to the ***Ca***S_1 foliation and shear plane.

- The ***Ca***D_2 event was a pervasive deformational episode, that contributed largely to the formation of the high strain zone. During ***Ca***D_2, the south-directed transport of allochthonous and parautochthonous slices continued. The differing origins of the various blocks led to variation in the metamorphic conditions, however in general the ***Ca***D_2 event is characterised by low to medium grade metamorphic temperatures and pressures, and high strain, resulting in intense structural deformation. ***Ca***D_2 overprinted the ***Ca***D_1 event, and obliterated the textures and mineral assemblages attributed to ***Ca***D_1 in some areas. In some parautochthonous slices, metamorphism early in the ***Ca***D_2 event reached the highest temperatures (460-500°C), with pressures of 600-700 MPa. This grade of metamorphism, just in the greenschist-amphibolite facies transition zone, occurred in the eastern part of the Bowry Formation and the western part of the

AGC. In some parts of these slices, metamorphism during early ***Ca***D_2 was in the garnet stability field. In the parautochthonous "eastern" Ahrberg Group, as well as parts of the Bowry Formation and the AGC, the metamorphic grade was in the upper greenschist facies, and did not reach the garnet stability field. Temperatures of 400-450°C and pressures of around 500 MPa prevailed during the early ***Ca***D_2 event in these slices. The variation in metamorphic histories in the different parts of the Bowry Formation, and AGC is significant, as it indicates that these are not coherent units. They are complexes, made up of blocks which have undergone different metamorphic conditions, and therefore must have been separate during the ***Ca***D_1 and early ***Ca***D_2 events.

Late ***Ca***D_2 was a uniform metamorphic event. It produced greenschist facies metamorphism, across the Arthur Lineament, with temperatures of approximately 350-400°C, and pressures of 300-400 MPa. In the "western" Ahrberg Group, peak metamorphism was in the lower greenschist facies. The common late ***Ca***D_2 assemblage and metamorphic grade in all the units of the lineament suggest that at this stage, in contrast to the ***Ca***D_1 and early ***Ca***D_2 events, the present 'stack' of tectonostratigraphic units had been assembled.

Whereas the ***Ca***D_2 metamorphism has been divided into early and late stages, this has not been possible for structural deformation during this event. Alignment of minerals with the intense, pervasively developed ***Ca***S_2 foliation indicates that the structural deformation and metamorphism attributed to the ***Ca***D_2 event are directly related. ***Ca***D_2 produced tight to isoclinal folds, with a pervasive schistose axial planar cleavage, that overprints the ***Ca***S_1 foliation. The cleavage is sub-parallel to bedding and the ***Ca***S_1 foliation, due to the near co-axial refolding by ***Ca***F_2. Syn-***Ca***D_2 shearing, parallel to the ***Ca***S_2 foliation, accompanied folding. The ***Ca***F_2 fold style and orientation infers that south-directed transport persisted during the ***Ca***D_2 event. Thus the allochthonous and parautochthonous slices, originating to the north of their current position, continued their movement towards the south.

During the ***Ca***D_1 and ***Ca***D_2 events the strain was localised, with the most strongly deformed (high strain) zones developing within the package of

allochthonous and parautochthonous slices, and close to the décollement surfaces. In these areas within the Arthur Lineament, the ***Ca***F_1 and ***Ca***F_2 folds plunge to the south, and their axial surfaces dip variably to the east. This differs in orientation to outside the lineament in the more weakly deformed (low strain) zones. To the east of the lineament, in areas of low strain, fold axes are east-west trending, and sub-horizontal, and axial planes dip gently to the south. The folds are close to recumbent, and are downward facing, as a result of continued movement to the south in a nappe-style fold and thrust system.

- The ***Ca***D_3 event followed the main deformation of the Tyennan Orogeny. The age of ***Ca***D_3 is indirectly constrained as late Cambrian. ***Ca***D_3 is best developed to the west of the lineament, in the Rocky Cape Group and correlates. It is a locally developed deformation, and produced meso- to macroscopic asymmetric folds with west-dipping axial planes and thrust faults that imply an east-directed transport (Figure 5.5(d)). In areas where the ***Ca***D_3 event is weakly developed, such as on the north coast in the Somerset-Doctors Rocks region, the ***Ca***S_1 and ***Ca***S_2 foliations are gently east-dipping. However, in areas where the ***Ca***D_3 event is strongly developed, the ***Ca***S_1 and ***Ca***S_2 foliations are steeply east-dipping. The ***Ca***D_3 event was responsible for the uplifting of the high strain zone, resulting in the steep east-dip of the ***Ca***S_1 and ***Ca***S_2 foliations and associated detatchment surfaces. This ***Ca***D_3 event produced the linear expression of the Arthur Lineament.

- Subsequent Devonian deformation, associated with granitoid intrusion, caused localised refolding of the lineament, although this event was relatively weak, and did not play a significant role in the development of the Arthur Lineament.

In summary, following the Cambrian arc-continent collision, the blueschist grade allochthonous slices were transported (obducted) to the south of the subduction zone (***Ca***D_1)(Figure 5.5(c)). Other parautochthonous rocks were also transported to the south during this high strain event, with associated intense shearing and folding occurring at greenschist grade metamorphic conditions. Following this, a near coaxial high strain deformational event took place, detaching and overthrusting other

parautochthonous slices to the south, as they were variably metamorphosed to greenschist and upper greenschist-amphibolite grade (early ***Ca***D_2)(Figure 5.5(c)). During these events, strain-related rotation of the developing folds took place, resulting in a change in orientation of the fold axes from east-west to north south, and foliations from south-dipping to east-dipping, from the low strain zones into the high strain zones. The revised metamorphic geochronology of the Arthur Lineament indicates the early ***Ca***D_2 event occurred around 505-510 Ma. During ***Ca***D_1 and early ***Ca***D_2, the parautochthonous lithologies were structurally emplaced on top of the less deformed, autochthonous units. In the final stage of assembling the tectonostratigraphic 'pile', the various slices were stacked together, and lower greenschist facies metamorphic conditions were developed uniformly in all allochthonous, parautochthonous and autochthonous blocks (late ***Ca***D_2). Subsequent to this, the ***Ca***D_3 event caused the tilting of the tectonostratigraphy, to complete the development of the Arthur Lineament (Figure 5.5(d)).

REFERENCES

Adams C.J., Black L.P., Corbett K.D. Green G.R. 1985. Reconnaissance isotopic studies bearing on the tectonothermal history of Early Palaeozoic and Late Proterozoic sequences in Western Tasmania. *Australian Journal of Earth Sciences*, **32**, 7-36.

Aitchison J.C., Clarke G.L., Cluzel D. & Meffre S. 1995. Eocene arc-continent collision in New Caledonia and implications for regional SW Pacific tectonic evolution. *Geology*, **23**, 161-164.

Alabaster T., Pearce J.A. & Malpas J. 1982. The volcanic stratigraphy and the petrogenesis of the Oman ophiolite complex. *Contributions to Mineralogy and Petrology*, **81**, 168-183.

Bain, J., & Draper, J., 1997, North Queensland geology. *Australian Geological Survey Organisation Bulletin*, **240**, 1-600.

Baker B.H., Goles G.G., Leeman W.P. & Lindstrom M.M. 1977. Geochemistry and petrogenesis of a basalt-benmoreite-trachyte suite from the southern part of the Gregory Rift, Kenya. *Contributions to Mineralogy and Petrology*, **64**, 303-332.

Baldwin S. & Ireland T. A. 1995. Tale of two eras: Pliocene-Pleistocene unroofing of Cenozoic andesite Archean zircons from active metamorphic core complexes, Solomon Sea, Papua New Guinea. *Geology*, **23**, 1023-1026.

Bell R. & Jefferson C. 1987. An hypothesis for an Australian-Canadian connection in the Late Proterozoic and the birth of the Pacific Ocean. *Proceedings Pacific Rim Congress '87*, Melbourne, Australian Institute Mining Metallurgy, 39-50.

Berry R.F. 1989. Microstructural evidence for a westward transport direction during middle Cambrian obduction in Tasmania. *Geological Society of Australia Abstracts*, 24, 8-9.

Berry R.F. 1994. Tectonics of western Tasmania: Late Precambrian – Devonian. *Geological Society of Australia Abstracts*, **39**, 6-8.

Berry R.F & Crawford A.J. 1988. The tectonic significance of Cambrian allochthonous mafic-ultramafic complexes in Tasmania. *Australian Journal of Earth Sciences*, **35**, 523-533.

Berry R.F., Jenner G.A., Meffre S. & Tubrett M.N. 2001. A North American provenance for Neoproterozoic to Cambrian sandstones in Tasmania? *Earth and Planetary Science Letters*, **192**, 207-222.

Berry R.F, Meffre S. & Kreuzer H. 1997. Metamorphic rocks from the southern margin of Tasmania and their tectonic significance. *Australian Journal of Earth Sciences*, **44**, 609-619.

Bevins R.E., Kokelaar B.P. & Dunkley P.N. 1984. Petrology and geochemistry of lower to middle Ordovician igneous rocks in Wales: a volcanic arc to marginal basin transition. *Proceedings of the Geological Association*, **95**, 337-347.

Black L.P. 1994. The significance of current and proposed SHRIMP dating. *Mineral Resources Tasmania unpublished report* **1994/16**.

Black L.P., Seymour D.B. & Corbett K.D. 1997. Dating Tasmania's oldest geological events. *Australian Geological Survey Organisation Record* **1997/15**.

Blackney P.J.C. 1982. Metamorphic petrology of S.W. King Island. B. Sc Hons. Thesis, *University of Tasmania*, (unpublished).

Blake F. 1939. Report on the Corinna Alluvial Goldfield. *Tasmanian Department of Mines Report* 1939.

Blewett R., Black L.P., S.S., Knutson J., Hutton L. J. & Bain J. H. 1998. U-Pb zircon and Sm-Nd geochronology of the Mesoproterozoic of North Queensland implications for a Rodinian connection with the Belt Supergroup of North America. *Precambrian Research*, **89**, 101-127.

Bons A.J. 1988. Intracrystalline deformation and slaty cleavage development in very low grade slates from the central Pyrenees. *Geologica Ultraiectina*, **56**.

Borg S. & DePaolo D. 1994. Laurentia, Australia and Antarctica as a Late Proterozoic supercontinent. *Geology*, **22**, 307-310.

Borradaile G.J., Bayly M.B. & Powell C.McA 1982. Atlas of deformational and metamorphic rock fabrics. *Springer-Verlag*, 551p.

Brookfield M. 1993. Neoproterozoic Laurentia-Australia fit. *Geology*, **21**, 683-686.

Brown A.V. 1986. Geology of the Dundas-Mt Lindsay-Mt Youngbuck area. *Bulletin of the Geological Survey of Tasmania*, **62**.

Brown A.V. 1989. Eo-Cambrian-Cambrian. In: Burrett C.F. & Martin E.L. eds. Geology and Mineral Resources of Tasmania. *Geological Society of Australia, Special Publication*, **15**, 47-84.

Brown A.V. & Jenner G.A. 1988. Tectonic implications of the re-interpretation of Eocambrian-Cambrian mafic volcanic and associated ultramafic rocks in Western Tasmania. *Geological Society of Australia Abstracts,* 23-26.

Brown A.V., Calver C.R., Corbett K.D., Forsyth S.M., Goscombe B.A., Green G.R., McLenaghan M.P., Pemberton J. & Seymour D.B. 1995. Geological Atlas 1:250000 digital series. *Tasmania Geological Survey.*

Brown E.H. 1974. Comparison of the mineralogy and phase relations of blueschists from the north Cascades, Washington, and the greenschists from Otago, New Zealand. *Bulletin of the Geological Society of America*, **85**, 333-344.

Brown E.H. 1977. The crossite content of Ca-amphibole as a guide to pressure of metamorphism. *Journal of Petrology*, **18**, 53-72.

Bucher K. & Frey M. 1994. Petrogenesis of Metamorphic Rocks, 6th edition, complete revision of Winkler's textbook, *Springer Verlag*, 318pp.

Burk C.A. & Darke C.L. 1974. The geology of continental margins. *Springer-Verlag*, 1009p.

Burrett C. & Berry R.F. 2000. Proterozoic Australia-Western United States (AUSWUS) fit between Laurentia and Australia. *Geology*, **28**, 103-106.

Calver C.R. 1996. Reconnaissance isotope chemostratigraphy of Neoproterozoic carbonates in western Tasmania. *Geological Survey of Tasmania Record* **1996/10.**

Calver C.R. 1998. Isotope stratigraphy of the Neoproterozoic Togari Group, Tasmania. *Australian Journal of Earth Sciences*, **45**, 865-874.

Calver C.R., Corbett K.D., Everard J.L., Goscombe B.A., Pemberton J. & Seymour D.B. (comp) 1995. Geological Atlas 1:250 000 digital series. Geology of northwest Tasmania. *Tasmanian Geological Survey.*

Calver C.R. & Walter M.R. 2000. The late Neoproterozoic Grassy Group of King Island, Tasmania: correlation and palaeogeographic significance. *Precambrian Research*, **100**, 299-312.

Carey S.W & Banks M.R. 1954. Lower Palaeozoic unconformities in Tasmania. *Papers and Proceedings of the Royal Society of Tasmania*, **88**, 245-269.

Carpenter P.K. 1999. Status report on Corning standard glasses 95IRV, 95IRW and 95IRX. *Microscopy and Microanalysis*, **5**, 580-581.

Cawood P.A. 1991. Processes of ophiolite emplacement in Oman and Newfoundland. In: Peters J., Nicolas A. & Coleman R.G. eds. Ophiolite

Genesis and Evolution of the Oceanic Lithosphere. *Kluwer Academic Publishers*, 501-516.

Chemenda A.I., Mattauer M. & Bokun A.N. 1996. Eclogites and blueschists of the Pam Peninsula NE New Caledonia: a reappraisal. *Journal of Petrology*, **38**, 843-876.

Condie K.C. 1992. Proterozoic terranes and continental accretion in southwestern North America, *in* Condie, K.C., ed., Proterozoic continental evolution: Amsterdam. *Elsevier*, 447-480.

Corbett K.D. & Turner N.J. 1989. Early Palaeozoic deformation and tectonics. In: Burrett C.F. & Martin E.L. eds. Geology and Mineral Resources of Tasmania. *Geological Society of Australia, Special Publication*, **15**, 154-181.

Cox S.F. 1973. The structure and petrology of the Cape Wickham area, King Island. B.Sc. Hons. thesis, *University of Tasmania* (unpublished).

Cox S.F. 1989. Cape Wickham. In: Burrett C.F. & Martin E.L. eds. Geology and Mineral Resources of Tasmania. *Geological Society of Australia Special Publication*, **15**, 154-181.

Crawford A.J. 1992. Geochemistry and implications of mafic metavolcanics in the Corinna-Savage River area. In Turner, N.J., ed. Corinna 1:50 000 geological map. Field guide to selected rock exposures, pp. 27-37. *Tasmania Department of Mines Report* **1992/06**.

Crawford A.J. & Berry R.F. 1992. Tectonic implications of Late Proterozoic-Early Palaeozoic igneous rock associations in western Tasmania. *Tectonophysics*, **214**, 37-56.

Crawford A.J. & Hilyard D. 1990. Geochemistry of Late Proterozoic tholeiitic flood basalts, Adelaide Geosyncline, South Australia. In: Jago J.B & Moore P.S., eds. The evolution of a Late Precambrian-Early Palaeozoic rift complex: the Adelaide Geosyncline. *Geological Society of Australia Special Publication*, **16**, 49-68.

Crawford A.J., Stevens B.P.J. & Fanning M. 1997. Geochemistry and tectonic setting of some Neoproterozoic and Early Cambrian volcanics in western New South Wales. *Australian Journal of Earth Sciences*, **44**, 831-852.

Crook K.A.W. 1979. Tectonic implications of some field relationships of the Adelaidean Cooee Dolerite, Tasmania. *Journal of the Geological Society of Australia*, **26**, 353-361.

Dalziel I.W.D. 1991. Pacific margins of Laurentia and East Antarctica as a conjugate rift pair: Evidence for an Eocambrian supercontinent. *Geology*, **19**, 598-601.

Davies H.L. & Jaques A.L. 1984. Emplacement of ophiolite in Papua New Guinea. In: Gass I.G., Lippard S.J. & Shelton A.W. eds. Ophiolites and Oceanic Lithosphere. *Blackwell Scientific Publications*, 341-349.

Deer W.A., Howie R.A. & Zussman J. 1992. An introduction to the rock-forming minerals. 2nd ed. *Longman Scientific Technical*, 696

Deniel C., Vidal P., Coulon C., Vellutini P. & Piguet P. 1994. Temporal evolution of mantle sources during continental rifting: the volcanism of Djibouti (Afar). *Journal of Geophysical Research*, **99**, B2, 2853-2869.

Dewey J.F., Holdsworth R.E. & Strachan R.A. 1998. Transpression and transtension zones. In: Holdsworth R.E., Strachan R.A. & Dewey J.F. eds. Continental Transpressional and Transtensional Tectonics. *Geology Society London, Special Publications*, **135**, 1-14.

Doughty P., Price R. & Parrish R. 1998. Geology and U-Pb geochronology of Archean basement and Proterozoic cover in the Priest River Complex, northwestern USA and their implications for Cordilleran structure and Precambrian continent reconstructions. *Canadian Journal of Earth Sciences*, **35**, 39-54.

Drake M.J. & Weill D.F. 1972. New rare earth element standards for electron microprobe analysis. *Chemical Geology*, **10**, 179-181.

Eusden J.D. & Barreiro B. 1988. The timing of peak high grade metamorphism in central-eastern New England. *Maritime Sediments and Atlantic Geology*, **24**, 241-255.

Everard J.L, Seymour D.B., Brown A.V. & Calver C.R. 1996. Geological Atlas 1:50 000 Series. Sheet 27 (7915N). Trowutta. *Geological Survey of Tasmania.*

Everard J.L., McClenaghan M.P., Reed A.R. & Seymour D.B. 2000. Field excursion guide notes for the Roger, Sumac and Dempster digital 1:25,000 scale geological map sheets, northwestern Tasmania. *Mineral Resources Tasmania Record* **2000/02**.

Fanning C.M., Flint R.B. & Preiss W.V. 1986. Single and multiple frain U-Pb zircon analyses for the early Adelaidean Rook Tuff, Willouran Ranges, South Australia, *Geological Society of Australia Abstracts*, **15**, 71-72.

Floyd P.A. & Winchester J.A. 1975. Magma type and tectonic setting discrimination using immobile elements. *Earth and Planetary Science Letters*, **27**, 211-218.

Floyd P.A. & Winchester J.A. 1978. Identification and discrimination of altered and metamorphosed volcanic rocks using immobile elements. *Chemical Geology*, **21**, 291-306.

Gee R.D. 1967a. The Proterozoic rocks of the Rocky Cape Geanticline. In: The Geology of Western Tasmania – a Symposium. *University of Tasmania, Hobart* (unpublished).

Gee R.D. 1967b. The tectonic evolution of the Rocky Cape Geanticline in northwest Tasmania. Ph.D. Thesis, *University of Tasmania* (unpublished).

Gee R.D. 1968. A revised stratigraphy for the Precambrian of northwest Tasmania *Papers Proceeding the Royal Society of Tasmania*, **102**, 7-10.

Gee R.D. 1977. Burnie, Tasmania. *Tasmania Department of Mines Geological Atlas 1 Mile Series Explanatory Report,* Sheet 22 (8015N).

Gee R.D. 1989. The Rocky Cape Region and Nearby Inliers. In: Burrett C.F. & Martin E.L. eds. Geology and Mineral Resources of Tasmania. *Geological Society of Australia Special Publication,* **15**, 10-14.

Gee R.D., Gulline A.B. & Bravo A.P. 1967. Burnie, Tasmania. *Tasmanian Department of Mines Geological Atlas 1 Mile Series*, Sheet 28 (8015N).

Green T.H. & Spiller A.R. 1977. Blue amphibole from Precambrian metabasalts, Savage River, Tasmania. *American Mineralogist*, **62**, 164-166.

Gresham J.J. 1972. The regional geology of King Island. Geopeko Ltd. (unpublished).

Griffin B.J., 1974. Cambrian tectonism and vulcanism in the Smithton Basin. B.Sc. Hons. Thesis. *University of Tasmania* (unpublished).

Groves D.I. 1971. The regional significance of the Don Hill fault zone of Mt Bischoff, Tasmania. *Tasmania Department of Mines Technical Reports*, **14**, 111-121.

Guidotti C.V., Yates M.G., Dyar M.D. & Taylor M.E. 1994. *American Mineralogist*, **79**, 793-795.

Hacker B.P. Mosenfelder J.L. & Gnos E. 1996. Rapid emplacement of the Oman ophiolite : thermal and geochronologic constraints. *Tectonics*, **15**, 1230-1247.

Harcourt Smith J., 1897. Report on the mineral district between Corinna and Waratah. *Report of the Secretary of Mines* 1896-1897.

Hills C.L., & Carey S.W. 1949. Geology and Mineral Industry. *Handbook for Tasmania, A.N.Z.A.A.S.*, 21-44.

Hobbs B.E., Means W.D. & Williams P.F. 1976. An outline of structural geology. *John Wiley and Sons Ltd.*, 571p.

Holland T.J.B. & Powell R. 1998. An internally consistent thermodynamic data set for phases of petrological interest. *Journal of Metamorphic Geology*, **16**, 309-343.

Hoffman P. 1991. Did the breakout of Laurentia turn Gondwanaland inside-out? *Science*, **252**, 1409-1412.

Hoffman P. 1988. The United Plates of America, the birth of a craton: *Annual Review of Earth and Planetary Science*, **16**, 543-603.

Holm O.H. & Berry R.F. 2002. Structural history of the Arthur Lineament, Northwest Tasmania, Australia: an analysis of critical outcrops. *Australian Journal of Earth Sciences*, **49**,167-185.

Holm O.H., Berry R.F. & Steele D.A. 2001. Defining Tasmania's deformation history-geochronology of metamorphic monazites. *Geological Society of Australia Abstracts*, **64**, 89-90.

Idnurm M. & Giddings J. W. 1995. Paleoproterozoic-Neoproterozoic North America-Australia link; new evidence from paleomagnetism. *Geology*, **23**, 149-152.

Jago J.B. & Brown A.V. 1989. Middle to Upper Cambrian fossiliferous sedimentary rocks. In: Burrett C.F. & Martin E.L. eds. Geology and Mineral Resources of Tasmania. *Geological Society of Australia Special Publication*, **15**, 74-83.

Jarosewich E. & Boatner L.A. 1991. Rare-earth element reference samples for electron microprobe analyses. *Geostandards Newsletter*, **15**, 397-399.

Jefferson C.W. & Parrish R.R. 1989. Late Proterozoic stratigraphy, U-Pb zircon ages and rift tectonics, Mackenzie Mountains, northwestern Canada. *Canadian Journal of Earth Sciences*, *26*, 1784-1801.

Kamperman M. 1984. The Precambrian metamorphic geology of the Lyell Highway-Collingwood River area. Hons. Thesis. *University of Tasmania* (unpublished).

Karlstrom K. E., Harlan S. S., Williams M. L., McLelland J., Geissman J. W. & Åhäll K-I. 1999. Refining Rodinia: Geologic evidence for the Australia - western U.S. connection in the Proterozoic. *GSA Today*, **9-10**, 1-7.

Khin Zaw, Turner N.J., Large R.R., Nolan H. & Mernagh T. 1992. Geology and genesis of silica flour and gold in the Corinna district, western Tasmania. *Bulletin of the Geological Survey of Tasmania*, **70**, 96.

Kingsbury J.A., Miller C.F., Wooden J.L. & Harrison T.M. 1993. Monazite paragenesis and U-Pb systematics in rocks of the eastern Mojave Desert, California, USA: implications for thermochronometry. *Chemical Geology*, **110**, 147-167.

Laird J. & Albee A.L. 1981a. High-pressure metamorphism in mafic schist from northern Vermont. *American Journal of Science*, **281**, 97-126.

Laird J. & Albee A.L. 1981b. Pressure, temperature, and time indicators in mafic schist: their application to reconstructing the polymetamorphic history of Vermont. *American Journal of Science*, **281**, 127-175.

Leake B.E., Woolley A.R., Arps C.E.S., Birch W.D., Gilbert M.C., Grice J.D., Hawthorne F.C., Kato A., Kisch H.J., Krivovichev V.G., Linthout K., Laird J., Mandarino J.A., Maresch W.V., Nickel E.H., Rock N.M.S., Schumacher J.C., Smith D.C., Stephenson N.C.N., Ungaretti L., Whittaker E.J.W. & Guo Y. 1997. Nomenclature of amphiboles; report of the subcommittee on amphiboles of the International Mineralogical Association, Commission on New Minerals and Mineral Names. *Mineralogical Magazine*, **61**; 2(405), 295-321.

Lewis R. 1991. Structure and metamorphic petrology of the Forth Metamorphic Complex. BSc. Hons. Thesis. *University of Tasmania* (unpublished).

Li Z-X., Zhang L. & Powell C. 1995. South China in Rodinia: Part of the missing link between Australia-east Antarctica and Laurentia? *Geology*, **23**, 407-410.

Li Z.X., Zhang L. & Powell C.McA. 1996. Positions of the East Asian cratons in the Neoproterozoic supercontinent Rodinia. *Australian Journal of Earth Sciences*, **43**, 593-604.

Li Z.X., Baillie P.W. & Powell C.McA. 1997. Relationships between northwestern Tasmania and East Gondwanaland in the Late Cambrian/Early Ordovician: Palaeomagnetic evidence. *Tectonics*, **16**, 161-171.

Luff I.W. 1982. Petrogenesis of the island arc tholeiite series of the South Sandwich Islands. PhD thesis, *University of Leeds* (unpublished).

McClay K.R. 1997. The mapping of geological structures. Geological Society of London handbook. *John Wiley and Sons Ltd.*, 161p.

McDougall I. & Leggo P.J. 1965. Isotopic age determinations in granitic rocks from Tasmania. *Journal of the Geological Society of Australia*, **12**, 295-332.

Mason R. 1978. Petrology of the metamorphic rocks. *Allen and Unwin Ltd.*, 254p.

Meffre S., Berry R.F. & Hall M. 2000. Cambrian metamorphic complexes in Tasmania: tectonic implications. *Australian Journal of Earth Sciences*, **47**, 971-985.

Miyashiro A. & Shido F. 1975. Tholeiitic and calc-alkali series in relation to the behaviours of titanium, vanadium, chromium and nickel. *American Journal of Science*, **275**, 265-277.

Montgomery A. 1894. Report on the Corinna Goldfield. *Report of the Secretary of Mines*, 1893-1894.

Moores E.M. 1991. Southwest U.S.-East Antarctica connection: a hypothesis. *Geology*, **19**, 425-428.

Mueller A.M. 1998. Sedimentology of the Oonah Formation, western Tasmania. B.Sc. Hons. Thesis. *University of Tasmania* (unpublished).

Osborn E.F. 1962. Reaction series for subalkaline igneous rocks based on different oxygen pressure conditions. *American Mineralogist*, **47**, 211-226.

Overstreet W.C. 1967. The geological occurrence of monazite. *United States Geological Survey, Professional Paper* **530**.

Park J.K., Buchan K.L. & Harlan S.S. 1995. A proposed giant radiating dyke swarm fragmented by the separation of Laurentia and Australia based on palaeomagnetism of ca. 780 Ma mafic intrusions in western North America. *Earth and Planetary Science Letters*, **132**, 129-139.

Parrish R.R. 1990. U-Pb dating of monazite and its applications to geological problems. *Canadian Journal of Earth Sciences*, **27**, 1431-1454.

Passchier C.W & Trouw R.A.J. 1996. Microtectonics. *Springer -Verlag*, 289p.

Pearce J.A. 1983. Role of the sub-continental lithosphere in magma genesis at active continental margins. In: Hawkesworth C.J. & Norry M.J. eds. Continental basalts and mantle xenoliths. *Shiva, Nantwich*, 230-249.

Pearce J.A. & Cann J.R. 1973. Tectonic setting of basic volcanic rocks determined using trace element analyses. *Earth and Planetary Science Letters*, **19**, 290-300.

Pearce J.A. & Gale G.H. 1977. Identification of ore-deposition environment from trace element geochemistry of associated igneous host rocks. *Geological Society Special Publication*, **7**, 14-24.

Pearce J.A.., Harris N.B.W. & Tingle A.G. 1984. Trace element discrimination diagrams for the tectonic interpretation of granitic rocks. *Journal of Petrology*, **25**, 956-983.

Perfit M.R., Gust D.A., Bence A.E., Arculus R.J. & Taylor S.R. 1980. Chemical characteristics of island arc basalts: implications for mantle sources. *Chemical Geology*, **30**, 256-277.

Pouchou J.L. & Pichoir F. 1984. Un nouveau modele de calcul pour la microanalyse quantitative par spectrometrie de rayons X. L'application a l'analyses d'echantillons homogenes. *Recherche Aerospatiale*, **3**, 167-192.

Powell C.McA. 1979. A morphological classification of rock cleavage. *Tectonophysics*, **58**, 21-34.

Powell C.McA. 1998. Tectonic Framework of Eastern Australia from ~1100 to ~320 Ma (abstract). In Finlayson D.M. & Jones L.E.A. eds. Mineral Systems and the Crust-Upper Mantle of Southeast Australia. *Australian Geological Survey Organisation Record* **1998/02**, 147-150.

Powell C.McA, Li Z.X., McElhinny M.W., Meert J.G. & Park J.K. 1993. Palaeomagnetic constraints on the timing of the Neoproterozoic break-up of Rodinia and the Cambrian formation of Gondwana. *Geology*, **21**, 889-892.

Powell C.McA, Baillie P.W., Preiss W.V., Gatehouse C.G., Krapez B. & Li Z.X. 1994a. South Australian Record of a Rodinian epicontinental basin and its mid-Neoproterozoic break-up to form the Palaeopacific Ocean. *Tectonophysics*, **237**, 113-140.

Powell C.McA, Baillie P.W. & Li Z.X. 1994b. Tasmania: a continental ribbon in the Neoproterozoic Pacific Ocean. *Geological Society of Australia Abstracts*, **36**, 130-131.

Powell R. & Holland T.J.B. 1998. THERMOCALC v.2.7

Powell R. & Holland T.J.B. 2000. THERMOCALC v.3.1

Preiss W.V. 2000. The Adelaide Geosyncline of South Australia and its significance in Neoproterozoic continental reconstruction. *Precambrian Research*, **100**, 21-63.

Råheim A. & Compston W. 1977. Correlations between metamorphic events and Rb-Sr ages in metasediments and eclogite from western Tasmania. *Lithos*, **10**, 271-289.

Ramsay J.G. 1967. Folding and Fracturing of Rocks. *McGraw-Hill*, 568p.

Reed A.R. 2001. Structure and setting of Proterozoic and Palaeozoic rocks in the Tamar region, northern Tasmania. *Geological Society of Australia*. SGTSG Field Guide **9**, 101pp.

Reed J. C., Bickford M. E., Houston R.S & Link P.K. (eds) 1993. Precambrian Conterminous U.S.: The Geology of North America, Boulder Colorado, *Geological Society of America*, **C-2**, 603p.

Reid A.M. 1924. Preliminary Report on the Occurrence of Iron Ore at Meredith, Paradise, Rocky, and Whyte Rivers *Tasmanian Department of Mines Report* 1924.

Ridley J. & Casey M. 1989. Numerical modelling of folding in rotational strain histories: Strain regimes expected in thrust belts and shear zones. Geology, **17**, 875-878.

Rollinson H.R. 1993. Using geochemical data: evaluation, presentation, interpretation. *Longman Ltd.*, 352p.

Ross G. 1991. Precambrian basement in the Canadian Cordillera: an introduction: *Canadian Journal Earth Science*, **28**, 1133-1139.

Ross G., Parrish R. & Winston D. 1992. Provenance and U-Pb geochronology of the Mesoproterozoic Belt Supergroup (United States): Implications for age of deposition and pre-Panthalassa plate reconstructions. *Earth and Planetary Science Letters*, **113**, 57-76.

Scherrer N.C., Engi M., Gnos E., Jakob V. & Liechti A. 2000. Monazite analysis; from sample preparation to microprobe dating and REE quantification. *Schweiz. Mineral. Petrogr. Mitt.*, **80**, 93-105.

Scott J.B. 1926. Report on Brown and Little Plains, Rocky River District. *Tasmanian Department of Mines Report* 1926.

Seymour D.B. & Calver C.R. 1995. Explanatory notes for the Time-Space Diagram and Stratotectonic Elements Map of Tasmania. *Tasmanian Geological Survey Record* **1995/01**.

Shaw R., Wellman P., Gun P., Whitaker A., Tarlowski C. & Morse M. 1996. Guide to using the Australian crustal elements map. *Australian Geological Survey Organisation Record*, **1996/30**, 1-20.

Sheraton J.W., Tingey R.J., Oliver R.L. & Black L.P. 1996. Geology of the Bunger Hills-Denman Glacier region, East Antarctica, *Australian Geological Survey Organisation Bulletin,* **244**, 70-81.

Shervais J.W. 1982. Ti-V plots and the petrogenesis of modern and ophiolitic lavas. *Earth and Planetary Science Letters*, **59**, 101-118.

Smith H.A. & Barreiro B. 1990. Monazite U-Pb dating of staurolite grade metamorphism in pelitic schists. *Contributions to Mineralogy and Petrology*, **105**, 602-615.

Solomon M. & Griffiths J.R. 1974. Aspects of the early history of the southern part of the Tasman Orogenic Zone. In: Denmead, A.K., Tweedale, G.W., & Wilson, A.F., eds. The Tasman Geosyncline – a Symposium, *Geological Society of Australia, Qld Division*, 19-44.

Spear F.S. 1993. Metamorphic Phase Equilibria and Pressure-Temperature-Time Paths. *Mineralogical Society of America*. Washington, DC, United States. 799.

Spiller A.R. 1974. The petrology of the Savage River iron ore deposit, Tasmania. B.A. Hons. Thesis, *Macquarie University* (unpublished).

Spry A.H. 1957a. Lower Pieman Hydro-Electric Development: Geology of Part of the Lower Pieman River. *Report to the Hydro-Electricity Commission Tasmania.*

Spry A.H. 1957b. The Precambrian Rocks of Tasmania, Part 1, Dolerites of the North-West Coast of Tasmania. *Papers Proceeding the Royal Society of Tasmania*, **91**, 81-93.

Spry A.H. 1957c. Precambrian Dolomites in Tasmania. *Mineral Resources Tasmania Report*, **10**, 32-38.

Spry A.H. 1958a. Lower Pieman Hydro-Electric Development: Geology of the Mt Donaldson area. *Report to the Hydro-Electricity Commission Tasmania.*

Spry A.H. 1962. The Precambrian rocks. In Spry, A.H. & Banks, M.R., eds. The Geology of Tasmania. *Journal of the Geological Society of Australia.* **9**(2): 107-145.

Spry A.H. 1964. Precambrian rocks of Tasmania, Part VI, the Zeehan - Corinna area. *Papers Proceeding the Royal Society of Tasmania*, **98**, 23-48.

Spry A.H. & Ford R.J. 1957. A reconnaissance of the Corinna-Pieman Heads area. *Papers Proceeding the Royal Society of Tasmania*, **91**, 1-7.

Storey B.C., Alabaster T., Macdonald D.I.M., Millar I.L., Pankhurst R.J. & Dalziel I.W. 1992. Upper Proterozoic rift-related rocks of the Pensacola Moutains, Antarctica: precursors to supercontinental break-up? *Tectonics*, **11**, 1392-1405.

Streit J.E. & Cox S.F. 1998. Fluid infiltration and volume change during mid-crustal mylonitization of Proterozoic granite, King Island, Tasmania. *Journal of Metamorphic Geology* **16**, 197-212.

Sun S.S. & McDonough W.F. 1989. Chemical and isotopic systematics of oceanic basalts: implications for mantle composition and processes. In: Saunders A.D. & Norry M.J., eds. Magmatism in ocean basins. *Geological Society of London Special Publication*, **42**, 313-345.

Suppe J. 1985. Principles of Structural Geology. *Prentice-Hall Inc.*, 537p.

Thureau G. 1884. Mount Cleveland and Corinna Gold Fields. *Parliamentary Papers, Tasmania.* **104**.

Turner N.J. 1979. The boundary relationship of the Concert Schist and the Oonah Quartzite and Slate correlate at Dundas. *Papers Proceeding the Royal Society of Tasmania*, **113**, 15-20.

Turner N.J. 1984. Proterozoic sequences in the southern part of the Rocky Cape region. In Baillie P.W., & Collins P.L.F., eds. Mineral Exploration and Tectonic Processes in Tasmania. *Geological Society of Australia, Tasmania Division, Hobart.*

Turner N.J. 1989. The Precambrian. In: Burrett C.F. & Martin E.L. eds. Geology and Mineral Resources of Tasmania. *Geological Society of Australia, Special Publication*, **15**, 5-46.

Turner N.J. 1990. Late Proterozoic of northwest Tasmania – regional geology and mineral deposits. In: F.E. Hughes, ed. Geology of the Mineral Deposits of Australia and Papua New Guinea. *The Australasian Institute of Mining and Metallurgy* 1169-1174

Turner N.J. 1992. Corinna 1:50 000 geological map. Field guide to selected rock exposures. *Tasmania Department of Mines Report* **1993/06**.

Turner N.J. 1993. K-Ar geochronology in the Arthur Metamorphic Complex, Ahrberg Group and Oonah Formation, Corinna district. *Tasmania Department of Mines Report* **1992/27**.

Turner N.J., Brown A.V., McClenaghan M.P. & Soetrisno I.R. 1991. Geological Atlas 1:50 000 Series. Sheet 43 (7914N). Corinna. *Department of Resources and Energy, Tasmania.*

Turner N.J., Botrill R.S., Crawford A.J. & Villa I. 1992. Geology and prospectivity of the Arthur Mobile Belt. *Bulletin of the Geological Survey of Tasmania*, **70**, 227-233.

Turner N.J. & Bottrill R.S. 1993. Blue amphibole in the Proterozoic to Cambrian Arthur Metamorphic Complex, northwest Tasmania. *Mineral Resources Tasmania Report.* **1993/26.**

Turner N.J. & Crawford A.J. 1993. General features and chemical analyses of mafic and other rocks, Corinna geological map quadrangle. *Mineral Resources Tasmania Report.* **1993/23.**

Turner N.J., Black L.P. & Kamperman M. 1994. Pre-Middle Cambrian stratigraphy, orogenesis and geochronology in western Tasmania. In: Cooke, D.R. & Kitto, P.A., eds. Contentious Issues in Tasmanian geology. *Geological Society of Australia Abstract Series*, **39**, 51-56.

Turner N.J., Black L.P. & Kamperman M. 1998. Dating of Neoproterozoic and Cambrian orogenies in Tasmania. *Australian Journal of Earth Sciences*, **45**, 789-806.

Turner N.J & Bottrill R.S. 2001. Blue amphibole, Arthur Metamorphic Complex, Tasmania: composition and regional tectonic setting. *Australian Journal of Earth Sciences*, **48**, 167-181.

Twelvetrees W.H. 1900. Report on the mineral fields between Waratah and Corinna. *Report of the Secretary of Mines, Tasmania.* 1899-1900.

Twelvetrees W.H. 1903. Report on the mineral fields between Waratah and Long Plains. *Tasmanian Department of Mines Report.* **207.**

Twelvetrees W.H. 1905. Report on the North-West Coast Mineral Deposits. *Report of the Secretary of Mines, Tasmania.* 1904-1905.

Veevers J.J., Walter M.R. & Scheibner E. 1997. Neoproterozoic tectonics of Australia-Antarctica and Laurentia and the 560 Ma birth of the Pacific Ocean reflect the 400 m.y. Pangaean Supercycle. *Journal of Geology*, **105**, 225-242.

von der Borsch C.C. 1980. Evolution of Late Proterozoic to Early Paleozoic Adelaide Foldbelt, Australia: comparisons with post-Permian rifts and passive margins. *Tectonophysics*, **70**, 115-134.

Williams E., McClenaghan M.P. & Collins P.L.F. 1989. Mid-Palaeozoic deformation, granitoids and ore deposits. In: Burrett C.F. & Martin E.L. eds. Geology and Mineral Resources of Tasmania. *Geological Society of Australia, Special Publication*, **15**, 239-292.

Williams P.R. 1989. Areas north and south of Mt Bischoff. In: Seymour D.B. compiler. Geological Atlas 1:50 000 Series Sheet 36 (8015N), St Valentines. *Geological Survey of Tasmania Explanatory Report.* 12-13.

Winchester J.A & Floyd P.A. 1976. Geochemical magma type discrimination; application to altered and metamorphosed basic igneous rocks. *Earth and Planetary Science Letters*, **28**, 459-469.

Winchester J.A & Floyd P.A. 1977. Geochemical discrimination of different magma series and their differentiation products using immobile elements. *Chemical Geology*, **20**, 325-343.

Wise D.U., Dunn D.E., Engelder J.T., Geiser P.A., Hatcher R.D., Kish S.A., Odom A.L. & Schamel S. 1984. Fault-related rocks: Suggestions for terminology. *Geology*, **12**, 391-394.

Yardley B.W.D. 1989. An introduction to metamorphic petrology. *Longman Group U.K. Ltd*, 248p.

Young G. 1992. Late Proterozoic stratigraphy and the Canada-Australia connection *Geology*, **20**, 215-218.

Zhao J. & McCulloch M.T. 1993. Sm-Nd isochron ages of Late Proterozoic dyke swarms in Australia: evidence for two distinctive events of mafic magmatism and crustal extension. *Chemical Geology*, **109**, 341-354.

Zhao J., McCulloch M.T. & Korsch R.J. 1994. Characterisation of a plume-related ~800 Ma magmatic event and its implications for basin formation in central-southern Australia. *Earth and Planetary Science Letters*, **121**, 349-367.

Zhu C. & Sverjensky D.A. 1991. Partitioning of F-Cl-OH between minerals and hydrothermal fluids. *Geochimica et Cosmochimica Acta,* **55**, 1837-1858.

Zhu X.K. & O'Nions R.K. 1999. Monazite chemical compositions: some implications for monazite geochronology. *Contributions to Mineralogy and Petrology,* **137**, 351-363.